INTRODUCTION TO FLUID MOTIONS AND SEDIMENT TRANSPORT



John Southard
Massachusetts Institute of Technology



Massachusetts Institute of Technology

Introduction to Fluid Motions and Sediment Transport

John Southard

This text is disseminated via the Open Education Resource (OER) LibreTexts Project (https://LibreTexts.org) and like the thousands of other texts available within this powerful platform, it is freely available for reading, printing, and "consuming."

The LibreTexts mission is to bring together students, faculty, and scholars in a collaborative effort to provide an accessible, and comprehensive platform that empowers our community to develop, curate, adapt, and adopt openly licensed resources and technologies; through these efforts we can reduce the financial burden borne from traditional educational resource costs, ensuring education is more accessible for students and communities worldwide.

Most, but not all, pages in the library have licenses that may allow individuals to make changes, save, and print this book. Carefully consult the applicable license(s) before pursuing such effects. Instructors can adopt existing LibreTexts texts or Remix them to quickly build course-specific resources to meet the needs of their students. Unlike traditional textbooks, LibreTexts' web based origins allow powerful integration of advanced features and new technologies to support learning.



LibreTexts is the adaptable, user-friendly non-profit open education resource platform that educators trust for creating, customizing, and sharing accessible, interactive textbooks, adaptive homework, and ancillary materials. We collaborate with individuals and organizations to champion open education initiatives, support institutional publishing programs, drive curriculum development projects, and more.

The LibreTexts libraries are Powered by NICE CXone Expert and were supported by the Department of Education Open Textbook Pilot Project, the California Education Learning Lab, the UC Davis Office of the Provost, the UC Davis Library, the California State University Affordable Learning Solutions Program, and Merlot. This material is based upon work supported by the National Science Foundation under Grant No. 1246120, 1525057, and 1413739.

Any opinions, findings, and conclusions or recommendations expressed in this material are those of the author(s) and do not necessarily reflect the views of the National Science Foundation nor the US Department of Education.

Have questions or comments? For information about adoptions or adaptions contact info@LibreTexts.org or visit our main website at https://LibreTexts.org.

The LibreTexts name, logo, and book covers are trademarked by LibreTexts, Inc. (a 501(c)(3) not-for-profit organization) and protected against unauthorized use.

This text was compiled on 10/20/2026

TABLE OF CONTENTS

Licensing

1: Introduction

1.1: The Nature of Fluids

1.2: Pressure

1.3: Viscosity

1.4: Diffusion

2: Flow Past a Sphere I - Dimensional Analysis, Reynolds Numbers, and Froude Numbers

2.1: Introduction

2.2: Which Variables are Important?

2.3: Some Dimensional Reasoning and its Consequences

2.4: How to Construct Dimensionless Variables

2.5: What if You Choose the Wrong Variables?

2.6: "Dimensional Analysis"

2.7: Significance of Reynolds Numbers and Froude Numbers

3: Flow Past a Sphere II - Stokes' Law, The Bernoulli Equation, Turbulence, Boundary Layers, Flow Separation

3.1: Introduction and the Navier-Stokes Equation

3.2: Flow Past a Sphere at Low Reynolds Numbers

3.3: Inviscid Flow

3.4: The Bernoulli Equation

3.5: Turbulence

3.6: Boundary Layers

3.7: Flow Separation

3.8: Flow Past a Sphere at High Reynolds Numbers

3.9: Settling of Spheres

4: Flow in Channels

4.1: Introduction to Flow in Channels

4.2: Laminar Flow Down an Inclined Plane

4.3: Turbulent Flow in Channels - Initial Material

4.4: Turbulent Shear Stress

4.5: Structure of Turbulent Boundary Layers

4.6: Flow Resistance

4.7: Velocity Profiles

4.8: More on the Structure of Turbulent Boundary Layers- Coherent Structures in Turbulent Shear Flow

5: Open-Channel Flow

5.1: Introduction to Open-Channel Flow

5.2: Two Practical Problems
5.3: Uniform Flow
5.4: Energy in Open-Channel Flow
5.5: The Hydraulic Jump
5.6: Hydraulic Regimes of Open-Channel Flow
5.7: Gradually Varied Flow

6: Oscillatory Flow

6.1: Introduction
6.2: The Nature of Waves
6.3: Water Motions Due to Waves
6.4: Wave Boundary Layers
6.5: Combined Flow (Waves plus Current)

7: Flow in Rotating Environments

7.1: Playing on a Rotating Table
7.2: The Coriolis Effect on the Earth's Surface
7.3: The Rossby Number and Inertia Currents
7.4: The Ekman Spiral
7.5: Geostrophic Motion
7.6: Ekman Layers
7.7: Planetary Boundary Layers- The Ekman Layer, The Logarithmic Layer, and The Mixed Layer

8: Sediments, Variables, and Flumes

8.1: Introduction to Sediments, Variables, and Flumes
8.2: Hydrodynamic Perspective
8.3: Particle Motions vs. Turbulence
8.4: Observing Sediment Transport
8.5: Variables
8.6: Flumes

9: Threshold of Movement

9.1: Introduction to Threshold of Movement
9.2: Forces on Bed Particles
9.3: Balance of Forces and Dimensional Analysis
9.4: Movement Threshold
9.5: Recasting the Shields Diagram
9.6: The Effect of Density Ratio

10: Movement of Sediment by Water Flows

10.1: Introduction to the Movement of Sediment by Water Flows
10.2: The Bed, the Flow, and the Load
10.3: Transport Mode Versus Flow Intensity
10.4: Bed Load

10.5: Suspension in a Shear Flow- The Diffusional Theory of Suspension

11: Movement of Sediment by the Wind

11.1: Introduction

11.2: Saltation I

11.3: Saltation II

12: Bed Configurations Generated by Water Flows and the Wind

12.1: Introduction to Bed Configurations

12.2: Unidirectional-Flow Bed Configurations

12.3: Velocity Profiles over Ripples

12.4: Movement of Ripples and Dunes

12.5: 2D Dunes and 3D Dunes

12.6: Oscillatory-Flow and Combined-Flow Bed Configurations

12.7: Wind Ripples and Eolian Dunes

12.8: Works Cited and Reading List

13: The Sediment Transport Rate

13.1: Introduction to Sediment Transport Rates

13.2: The Sediment Load and the Sediment Transport Rate

13.3: Predicting the Sediment Transport Rate

14: Mixed-Size Sediments

14.1: Introduction

14.2: Several Consequences of Size

14.3: A Look at Some Real Data on Fractional Transport Rates, From the Flume and From the Field

14.4: Movement Threshold in Mixed-Sized Sediments

14.5: Deviations from the Condition of Equal Mobility

15: Deposition

15.1: Introduction to Deposition

15.2: Modes of Deposition

15.3: Why Deposition or Erosion?

16: Cross Stratification

16.1: Stratification and Cross Stratification

16.2: The Nature of Cross Stratification

16.3: The Basic Idea Behind Climbing-Bed-Form Cross Stratification

16.4: Important Kinds of Climbing-Bed-Form Cross Stratification

16.5: Cross Stratification Not Produced by Climbing Bed Forms

17: Planar Stratification

17.1: Introduction to Planar Stratification

17.2: The Origin of Planar Lamination in Sands and Sandstones

17.3: Planar Lamination in Fine Sediments

Index
Index
Glossary
Detailed Licensing

This page titled Introduction to Fluid Motions and Sediment Transport (Southard) is shared under a CC BY-NC-SA 4.0 license and was authored, remixed, and/or curated by John Southard via source content that was edited to the style and standards of the LibreTexts platform.

Licensing

A detailed breakdown of this resource's licensing can be found in ***Back Matter/Detailed Licensing***.

This page titled Licensing is shared under a license and was authored, remixed, and/or curated by LibreTexts.

1: INTRODUCTION

1.1: The Nature of Fluids
1.2: Pressure
1.3: Viscosity
1.4: Diffusion

This page titled 1: Introduction is shared under a CC BY-NC-SA 4.0 license and was authored, remixed, and/or curated by John Southard (MIT OpenCourseware) via source content that was edited to the style and standards of the LibreTexts platform.

1.1: The Nature of Fluids

Fluids are substances that deform continuously and permanently when they are subjected to forces that vary spatially in magnitude or direction. The nature of the relationship between the deforming forces and the geometry of deformation varies from fluid to fluid; you will see in this chapter that the relationship is a simple linear one for air and water. Fluids can be classified as either **liquids**, which are relatively dense and maintain a definite volume, and **gases**, which are less dense and expand to fill their container. Fluids, both liquids and gases, are distinguished from solids by their inability to withstand deforming forces: in contrast to solids, they continue to deform for as long as the deforming forces are applied. This distinction is actually not as neat as I have made it out to be, but we would become sidetracked into the field of rheology for elaboration.

Liquids and gases differ greatly in their structure on the atomic scale: liquids consist of closely packed molecules that exert strong forces on their neighbors as they weave around one another, sometimes forming fleeting and very small bonded aggregates, whereas gases, unless they are very compressed, consist of atoms or molecules that are almost always far apart from one another as they zip around along their free paths of motion, colliding with the walls of their container and occasionally with one another.

How is it, then, that the *macroscopic motions of liquids and gases need not be considered separately*? The answer is that fluids can be treated as if they were 2—as if their constituent matter, which is actually distributed discontinuously as atoms and molecules, were smeared uniformly throughout space. The idea here is that the forces among the constituent particles, which vary enormously in space on the scale of the particles themselves, average out to look as though they vary smoothly on scales much larger than the particles but very small relative to the macroscopic scales of problems in fluid dynamics—which themselves can be very small. To phrase this in a slightly different way: *the structure of fluids is on such a fine scale that the actual intermolecular forces can just as well be treated as continuously and smoothly varying*, from the standpoint of all problems in fluid dynamics on *scales much larger than the molecules*. The justification for this approach is that it works extremely well for fluid flows on scales that are much larger than the intermolecular spacing. So in these notes you never have to think again about the atoms and molecules of fluids! (Well, that's not quite true, but almost.)

This page titled 1.1: The Nature of Fluids is shared under a CC BY-NC-SA 4.0 license and was authored, remixed, and/or curated by John Southard (MIT OpenCourseware) via source content that was edited to the style and standards of the LibreTexts platform.

1.2: Pressure

The concept of fluid pressure is one of the most fundamental in fluid dynamics. Generally in physics the term **pressure** is used for a *force per unit area*. But we need to be more specific about the significance of pressure in fluids.

Fluid Pressure

Suppose that you immerse a solid test sphere in a container of fluid at rest, and suppose further that you have a little meter with which you can measure the normal force per unit area exerted by the fluid at some point on the surface of the sphere (Figure 1.2.1). That force per unit area is the pressure exerted by the fluid on the surface of the sphere. That probably seems like a simple enough concept. (Because the fluid is not moving relative to the sphere, the fluid exerts only a normal component of force, not a tangential component; we will start looking at the nature of the tangential force exerted by moving fluid on a solid surface in the following section.) But there is more to fluid pressure than just that.

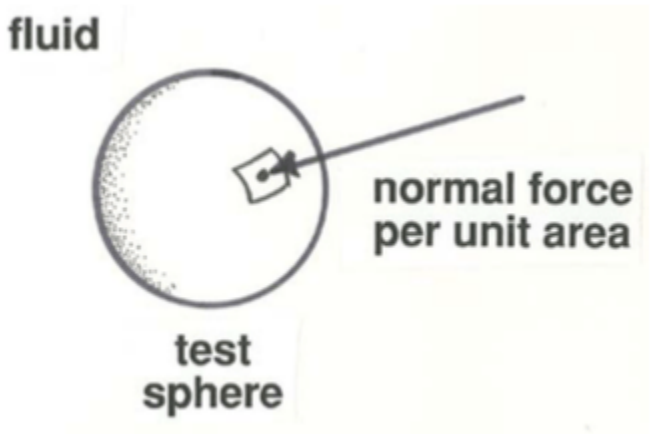


Figure 1.2.1: Normal force per unit area exerted by the fluid at a point on the surface of a tests sphere immersed in the fluid.

Now suppose that you make the solid sphere smaller and smaller. You can think of it as eventually becoming just a point. Then, associated with each line through that point there is a compressive force per unit area, directed inward from both directions along the line toward the point, with the same value as the force per unit area you measured on the surface of the test sphere (Figure 1.2.2). And the value of this compressive force per unit area is the same for every orientation of the line through the point. This is the essence of the concept of **fluid pressure**: *it is a compressive force per unit area that acts equally in all directions at a point in the fluid*, whether or not there is a solid surface at that point upon which the force acts. If there is no solid surface, you just have to think in terms of one part of the fluid continuum exerting a compressive force on the adjacent part of the fluid continuum.

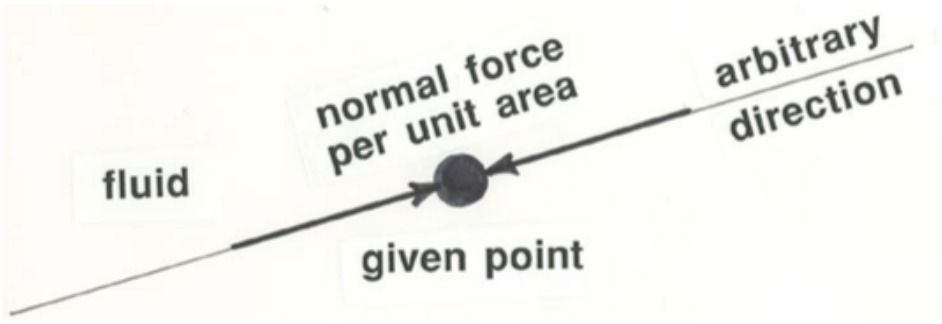


Figure 1.2.2: The compressive force per unit area associated with each line through a point in the fluid.

Pressure of a Moving Fluid

The concept of fluid pressure introduced above holds equally well for a moving fluid. Then you just have to imagine measuring the pressure at a point that is *moving along with the fluid*. It is convenient and natural to think of the pressure in a moving fluid as being made up of two parts, the static pressure and the dynamic pressure. The **static pressure** is the pressure that would be measured at the given point in the fluid if the fluid were not moving. The **dynamic pressure** is the difference between the total pressure—that is, the pressure you would actually measure at the given point in the moving fluid, with some appropriate instrument—and the static pressure. The dynamic pressure is the part of the pressure that is associated with the motion of the fluid. There will be much more to say about the relationship between fluid motion and dynamic pressure later in these notes; suffice it to say here that the dynamic pressure is zero in a stationary fluid, and also in a fluid that is in *uniform motion*, in the sense that there are no accelerations anywhere in the fluid (Figure 1.2.3).

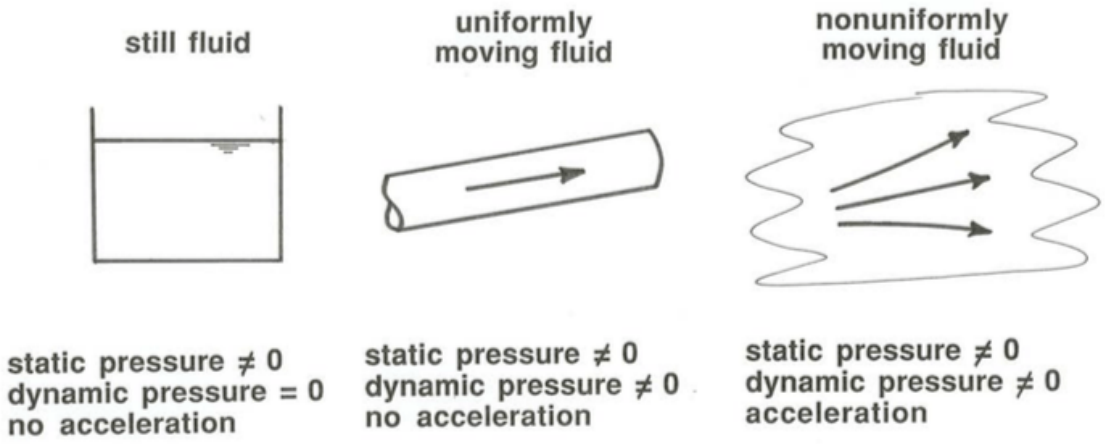


Figure 1.2.3: Static pressure and dynamic pressure in fluids at rest, in uniformly moving fluids, and in non-uniformly moving fluids.

Static Pressure

It is not difficult to understand here, however, what determines the static pressure. In the case of fluid in a closed container, one part of the static pressure has to do just with the external compression imposed upon the walls of the container. When you blow up a balloon, the air pressure inside the balloon is greater than outside, because the distended walls of the balloon are trying to re-shrink, and as a consequence they are everywhere pushing inward against the air inside (Figure 1.2.4). The pressure on the walls becomes adjusted to be the same at all points, because if that were not the case, then there would be pressure differences from point to point within the fluid, and by Newton's second law that would cause motions in the fluid.

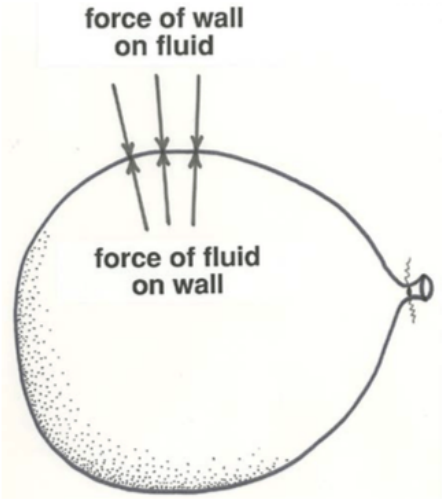


Figure 1.2.4: Forces at the wall of a blown-up balloon.

The other part of the static pressure has to do with the weight of fluid that overlies a given point in the fluid. Think about a tall upright cylindrical container filled with a liquid (Figure 1.2.5). You can easily compute the weight of liquid in the vertical column that overlies a little unit area on the bottom of the container: it is equal to $p = \rho g h$ (1.2.1), where ρ is the density of the liquid, g is the acceleration of gravity, and h is the height of the liquid column above the bottom:

$$p = \rho g h \tag{1.2.1}$$

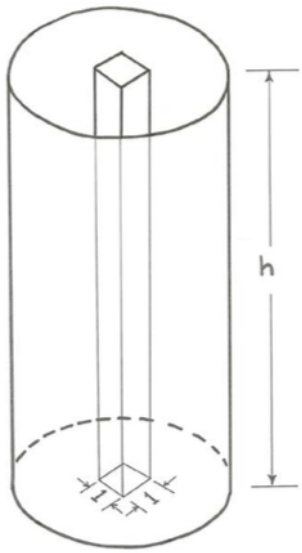


Figure 1.2.5: Hydrostatic pressure in a column of water.

It is just a matter of multiplying the weight per unit volume of the liquid, ρg, by the volume of liquid in the vertical column, h (1.2.1). This part of the static pressure caused by the weight of overlying fluid, called the **hydrostatic pressure**, is given by the same equation not just on the bottom but also at all points in the fluid, and on the sides of the container as well; refer to the discussion, above, of the nature of pressure as a compressive force per unit area acting equally in all directions at any point in the fluid.

So by Equation (1.2.1), called the **hydrostatic equation**, the hydrostatic pressure in the liquid increases linearly with depth, from zero at the surface (Figure 1.2.6). Compressible fluids like gases, however, are trickier; the vertical distribution of density and pressure in the atmosphere, for example, is the outcome of the balance between pressure and weight of overlying fluid, on the one hand, and the relationship between pressure and density, on the other hand.

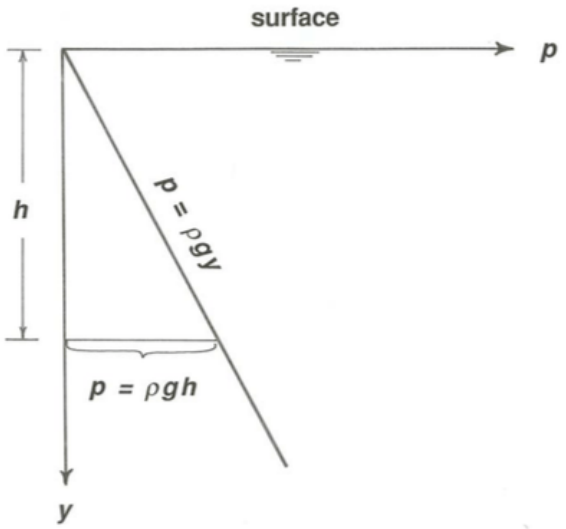


Figure 1.2.6: The linear increase in hydrostatic pressure with depth.

Look again at the container of motionless liquid. In your imagination, isolate a volume of liquid, bounded at the top and bottom by imaginary horizontal planes and around the sides by an imaginary vertical cylinder. Now examine the balance of forces in the vertical direction on the mass of liquid contained within that volume. One thing we know for sure is that the sum of all the vertically directed forces, upward and downward, on that mass of liquid has to be zero, because the liquid is at rest, and Newton's second law tells us that the net force acting on the volume of liquid must be zero. (This technique of isolating an imaginary volume of material, called a **free body**, and examining the forces on it and the motions it undergoes is a common technique in the mechanics of continuous media, whether solids or fluids.)

There are vertically directed pressure forces on the top and bottom of the cylinder, but not on the sides of the cylinder, because the pressure forces on the sides of the cylinder are all horizontal. Remember that by the hydrostatic equation the pressure on the bottom of the free body is greater than the pressure on the top. Why, then, does the body not accelerate upward, in accordance with Newton's second law? The answer is that this upward-directed pressure force is exactly balanced by the weight of the liquid in the body. This is a manifestation of what is called the **hydrostatic balance**.

Buoyancy

Now suppose that you replace the imaginary free body of liquid with a real body of the same shape, with vanishingly thin but rigid walls and just empty space (if we ignore the density of air) within. The weight of the body is effectively zero, so there is no weight to balance the upward-directed net pressure force. As you all know, the body floats up to the surface. This effect, termed **buoyancy**, holds for all fluids, gases as well as liquids. It should be easy for you to imagine the great many environments, in and on the Earth, where buoyancy is an important effect.

If you want a real-life demonstration of the magnitude of the buoyancy force, try taking a watertight and lightweight pail and pushing it down into a tub full of water, with its open end facing upward (Figure 1.2.7). You know that the farther in you push it, the more difficult it is to push it. What is going on here is that you are pushing against the force of the hydrostatic pressure summed over the entire bottom surface of the pail. There is no water in the pail to balance that hydrostatic pressure force, so you have to establish the balance with your own hands and arms.

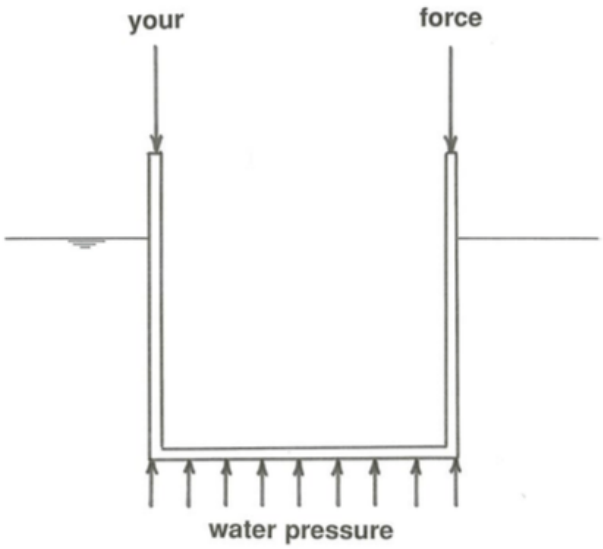


Figure 1.2.7: The force of buoyancy when you push an airtight empty box into the water.

The various bodies within the fluid we have been dealing with need not be of the special shape, with only vertical and horizontal surfaces, we have been assuming. The same considerations hold true for bodies of arbitrary shape. At a point on a sloping part of the surface of such a body, you just have to take the vertical component of the pressure that is acting normal to the surface at the given point, and therefore in a sloping direction (Figure 1.2.8).

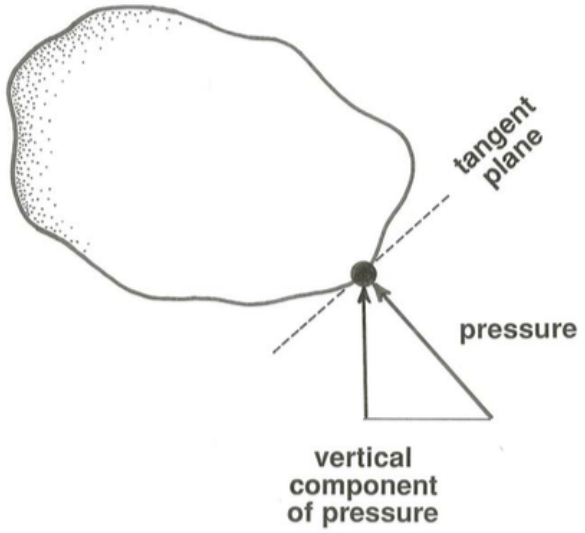


Figure 1.2.8: The vertical component of the fluid pressure on a submerged object of arbitrary shape.

Specific Weight

One final matter has to do with the weight per unit volume, or **specific weight**, of an object or of some part of a continuous material, usually denoted by γ. Because the weight of a body is mg, the specific weight is $mg/volume$, which can be rearranged as $(m/volume)g$, or ρg, because density ρ is just mass per unit volume. So the relationship between density (mass per unit volume) and specific weight (weight per unit volume) is $\gamma = \rho g$. (Minor note: density could be called “specific mass”, but it never is—although its inverse, the volume per unit mass, is indeed called the specific volume.)

You also have to think about the submerged specific weight of an object that is entirely immersed in a fluid. It should make sense to you, and it follows from the earlier considerations on the pressure forces on submerged bodies, that the effective weight of a submerged body is less than its actual weight by the weight of the fluid it displaces. (This is the effect that I think is supposed to

have caused Archimedes to shout “Eureka!” in his bathtub.) In these notes the submerged specific weight is denoted by γ'. Here is the mathematics:

$$\gamma' = \rho_{body} g - \rho_{fluid} g = (\rho_{body} - \rho_{fluid})\, g \tag{1.2.2}$$

If this does not make immediate sense to you, just imagine that the density of a certain submerged body, initially denser than the fluid, is gradually decreased somehow until its density is the same as that of the fluid, whereupon it has the same specific weight as the fluid and is in hydrostatic balance, and therefore neither rises nor sinks. A body of this kind is said to be *neutrally buoyant*. Tiny neutrally buoyant particles make excellent markers for tracing and visualizing the motions of fluids, both in reality and in the imagination.

This page titled 1.2: Pressure is shared under a CC BY-NC-SA 4.0 license and was authored, remixed, and/or curated by John Southard (MIT OpenCourseware) via source content that was edited to the style and standards of the LibreTexts platform.

1.3: Viscosity

Another concept in fluid dynamics, viscosity, is one that is less likely to be within your range of intuition and experience than pressure. **Viscosity** is a property of fluids that characterizes their resistance to deformation. This section is devoted to making that idea clear to you, and to making a start on exploring its consequences for fluid motions.

Parallel Plate Experiment

For a first look at how fluids behave when they are deformed, here is an experiment you could attempt on your own kitchen table. Arrange two horizontal parallel plates, spaced a distance L apart, with a fluid at rest between them (Figure $1.3.1$). You could justifiably argue that it would be hard to make such an experiment, because how could you keep the fluid from leaking out at the margins of the plates? Do not worry about such practicalities; just suppose that the plates are very broad relative to their spacing, or that the fluid you have chosen is "thick", i.e., has a high viscosity (you are likely to have a number of high- viscosity household fluids, like honey, or molasses, or corn syrup, or motor oil, available), which would ooze out from the between the plates only slowly, giving you time to do the experiment described below.

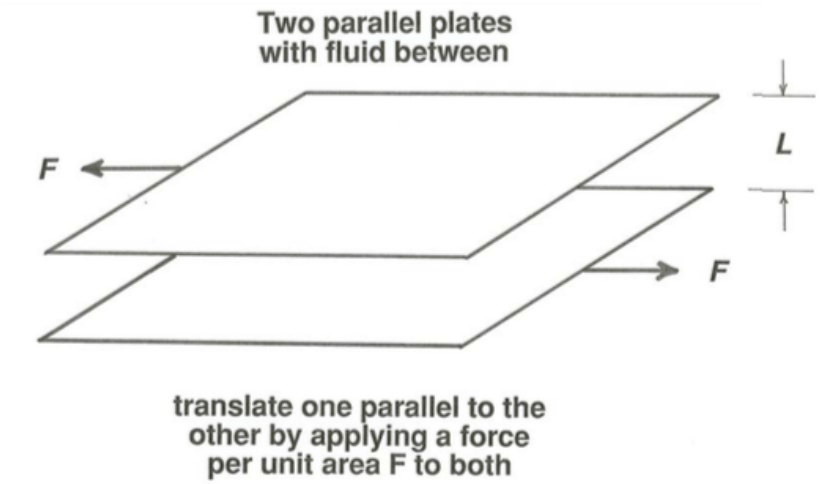


Figure $1.3.1$: Shearing a fluid between two parallel plates.

Accelerate the upper plate rapidly to a constant velocity V parallel to itself by applying a force per unit area, call it F, over its entire surface, while you hold the lower plate fixed by applying to it an equal and opposite force per unit area. You could do that by taping the lower plate to the table and attaching handles with suction cups to the top of the upper plate. The fluid is set in motion by friction from the moving plate.

How does the fluid move? You might picture the motion as a series of tabular layers of fluid, parallel to the bounding plates, sliding past one another in a shearing motion, but of course in reality the shearing is continuous rather than as discrete layers. Shear of this kind always acts whenever fluids are in motion relative to solid boundaries—which is just about all the flows we will consider in these notes. If you were somehow able to measure the velocity of the fluid at a large number of points along some imaginary line normal to the plates (Figure $1.3.2$), what would be the distribution of velocity? You would find that after an initial transient period of adjustment during which progressively lower layers of the fluid are brought into motion, the velocity would vary linearly from zero at the stationary plate to V at the moving plate.

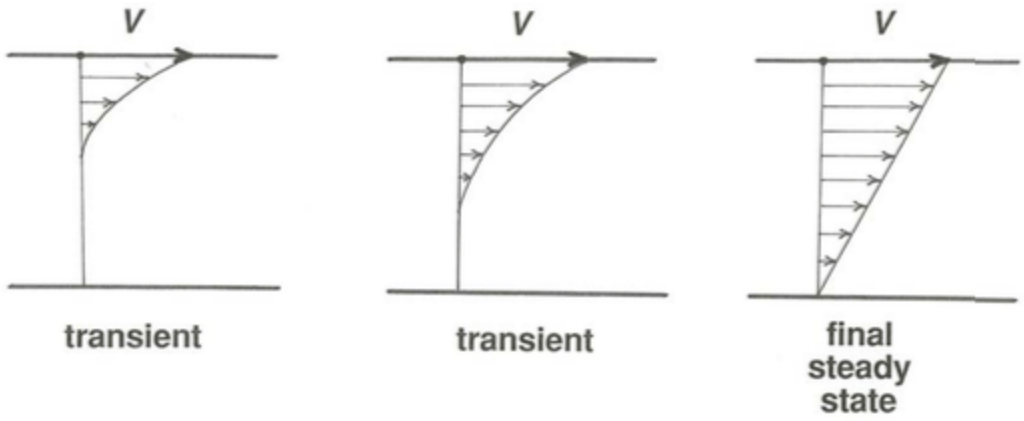


Figure 1.3.2: Development of the velocity profile in a fluid sheared between two parallel plates.

From Figure 1.3.2 you can see that the fluid in contact with each of the plates has exactly the same velocity as the plates themselves. This is a manifestation of what is known as the **no-slip condition**: fluid in contact with a solid boundary has exactly the same velocity as that boundary. Although this no- slip condition might seem counterintuitive to you, it is a fact of observation, and it can be justified by considerations on intermolecular forces. The flow of the continuously deforming fluid past the solid boundary is not the same as sliding a rigid slab, like a brick, across a table top. Intermolecular forces act between the fluid and the solid at the boundary just as they do across planes of shearing in the interior of the fluid, so there's no more reason to expect a discontinuity in velocity at the boundary than within the fluid.

Shear Stress

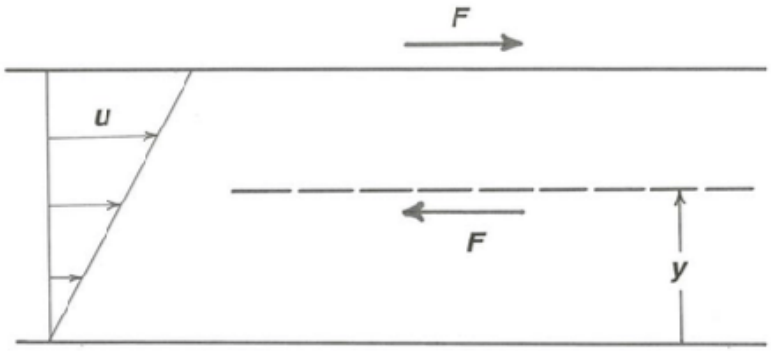


Figure 1.3.3: An imaginary plane, parallel to the plates, in the sheared fluid. F is the shearing force per unit area.

To see why the velocity distribution between the plates is linear, pass an imaginary plane, parallel to the plates, anywhere through the fluid (Figure 1.3.3). Because the fluid contained between this plane and either the lower plate or the upper plate is not being accelerated after the steady state is attained, the fluid on either side of this plane must be exerting on the fluid on the other side of the plane the same force per unit area F as that on the plates themselves. Because the imaginary plane can be located anywhere between the two plates, the shearing force per unit area across all such planes in the fluid, called the **shear stress**, must be the same. (From here on, keep firmly in mind the distinction between *shear*, an aspect of the geometry of fluid deformation, and *shear stress*, the shearing force per unit area associated with the shearing.) And because the fluid must be expected to shear or deform at the same rate for the same applied shearing force, the rate of change of velocity normal to the plates must be constant: assuming the y axis to be normal to the plates, and letting u be the velocity of the fluid at a point,

$$du/dy = k \tag{1.3.1}$$

where k is some constant. So the velocity itself must vary linearly: taking $y = 0$ at the lower plate,

$$u = \int k dy = ky + c \tag{1.3.2}$$

Evaluating the constant of integration c by using the no-slip condition that $u = 0$ at $y = 0$, we find $c = 0$, so

$$u = ky \tag{1.3.3}$$

For more on what determines the magnitude of that constant k, see a later paragraph.

Viscosity

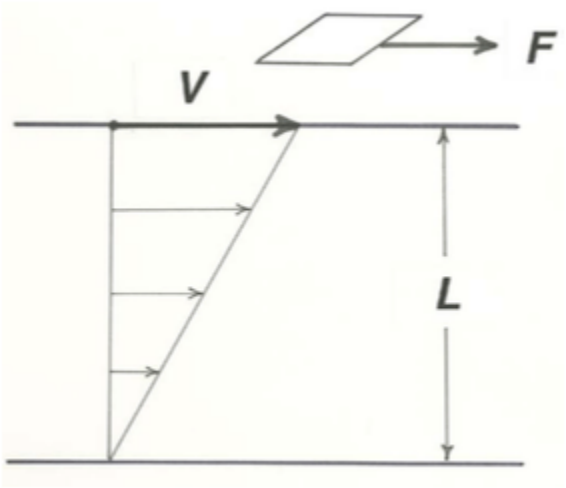


Figure 1.3.4: The force per unit area F needed to produce a given difference in velocity between two parallel plates with sheared fluid between.

What determines the value of F needed to produce a given difference in velocity between the two plates (Figure 1.3.4)? For many fluids the ratio of F to the quantity V/L, which represents the rate of shear in the fluid, would be found to be the same for all values of F:

$$F/(V/L) = \text{const}, \text{or} F = \text{const} \cdot (V/L) \tag{1.3.4}$$

This constant ratio, the ratio of applied shear stress to the resulting rate of shear, usually denoted by μ, is called the **viscosity** of the fluid. The viscosity is this the fluid property that characterizes the resistance of the fluid to deformation. For fluids like air and water, the viscosity is indeed an intrinsic property of the fluid, in that it does not depend on the state of motion but only on the nature of the fluid itself. Different fluids have different viscosities. Fluids with higher viscosities require a greater shearing force per unit area to produce a given rate of shearing, and fluids with higher viscosities have a greater rate of shearing for a given shearing force per unit area. For a given fluid the viscosity is a function of temperature; for water, viscosity decreases with temperature, but for air, viscosity increases with temperature.

Universal Case

Now we need to generalize beyond the kitchen-table experiment. Here comes a substantial conceptual jump. The parallel-plate experiment is a rather specialized case of shearing in a fluid. In a more general flow, the geometry of the flow is more complicated and the rate of shear and the corresponding shearing force per unit area generally varies from place to place. Even so, the deformation of the fluid in any tiny volume can be visualized in the same way as in the parallel-plate experiment. A relationship like Equation 1.3.4 holds at every point in a sheared fluid, no matter how much the rate and orientation of the shearing vary from place to place:

$$\frac{\tau}{du/dy} = \mu \tag{1.3.5}$$

or

$$\tau = \mu \frac{du}{dy} \tag{1.3.6}$$

where τ is the shear stress (i.e., the local shearing force per unit area) exerted across the shearing surfaces at some point in the

fluid, and du/dy is the rate of change of the local fluid velocity u in the direction y normal to the shearing surfaces at the point (Figure 1.3.5). We will often have occasion to make use of Equation 1.3.6 later in the course. I have sidestepped its derivation from first principles; that would necessitate starting from Newton's second law, written in differential form, for the general fluid motion. I hope that the shortcut I have presented here gives you a good understanding of the significance of Equation 1.3.6.

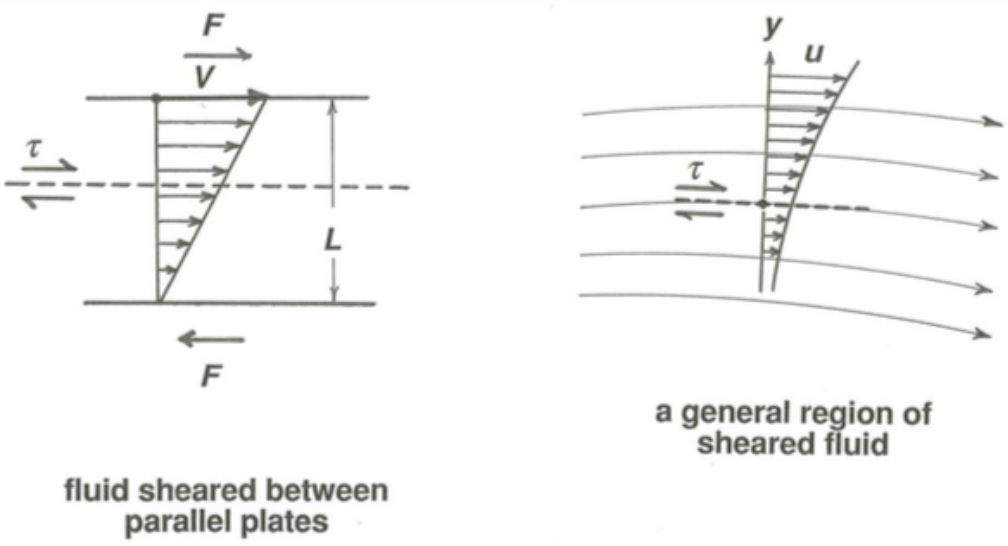


Figure 1.3.5: Viscosity as the ratio of applied shear stress to rate of shear at a point in a sheared fluid.

You can see now the significance of k in the linear velocity distribution in Equation 1.3.3 for shearing of a fluid between parallel plates. Combine Equation 1.3.6, the general relationship between shear stress and shear rate, with the result, found above for the parallel-plate experiment, that $du/dy = k$ (Equation 1.3.1), which expresses that the spatial rate of change, in the direction normal to the planes of shearing, of local fluid velocity is the same at all levels between the plates:

$$\frac{du}{dy} = k = \frac{\tau}{\mu} \tag{1.3.7}$$

So the constant k reflects the relative magnitude of the applied shearing force per unit area and the viscosity: for given viscosity, a greater applied shearing force per unit area on the upper plate produces a steeper velocity gradient in the fluid, and for given applied force per unit area, a given viscosity produces a less steep velocity gradient.

Why do fluids resist deformation? The shear stress that is mutually exerted across the surfaces of shear in the fluid, like the shear planes in the fluid between the parallel plates on your kitchen table, can be thought of as **internal friction**. For liquids, to account for the origin of this internal friction you can appeal to the necessity of stretching and breaking the fleeting bonds between the adjacent close-lying molecules of the fluid whose centers lie on one side or other of the imaginary shear plane. For gases, however, the picture is not as straightforward (although ultimately simpler mechanically!) because gases consist of isolated atoms or molecules pursuing their free paths and interacting among themselves only relatively infrequently. In gases, the shear planes pass through mostly empty space, and the constituent particles are for the most part moving freely as they pass across the shear planes in one direction or the other. To present a satisfactory account of the origin of internal friction in sheared gases, we have to deal with the phenomenon of *diffusion*. Diffusion is an important physical process that will figure in a number of later topics in these notes as well, so this is a good place, in the following section, to address it.

This page titled 1.3: Viscosity is shared under a CC BY-NC-SA 4.0 license and was authored, remixed, and/or curated by John Southard (MIT OpenCourseware) via source content that was edited to the style and standards of the LibreTexts platform.

1.4: Diffusion

Diffusion is the process by which matter, or properties carried by matter, like momentum, heat, solute, or suspended sediment, is transported from one part of a medium to another by random motions, molecular or macroscopic, in the presence of a spatial variation, or gradient, in average concentration of matter or the property. The essential factors in diffusion are thus the presence of random movements within the medium and a spatial gradient of some quantity or property. There cannot be diffusive transport without the concurrent existence of both conditions.

A good way to understand the nature of diffusion is to think about a simple hypothetical example. Suppose that you erect a vertical wall or barrier across the middle of a large room and manage somehow to fill one side of the room with white air molecules and the other side of the room with black air molecules (Figure 1.4.1). At some particular time you instantaneously remove the barrier. Watch the exchange of speeding molecules across the plane once occupied by the barrier. In any small time interval the numbers of molecules passing in one direction across that plane is almost exactly equal to the numbers of molecules passing in the other direction, because the concentration of molecules stays the same everywhere, on the average, or else pressure differences from place to place would cause a net movement of air from higher pressure to lower pressure.

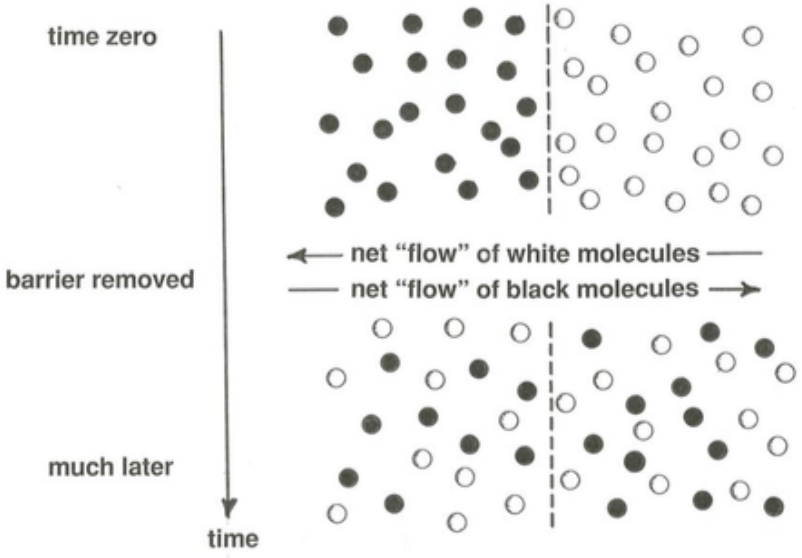


Figure 1.4.1: Diffusion of air molecules.

Immediately after the barrier is removed, all of the molecules moving from the "white" side to the "black" side are white and all of the molecules moving from the "black" side to the "white" side are black. At later times, after some of the white molecules have made their way over to the originally black side and some of the black molecules have made their way over to the white side, both white and black molecules move across the plane in each direction, but for a long time more white molecules than black move from the originally white side to the originally black side, and likewise more black molecules than white move from the originally black side to the originally white side.

This reveals the essence of diffusive transport: as the gradient of concentration of black and white molecules normal to the plane is made smaller by the diffusive transport, the rate of diffusive transport itself decreases; gradually the concentration gradients are evened out. Eventually, equal numbers of blacks and whites pass across the plane in either direction, and there is no more diffusive transport.

In simple diffusion of the kind exemplified above, the rate of diffusive transport, expressed as mass per unit time per unit area normal to the direction of diffusion (called the **diffusive flux**) is directly proportional to the concentration gradient in the direction of the diffusive flux. In the example above, you could convince yourself of this with just a little thought. This is expressed by the equation

$$F = -D\frac{\partial c}{\partial x} \tag{1.4.1}$$

where F is the rate of transport of mass per unit area, c is the mass concentration of the diffusing substance, and D is a proportionality coefficient called the **diffusion coefficient**. The minus sign is there because the diffusive transport is in the direction of decrease in c ("down the gradient", in the parlance of physics). Diffusion can be more complicated than this: the diffusion coefficient might be a function of the concentration, and it might vary with direction at a point. We will not need to deal with such complications in these notes.

Viscosity as a Diffusion Coefficient

Viscosity can be interpreted as a *diffusion coefficient for molecular momentum*. Look at a small region of sheared fluid, and focus in on the collection of molecules in the vicinity of one of the shear planes (Figure 1.4.2). Molecules are continually passing back and forth across the plane. The total mass of molecules passing in one direction is the same as the total mass passing in the other direction, but (and this is the essential point) the same kind of statement isnot true for transport, in the direction normal to the shear plane, of the component of molecule momentum taken normal to the shear plane and in the direction of average movement—just because, by the nature of shearing, the average velocity is greater on one side of the plane than the other. So random movements of molecules across the shear plane cause a normal-to-the-shear-plane transport of downflow component of momentum in the direction from higher flow speed to lower flow speed.

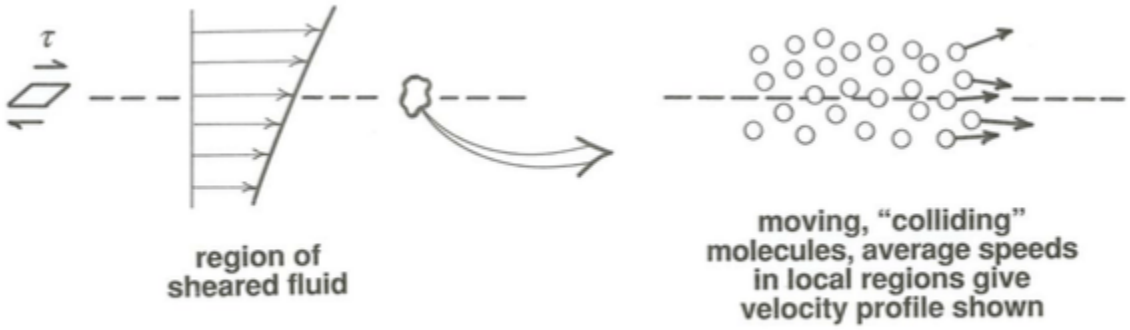


Figure 1.4.2: How the random motions of fluid molecules in the presence of macroscopic shear in a fluid continuum gives rise to shear stress.

Applying the diffusion equation (Equation 1.4.1) here, momentum transport rate $= D\frac{d(\rho u)}{dy}$

$$= \rho D \frac{du}{dy} \tag{1.4.2}$$

By Newton's second law this spatial rate of change of momentum is equivalent to a force per unit area τ on the shear planes:

$$\tau = \rho D \frac{du}{dy} \tag{1.4.3}$$

By comparing Equation 1.4.2 with Equation 1.4.3 you see that the viscosity μ can be viewed as the diffusion coefficient for downflow momentum, multiplied by the fluid density ρ. The physical interpretation here is that the on-the-average faster molecules that pass across the shear plane from the higher-velocity side to the lower-velocity side tend to speed up the molecules on the lower-velocity side, by eventually colliding with them and exerting actual forces on them, and conversely the on-the-average slower molecules that pass across the shear plane from the lower-velocity side to the higher-velocity side tend to slow down the molecules on the higher-velocity side. This mutual speeding-up and slowing-down has the effect of an actual surface contact force across the plane, of the sort you would associate with, say, the sliding of a brick on a tabletop—but remember that there is no slip along the shear planes in the fluid.

This page titled 1.4: Diffusion is shared under a CC BY-NC-SA 4.0 license and was authored, remixed, and/or curated by John Southard (MIT OpenCourseware) via source content that was edited to the style and standards of the LibreTexts platform.

2: FLOW PAST A SPHERE I - DIMENSIONAL ANALYSIS, REYNOLDS NUMBERS, AND FROUDE NUMBERS

2.1: Introduction

2.2: Which Variables are Important?

2.3: Some Dimensional Reasoning and its Consequences

2.4: How to Construct Dimensionless Variables

2.5: What if You Choose the Wrong Variables?

2.6: "Dimensional Analysis"

2.7: Significance of Reynolds Numbers and Froude Numbers

This page titled 2: Flow Past a Sphere I - Dimensional Analysis, Reynolds Numbers, and Froude Numbers is shared under a CC BY-NC-SA 4.0 license and was authored, remixed, and/or curated by John Southard (MIT OpenCourseware) via source content that was edited to the style and standards of the LibreTexts platform.

2.1: Introduction

Steady flow past a solid sphere is important in many situations, both in the natural environment and in the world of technology, and it serves as a good reference case for extension to more complicated situations, involving unsteady flows and/or nonuniform flows and/or nonspherical bodies. It is also an excellent starting point for development of a number of important principles and techniques that are essential for later development in these notes. In particular, I hope to be able to convince you of the importance and utility of careful dimensional reasoning about flows of fluids.

You can think in terms of fluid flowing past a stationary sphere, or of a sphere moving through stationary fluid. The two cases are almost, but not quite, equivalent. And in the latter case you could imagine the sphere being moved through the fluid in three different ways: fastened to a rigid strut, or towed with a flexible line, or pulled downward through the fluid under its own weight. For now, do not worry about these distinctions; just view the fluid from the standpoint of the sphere. I will return to the differences briefly later. For the sake of definiteness, assume here that the sphere is towed or pushed through still fluid. All that is said here about the flow is then with reference to a point fixed relative to the moving sphere.

Just from considerations of space and motion, it is clear that the approaching fluid must both move faster and be displaced laterally as it flows past the sphere. On the other hand, the no-slip condition requires that the fluid velocity be zero everywhere at the surface of the sphere; this implies the existence of gradients (that is, spatial rates of change) of velocity, very sharp under some conditions, at and near the surface of the sphere. These velocity gradients produce a shear stress on the surface of the sphere; see Equation 1.3.6. When summed over the surface, the shear stress exerted by the fluid on the sphere represents the part of the total drag force on the sphere called the **viscous drag**. Your intuition probably tells you (correctly in this case) that the pressure of the fluid, the normal force per unit area, is greater on the front of the sphere than on the back. The sum of the pressure forces over the entire surface of the sphere represents the other part of the drag force, called the **pressure drag** or **form drag**. You will see later that the relative importance of viscous drag and pressure drag, as well as the qualitative flow patterns and the distance out into the fluid the sphere makes its presence felt, are greatly different in different ranges of flow.

You can see now that even in such a seemingly simple flow as the passage of a steady and uniform approach flow around a smooth sphere there is a great variation in flow phenomena. Complexity of this kind in deceptively simple flows is common in fluid dynamics; you need to be on your guard against theorizing about phenomena of fluid flow without the ground truth of experiment and observation.

This page titled 2.1: Introduction is shared under a CC BY-NC-SA 4.0 license and was authored, remixed, and/or curated by John Southard (MIT OpenCourseware) via source content that was edited to the style and standards of the LibreTexts platform.

2.2: Which Variables are Important?

Think first about the resultant drag force F_D exerted on the sphere by the fluid (Figure 2.2.1). To account fully for the value assumed by F_D for a given sphere in a given fluid, we have to specify the values of certain other variables. (This carefully phrased sentence should not be interpreted as implying that F_D is necessarily the "dependent variable" in the problem; for a sphere settling under its own weight, it is more natural to think of F_D as an independent variable and settling velocity as the dependent variable. What is important here is that there is a one-to-one correspondence between the values of F_D and the values of those other variables, irrespective of their dependence or independence. That said, however, for convenience I will refer to such variables as independent variables.)

- The velocity U of the sphere relative to the fluid is important because it affects the shear in the fluid near the surface of the sphere, and therefore by Equation 1.3.7 the shear stress.
- Sphere diameter D is important for the same reason.
- Viscosity μ is important because it determines the shear force associated with a given rate of shear.
- Fluid density ρ must also be included, because the forces associated with the accelerations in the fluid depend upon ρ: the response of a body to a force exerted on it depends on the mass of the body; that is the essence of Newton's second law. If the sphere is in steady motion far from solid walls or a free surface, you can assume that no other variables are important.

So

$$F_D = f(U, D, \rho, \mu) \tag{2.2.1}$$

where f is some function with one or more terms involving the four independent variables (Figure 2.2.1). (I will often use the same symbol f for unrelated functions. In Chapter 4, f is also used for a quantity called the friction factor.)

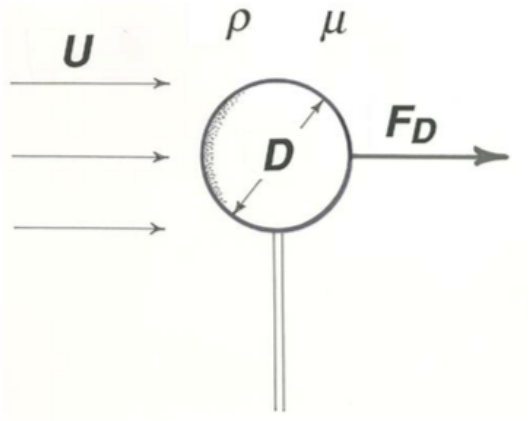


Figure 2.2.1: The drag force F_D on a sphere moving relative to a viscous fluid.

You might reasonably ask why neither sphere density nor acceleration of gravity are on the list. These are relevant only if the sphere settles under its own weight, and then only because they determine the weight of the sphere, to which F_D is then equal after a steady state of settling is attained. Variables that enter the problem only by their effect on other variables already on the list and not because of some separate effect need not be included in the analysis. And there is no reason to think that either of these has any such significance.

If we are lucky in problems like this, we can use theory to derive an analytical form for the function in Equation 2.2.1 that agrees well with observation. If not, we have to attempt a numerical solution or rely solely on experiment. For flow past a sphere there is indeed an analytical solution, described later in this chapter, that agrees beautifully with experimental data, but it holds over only a limited range of the independent variables; over the rest of the range we can obtain the function by experiment, as is commonly the case in problems of flow of real fluids. With flow past the sphere as an example we need to consider how we can best go about organizing both data and thought by resorting to dimensional reasoning.

This page titled 2.2: Which Variables are Important? is shared under a CC BY-NC-SA 4.0 license and was authored, remixed, and/or curated by John Southard (MIT OpenCourseware) via source content that was edited to the style and standards of the LibreTexts platform.

2.3: Some Dimensional Reasoning and its Consequences

Obtaining the Correct Dimensions

Like every physically correct equation, Equation 2.2.1 must represent equality not only of *magnitudes* but also of *dimensions*. In most mechanical systems three basic dimensions are needed to express forces, motions, and system properties; these are usually taken to be mass (M), length (L), and time (T). So whatever the form of the term or terms on the right side of Equation 2.2.1, the variables U, D, ρ, and μ must combine in such a way that each term has the dimensions of force, because the left side has the dimensions of force. The following list gives the dimensions of each of the five variables involved in flow past a sphere, in terms of mass M, length L, and time T:

$$\begin{aligned} F_D &- \mathrm{ML/T^2} \\ U &- \mathrm{L/T} \\ D &- \mathrm{L} \\ \rho &- \mathrm{M/L^3} \\ \mu &- \mathrm{M/LT} \end{aligned}$$

The only variable here whose dimensions are not straightforward is μ; the dimensions $\mathrm{M/LT}$ are obtained by use of Equation 1.3.6, by which μ is defined.

It is advantageous to rewrite equations like Equation 2.2.1 in dimensionless form. To do this, first make the left side dimensionless by dividing F_D by some product of independent variables that itself has the dimensions of force. Using the list of dimensions above, you can verify that $\rho U^2 D^2$ has the dimensions of force:

$$\rho U^2 D^2 : (\mathrm{M/L^3})\,(\mathrm{L/T})^2(\mathrm{L})^2 = \mathrm{ML/T^2}$$

So dividing the left side of Equation 2.2.1 by $\rho U^2 D^2$ makes the left side of the equation dimensionless. The result, $F_D/\rho U^2 D^2$, can be viewed as a dimensionless form of F_D. That leaves the right side of Equation 2.2.1 to be made dimensionless. There is one and only one way the four variables U, D, ρ, and μ can be combined into a dimensionless variable, namely $\rho UD/\mu$:

$$\rho UD/\mu\text{: } (\mathrm{M/L^3})\,(\mathrm{L/T})(\mathrm{L})/(\mathrm{M/LT}) \text{ ... M, L, T cancel}$$

(That statement is not strictly true—but all the other possibilities are just $\rho UD/\mu$ raised to some power, and they are not independent of $\rho UD/\mu$.) So whatever the form of the function f, the right side of the dimensionless form of Equation 2.2.1 can be written using just one dimensionless variable:

$$\frac{F_D}{\rho U^2 D^2} = f\left(\frac{\rho UD}{\mu}\right) \tag{2.3.1}$$

A Simplified Function

Equation 2.3.1 is an equivalent but dimensionless form of Equation 2.2.1. The great advantage of the dimensionless equation is that it involves only two variables—a dependent dimensionless variable $F_D/\rho U^2 D^2$ and an independent dimensionless variable $\rho UD/\mu$—instead of the original five. Think of the enormous saving in effort this implies for an experimental program to characterize the drag force. If you had to measure F_D as a function of each one of the four variables while holding the other three constant, you would generate mountains of data and graphs. But Equation 2.3.1 tells you that U, D, ρ, and μ need only be varied so as to make $\rho UD/\mu$ vary. All of the experimental points for $F_D/\rho U^2 D^2$ obtained by varying $\rho UD/\mu$ should plot as a curve in a two-dimensional graph with these two variables along the axes. Whatever the values of U, D, ρ, and μ, all possible realizations of flow past a sphere are expressed by just one curve. This curve is shown in Figure 2.3.1 together with some of the experimental points that have been used to define it. The physics behind the curve is discussed in Chapter 3, after more background in the principles of fluid dynamics. And you could find the curve by varying only one of the four variables U, D, ρ, and μ—although you may not be able to get a very wide range of values of $\rho UD/\mu$ by varying only one of those variables. A fairly small number of experiments involving values of the original independent variables that combined to span a wide range of $\rho UD/\mu$ would suffice to characterize all other possible combinations of independent variables. This is because each point in the dimensionless graph represents a

great many different possible combinations of the original variables—an infinity of these, in fact. You thus gain a far-reaching predictive capability on the basis of relatively little observational effort.

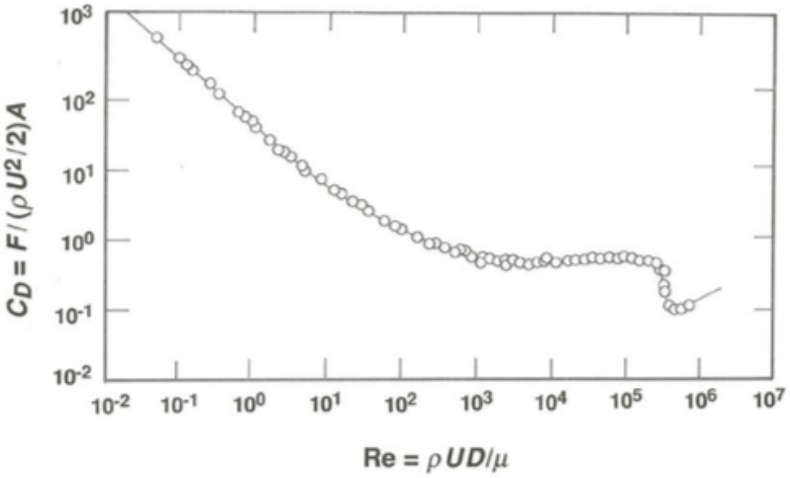


Figure 2.3.1: Plot of dimensionless drag force vs. Reynolds number for flow of a viscous fluid past a sphere. The dimensionless drag force is expressed in the form of a conventionally defined drag coefficient rather than as the dimensionless drag force F_D; see further in the text. Experimental points are from several sources, and are somewhat generalized. Some of the data points are from settling of a sphere through a still fluid, and others are from flow past a sphere held at rest. For a more detailed plot, see, for example, Schiller (1932).

A skeptic might find all this to be too good to be true. But the fact is that this is how things work, and the analysis of flow past a sphere is just one good example. A note of caution is in order, however. It is prudent to vary as many of the variables over as wide a range as possible; this does not take an enormous number of observations, and it is a check on the correctness of your analysis. You will see below in more detail that if there is a larger number of important variables than you think, your data points would form a scattered band rather than a single curve. Then if you varied just one variable to try to find the curve, you would indeed get a curve, but it would not be the curve you were after; you would be missing the scatter that would manifest itself if you varied the other variables as well.

Several notes

First, variables of the form $\rho UD/\mu$ are called **Reynolds numbers**, usually denoted by Re. Whenever both density and viscosity are important in a problem and both a length variable and a velocity are involved, a Reynolds number can be formed and used. There are thus many different Reynolds numbers, with different length and velocity variables depending on the particular problem. You will encounter others in later chapters.

Second, for the steady flow we have assumed, the variables U, D, ρ, and μ characterize not only everything about the distributions of shear stress and pressure over the entire surface of the sphere, which add up to F_D, but also the distributions of shear stress, pressure, and fluid velocity at every point in the surrounding fluid. Because $\rho UD/\mu$ replaces these four variables on the right side of Equation 2.3.1, the same can be said of the Reynolds number. Anything about forces and motions you might want to consider can be viewed as being specified completely by the Reynolds number.

Third, there is a further important consequence of the fact that each point on the curve of $F_D/\rho U^2 D^2$ vs. $\rho UD/\mu$ represents an infinity of combinations of U, D, ρ, and μ. Suppose that you wanted to find the drag force exerted by a certain flow on a sphere that is too large to fit into your laboratory or your basement. You could work with a much smaller sphere by adjusting the values of U, ρ, and μ so that $\rho UD/\mu$ is the same as in the flow in question past the large sphere (Figure 2.3.2). Then from the curve in Figure 2.3.1 the value of $F_D/\rho U^2 D^2$ is also the same, and from it you could find the drag force F_D on the large sphere by substituting the corresponding values of U, D, and ρ. Or, on the other hand, you could study the flow around a very small sphere by use of a much larger sphere, with the same complete confidence in the results (Figure 2.3.2). This is the essence of scale modeling: the study of one physical system by use of another at a smaller or larger physical scale but with variables adjusted so that all forces and motions in the two systems are in the same proportions. Figure 2.3.2 shows how you might use flow around a small sphere with diameter D_m to model flow around a much larger sphere with diameter D_o. You would have to adjust the flow velocities U_m and U_o, as well as the fluid viscosities μ_m and μ_o and the fluid densities ρ_m and ρ_o, so that the Reynolds number Re_m, equal to $\rho_m U_m D_m/\mu_m$, in the model is the same as the Reynolds number Re_o, equal to $\rho_o U_o D_o/\mu_o$, in the large-scale flow. Then all forces and motions are in the same proportion in the two flows, and, specifically, the dimensionless drag force, or the

drag coefficient, is the same in the two flows. Despite the great difference in physical scale, both of the flows are represented by the same point on the graph of drag coefficient vs. Reynolds number, so anything about the two flows, provided only that it is expressed in dimensionless form, is the same in the two flows. Each point on the curve of $F_D/\rho U^2 D^2$ vs. $\rho UD/\mu$ represents an infinite number of possible experiments, each of which is a scale model of all the others!

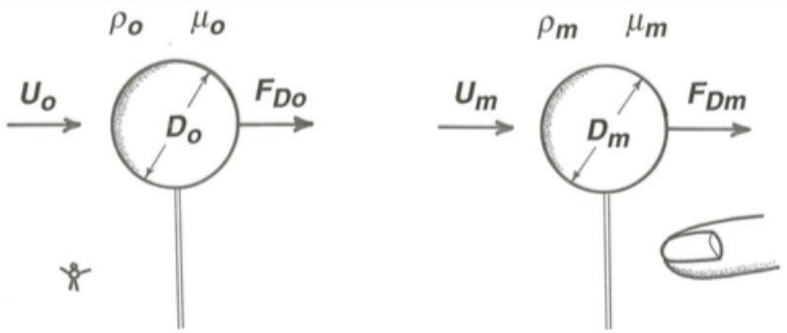


Figure 2.3.2: An example of scale modeling: using flows around a small sphere to model flow around a large sphere. (The object in the lower right is supposed to be someone's fingertip.)

Fourth, in Figure 2.3.1 the dimensionless drag force is written in a conventional form that is slightly different from that derived above: $F_D/\left(\rho U^2/2\right) A$, where A is the cross-sectional area of the sphere, equal to $\pi D^2/4$. This differs from $F_D/\rho U^2 D^2$ by the factor $\pi/8$, but its dimensions are exactly the same. It is usually called a **drag coefficient**, denoted by C_D; you can see why that term came about by writing

$$F_D = C_D \frac{\rho U^2}{2} A \tag{2.3.2}$$

where the factor $\left(\rho U^2/2\right) A$ on the right side has dimensions of force. The functional relationship between dimensionless drag force and Reynolds number in Equation 2.3.1 can be written in an entirely equivalent form using C_D:

$$C_D = \frac{FD}{\frac{\rho U^2}{2} A} = f\left(\frac{\rho UD}{\mu}\right) \tag{2.3.3}$$

Fifth, there are alternative versions of the dependent dimensionless variable. Dividing by $\rho U^2 D^2$ is not the only way to nondimensionalize F_D. You can check for yourself that $F_D/\mu UD$, $\rho F_D/\mu^2$, and $F_D/\mu U$ are other possibilities, obtained by combining F_D with the four variables ρ, μ, U, and D taken three at a time. (You will see in the next section how to derive such variables.) Sometimes, as in the last two cases, one of the variables drops out; this happens when M or L or T appears in only one of the four variables chosen. Any of these three alternative dependent dimensionless variables would serve just as well as $F_D/\rho U^2 D^2$ to represent the data. You will see below, however, that sometimes one is more revealing than the others.

This page titled 2.3: Some Dimensional Reasoning and its Consequences is shared under a CC BY-NC-SA 4.0 license and was authored, remixed, and/or curated by John Southard (MIT OpenCourseware) via source content that was edited to the style and standards of the LibreTexts platform.

2.4: How to Construct Dimensionless Variables

You may be wondering about how you could have constructed the dimensionless variable $\rho UD/\mu$ on your own instead of having it presented to you. Start with a very general product $\rho^a U^b D^c \mu^d$. The exponents a through d have to be adjusted so that the M, L, and T dimensions of the product cancel out. One of the exponents can be chosen arbitrarily, say $d = 1$, but then a, b, and c have to be adjusted by solving three equations, one each for M, L, and T, expressing the condition that the product be dimensionless. Using length as an example, you can see from the list of dimensions above that length enters into ρ to the power -3, into U to the power $+1$, into D to the power $+1$, and into μ to the power -1. So for the length dimension to cancel out of $\rho^a U^b D^c \mu$, the following condition must be met: $-3a + b + c - 1 = 0$. (Keep in mind that we have already chosen d to be 1. Two more conditions, one for M and one for T, give three linear equations in the three unknowns a, b, and c:

$$\begin{array}{rrrrll} -3a & +b & +c & -1 & = 0 & (\text{ for } L) \\ +a & & & +1 & = 0 & (\text{ for } M) \\ & -b & & -1 & = 0 & (\text{ for } T) \end{array} \tag{2.4.1}$$

The solution is $a = -1$, $b = -1$, $c = -1$, so the product takes the form $\mu/\rho UD$. This is the inverse of the Reynolds number introduced above. If d had been taken as -1 at the outset, the result would have been the Reynolds number itself.

This page titled 2.4: How to Construct Dimensionless Variables is shared under a CC BY-NC-SA 4.0 license and was authored, remixed, and/or curated by John Southard (MIT OpenCourseware) via source content that was edited to the style and standards of the LibreTexts platform.

2.5: What if You Choose the Wrong Variables?

Including an Irrelevant Variable

What would be the consequences of including an irrelevant variable in analyzing the dimensional structure of a problem like that of flow past a sphere? Suppose, contrary to fact but just for the sake of discussion, that viscosity is not important in determining F_D. Then the functional relationship for F_D would be

$$F_D = f(U, D, \rho) \tag{2.5.1}$$

As before, you can start to make this equation dimensionless by forming the same dimensionless drag force $F_D/\rho U^2 D^2$ on the left-hand side. But how about the right-hand side? The three variables U, D, and ρ cannot be combined to form a dimensionless variable, because there is not enough freedom to adjust exponents to make a product $U^a D^b \rho^c$ dimensionless; this should be clear from the formal procedure described above for obtaining $\rho UD/\mu$. Then what takes the place of the Reynolds number on the right side? The answer is that the right side must be a numerical constant: there is no independent dimensionless variable. So if μ were not important in flow past a sphere, the dimensionless force $F_D/\rho U^2 D^2$ would be a constant rather than a function of the Reynolds number. To generalize: *if one original variable is eliminated from the problem, one dimensionless variable must be eliminated as well*. In a graph of C_D vs. Re the experimental points would fall along a straight line parallel to the Re axis, as shown schematically in Figure $2.5.1$. Now look back at the actual graph of C_D vs. Re in Figure 2.3.1. Over a wide range of Reynolds numbers from about 10^2 to greater than 10^5, C_D is nearly independent of the Reynolds number. Because μ is the only variable that appears in the Reynolds number but not in C_D, this tells you that μ is indeed not important in determining F_D at large Re. The reasons for this are discussed in Chapter 3.

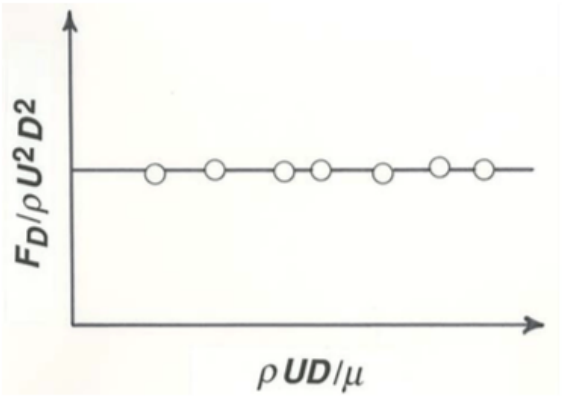


Figure $2.5.1$: What the plot of dimensionless drag force vs. Reynolds number for flow around a sphere would look like if the viscosity were not important.

Now you can see why there is some practical advantage to using $F_D/\rho U^2 D^2$ as the dependent dimensionless variable. The other three mentioned above contain μ, and so in a plot of any one of them against $\rho UD/\mu$ the segment of the curve for which μ is not important would plot as a sloping line rather than as a horizontal line, and the unimportance of μ would not be as easy to recognize.

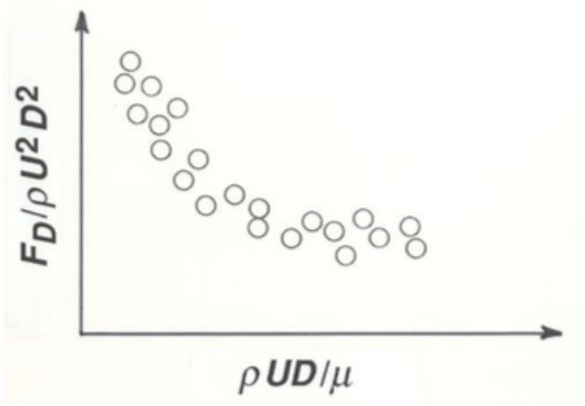


Figure 2.5.2: What the plot of dimensionless drag force vs. Reynolds number for flow around a sphere towed near a solid wall in a still body of water would look like if the distance of the sphere from the wall is not held constant from trial to trial.

Omitting a Relevant Variable

You should also consider the consequences of omitting an important variable from consideration. For example, if you had not been careful to keep the sphere well away from the wall of the vessel containing the fluid, you would find (Figure 2.5.2) that the experimental points plot in a scattered band around the curve of C_D vs. Re in Figure 2.3.1. This tells you that some other variable is important in determining F_D and that you have inadvertently let it vary—assuming, of course, that your measurements are free of errors in the first place. The obvious culprit is y, the distance of the center of the sphere from the wall (Figure 2.5.3), because the proximity of the sphere to the solid wall distorts the pattern of flow around the sphere and thus changes the fluid forces on the sphere to some extent. With y included in the analysis, the functional relationship for F_D is of the form

$$F_D = f(U, D, \rho, \mu, y) \tag{2.5.2}$$

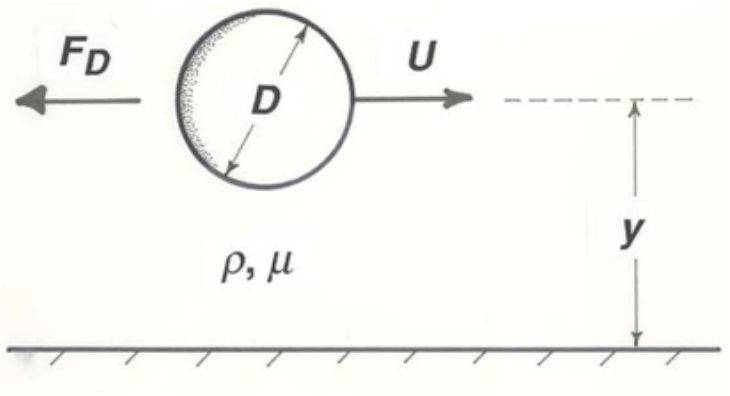


Figure 2.5.3: Towing a sphere parallel to a nearby solid planar wall.

In nondimensionalizing Equation 2.5.2 you should again expect to have a dimensionless drag force on the left and the Reynolds number on the right. But what happens to the new variable y? You can use it to form one more independent dimensionless variable, in the same way you formed the Reynolds number. There has to be at least one other such variable, because y has to appear somewhere on the right side of the nondimensionalized version of Equation 2.5.2. A natural choice for this new variable is y/D (or D/y). You could instead form another Reynolds number, $\rho Uy/\mu$. But only two of the three variables $\rho UD/\mu$, $\rho Uy/\mu$, and y/D are independent of each other: addition of one new independent variable to the problem adds only one new independent dimensionless variable. It is also worth pointing out that you can arrive at the second Reynolds number, $\rho Uy/\mu$, by multiplying the first, $\rho UD/\mu$, by the new dimensionless variable y/D. This is an illustration of the principle that you can always replace a dimensionless variable in a set of dimensionless variables by another one formed by multiplying or dividing it by one of the others, or with some power or root of one of the others. So in dimensionless form Equation 2.5.2 is then

$$\frac{F_D}{\rho U^2 D^2} = f\left(\frac{\rho UD}{\mu}, \frac{y}{D}\right) \tag{2.5.3}$$

The function in Equation 2.5.3 would plot as a curved surface in a three-dimensional graph with C_D, Re, and y/D along the axes (Figure 2.5.4). The two planes perpendicular to the y/D axis in Figure 2.5.4 show the range over which y/D varied in your experiments without your realizing that it is important. The projection of the segment of the surface between these two planes onto the C_D–Re plane is the band in which your experimental points would fall. The intersection of the surface with the plane $y/D = 0$, also shown on the projection, represents the curve you would have gotten if you had always kept the sphere very far away from the wall; it is the same as the curve in Figure 2.3.1.

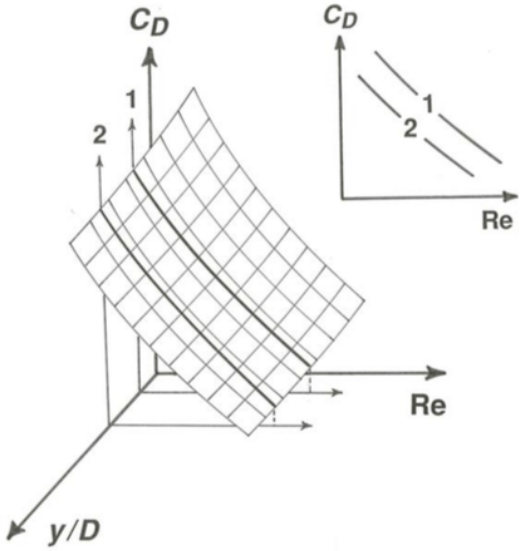


Figure 2.5.4: For towing of a sphere parallel to a nearby solid planar wall, data from a large number of trials would plot as a surface in a three-dimensional graph of drag coefficient, Reynolds number, and ratio of distance from wall to sphere diameter. The graph in the upper right shows, in a plot of drag coefficient vs. Reynolds number, two curves corresponding to two different values of the ratio of distance from wall to sphere diameter. These curves are the intersections of the full surface with planes parallel to the C_D–Re plane.

Involving Gravity

You could carry the analysis one step further by moving the sphere horizontally just beneath the free surface of a liquid at rest in a gravitational field (Figure 2.5.5). Of importance now is not only the distance y of the sphere below the free surface but also the acceleration of gravity g: if the movement of the sphere distorts the free surface, unbalanced gravity forces would tend to flatten the surface again, and surface gravity waves may be generated. Then

$$F_D = f(U, D, \rho, \mu, y, g) \tag{2.5.4}$$

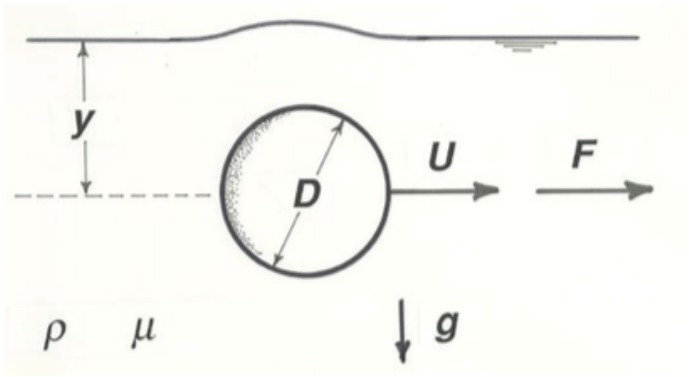


Figure 2.5.5: Towing a sphere horizontally through a still liquid, not far below the free surface of the liquid.

This adds still another independent dimensionless variable, and that variable must include g. There are five possibilities: $\mu g/\rho U^3$, $\rho^2 g D^3/\mu^2$, $\rho^2 g y^3/\mu^2$, U^2/gD, and U^2/gy, plus obvious variants obtained by inversion and exponentiation. (You could try constructing

these by combining U, ρ, μ, D, and y three at a time with g and going through the procedure described above for Re. You would also get y/D again in the process.) Any one of these five would suffice to express the effect of g on the drag force. Again only one is independent, because the others can all be obtained by combining that one (whichever you choose) with either $\rho UD/\mu$ or y/D. It would be conventional, in a problem like this, to use $U/(gy)^{1/2}$ as the added independent variable. The dimensionless form of Equation 2.5.4 is then

$$\frac{FD}{\rho U^2 D^2} = f\left(\frac{\rho UD}{\mu}, \frac{U^2}{gy}, \frac{y}{D}\right) \tag{2.5.5}$$

The square root of a variable like U^2/gy or U^2/gD, with a velocity, a length variable, and g, is called a **Froude number**, usually denoted by Fr. It is natural, although not essential, to use U^2/gy here because then each of the four dimensionless variables in the functional relationship can be viewed as being formed by combining F_D, μ, y, and g in turn with the three variables ρ, U, and D; see the following paragraph for details.

Note

The function in Equation 2.5.5 would plot as a four-dimensional "surface" in a graph of C_D vs. Re, Fr, and y/D. It is difficult to visualize such a graph. A good substitute would be to plot a three-dimensional graph for each of a series of values of one of the independent dimensionless variables. The trouble is that there is an infinite number of these three-dimensional graphs. (I remember once reading somewhere that to express graphically the relationship between two variables you need a page, and to express the relationship among three variables you need a book of pages, and to express the relationship among four variables you need a library of books. For five variables you would need a world of libraries!

Handling Multiple Variables

Suppose that you had realized at the outset that all seven variables in Equation 2.5.4 are important in the problem. The systematic way of obtaining four dimensionless variables all at once is just an extension of the method described in an earlier section for obtaining the Reynolds number. Form four products by choosing three of the seven variables (the "repeating" variables) to be those raised to the exponents a, b, and c and using each of the remaining four variables in turn as the one that is raised to the exponent 1 (or to any other fixed exponent, for that matter). You can verify for yourself that if you choose ρ, U, and D as the three repeating variables, the four products $\rho^a U^b D^c F_D$, $\rho^a U^b D^c \mu$, $\rho^a U^b D^c y$, and $\rho^a U^b D^c g$ would produce the four dimensionless variables in Equation 2.5.5, except that U^2/gD appears instead of U^2/gy. It turns out that for this procedure to work, the constraints on the choice of the three repeating variables are that (1) among them they include all three dimensions M, L, T, and (2) they be dimensionally independent of each other, in the sense that you cannot obtain the dimensions of any one by multiplying together the dimensions of the other two after raising them to some exponents. These constraints just ensure that you get solvable sets of simultaneous equations.

This page titled 2.5: What if You Choose the Wrong Variables? is shared under a CC BY-NC-SA 4.0 license and was authored, remixed, and/or curated by John Southard (MIT OpenCourseware) via source content that was edited to the style and standards of the LibreTexts platform.

2.6: "Dimensional Analysis"

Most kinds of fluid flow that are important in natural environments do not lend themselves to analytical solutions, even when no sediment is moved, so experiment and observation are a valuable way to learn something about them. I have expatiated upon dimensionless variables and their use in expressing experimental results because this sort of analysis, usually called dimensional analysis, is so useful in dealing with problems of fluid flow and sediment movement. **Dimensional analysis** is a way of getting some useful information about a problem when you cannot obtain an analytical solution and may not even know anything about the form of the solution, but you have some ideas about important physical effects or variables. You will encounter many examples of its use in later chapters.

Suppose that you are dealing with a fluid-flow problem that can be simplified somehow, perhaps in geometry or in time variability, to be manageable but still representative. Use your experience and physical intuition to identify the important variables. Form a set of dimensionless variables by which the observational results can be expressed. This represents the most efficient means of dealing with experimental data, and it usually makes it possible to get some idea of the ranges in which certain physical effects are important or unimportant. Do not worry too much about guessing wrong about important variables; the example of flow past a sphere shows how you can find out and change course.

The number of dimensionless variables equivalent to a given set of original variables is given by the **Pi theorem**, also called Buckingham's theorem. By the Pi theorem, the number of dimensionless variables corresponding to a number n of original variables that describe some physical problem is equal to $n - m$, where m is the number of dimensions by which the problem must be expressed. If you want to go back to the original source of the proofs (the theorem was not proved in the foregoing material, just demonstrated), see Buckingham (1914, 1915).

This page titled 2.6: "Dimensional Analysis" is shared under a CC BY-NC-SA 4.0 license and was authored, remixed, and/or curated by John Southard (MIT OpenCourseware) via source content that was edited to the style and standards of the LibreTexts platform.

2.7: Significance of Reynolds Numbers and Froude Numbers

Some further insight into the significance of Reynolds numbers and Froude numbers is afforded by showing that dimensionless variables of this form always arise in problems involving viscous forces and gravity forces. But first I want to make sure you know what an equation of motion is.

Equations of Motion

The **equation of motion** for some body of matter, whether solid or fluid, whether discrete or continuous, is just Newton's second law written for that body. You write out the sum of all the forces acting on the body and set that sum equal to the mass times the acceleration. The equation of motion for a continuous medium like a fluid comes out to be a differential equation. Why? Because to derive the equation you have to write it for some element of fluid with finite volume, and then watch what happens to the equation as the volume element shrinks to a point.

Think about the balance of forces on some small element of fluid in any fluid-flow problem (for example, that of a sphere moving near a free surface) that involves fluid shear forces and also gravity forces that are not simply balanced out by hydrostatic pressure. Whatever the exact nature of the problem, Newton's second law must hold for this small element of fluid, so we can write for it a general equation of motion in words:

$$\text{viscous force} \;+\; \text{gravity force} \;+\; \text{any other forces} = \;\text{rate of change of momentum} \tag{2.7.1}$$

All of the terms in this equation have the same dimensions, so we can divide all the terms by any one of them to obtain an equation with all terms dimensionless. Dividing by the term on the right,

$$\frac{\text{viscous force}}{\text{ROC of momentum}} + \frac{\text{gravity force}}{\text{ROC of momentum}} + \frac{\text{other forces}}{\text{ROC of momentum}} = 1 \tag{2.7.2}$$

What will be the form of the first two dimensionless terms on the left side of Equation 2.7.2, in terms of representative variables that might be involved in any given flow problem? Assuming that there is some characteristic length variable L in the problem like a sphere size or flow depth, and some characteristic velocity V like the approach velocity in flow past a sphere or the mean velocity or surface velocity in flow in a channel, then the rate of change of momentum, which has dimensions of momentum divided by a characteristic time T, can be written as proportional to $rhoL^3V/T$. (Remember that the mass can be expressed as density times volume and the volume as the cube of a length.) And this can further be written $rhoL^2V^2$, because velocity has the dimensions L/T. The viscous force is the product of the viscous shear stress and the area over which it acts. Area is proportional to the square of the characteristic length, and by Equation 1.3.7 the shear stress is proportional to the viscosity and the velocity gradient, so the viscous force is proportional to $\mu(V/L)L^2$, or μVL. The first term in Equation 2.7.2 is then proportional to $\mu VL/\rho L^2V^2$, or $\mu/\rho LV$. This is simply the inverse of a Reynolds number. The Reynolds number in any fluid problem is therefore inversely proportional to the ratio of a viscous force and a quantity with the dimensions of a force, the rate of change of momentum, which is usually viewed as an "inertial force".

How about the second term in Equation 2.7.2? The gravity force is the weight of the fluid element, which is proportional to ρgL^3. The second term is then proportional to $\rho gL^3/\rho L^2V^2$, or gL/V^2. This is the square of the inverse of a Froude number. The square of the Froude number is therefore proportional to the ratio of a gravity force and a rate of change of momentum or an "inertial force".

This probably strikes you as not a very rigorous exercise—and indeed it is not. It is intended only to give you a general feel for the significance of Reynolds numbers and Froude numbers. At the expense of lengthening this chapter considerably, the general differential equation of motion for flow of a viscous fluid could be derived and then made dimensionless by introducing the same characteristic length and characteristic velocity, and a reference pressure as well. You would see that the Reynolds number and the Froude number then emerge as coefficients of the dimensionless viscous-force term and dimensionless gravity-force term, respectively. This is done especially lucidly by Tritton (1988, Chapter 7). The value of such an exercise is that then the magnitudes of the Reynolds number and Froude number tell you whether the viscous-force term or the gravity-force term in the equation of motion can be neglected relative to the mass-times-acceleration term. This is a productive way of simplifying the equation of motion to gain some insight into the physics of the flow.

When you are deciding which set of dimensionless variables to work with in problems like that of flow past a sphere, introduced

above, it makes sense to use dimensionless variables that have their own physical significance, like Reynolds numbers and Froude numbers. In later chapters, other dimensionless variables are introduced that represent ratios of two forces in specific problems.

Conclusion

Before you are confronted any further with the physics of flow past spheres, you need to be introduced to quite a bit more material on fluid flow. The first part of the next chapter, Chapter 3, is devoted to this material, before more on the topic of flow past spheres.

References Cited

- Buckingham, E., 1914, On physically similar systems; illustrations of the use of dimensional equations: Physical Review, ser. 2, v. 4, p. 345-376.
- Buckingham, E., 1915, Model experiments and the forms of empirical equations: American Society of Mechanical Engineers, Transactions, v. 37, p. 263- 292.
- Schiller, L., 1932, Fallversuche mit Kugeln und Scheiben, in Schiller, L., ed., Handbuch der Experimentalphysik, Vol. 4, Hydro- und Aeromechanik, Part 2, Widerstand und Auftrieb, p. 339-398: Leipzig, Akademische Verlagsgesellschaft, 443 p.
- Tritton, D.J., 1988, Physical Fluid Dynamics, 2nd Edition: Oxford, U.K., Oxford University Press, 519 p.

This page titled 2.7: Significance of Reynolds Numbers and Froude Numbers is shared under a CC BY-NC-SA 4.0 license and was authored, remixed, and/or curated by John Southard (MIT OpenCourseware) via source content that was edited to the style and standards of the LibreTexts platform.

3: FLOW PAST A SPHERE II - STOKES' LAW, THE BERNOULLI EQUATION, TURBULENCE, BOUNDARY LAYERS, FLOW SEPARATION

3.1: Introduction and the Navier-Stokes Equation

3.2: Flow Past a Sphere at Low Reynolds Numbers

3.3: Inviscid Flow

3.4: The Bernoulli Equation

3.5: Turbulence

3.6: Boundary Layers

3.7: Flow Separation

3.8: Flow Past a Sphere at High Reynolds Numbers

3.9: Settling of Spheres

This page titled 3: Flow Past a Sphere II - Stokes' Law, The Bernoulli Equation, Turbulence, Boundary Layers, Flow Separation is shared under a CC BY-NC-SA 4.0 license and was authored, remixed, and/or curated by John Southard (MIT OpenCourseware) via source content that was edited to the style and standards of the LibreTexts platform.

3.1: Introduction and the Navier-Stokes Equation

So far we have been able to cover a lot of ground with a minimum of material on fluid flow. At this point I need to present to you some more topics in fluid dynamics—inviscid fluid flow, the Bernoulli equation, turbulence, boundary layers, and flow separation—before returning to flow past spheres. This material also provides much of the necessary background for discussion of many of the topics on sediment movement to be covered in Part II. But first we will make a start on the nature of flow of a viscous fluid past a sphere.

The Navier-Stokes Equation

The idea of an equation of motion for a viscous fluid was introduced in the Chapter 2. It is worthwhile to pursue the nature of this equation a little further at this point. Such an equation, when the forces acting in or on the fluid are those of viscosity, gravity, and pressure, is called the **Navier–Stokes equation**, after two of the great applied mathematicians of the nineteenth century who independently derived it.

It does not serve our purposes to write out the Navier–Stokes equation in full detail. Suffice it to say that it is a *vector partial differential equation*. (By that I mean that the force and acceleration terms are vectors, not scalars, and the various terms involve partial derivatives, which are easy to understand if you already know about differentiation.) The single vector equation can just as well be written as three scalar equations, one for each of the three coordinate directions; this just corresponds to the fact that a force, like any vector, can be described by its scalar components in the three coordinate directions.

The Navier–Stokes equation is notoriously difficult to solve in a given flow problem to obtain spatial distributions of velocities and pressures and shear stresses. Basically the reasons are that the acceleration term is nonlinear, meaning that it involves products of partial derivatives, and the viscous-force term contains second derivatives, that is, derivatives of derivatives. Only in certain special situations, in which one or both of these terms can be simplified or neglected, can the Navier–Stokes equation be solved analytically. But numerical solutions of the full Navier–Stokes equation are feasible for a much wider range of flow problems, now that computers are so powerful.

This page titled 3.1: Introduction and the Navier-Stokes Equation is shared under a CC BY-NC-SA 4.0 license and was authored, remixed, and/or curated by John Southard (MIT OpenCourseware) via source content that was edited to the style and standards of the LibreTexts platform.

3.2: Flow Past a Sphere at Low Reynolds Numbers

We will make a start on the flow patterns and fluid forces associated with flow of a viscous fluid past a sphere by restricting consideration to low Reynolds numbers $\rho UD/\mu$ (where, as before, U is the uniform approach velocity and D is the diameter of the sphere).

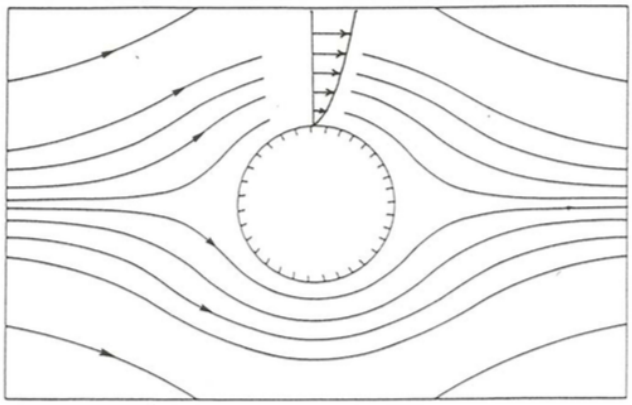


Figure $3.2.1$: Steady flow of a viscous fluid at very low Reynolds numbers ("creeping flow") past a sphere. The flow lines are shown in a planar section parallel to the flow direction and passing through the center of the sphere.

At very low Reynolds numbers, $\mathrm{Re} \ll 1$, the flow lines relative to the sphere are about as shown in Figure $3.2.1$. The first thing to note is that for these very small Reynolds numbers *the flow pattern is symmetrical front to back*. The flow lines are straight and uniform in the free stream far in front of the sphere, but they are deflected as they pass around the sphere. For a large distance away from the sphere the flow lines become somewhat more widely spaced, indicating that the fluid velocity is less than the free-stream velocity. Does that do damage to your intuition? One might have guessed that the flow lines would be more crowded together around the midsection of the sphere, reflecting a greater velocity instead—and as will be shown later in this chapter, that is indeed the case at much higher Reynolds numbers. (See a later section for more on what I have casually called flow lines here.) For very low Reynolds numbers, however, the effect of "crowding", which acts to increase the velocity, is more than offset by the effect of viscous retardation, which acts to decrease the velocity.

The velocity of the fluid is zero everywhere at the sphere surface (remember the no-slip condition) and increases only slowly away from the sphere, even in the vicinity of the midsection: at low Reynolds numbers, the retarding effect of the sphere is felt for great distances out into the fluid. You will see later in this chapter that the zone of retardation shrinks greatly as the Reynolds number increases, and the "crowding" effect causes the velocity around the midsection of the sphere to be greater than the free-stream velocity except very near the surface of the sphere; more on that later.

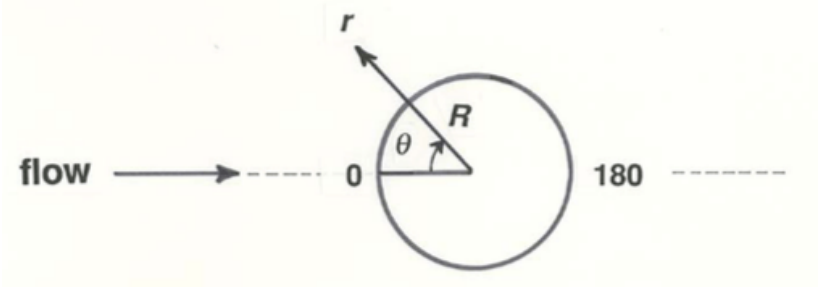


Figure $3.2.2$: Coordinates for description of the theoretical distribution of velocity in flow past a sphere at very low Reynolds numbers (creeping flow).

Using the Navier-Stokes Equation to Describe Velocity and Pressure of a Creeping Flow

If you would like to see for yourself how the velocity varies in the vicinity of the sphere, Equations 3.2.1 give the theoretical distribution of velocity v, as a function of distance r from the center of the sphere and the angle θ measured around the sphere from 0° at the front point to 180° at the rear point (Figure 3.2.2):

$$\begin{aligned} u_r &= -U\cos\theta\left(1-\tfrac{3R}{2r}+\tfrac{R^3}{2r^3}\right) \\ u\theta &= U\sin\theta\left(1-\tfrac{3R}{4r}-\tfrac{R^3}{4r^3}\right) \end{aligned} \tag{3.2.1}$$

This result was obtained by Stokes (1851) by specializing the Navier–Stokes equations for an approaching flow that is so slow that accelerations of the fluid as it passes around the sphere can be ignored, resulting in an equation that can be solved analytically. I said in Chapter 2 that fluid density ρ is needed as a variable to describe the drag force on a sphere because accelerations are produced in the fluid as the sphere moves through it. If these accelerations are small enough, however, it is reasonable to expect that their effect on the flow and forces can be neglected. Flows of this kind are picturesquely called creeping flows. The reason, to which I alluded in the previous section, is that in the Navier–Stokes equations the term for rate of change of momentum becomes small faster than the two remaining terms, for viscous forces and pressure forces, as the Reynolds number decreases.

You can see from Equations 3.2.1 that as $r \to \infty$ the velocity approaches its free-stream magnitude and direction. The $1/r$ dependence in the second terms in the parentheses on the right-hand sides of Equations 3.2.1 reflects the appreciable distance away from the sphere the effects of viscous retardation are felt. A simple computation using Equations 3.2.1 shows that, at a distance equal to the sphere diameter from the surface of the sphere at the midsection in the direction normal to the free-stream flow, the velocity is still only 50% of the free-stream value.

At every point on the surface of the sphere there is a definite value of fluid pressure (normal force per unit area) and of viscous shear stress (tangential force per unit area). These values also come from Stokes' solution for creeping flow around a sphere. For the shear stress, you could use Equations 3.2.1 to find the velocity gradient at the sphere surface and then use Equation 1.3.7 to find the shear stress. For the pressure, Stokes found a separate equation,

$$p - p_0 = \frac{3}{2}\frac{\mu U R}{r^2}\cos\theta \tag{3.2.2}$$

where p_0 is the free-stream pressure. Figures 3.2.3 and 3.2.4 give an idea of the distribution of these forces. It is easy to understand why the viscous shear stress should be greatest around the midsection and least on the front and back surface of the sphere, because that is where the velocity near the surface of the sphere is greatest. The distribution of pressure, high in the front and low in the back, also makes intuitive sense. It is interesting, though, that there is a large front-to-back difference in pressure despite the nearly perfect front-to-back symmetry of the flow.

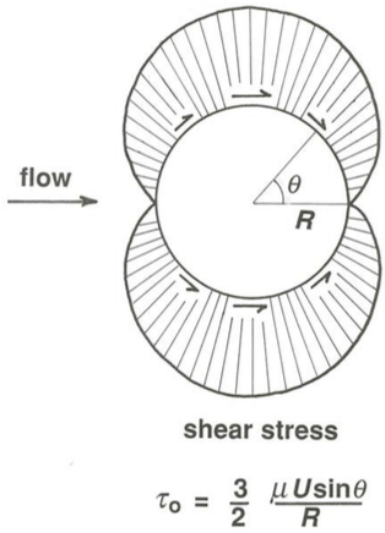


Figure 3.2.3: Distribution of shear stress on the surface of a sphere in a flow of viscous fluid at very low Reynolds numbers (creeping flow). The distribution is shown in a planar section parallel to the flow direction and passing through the center of the sphere.

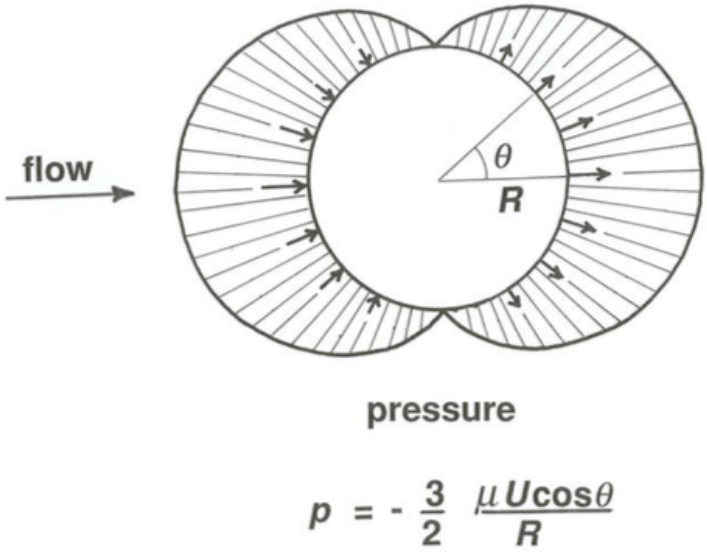


Figure 3.2.4: Distribution of pressure on the surface of a sphere in a flow of viscous fluid at very low Reynolds number (creeping flow). The distribution is shown in a planar section parallel to the flow direction and passing through the center of the sphere.

Using the Navier-Stokes Equation to Describe Drag Force (Stoke's Law)

You can imagine adding up both pressures and viscous shear stresses over the entire surface, remembering that both magnitude and direction must be taken into account, to obtain a resultant pressure force and a resultant viscous force on the sphere. Because of the symmetry of the flow, both of these resultant forces are directed straight downstream. You can then add them together to obtain a grand resultant, the total drag force F_D. Using the solutions for velocity and pressure given above (Equations 3.2.1 and 3.2.2), Stokes obtained the result

$$F_D = 6\pi\mu UR \tag{3.2.3}$$

for the total drag force on the sphere. Density does not appear in Stokes' law because it enters the equation of motion only the mass-time-acceleration term, which was neglected. For Reynolds numbers less than about one, the result expressed by Equation 3.2.3 (called **Stokes' law**) is in nearly perfect agreement with experiment. It turns out that in the Stokes range, for $Re \ll 1$, exactly one-third of F_D is due to the pressure force and two-thirds is due to the viscous force.

Now pretend that you do not know anything about Stokes' law for the drag on a sphere at very low Reynolds numbers. If you reason, as discussed above, that ρ can safely be omitted from the list of variables that influence the drag force, then you are left with four variables: F_D, U, D, and μ. The functional relationship among these four variables is necessarily

$$f\left(F_D, U, D, \mu\right) = \text{const} \tag{3.2.4}$$

You can form only one dimensionless variable out of the four variables F_D, U, D, and μ, namely $F_D/\mu UD$. So, in dimensionless form, the functional relationship in Equation 3.2.4 becomes

$$\frac{F_D}{\mu UD} = \text{const} \tag{3.2.5}$$

You can think of Equation 3.2.5 as a special case of Equation 2.3.1. If you massage Stokes' law (Equation 3.2.3) just a bit, by dividing both sides of the equation by μUR to make the equation dimensionless, and using the diameter D instead of the radius R, you obtain

$$\frac{F_D}{\mu UD} = 3\pi \tag{3.2.6}$$

Compare this with Equation 3.2.5 above. You see that dimensional analysis alone, without recourse to attempting exact solutions, provides the equation to within the proportionality constant. Stokes' theory provides the value of the constant.

The flow pattern around the sphere and the fluid forces that act on the sphere gradually become different as the Reynolds number is increased. The progressive changes in flow pattern with increasing Reynolds number are discussed in more detail later in this chapter, after quite a bit of necessary further background in the fundamentals of fluid dynamics.

This page titled 3.2: Flow Past a Sphere at Low Reynolds Numbers is shared under a CC BY-NC-SA 4.0 license and was authored, remixed, and/or curated by John Southard (MIT OpenCourseware) via source content that was edited to the style and standards of the LibreTexts platform.

3.3: Inviscid Flow

Over the past hundred and fifty years a vast body of mathematical analysis has been devoted to a kind of fluid that exists only in the imagination: an **inviscid fluid**, in which no viscous forces act. This fiction (in reality there is no such thing as an inviscid fluid) allows a level of mathematical progress not possible for viscous flows, because the viscous-force term in the Navier–Stokes equation disappears, and the equation becomes more tractable. The major outlines of mathematical analysis of the resulting simplified equation, which is mostly beyond the scope of these notes, were well worked out by late in the 1800s. Since then, fluid dynamicists have been extending the results and applying or specializing them to problems of interest in a great many fields.

Fluid Velocity for Inviscid Flow

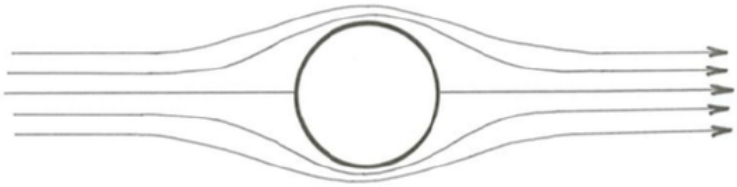


Figure 3.3.1: Flow of an inviscid fluid past a sphere. The flow lines are shown in a planar section parallel to the flow direction and passing through the center of the sphere.

The pattern of inviscid flow around a sphere, obtained as noted above by solving the equation of motion for inviscid flow, is shown in Figure 3.3.1. The arrangement of flow lines differs significantly from that in creeping viscous flow around the sphere (Figure 3.2.1): the symmetry is qualitatively the same, but, in contrast to creeping flow, the flow lines become more closely spaced around the midsection, reflecting acceleration and then deceleration of the flow as it passes around the sphere. Figure 3.3.2 is a plot of fluid velocity along the particular flow line that meets the sphere at its front point, passes back along the surface of the sphere, and leaves the sphere again at the rear point. The velocity varies symmetrically with respect to the midsection of the sphere: it falls to zero at the front point, accelerates to a maximum at the midsection, falls to zero again at the rear point, and then attains its original value again downstream. The front and rear points are called **stagnation points**, because the fluid velocity is zero there. Note that elsewhere the velocity is *not* zero on the surface of the sphere, as it is in viscous flow. Do not let this unrealistic finite velocity on the surface of the sphere bother you; it is a consequence of the unrealistic assumption that viscous effects are absent, so that the no-slip condition is not applicable.

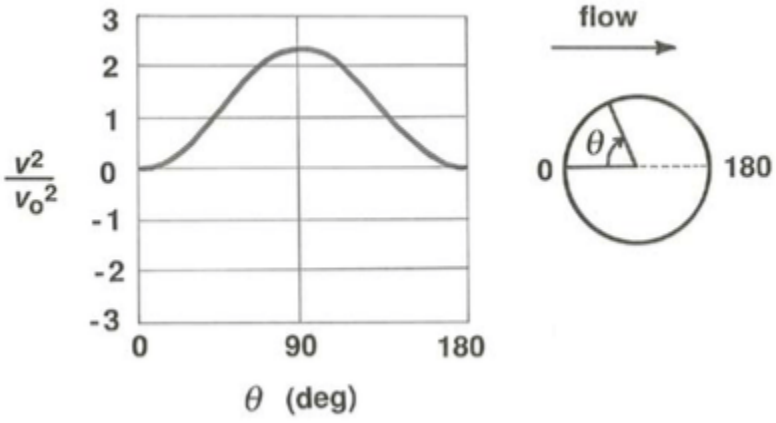


Figure 3.3.2: Plot of fluid velocity at the surface of a sphere that is held fixed in steady inviscid flow. The velocity, nondimensionalized by dividing by the stagnation velocity, is plotted as a function of the angle θ between the center of the sphere and points along the intersection of the sphere surface with a plane parallel to the flow direction and passing through the center of the sphere. The angle θ varies from zero at the front stagnation point of the sphere to 180° at the rear stagnation point.

Fluid Pressure for Inviscid Flow

Figure 3.3.3 shows the distribution of fluid pressure around the surface of a sphere moving relative to an inviscid fluid. As with velocity, pressure is distributed symmetrically with respect to the midsection, and its variation is just the inverse of that of the velocity: relative to the uniform pressure far away from the sphere, it is greatest at the stagnation points and least at the midsection. One seemingly ridiculous consequence of this symmetrical distribution is that the flow exerts no net pressure force on the sphere, and therefore, because there are no viscous forces either, it exerts no resultant force on the sphere at all! This is in striking contrast to the result noted above for creeping viscous flow past a sphere (Figure 3.2.3), in which the distribution of pressure on the surface of the sphere shows a strong front-to-back asymmetry; it is this uneven distribution of pressure, together with the existence of viscous shear forces on the boundary, that gives rise to the drag force on a sphere in viscous flow.

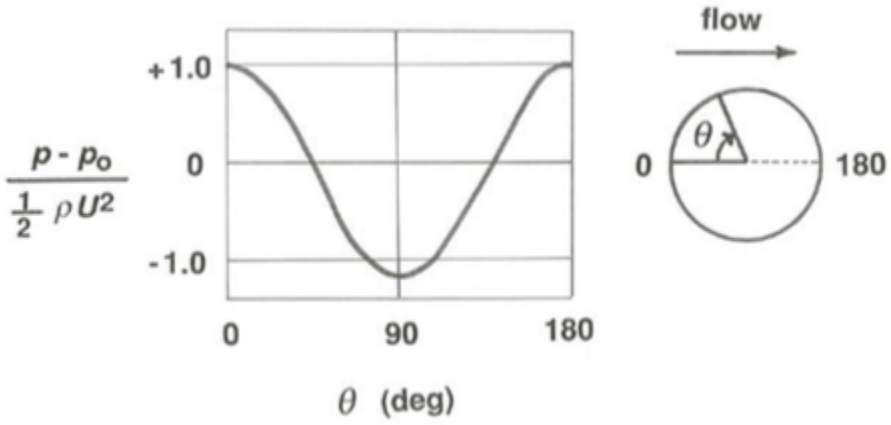


Figure 3.3.2.

Value of Inviscid Theory

So the distributions of velocity and pressure in inviscid flow around a sphere, and therefore of the fluid forces on the sphere, are grossly different from the case of flow of viscous fluid around the sphere. Then what is the value of the inviscid approach? You will see in the section on flow separation later on that at higher real-fluid velocities the boundary layer in which viscous effects are concentrated next to the surface of the sphere is thin, and outside this thin layer the flow patterns and the distributions of both velocity and pressure are approximately as given by the inviscid theory. Moreover, the boundary layer is so thin for high flow velocities that the pressure on the surface of the sphere is approximately the same as that given by the inviscid solution just outside the boundary layer. And because at these high velocities the pressure forces are the main determinant of the total drag force, the inviscid approach is useful in dealing with forces on the sphere after all. Behind the sphere the flow patterns given by inviscid theory are grossly different from the real pattern at high Reynolds numbers, but you will see that one of the advantages of the inviscid assumption is that it aids in a rational explanation for the existence of this great difference.

In many kinds of flows around well streamlined bodies like airplane wings, agreement between the real viscous case and the ideal inviscid case is much better than for flow around blunt or bluff bodies like spheres. In flow of air around an airplane wing, viscous forces are important only in a very thin layer immediately adjacent to the wing, and outside that layer the pressure and velocity are almost exactly as given by inviscid theory (Figure 3.3.4). It is these inviscid solutions that allow prediction of the lift on the airplane wing: although drag on the wing is governed largely by viscous effects within the boundary layer, lift is largely dependent upon the inviscid distribution of pressure that holds just outside the boundary layer. To some extent this is true also for flow around blunt objects resting on a planar surface, like sand grains on a sand bed under moving air or water.

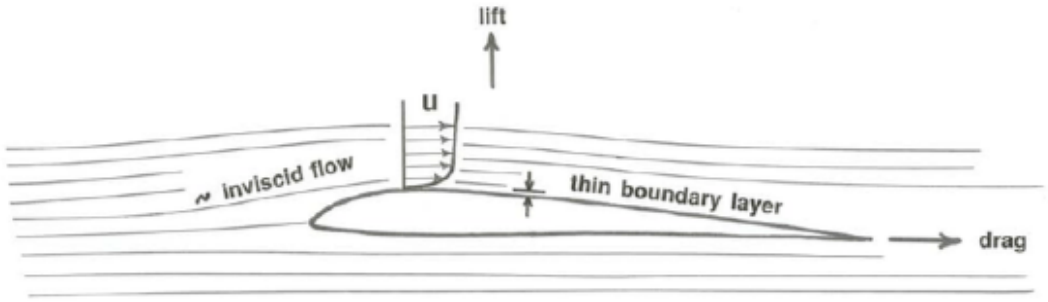


Figure 3.3.4: Flow of a real fluid past an airfoil, showing an overall flow pattern almost identical to that of an inviscid flow except very near the surface of the airfoil, where a thin boundary layer of retarded fluid is developed. Note that the velocity goes to zero at the surface of the airfoil.

This page titled 3.3: Inviscid Flow is shared under a CC BY-NC-SA 4.0 license and was authored, remixed, and/or curated by John Southard (MIT OpenCourseware) via source content that was edited to the style and standards of the LibreTexts platform.

3.4: The Bernoulli Equation

In the example of inviscid flow past a sphere described in the preceding section, the pressure is high at points where the velocity is low, and vice versa. It is not difficult to derive an equation, called the **Bernoulli equation**, that accounts for this relationship. Because this will be useful later on, I will show you here how it comes about.

Flowlines

First I have to be more specific about what I have casually been calling flow lines. Fluid velocity is a vector quantity, and, because the fluid behaves as a continuum, a velocity vector can be associated with every point in the flow. (Mathematically, this is described as a *vector field*.) Continuous and smooth curves that can be drawn to be everywhere tangent to the velocity vectors throughout the vector field are called **streamlines** (Figure 3.4.1). One and only one streamline passes through each point in the flow, and at any given time there is only one such set of curves in the flow. There obviously is an infinity of streamlines passing through any region of flow, no matter how small; usually only a few representative streamlines are shown in sketches and diagrams. An important property of streamlines follows directly from their definition: the flow can never cross streamlines.

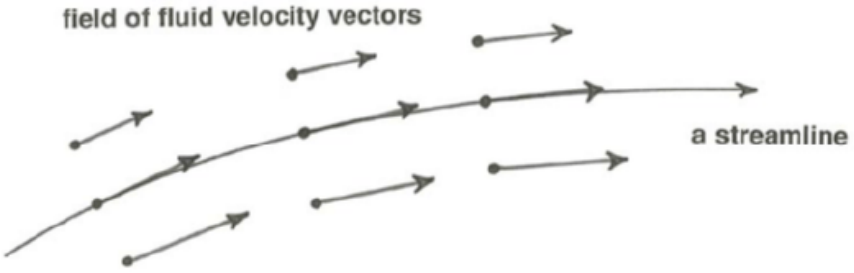


Figure 3.4.1: Streamlines.

If the flow is steady, the streamline pattern does not change with time; if the streamline pattern changes with time, the flow is unsteady. But note that the converse of each of these statements is not necessarily true, because an unsteady flow can exhibit an unchanging pattern of streamlines as velocities everywhere increase or decrease with time.

There are two other kinds of flow lines, with which you should not confuse streamlines (Figure 3.4.2): **pathlines**, which are the trajectories traced out by individual tiny marker particles emitted from some point within the flow that is fixed relative to the stationary boundaries of the flow, and **streaklines**, which are the streaks formed by a whole stream of tiny marker particles being emitted continuously from some point within the flow that is fixed relative to the stationary boundaries of the flow. In steady flow, streamlines and pathlines and streaklines are all the same; in unsteady flow, they are generally all different.

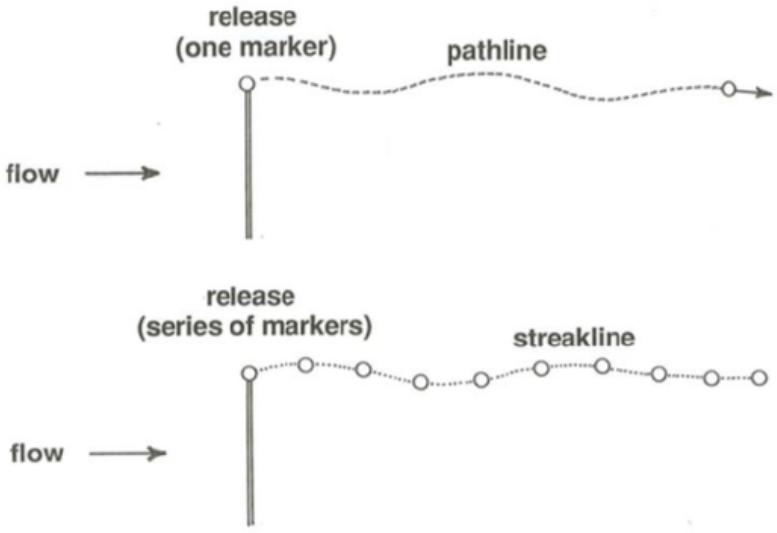


Figure 3.4.2: Pathlines and streaklines.

Streamtubes and the Bernoulli Equation

You also can imagine a tube-like surface formed by streamlines, called a stream tube, passing through some region (Figure 3.4.3). This surface or set of streamlines can be viewed as functioning as if it were a real tube or conduit, in that there is flow through the tube but there is no flow either inward or outward across its surface.

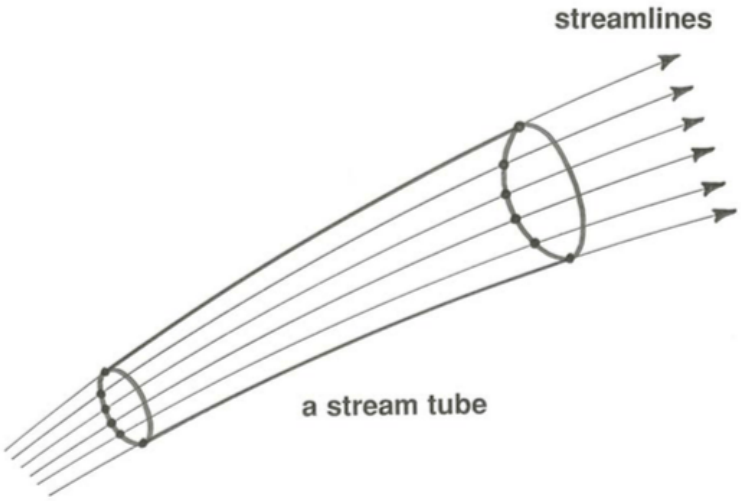


Figure 3.4.3: A streamtube.

Consider a short segment of one such tiny stream tube in a flow of incompressible fluid (Figure 3.4.4). Write the equation of motion (Newton's second law) for the fluid contained at some instant in this stream-tube segment. The cross-sectional area of the tube is ΔA, and the length of the segment is Δs. If the pressure at cross section 1, at the left-hand end of the segment, is p, then the force exerted on this end of the segment is $p\Delta A$. It is not important that the area of the cross section might be slightly different at the two ends (if the flow is expanding or contracting), or that p might vary slightly over the cross section, because you can make the cross-sectional area of the stream tube as small as you please. What is the force on the other end of the tube? The pressure at cross section 2 is different from that at cross section 1 by $(\partial p/\partial s)\Delta s$, the rate of change of pressure in the flow direction times the distance between the two cross sections, so the force on the right-hand end of the tube is

$$\left(p + \frac{\partial p}{\partial s}\Delta s\right)\Delta A \tag{3.4.1}$$

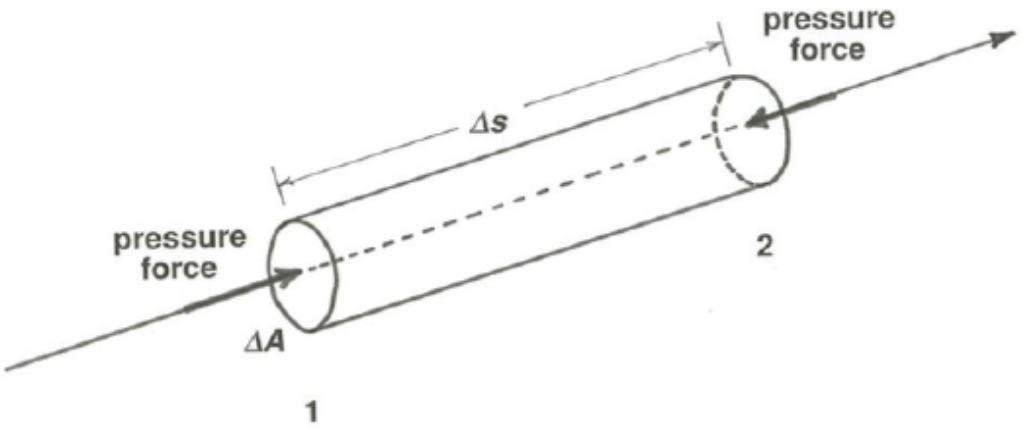


Figure 3.4.4: Definition sketch for derivation of the Bernoulli equation for incompressible inviscid flow.

The net force on the stream tube in the flow direction is then

$$p\Delta A - \left(\mathrm{p} + \frac{\partial p}{\partial s}\Delta s\right)\Delta A = -\frac{\partial p}{\partial s}\Delta s \Delta A \tag{3.4.2}$$

The pressure on the lateral surface of the tube is of no concern, because the pressure force on it acts normal to the flow direction.

Newton's second law, $F = d(mv)/dt$, for the fluid in the segment of the stream tube, where v is the velocity of the fluid at any point (in this section v is used not as the component of velocity in the y direction but as the component of velocity tangent to the streamline at a given point), is then

$$-\frac{\partial p}{\partial s}\Delta s \Delta A = \frac{d}{dt}[v(\rho \Delta s \Delta A)] \tag{3.4.3}$$

Simplifying Equation 3.4.3 and making use of the fact that ρ is constant and so can be moved outside the derivative,

$$-\frac{\partial p}{\partial s} = \rho \frac{dv}{dt} \tag{3.4.4}$$

The derivative on the right side of Equation 3.4.4 can be put into more convenient form by use of the chain rule and a simple "undifferentiation" of one of the resulting terms:

$$\begin{aligned} -\frac{\partial p}{\partial s} &= \rho \frac{dv}{dt} \\ &= \rho\left[\frac{\partial v}{\partial t}\frac{dt}{dt} + \frac{\partial v}{\partial s}\frac{ds}{dt}\right] \\ &= \rho\left[\frac{\partial v}{\partial t} + v\frac{\partial v}{\partial s}\right] \end{aligned} \tag{3.4.5}$$

$$= \rho\left[\frac{\partial v}{\partial t} + \frac{1}{2}\frac{\partial\left(v^2\right)}{\partial s}\right] \tag{3.4.6}$$

Equation 3.4.6 is strictly true only for the single streamline to which the stream tube collapses as we let ΔA go to 0, because only then need we not worry about possible variation of either p or v over the cross sections. Assuming further that the flow is steady, $\partial v/\partial t = 0$, and Equation 3.4.6 becomes

$$-\frac{\partial p}{\partial s} = \frac{\rho}{2}\frac{\partial\left(v^2\right)}{\partial s} \tag{3.4.7}$$

It is easy to integrate Equation 3.4.7 between two points 1 and 2 on the streamline (remember that this equation holds for any streamline in the flow):

$$-\int_1^2 \frac{\partial p}{\partial s} ds = \frac{\rho}{2}\int_1^2 \frac{\partial(v^2)}{\partial s} ds$$

$$p_2 - p_1 = -\frac{\rho}{2}\left(v_2^2 - v_1^2\right) \tag{3.4.8}$$

or, viewed in another way,

$$p + \frac{\rho v^2}{2} = \text{const} \tag{3.4.9}$$

You can see from Equation 3.4.8 that if the flow is steady and incompressible there is an inverse relationship between fluid pressure and fluid velocity along any streamline. Equation 3.4.8 or Equation 3.4.9 is called the **Bernoulli equation**. Remember that it holds only along individual streamlines, not through the entire flow. In other words, the constant in the Equation 3.4.9 is generally different for each streamline in the flow. And it holds only for inviscid flow, because if the fluid is viscous there are shearing forces across the lateral surfaces of stream tubes, and Newton's second law cannot be written and manipulated so simply. But often in flow of a real fluid the viscous forces are small enough outside the boundary layer that the Bernoulli equation is a good approximation.

Note

Note that the right-hand side of Equation 3.4.8 is the negative of the increase in kinetic energy per unit volume of fluid between point 1 and point 2. The Bernoulli equation is just a statement of the work–energy theorem, whereby the work done by a force acting on a body is equal to the change in kinetic energy of the body. In this case, fluid pressure is the only force acting on the fluid.

In discussing inviscid flow around a sphere I called the front and rear points of the sphere the stagnation points, because velocities relative to the sphere are zero there. Using the Bernoulli equation it is easy to find the corresponding *stagnation pressures*. Taking the free-stream values of pressure and velocity to be po and vo, writing Equation 3.4.8 in the form

$$p - p_o = -\frac{\rho}{2}\left(v^2 - v_o^2\right) \tag{3.4.10}$$

and substituting $v = 0$ at the stagnation points, the stagnation pressures (the same for front and rear points) are

$$p = p_o + \frac{\rho v_o^2}{2} \tag{3.4.11}$$

This page titled 3.4: The Bernoulli Equation is shared under a CC BY-NC-SA 4.0 license and was authored, remixed, and/or curated by John Southard (MIT OpenCourseware) via source content that was edited to the style and standards of the LibreTexts platform.

3.5: Turbulence

Most of the fluid flows of interest in science, technology, and everyday life are turbulent flows—although there are many important exceptions to that generalization, like the flow of groundwater in the porous subsurface, or the flow of blood in capillaries, or the flow of lubricating fluid in thin clearances between moving parts of a machine, or the flow of that thin, slow-moving sheet of water you see on the paved surface of the shopping-mall parking lot after a rain. Because of the range and complexity of problems in turbulent flow, the approach here will necessarily continue to be selective. The introductory material on the description and origin of turbulence in this section is background for the important topic of turbulent flow in boundary layers in the following section and in Chapter 4. The emphasis in all this material on turbulence is on the most important physical effects. Mathematics will be held to a minimum, although some is unavoidable in the derivation of useful results on flow resistance and velocity profiles in Chapter 4.

What is Turbulence?

It is not easy to devise a satisfactory definition of turbulence. **Turbulence** might be loosely defined as an irregular or random or statistical component of motion that under certain conditions becomes superimposed on the mean or overall motion of a fluid when that fluid flows past a solid surface or past an adjacent stream of the same fluid with different velocity. This definition does not convey very well what turbulence is really like; it is much easier to describe turbulence than to define it.

Describing Turbulence

My goal in this section is to present to you as clear a picture as possible of what turbulence is like. Suppose that you were in possession of a magical instrument that allowed you to make an exact and continuous measurement of the fluid velocity at any point in a turbulent flow as a function of time. I am calling the instrument magical because all of the many available methods of measuring fluid velocity at a point, some of them fairly satisfactory, inevitably suffer to some extent from one or both of two drawbacks:

1. The presence of the instrument distorts or alters the flow one is trying to measure.
2. The effective measurement volume is not small enough to be regarded as a “point”.

What would your record of velocities look like? Figure $3.5.1$ is an example of a record, for the component u of velocity in the downstream direction. The outstanding characteristic of the velocity is its *uncertainty*: there is no way of predicting at a given time what the velocity at some future time will be. But note that there is a readily discernible (although not precisely definable) range into which most of the velocity fluctuations fall, and the same can be said about the time scales of the fluctuations.

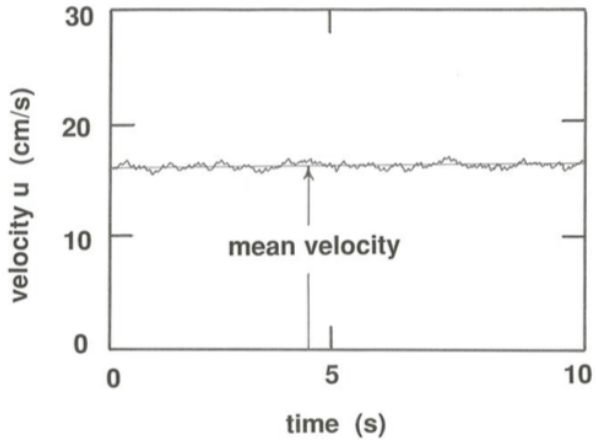


Figure $3.5.1$: Typical record of streamwise instantaneous flow velocity measured at a point in a turbulent channel flow.

Turbulence measurements present a rich field for statistical treatment. First of all, a mean velocity $\overline{u}$ can be defined from the record of u by use of an averaging time interval that is very long with respect to the time scale of the fluctuations but not so long

that the overall level of the velocity drifts upward or downward during the averaging time. A fluctuating velocity u' can then be defined as the difference between the instantaneous velocity u and the mean velocity $\overline{u}$:

$$u' = u - \overline{u} \tag{3.5.1}$$

where the overbar denotes a time average. The time-average value of u' must be zero (by definition!). Now look at the component of velocity in any direction normal to the mean flow direction. You would see a record similar to that shown in Figure 3.5.1, except that the average value would always have to be zero; the normal-to-boundary velocity is usually called v, and the cross-stream velocity parallel to the boundary and normal to flow) is usually called w. Equations just like Equation 3.5.1 can be written for the components v and w:

$$\begin{aligned} v' &= v - \overline{v} = v \\ w' &= w - \overline{w} = w \end{aligned} \tag{3.5.2}$$

A good measure of the *intensity* of the turbulence is the root-mean- square value of the fluctuating components of velocity:

$$\begin{aligned} \text{rms}\,(u') &= \left(u'^2\right)^{1/2} \\ \text{rms}\,(v') &= \left(v'^2\right)^{1/2} \\ \text{rms}\,(w') &= \left(w'^2\right)^{1/2} \end{aligned} \tag{3.5.3}$$

These are formed by taking the square root of the time average of the squares of the fluctuating velocities; for those who are familiar with statistical terms, the rms values are simply standard deviations of instantaneous velocities. They are always positive quantities, and their magnitudes are a measure of the strength or intensity of the turbulence, or the spread of instantaneous velocities around the mean. Turbulence intensities are typically something like five to ten percent of the mean velocity $\overline{u}$ (that is, again in the parlance of statistics, the coefficient of variation of velocity is 5–10%).

Several Ways of Analyzing Turbulence

Statistical analysis of turbulence can be carried much further than this. But now suppose that you measured velocity in a different way, by following the trajectories of fluid "points" or markers as they travel with the flow and measuring the velocity components as a function of time (Figure 3.5.2). It is straightforward, though laborious, to do this sort of thing by photographing tiny neutrally buoyant marker particles that represent the motion of the fluid well and then measuring their travel and computing velocities. Velocities measured in this way, called *Lagrangian* velocities, are related to those measured at a fixed point, called *Eulerian* velocities, and the records would look generally similar. The trajectories themselves would be three-dimensionally sinuous and highly irregular, as shown schematically in Figure 3.5.2, although angles between tangents to trajectories and the mean flow direction are usually not very large, because u' is usually small relative to $\overline{u}$.

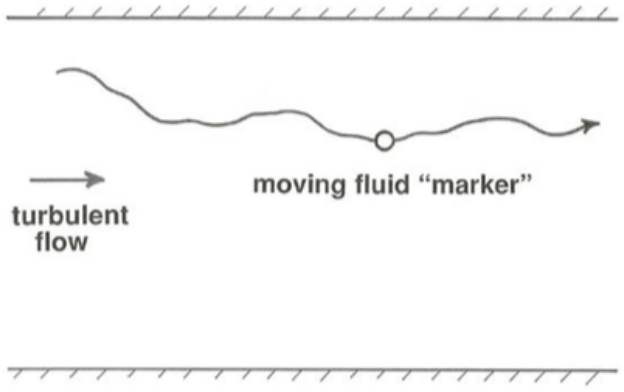


Figure 3.5.2: Typical trajectory of a small fluid element or neutrally buoyant marker particle in a turbulent channel flow.

You can also imagine releasing fluid markers at some fixed point in the flow and watching a succession of trajectories traced out at different times (Figure 3.5.3). Each trajectory would be different in detail, but they would show similar features.

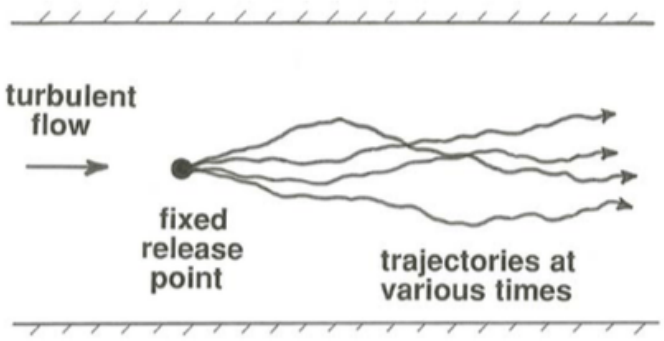


Figure 3.5.3: A series of trajectories of small, neutrally buoyant markers in a turbulent channel flow, all released from the same point.

One thing you can do to learn something about the spatial scale of the fluctuations revealed by velocity records like the one in Figure 3.5.1 is to think about the distance over which the velocity becomes "different" or uncorrelated with distance away from a given point (Figure 3.5.4). Suppose that you measured the velocity component u simultaneously at two points 1 and 2 a distance x apart in the flow and computed the correlation coefficient by forming products of a large number of pairs of velocities, each measured at the same time, taking the average of all the products, and then normalizing by dividing by the rms value. If the two points are close together compared to the characteristic spatial scale of the turbulence, the velocities at the two points are nearly the same, and the coefficient is nearly one. But if the points are far apart the velocities are uncorrelated (that is, they have no tendency to be similar), and the coefficient is zero or nearly so. The distance over which the coefficient falls to its minimum value, a bit less than one, before rising again to zero is roughly representative of the spatial scale of the turbulent velocity fluctuations. The gentle minimum is an indication that the distance out from the original point corresponds to adjacent eddies, which tend to have an opposing velocity, hence the minimum. A similar correlation coefficient can be computed for Lagrangian velocities, and correlation coefficients can also be based on time rather than on space.

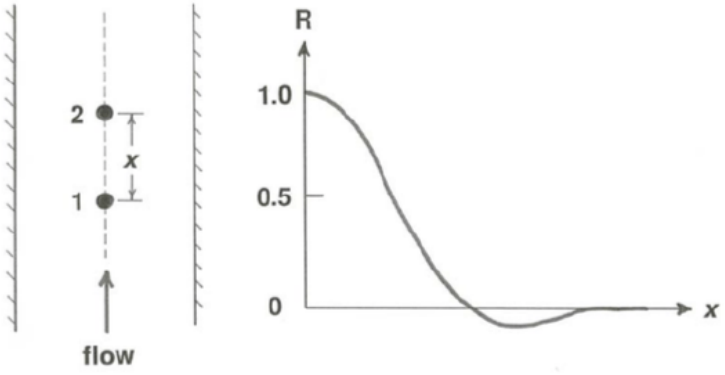


Figure 3.5.4: Correlation coefficient R for fluid velocity measured at two points, 1 and 2, separated by a streamwise (i.e., alongstream) distance x.

Eddies

One of the very best ways to get a qualitative idea of the physical nature of turbulent motions is to put some very fine flaky reflective material into suspension in a well illuminated flow. The flakes tend to be brought into parallelism with local shearing planes, and variations in reflected light from place to place in the flow give a fairly good picture of the turbulence. Although it is easier to appreciate than to describe the pattern that results, the general picture is one of intergrading swirls of fluid, with highly irregular shapes and with a very wide range of sizes, that are in a constant state of development and decay. These swirls are called turbulent **eddies**. Even though they are not sharply delineated, they have a real physical existence.

The swirly nature of the eddies is most readily perceived when the eye attempts to follow points moving along with the flow; if instead the eye attempts to fix upon a point in the flow that is stationary with respect to the boundaries, fluid elements (if there are some small marker particles contained in the fluid to reveal them) are seen to pass by with only slightly varying velocities and directions, in accordance with the Eulerian description of turbulent velocity at a point.

Each eddy has a certain sense and intensity of rotation that tends to distinguish it, at least momentarily, from surrounding fluid. The property of solid- body-like *rotation of fluid at a given point* in the flow is termed **vorticity**. Think in terms of the rotation of a small element of fluid as the volume of the element shrinks toward zero around the point. The vorticity varies smoothly in both magnitude and orientation from point to point. The eddy structure of the turbulence can be described by how the vorticity varies throughout the flow; the vorticity in an eddy varies from point to point, but it tends to be more nearly the same there than in neighboring eddies.

Laminar and Turbulent Flow

At first thought it seems natural that fluids would show a smooth and regular pattern of movement, without all the irregularity of turbulence. Such regular flows are called **laminar flows**. You will see over and over again in these notes that flows in a given setting or system are laminar under some conditions and turbulent under other conditions. Now that you have some idea of the kinematics of turbulent flow, you might consider what it is that governs whether a given flow is laminar or turbulent in the first place, and what the transition from laminar to turbulent flow is like. Osborne Reynolds did the pioneering work on these questions in the 1880s in an experimental study of flow through tubes with circular cross section (Reynolds, 1883).

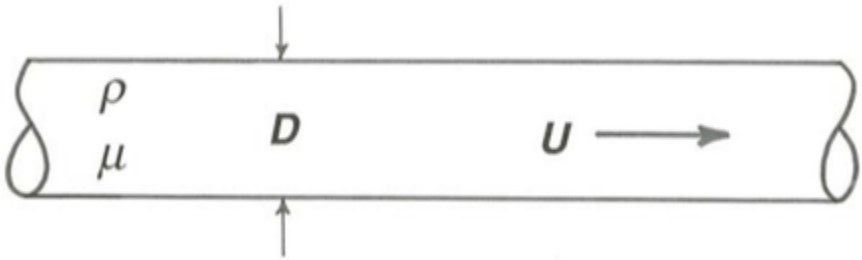


Figure $3.5.5$: Variables associated with steady flow through a circular tube.

Think first about the variables that must be important in steady flow through a straight circular tube (Figure $3.5.5$). Density ρ must be taken into account, because of the possibility of turbulent flow in the tube and therefore local fluid accelerations. Viscosity μ must be taken into account because it affects the shearing forces within the fluid and at the wall. A variable that describes the speed of movement of the fluid is important, because this governs both fluid inertia and rates of shear. A good variable of this kind is the mean velocity of flow U in the tube; this can be found either by averaging the local fluid velocity over the cross section of the tube or by dividing the discharge (the volume rate of flow) by the cross-sectional area of the tube. The diameter D of the tube is important because it affects both the shear rate and the scale of the turbulence. Gravity need not be considered explicitly in this kind of flow because no deformable free surface is involved. By dimensional analysis, as discussed in Chapter 2, the four variables U, D, ρ, and μ can be combined into a single dimensionless variable $\rho UD/\mu$ on which all of the characteristics of the flow, including the transition from laminar to turbulent flow, depend. Reynolds first deduced the importance of this variable, now called the **Reynolds number**, by considering the dimensional structure of the equation of motion in the way I alluded to briefly at the end of Chapter 2.

Reynolds made two kinds of experiments. The first, to study the development of turbulent flow from an originally laminar flow, was made in an apparatus like that shown in Figure $3.5.6$: a long tube leading from a reservoir of still water by way of a trumpet-shaped entrance section, through which a flow with varying mean velocity could be passed with a minimum of disturbance. Three different tube diameters ($1/4''$, $1/2''$, and $1''$; 0.64, 1.27, and 2.54cm) and water of two different temperatures, and therefore of two different viscosities, were used. For each combination of D and μ, U was gradually increased until the originally laminar flow became turbulent. The transition was observed with the aid of a streak of colored water introduced at the entrance of the tube.

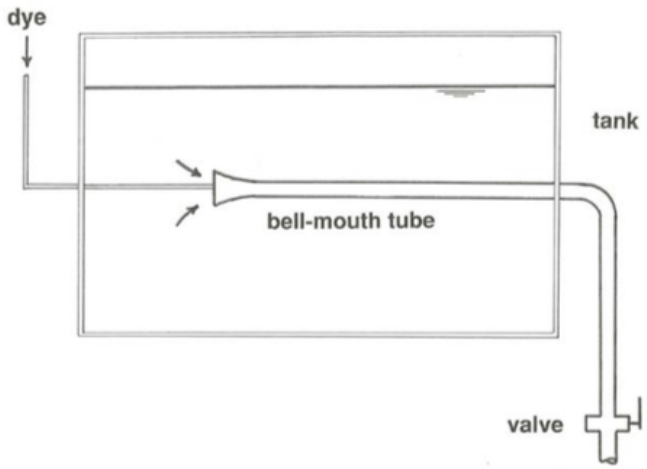


Figure 3.5.6: Apparatus (schematic) used by Osborne Reynolds in his study of the transition from laminar to turbulent flow in a circular tube.

> When the velocities were sufficiently low, the streak of color extended in a beautiful straight line through the tube [Figure 3.5.7A].... As the velocity was increased by small stages, at some point in the tube, always at a considerable distance from the trumpet or entrance, the color band would all at once mix up the surrounding water and fill the rest of the tube with a mass of colored water [Figure 3.5.7B].... On viewing the tube by the light of an electric spark, the mass of water resolved itself into a mass of more or less distinct curls, showing eddies [Figure 3.5.7C] - (Reynolds, 1883, p. 942)

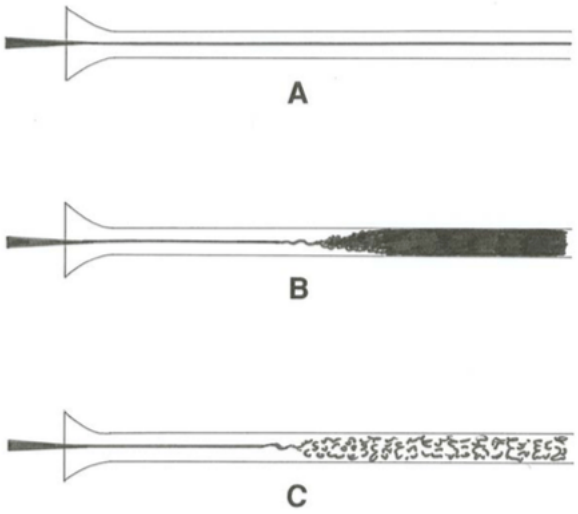


Figure 3.5.7: The results of Reynolds' experiments on the transition from laminar to turbulent flow in a circular tube.

Reynolds found that for each combination of D and U the point of transition was characterized by almost exactly the same value of Re, around $12,000$. Subsequent experiments have since confirmed this over a much wider range of U, D, ρ, and μ.

Reynolds suspected that, because the transition from laminar to turbulent flow was so abrupt and the resulting turbulence was so well developed, the laminar flow became potentially unstable to large disturbances at a much lower value of Re than he found for the transition when he minimized external disturbances, and in fact he observed that the transition took place at much lower values of Re if there was residual turbulence in the supply tank or if the apparatus was disturbed in any way. Similar experiments made with even greater care in eliminating such disturbances have since shown that laminar flow can be maintained to much higher values of Re, up to about $40,000$, than in Reynolds' original experiments.

To circumvent the persistence of laminar flow into the range of Re for which it is unstable, Reynolds made a separate set of experiments to study the transition of originally turbulent flow to laminar flow as the mean velocity in the tube was gradually decreased. To do this he passed turbulent flow through a very long metal pipe and gradually decreased the mean velocity until

at some point along the pipe the flow became laminar. The occurrence of the transition was detected by measuring the drop in fluid pressure between two stations about two meters apart near the downstream end of the pipe. (It had been known long before Reynolds' work—and you yourselves will soon be seeing why—that in laminar flow through a horizontal pipe the rate at which fluid pressure drops along the pipe is directly proportional to the mean velocity, whereas in turbulent flow it is approximately proportional to the square of the mean velocity. Thus, although Reynolds could not see the transition he had a sensitive means of detecting its occurrence.) Again many different combinations of D and μ were used, and in every case the transition from turbulent to laminar flow occurred at values of Re close to 2000. This is the value for which laminar flow can be said to be *unconditionally stable*, in the sense that no matter how great a disturbance is introduced, the flow always reverts to being laminar.

Origin of Turbulence

Mathematical theory for the origin of turbulence is intricate, and only partly successful in accounting for the transition to turbulent flow at a certain critical Reynolds number. One of the most successful approaches involves analysis of the stability of a laminar flow against very small-amplitude disturbances. The mathematical technique involves introducing a small wavelike disturbance of a certain frequency into the equation of motion for the flow and then seeing whether the disturbance grows in amplitude or is damped. The assumption is that if the disturbance tends to grow it will eventually lead to development of turbulence.

Although a satisfactory explanation would take us off the track at this point, in laminar flow there is a tendency for a wave-shaped distortion like the one in Figure $3.5.8$ to be amplified with time: applying the Bernoulli equation along the streamlines shows that fluid pressure is lowest where the velocity is greatest in the region of crowded flow lines, and highest where the velocity is smallest in the region of uncrowded flow lines, and the resulting unbalanced pressure force tends to accelerate the fluid in the direction of convexity and thereby accentuate the distortion. But at the same time the viscous resistance to shearing tends to weaken the shearing in the high-shear part of the distortion and thus tends to make the flow revert to uniform shear. It should therefore seem natural that the Reynolds number, which is a measure of the relative importance of viscous shear forces and accelerational tendencies, should indicate whether disturbances like this are amplified or damped.

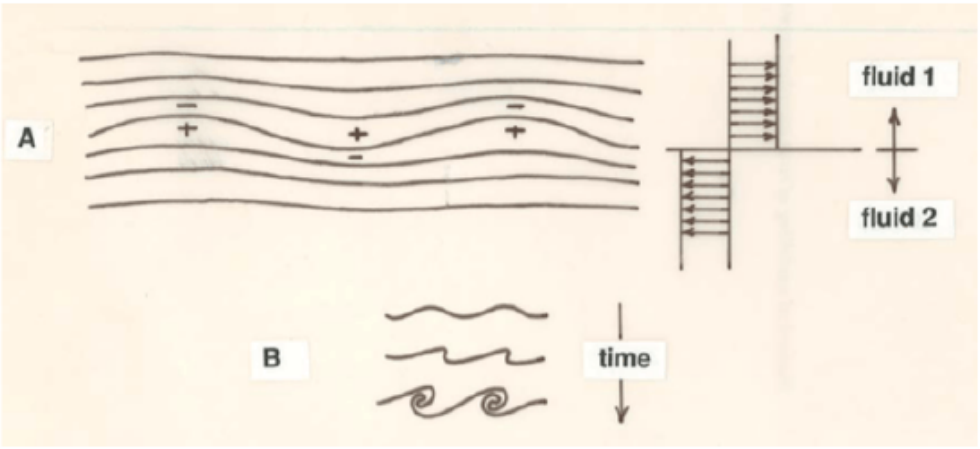


Figure $3.5.8$: Amplification of a wave-shaped disturbance on an interface of velocity discontinuity in laminar flow (schematic). **A)** Pressure forces acting to deform the surface. Plus and minus signs indicate high and low pressures, respectively. **B)** Evolution of the disturbance with time in a series of vortices.

Figure $3.5.9$ is a stability diagram for a laminar shear layer or boundary layer (see next section) developed next to a planar boundary. The diagram shows the results of both the mathematical stability analysis described above and experimental observations on stability. The experiments were made by causing a small metal band to vibrate next to the planar boundary at a known frequency and observing the resulting velocity fluctuations in the fluid. Agreement between theory and experiment is good but not perfect; if the experimental results were completely in agreement with the calculated curve, they would all fall on it. The diagram shows that there is a well-defined critical Reynolds number, Re_{crit}, below which the laminar flow is always stable but above which there is a range of frequencies at any Reynolds number for which the disturbance is amplified, so that the laminar flow is potentially unstable and becomes turbulent provided that disturbances with frequencies in that range are present.

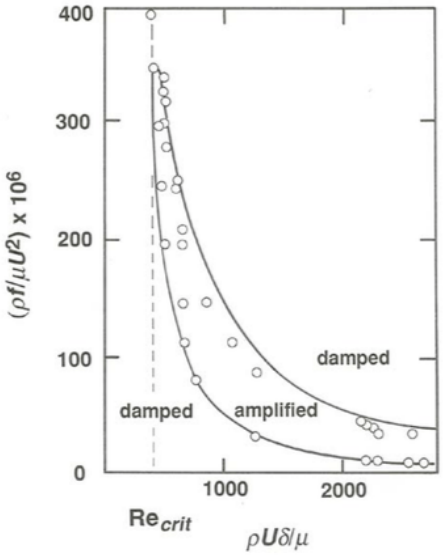


Figure 3.5.9: Diagram showing stability of a laminar shear layer (boundary layer) developed next to a planar boundary. The vertical axis is a dimensionless measure of the frequency f of the imposed small-amplitude disturbances. The horizontal axis is a Reynolds number based on the thickness δ of the boundary layer and free-stream velocity at the outer edge of the boundary layer. The solid curve is the calculated curve for neutral stability (Lin, 1955); the points represent experimental determinations of neutral stability (Schubauer and Skramstad, 1947).

This page titled 3.5: Turbulence is shared under a CC BY-NC-SA 4.0 license and was authored, remixed, and/or curated by John Southard (MIT OpenCourseware) via source content that was edited to the style and standards of the LibreTexts platform.

3.6: Boundary Layers

Introduction

A **boundary layer** is the zone of flow in the immediate vicinity of a solid surface or boundary in which the motion of the fluid is affected by the frictional resistance exerted by the boundary. The no-slip condition requires that the velocity of fluid in direct contact with solid boundary be exactly the same as the velocity of the boundary; the boundary layer is the region of fluid next to the boundary across which the velocity of the fluid grades from that of the boundary to that of the unaffected part of the flow (often called the **free stream**) some distance away from the boundary.

Probably the simplest example of a boundary layer is the one that develops on both surfaces of a stationary flat plate held parallel to a uniform free stream of fluid (Figure $3.6.1$). Just downstream of the leading edge of the plate the boundary layer is very thin, and the shearing necessitated by the transition from zero velocity to free-stream velocity is compressed into a thin zone of strong shear, so the shear stress at the surface of the plate is large (cf. Equation 1.3.6). Farther along the plate the boundary layer is thicker, because the motion of a greater thickness of fluid is retarded by the frictional influence of the plate, in the form of shear stresses exerted from layer to layer in the fluid; the shearing is therefore weaker, and the shear stress at the surface of the plate is smaller.

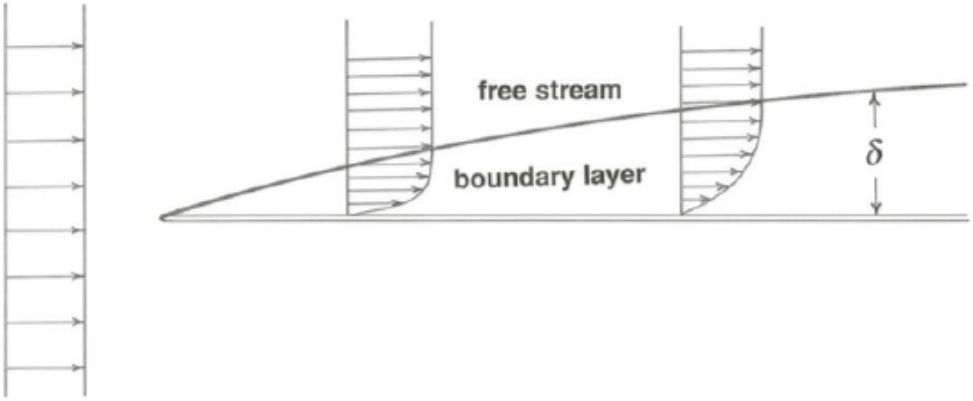


Figure $3.6.1$: Development of a laminar boundary layer on a flat plate at zero incidence (i.e., held edgewise to the flow). A boundary layer develops on both sides of the plate; only one side is shown.

Boundary layers develop on objects of any shape immersed in a fluid moving relative to the object: flat plates as discussed above, airplane wings and other streamlined shapes, and blunt or bluff bodies like spheres or cylinders or sediment particles. Boundary layers also develop next to the external boundaries of a flow: the walls of pipes and ducts, the beds and bottoms of channels, the ocean bottom, and the land surface under the moving atmosphere. In every case the boundary layer has to start somewhere, as at the front surface or leading edge of a body immersed in the flow or at the upstream end of any solid boundary to the flow. And in every case it grows or expands downstream, until the flow passes by the body (the shearing motion engendered in the boundary layer is then degraded by viscous forces), or until it meets another boundary layer growing from some other surface, or until it reaches a free surface, or until it is prevented from further thickening by encountering a stably density-stratified layer of the medium—as is commonly the case in the atmosphere and in the deep ocean.

Laminar Boundary Layers and Turbulent Boundary Layers

Flow in boundary layers may be either laminar or turbulent. A boundary layer that develops from the leading part of an object immersed in a free stream or at the head of a channel or conduit typically starts out as a laminar flow, but if it has a chance to grow for a long enough distance along the boundary it abruptly becomes turbulent. In the example of a flat-plate boundary layer (Figure $3.6.2$) we can define a Reynolds number $\mathrm{Re}_\delta = \rho U \delta / \mu$ based on free-stream velocity U and boundary-layer thickness δ; just as in flow in a tube, discussed in a previous section, past a certain critical value of Re_δ the laminar boundary layer is potentially unstable and may become turbulent. If there are no large turbulent eddies in the free stream, the laminar boundary layer may persist to very high Reynolds numbers; if the free stream is itself turbulent, or if the solid boundary surface is very rough, the

boundary layer may become turbulent a very short distance downstream of the leading edge. Turbulence in the form of small spots develops at certain points in the laminar boundary layer, spreads rapidly, and soon engulfs the entire boundary layer.

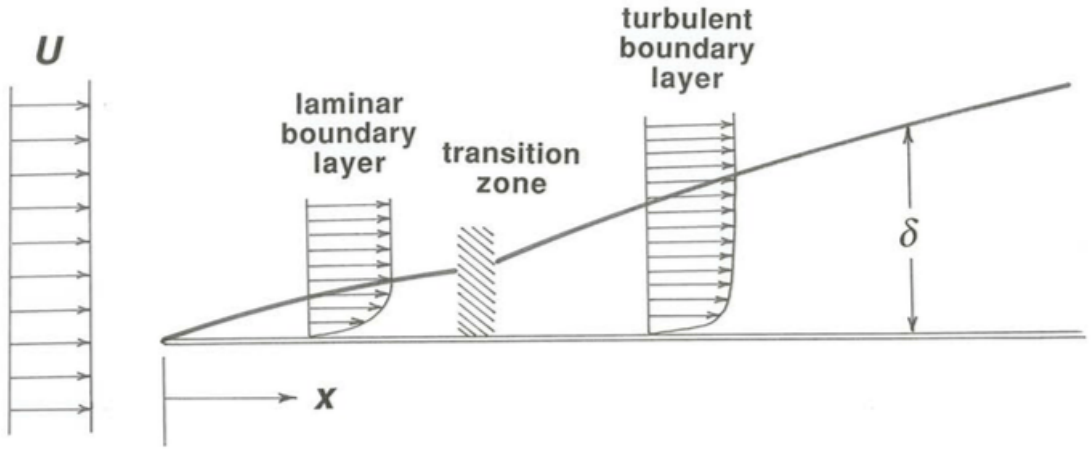


Figure 3.6.2: Transition from a laminar boundary layer to a turbulent boundary layer on a flat plate at zero incidence.

Once the boundary layer becomes turbulent it thickens faster, because fluid from the free stream is incorporated into the boundary layer at its outer edge in much the same way that clear air is incorporated into a turbulent plume of smoke (Figure 3.6.3). That effect is in addition to, and as important as, the effect of incorporation of new fluid into the boundary layer just by local frictional action—which is the *only* way a laminar boundary layer can thicken. But the thickness of even a turbulent boundary layer grows fairly slowly relative to downstream distance; the angle between the average position of the outer edge of the boundary layer and the boundary itself is not very large, typically something like a few degrees.

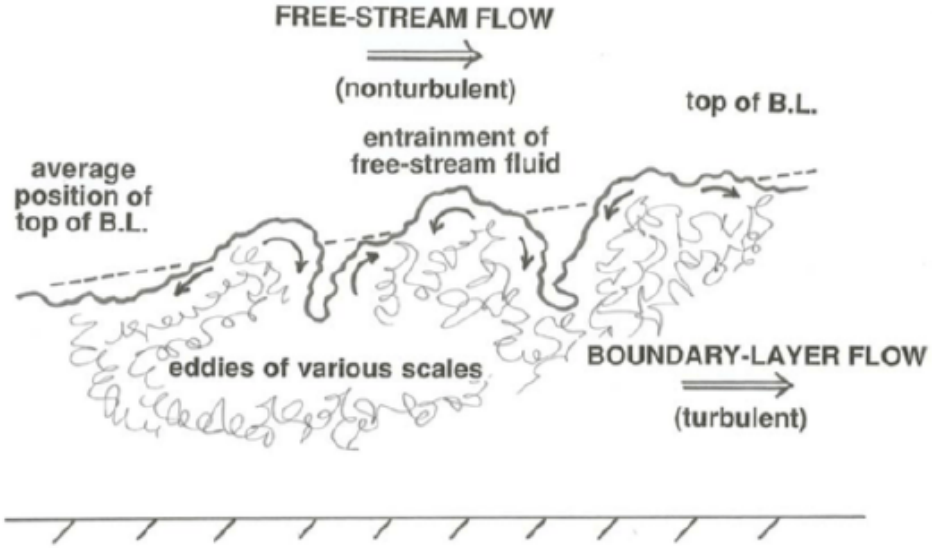


Figure 3.6.3: Sketch of processes acting to thicken a turbulent boundary layer on a flat plate at zero incidence.

Wakes

In situations where the flow passes all the way past some object of finite size surrounded by the flow, the boundary layer does not have a chance to develop beyond the vicinity of the body itself (Figure 3.6.4). Downstream of the object the fluid that was retarded in the boundary layer is gradually reaccelerated by the free stream, until far downstream the velocity profile in the free stream no longer shows any evidence of the presence of the object upstream. The zone of retarded and often turbulent fluid downstream of the object is called the **wake**.

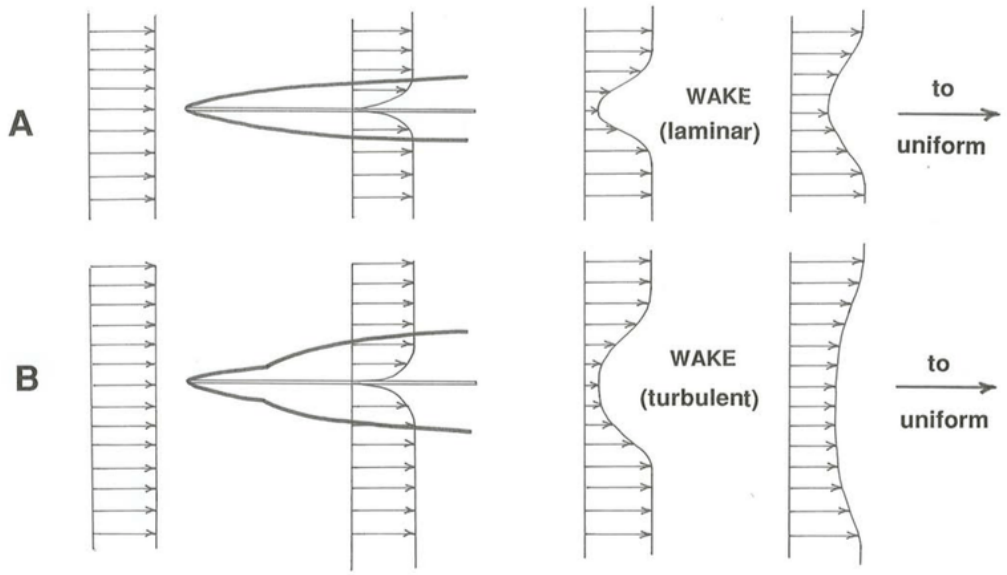


Figure 3.6.4: Development of a wake downstream of a flat plate at zero incidence.

How Thick are Boundary Layers?

One usually thinks of a boundary layer as being thin compared to the scale of the body on which it develops. This is true at high Reynolds numbers, but it is not true at low Reynolds numbers. I will show you here, by a fairly simple line of reasoning, that the boundary-layer thickness varies inversely with the Reynolds number.

The thickness of the boundary layer is determined by the relative magnitude of two effects:

1. The slowing of fluid farther and farther away from the solid surface by the action of fluid friction.
2. The sweeping of that low-momentum fluid downstream and its replacement by fluid from upstream moving at the free-stream velocity.

The greater the second effect compared with the first, the thinner the boundary layer.

Think in terms of the downstream component of fluid momentum at some distance away from the solid boundary and at some distance downstream from the leading edge of the boundary layer. The rate of downstream transport of fluid momentum (written per unit volume of fluid) at the outer edge of the boundary layer is $U(\rho U)$, where U is the free-stream velocity. The slowing of fluid by friction is a little trickier to deal with. Think back to Chapter 1, where I introduced the idea that the viscosity can be thought of as a cross-stream diffusion coefficient for downstream fluid momentum. In line with that idea, within the boundary layer the downstream fluid momentum is all the time diffusing toward the boundary. (Fluid dynamicists like to say that the boundary is a sink for momentum.) So the rate of cross-stream momentum diffusion is approximately equal to $\mu(U/\delta)$, where U/δ represents in a crude way the velocity gradient du/dy within the boundary layer.

The rate of thickening of the boundary layer is crudely represented by the ratio of downstream transport of momentum, on the one hand, to the rate of decrease of momentum at a place on account of the diffusion of momentum toward the boundary, both of these quantities having been derived in the last paragraph:

$$\frac{\text{cross-stream diffusion}}{\text{downstream transport}} = \frac{\mu U/\delta}{\rho U^2}$$

$$= \frac{\mu}{\rho U \delta}$$

$$= 1/\operatorname{Re}\delta \tag{3.6.1}$$

Equation 3.6.1 shows that the rate of boundary-layer thickening varies as the inverse of the Reynolds number based on boundary-layer thickness. This means that the boundary layer thickens more and more slowly in the downstream direction, so the cartoon of the flat-plate boundary layer in Figure 3.6.1, with the top of the boundary layer describing a curve that is concave toward the plate, is indeed qualitatively correct.

Equation 3.6.1 also tells you that the larger the Reynolds number based on the mean flow and the size of the solid object on which the boundary layer is growing, the thinner the boundary layer is at a given point—because for given δ, Re_δ is proportional to this Reynolds number. (For the flat plate, this Reynolds number is based on the distance from the leading edge; for the sphere, it is based most naturally on sphere diameter.) So the faster the free stream velocity and the larger the sphere (or the farther down the flat plate), and the smaller the viscosity, the thinner the boundary layer.

Keep in mind, as a final note, that all of the foregoing is for a laminar boundary layer—although the second part of the conclusion, that boundary-layer thickness is proportional to some Reynolds number defined on the size of the body, is qualitatively true for a turbulent boundary layer as well.

You might be wondering how thick boundary layers really are. This is something you can think about the next time you are sitting in a window seat over the wing, several miles above the Earth. How thick is the boundary layer at a distance of, say, one meter from the leading edge of the wing, when the plane is traveling at 500 miles an hour? There is an exact solution for the thickness of a laminar boundary layer as a function of the Reynolds number Re_x based on free- stream velocity and distance from the leading edge:

$$\delta = 4.99\mathrm{Re}_x^{-1/2} \tag{3.6.2}$$

(The derivation of Equation 3.6.2 is a little beyond this course; see Tritton, 1988, p. 127–129 if you are interested in pursuing it further.) Assuming an air temperature of $-50^\circ\mathrm{C}$ and an altitude of $35,000$ feet, the density of the air is about $10^{-3}\mathrm{g/cm}^3$ and the viscosity is something like 1.5×10^{-4} poise. Substituting the various values into Equation 3.6.2, we find that the boundary-layer thickness is a few hundredths of a millimeter. The boundary layer on the roof of your car at $65\mathrm{mph}$ is much thicker, by about an order of magnitude, because the air speed is so much slower.

Some Flows are "All Boundary Layer"

An example of the boundary layer growing to fill the entire flow is an open-channel flow that has just emerged from a sluice-like outlet at the bottom of a large reservoir of water (Figure 3.6.5). Right at the inlet, the entire flow could be considered the “free stream”. As the flow passes down the channel, a boundary layer grows upward into the flow from the bottom. If the minor effect of friction with the atmosphere is neglected, no boundary layer develops at the upper surface of the flow. Eventually the growing boundary layer reaches the surface, and from that point downstream the river is all boundary layer!

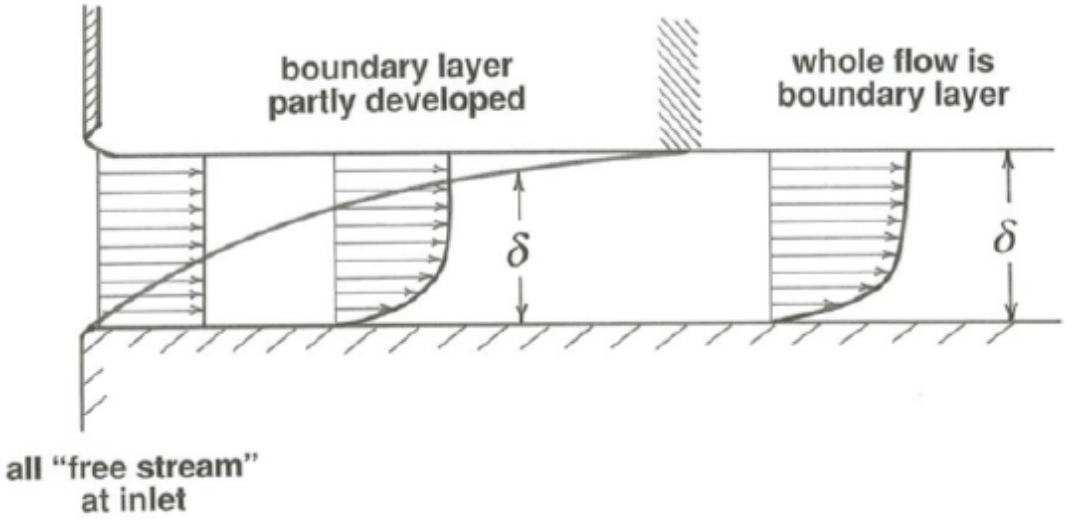


Figure 3.6.5: Downstream development of a boundary layer in an open-channel flow that begins at the outlet of a sluice gate.

In a situation like this, boundary-layer development is typically complete in a downchannel distance equal to something like a few tens of flow depths. Upstream, in the zone of boundary-layer growth, the boundary layer is nonuniform, in that it is different at each section; downstream, in the zone of fully established flow, the boundary layer is uniform, in that it looks the same at every cross section.

Internal Boundary Layers

Finally, there can be boundary layers within boundary layers. Such boundary layers are called **internal boundary layers**. Suppose that a thick boundary layer is developing on a broad surface in contact with a flow, or a boundary layer has already grown to the full lateral extent of the flow, as in a river. Any solid object of restricted size immersed in that boundary layer, located either on the boundary, like some kind of irregularity or protuberance, or within the flow, like part of a submarine structure, causes the local development of another boundary layer (Figure 3.6.6).

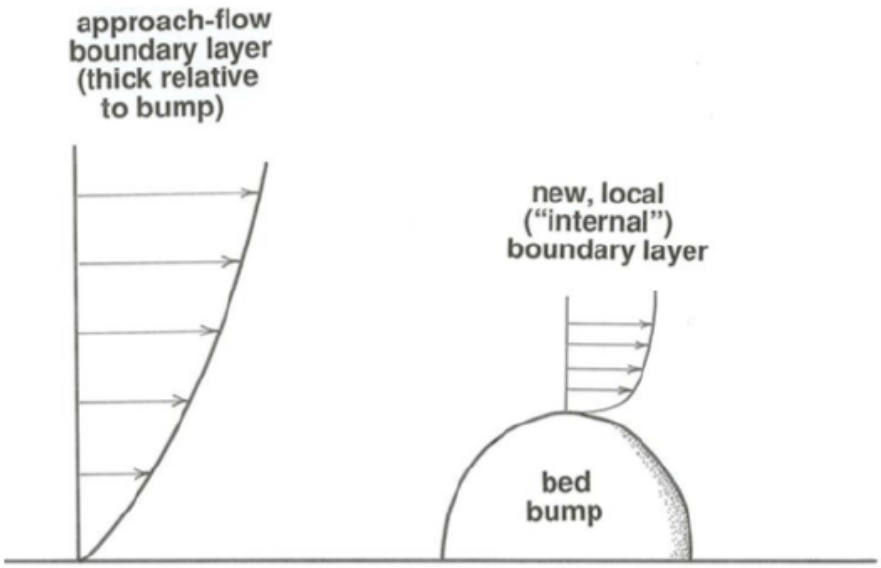


Figure 3.6.6: *Development of an internal boundary layer on a hemispherical roughness element on the bed of a channel flow.*

This page titled 3.6: Boundary Layers is shared under a CC BY-NC-SA 4.0 license and was authored, remixed, and/or curated by John Southard (MIT OpenCourseware) via source content that was edited to the style and standards of the LibreTexts platform.

3.7: Flow Separation

The overall pattern of flow at fairly high Reynolds numbers past blunt bodies or through sharply expanding channels or conduits is radically different from the pattern expected from inviscid theory, which I have said is often a good guide to the real flow patterns. Figure 3.7.1 shows two examples of such flow patterns, one for a sphere and one for a duct or pipe that has a downstream expansion at some point. Near the point where the solid boundary begins to diverge or fall away from the direction of the mean flow, the boundary layer separates or breaks away from the boundary. This phenomenon is called **flow separation**.

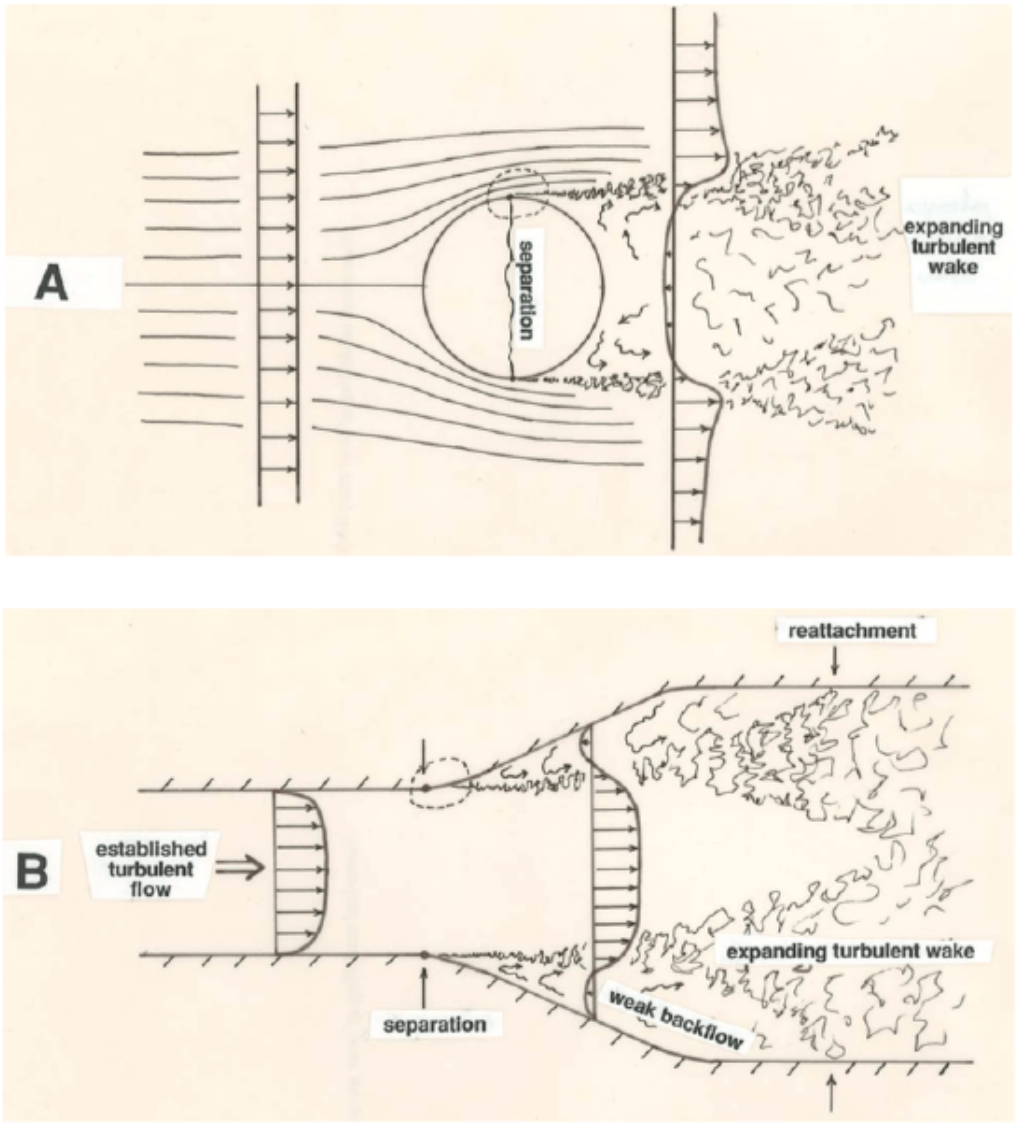


Figure 3.7.1: Two examples of flow separation: **A)** flow around a sphere; **B)** flow through an expansion in a planar duct.

In all cases the flow separates from the boundary in such a way that the fluid keeps moving straight ahead as the boundary surface falls away from the direction of flow just upstream. The main part of the flow, outside the boundary layer, diverges from the solid boundary correspondingly. If you look only at the regions enclosed by the dashed curves in Figure 3.7.1 you can appreciate that flow separation is dependent not so much on the overall flow geometry as on the change in the orientation of the boundary relative to the overall flow—a change that involves a curving away of the boundary from the overall flow direction. Separation takes place at or slightly downstream of the beginning of this curving away.

The region downstream of the separation point is occupied by stagnant fluid with about the same average velocity as the boundary itself. In this region the fluid has an unsteady eddying pattern of motion, with only a weak circulation as shown in Figure

3.7.1. As soon as the boundary layer leaves the solid boundary it is in contact with this slower-moving fluid across a surface of strong shear. This surface of shearing is unstable, and a short distance downstream of the separation point it becomes wavy and then breaks down to produce turbulence. This turbulence is then mixed or diffused both into the main flow and into the stagnant region, and it is eventually damped out by viscous shearing within eddies, but its effect extends for a great distance downstream. The stagnant region of fluid inside the separation surface, together with the region of strong turbulence developed on the separation surface, is called a **wake**. Far downstream from a blunt body like a sphere (Figure 3.7.1A) the wake turbulence is weak and the average fluid velocity along a profile across the mean flow is slightly less than the free-stream velocity. In flow past an expansion in a duct or channel (Figure 3.7.1B), the expanding zone of wake turbulence eventually impinges upon the boundary; downstream of this point, where the flow is said to *reattach* to the boundary, the flow near the boundary is once again in the downstream direction, and a new boundary layer develops until far downstream of the expansion the flow is once again fully established.

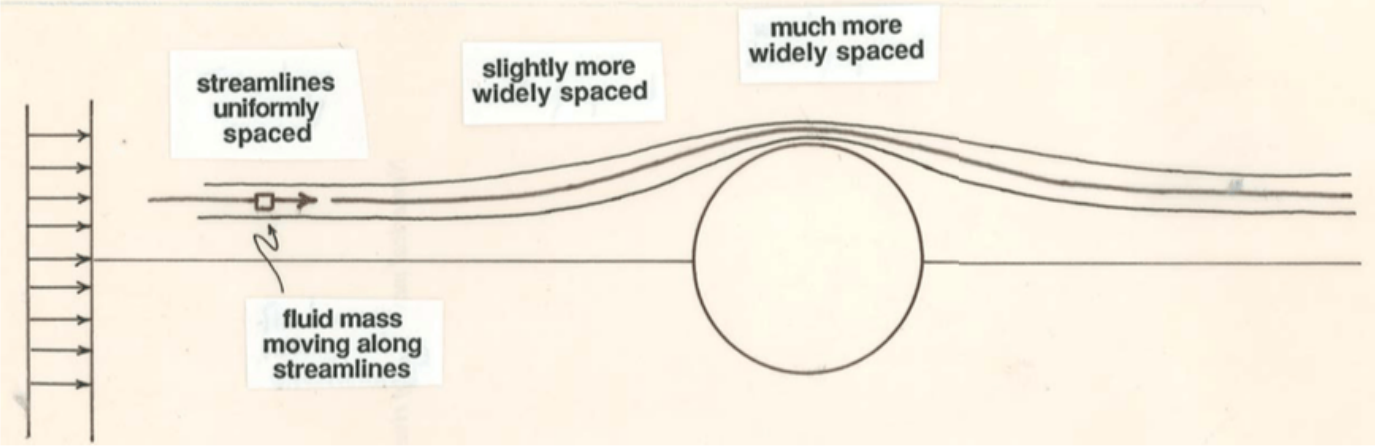


Figure 3.7.2: Pattern of streamlines in steady inviscid flow past a sphere.

You can understand why flow separation takes place by reference to steady inviscid flow around a sphere (Figure 3.7.2). Remember that variations in fluid velocity can be deduced qualitatively just from variations in spacing of neighboring streamlines. As a small mass of fluid approaches the sphere along a streamline that will take it close to the surface of the sphere, it decelerates slightly from its original uniform velocity and then accelerates to a maximum velocity at the midsection of the sphere (Figure 3.7.3A). Beyond the midsection it experiences precisely the reverse variation in velocity: it decelerates to minimum velocity and then accelerates slightly back to the free-stream velocity. We can apply the Bernoulli equation (Equation 3.4.7 or 3.4.8) to find the corresponding variation in fluid pressure (Figure 3.7.3B). The pressure is slightly greater than the free-stream value at points just upstream and just downstream of the sphere but shows a minimum at the midsection. It is this variation in pressure that causes strong accelerations and decelerations as the fluid passes around the sphere. In front of the sphere the pressure decreases along the streamline (the spatial rate of change or gradient of pressure is said to be negative or favorable), so there is a net force on the fluid mass in the direction of motion, causing an acceleration. In back of the sphere the pressure increases along the streamline (the pressure gradient is positive or adverse), so there is a net force opposing the motion, and the fluid mass decelerates.

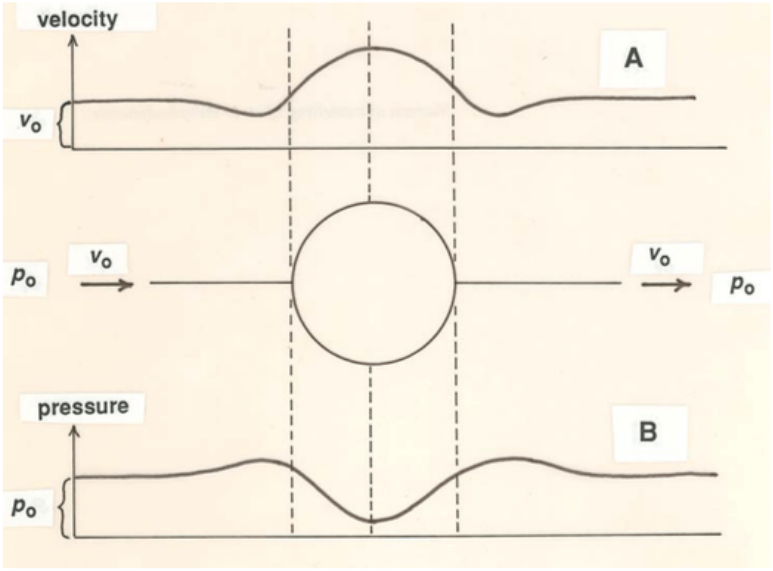


Figure 3.7.3: Variation in **A)** velocity and **B)** pressure along a streamline passing close to the surface of a sphere, for steady inviscid flow past the sphere (schematic).

In inviscid flow the pressure is the only force in the fluid. But in the real world of viscous fluids, a boundary layer develops next to the sphere (Figure 3.7.4). If the boundary layer is thin, the streamwise variation in fluid pressure given by the Bernoulli equation along streamlines just outside the boundary layer is approximately the same as the pressure on the boundary; the pressure outside the boundary layer is said to be *impressed* on the boundary. If now you follow the motion of a fluid mass along a streamline that is close enough to the sphere to become involved in the boundary layer, a viscous force as well as the impressed pressure force acts on the fluid mass. Because the viscous force everywhere opposes the motion, the fluid mass cannot ultimately regain its uniform velocity after passing the sphere, as in inviscid flow. The fluid cannot accelerate as much in front of the sphere as in the inviscid flow, and it reaches the midsection with lower velocity; then the adverse pressure gradient in back of the sphere, which is augmented by the viscous retardation, decelerates the fluid to zero velocity and causes it to start to move in reverse. This reverse flow forms a barrier to the continuing flow from the front of the sphere, and so the flow must break away from the boundary to pass over the obstructing fluid. Because velocities are small along streamlines close to the boundary, this deceleration to zero velocity occurs only a short distance downstream of the onset of the adverse pressure gradient where the boundary curves away from the mean flow direction.

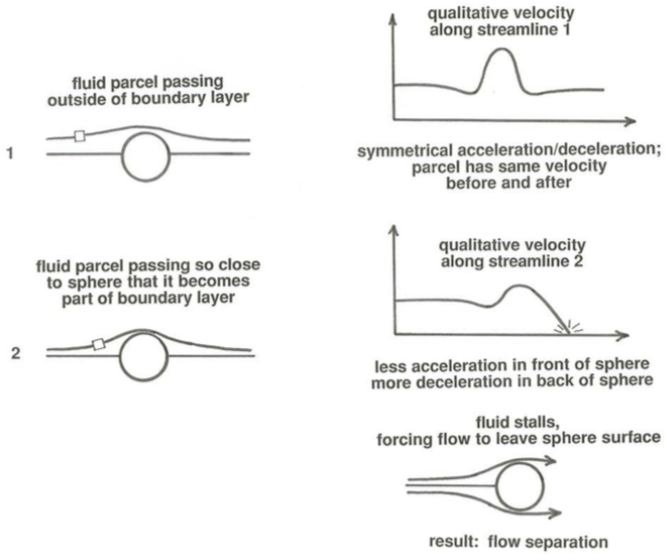


Figure 3.7.4: Flow processes leading to the onset of flow separation.

Once the separated flow is established, the flow pattern looks something like that shown in Figure 3.7.5. This figure is just a detail of the region enclosed by the dashed curves in Figure 3.7.1.

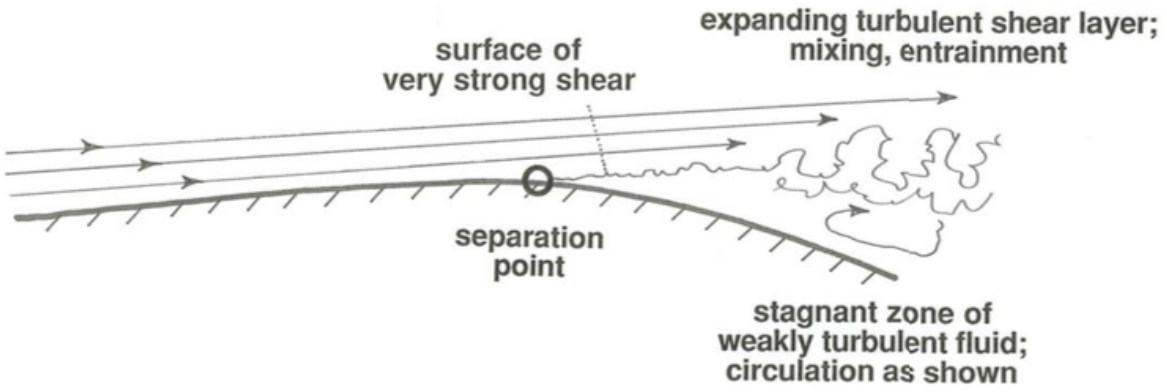


Figure 3.7.5: Close-up view of flow separation (schematic).

You might justifiably ask why this same explanation should not hold just as well for slow flow around a sphere at Reynolds numbers small enough to be in the Stokes range. A superficial answer would be that according to Stokes' law for slow viscous flow around a sphere the distributions of pressure and shear stress are such that the flow passes around the sphere without reversal. A more basic explanation, which is qualitatively true but may not be very helpful, is as follows. As noted earlier in this chapter, flow around a sphere at low velocities is characterized by fluid accelerations that are everywhere so small compared to fluid velocities that the viscous forces are everywhere closely balanced by pressure forces, so that there is no tendency for fluid to decelerate to a stall. At these low velocities, retardation by viscous shearing in the fluid caused by the presence of the solid boundary extends for a great distance away from the surface of the sphere. As the velocity around the sphere increases, this retarded fluid is to a progressively greater extent swept or advected back around the sphere, to be "replaced" by faster-moving fluid, thus concentrating the region of retardation into a relatively thin layer near the solid boundary. The pressure distribution in the fluid outside this thin boundary layer becomes more and more like that predicted by inviscid theory. Think in terms of a balance between spreading of retardation outward from the solid boundary, on the one hand, and delivery of faster-moving fluid from upstream, on the other hand. As the Reynolds number increases, the latter effect becomes more and more important relative to the former. Ultimately, flow separation develops for the reasons outlined above.

This page titled 3.7: Flow Separation is shared under a CC BY-NC-SA 4.0 license and was authored, remixed, and/or curated by John Southard (MIT OpenCourseware) via source content that was edited to the style and standards of the LibreTexts platform.

3.8: Flow Past a Sphere at High Reynolds Numbers

So far we have considered flow past a sphere only from the standpoint of dimensional analysis, in Chapter 2, to derive a relationship between drag coefficient and Reynolds number, and we have looked at flow patterns and fluid forces only at very low Reynolds numbers, in the Stokes range. You are now equipped to deal with flow past a sphere at higher Reynolds numbers.

As the Reynolds number increases, flow separation gradually develops, and this corresponds to a change from a regime of flow dominated by viscous effects, with viscous forces and pressure forces about equally important, to a regime of flow dominated by flow-separation effects, with pressure forces far larger than viscous forces. This gradual change in the flow regime is manifested in the change from the descending-straight-line branch of the curve for drag coefficient C_D as a function of Reynolds number (see Figure 2.3.1) to the approximately horizontal part of the curve at higher Reynolds numbers. Even before separation is fully developed, there are deviations of the observed drag coefficient from that predicted by Stokes' law (Figure $3.8.1$), but, after flow separation well established, the curve for C_D shows no relationship whatsoever to Stokes' law (Figure 2.3.1).

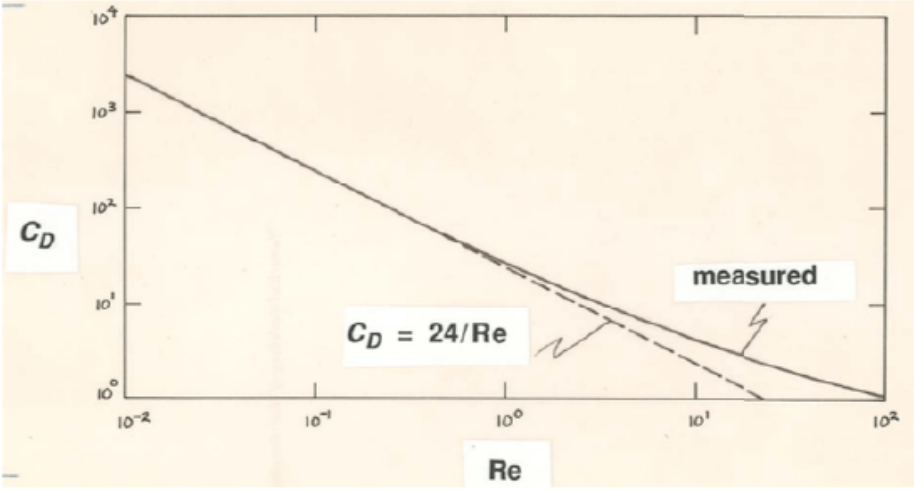


Figure $3.8.1$: Deviation of drag coefficient C_D from Stokes' law at Reynolds numbers between 1 and 100.

In this section we will examine in a qualitative way the gradual but fundamental ways the flow pattern around the sphere changes as the Reynolds number increases. These changes can be classified or subdivided into several stages, which could well be called flow regimes. **Flow regimes** are distinctive or characteristic patterns of flow, which are manifested in certain definite ranges of flow conditions and which are qualitatively different from other regimes that are manifested in neighboring ranges of flow conditions. The flow regimes associated with flow around a sphere are intergradational but distinctive. Keep in mind that they are characterized or described completely by the Reynolds number, and only by the Reynolds number: it is not just the size of the sphere, or the velocity of flow around it, or the kind of fluid; it is how all of these combine to give a particular value of the Reynolds number.

Figure $3.8.2$ shows a cartoon series of flow patterns with increasing Re, and the corresponding position on the drag-coefficient curve (Figure 2.3.1). Looking ahead to the following section on settling of spheres, these figures also give approximate values of the diameters of quartz spheres settling in water at the given Reynolds numbers, and the corresponding settling velocity, in centimeters per second.

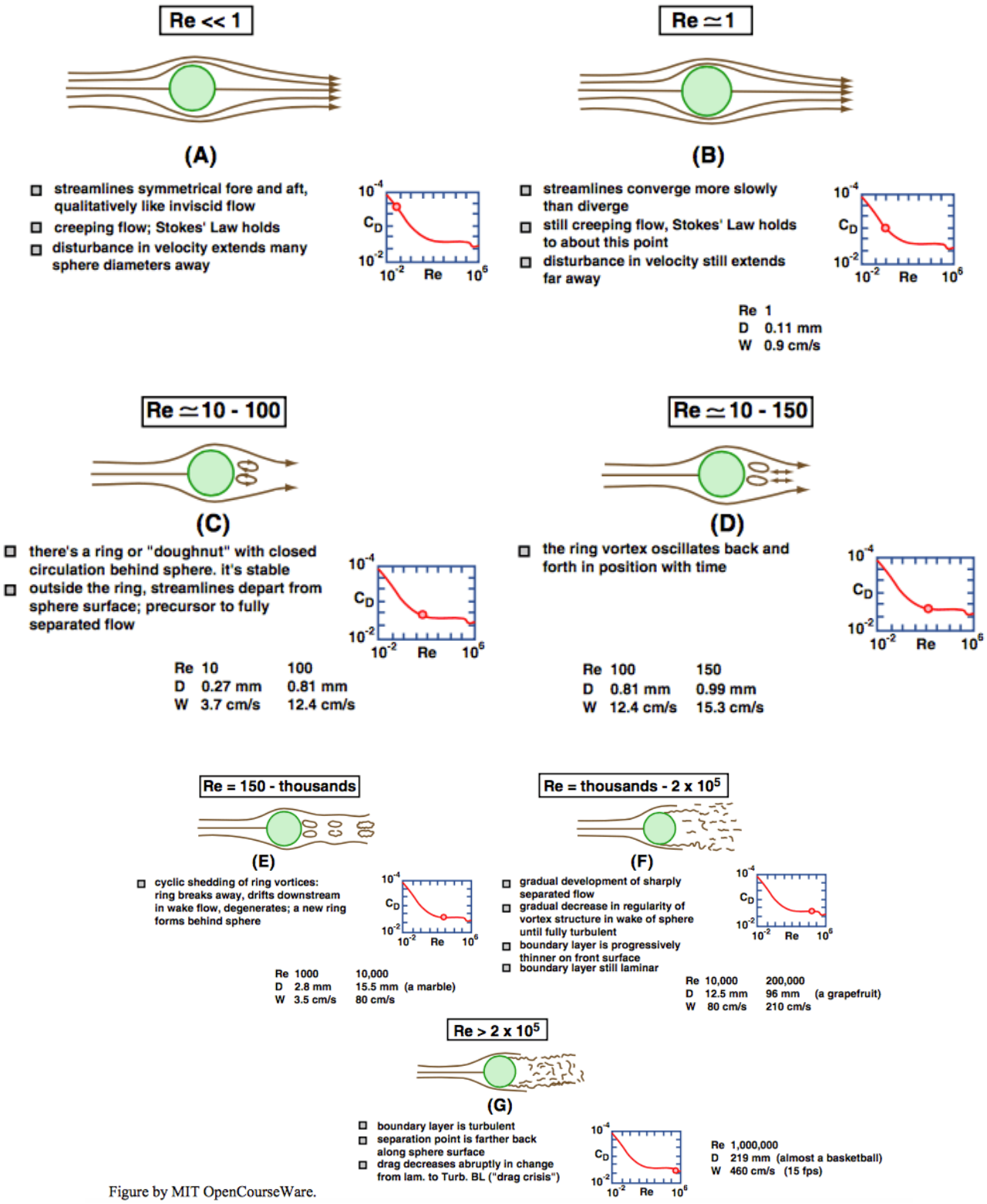


Figure by MIT OpenCourseWare.

Figure 2-2) is shown, as well as settling velocities and sizes of quartz spheres settling through room-temperature water at various values of Reynolds number.

Figure 3.8.2A shows the picture for creeping flow at $\mathrm{Re} << 1$, as already discussed. The streamlines show a symmetrical pattern front to back. Although not shown in the figure, the flow velocity increases only gradually away from the surface of the sphere; in other words, there is no well-defined boundary layer at these low Reynolds numbers.

In Figure 3.8.2B, for $\mathrm{Re} \approx 1$, the picture is about the same as at lower Re, but streamlines converge more slowly back of the sphere than they diverge in front of the sphere. Corresponding to this change in flow pattern, it is in about this range that the front-to-back pressure forces begin to increase more rapidly than predicted by Stokes' Law.

Flow separation can be said to begin at a Reynolds number of about 24. The point of separation is at first close to the rear of the sphere, and separation results in the formation of a ring eddy attached to the rear surface of the sphere. Flow within the eddy is at first quite regular and predictable (Figure 3.8.2C), thus not turbulent, but, as Re increases, the point of separation moves to the side of the sphere, and the ring eddy is drawn out in the downstream direction and begins to oscillate and become unstable (Figure 3.8.2D). At Re values of several hundred, the ring eddy is cyclically shed from behind the sphere to drift downstream and decay as another forms (Figure 3.8.2E). Also in this range of Re, turbulence begins to develop in the wake of the sphere. At first turbulence develops mainly in the thin zone of strong shearing produced by flow separation and then spreads out downstream, but as Re reaches values of a few thousand the entire wake is filled with a mass of turbulent eddies (Figure 3.8.2F).

In the range of Re from about 1000 to about $200,000$ (Figure 3.8.2F) the pattern of flow does not change much. The flow separates at a position about 80° from the front stagnation point, and there is a fully developed turbulent wake. The drag is due mainly to the pressure distribution on the surface of the sphere, with only a minor contribution from viscous shear stress. The pressure distribution is as shown in Figure 3.8.3 and does not vary much with Re in this range, so the drag coefficient remains almost constant at about 0.5.

At very high Re, above about $200,000$, the boundary layer finally becomes turbulent before separation takes place, and there is a sudden change in the flow pattern (Figure 3.8.2G). The distinction here is between **laminar separation**, in which the flow in the boundary layer is still laminar where separation takes place, and **turbulent separation**, in which the boundary layer has already changed from being laminar to being turbulent at some point upstream of separation. Turbulent separation takes place farther around toward the rear of the sphere, at a position about 120–130° from the front stagnation point. The wake becomes contracted compared to its size when the separation is laminar, and consequently the very low pressure exerted on the surface of the sphere within the separation region acts over a smaller area. Also, the pressure itself in this region is not as low (Figure 3.8.3). The combined result of these two effects is a sudden drop in the drag coefficient C_D, to a minimum of about 0.1. This is sometimes called the **drag crisis**.

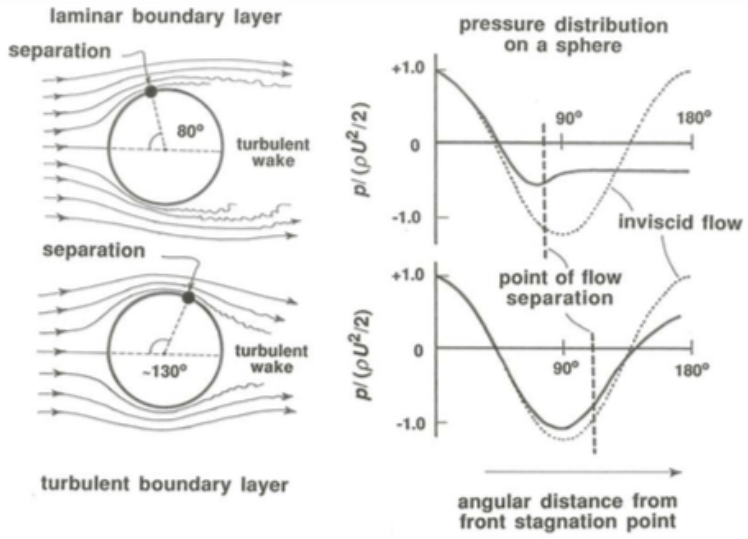


Figure 3.8.3: Flow patterns and pressure distributions around a sphere at high Reynolds numbers. A) Experimental results for a laminar boundary layer; B) results for a turbulent boundary layer. In each case, the theoretical pressure distribution for inviscid flow is shown for comparison. The pressure is scaled by the stagnation pressure, $\rho U^2/2$.

Have you ever wondered why golf balls have that pattern of dimples on them? It is to make them go faster and farther, but why? It is because the Reynolds number of the flying golf ball is just about in the range of transition from a laminar boundary layer to a turbulent boundary layer, and the dimples help to trigger the transition and thus reduce the air drag on the flying ball.

This page titled 3.8: Flow Past a Sphere at High Reynolds Numbers is shared under a CC BY-NC-SA 4.0 license and was authored, remixed, and/or curated by John Southard (MIT OpenCourseware) via source content that was edited to the style and standards of the LibreTexts platform.

3.9: Settling of Spheres

Introduction

This section deals with some basic ideas about settling of solid spheres under their own weight through still fluids. This is an important topic in meteorology (hailstones), sedimentology (sediment grains), and technology (cannon balls and spacecraft). In this section we will look at the terminal settling velocity of spheres as an applied problem. At the end I will make some comments about the complicated matter of the time and distance it takes for a sphere to attain its terminal settling velocity.

If placed in suspension in a viscous fluid, a solid body denser than the fluid settles downward and a solid body less dense than the fluid rises upward. A qualification is needed here, however: the body must not be so small that its submerged weight is even smaller than the random forces exerted on it by bombardment by the fluid molecules in thermal motion. Such small weights are generally associated only with the finest particles, in the colloidal size range of small fractions of a micron.

When a nonneutrally buoyant body is released from rest in a still fluid, it accelerates in response to the force of gravity. As the velocity of the body increases, the oppositely directed drag force exerted by the fluid grows until it eventually equals the submerged weight of the body, whereupon the body no longer accelerates but falls (or rises) at its **terminal velocity**, also called the **fall velocity** or **settling velocity** in the case of settling bodies (Figure $3.9.1$).

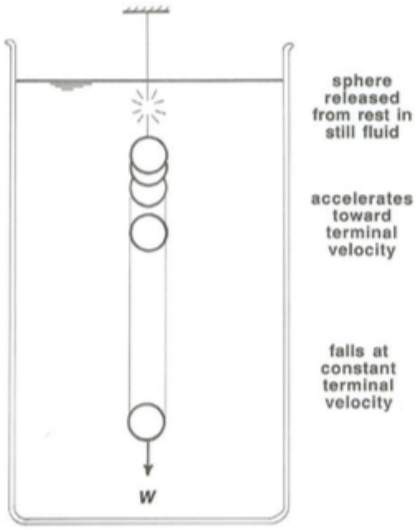


Figure $3.9.1$: Attainment of terminal fall velocity when a sphere is dropped from rest in a vessel of still liquid.

Towing vs. Settling

I promised you in Chapter 2 that I would make some comments later about the differences between moving a sphere through still fluid and passing a moving fluid by a stationary sphere. This topic has relevance to the settling of spheres, so I will say some things about it at this point.

It should make sense to you that towing a sphere at velocity U through a still fluid by exerting a constant force F_D on it is equivalent to passing a steady and uniform stream of fluid at velocity U around a sphere that is held fixed relative to the boundaries of the flow. This is largely true, but there are two complications. First, if the sphere is held fixed and the flow passes by it, the drag force can be influenced by even weak turbulence in the approaching flow, whereas if the sphere is towed through still fluid there can be no such effect. Second, you have seen that, in some ranges of relative velocity, eddies can form behind the sphere and break away irregularly; if the sphere is fixed and the fluid is flowing by, this causes the force to fluctuate about some average value but does not affect the relative velocity, whereas if the sphere is towed, either the velocity fluctuates along with the force or, if by definition we tow with a constant force, the velocity fluctuates but the force is steady.

Settling of a sphere through still fluid under its own weight is exactly like towing the sphere vertically downward by applying a constant towing force, namely the weight of the sphere, which is simply the Earth's gravitational attractive force on the sphere. The weight of the sphere is constant and entirely independent of the state of motion, and the sphere responds by settling downward at some velocity through the fluid. (As noted above, this velocity may fluctuate slightly with time.) For spheres the differences between the fixed-sphere case and the settling-sphere case are usually assumed to be minor. Indeed, some of the data in Figure 2.3.1 for dimensionless drag force as a function of Reynolds number are from settling experiments and some are from wind-tunnel experiments with fixed spheres, and it can be seen that there is very little scatter of the combined experimental curve.

Dimensional Analysis

To obtain an experimental curve for settling velocity we can simply transform the curve in Figure 2.3.1 for drag coefficient vs. Reynolds number for towed spheres into a curve based on settling velocity. In fact, much of this curve, especially for low Reynolds numbers, was obtained by settling experiments in the first place, with the experimental results recast into the form of drag coefficients.

When a sphere falls at terminal velocity the drag force F_D is equal to the submerged weight of the particle, $(1/6)\pi D^3\gamma'$, where γ' is the submerged weight per unit volume of the particle, equal to $g(\rho_s - \rho)$. Substituting this for F_D in the definition of the drag coefficient C_D in Equation 2.3.2, using settling velocity w in place of U, and then solving for C_D,

$$C_D = \frac{4}{3}\frac{\gamma' D}{\rho w^2} \tag{3.9.1}$$

This expression for C_D, which can be viewed as the "settling drag coefficient", can be used in the relationship for dimensionless drag force as a function of Reynolds number (Equation 2.3.2) for spheres moving through a viscous fluid:

$$\frac{\gamma' D}{\rho w^2} = f\left(\frac{\rho w D}{\mu}\right) \tag{3.9.2}$$

where the factor $4/3$ has been absorbed into the function, just for convenience. Figure $3.9.2$, which is the same as Figure 2.3.1 with axes relabeled and adjusted in scale to take account of the factor $4/3$, is the corresponding graph of this function. No data points are shown, because the curve is exactly the same as in Figure 2.3.2. Figure $3.9.2$ gives settling velocity was an implicit function of ρ, U, D, and γ'.

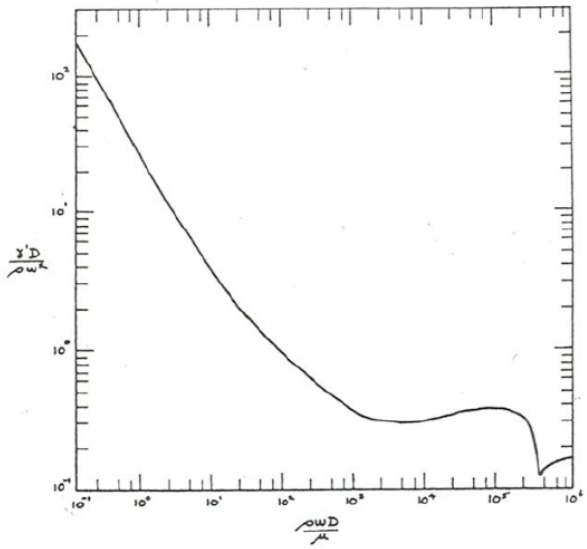


Figure $3.9.2$: "Settling drag coefficient" $\gamma' D/\rho w^2$ vs. Reynolds number $\rho w D/\mu$ based on settling velocity.

The curve in Figure $3.9.2$ is still not very convenient for finding the settling velocity when the other variables are given. This is because both w and D appear in the dimensionless variables along both axes. Finding w in an actual problem would necessitate laborious trial-and-error computation. To get around this problem the graph can be further recast into a more convenient form in which w appears in only one of the two dimensionless variables. Also, because usually what is desired is w as a function of D, or

vice versa, it is convenient to arrange for D to appear only in the other variable.

Recall from Chapter 2 that if you have a set of dimensionless variables for a problem you can multiply or divide any one of them by any others in the set to get a new variable to replace the old one. To get a dimensionless variable with w but not D, invert the left-hand variable in Equation 3.9.2 and multiply the result by the right-hand variable:

$$\left(\frac{\rho w^2}{\gamma' D}\right)\left(\frac{\rho w D}{\mu}\right) = \frac{\rho^2 w^3}{\gamma' \mu} \tag{3.9.3}$$

And to get a dimensionless variable with D but not w, square the right-hand variable in Equation 3.9.2 and multiply it by the left-hand variable:

$$\left(\frac{\rho w D}{\mu}\right)^2\left(\frac{\gamma' D}{\rho w^2}\right) = \frac{\rho \gamma' D^3}{\mu^2} \tag{3.9.4}$$

It is convenient, but not necessary, to take these two variables to the one-third power, so that w and D appear to the first power; $w\left(\rho^2/\gamma'\mu\right)^{1/3}$ can be viewed as a dimensionless settling velocity, and $D\left(\rho\gamma'/\mu^2\right)^{1/3}$ as a dimensionless sphere diameter. Because these two new variables are equivalent to C_D and Re, the functional relationship for C_D vs. Re can just as well be written

$$\left(\frac{\rho^2}{\gamma'\mu}\right)^{1/3} w = f\left(\frac{\rho\gamma'}{\mu^2}\right)^{1/3} D \tag{3.9.5}$$

The usefulness of Equation 3.9.5 is that the settling velocity appears only on the left side and the sphere diameter appears only on the right side.

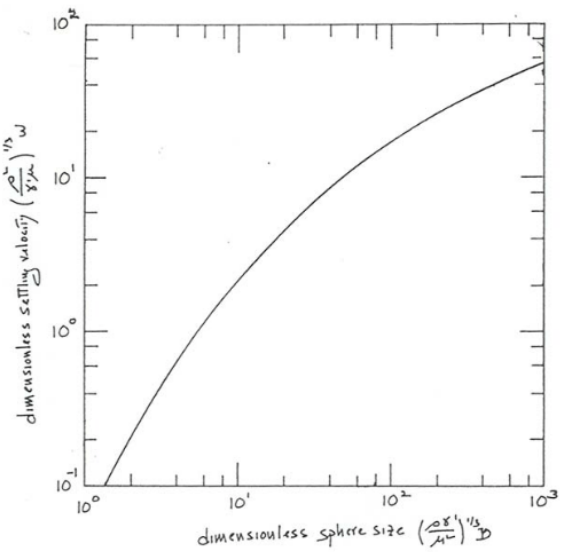


Figure 3.9.3: Dimensionless settling velocity vs. dimensionless sphere size for settling of a sphere in a vessel of still liquid.

It is now a simple matter to find w for a given fluid, sphere size, and submerged specific weight by use of Figure 3.9.3, which is a plot of dimensionless setting velocity vs. dimensionless sphere diameter. This curve is obtained directly from that in Figure 3.9.2; you can imagine taking the original data points and forming the new dimensionless variables rather than the old ones to plot the curve in the new coordinate axes of Figure 3.9.3. This emphasizes that these two curves are equivalent because they are based on the same set of experimental data.

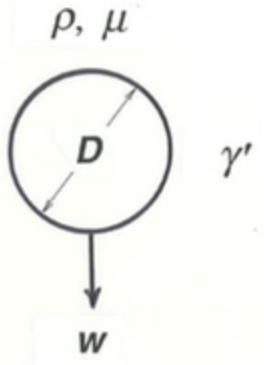


Figure 3.9.4: Definition sketch for dimensional analysis of a sphere settling through a still fluid.

If you are unsatisfied by the roundabout way of arriving at the functional relationship expressed in Equation 3.9.3, you might consider making a fresh start on dimensional analysis of the problem of settling of a sphere through a still fluid at terminal velocity (Figure 3.9.4). Settling velocity w, the dependent variable, must depend on fluid density ρ, fluid viscosity μ, sphere diameter D, and submerged weight per unit volume γ' of the sphere. Each of these must be included for the reasons given in Chapter 2. As before, acceleration of gravity and sphere density do not have to appear separately in the list of variables because they are important only by virtue of their combined effect on γ'. The five variables w, ρ, μ, D, and γ' should then combine into two dimensionless variables. You can conveniently arrange for one to contain w but not D and the other to contain D but not w by using the other three variables as the "repeating" variables. You might verify for yourself that this procedure leads to the two dimensionless variables in Equation 3.9.5.

Settling at Low Reynolds Numbers

Remember from Chapter 3 that if the Reynolds number based on sphere diameter and relative flow velocity is less than about one, the drag force on the sphere is given exactly by Stokes' Law, $F_D = 3\pi\mu UD$. This holds in particular for spheres settling under their own weight. Using Stokes' Law it is easy to develop a useful formula for the settling velocity of spheres that is valid in the Stokes range ($\mathrm{Re} < 1$). Write an equation that balances the submerged weight of the sphere, $(\pi D^3/6)\,\gamma'$, by the drag force, given by Stokes' Law, $3\pi D\mu w$, where I have used the settling velocity w as the relative velocity of the fluid and the sphere. Solving for w,

$$w = \frac{1}{18}\frac{\gamma' D^2}{\mu} \tag{3.9.6}$$

This equation is widely cited and widely used in books and papers on settling of spheres and other bodies, like sediment particles, that have the approximate shape of a sphere, but keep firmly in mind that it applies *only* in the Stokes range of settling Reynolds numbers $\rho w D/\mu$.

The Effect of Turbulence on Particle Settling

One clear effect of turbulence on particle setting is the possibility of dispersion. Think about arranging an experiment in which a batch or continuing supply of sediment particles is introduced at the free surface of a channel flow. If the flow is laminar, the particles (if they are identical in size, shape, and density) are identical also in their settling behavior as well, and they all land on the bottom boundary of the flow at the same point,. If the flow is turbulent, however, the settling particles land on the bottom over a wide streamwise range of points, the obvious reason being that each particles traverses (or, perhaps more accurately, finds itself within the domain of) a different set of eddies during its descent, and so it experiences a different set of local fluid velocities. Both the vertical and the horizontal components of fluid velocities within eddies act to spread out, or disperse, the particle trajectories around the overall average trajectory.

It might seem intuitively reasonable to you to assume that the average settling time of the particles in the turbulent flow is the same as the single, well- defined settling time in the laminar flow, because the particles in the turbulent flow are, when viewed on the scale of the particles themselves, just settling through surrounding fluid that is the same as in the laminar case, and the "ups" should balance out the "downs", on average. That cannot be quite true, however, if only for the reason that the drag coefficient of a sphere moving through a fluid is non-negligibly affected by accelerations and decelerations of the fluid that is moving relative

to the particle, and that is exactly what is happening when the particle is in a turbulent flow field.

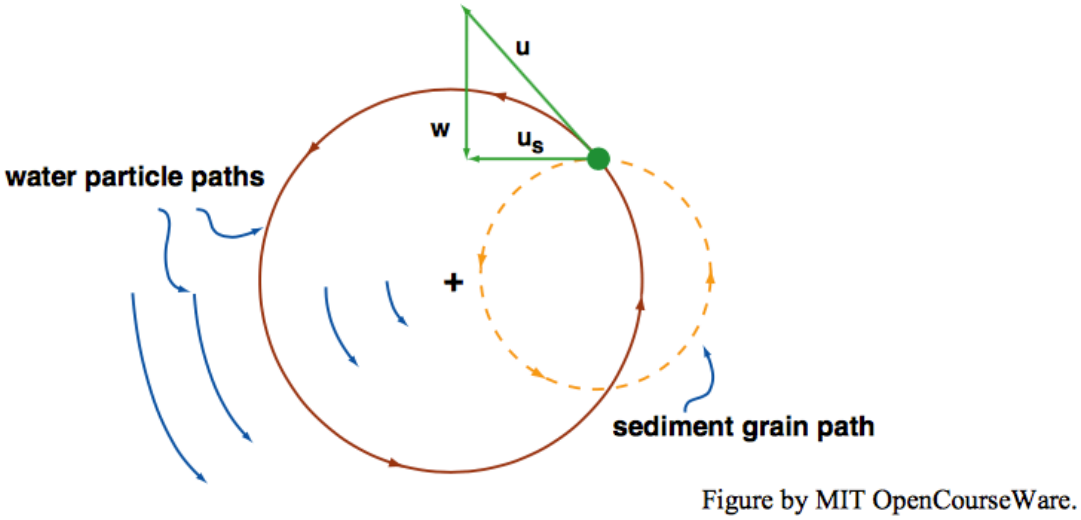


Figure from G.V. Middleton.)

But there is another effect, and one that cannot be ignored, that almost certainly lies outside of your intuition: under certain conditions, a settling particle that finds itself within a rotating eddy tends to become trapped within that eddy! This effect has been studied by Tooby et al. (1977) and Nielsen (1984). In an ideal vortex, rotating about a horizontal axis, a particle within the rising limb describes a circular orbit, which ideally would be closed and would not exhibit any net downward motion (Figure $3.9.5$). In Figure $3.9.5$, the tangential velocity of the fluid, u, is proportional to the distance from the center of the vortex.
Simple vector addition of u and w, the settling velocity of the particle, products a circular trajectory of the sediment particle, with no net settling. In the experiment by Tooby et al. (1977), particles tended to spiral slowly outwards, so that they would ultimately diffuse out of the vortex, but sufficiently fine sediment would be trapped in vortices and would move with the vortex until it dissipated. The mechanism is not very sensitive to the size of the trapped particles, and it should tend to produce less vertical segregation by size than the classical diffusional theory predicts.

References Cited

Lin, C.C., 1955, The Theory of Hydrodynamic Instability: Cambridge, U.K., Cambridge University Press, 155 p.

Nielsen, P., 1984, On the motion of suspended sand particles: Journal of Geophysical Research, v. 89, p. 616-626.

Reynolds, O., 1883, An experimental investigation of the circumstances which determine whether the motion of water shall be direct or sinuous, and the law of resistance in parallel channels: Royal Society [London], Philosophical Transactions, v. 174, p. 935-982.

Schubauer, G.B., and Skramstad, H.K., 1947, Laminar boundary-layer oscillations and stability of laminar flow: Journal of Aeronautical Science, 14 (2), p. 69-78.

Stokes, G.G., 1851, On the effect of the internal friction of fluids on the motion of pendulums: Cambridge Philosophical Society, Transactions, v. 9, no. 8, p. 287.

Tooby, P.F., Wick, G.L., and Isaacs, J.D., 1977, The motion of a small sphere in a rotating velocity field: a possible mechanism for suspending particles in turbulence: Journal of Geophysical Research, v. 82, p. 2096-2100.

Tritton, D.J., 1988, Physical Fluid Dynamics, 2nd Edition: Oxford, U.K., Oxford University Press, 519 p.

This page titled 3.9: Settling of Spheres is shared under a CC BY-NC-SA 4.0 license and was authored, remixed, and/or curated by John Southard (MIT OpenCourseware) via source content that was edited to the style and standards of the LibreTexts platform.

4: FLOW IN CHANNELS

This chapter focuses on two of the most important aspects of channel flow: *boundary resistance to flow*, and the *velocity structure of the flow*. The discussion is built around two reference cases: steady uniform flow in a circular pipe, and steady uniform flow down an inclined plane. Flow in a circular pipe is clearly of great practical and engineering importance, and it is given lots of space in fluid-dynamics textbooks. Flow down a plane is more relevant to natural Earth-surface settings (sheet floods come to mind), and it serves as a good reference for river flows.

4.1: Introduction to Flow in Channels

4.2: Laminar Flow Down an Inclined Plane

4.3: Turbulent Flow in Channels - Initial Material

4.4: Turbulent Shear Stress

4.5: Structure of Turbulent Boundary Layers

4.6: Flow Resistance

4.7: Velocity Profiles

4.8: More on the Structure of Turbulent Boundary Layers- Coherent Structures in Turbulent Shear Flow

This page titled 4: Flow in Channels is shared under a CC BY-NC-SA 4.0 license and was authored, remixed, and/or curated by John Southard (MIT OpenCourseware) via source content that was edited to the style and standards of the LibreTexts platform.

4.1: Introduction to Flow in Channels

Flows in conduits or channels are of interest in science, engineering, and everyday life. Flows in closed conduits or channels, like pipes or air ducts, are entirely in contact with rigid boundaries. Most closed conduits in engineering applications are either circular or rectangular in cross section. **Open-channel flows**, on the other hand, are those whose boundaries are not entirely a solid and rigid material; the other part of the boundary of such flows may be another fluid, or nothing at all. Important open-channel flows are rivers, tidal currents, irrigation canals, or sheets of water running across the ground surface after a rain.

In both closed conduits and open channels, the shape and area of the cross section of the flow can change along the stream; such flows are said to be **nonuniform**. Flows are those that do not change in geometry or flow characteristics from cross section to cross section are said to be **uniform**. Remember that flows can be either **steady** (not changing with time) or **unsteady** (changing with time). In this chapter we will look at laminar and turbulent flows in conduits and channels. The emphasis in this chapter is on steady uniform flow in straight channels. That's a simplification of flows in the natural world, in rivers and in the ocean, but it will reveal many fundamental aspects of those more complicated flows. The material in this chapter is applicable to a much broader class of flows, in pipes and conduits, as well; such matters are covered in standard textbooks on fluid dynamics.

This chapter focuses on two of the most important aspects of channel flow: *boundary resistance to flow*, and the *velocity structure of the flow*. The discussion is built around two reference cases: steady uniform flow in a circular pipe, and steady uniform flow down an inclined plane. Flow in a circular pipe is clearly of great practical and engineering importance, and it is given lots of space in fluid-dynamics textbooks. Flow down a plane is more relevant to natural Earth-surface settings (sheet floods come to mind), and it serves as a good reference for river flows.

The first section looks at laminar flow in a planar open channel, to derive expressions for the distributions of shear stress and velocity across the cross section. There are two equivalent ways of doing that: specializing the Navier–Stokes equations (which, remember, are a general statement of Newton's second law as applied to fluid flows) to the given kind of flow, or writing Newton's second law directly for the given kind of flow. We will take the second approach here. Then in further sections we will tackle the much more difficult problem of resistance and velocity in turbulent flows in pipes and channels. That will necessitate a deeper examination of the nature of shear stresses in turbulent flow, and a careful consideration of the differences between what I will call smooth flow and rough flow. The outcome will be some widely useful techniques as well as greatly increased understanding. The section on velocity distributions is intricate and lengthy, and may not seem as directly useful, but it reveals some really fundamental concepts.

This page titled 4.1: Introduction to Flow in Channels is shared under a CC BY-NC-SA 4.0 license and was authored, remixed, and/or curated by John Southard (MIT OpenCourseware) via source content that was edited to the style and standards of the LibreTexts platform.

4.2: Laminar Flow Down an Inclined Plane

In this section we apply Newton's second law to steady and uniform flow down an inclined plane. The strategy is to look at a block of the flow, bounded by imaginary planes normal to the bottom, with unit cross-stream width and unit streamwise distance (Figure $4.2.1$). In fluid dynamics, such a block of fluid is said to be a "free body". Because the flow is assumed to be steady and uniform, all of the forces in the streamwise direction that are exerted upon the fluid within the free body at any given time must add up to be to zero.

I should mention at the outset that for now I will not address how the flow is arranged so that the flow is uniform. If you just pour a sheet of water onto the plane along some particular horizontal line on the plane, you should not expect that uniform flow will automatically be established downslope of that line in the sense that the flow depth is the same at all normal-to-flow sections farther down the plane, and in general it is not: you would need to adjust the slope of the plane to attain a state of uniformity. This is not a trivial problem, and it should await some more detailed material, later in this chapter, on flow resistance. On the other hand, it should make intuitive sense to you that if the plane is very long the degree of nonuniformity would be very small whatever the slope: just imagine pouring water from a row of little faucets onto a plane a mile long and sloping a few degrees.

Obviously only liquids, not gases, can flow as open-channel flows. The freely deformable upper surface of the liquid, called the **free surface**, is open to the air. We will neglect the minor forces exerted by the overlying air on the moving liquid. Our idealized channel flow is of infinite width, with no side boundaries, and it is therefore just a convenient abstraction. But a flow in a channel of rectangular cross section with the width of flow much greater than the depth of flow is a good approximation to a flow with infinite width.

Take the x direction to be downstream and the y direction to be normal to the boundary, with $y = 0$ at the bottom of the flow (Figure 4-1). By the no-slip condition, the velocity is zero at $y = 0$, so the velocity must increase upward in the flow. It is also clear that the flow is everywhere directed straight down the plane. Think about the forces acting on the fluid contained at a given instant in the free body within the rectangular volume formed by the free surface, the bottom boundary, and two pairs of imaginary planes normal to the bottom and with unit spacing, one pair parallel to the flow and spaced a distance B apart, and the other normal to the flow and spaced a distance L apart (Figure $4.2.1$).

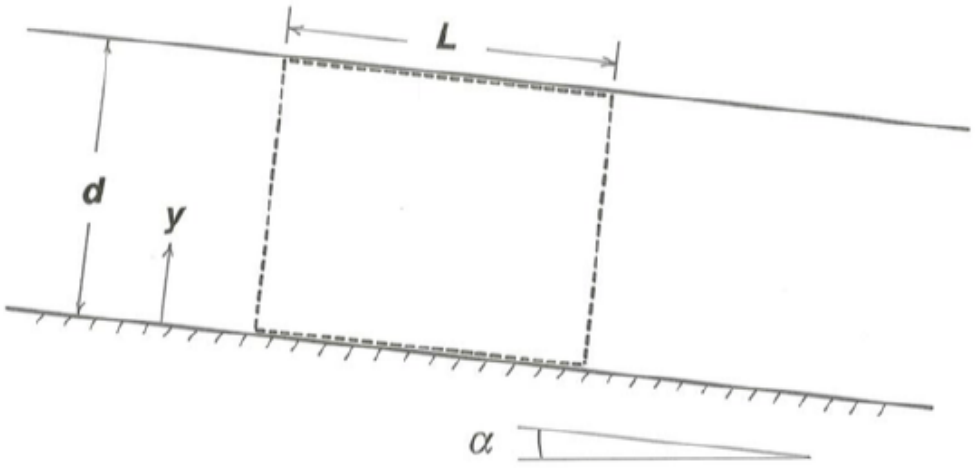


Figure $4.2.1$: Definition sketch for deriving the boundary shear stress in steady uniform flow down an inclined plane.

Writing Newton's second law for the balance of forces on this free body means equating the downslope driving force, caused by the downslope component of the weight of the fluid in the free body, with the resistance force exerted by the planar boundary on the lower surface of the free body. The weight of the fluid in the free body is γBLd, where d is the depth of flow. The downslope component of this weight is $\gamma \sin \alpha BLd$, where α is the slope angle of the plane (Figure $4.2.2$).

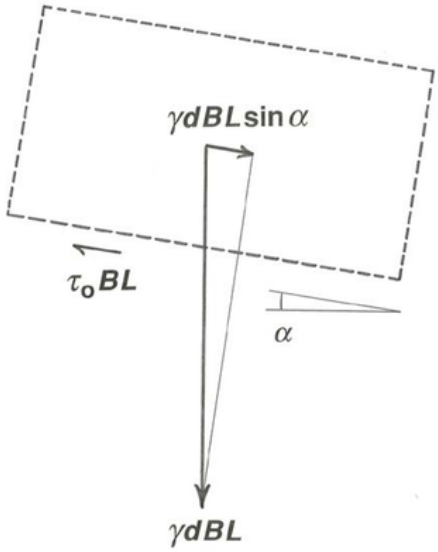


Figure 4.2.2: *Forces on a free body of fluid in steady uniform flow down an inclined plane.*

This is balanced by the frictional force $\tau_o BL$ exerted by the bottom boundary. There are also pressure forces acting parallel to the flow direction on the upstream and downstream faces of the free body, but because by our assumption of uniformity the vertical distribution of these pressure forces is the same at every cross section, they balance each other out and cause no net force on the free body. Setting $\gamma \sin \alpha BLd$ equal to $\tau_o BL$ and solving for τ_o,

$$\tau_o = \gamma d \sin \alpha \tag{4.2.1}$$

so the boundary shear stress is directly proportional to the product of the flow depth, the specific weight of the liquid, and the sine of the slope angle.

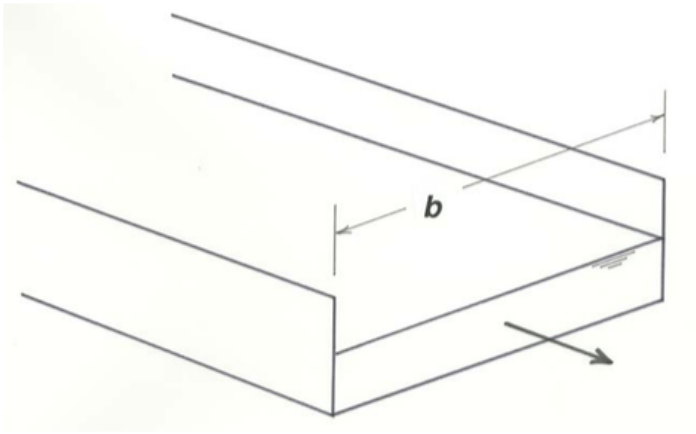


Figure 4.2.3: Sketch of a rectangular open channel of width b*, to aid in the definition of the hydraulic radius.*

Before we continue with the development, we will make the resistance equation more relevant to the real world by writing a similar equation for a channel with rectangular cross section and then for a channel with arbitrary (but unvarying) cross section. To generalize Equation 4.2.1 to a rectangular channel, take the flow width to be b (Figure 4.2.3) and write the force balance for a free body that fills the channel, from wall to wall, in a segment of length L along the flow. Doing the same mathematics as above gives the result

$$\tau_o = \gamma \sin \alpha \frac{bd}{2d + b} \tag{4.2.2}$$

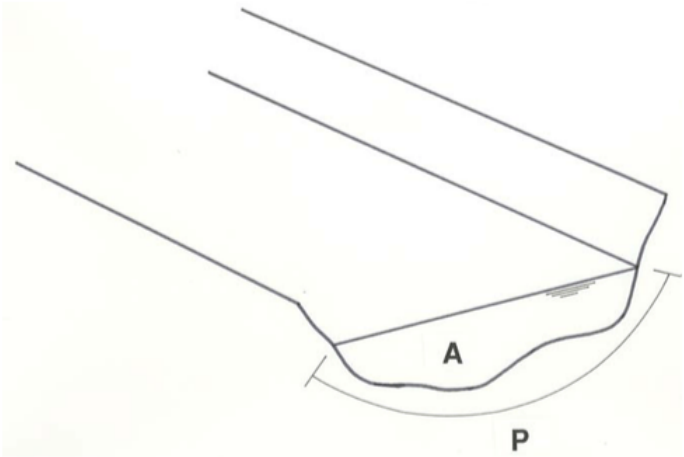


Figure 4.2.4: The wetted perimeter of a straight open channel flow.

To generalize Equation 4.2.1 to a channel of arbitrary cross-section shape, assume that the area of the cross section is A and the wetted perimeter (the distance along the submerged part of the boundary from waterline to waterline) is P (Figure 4.2.4). The same balance of forces gives

$$\tau_o = \gamma \sin \alpha \frac{A}{P} \tag{4.2.3}$$

Equations 4.2.1, 4.2.2, and 4.2.3 look rather different, but they can easily be unified by defining a quantity called the **hydraulic radius** R_H formed by dividing the cross-sectional area of the flow by the wetted perimeter. You can verify for yourself that the hydraulic radius of flow in a rectangular channel is $bd/(2d + b)$. It is a little more difficult to see that the hydraulic radius of an infinitely wide channel flow is just the flow depth d. You can reason that as the width b increases relative to the depth d, the term $2d$ in the denominator $2d + b$ becomes a smaller and smaller part of the denominator, so the hydraulic radius $bd/(2d + b)$ tends toward bd/b, or just d, as the width increases relative to the depth. The right-hand sides of all three equations, 4.2.1, 4.2.2, and 4.2.3 , become $\gamma \sin \alpha R_H$.

Equation 4.2.3, or its special cases Equation 4.2.1 or Equation 4.2.2, is the basic resistance equation for steady uniform flow in an open channel. Not many useful results in fluid mechanics are so easily derived! It is the principal way that the boundary shear stress is found in rivers (although to use it that way you need to do some surveying to establish the elevation of the water surface at two points along the channel, at least hundreds if not thousands of meters apart). Sometimes the three equations are written in terms of the slope, $\tan \alpha$, rather than the sine of the slope angle, $\sin \alpha$, because for very small α (the usual case), the approximation $\sin \alpha \approx \tan \alpha$ is a good one.

Now back to the infinitely wide flow down a plane: now that you know how to find the boundary shear stress, what can be said about how the shear stress and flow velocity within the flow vary with height above the bottom? One thing you already know for sure: by the no-slip condition, *the velocity at the very bottom must be zero*. Another thing you can say without further derivation is that *the velocity must be at its maximum at the free surface*. Why? Because the downslope driving force of gravity is a “body force” that acts throughout the flow, whereas resisting friction force acts only at the bottom. The flow velocity must therefore increase monotonically upward in the flow.

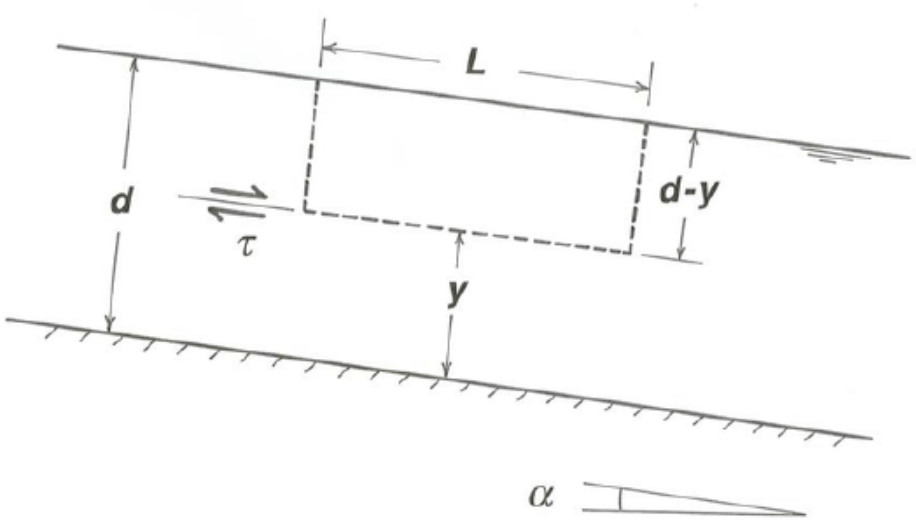


Figure 4.2.5: Definition sketch for deriving the distribution of shear stress in steady uniform laminar open-channel flow.

We can find the shear stress and velocity at all points up in the flow by applying the same force-balancing procedure to a free body of fluid similar to that used above but with its lower face formed by an imaginary plane a variable distance y above the bottom and parallel to it (Figure 4.2.5). The shear stress τ across the plane is given directly by the force balance:

$$\tau = \gamma \sin \alpha (d - y) \tag{4.2.4}$$

Using Equation 4.2.1 to eliminate $\gamma \sin \alpha$ from Equation 4.2.4, we can write τ in terms of the boundary shear stress τ_o:

$$\tau = \tau_o \left(1 - \frac{y}{d}\right) \tag{4.2.5}$$

Equation 4.2.5 shows that τ varies linearly from a maximum of $\gamma \sin \alpha$ at the bottom to zero at the surface (Figure 4-6).

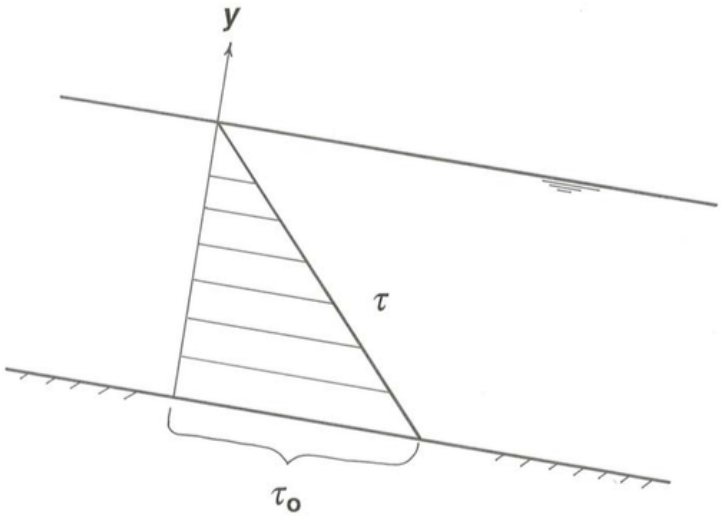


Figure 4.2.6: The distribution of shear stress in steady uniform laminar open- channel flow. (It is noted later in the text that this distribution holds for turbulent flow as well.)

Eliminating τ from Equation 4.2.4 by use of Equation 1.3.6 gives an expression for the velocity gradient du/dy:

$$\mu \tfrac{du}{dy} = \gamma \sin \alpha (d - y)$$

$$\frac{du}{dy} = \frac{\gamma \sin \alpha}{\mu} (d - y) \tag{4.2.6}$$

Equation 4.2.6 can be integrated to give the velocity distribution from the bottom boundary to the free surface:

$$\begin{aligned} u &= \int \frac{du}{dy} dy \\ &= \int \frac{\gamma \sin \alpha}{\mu} (d - y) dy \\ &= \frac{\gamma \sin \alpha}{\mu} \left(d \int dy + \int y dy \right) \\ &= \frac{\gamma \sin \alpha}{\mu} \left(yd + \frac{1}{2} y^2 \right) + c \end{aligned}$$

We can evaluate the constant of integration c by use of the boundary condition that $u = 0$ at $y = 0$; we find that $c = 0$, so

$$u = \frac{\gamma \sin \alpha}{\mu} \left(yd + \frac{1}{2} y^2 \right) \tag{4.2.7}$$

For given values of γ, α, μ, and d, the velocity u thus varies parabolically from zero at the bottom boundary to a maximum at the surface (Figure 4.2.7). On the other hand, from Equation 4.2.7 the velocity gradient du/dy varies linearly from a maximum at the bottom to zero at the free surface, because it is directly proportional to the shear stress (Figure 4.2.7).

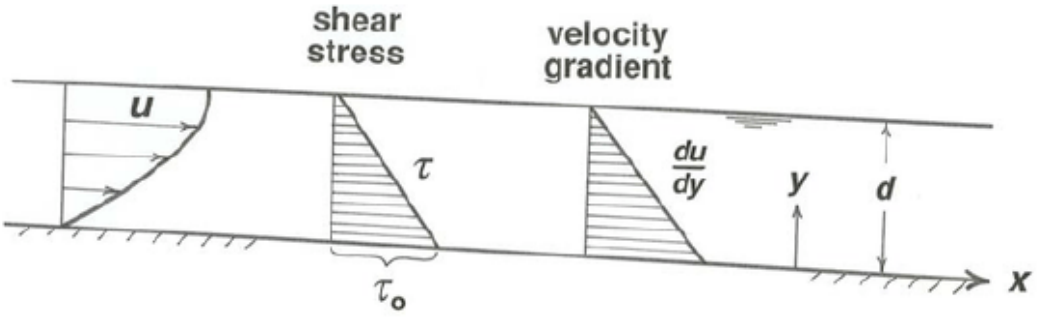


Figure 4.2.7: The vertical distribution of velocity, shear stress, and velocity gradient in steady uniform laminar open-channel flow.

Here is a reminder about shearing within a flowing fluid, which you first encountered back in Chapter 1. You can think, loosely, in terms of layers of the fluid sliding past one another. A good way of making that concrete is to obtain a very thick telephone book and "rack" its pages by putting you hands firmly on the front and back covers and sliding them parallel to one another in the direction perpendicular to the spine of book. In fluids, of course, the shearing is continuous rather than in the form of discrete layers.

This page titled 4.2: Laminar Flow Down an Inclined Plane is shared under a CC BY-NC-SA 4.0 license and was authored, remixed, and/or curated by John Southard (MIT OpenCourseware) via source content that was edited to the style and standards of the LibreTexts platform.

4.3: Turbulent Flow in Channels - Initial Material

The big question at this point is this: how applicable to real flows are the equations for the distribution of shear stress and velocity in steady uniform flows in circular pipes and open channels derived in the preceding section? If you made experiments with pipe flows and channel flows at very low Reynolds numbers, before the transition to turbulent flow (remember, this would necessitate combinations of low velocities, high viscosities, and small flow depths and diameters), you would find beautiful agreement between theory and observation—something that is always satisfying for both the theoretician and the experimentalist. But for turbulent flows, which is the situation in most flows that are of practical interest, the story is different.

Figure $4.3.1$ shows a comparison of velocity profiles, in both pipes and channels, between laminar and turbulent flows arranged to have the same discharge. It is clear that the turbulent-flow velocity profiles are much more nearly uniform over most of the flow but show a much sharper change in velocity near the boundary, where by the no-slip condition the velocity has to go to zero. It is easy to understand qualitatively why this is so: the exchange of turbulent eddies—macroscopic masses or parcels of fluid—across the surfaces of mean shearing normal to the solid boundaries is much better at ironing out cross-flow velocity differences than is just the exchange of molecules over short distances in laminar flow. But then the velocity gradient near the boundary, where the normal-to-boundary motions of eddies are inhibited by the presence of the boundary itself, must be even sharper than in laminar flow.

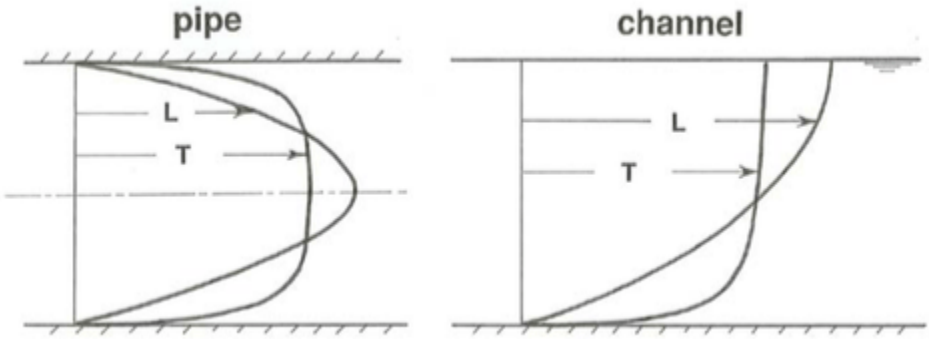


Figure $4.3.1$: Comparison of laminar and turbulent velocity profiles sin steady uniform flow in **A)** a circular pipe and **B)** an open-channel flow.

The story with shear stress is different. If you look back at the derivation of Equation 4.2.4 for the shear-stress distribution in a channel flow, there is nothing in the underlying assumptions that is specific to laminar flow, so the results—the linear distribution of shear stress—should hold just as well in turbulent flow as in laminar flow. I will be making use of that fact later in this chapter.

You might be tempted to ask why Equation 4.2.7 breaks down for turbulent flow. The most straightforward answer (although not the most important) is, with reference to the channel flow, that we can no longer assume that the shear stress across planes in the flow parallel to the bottom boundary is given by Equation 1.3.6, $\tau = \mu(du/dy)$, so we can no longer eliminate τ and perform the integration as in Equation 4.2.7.

Now to get down to more important reasons: part of the reason Equation 4.2.7 is no longer applicable is simply that on account of the irregularity of the fluid motion in the turbulent case the surfaces of local shear are oriented differently at each point on such a plane, and the rate or intensity of shear varies as well. But there is a more important reason that has to do with the basic nature of shear stress in turbulent flow past a solid boundary, which I will deal with in the next section. Suffice it to say here that in one important sense the viscosity is effectively much greater in turbulent flows, again because of the efficacy with which turbulent eddies transport fluid momentum across planes of mean shearing; remember that the basic nature of viscosity itself arises from such momentum exchange on the part of the constituent molecules of the fluid.

This inability to obtain a theoretical velocity distribution in turbulent flows is just one example of a general problem with such flows: it is not possible to solve the equations of motion to obtain exact solutions. The reason for this is basically similar to, although more general than, the problem with velocity profiles noted above: we know what equations we have to solve but we cannot solve them because of the uncertainty that turbulence introduces into the application of these equations. The great number of equations to be found in textbooks and papers on turbulent flow are *semi-empirical*: the general form of the equation may be suggested by physical reasoning, but the numerical constants in the equation, and therefore its specific form, must be found from experiments. And in many cases not even the general form of the equation is known, and the curve must be obtained

entirely by experiment. This should become abundantly clear in the material on resistance and velocity profiles in turbulent flow below.

This page titled 4.3: Turbulent Flow in Channels - Initial Material is shared under a CC BY-NC-SA 4.0 license and was authored, remixed, and/or curated by John Southard (MIT OpenCourseware) via source content that was edited to the style and standards of the LibreTexts platform.

4.4: Turbulent Shear Stress

One of the most significant effects of turbulence is the transport of such things as heat, momentum, solute, or suspended matter—material or properties that can be viewed as carried passively by the fluid—across planes parallel to the mean flow by the random motions of fluid masses back and forth across these planes. The mean normal-to-boundary velocity across such planes is by definition zero, so the net mass of fluid transferred back and forth in this way must balance to zero on the average. But if the material or property passively associated with the fluid is on the average unevenly distributed—if its average value varies in a direction normal to the mean motion—then the balanced turbulent transfer of fluid across the planes causes a diffusive transport or "flow" of this property, usually referred to as a **flux**, in the direction of decreasing average value. This kind of transport is called **turbulent diffusion**.

To see the turbulent diffusion of some material or property carried by the fluid, think about the result of an exchange of two fluid parcels or eddies with equal mass across a plane of mean shear parallel to the boundary in a turbulent boundary layer (Figure $4.4.1$). The eddy traveling from the side of the plane with higher average value of some property P tends to arrive on the other side with a higher value of P than its new surroundings, and conversely the eddy traveling from the side with lower average value tends to arrive with a lower value than its surroundings. The exchange thus tends to even out the distribution of P by means of a net transport of P in the direction of decreasing average value.

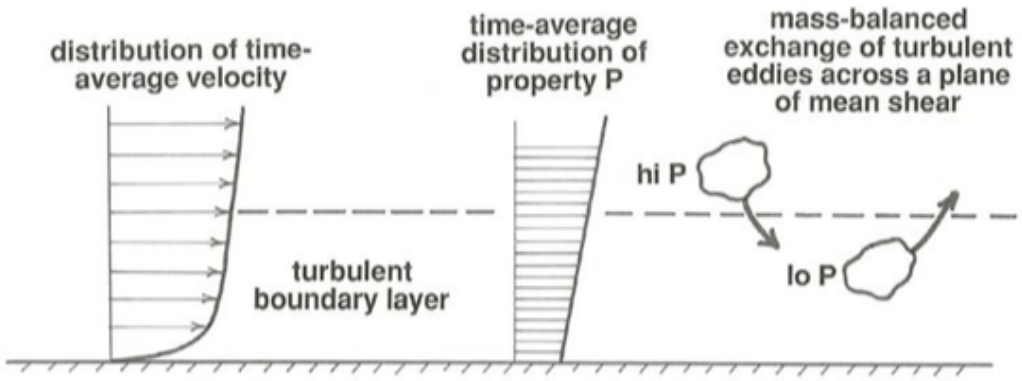


Figure $4.4.1$: Transport of a material or a property by turbulent diffusion in a turbulent boundary layer.

An irregular or nonuniform distribution of the property P at the scale of individual eddies is to be expected by the very nature of the diffusion process. So not every eddy that crosses the plane of mean shear shown in Figure $4.4.1$ from the side with higher average P arrives on the other side with a value of P higher than the new surroundings, and conversely not every eddy crossing in the other direction arrives with a lower value of P. But the important point is that there is a *tendency* for this to happen because there is a statistical correlation between values of P and position normal to the plane, and therefore an average gradient of P in that direction. That average gradient is maintained by some process unrelated to diffusion.

A simple but important example is that of sediment carried in suspension by a river or a tidal current or the atmosphere. (We will look at this problem in more detail in Part II.) You know that if a fluid flow is strong enough it can pick up particles of sand or dust from the lower boundary of the flow and carry them high up into the flow, whence they eventually settle back to the bed or the ground. The concentration of the suspended sediment decreases upward, because of the tendency of the sediment to settle through its surrounding fluid. There is a balance between downward settling and upward turbulent diffusion along the concentration gradient (Figure $4.4.2$). The correlation between suspended-sediment concentration and distance above the bottom is clear in Figure $4.4.2$.

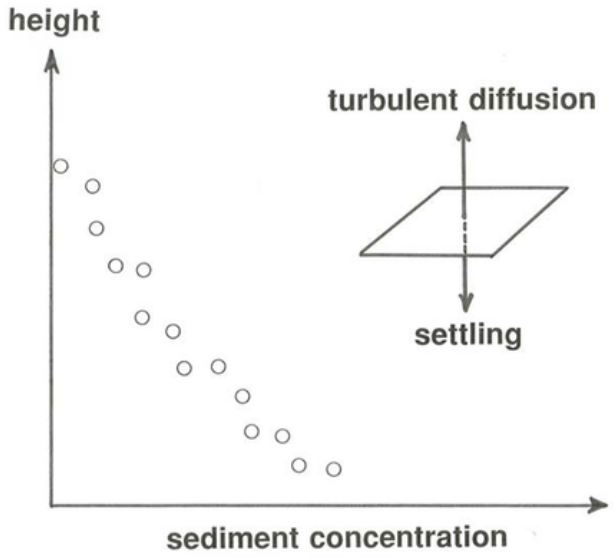


Figure 4.4.2: Balance between upward transport of suspended sediment by turbulent diffusion and downward transport by settling.

We can appeal to the idea of diffusion of fluid momentum to account for the differences in velocity distribution in laminar and turbulent flow down an inclined plane, discussed in an earlier section of this chapter. In laminar flow there are no eddies to be exchanged across shear planes parallel to the bottom, but the molecules themselves hurtle or weave randomly back and forth across these planes in loose analogy with the picture outlined above for the random motions of turbulent eddies. Because on average the molecules have a greater downchannel velocity in the region above a given shear plane than below it, molecular exchange across the plane tends to even out the distribution of fluid momentum and therefore also of fluid velocity. Fluid momentum is continuously created, by either the downslope forces of gravity or a driving downstream pressure gradient (or a combination of the two), then transported toward the bottom boundary by molecular diffusion, and in the process is "consumed" by the resistance force at the bottom boundary.

The tendency for molecular motions to even out the velocity distribution in a sheared fluid is in part the physical cause of the resistance of a fluid to shearing. In liquids the effect of transient molecular attractions in resisting shear is more important, but in gases the diffusive effect is the dominant one. The viscosity of a fluid is simply a measure of the effectiveness of molecular motions and/or molecular attractions in smoothing out an uneven velocity distribution or in maintaining the velocity distribution against the tendency for the fluid to accelerate downslope and intensify the shearing. The continuum hypothesis allows us to disregard the details of molecular forces and diffusion and regard the resulting shear stress as a point quantity.

In turbulent flow, on the other hand, there is an additional diffusional mechanism for transport of fluid momentum toward the boundary: exchange of macroscopic fluid eddies across the planes of mean shear parallel to the bottom tends to even out the velocity distribution by diffusion of momentum toward the bottom (Figure 4.4.3). By Newton's second law this rate of transport of momentum by turbulent motions is equivalent to a shear stress across the plane. This is called the **turbulent shear stress** or, usually, the **Reynolds stress**. It has exactly the same physical effect as an actual frictional force exerted directly between the two layers of fluid on either side of the plane: the faster-moving fluid above the plane exerts an accelerating force on the slower-moving fluid below the plane, and conversely the fluid below exerts an equal and opposite retarding force on the fluid above. It is true that the "range of operation" of this force is smeared out indefinitely for some distance on either side of the plane, but the result is the same as that of a force exerted directly across the plane.

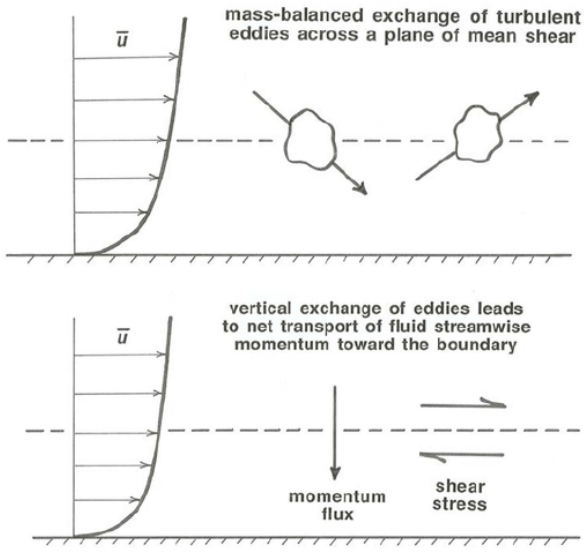


Figure 4.4.3: The origin of turbulent shear stress.

The total shear stress across a shear plane in the flow is the sum of the turbulent shear stress, caused by macroscopic diffusion of fluid momentum, and the viscous shear stress, caused in part by molecular diffusion of fluid momentum and in part by attractive forces between molecules at the shear plane. Owing to its macroscopic nature the turbulent shear stress can be associated with a given point on a shear plane only in a formal way; the viscous shear stress, although it has real physical meaning from point to point, must be regarded as an average over the area of the shear plane, because in turbulent flow both the magnitude and the orientation of shearing vary (continuously, and on the scale of eddies) from point to point.

In an earlier section of this chapter we derived expressions (Equation 4.2.3) for the shear stress across shear planes in laminar flow in a pipe or a channel. The shear stress in those two equations is the sum of the turbulent shear stress and the viscous shear stress. You may protest that the results in Equation 4.2.3 was obtained for laminar flow only. But in deriving the equations we did not assume anything at all about the internal nature of the flow, only that the flow is steady and uniform on the average. This is in contrast to the results for velocity distribution, Equation 4.2.7, which involve the assumption that the shear stress across a shear plane is given by Equation 1.3.6, an assumption that is inadmissible for turbulent flow because of the importance of the additional turbulent shear stress. The linear distribution of shear stress from zero at the surface to a maximum at the bottom should therefore hold just as well for turbulent flow as for laminar flow, provided only that the flow is steady and uniform on average.

Except very near the solid boundary, where the normal-to- boundary component of the turbulent velocity must go to zero, the turbulent shear stress is far greater than the viscous shear stress. This is because turbulent exchange of fluid masses acts on a much larger scale than the molecular motions involved in the viscous shear stress and therefore transports momentum much more efficiently. Figure 4.4.4 is a plot of the distribution of turbulent shear stress and viscous shear stress in steady uniform flow down a plane. The total shear stress is given by the straight line, and the turbulent shear stress is given by the curve that is almost coincident with the straight line all the way from the surface to very near the bottom but then breaks sharply away to become zero right at the bottom. The difference between the straight line for total shear stress and the curve for turbulent shear stress represents the viscous shear stress; this is important only very near the boundary.

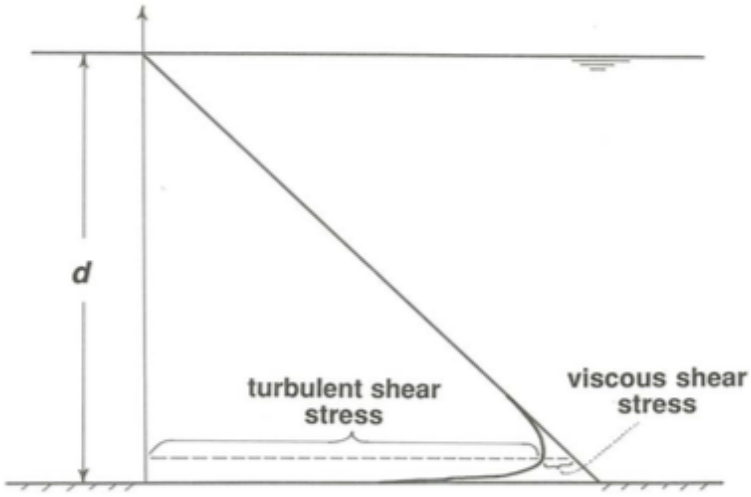


Figure 4.4.4: Distribution of total shear stress, turbulent shear stress, and viscous shear stress in a steady and uniform open-channel flow.

Because the turbulent shear stress is so much larger than the viscous shear stress except very near the boundary, differences in time- average velocity from layer to layer in turbulent flow are much more effectively ironed out over most of the flow depth than in laminar flow. This accounts for the much gentler velocity gradient du/dy over most of the flow depth in turbulent flow than in laminar flow; go back and look at Figure 4.3.1. But as a consequence of this gentle velocity gradient over most of the flow depth, near the bottom boundary, where viscous effects rather than turbulent effects are dominant, the velocity gradient is much steeper than in laminar flow, because the shearing necessitated by the transition from the still-large velocity *near* the boundary to the zero velocity *at* the boundary (remember the no-slip condition) is compressed into a thin layer immediately adjacent to the boundary.

Turbulence Closure Problem

When the Navier–Stokes equations are written for turbulent flow, and then instantaneous velocities are converted to their mean and fluctuating components, as was done in Chapter 3, time averages of products of fluctuating quantities (the Reynolds stresses mentioned in the previous section) emerge as new unknowns—and when one tries to characterize those new unknowns, further new unknowns arise! The result is that the equations of motion for turbulent flow can never form a closed system in which the number of equations is equal to the number of unknowns. This is called the **turbulence closure problem**. It is often said to be one of the great unsolved problems in all of physics. (That is a very strong statement.)

Various strategies have been devised to circumvent the closure problem, by making certain assumptions or parameterizations. A simple and widely used example must suffice here: parameterizing the nature of turbulent momentum transport in a turbulent shear flow by use of the eddy viscosity, and how it varies from the boundary of the flow into the interior.

This page titled 4.4: Turbulent Shear Stress is shared under a CC BY-NC-SA 4.0 license and was authored, remixed, and/or curated by John Southard (MIT OpenCourseware) via source content that was edited to the style and standards of the LibreTexts platform.

4.5: Structure of Turbulent Boundary Layers

Introduction

I have said quite a lot about what turbulence looks like in a general way, but now I need to be more specific about the structure of turbulence in turbulent boundary layers. (Another term I could use instead of turbulent boundary layers is **turbulent shear flow**: any turbulent flow that involves overall mean shearing, of the fluid, usually on account of the presence of a solid boundary to the flow.)

Many of the important things about turbulence in boundary layers have been known for a long time. Workable techniques for reliable measurement of instantaneous velocities in air were developed half a century ago, in the 1940s and 1950s. Comparable laboratory techniques for water flows became available in the 1960s, and reliable field measurements in water flows became possible later. It is still difficult to make detailed observations of the scales, shapes, motions, and interactions of turbulent eddies, especially the relatively small eddies near the boundary. Only in the last few decades has observational knowledge of the dynamics of near- boundary turbulent structure advanced from the stage of point measurements of velocities and their statistical treatment, to observations of the eddy structure of the turbulent flow as a whole by means of various flow-visualization techniques. Studies on the structure and organization of turbulent fluid motions in boundary layers has become an actively growing branch of fluid dynamics, and has resulted in much deeper understanding of the dynamics of turbulent flows.

In the following section are some of the most important facts and observations on the turbulence structure of turbulent boundary layers—with steady uniform flow down a plane as a reference case, but the differences between this and other kinds of boundary-layer flow lie only in minor details and not in important effects.

Vertical Organization of Flow Structure in Channel Flows

First of all, you should expect the nature of turbulence to vary strongly from surface to bottom in the flow, because the boundary is the place where the vertical turbulent fluctuations must go to zero and where by the no-slip condition the fluid velocity itself must go to zero. You have already seen that the relative contributions of turbulent shear stress and viscous shear stress change drastically in the vicinity of the boundary.

If the bottom boundary is physically smooth, or if it is rough but the height of the roughness elements is less than a certain value to be discussed presently, three qualitatively different but intergrading zones of flow can be recognized (Figure 4.5.1): a thin viscous sublayer next to the boundary, a turbulence-dominated outer layer occupying most of the flow depth, and a buffer layer between. If the boundary is too rough, the viscous sublayer is missing. Here I will only give a qualitative description of the flow in these layers; in later sections I will show their implications for flow resistance and velocity profiles.

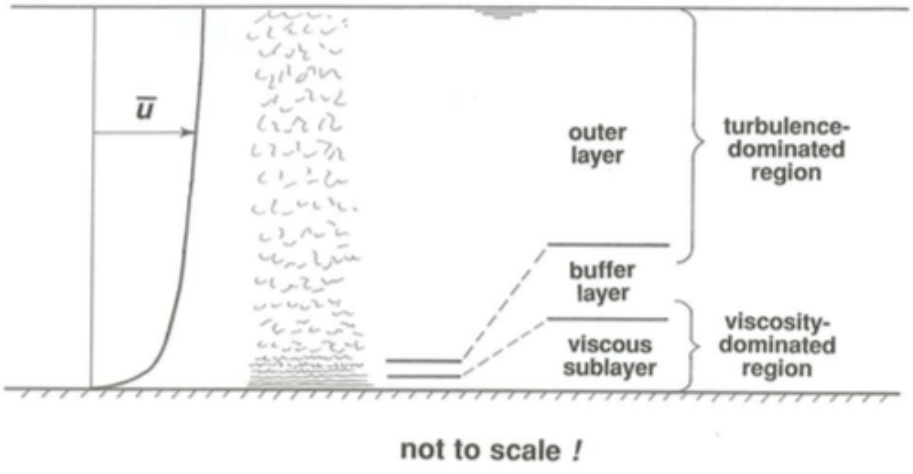


Figure 4.5.1: Division of turbulent open-channel flow into layers on the basis of turbulence structure.

The **viscous sublayer** is a thin layer of flow next to the boundary in which viscous shear stress predominates over turbulent shear stress. Shear in the viscous sublayer, as characterized by the rate of change of average fluid velocity as one moves away from the wall, is very high, because fast-moving fluid is mixed right down to the top of the viscous sublayer by turbulent diffusion.

The thickness of the viscous sublayer depends on the characteristics of the particular flow and fluid; it is typically in the range of a fraction of a millimeter to many millimeters. You will find out later how to ascertain the viscous-sublayer thickness.

The flow is not strictly laminar in the viscous sublayer because it experiences random fluctuations in velocity. What is important, however, is that because fluctuations in velocity normal to the boundary must decrease to zero at the boundary itself, molecular transport of fluid momentum is dominant over turbulent transport of momentum near the boundary. Fluctuations in velocity very close to the boundary must therefore be largely parallel to the boundary. Fluctuations in shear stress on the boundary itself caused by these fluctuations in velocity can be substantial. The turbulent fluctuations in velocity in the viscous sublayer are the result of advection of eddies from regions farther away from the wall; these eddies are damped out by viscous shear stresses in the sublayer.

When the boundary is physically smooth the thickness of the viscous sublayer can easily be defined, but when the boundary is covered with closely spaced roughness elements (like sediment particles, or corrosion bumps, or densely spaced buildings, or trees and shrubs) with heights greater than the thickness of the viscous sublayer (or, more precisely, what the sublayer thickness would be in the absence of the roughness), then no sublayer is actually present at all, and turbulence extends all the way to the boundary, in among the roughness elements.

Of course, if you zoomed in to look at the boundary even more closely, you would find very thin viscous sublayers right at the surfaces of each of the roughness elements: close enough to any solid surface, the flow has to be dominated by viscous effects. In the preceding paragraph I was talking about the presence or absence of a viscous sublayer over a whole larger area of the boundary, at lateral scales much greater than the individual roughness elements.

The **buffer layer** is a zone just outside the viscous sublayer in which the gradient of time-average velocity is still very high but the flow is strongly turbulent. Its outstanding characteristic is that both viscous shear stress and turbulent shear stress are too important to be ignored. With reference to Figure 4.5.1 you can see that this is the case only in a thin zone close to the bottom. Very energetic small-scale turbulence is generated there by instability of the strongly sheared flow, and there is a sharp peak in the conversion of mean-flow kinetic energy to turbulent kinetic energy, and also in the dissipation of this turbulent energy; for this reason the buffer layer is often called the **turbulence-generation layer**. (There will be more on kinetic energy in turbulent flows soon.) Some of the turbulence produced here is carried outward into the broad outer layer of flow, and some is carried inward into the viscous sublayer. The buffer layer is fairly thin but thicker than the viscous sublayer.

The broad region outside the buffer layer and extending all the way to the free surface is called the **outer layer**. (In pipe flow this is more naturally called the **core region**.) This layer occupies most of the flow depth, from the free surface down to fairly near the boundary. Here the turbulent shear stress is predominant, and the viscous shear stress can be neglected. Except down near the buffer layer, turbulence in this zone is of much larger maximum scale than nearer the boundary. Because of their large size, the turbulent eddies here are more efficient at transporting momentum normal to the flow direction than are the much smaller eddies nearer the boundary; this is why the profile of mean velocity is much gentler in this region than nearer the bottom. But it turns out that these large eddies contain much less kinetic energy per unit volume of fluid than in the buffer layer. The normal-to-boundary dimension of the largest eddies in this outer layer is a large fraction of the flow depth—but there are smaller eddies too, at a whole range of scales; see a later section for more discussion of eddy scales.

In terms of the relative importance of turbulent shear stress and viscous shear stress, it is convenient to divide the flow in a somewhat different way (Figure 4.5.1) into a **viscosity-dominated region**, which includes the viscous sublayer and the lower part of the buffer layer, where viscous shear stress is more important than turbulent shear stress, and a **turbulence-dominated region**, which includes the outer layer and the outer part of the buffer layer, where the reverse is true. In a thin zone in the middle part of the buffer layer the two kinds of shear stress are about equal. It is worth emphasizing that there are no sharp divisions in all this profusion of layers and regions: they grade smoothly one into another.

This page titled 4.5: Structure of Turbulent Boundary Layers is shared under a CC BY-NC-SA 4.0 license and was authored, remixed, and/or curated by John Southard (MIT OpenCourseware) via source content that was edited to the style and standards of the LibreTexts platform.

4.6: Flow Resistance

Introduction

This section takes account of what is known about the mutual forces exerted between a turbulent flow and its solid boundary. You have already seen that flow of real fluid past a solid boundary exerts a force on that boundary, and the boundary must exert an equal and opposite force on the flowing fluid. It is thus immaterial whether you think in terms of resistance to flow or drag on the boundary.

Forces Exerted by a Flow on its Boundary

What is the physical nature of the mutual force between the flow and the boundary? Remember that at every point on the solid boundary, no matter how intricate in detail the geometry of that boundary may be, two kinds of fluid forces act: *pressure*, acting normal to the local solid surface at the point, and *viscous shear stress*, acting tangential to the local solid surface at the point.

If the boundary is physically smooth (Figure $4.6.1$A) the downstream component of force the fluid exerts on the boundary can result only from the action of the viscous shear stresses, because the pressure forces can then have no component in the direction of flow. But the boundary may be strongly uneven or rough on a small scale at the same time it is planar or smoothly curving on a large scale; this unevenness or roughness might involve arrays of various kinds of bumps, corrugations, protuberances, or particulate masses. Most natural flows, and many in engineering practice also, like canals and corroded pipes, have physically rough boundaries. Then the picture is more complicated (Figure $4.6.1$B), because there is a downstream component of pressure force on the boundary in addition to a downstream component of viscous force: just as with the drag on spheres, considered in Chapters 2 and 3, if roughness elements are present on the boundary, local pressure forces are greater on the upstream sides than on the downstream sides, so each element is subjected to a resultant pressure force with a component in the downstream direction.

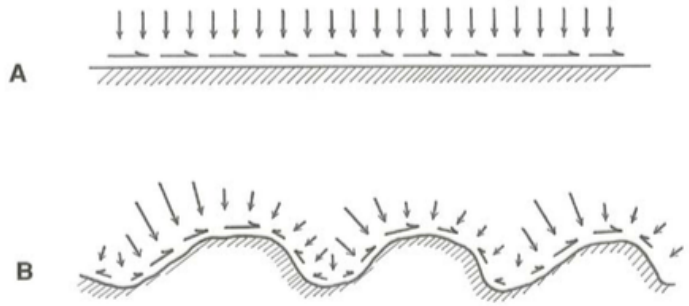


Figure $4.6.1$: Pressure forces and viscous forces on physically smooth and physically rough boundaries.

The details of pressure forces on roughness elements are complicated, because they depend not only on a Reynolds number based on the size of the roughness elements and the local velocity of flow around the elements (in generally the same way that the pressure forces depend on a Reynolds number in the case of unbounded and uniform flow around a sphere, as was discussed in earlier chapters), but also on the shape, arrangement, and spacing of the elements. Qualitatively, however, the picture is clear (Figure $4.6.2$): at low Reynolds numbers the pressure force on an element is of the same order as the viscous force, as in creeping flow past a sphere, whereas at higher Reynolds numbers the pressure forces are much greater than the viscous forces, as in separated flow past a sphere.

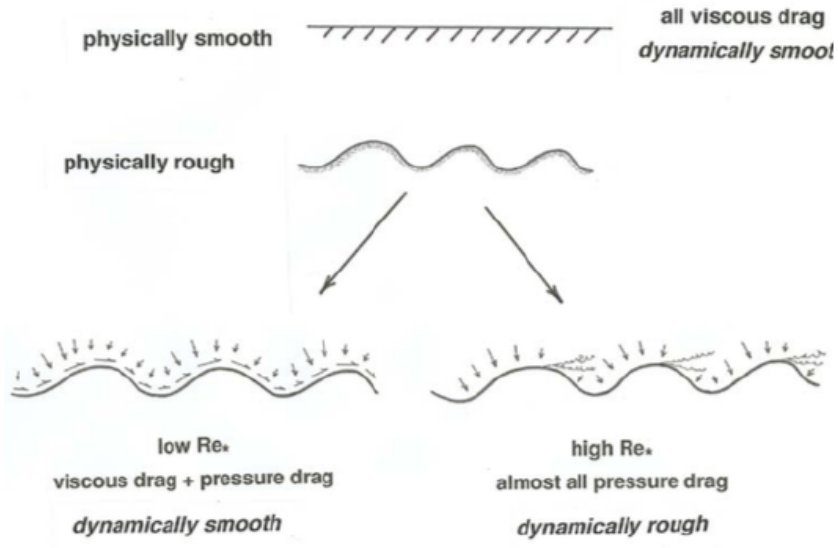


Figure 4.6.2: Differences in near-bed flow and forces in flow over a rough boundary, as a function of the roughness Reynolds number Re_*.

The sum of all the forces on individual roughness elements on the boundary (or, in the case of a physically smooth boundary, the sum of the viscous shear stresses at all points of the boundary) constitutes the overall drag on the boundary, or conversely the overall resistance to the flow; when expressed as force per unit area this boundary resistance is called the **boundary shear stress**, denoted by τ_o (usually pronounced *tau-zero* or *tau-naught*). It is important to remember that τ_o refers not to the viscous shear stress at any given point on the flow boundary—which seems to fit the description of "boundary shear stress" perfectly!—but to the average force per unit area, viscous forces plus pressure forces, over an area of the boundary large enough that the variations in local forces from point to point are suitably averaged out. That means an area many times the size of the individual roughness elements (Figure 4.6.3).

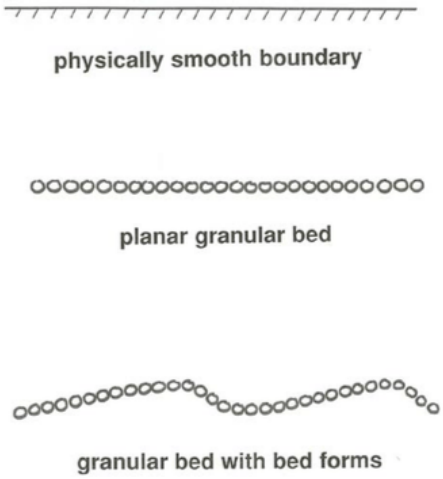


Figure 4.6.3: Boundary shear stress over physically smooth boundaries, granular-rough boundaries, and boundaries rough on the scale of bed forms as well as sediment particles.

It is worth considering at this point how the boundary shear stress τ_o is actually measured in pipes and channels. Direct measurement is difficult even in the laboratory: mechanical shear plates set flush with the boundary tend to cause some disturbance to the flow because of the inevitable gap or step at the edges. Hot-film sensors, which measure the shear at the fluid–solid interface indirectly via the conductive heat transfer from a heated solid surface, get around this problem nicely for smooth boundaries, but they do not work well for rough boundaries, especially when the roughness elements are in motion, like sediment grains. Direct measurement under field conditions has been limited.

Fortunately, there are other ways of measuring the boundary shear stress. In a horizontal closed conduit you can measure the downstream pressure gradient just by installing two pressure gauges some distance apart, reading the pressure drop, and dividing

by the distance between the gauges (Figure 4.6.4A). Then you can use an equation, analogous to Equation 4.2.1, that relates the boundary shear stress to the pressure gradient. If the conduit is not horizontal, be sure to subtract out the difference in hydrostatic pressure between the two stations, so that you are left with the dynamic pressure (Figure 4.6.4B). In a steady and uniform channel flow you can use Equation 4.2.1, the resistance equation for channel flow, to find τ_o without concern for the internal details of the flow simply by measuring the slope of the water surface; although not always a simple matter, this is possible in both field and laboratory with the proper surveying equipment. The problem is that the value of τ_o obtained in this way is the average around the wetted perimeter of the cross section, so it is not exactly the same as the boundary shear stress at any particular place on the wetted perimeter. Moreover, if the channel flow is not uniform—if the depth and velocity vary from section to section—then Equation 4.2.1 holds only approximately, not exactly; the error introduced depends on the degree of nonuniformity.

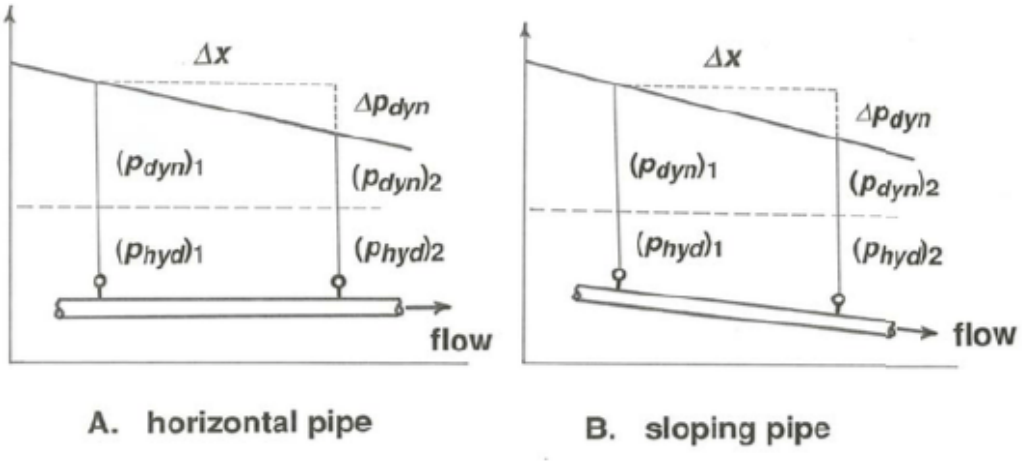


Figure 4.6.4: Static and dynamic pressure in **A)** a horizontal pipe and **B)** an inclined plane.

Another method of finding τ_o, suitable only for laboratory experiments with smooth flow, is to measure the velocity profile within the viscosity-dominated zone of flow very near the boundary, using various techniques, in order to determine velocity gradient at the boundary, which by Equation 1.3.6 is proportional to τ_o. One serious problem here is that the viscous sublayer is very thin, necessitating that the measuring device be extremely small for accurate results. Another problem is that this technique is not workable in situations where the roughness elements are larger than the potential thickness of the viscous sublayer—and that is true of most sediment-transporting flows of interest in natural environments.

Finally, you will see presently, after considering velocity profiles in turbulent flow, that τ_o can also be found indirectly in both rough and smooth flow by means of less demanding measurement of the velocity profile through part or all of the flow depth. This last method is the most useful of all.

Smooth Flow and Rough Flow

Two fundamentally different but intergrading cases of turbulent boundary-layer flow can be distinguished by comparing the thickness of the viscous sublayer and the height of granular roughness elements. (What I will say here is for sand-grain roughness, but the situation is about the same for close-packed roughness of any geometry.) The roughness elements may be small compared to the thickness of the sublayer and therefore completely enclosed within it (Figure 4.6.5A). Or they may be larger than what the sublayer thickness would be for the given flow if the boundary were physically smooth rather than rough (Figure 4.6.5B). In the latter case, flow over and among the roughness elements is turbulent, and the structure of this flow is dominated by effects of turbulent momentum transport. There can then be no overall viscous sublayer in the sense described in an earlier section, although, as noted earlier, a thin viscosity- dominated zone with thickness much smaller than the roughness size must still be present at the very surfaces of all of the roughness elements. In the transitional case the roughness elements poke up through a viscous sublayer that is of about the same thickness as the size of the elements.

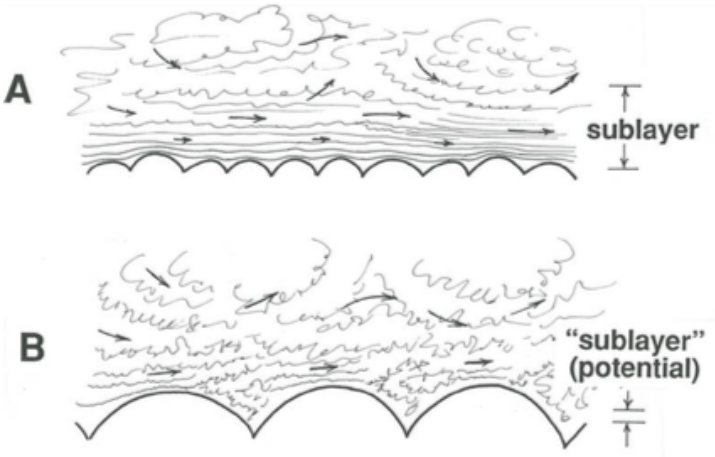


Figure 4.6.5: Differences in flow structure near a granular bed, depending upon whether **A)** the viscous sublayer is thicker than the heights of the particles or **B)** the heights of the particles are greater than what the thickness of the viscous sublayer would be in the absence of the particles.

If, in flow over a rough bed, the viscous-sublayer thickness is much greater than the size of the roughness elements, the overall resistance to flow turns out to be almost the same as if the boundary were physically smooth; such flows are said to be **dynamically smooth** (or hydraulically or hydrodynamically or aerodynamically smooth), even though they are in fact *geometrically* rough. (Obviously, flow over physically smooth boundaries is also dynamically smooth.) This is a consequence of the argument, introduced above, that if the Reynolds number of flow around individual roughness elements is small, as must be the case if the elements are much smaller than the viscous sublayer, pressure forces and viscous forces are of about the same magnitude, so that the presence of roughness makes little difference in the overall resistance to flow. If the elements are much larger than the potential thickness of the viscous sublayer, however, Reynolds numbers of local flow around the elements are large enough that pressure forces on the elements are much larger than viscous forces, and then the roughness has an important effect on flow resistance. Such flows are said to be **dynamically rough**. There is an intermediate range of conditions for which the flow is said to be **transitionally rough**.

It is convenient to have a dimensionless measure of distance from the boundary that can be used to specify the thicknesses of the viscous sublayer and the buffer layer. Assume for this purpose that the dynamics of flow near the boundary is controlled only by the shear stress τ_o and the fluid properties ρ and μ. This should seem at least vaguely reasonable to you, in that the dynamics of turbulence and shear stress in the viscous sublayer and buffer layer are a local phenomenon related to the presence of the boundary but not much affected by the weaker large-scale eddies in the outer layer. There will be more on this in the later section on velocity profiles. You can readily verify that the only possible dimensionless measure of distance y from the boundary would then be $\rho^{1/2}\tau_0^{1/2}y/\mu$, often denoted by y^+. A similar dimensionless variable $\rho^{1/2}\tau_0^{1/2}D/\mu$, involving the height D of roughness elements on the boundary, can be derived by the same line of reasoning about variables important near the boundary. This latter variable is called the **boundary Reynolds number** or the **roughness Reynolds number**, often denoted by Re_*.

The dimensionless distance y^+ and the roughness Reynolds number Re_* can be written in a more convenient and customary form by introduction of two new variables. The quantity $(\tau_0/\rho)^{1/2}$, usually denoted by u_* (pronounced u-star), has the dimensions of a velocity; it is called the **shear velocity** or the **friction velocity**. Warning: u_* is *not* an actual velocity; it is a quantity involving the boundary shear stress that conveniently has the dimensions of a velocity. The quantity μ/ρ, which you may have noticed commonly appears in Reynolds numbers, is called the **kinematic viscosity**, denoted by ν. The word *kinematic* is used because the dimensions of ν involve only length and time, not mass. If y^+ as defined above is rearranged slightly it can be written u_*y/ν and the roughness Reynolds number can be written u_*D/ν.

When expressed in the dimensionless form y^+, the transition from the viscous sublayer to the buffer layer is at a y^+ value of about 5, and the transition from the buffer layer to the turbulence-dominated layer is at a y^+ value of about 30. These transition values are about the same whatever the values of boundary shear stress τ_o and fluid properties ρ and μ; this confirms the supposition made above that over a wide range of turbulent boundary-layer flows the variables τ_o, ρ, and μ suffice to characterize the flow near the boundary. These values are known not from watching the flow but from plots of velocity profiles, as will be discussed presently.

The relative magnitude of the viscous-sublayer thickness and the roughness height D can be expressed in terms of the roughness Reynolds number u_*D/ν. To see this, take the top of the viscous sublayer to be at $u_*\delta_v/v \approx 5$, meaning that $\delta_v \approx 5v/u_*$ is the

distance from the boundary to the top of the viscous sublayer. Here I have replaced y by δ_v, the thickness of the viscous sublayer. The ratio of particle size to sublayer thickness is then $D/\delta_v \approx (u_* D/v)/5$. In other words, sublayer thickness and particle size are about the same when the roughness Reynolds number has a value of about 5. (But remember that if the roughness elements are this large or larger, there is no well developed viscous sublayer in the first place.) Another way of looking at this is that we can compare the particle size D with v/u_*, a quantity with dimensions of length called the **viscous length scale**, which is proportional to the thickness of the viscous sublayer.

The limits of smooth and rough flow can also be specified by values of the roughness Reynolds number. The upper limit of smooth flow is associated with the condition that the height of the viscous sublayer is about equal to that of the roughness elements. As noted above, at the top of the viscous sublayer $y^+ = u_* \delta_v / v \approx 5$, so the upper limit of roughness Reynolds numbers for smooth flow should be $u_* D/\nu \approx 5$, and in fact the value of 5 is in good agreement with results based on both boundary resistance and velocity profiles. Likewise, the lower limit of roughness Reynolds numbers for fully rough flows is found to be about 60. It is between these values $(5 < u_* D/v < 60)$ that the flow is said to be transitionally rough.

Some further discussion of smooth and rough flow can be found in the latter part of this chapter in the section on velocity profiles.

Dimensional Analysis of Flow Resistance

One circumstance that tends to make the standard treatments of flow resistance in fluid-dynamics textbooks seem more complicated than they really are is that the details of the equations for flow resistance (although not their general form) depend not only on the boundary roughness but also on the overall geometry of the flow. On the one hand, the flow may be a turbulent boundary layer growing into a free stream; on the other hand, it may be a fully established turbulent boundary layer that occupies all of a conduit or channel. In terms of flow mechanics in the boundary layer itself, these two kinds of flow can be treated together. In the latter case any number of boundary geometries are possible. The classic experiments on flow resistance were made using circular pipes with inside surfaces coated with uniform sand, and not much systematic work has been done on channel flow. The discussion here focuses on pipe flow, with the understanding that both the principles and the general form of the results are the same for any steady uniform flow whatever the boundary geometry.

In common with other aspects of turbulent boundary-layer flow, there is no theory we can draw on to find relationships for flow resistance. It is therefore again natural to start with a dimensional analysis of resistance to flow through a circular pipe or tube (Figure $4.6.6$) in order to develop a framework in which experimental data can provide dimensionless relationships that are expressible in the form of essentially empirical equations that are valid in certain ranges of flow.

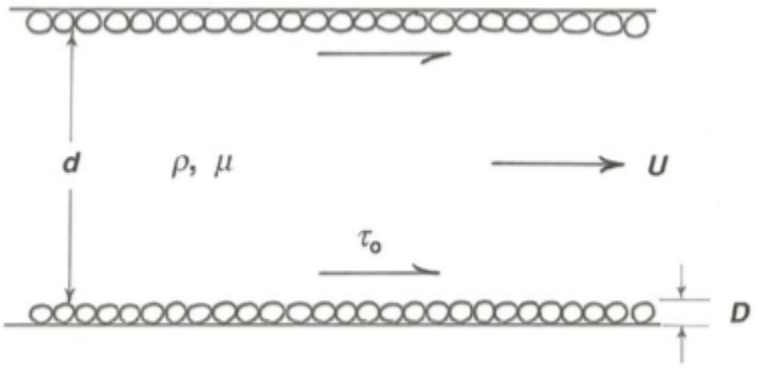


Figure $4.6.6$: Definition sketch for dimensional analysis of flow resistance in a circular pipe.

Which variables must be specified in order that the boundary shear stress τ_o can be fully characterized or determined? Pipe diameter d and mean flow velocity U are important because they affect the rate of shearing in the flow, both directly and through their effect on the structure of turbulence. Viscosity μ is obviously important because of its role in determining viscous shear stress at the boundary. Fluid density ρ is important because if the flow is turbulent there must be local fluid accelerations. Finally, the size D of boundary roughness elements may affect the turbulent forces and motions near the boundary. There are thus two important length scales in the problem of flow resistance: pipe diameter and roughness height. We will have to assume that shape, spacing, and arrangement of the roughness elements are either always the same or, if variable, are of secondary importance in determining flow resistance. Neither assumption is justified, but they form a good place to start. Never mind that if the boundary is rough there is some haziness about where the position of the wall should be taken in defining the pipe diameter; at least with respect to flow resistance, any reasonable choice produces consistent results provided that consideration is limited

to geometrically similar roughness.

Assuming that all of the important variables have been included,τo can be viewed as a function of the five variables U, d, D, ρ, and μ. You should then expect to have a dependent dimensionless variable as a function of two independent dimensionless variables. It should occur to you immediately that one of the independent dimensionless variables can be a Reynolds number based on U and d, which I will call the mean-flow Reynolds number. The other independent dimensionless variable is most naturally d/D, the ratio of pipe diameter to roughness height. This variable is called the **relative roughness**. The dependent dimensionless variable, which must involve τ_o, has exactly the same form and physical significance as the dimensionless drag force or drag coefficient that characterizes the drag on a sphere moving relative to a fluid (Chapter 2), except that here we are dealing with a force per unit area rather than with a force. You can verify that one possible dimensionless variable involving τ_o is $8\tau_0/\rho U^2$, and although this is not the only one possible (there are two others; you might at this point try to find them yourself) it is the most useful, and it is the one that is conventionally used. (The factor 8 is present for reasons of convenience that need not concern us here.) This dimensionless boundary shear stress is called the **friction factor**, denoted by f; it is one kind of flow-resistance coefficient.

The functional relationship for flow resistance can thus be written

$$f = \frac{8\tau_o}{\rho U^2} = F\left(\frac{\rho U d}{\mu}, \frac{d}{D}\right) \tag{4.6.1}$$

where F is a function that for turbulent flow has to be ascertained by experiment.

Resistance Diagrams

The relationship expressed in Equation 4.6.1 can be shown in a two-dimensional graph most easily by plotting curves of f vs. Reynolds number for a series of values of d/D. Figure 4.6.7 shows a graph of this kind, called a **resistance diagram**. The data were obtained by Nikuradse (1933) for flows through circular pipes lined with closely spaced sand grains of approximately uniform size. A version of Figure 4.6.7 is shown in just about all books on flow of viscous fluids.

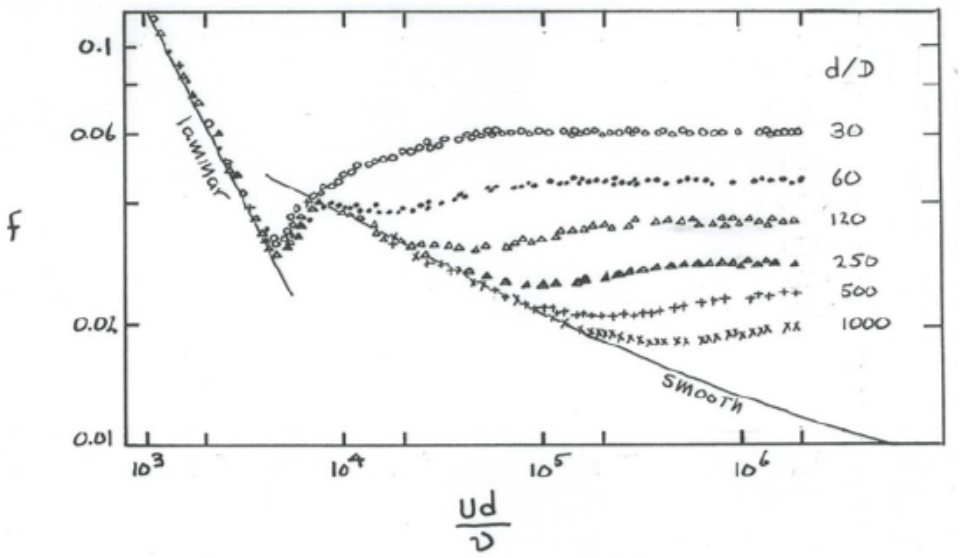


Figure 4.6.7: Graph of friction factor vs. mean-flow Reynolds number (pipe friction diagram) for a flow in a circular pipe with granular roughness.

Leaving aside the steeply sloping part of the curve on the far left (it holds for laminar flow in the pipe, for which we have already obtained an exact solution), you see that at fairly low Reynolds numbers the curve off vs. Re for any given d/D in Figure 4.6.7 at first slopes gently down to the right, then breaks away, and finally levels out to a horizontal straight line. The larger the relative roughness d/D the greater the Reynolds number at which the breakaway takes place. Physically smooth boundaries, for which $D/d = 0$, follow the descending curve to indefinitely high Reynolds numbers. Flows that plot on this descending curve are those I earlier termed dynamically smooth. Note that flows over physically rough boundaries can be dynamically smooth, provided that d/D is sufficiently large. If Re is fairly small and the pipe is fairly large, D can be absolutely large—millimeters or even centimeters—in smooth water flows. Flows that plot on the horizontal straight lines to the right are those I called fully rough, and

those at intermediate points are those I called transitionally rough. For a given d/D the flow is smooth at low Reynolds numbers but rough at sufficiently high Reynolds numbers.

Two questions need to be discussed at this point:

1. How would the results in Figure $4.6.7$ change for kinds of roughness elements different from glued-down uniform sand grains?
2. How would the results change for conduits or channels with geometry different from that of a circular pipe?

The answer to both of these questions is that the results are qualitatively the same, provided that the characteristics of the roughness are not grossly different and that the size of the roughness elements remains a small fraction of the conduit diameter or channel depth. The curves are merely shifted slightly in position or differ slightly in shape. To adapt the uniform- sand-roughness results to other kinds of roughness a quantity called the **equivalent sand roughness**, denoted by k_s, is defined as the fictitious roughness height that would make the results for the given kind of roughness expressible by the same plot as in Figure $4.6.7$ for uniform-sand-roughness pipes. And to compare the pipe results with those for conduits or channels with different geometry, it is customary to use the hydraulic radius in place of the pipe radius, although the results cannot be expected to be exactly the same. By applying the definition of hydraulic radius given earlier in this chapter you can verify that for a circular pipe the hydraulic radius specializes to one-fourth the pipe diameter. (You have already seen that for an infinitely wide channel flow the hydraulic radius specializes to the flow depth.)

There is an equivalent way of expressing resistance that is used specifically for open-channel flow. Combining the equation $\tau_o = (f/8)\rho U^2$ that defines the friction factor f with the equation $\tau_o = \rho g d \sin\alpha$ (Equation 4.2.1) for boundary shear stress in steady uniform flow down a plane, eliminating τ_o from the two equations, and then solving for U,

$$U = \left(\frac{8g}{f} \quad d \sin\alpha \right)^{1/2} \tag{4.6.2}$$

$$U = C(d \sin\alpha)^{1/2} \tag{4.6.3}$$

where

$$C = \left(\frac{8g}{f} \right)^{1/2} \tag{4.6.4}$$

Equation $4.6.4$, which relates mean velocity, flow depth, and slope for uniform flow in wide channels, is called the **Chézy equation**, after the eighteenth-century French hydraulic engineer who first developed it. The coefficient C, called the **Chézy coefficient**, is *not* a dimensionless number like the friction factor f; it has the dimensions $g^{1/2}$. But because g is very nearly a constant at the Earth's surface, C can be viewed as being a function only of f. I have introduced the Chézy C because it is in common use in work on open-channel flow, but you should understand that it adds nothing new.

This page titled 4.6: Flow Resistance is shared under a CC BY-NC-SA 4.0 license and was authored, remixed, and/or curated by John Southard (MIT OpenCourseware) via source content that was edited to the style and standards of the LibreTexts platform.

4.7: Velocity Profiles

Introduction

You have already seen that the profile of time-average local fluid velocity $\overline{u}$ from the bottom to the surface in turbulent flow down a plane is much blunter over most of the flow depth than the corresponding parabolic profile for laminar flow (Figure 4.3.1). This is the place to amplify and quantify the treatment of velocity profiles in turbulent boundary-layer flows.

First I will pose the following question: Can an equation for the velocity profile in a turbulent boundary-layer flow be found by writing an equation like Equation 1.3.6 for turbulent flow and solving for the velocity profile by integration? As noted earlier, Equation 4.2.4, for the distribution of total shear stress in the flow, is valid for turbulent flow as well as for laminar flow, because no assumptions were made about the nature of internal fluid motions in its derivation, just that the flow must be steady and uniform on the average. And an expression of the same kind as Equation 1.3.6, defining the shear stress, can also be written for turbulent flow:

$$\tau = \mu\frac{du}{dy} + \eta\frac{du}{dy} \tag{4.7.1}$$

The term $\mu(du/dy)$ is the *viscous shear stress* due to the mean shear across planes parallel to the boundary. (Actually it's is a spatial average over an area of such a plane that is large relative to eddy scales, because fluid shear varies from point to point in turbulent flow.) The term $\eta(du/dy)$ is a way of writing the *turbulent shear stress* across these planes that involves an artificial quantity η, called the **eddy viscosity**, that is formally like the molecular viscosity μ. Everywhere in a turbulent shear flow except very near the solid boundary the eddy viscosity is much larger than the molecular viscosity, because turbulent momentum transport is dominant over molecular momentum transport. (Often η is written as $\rho\varepsilon$, where ε can be viewed as the *kinematic eddy viscosity*, in analogy with ν; ε is also called the **eddy diffusion coefficient**.) Just as for laminar flow, the expressions for τ_o in Equation 4.7.1 and Equation 1.3.6 can be set equal to give a differential equation for u as a function of distance y from the boundary:

$$(\mu + \eta)\frac{du}{dy} = \gamma \sin\alpha(d - y) \tag{4.7.2}$$

Unfortunately there is always an insuperable problem in integrating Equation 4.7.2, or any other equation like it for turbulent flow in a conduit or channel with some other geometry, to find the velocity distribution. Unlike the molecular viscosity μ, the eddy viscosity η, rather than being a property of the fluid, depends upon the flow: it varies with height above the boundary, because the turbulent shear stress it represents is a function of the flow itself, for which we are trying to solve. We are therefore always forced to find the velocity distribution in turbulent flow by experiment.

It is important to realize, however, that experiments to find the velocity profile do not have to be blindly empirical: physical reasoning can be used to guess which effects and therefore which variables are important in governing the velocity distribution in the various layers of the flow. If the functional relationships thus specified by the dimensional structure of the problem are consistent with the observational results, then the correctness of that qualitative view of the physics is confirmed. In fact, much of what is known about turbulent flow past solid boundaries has been learned in this way.

We will stick with steady and uniform flow down a plane, but exactly the same kind of analysis could be made for flow in a closed conduit. Think about which variables you have to specify to take full account of the profile of time-average velocity u along an imaginary line through the flow, normal to the bottom boundary, stretching from the bottom to the free surface (Figure 4.7.1).

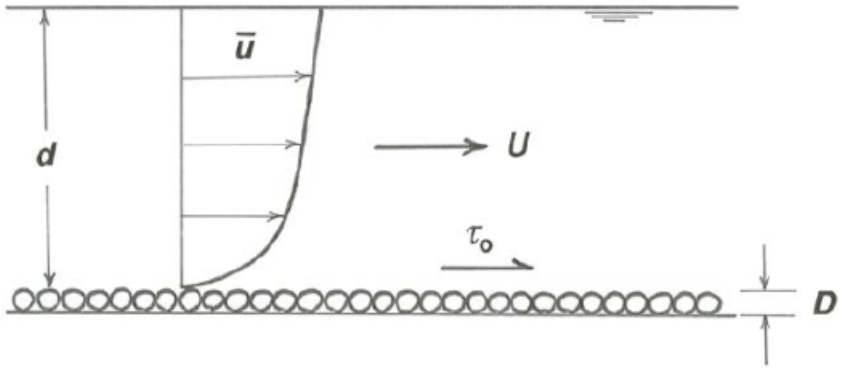


Figure 4.7.1: Definition sketch for dimensional analysis of velocity profiles in turbulent open-channel flow.

The bottom can be either smooth or rough. As in the flow-resistance problem, make the assumption (not a good one, but it gets us started) that the roughness can be characterized by the size D of the elements without having to worry about their shape and arrangement. The boundary shear stress τ_o is the best variable to use to characterize the strength of the flow. You should expect that in general the flow depth d would be needed as well. The viscosity μ is needed, because it is tied up with shearing in the fluid. Finally, as in all problems in turbulent flow, the fluid density ρ is needed, because the fluid experiences local accelerations (in the form of eddies), so fluid inertia is important. So $\overline{u}$ can be viewed as a function of τ_o, ρ, μ, d, and D, and of course the distance y above the bottom:

$$\overline{u} = f\left(\tau_0, \rho, \mu, D, d, y\right) \tag{4.7.3}$$

The dimensionless functional relationship for $\overline{u}$ is then

$$\frac{\overline{u}}{u.} = f\left(\frac{u_* D}{v}, \frac{d}{D}, \frac{y}{d}\right) \tag{4.7.4}$$

where we have made use of the shear velocity u_* and the kinematic viscosity ν introduced earlier in this chapter. Equation 4.7.4 says that $\overline{u}/u_*$, a dimensionless version of $\overline{u}$ (often denoted u^+), should be a function only of the roughness Reynolds number $u_* D/\nu$ and the relative roughness d/D for a given dimensionless position y/d in the flow. There are alternative possibilities for the three independent dimensionless variables (for example, all three could be put into the form of a Reynolds number, each with a different one of the three length variables), but this is the most natural.

I am sure that all the velocity data you could get your hands on would plot very nicely in a four-dimensional graph using the variables $\overline{u}/u_*$, $u_* D/\nu$, d/D, and y/d. But even though the number of variables has been reduced from seven to four, you would still have a burdensome plotting job and a product that would be unwieldy for practical use. Moreover, further careful study would be needed to decipher what the graph is telling you about the physics behind velocity profiles. This is a good place to think about whether the problem can be simplified further by a divide-and-conquer approach wherein certain of the variables are eliminated or modified in certain ranges of conditions to arrive at simpler functions that represent the data well under those conditions. This serves two purposes: it provides useful results, and it helps to clarify the physical effects that are important.

First off, in the next two sections, I will present some ideas about *energy in turbulent flow*. This may seem out of place here, but it leads to two conclusions that are of great importance for velocity profiles in turbulent flow: that of

1. the existence of overlapping inner and outer layers of the flow, in which separate equations for velocity profiles hold, and that of
2. the approximate independence of these profiles on the mean-flow Reynolds number.

Further subsections are devoted to the details of velocity profiles in the inner and outer layers of flows for which the diameter of the sediment on the bed is far smaller than the flow depth.

Energy

In making some simplifying assumptions it helps to take a closer look at the nature of turbulence in a channel flow. I will present some arguments that I hope will make some sense to you even though they cannot be developed rigorously here. In what follows,

remember that kinetic energy, a quantity $mv^2/2$ associated with a body with mass m moving with velocity v, is changed only when an unbalanced force does work on the body, and the change in kinetic energy is equal to the work done. The change in kinetic energy caused by the action of certain forces like gravity can be recaptured without any loss of mechanical energy, but the work done by frictional forces represents conversion of mechanical energy into heat.

I will start with laminar flow because the energy bookkeeping is simpler (Figure $4.7.2$A). The viscous shear stress acting across the shear planes does work against the moving fluid. (Remember that a force does work on a moving body provided that there is a component of the force in the direction of movement of the body, as is the case here.) The viscous shear stress is the mechanism that converts potential energy into heat, the heat then being transferred to the surroundings by conduction or radiation. The particular magnitude of kinetic energy in the flow in the process of this conversion is an outcome of the dynamics of the flow.

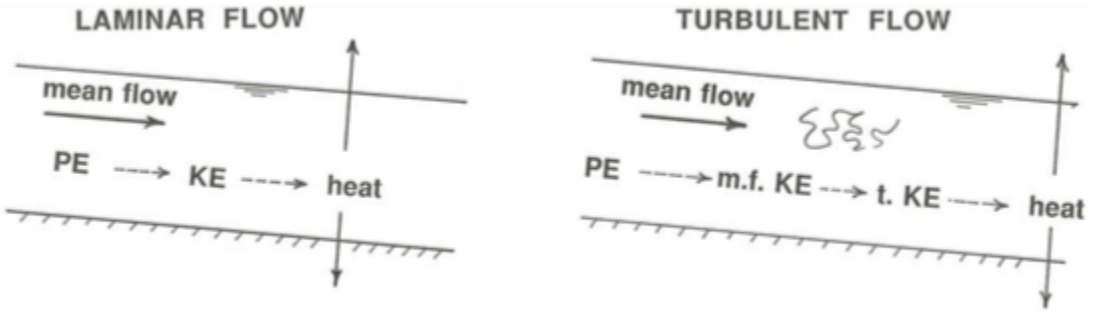


Figure $4.7.2$: Energetics of **A)** laminar open-channel flow and **B)** turbulent open-channel flow.

In turbulent flow (Figure $4.7.2$B), kinetic energy is contained not just in the mean flow but also in the turbulent fluctuations. Potential energy is again converted to heat, but the way the flow mediates this conversion, and therefore the picture of kinetic energy in the flow, is more complicated. This is because energy is extracted mainly by the work done against the mean motion by the turbulent shear stress rather than by the viscous stress, because at all levels in the flow except very near the bottom the former greatly overshadows the latter. This work done by the turbulent shear stress transforms the kinetic energy of the mean motion into kinetic energy associated mostly with the largest eddies, which have the dominant role in the turbulent shear stress because they are the longest-range carriers of fluid momentum. But not much of this turbulent kinetic energy is converted directly into heat in these large eddies, because they are so large relative to the velocity differences across them that shear rates in them are very small.

Then where does the kinetic energy go? Answer: it is handed down to smaller eddies. This phrase “handed down” might strike you as plausible but unilluminating. Large eddies degenerate or become distorted into smaller eddies in ways not elaborated here, and when this happens the kinetic energy that was associated with the large eddies becomes “transferred to” (that is, is now associated with) the smaller eddies. But the odds are all against smaller eddies organizing themselves again into larger eddies—just watch the breakup of regular flow in a smoke plume to get the sense that the natural tendency in turbulent motions is for larger-scale motions to be broken up into smaller-scale motions. So in terms of kinetic energy, turbulence is largely a one-way street: it passes energy mostly from large scales to small scales, not in the other direction. This effect is called an **energy cascade**. Shear rates are greatest in the smallest eddies because of their small size relative to the velocity differences across them, and it is in these smallest eddies that most of the kinetic energy is finally converted into heat. In fact, the reason why there is a lower limit to eddy size is that below a certain scale the viscous shear stresses are so strong that they damp out the velocity fluctuations.

A very significant consequence is that viscosity has a direct effect on turbulence only at the smallest scales of turbulent motion. If the mean- flow Reynolds number is increased, the energy cascade is lengthened at the smallest scales by development of even smaller eddies, but the structure of turbulence at larger scales is not much changed (Figure $4.7.3$). So any bulk characteristic of the flow that is governed by the large-scale turbulence— like the velocity profile, which depends mainly on the turbulent exchange of fluid momentum—should be only slightly dependent on the Reynolds number. This effect is called **Reynolds-number similarity**.



Figure 4.7.3: Increase in the range of eddy scales as a function of mean- flow Reynolds number.

Inner and Outer Layers

Now back to velocity profiles. I want to convince you that two different but overlapping regions or layers of the flow can be recognized (Figure 4.7.4) in which the velocity profile depends not on the full list of variables τ_o, ρ, μ, D, y, and d used in the dimensional analysis above but on certain subsets. The advantage is that in each of these layers there is then a simpler functional relationship for the velocity profile, one that leads to a curve in a two-dimensional graph that holds very well for almost the entire range of turbulent channel flows. I will wave my arms a little about the various variables, but of course the most convincing evidence is that this is how things actually work out, as you will see.

Near the bottom boundary, in what I called the buffer zone and for a ways outside it, the turbulence is small-scale and intense, and both production and dissipation of turbulent kinetic energy are known from actual measurements to be at a peak. It is reasonable to view the dynamics of the turbulence, and therefore the nature of the velocity profile, as being controlled by local effects and substantially independent of the nature of the turbulence in the rest of the flow, all the way up to the free surface. This is also true of the viscous sublayer, if one is present, because there the velocity profile is controlled by the strong viscous shear adjacent to the solid boundary. The velocity profile in this inner layer thus depends on τ_o, D, ρ, μ, and y, but not on d.

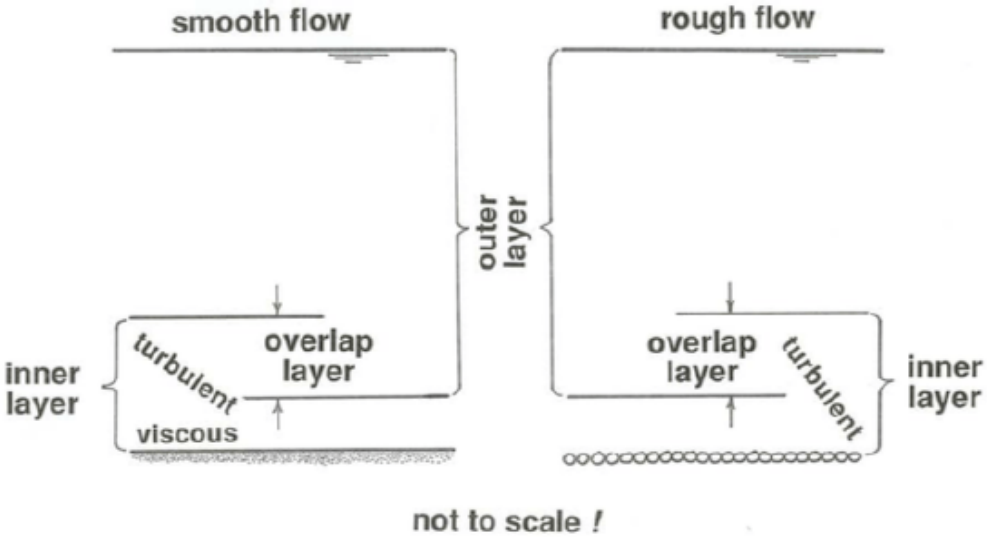


Figure 4.7.4: Layers in turbulent open-channel flow.

On the other hand, over most of the flow depth, from the free surface all the way down to the top of the buffer layer in smooth flow, you have seen already from the discussion of turbulent energy that the velocity profile should be largely independent of μ. If the boundary is rough, the profile should be independent of D as well as of μ down to a position just far enough above the roughness elements that the turbulence shed by the elements is not important in the turbulence dynamics. But you should expect the profile to depend on d, because the size of the largest eddies is proportional to the flow depth. The velocity profile in this outer layer (here I have generalized the significance of the concept of the outer layer introduced in an earlier section) should thus depend on τ_o, ρ, d, and y, but not on D or μ.

If you scrutinize the definitions of the inner and outer layers in the last two paragraphs in the light of what I have said about the structure of the flow, you will see that *they are likely to overlap*. In other words, there is a zone where the velocity profile is at the same time independent of all three variables d, μ, and D. This should be true so long as the mean-flow Reynolds number is high

enough (well beyond the laminar–turbulent transition) that the viscosity-dominated zone near the boundary is very thin relative to the flow depth. (Remember that the thickness of the viscous sublayer decreases as the Reynolds number increases, because the Reynolds number is a measure of the relative importance of inertial forces and viscous forces.)

You are probably thinking by now that I have presented you with a confusion of layers. I will summarize them at this point. On the one hand, in terms of the relative importance of viscous shear stress and turbulent shear stress it is natural to recognize three intergrading but well defined zones (the viscous sublayer, the buffer layer, and the outer layer) or, more generally, a viscosity-dominated layer below and a turbulence- dominated layer above. On the other hand, in terms of importance or unimportance of variables (a related but not identical matter), two overlapping layers can be recognized: an inner layer in which the mean velocity, and other mean characteristics of the flow as well, depends on μ or D (or both) but not d, and the same outer layer in which the mean velocity depends on d but not on μ or D. In rough flow the entire thickness of the flow is dominated by turbulence, and there is no viscosity-dominated layer—but there are still inner and outer layers.

The Law of the Wall for Smooth Boundaries

Look first at the inner-layer velocity profile over a physically smooth bottom boundary. From what was just said about the inner layer,

$$\overline{u} = f\left(\tau_0, \rho, \mu, y\right) \tag{4.7.5}$$

or in dimensionless form,

$$\frac{\overline{u}}{u} = f\left(\frac{\rho u_* y}{\mu}\right) \tag{4.7.6}$$

Equation 4.7.6 states that the velocity u , nondimensionalized using u_*, depends only on y^+, the dimensionless distance from the bottom. So the velocity profile should be expressible as a single curve for all turbulent channel flows with smooth bottom boundaries. Equation 4.7.6 is the general form of what is called **the law of the wall for smooth boundaries**.

You should expect the velocity profile expressed in Equation 4.7.6 to be in two parts, one corresponding to the viscous sublayer and the other to the outer part of the inner layer, where turbulent shear stress predominates over viscous shear stress. These two parts of the profile have to pass smoothly one from the other in the intervening buffer layer. Because fluid accelerations are unimportant in the viscous sublayer, u there depends on τ_o, μ, and y, but not on ρ:

$$\overline{u} = f\left(\tau_0, \mu, y\right) \tag{4.7.7}$$

The only way to write Equation 4.7.7 in dimensionless form is

$$\frac{\mu u}{\tau_o y} = \text{const} \tag{4.7.8}$$

because there is only one way to form a dimensionless variable from the four variables $\overline{u}$, τ_o, μ, and y. Equation 4.7.8 can be juggled algebraically a little by introducing ρ on both sides, for no other reason than to put it in the same form as Equation 4.7.6:

$$\frac{\overline{u}}{u_*} = \text{const}\frac{\rho u_* y}{\mu} \tag{4.7.9}$$

The constant in Equation 4.7.9 turns out to be unity. To get an idea why, go back to Equation 4.2.7, the exact solution for the velocity profile in laminar channel flow. It is reasonable to expect that the velocity profile in the viscous sublayer of a turbulent channel flow is like the velocity profile near the boundary in a laminar channel flow. Points near the boundary in laminar flow, where the velocity gradient $d\overline{u}/dy$ is very large, are way out on the limb of the parabola in Equation 4.2.7, so the second term on the right in Equation 4.2.7 can be neglected and u assumed to be a linear function of y/d:

$$\overline{u} = \frac{\tau_o}{\mu d}(yd) \tag{4.7.10}$$

When cast in the same form as Equation 4.7.9, this becomes

$$\frac{\overline{u}}{u_*} = \frac{\rho u_* y}{\mu} \tag{4.7.11}$$

Equation 4.7.11 represents the specific part of the law of the wall for a dynamically smooth flow inside the viscous sublayer. Figure 4.7.5 shows that Equation 4.7.11 is in good agreement with careful velocity measurements in the viscous sublayer.

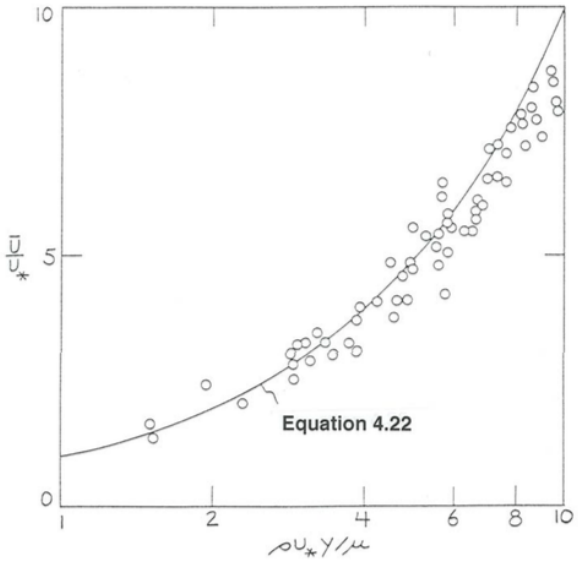


Figure 4.7.5: Plot of dimensionless mean flow velocity $\overline{u}/u_*$ vs. dimensionless distance from boundary, $\rho u_* y/\mu$, for the viscous sublayer in turbulent open-channel flow. This plot represents the law of the wall inside the viscous sublayer.

In the outer, turbulence-dominated part of the inner layer over a physically smooth bottom, we can assume that $d\overline{u}/dy$ does not depend on μ, because the shear stress and therefore the velocity gradient is determined almost entirely by turbulent momentum exchange (see Equation 4.7.1). On the other hand, u itself must depend on μ, because the velocity profile in the turbulence-dominated part of the inner layer must be connected to that in the viscosity-dominated part, and you have just seen that the velocity profile in the viscous sublayer depends on μ. In other words, the velocity at the base of the turbulence-dominated part of the inner layer depends on the velocity at the top of the viscous sublayer, which in turn depends on μ. The viscosity-dominated part of the profile can be viewed as "anchoring" the turbulence-dominated part of the profile to the bottom, where the velocity is zero by the no-slip condition. So to get the velocity profile we have to start with the velocity gradient, rather than the velocity itself, and write $d\overline{u}/dyy = f(\tau_0, \rho, y)$ in dimensionless form as

$$\frac{y}{u_*}\frac{du}{dy} = A \tag{4.7.12}$$

where A is a dimensionless constant that should hold in this particular layer for all turbulent channel flows over smooth boundaries, and then integrate to obtain the dimensionless velocity profile:

$$\frac{\overline{u}}{u_*} = A\ln y + A_1 \tag{4.7.13}$$

where A_1, also dimensionless, is a constant of integration. By the concept of Reynolds-number similarity discussed above, A should be very nearly constant provided that the Reynolds number is high enough for the turbulence to be fully developed.

Note that Equation 4.7.13 does not contain μ explicitly, but from what was said above, μ has to be in there somewhere. The resolution of this seeming paradox is that the constant of integration A_1 must depend upon μ. You can verify that this is so by noting that Equation 4.7.13 can be put into the general form of the law of the wall given by Equation 4.7.6 if and only if A_1 is equal to $A\ln(\rho u_*/\mu) + B$: putting this expression for A_1 into Equation 4.7.13,

$$\begin{aligned}\tfrac{\overline{u}}{u_*} &= A\ln y + A\ln\tfrac{\rho u_*}{\mu} + \mathrm{B}\\ &= A\ln\frac{\rho u_* y}{\mu} + B\end{aligned} \tag{4.7.14}$$

The constant B is just the residuum of the constant of integration after $A\ln(\rho u_*/\mu)$ has been extracted.

There is no universal agreement in the literature on the values of the constants A and B: A is usually taken to be between 2.4 and

2.5, and B is taken to be between 5 and 6. The small differences in A and the larger differences in B from source to source are an understandable result of fitting straight lines in semilogarithmic plots of slightly scattered data from diverse experimental studies. Discussions on the values of these constants can be found in Monin and Yaglom (l971) and Hinze (1975). With the commonly used values $A = 2.5$, $B = 5.1$, Equation 4.7.14 becomes

$$\frac{\overline{u}}{u_*} = 2.5 \ln \frac{\rho u_* y}{\mu} + 5.1 \tag{4.7.15}$$

The constant A, which is a reflection of the nature of turbulent momentum transport in the inner layer, is often written $1/\kappa$, and κ is called **von Kármán's constant**. Thus, κ has a value very nearly 0.4. The reason A is written as $1/\kappa$ is historical, not fundamental. Also, you should expect a weak dependence of A on the mean-flow Reynolds number. The exact nature of variation of A with the Reynolds number, and with the suspended- sediment concentration in sediment-transporting flows as well, has been controversial.

Equation 4.7.15 shows that the velocity profile is expressed by a single curve for the turbulence-dominated part of the inner layer, just as was the case for the viscosity-dominated part. It is the profile given by Equation 4.7.15 that is usually called the law of the wall, although that term more properly describes the whole inner-layer profile, viscosity-dominated and turbulence-dominated, plus the transition between.

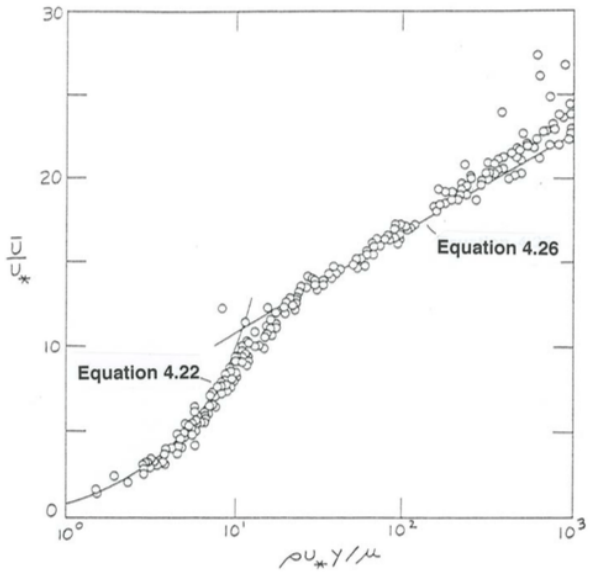


Figure 4.7.6: Plot of dimensionless mean flow velocity $\overline{u}/u_*$ vs. dimensionless distance from the boundary, $\rho u_* y/\mu$, for the inner layer over a smooth boundary in turbulent open-channel flow. This plot represents the law of the wall for dynamically smooth flow.

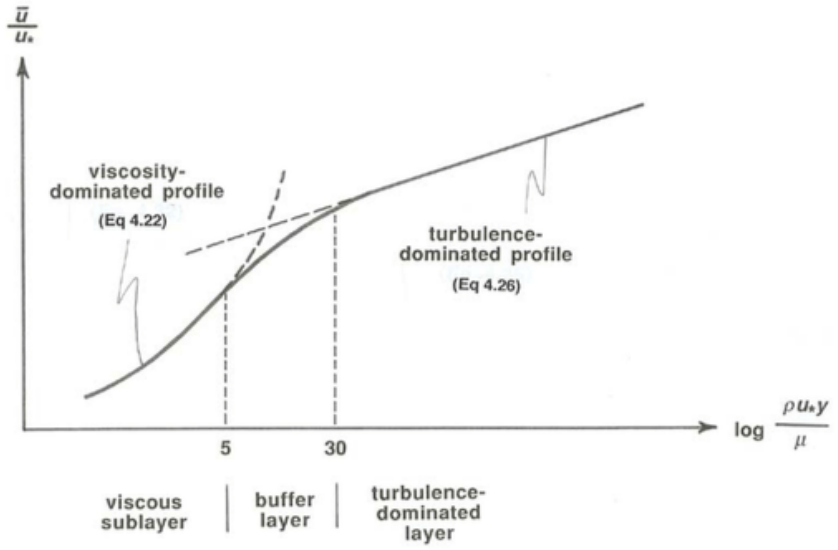


Figure $4.7.6$.

In summary, time-average velocity u in the inner layer over a smooth boundary, when nondimensionalized by dividing by u_*, should plot as a single curve as a function of y^+, the dimensionless distance above the bottom. Figure $4.7.6$, which incorporates the data already plotted in Figure $4.7.5$ for the viscous sublayer, shows the velocity profile through the whole of the inner layer over a smooth boundary. This profile represents the complete law of the wall for smooth boundaries. The data points in the viscosity-dominated part of the inner layer follow Equation $4.7.11$; the data points in the turbulence-dominated part of the inner layer follow Equation $4.7.15$, which plots here as a straight line because of the semilogarithmic coordinates.

Between y^+ values of about 5 and about 30 in Figure $4.7.6$ there is a smooth transition between the viscosity-dominated profile (Equation $4.7.11$) and the turbulence-dominated profile (Equation $4.7.15$); see Figure $4.7.7$. This is the buffer layer, where viscous shear stress and turbulent shear stress are both important. For $y^+ < 5$ the turbulent shear stress is negligible, and Equation $4.7.11$ describes the profile; for $y^+ > 30$ the viscous shear stress is negligible, and Equation $4.7.15$ describes the profile. It is in wall-law plots like Figure $4.7.6$ that the lower and upper limits of the buffer layer are most clearly manifested. You will see a variety of lower and upper limiting y^+ values mentioned in the literature; this is understandable, because the divergence of the curves given by Equations $4.7.11$ and $4.7.15$ from the actual profile is gradual. Although it is of no great physical significance, the height of intersection of Equations $4.7.11$ and $4.7.15$ in the buffer layer is at $y^+ = 11$, as you can see from Figure $4.7.6$. What is of greater significance is that the turbulent shear stress and the viscous shear stress are found experimentally to be equal at a slightly larger y^+ value of about 12; this is in a sense the "middle" of the buffer layer.

The dimensionless height y^+ above the boundary at which $\overline{u}/u_*$ begins to deviate from the law of the wall depends on the mean-flow Reynolds number Re; it ranges upward from around 500 at small Re to over 1000 at larger Re. For y^+ greater than this, $\overline{u}/u_*$ is greater than predicted by the law of the wall.

How thick is the inner layer? The upper limit of y^+ for the law of the wall at high Reynolds numbers for open-channel flow is not well established, but assume a y^+ value of 1000 in a flow of room-temperature water $1\ \mathrm{m}$ deep at a mean flow velocity of $0.5\ \mathrm{m/s}$. Then y at the outer limit of the inner layer is about $5\ \mathrm{cm}$. (To figure this out, compute Re, use the smooth-flow curve in Figure 4.6.7 to get f and therefore τ_o, and put that into y^+.) So the inner layer occupies only a small percentage of the flow depth, no more than $10 - 20\%$. And the viscous sublayer in this flow is only a fraction of a millimeter thick. Note that the logarithmic abscissa axis in plots like Figure $4.7.6$ crowds the whole outer layer, in which Equation $4.7.15$ no longer holds, into a small part of the graph.

Most of the data points in Figure $4.7.6$ are from flows in circular pipes and rectangular ducts rather than from open-channel flows. But data from open-channel flows, and from boundary layers developing on flat plates as well, are consistent with those from flow in pipes and ducts. This emphasizes the important point that the law of the wall holds for a wide variety of geometries of outer-layer flow. From the earlier discussion of variables important in the inner and outer layers, this should be no surprise: the flow in the inner layer is governed by local effects and is independent of the nature of the outer flow. In fact, the law of the wall is even more general: although we won't pursue the matter here, the law of the wall holds even when there is a substantial pressure gradient (negative or positive) in the direction of flow, resulting in downstream acceleration or deceleration.

The Law of the Wall for Rough Boundaries

In many turbulent boundary-layer flows, the boundary is not physically smooth but instead is occupied by, or is covered by, or consists of, roughness elements of some kind. By the term **roughness element** I mean any local part of the boundary that protrudes above the overall or average boundary surface. Such things as buildings, trees, crops, people, water waves, sand particles, boulders, or corrosion scales come readily to mind. In what follows, we will assume (Figure 4.7.8) that the roughness elements are much smaller than the flow depth $(D << d)$ and that the layer of the flow we will consider, for now, has a thickness that is not a large fraction of the flow depth $(y << d)$. Provided that the roughness elements are not much smaller than the thickness of the viscous sublayer, the velocity profile in the boundary layer depends on the size, shape, and arrangement of the roughness elements as well as on τ_o, ρ, μ, and y:

$$\overline{u} = f\left(\tau_o, \rho, \mu, y, \text{ roughness geometry}\right) \tag{4.7.16}$$

where the roughness geometry is specified by the size distribution, the shape distribution, and the plan-view packing or arrangement of the roughness elements.

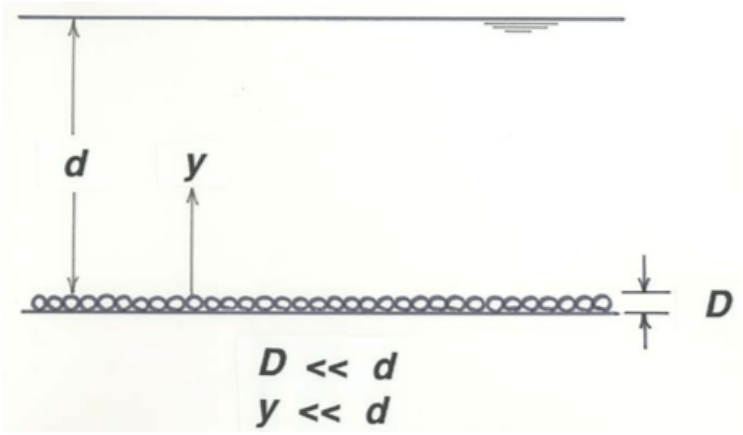


Figure 4.7.8: Definition sketch for analysis of mean velocity profiles in dynamically rough flow.

To make any progress we have to be specific about the nature of the roughness. Assume here that the roughness is composed of fairly well sorted mineral sediment particles with the usual natural range of particle shape and roundness, and that the particles form a full sediment bed that is planar on a large scale. Roughness of this kind, called *close-packed granular roughness* by fluid dynamicists, is fairly well characterized by the single variable D, the mean or median particle size. This roughness is the best-studied kind, and it is important in a great many natural water flows over sediments, but there are many other kinds of roughness, in both nature and technology.

With the above simplifications, Equation 4.7.16 becomes

$$\overline{u} = f\left(\tau_0, \rho, \mu, y, D\right) \tag{4.7.17}$$

or, in dimensionless form,

$$\frac{\overline{u}}{u_*} = f\left(\frac{\rho u_* y}{\mu}, \frac{\rho u_* D}{\mu}\right) \tag{4.7.18}$$

So for flow over rough boundaries the dimensionless velocity u/u_* generally depends not only on y^+ but also on the boundary Reynolds number. Equation 4.7.17, which could also be written using y/D instead of $\rho u_* D/\mu$, is called **the law of the wall for granular-rough boundaries**.

Two different aspects of the effect of the roughness on the velocity profile become apparent upon examination of Equation 4.7.18. First, the size of the roughness elements relative to the thickness of the viscous sublayer is important. Remember from the section on smooth flow and rough flow earlier in this chapter that if D is much smaller than the viscous length scale $\mu/\rho u_*$ the roughness elements are embedded in the viscous sublayer, whereas if D is much larger than $\mu/\rho u_*$ there is no viscous sublayer and the roughness elements are enveloped in turbulence generated by flow separation around upstream elements. You should suspect, then, that for very small $\rho u_* D/\mu$ (less than about 5, for which viscous-sublayer thickness and roughness height are about equal),

the roughness has no effect on the velocity profile. Under these conditions the velocity profile over physically rough boundaries is indeed found to coincide with that over physically smooth boundaries—provided that we do not place our velocity meter so close to the bed that individual roughness elements distort the velocity field. The law of the wall for smooth boundaries, Equations 4.7.11 and 4.7.15 together with the transition between them through the buffer layer, therefore holds for flows with $\rho u_* D/\mu < 5$ over physically rough boundaries also. These are the flows that in the section on flow resistance were termed dynamically smooth even though physically rough and were shown to fall on the curve for physically smooth boundaries in the resistance diagram in Figure 4.6.7. For very large $\rho u_* D/\mu$, however, there is no viscous sublayer and therefore no effect of μ on the velocity profile, and you should expect to see a velocity profile that is rather different from the law of the wall for smooth flow. The next two subsections are devoted to the velocity profile in these dynamically rough flows.

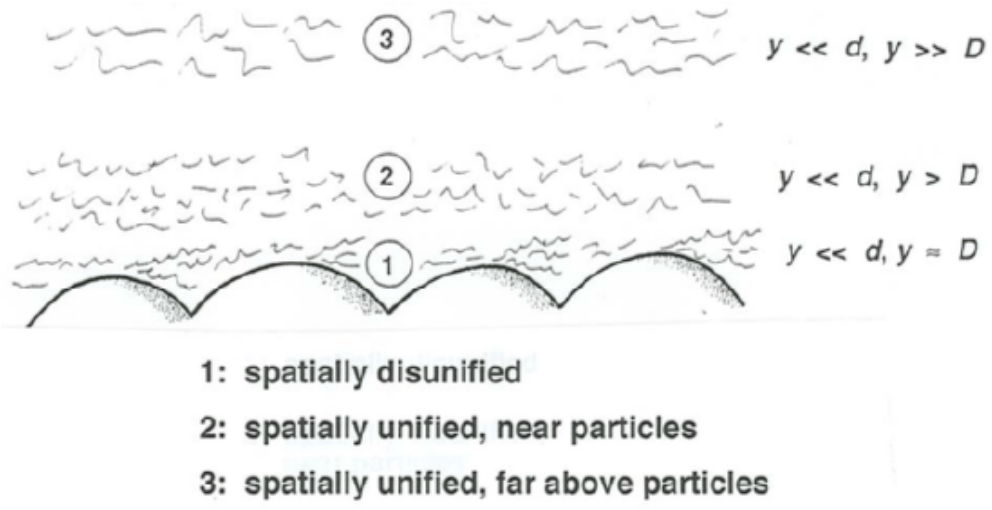


Figure 4.7.9: Differing regions of flow as a function of distance from the boundary in dynamically rough flow.

Second, in the case of rough flow the value of y relative to D is important (Figure 4.7.9). For $y \approx D$, at points in the flow that are nestled among the roughness elements themselves or are just a few roughness heights above the tops of the roughness elements, the velocity depends in a complicated way on the shapes of the roughness elements and on the position of the profile relative to individual elements, and we should not expect to find any generally applicable profile; the velocity profile could be said to be *spatially disunified*. A bit higher in the flow, several diameters above the tops of the elements, the wakes shed by individual elements blend together in such a way that the velocity profile is about the same at all positions, but the flow structure is still affected by the roughness- generated turbulence. Far above the tops of the elements, however, for $y >> D$, it is reasonable to expect that the turbulence structure is governed by local dynamics, as in smooth flow, and not by the wakes from the little roughness elements far below. If D is sufficiently smaller than the flow depth d, there should then be a layer of the flow for which $y << d$ and $y >> D$ at the same time—that is, a part of the inner layer in which roughness-generated turbulence is not of direct importance. Remember, however, that by analogy with what was said about smooth flow above, this part of the profile still has to be anchored at its lower end to that part of the velocity profile controlled by the roughness-generated turbulence.

In the following I will present the velocity profile in rough flows for which there is indeed a zone for which $y << d$ but at the same time $y >> D$ (or, more precisely, above the near-bed layer of spatial disunification of the profile, which is something like several roughness heights above the tops of the roughness elements). I will deal only with the region far enough above the bed that the roughness elements do not affect the profile shape; this could be called “the inner layer far above the roughness elements”. I will make only a few brief comments about the equally important flows in which there is no zone for which $y << d$ and $y >> D$, examples being shallow flows in gravel-bed streams.

In the part of the inner layer for which $y >> D$, neither μ nor D affects the slope of the velocity profile. We can therefore make exactly the same statement as for the turbulence-dominated part of the inner layer in physically smooth flow: the velocity gradient $d\overline{u}/dy$ depends only on τ_o, ρ, and y. This leads again to Equation 4.7.12, and upon integration, to Equation 4.7.13. We should even expect the constant A to be the same, because it is a manifestation of the vertical turbulent transport of streamwise fluid momentum, and we just concluded that sufficiently far from the boundary the structure of the turbulence depends only on local effects and is independent of the turbulence shed by the boundary roughness. The constant of integration A_1, however, is *different*, because it depends on the nature of the connecting velocity profile nearer the boundary, which is different from that in smooth flow. This latter difference has to do with the relative importance of viscous shear stress and turbulent shear stress near the boundary, and with the relative importance of viscous drag and pressure drag at the boundary: if $D >> \mu/\rho u_*$ (I termed

such flows fully rough), viscous shear stress in the flow and viscous drag on the boundary are negligible, so not only the velocity gradient but also the velocity itself is unaffected by μ in the layer under consideration here.

We can rearrange Equation 4.7.13 to obtain Equation 4.7.14 just as in the case of smooth flow, but with one important difference: by comparison with the general form of the law of the wall for rough flow (Equation 4.7.18), the term B is now not a constant but instead a function of the boundary Reynolds number:

$$\frac{\overline{u}}{u_*} = A \ln \frac{\rho u_* y}{\mu} + f\left(\frac{\rho u_* D}{\mu}\right) \tag{4.7.19}$$

Equation 4.7.19 can be put into an equivalent but more revealing and more useful form by splitting $f(\rho u_* D/\mu)$ into two parts: $-A \ln (\rho u_* D/\mu)$ plus a remainder that is some different function of $\rho u_* D/\mu$, which I will call B'. The only reason for this otherwise arbitrary choice is that now Equation 4.7.19 can be written

$$\begin{aligned} \frac{\overline{u}}{u_*} &= A\left(\ln \frac{\rho u_* y}{\mu} - \ln \frac{\rho u_* D}{\mu}\right) + \mathrm{B}' \\ &= A \ln \frac{y}{D} + B' \end{aligned} \tag{4.7.20}$$

Equation 4.7.20 is neater than Equation 4.7.19, but remember that B' is a function of $\rho u_* D/\mu$. If $\rho u_* D/\mu$ is sufficiently large, however, so that D is large relative to what the viscous-sublayer thickness would be, turbulence extends down among the roughness elements and there is no viscosity-dominated layer next to the bottom. The velocity profile then cannot depend on μ and therefore not on $\rho u_* D/\mu$, so B' in Equation 4.7.20 is a constant, which has a value of about 8.5 for uniform, close-packed sand-grain roughness. (There is about as much uncertainty about this constant as there is about the constant B in Equation 4.7.14 .) The value of B has indeed been found experimentally to become constant for $\rho u_* D/\mu > 60$. It is under these conditions that the flow was termed fully rough in the earlier section on flow resistance. Equation 4.7.20 can then be written as Equation 4.7.21, *the law of the wall for fully rough flow*:

$$\frac{\overline{u}}{u_*} = 2.5 \ln \frac{y}{D} + 8.5 \tag{4.7.21}$$

Figure 4.7.10 shows Equation 4.7.21 together with the data from Nikuradse (1933) on which the value of 8.5 for B' was originally derived. Nikuradse's data were obtained for a particular geometry of granular roughness manufactured by gluing a somewhat open monolayer of subrounded and almost single-size sand to the inner walls of circular pipes. You should expect the value of B' to be different for different roughness geometries, even if the average roughness height is the same, because the shape and arrangement of the roughness elements would be different, and this affects the details of the turbulence structure right near the boundary and thus also the velocity profile right near the boundary.

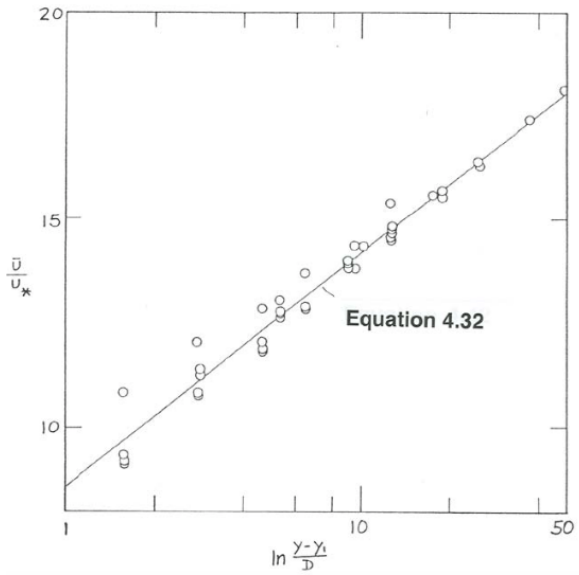


Figure 4.7.10: Plot of $\overline{u}/u^*$ vs. y/D for the inner layer over granular-rough boundaries. Data are from Nikuradse (1933) for runs with pipe radius $> 60D$. Only data for which $\mathrm{Re}^* > 60$ are shown, so this plot represents the law of the wall for dynamically fully rough flow. All points up to 0.2 times the pipe radius are shown. Included are eight profiles from four sand-lined pipes. As described in a later section, the $y = 0$ level has been adjusted downward from the tops of he grains a distance $y/D = -0.36$ to extend the straight-line fit as close to the bed as possible.

Figure 4.7.11 is another plot of Equation 4.7.21, this time without the data points. It is meant to serve as a warning about how close to the boundary Equation 4.7.21 actually applies. Recall that at heights no greater than a few roughness-element sizes, the flow can be said to be spatially disunified (see Paragraph 114 above), and in that region the basis for derivation of Equation 4.7.21 no longer holds. That is emphasized, in cartoon form, by the blurring of the profile near the rough boundary.

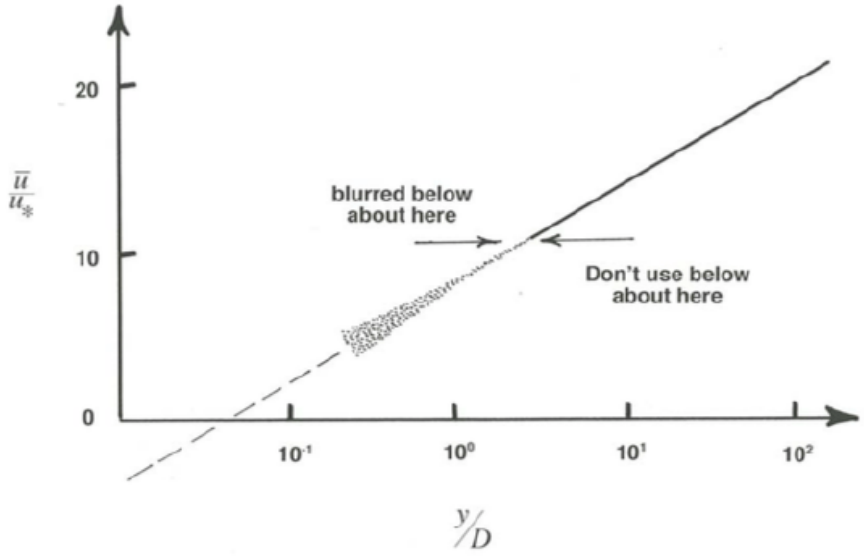


Figure 4.7.11: Plot of $\overline{u}/u^*$ vs. y/D for the inner layer over granular-rough boundaries (Equation 4.7.21), showing the region near the bed where the profile fails to follow Equation 4.7.21.

As is commonly done, you can preserve the value of 8.5 for B' in Equation 4.7.20 and use for D the fictitious diameter of single-size sand grains in a uniform monolayer that makes Equation 4.7.20 fit the velocity data best. That size is called the equivalent sand roughness, usually denoted k_s. (A more descriptive term would be the "equivalent Nikuradse- style sand roughness".) In other words, k_s for any given bed roughness, of any kind whatever, is the uniform-sand-grain height that gives the same wall-law velocity distribution for a given value of τ_o. On the face of it this seems like a neat way around the problem of what the value of B' is, but keep in mind that to determine B' in the first place you need to measure both the velocity profile and the boundary shear stress, independently, at the same time.

For $5 < \rho u_* D/\mu < 60$ the flow is said to be *transitionally rough*. The velocity profile is still a semilog straight line for $y >> D$, whether $\overline{u}/u_*$ is plotted against $\rho u_* y/\mu$ as in Figure 4.7.6 or against y/D as in Figure 4.7.10, and it still has the same slope given by the universal constant A. But the position of the straight line varies as the near-bed part of the profile changes from the smooth-flow profile shown in Figure 4.7.6 to the fully rough profile shown in Figure 4.7.10. For transitionally rough flows, the law of the wall in the innermost region, where there is some dependence on μ, cannot be derived in the form of a simple equation like Equation 4.7.15 or Equation {4.31}; keep in mind, however, that some form of the general law of the wall for rough boundaries (Equation 4.7.19) holds there nonetheless.

Finally, if $\rho u_* D/\mu$ is very small the roughness elements are deeply embedded in the viscous sublayer and can have no effect on the structure of the turbulence and the shape of the velocity profile above the viscous sublayer. The velocity profile is then the same as if the boundary were physically smooth. As discussed earlier in the section on flow resistance, the flow is dynamically smooth even though physically rough.

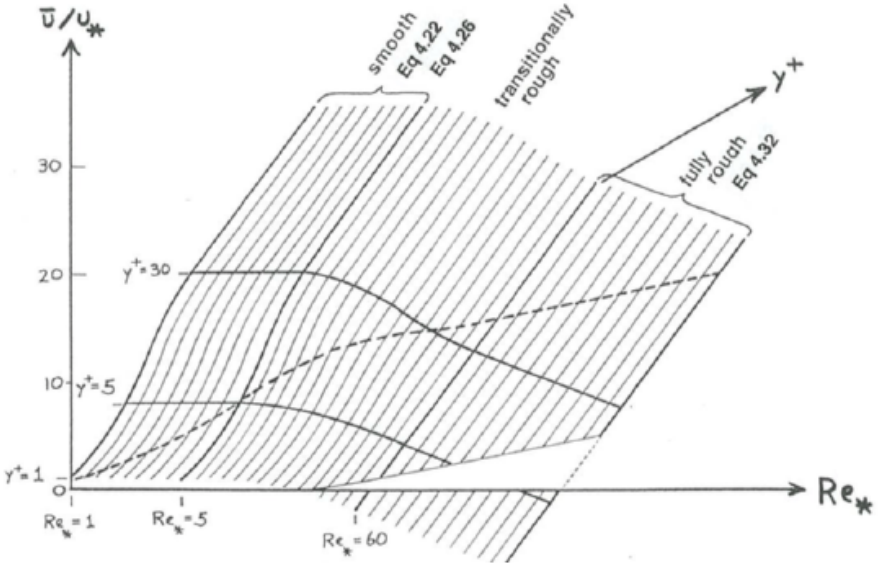


Figure 4.7.12: Combined plots of the law of the wall in smooth, transitionally rough, and fully rough flows.

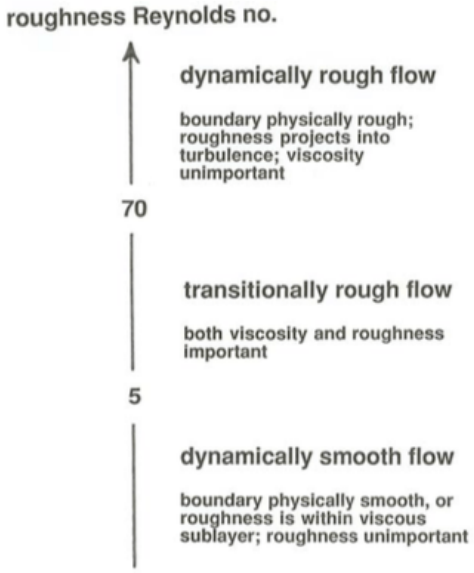


Figure 4.7.13: Ranges of roughness Reynolds number for dynamically smooth flows, transitionally rough flows, and fully rough flows.

Figure 4.7.12, a combined plot of the law of the wall in smooth and rough flows, summarizes much of what is in this section and the previous one (see also Figure 4.7.13). The three-dimensional surface in Figure 4.7.12, drawn by use of Equations 4.7.11, 4.7.15, and 4.7.21, shows $\overline{u}/u_*$ as a function of $y^(+)$ and Re_*. In smooth flows, represented by the left-hand part of the surface, the velocity profiles do not depend on Re_*, so the surface is a cylinder whose elements are parallel to the Re_* axis. Each of the

several profiles shown, which represent intersections of the surface with planes for which $\mathrm{Re}_* = const$, is exactly the same as that in Figure 4.7.6. In fully rough flows, represented by the region to the right of the plane $\mathrm{Re}_* = 60$, the velocity profiles depend only on y/D. To see why the right-hand part of the surface slopes downward to the right, write $\ln(y/D)$ as $\ln(\rho u_* y/\mu) - \ln(\rho u_* D/\mu)$, or $\ln y^+ - \ln \mathrm{Re}_*$; thus, the larger the value of Re^*, the smaller the value of $\overline{u}/u_*$ for a given value of y^+. Because there is no viscous sublayer or buffer layer to contend with, the profiles are straight lines all the way down to positions not far above the tops of the roughness elements. The rough-wall profile deviates from a semilog straight line within several roughness heights above the tops of the roughness elements—to say nothing of the spatial disunification of the velocity profile that sets in at a level just above the tops of the roughness elements. Only at points on the surface in Figure 4.7.12 well above the dashed curve that expresses the condition $y = D$ are the profiles valid; the part of the surface shown in the lower right is therefore useful only hypothetically, for displaying the nature of the relationships. Finally, in the middle part of the surface the profiles are transitional between the smooth and the fully rough profiles. Here the lines for $y^+ = 5$ and $y^+ = 30$ shown on the left-hand part of the surface lose their physical significance as the viscous sublayer disappears.

Note in Figure 4.7.12 that at any value of y^+ well up in the inner layer $\overline{u}/u_*$ in any rough flow is less than $\overline{u}/u_*$ in any smooth flow, although the slopes of the profiles for the two flows are the same at that height. This is because nearer the bottom the velocity increases more sharply with distance from the bottom in smooth flow than in rough flow. Figure 4.7.14 shows that effect, in cartoon form: the profile for rough flow lies everywhere below the profile for smooth flow. You can think of the two profiles shown in Figure 4.7.14 as being representative of the left and right extremes of the surface shown in Figure 4.7.12, given that the surface slopes downward to the right in Figure 4.7.12.

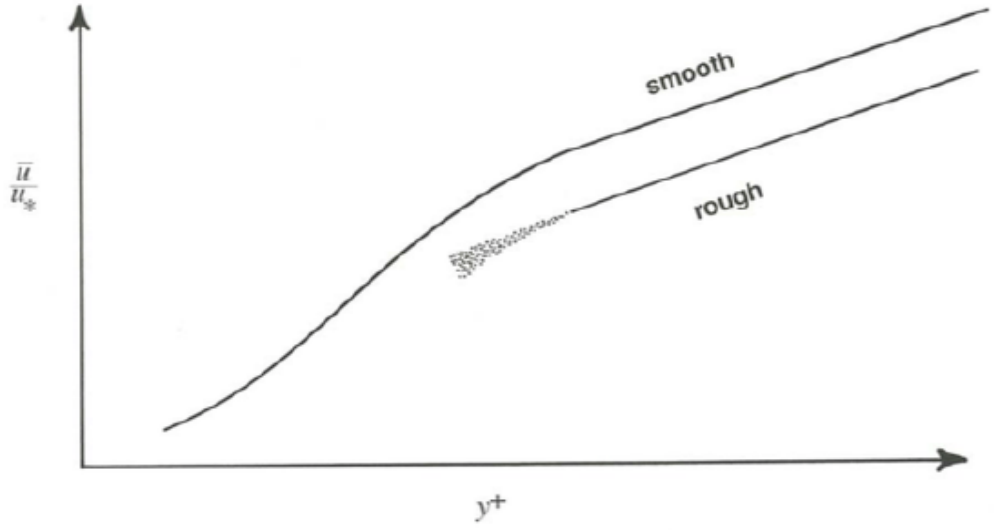


Figure 4.7.14: Cartoon plot showing the comparison between velocity profiles for smooth flow and rough flow.

A conventional additional step that is taken with Equation 4.7.20 is to write B' in the form $-A\ln(y_0/D)$, where the quantity y_o, with the dimensions of length, is called the **roughness length**. (Outdoors fluid dynamicists like meteorologists take the normal-to-boundary coordinate direction to be z, so they deal with z_o, not y_o.) Note: if you read the literature on velocity profiles in natural flow environments, you are likely to encounter this roughness length, rather than the equivalent quantities I have used earlier in this section.

Use of y_o allows B' to be completely absorbed into the log term in Equation 4.7.21:

$$\begin{aligned} \frac{\overline{u}}{u_*} &= A\ln\frac{y}{D} - A\ln\frac{y_o}{D} \\ &= A\ln\frac{y}{y_o} \end{aligned} \tag{4.7.22}$$

By the definition of the natural logarithm, y_o can be written in terms of B' as $y_0 = D\exp(-B'/A)$.

If the flow is only transitionally rough, y_o is a function of $\rho u_* D/\mu$, as is B'. If the flow is fully rough, however, y_o is independent of $\rho u_* D/\mu$ for the same reason that B' in Equation 4.7.19 is independent of $\rho u_* D/\mu$.

Note

Warning: don't confuse y_o with the actual roughness height D: for a given geometry of roughness in fully rough flow y_o is proportional to D (for close-packed uniform sand-grain roughness $y_0 = D/30$), but the proportionality coefficient varies considerably depending upon the particular geometry of the roughness.

Setting y equal to y_o in Equation 4.7.22 gives $\overline{u}/u_* = 0$. So another way of looking at y_o is that it is the height at which the velocity would become zero if the logarithmic rough-wall equation for the velocity profile could be extended down to that height. It is important to remember, however, that Equation 4.7.22 becomes inapplicable far above that position, which is nestled in among the roughness elements. (That is why I used the contrary-to-fact "subjunctive" verb construction in the preceding sentence.) See the very brief comments in the next paragraph.

We still have not considered the lowermost part of the inner layer, not far above the tops of the roughness elements. For sand-size bed roughness this region is not much more than a few millimeters thick, but for water flowing over gravels or for wind blowing over large ground-surface roughness like buildings or vegetation it may be decimeters or even meters thick, and no sophisticated, miniaturized velocity meters are needed to include it in measured velocity profiles. At positions this close to the bed, two complications arise: the logarithmic profile becomes distorted, and there is no obvious choice for $y = 0$.

Velocity Defect Law

Now look at the velocity profile in the outer layer. There the velocity is most naturally specified relative to that at the boundary with the free stream (or, in the case of free-surface flow, relative to the surface velocity, or in the case of pipe flow, relative to the centerline velocity), because we have seen that the inner layer, with a different relationship for the velocity, intervenes between the outer layer and the bottom boundary. In other words, if we look at the velocity relative to that at the surface we do not have to worry about how the velocity is anchored to the bottom through the inner layer. So instead of $\overline{u}$ we use $U_s - \overline{u}$, called the **velocity defect**, where U_s is the surface (i.e., maximum) velocity.

If you go back and review the discussion in the section on inner and outer layers you will see that the structure of the turbulence in the outer layer should depend on τ_o, ρ, y, and d, but not on μ, for the same reason that the velocity profile in the turbulence-dominated part of the inner layer does not depend on μ. Because this is true from the free surface down to the bottom of the outer layer, and because $U_s - \overline{u}$ characterizes the velocity relative to the free surface rather than the bottom, then not just the velocity gradient $d\overline{u}/dy$ (as in the turbulent part of the inner layer) but also $U_s - \overline{u}$ itself is independent of μ. Turbulence structure and $U_s - \overline{u}$ should not depend on D either, provided that $D << d$. So the general form of the velocity-defect profile is

$$U_s - \overline{u} = f\left(\tau_o, \rho, y, d\right) \tag{4.7.23}$$

or in dimensionless form

$$\frac{U_s - \overline{u}}{u_*} = f\left(\frac{y}{d}\right) \tag{4.7.24}$$

Equation 4.7.24 tells us that the dimensionless velocity defect depends only on the dimensionless height above the bottom. This relationship for the velocity profile in the outer layer is called the **velocity-defect law**. I will defer further discussion of velocity profiles in the outer part of the flow until the following section, where an examination of the region of overlap between the inner and outer layers affords further insight into the form of the velocity-defect law.

The Overlap Layer; More on the Velocity-Defect Law

One more matter to consider in this exposition of velocity profiles has to do with the **overlap layer**, where at sufficiently high mean- flow Reynolds numbers the conditions defining the inner and outer layers hold simultaneously; I refer you once more to the earlier section on inner and outer layers. This overlap layer is far enough from the bottom that the flow structure is independent of both viscosity and the characteristics of the bottom roughness but close enough to the bottom that the flow structure is independent of the flow depth (Figure 4.7.15). Here the inner-layer and outer-layer velocity profiles must *match*—that is, the velocities given by the law of the wall and by the velocity-defect law at any level in the overlap layer must be the same. The upper limit of the overlap layer is at the top of the inner layer. In smooth flow the lower limit is at the top of the buffer layer. With regard to the lower limit in rough flow, presumably the velocity-defect representation of the velocity profile, which looks downward from

the free surface and can ignore the details of the bottom roughness, must start to break down when it reaches the lower part of the inner layer, where you have seen that the roughness causes the inner-layer profile to curve away from a semilog straight line.

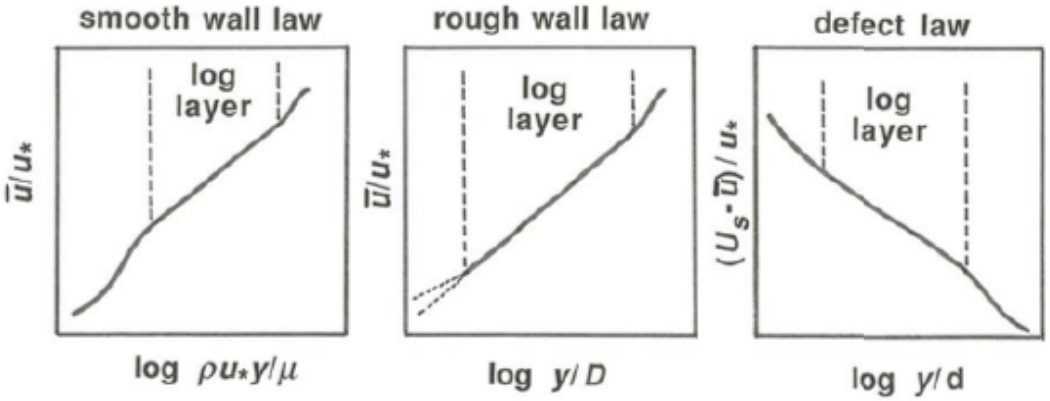


Figure 4.7.15: The overlap layer (the logarithmic layer) for smooth wall law, rough wall law, and velocity defect law.

The constraints imposed by the matching requirement on the form of both the wall law and the velocity-defect law in the overlap layer were first perceived by Izakson (1937) and Millikan (1939). The mathematical consequence of this matching, which I will not detail here, is that in the overlap layer—but not farther out, beyond the inner layer—the velocity-defect law as well as the wall law is of logarithmic form. The overlap layer is often called the **logarithmic layer**, because in it both the wall law and the defect law are logarithmic.

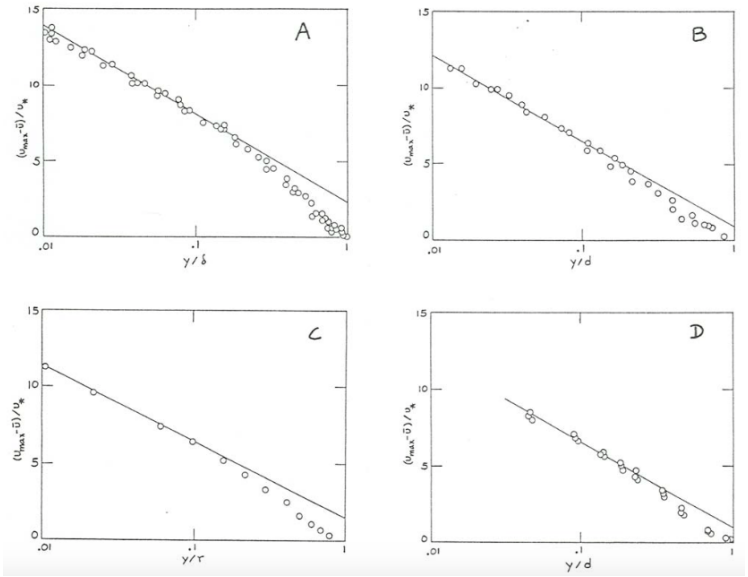


Figure 4.7.16: Velocity-defect profiles: plots of $(U_s - \overline{u})/u_*$ versus y/D in boundary-layer flows with four geometries: **A)** flat plate; **B)** circular pipe; **C)** wide planar duct; and **D)** open-channel flow. After Monin and Yaglom (1971) (various sources), and Coleman (1981). Straight lines with slopes of $-A(=-1/\kappa)$ are fitted to points for $y/d < 0.2$.

Figure 4.7.16 shows velocity-defect profiles on flat plates and in pipes, wide planar ducts, and open channels. The open-channel data, from Coleman (1981), are for a width-to-depth ratio of only about 2, but I have not been able to find any better data; the scarcity of good published data on complete velocity profiles from surface to bottom in steady uniform open-channel flows at large ratios of width to depth is striking. In each graph in Figure 4.7.16 the data points define a single curve that holds for a wide range of mean-flow Reynolds numbers, indicating that our assumptions about the controls on velocity and turbulence in the outer layer are justified. In each graph there is a well-defined semilog straight-line segment for fairly small y/d; that is the log layer. Toward the position of maximum velocity at $y/d = 1$ the profile breaks away from the semilog straight line to reach the point $(U_s - \overline{u})/u_* = 0$ at the position of maximum velocity.

The differing shape of the outer part of the velocity-defect profile in different geometries of flow is to be expected because of differing physical effects in the movement and geometry of large eddies in the region of the flow farthest from the solid boundary. Because the outer edge of a freely growing turbulent boundary layer is highly irregular in shape (Chapter 3), at any point near the

outer edge passage of large turbulent eddies alternates with passage of nonturbulent fluid, so the efficacy of turbulent momentum exchange is less and the velocity gradient correspondingly steeper than in regions closer to the boundary; this explains the large divergence of the profile from the semilog straight-line segment in Figure \({4{.}7{.}\eatSpaces{16} \endSpaces}\A. In pipes and planar ducts the similar but smaller divergence might be explained by the free passage of large eddies across the centerline or center plane from the opposite sides of the flow. In open- channel flow a similar effect might be produced by flattening of large eddies moving toward the free surface. The meager data from open channels suggest an effect similar in magnitude to that in pipes and planar ducts, or perhaps even smaller. There seems to be no reason to expect a perfectly logarithmic profile all the way to the free surface, but the deviations clearly are insubstantial, at least for practical work.

Effects of Roughness Height and Spacing

It is in some ways discouraging to sit back and consider that just about everything said so far about velocity profiles is limited to the case of sediment-free flow over close-packed roughness elements whose size is a tiny fraction of the flow depth. Obviously this is only a small subset of turbulent boundary-layer flows over rough boundaries. The discussion in this section emphasizes mostly the qualitative effects to be expected as

1. The height of the roughness elements increases relative to the flow depth.
2. The spacing of the roughness elements increases relative to their height.

Figure $4.7.17$ summarizes the changes in velocity profile as the size of close-packed granular roughness increases relative to flow depth. In Figure $4.7.17$A the particles are so small (or, more precisely, the roughness Reynolds number $\rho u_* D/\mu$ is so small) that the particles are embedded in a viscous sublayer, and the flow is dynamically smooth. In Figure $4.7.17$B the particles are larger and the flow is dynamically rough, but the particle size is still so small relative to the flow depth that there is a well developed outer layer beyond the overlap layer in which the velocity-defect profile holds but the inner-layer profile does not. These first two cases are covered by the preceding detailed treatment of velocity profiles.

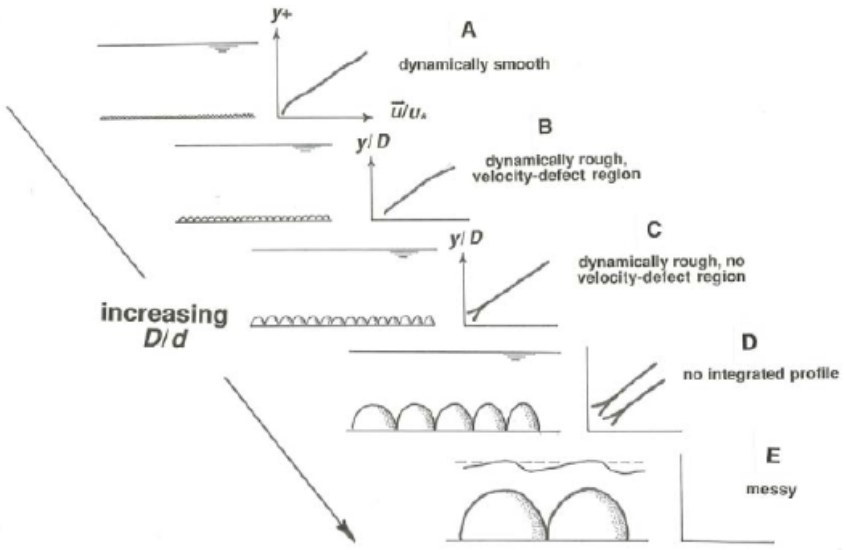


Figure $4.7.17$: Changes in velocity profile as the size of the close-packed granular roughness increases relative to flow depth.

In Figure $4.7.17$C, as the ratio of flow depth to particle size decreases still further, the distinction between inner and outer layers begins to be blurred, and eventually a situation is reached where the entire profile, from bottom to free surface, is affected by the details of the roughness. The whole profile then looks like just the lower part of the wall-law profile in flows with very large values of d/D. This effect begins to become appreciable at d/D values of something like 10 to 15.

As d/D decreases further, an increasingly large fraction of the total flow depth is occupied by the zone of the flow, within one or perhaps two grain diameters above the tops of the roughness particles, where the velocity profile is spatially disunified, in the sense that it varies with position relative to the layout of the particles. As shown in Figure $4.7.17$D in exaggerated form, for d/D values below about 2 or 3 most or all of the velocity profile is spatially variable in this way.

What happens as d/D decreases further (Figure $4.7.17$E) depends on the value of the mean-flow Froude number $U/(gD)^{1/2}$. (For

full appreciation of this point you will have to wait until I have presented more about free-surface flow later, in the next chapter.) For Froude numbers close to or greater than one (i.e., for supercritical or nearly supercritical flow), the free surface is strongly deformed by the presence of the particles just below the surface; think of a shallow fast-flowing mountain stream with a bed of cobbles and boulders. For the same very small d/D but low Froude numbers, however, the grains rest just beneath a relatively placid water surface, or in the extreme case project above the surface as islands.

Figure $4.7.18$ is a cartoon showing the changes in the structure of the flow as the roughness spacing decreases relative to the roughness height. Start with a physically smooth and planar bottom; the flow is dynamically smooth, and $y = 0$ is naturally taken at the planar bottom. Now take a set of roughness elements whose heights are a very small fraction of the flow depth and begin to place them either randomly or in a regular pattern on the bed. The elements could be three-dimensional bluff bodies or two-dimensional ridges transverse to the flow; the effects are qualitatively the same, at least until the ratio of spacing to height becomes very small.

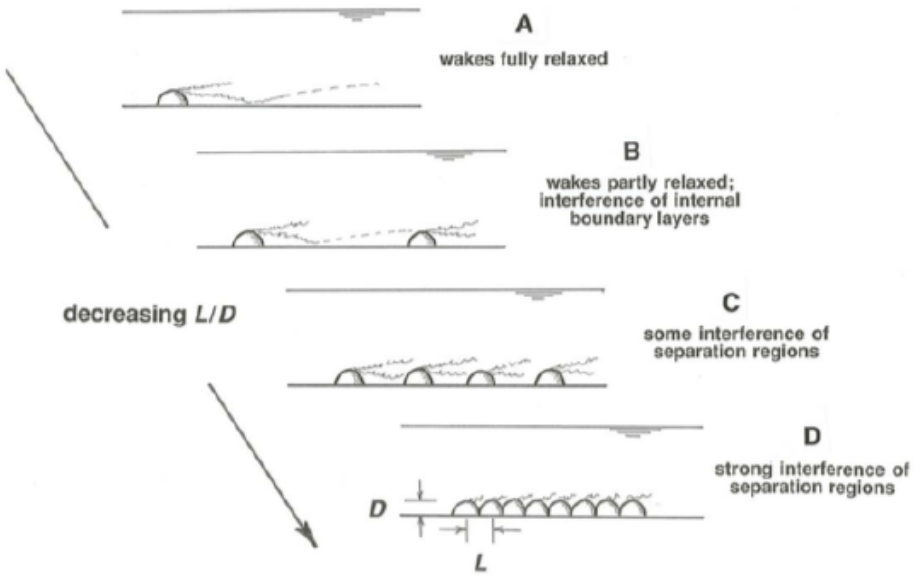


Figure $4.7.18$: Changes in flow structure as roughness spacing decreases relative to roughness height.

Provided that the roughness Reynolds number (based on the height of the roughness elements being added) is sufficiently large, each element creates a wake as the flow separates around it. From the discussion of flow separation in Chapter 3 you can see that the flow structure downstream of each roughness element is very complicated: the smooth- flow boundary layer is profoundly modified by the development of a highly turbulent shear layer that extends downstream from the separation point. Downstream from each element the flow gradually readjusts toward the boundary-layer structure that would exist in the absence of roughness; the wakes shed by the elements are said to relax. This readjustment or relaxation takes the form of a new lowest layer of the flow, expanding upward at the expense of the turbulent shear layer, in which a turbulence- dominated wall-law profile is established in just the same way as in a boundary layer growing on a flat plate. It takes a surprisingly large number of element heights downstream, something of the order of a hundred, for the process to be completed, whereupon the local structure of the flow shows no trace of the presence of the roughness element upstream and the wall-law layer extends without interruption from the planar bottom up into the region of the flow far above the level of the tops of the large roughness elements. The case of low roughness Reynolds numbers is of less interest here, because then the elements are embedded in a viscous sublayer, but in that case also a deficit in fluid momentum is created downstream of each element even though the flow does not separate, and this deficit is ironed out downstream by viscous shear until the original viscosity-dominated velocity profile is reestablished.

If the roughness elements are sufficiently far apart (Figure $4.7.18$A) each has a long wake extending downstream, but the flow is able to return to normal before it encounters the next roughness element. This has been called *isolated-roughness flow* (Morris, 1955). The velocity profile measured above a given point on the bed depends on the position of that point relative to the wakes behind the elements. You would have to measure a large number of profiles and average them spatially to obtain a profile that represents the entire flow. Compared with the original smooth- flow profile before emplacement of any roughness elements, the spatially averaged profile shows a deficit of velocity within one or two roughness heights of the bed.

The spatially averaged boundary shear stress τ_o is still dominantly viscous, as in the absence of roughness elements, but the contribution of pressure drag to τ_o increases with the roughness density. The flow could now be termed transitionally rough, although in a rather different sense from the use of that term in flow over close-packed roughness in earlier sections. Note also

that the original flow, before emplacement of roughness elements, can itself be dynamically rough, if the bottom is covered with close-packed roughness that is much smaller than the large, isolated roughness we are adding. Then τ_0 is dominated from the start by pressure drag, but this pressure drag is of two parts: a spatially uniform part produced by the underlying small and close-packed roughness, and a spatially nonuniform part produced by the large and isolated roughness. It takes only a low density of large roughness elements for their contribution to the pressure drag to outweigh that of the close-packed elements.

As we continue to add large roughness elements, a point is reached where the wakes shed by the elements do not relax completely before encountering another roughness element downstream, and with some further increase in density most points in the near-bed flow are within wakes in various stages of relaxation (Figure $4.7.18$B). Now there iss no place on the bed that shows the relatively simple velocity profile of the original smooth flow without roughness elements. A flow of this kind has been called **wake-interference flow** (Morris, 1955). Again you have to take a large number of local velocity profiles and spatially average them to get a profile representative of the entire bed. Because most of the area of the bed is overlain by reattached and relaxing wakes, the spatially averaged profile shows two distinct segments: one, adjacent to the bed and extending upward for some fraction of the roughness height, represents the spatial average of the local wall-law profiles in the relaxing wakes, and the other, starting well above the tops of the large roughness elements and extending far above, represents the wall law above the zone in which the upward- diffusing wake turbulence blends into a spatially uniform layer—the case that was treated at length in the earlier part of this chapter. These two distinctive parts of the profile tend to plot as semilog straight lines with a transition at heights somewhat below to somewhat above the tops of the roughness elements. See Nowell and Church (1979) for a good example. As the roughness spacing decreases, the height of the $y = 0$ level for the overall wall-law profile above the tops of the roughness elements rises higher and higher above the planar bottom.

With increasing roughness density, eventually most of the area of the bed between roughness elements is overlain by the parts of the wakes that lie upstream rather than downstream of reattachment (Figures $4.7.18$C, $4.7.18$D); this condition sets in when the ratio of roughness spacing to roughness height is of the order of ten or less. Well before this stage the lower straight-line segment of the spatially averaged velocity profile loses its distinctive character. The turbulent shear layers downstream of loci of separation then impinge mostly upon the surfaces of roughness elements downstream rather than on the planar bottom; viscous shear stresses on the planar bottom are almost nonexistent, and the geometry of the bottom in the areas between the roughness elements is irrelevant to the dynamics of the flow. For three-dimensional granular roughness this condition is maintained with no qualitative change as the elements become so closely spaced that their bases are touching—a good approximation to the condition of a loose granular bed treated in detail earlier. If the roughness consists of transverse ridges, however, the ratio of spacing to height can continue to decrease toward zero, and as it becomes smaller than about one the flow skims across the crests of the ridges and drives a circulation of stable vortices located in the deep and narrow troughs between the ridges; this has been called **skimming flow** (Morris, 1955).

This page titled 4.7: Velocity Profiles is shared under a CC BY-NC-SA 4.0 license and was authored, remixed, and/or curated by John Southard (MIT OpenCourseware) via source content that was edited to the style and standards of the LibreTexts platform.

4.8: More on the Structure of Turbulent Boundary Layers- Coherent Structures in Turbulent Shear Flow

There was a time, until the 1960s, when the emphasis in turbulence research was statistical: turbulence was largely viewed as a strictly *random phenomenon*, one that can be analyzed only by statistical methods. Implicit in such an approach is that turbulence has no apparent regularity or "ordered-ness" in its structure.

Beginning in the 1960s, however, there have been many studies on what are now termed **coherent structures** in turbulent shear flow. (I postponed this material until now, so that you would have more background in turbulent shear flow to bring to it.) It has become clear that shear turbulence is not merely a random assemblage of eddies of all sizes, shapes, and magnitudes and orientations of vorticity; rather, these are irregular but repetitive eddy structures, or flow patterns, in time and space, with distinctive shapes and histories of formation, evolution, and dissipation. These coherent structures are not strictly regular in geometry or periodic in time, but nonetheless they have a strong and distinctive element of non- randomness. One way of describing these coherent structures is that they are quasi-regular, or quasi-periodic, or quasi-deterministic. (The word *quasi* in Latin means "almost".) Admittedly the foregoing characterization does not give you much basis for imagining or visualizing what the coherent structures look like; see below for more concrete material.

Recall from Chapter 3 that turbulence can be viewed as an assemblage of swirling and intergrading parcels of fluid, called eddies, on a wide range of scales. Eddies have **vorticity**: the fluid in the eddies undergoes rotational motion, which is described by the local rate and orientation of rotation, varying from continuously from point to point. To appreciate the nature of coherent structures in shear turbulence, you need to deal with the shapes and also the vorticity of the structures, and how the shape and the vorticity develop ands change during the lifetime of a given element of structure.

The best way to perceive or capture ordered structures is to visualize them, by supplying the flow with marker material that reveals or distinguishes differently moving regions of fluid. Studies of ordered structures in turbulent flow have mostly used three techniques flow visualization:

1. dye injection, at points or along lines
2. generation of lines of tiny hydrogen bubbles in water by passing a current through a fine platinum wire immersed in the flow
3. high-speed motion-picture photography of very small opaque solid particles suspended in the flow

It is generally agreed that flow near the boundary in a turbulent shear flow tends to be characterized by the following sequence of events, commonly called the **burst–sweep cycle**. A high-velocity eddy or vortex (called a **sweep**) moves toward the boundary and interacts with low velocity fluid near the boundary to cause acceleration, increase in shear, and development of small-scale turbulence; this accelerated fluid is then lifted from the boundary and ejected as a turbulent **burst** into a region of flow farther from the boundary. The sweeps are inrushes of high-seed fluid at at a shallow angle toward the wall; the bursts are violent ejections of low- speed fluid outward from the vicinity of the wall.

Close to the boundary the high-velocity and low-velocity vortices or eddies tend to be elongated or streaked out in the streamwise direction, and their manifestation is a streaky or ribbon-like pattern of high and low fluid velocities, and therefore of boundary shear stresses as well. Owing to the substantial changes in velocity, shear, and turbulence above a given point on the boundary occasioned by the bursting cycle, the effective thickness of the viscous sublayer varies with time. Because of the existence of the burst–sweep cycle, the picture of the viscous sublayer developed earlier in this chapter is oversimplified: it has a definite thickness only as a time average at a given point. At a given time, the viscosity-dominated layer near the bottom is in some regions thin (and in those regions, shear near the bed, and shear stress on the bed, are temporarily high), and in adjacent regions it is thicker (and in those regions, the shear and the bed shear stress are temporarily smaller).

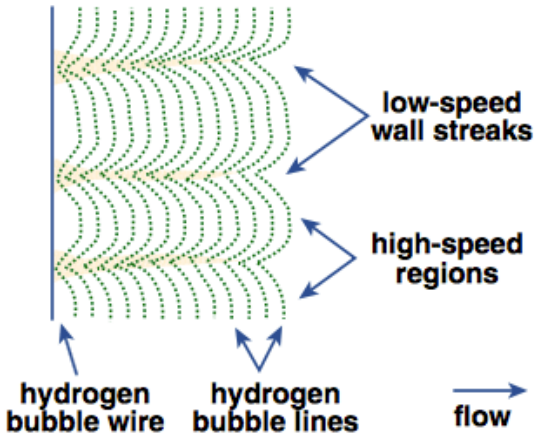


Figure by MIT OpenCourseWare.

Figure 4.8.1: Low-speed wall streaks and high-speed regions, as seen from above, revealed by the distortion of a horizontal cross-stream line of hydrogen bubbles generated along the left-hand line just above the wall. (From Smith, 1996.)

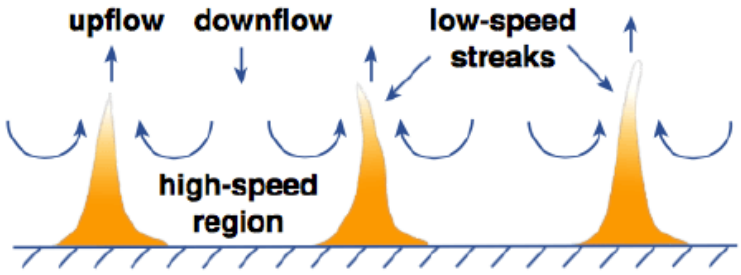


Figure by MIT OpenCourseWare.

Figure 4.8.2: Cartoon of low-speed wall streaks and intervening high-speed regions, as seen looking horizontally downstream near a horizontal wall. (From Smith, 1996.)

The common visual manifestation of the burst–sweep cycle is the existence of streamwise-oriented **low-speed streaks** (also called wall-layer streaks, or just streaks) just above the flow boundary. These streaks are low-speed zones that lie between intervening high-speed zones. In the low- speed zones, slow-moving fluid has an upward (that is, in the direction away from the boundary) component of motion as a result of downward flow in the high-speed zones (Figures 4.8.1, 4.8.2). Sediment particles tend to be swept into the low-speed streaks as the faster-moving fluid in the high-speed zones moves slightly obliquely toward the low-speed zones.

You might have seen such low-speed streaks on a cold winter day, with temperatures well below freezing, when a wind-driven light snow first falls upon are pavement, or in the desert when a strong wind blows fine sediments across the road surface. It is not difficult to set up a beautiful visual demonstration of low-speed streaks in a laboratory flume, where a small concentrations of brilliant white sediment particles are transported across a dark-colored bare flume bottom.

The strong message from such visualizations is that

- the streaks are strongly elongated parallel to the flow direction;
- the streaks waver and shift irregularly from side to side; and
- the streaks appear and disappear with time.

Much effort has gone into study of the scale of the streaks. It is clear that for dynamically smooth flow the average spacing λ of the streaks, when nondimensionalized as $\lambda^+ = \rho\lambda u_*/\mu$, is in the range somewhat above or below 100, and only weakly dependent upon the mean- flow Reynolds number. The streaks are also present when the flow is dynamically fully rough; the spacing of the streaks, when nondimensionalized by dividing by the size of the close-packed roughness elements, is between 3 and 4. In transitionally rough flow, the situation is less straightforward.

The burst–sweep cycle and its associated streak structure is a feature of the near-boundary part of the inner layer, in what was called in an earlier section the viscous sublayer (if one is present) and the buffer layer. Farther away from the boundary, where eddy scales range to larger size and where both production and dissipation of turbulent kinetic energy are less, there seems to be less coherence in the structure of the turbulence.

It remains to look into how the counter-rotating vortices, stretched out in the streamwise direction, originate, and how their shapes evolve. It is generally accepted that the key features in this regard are vortices variously called **horseshoe vortices** or **hairpin vortices**, owing to their characteristic shape (Figures 4.8.3, 4.8.4). These vortices develop, in ways not yet well understood, and then become stretched downstream by the strong mean shear, and as they are stretched, the vorticity in the limbs increases. (In an approximate sense, as the diameter of the spinning fluid is decreased, the spinning is compressed into a smaller cross section, and the rate of spinning increases.) These elongated vortex limbs are generally believed to be responsible for the fluid motions in the burst–sweep cycle.

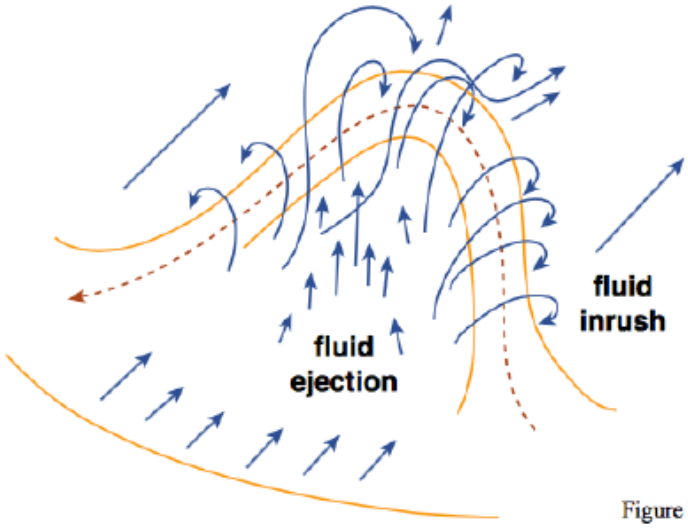


Figure by MIT OpenCourseWare.

Figure 4.8.3: Model of a near-wall horseshoe vortex. (Modified from Grass and Mansour-Tehrani, 1991; originally from Theodorsen, 1952.)

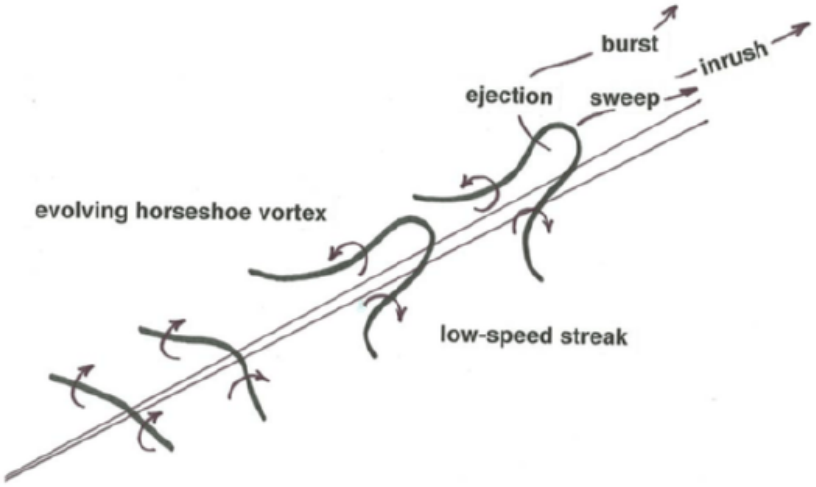


Figure 4.8.4: Formation and evolution of a horseshoe–hairpin vortex, showing its role in the burst–sweep cycle. (Modified from Hinze, 1975.)

The study of coherent structures in turbulent shear flows is an active area of research. For informative reviews of the status of understanding, see Robinson (1991), Grass and Mansouri-Tehrani (1996), and Smith (1996). Also on the reading list at the end of the chapter are some of the classic papers: Kline et al. (1967), Corino and Brodkey (1969), Grass (1971), and Offen and Kline (1974, 1975).

Chapter 4 References Cited

Coleman, N.L., 1981, Velocity profiles with suspended sediment: Journal of Hydraulic Research, v. 19, p. 211-229.

Corino, E.R., and Brodkey, R.S., 1969, A visual investigation of the wall region in turbulent flow: Journal of Fluid Mechanics, v. 37, p. 1-30.

Grass, A,J,, and Mansour-Tehrani, M, 1996, Generalized scaling of coherent bursting structures in the near-wall region of turbulent flow over smooth and rough boundaries, in Ashworth, P.J., Bennett, S.J., Best, J.L., and McLelland, S.J., Coherent Flow Structures in Open Channels: Wiley, p. 41-61

Grass, A.J., 1971, Structural features of turbulent flow over smooth and rough boundaries: Journal of Fluid Mechanics, v. 50, p. 233-255.

Grass, A.J., Stuart, R.J., and Mansour-Tehrani, M, 1991, Vortical structures and coherent motion in turbulent flow over smooth and rough boundaries: Royal Society (London), Philosophical Transactions, v. A336, p. 35-65.

Hinze, J.O., 1975, Turbulence, Second Edition: McGraw-Hill, 790 p.

Izakson, A., 1937, Formula for the velocity distribution near a wall [in Russian]: Zhurnal' Eksperimental'noi i Teoreticheskoi Fiziki, v. 7, p. 919-924.

Kline, S,J., Reynolds, W.C., Schraub, F.A., and Runstadler, P.W., 1967, The structure of turbulent boundary layers: Journal of Fluid Mechanics, v. 95, p. 741-773.

Millikan, C.B., 1939, A critical discussion of turbulent flow in channels and circular tubes: Fifth International Congress on Applied Mechanics, Cambridge, Massachusetts, Proceedings, p. 386-392.

Monin, A.S., and Yaglom, A.M., 1971, Statistical Fluid Mechanics, Volume 1: Cambridge, Massachusetts, MIT Press, 769 p.

Morris, H.M., 1955, Flow in rough conduits: American Society of Civil Engineers, Transactions, v. 120, p. 373-398.

Nikuradse, J., 1933, Gesetzmässigkeiten der Turbulente Strömung in glatten Rohren: VDI Forschungsheft 356.

Offen, G.R., and Kline, S.J., 1974, Combined dye-streak and hydrogen- bubble visual observations of a turbulent boundary layer: Journal of Fluid Mechanics, v. 62, p. 223-239.

Offen, G.R., and Kline, S.J., 1975, A proposed model of the bursting process in turbulent boundary layers: Journal of Fluid Mechanics, v. 70, p. 209-228.

Robinson, S.K., 1991, Coherent motions in the turbulent boundary layer: Annual Review of Fluid Mechanics, v. 23, p. 601-639.

Smith, C.R., 1996, Coherent flow structures in smooth-wall turbulent boundary layers: facts, mechanisms and speculation, in Ashworth, P.J., Bennett, S.J., Best, J.L., and McLelland, S.J., Coherent Flow Structures in Open Channels: Wiley, p. 1-39.

Tennekes, H., and Lumley, J.L., A First Course in Turbulence: Cambridge, Massachusetts, MIT Press, 300 p.

Theodorsen, T., 1952, Mechanisms of Turbulence: 2nd Midwestern Conference on Fluid Mechanics, Ohio Sate University, Columbus, Ohio, Proceedings, p. 1-18.

Tritton, D.J., Physical Fluid Dynamics, Second Edition: Oxford University Press, 519 p.

This page titled 4.8: More on the Structure of Turbulent Boundary Layers- Coherent Structures in Turbulent Shear Flow is shared under a CC BY-NC-SA 4.0 license and was authored, remixed, and/or curated by John Southard (MIT OpenCourseware) via source content that was edited to the style and standards of the LibreTexts platform.

5: OPEN-CHANNEL FLOW

This chapter is a selective presentation of some important topics in free- surface flow. I will defer consideration of the generation and propagation of gravity waves on the free surface of a standing or flowing body of liquid until Chapter 6, on oscillatory flow.

5.1: Introduction to Open-Channel Flow

5.2: Two Practical Problems

5.3: Uniform Flow

5.4: Energy in Open-Channel Flow

5.5: The Hydraulic Jump

5.6: Hydraulic Regimes of Open-Channel Flow

5.7: Gradually Varied Flow

This page titled 5: Open-Channel Flow is shared under a CC BY-NC-SA 4.0 license and was authored, remixed, and/or curated by John Southard (MIT OpenCourseware) via source content that was edited to the style and standards of the LibreTexts platform.

5.1: Introduction to Open-Channel Flow

Open-channel flows are those that are not entirely included within rigid boundaries; a part of the flow is in contract with nothing at all, just empty space (Figure 5.1.1). The surface of the flow thus formed is called a **free surface**, because that flow boundary is freely deformable, in contrast to the solid boundaries. The boundary conditions at the free surface of an open-channel flow are always that both the pressure and the shear stress are zero everywhere. But a flow can have a free surface but not be an open-channel flow. Closed-conduit flows that consist of two immiscible fluid phases of differing density in contact with each other along some bounding surface are not open-channel flows, because they are nowhere in contact with open space, but they do have a freely deformable boundary within them. Such flows are free-surface flows but not open-channel flows (Figure 5.1.2), although they are usually called **stratified flows**, because the density difference between the two fluids gives rise to gravitational effects in the flow. On the other hand, open-channel flows are by their definition also free- surface flows.

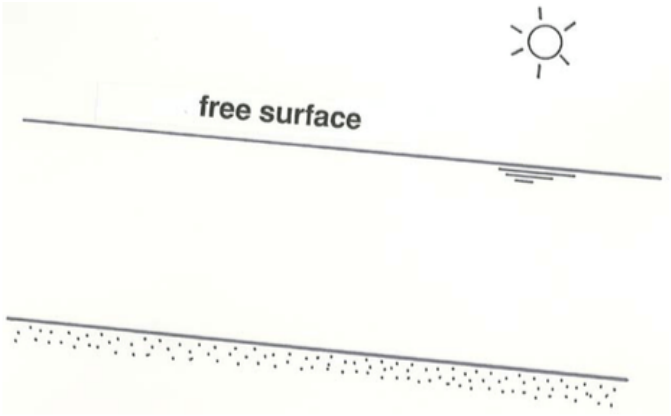


Figure 5.1.1: An open-channel flow.

In a narrow technical sense, flows of liquid at the Earth's surface, like ocean-surface currents or rivers, are not open-channel flows, because they are in contact with another fluid—the atmosphere—at a free surface within a two-phase fluid medium. But the contrast in density between water and air is so great that in studying Earth-surface liquid flows we usually ignore the presence of the overlying atmosphere.

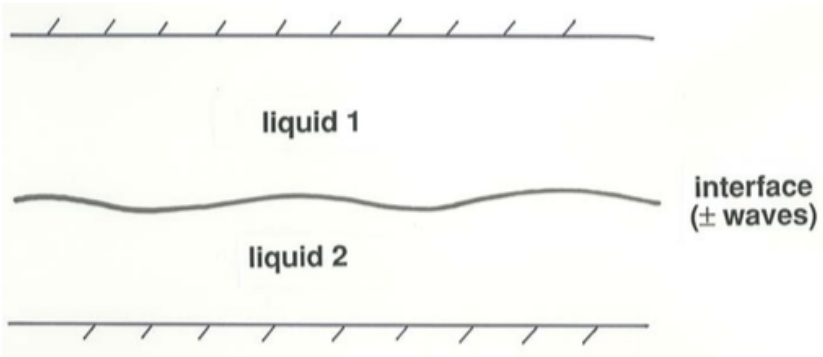


Figure 5.1.2: A free-surface flow that is not an open-channel flow.

All of the principles and techniques for dealing with velocity structure and boundary resistance that were developed for closed-conduit flows in earlier chapters hold as well for open-channel flows. In fact, much of the material in Chapter 4, on flow resistance and velocity structure, is about open-channel flows. But open-channel flows involve an important added element of complexity beyond what we have covered on laminar and turbulent flows in closed conduits: the presence of the free surface means that the geometry of the flow can change in the flow direction not just by being constrained to do so by virtue of the geometry of the boundaries but also by the behavior of the flow itself. This means that the acceleration of gravity can no longer be ignored by the expedient of subtracting out the hydrostatic pressure, as with closed-conduit flows, because the force of gravity helps to shape the free surface. So gravity must therefore be included as an additional independent variable in dealing with free-surface flows. You have already seen an example of this back in Chapter 2, when a sphere was towed underwater but near the free surface.

Also, under the right conditions gravity waves can be generated on the free surface, whether or not the fluid is flowing. When the deformable free surface is momentarily deformed in some small area by a deforming force of some sort—by the force of the wind, or by your agitating the water with your hand—the force of gravity acts to try to restore the free surface to its original planar condition. Provided that the viscosity of the liquid is not too high (have you ever tried to make waves in a vat of molasses?) this attempt at restoration of a deformed free surface leads to the propagation of gravity waves away from the region of surface disturbance.

This page titled 5.1: Introduction to Open-Channel Flow is shared under a CC BY-NC-SA 4.0 license and was authored, remixed, and/or curated by John Southard (MIT OpenCourseware) via source content that was edited to the style and standards of the LibreTexts platform.

5.2: Two Practical Problems

One of the interesting things about open-channel flow is the effect of gravity on the shape of the free surface relative to the solid boundary. Babbling brooks and white-water rivers clearly have complex free-surface geometries governed by bed relief, expansions and contractions of the channel, and, less obviously, upstream and downstream conditions. But all open-channel flow, even broad, majestic rivers like the Mississippi, or flows in laboratory channels we try to keep as nearly uniform as possible, are subject to such effects of gravity. To make this effect concrete, I will pose two questions at this point for you to think about. Both are of great practical importance to engineers dealing with open- channel flows.

Your intuition might have some trouble with the first question. Suppose that you set up a nice open-channel flow, in a wide rectangular channel, just for the sake of definiteness, with a planar bottom, which may or may not be sloping. Then, at a particular position down along the channel you introduce a smooth and gentle step in the channel bottom, either upward or downward (Figure 5.2.1). The question is: does the water surface rise or fall over the step, relative to its upstream level?

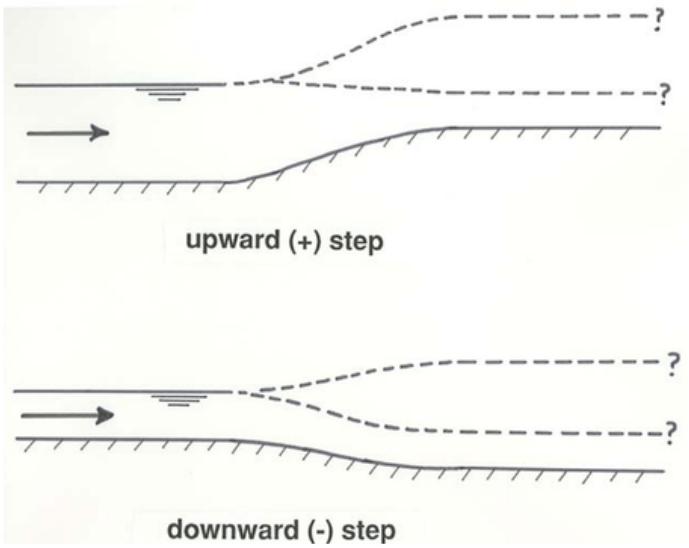


Figure 5.2.1: A positive step and a negative step in a channel bottom.

You will probably feel more comfortable with the second question. A river with a constant bottom slope is dammed at a certain point, so that the river has to merge somehow into a deep reservoir formed in the river valley (Figure 5.2.2). You can assume that far upstream in the channel the flow is very nearly uniform. That sloping water surface upstream has to pass continuously into the horizontal water surface of the reservoir, where the water velocity is negligible. What would the water-surface profile look like along a streamwise vertical cross section through the channel and the reservoir? Would it change very gradually, all the while sloping monotonically down toward the reservoir? Or would it continue unchanged all the way to the reservoir level, to meet the water surface in the reservoir by an abrupt change in water-surface slope?

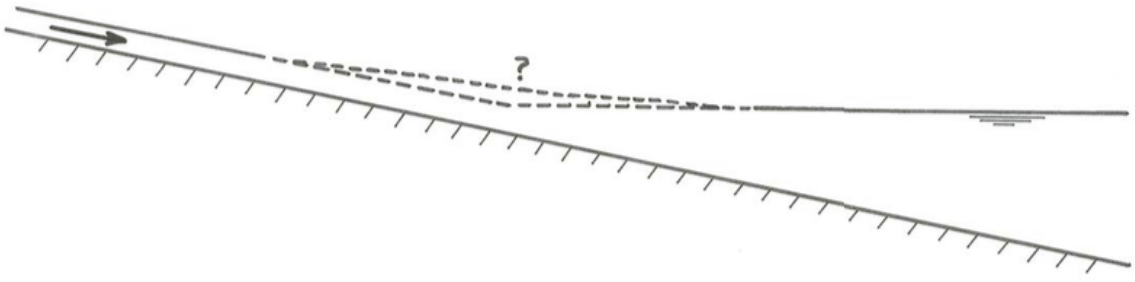


Figure 5.2.2: When a river enters a lake or reservoir, does the water surface in he river meet the water surface in the lake or reservoir in a smooth transition, or abruptly?

Before attacking these problems, you need a brief look at *uniform flow*, which is a useful reference for study of the nonuniformities introduced by the joint effect of gravity and the changing boundary geometry. Then I will have to expose you to more material on *flow energy*, because it turns out that this is the key to the problems posed above.

This page titled 5.2: Two Practical Problems is shared under a CC BY-NC-SA 4.0 license and was authored, remixed, and/or curated by John Southard (MIT OpenCourseware) via source content that was edited to the style and standards of the LibreTexts platform.

5.3: Uniform Flow

Uniform flow serves as a good reference case from which to think about the effect of gravity on the free surface in an open-channel flow. Only if an open- channel flow can somehow be adjusted to be strictly **uniform**, in the sense that the water surface is planar and the flow depth is the same at all cross sections along the flow (Figure $5.3.1$), can the effect of gravity in shaping the flow be ignored.

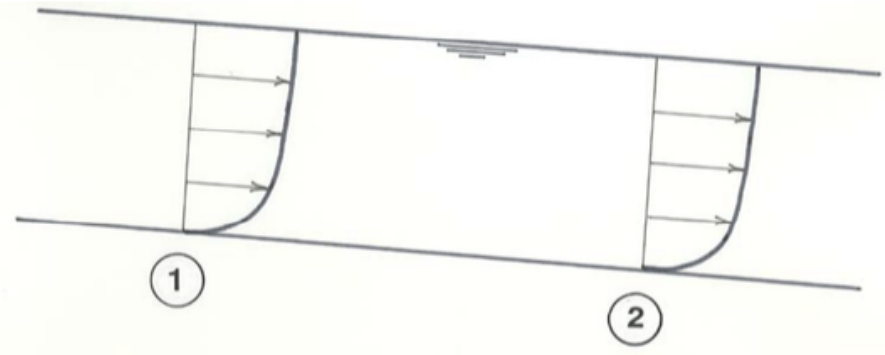


Figure $5.3.1$: A uniform open-channel flow: the depth and the velocity profile is the same at all sections along the flow.

Flows in the laboratory can be set up to be very nearly uniform, and outdoors flows like those in long canals are often also close to being uniform. But uniformity is an abstraction: real flows are never perfectly uniform, because, no matter how closely the conditions of flow are adjusted, there are always subtle free-surface effects that extend downstream from the source of the flow and upstream from the sink for the flow, or upstream and downstream from places where the channel geometry changes, like dams or bridge piers.

One kind of problem that is associated with uniform flow is what the channel slope will be if discharge Q, water depth d, and bed sediment size D are specified or imposed upon the flow. You can investigate this by building an open channel in your back yard, just nailed together out of wood, as if you were going to pan for gold. Try to make the channel several meters long and something like a meter wide, with a planar bottom and planar vertical sidewalls. Immerse the downstream end of the channel in one of those big above-ground swimming pools so many people have in their yards these days. (This is the key to imposing the flow depth on the channel upstream: the higher the water level in the swimming pool relative to the sediment bed in the channel, the deeper the flow in the channel.) Put a submersible pump in the pool to recirculate the water, and the transported sediment as well, to the upstream end of the channel at a given discharge Q. Lay a full bed of sand in the channel, thick enough so that the flow can redistribute it by erosion and deposition if it so desires, without exposing the channel bottom. Mount the upstream end of the channel on a scissors jack or the like, so that you can vary the slope of the channel.

It should seem obvious to you that for a given discharge, and an arbitrary channel-bottom slope you set at the beginning, the flow depth in the channel would vary from upstream to downstream: in general the flow in your channel is *nonuniform*, before the flow erodes sand from one end of the channel and deposits in at the other end in its desire to establish uniform flow. If that does not seem obvious to you, imagine that for a given discharge you first increased the channel slope; eventually you would have a condition in which the flow was relatively shallow at the upstream end and relatively deep at the downstream end (Figure $5.3.2$ A). On the other hand, if you decreased the channel slope to be very gentle, you would eventually have a condition in which the flow was relatively deep at the upstream end and relatively shallow at the downstream end (Figure $5.3.2$B). Somewhere in between those two extreme conditions there would be a slope for which the flow was nearly uniform. The question then is: *what governs what the slope is for uniform flow?*

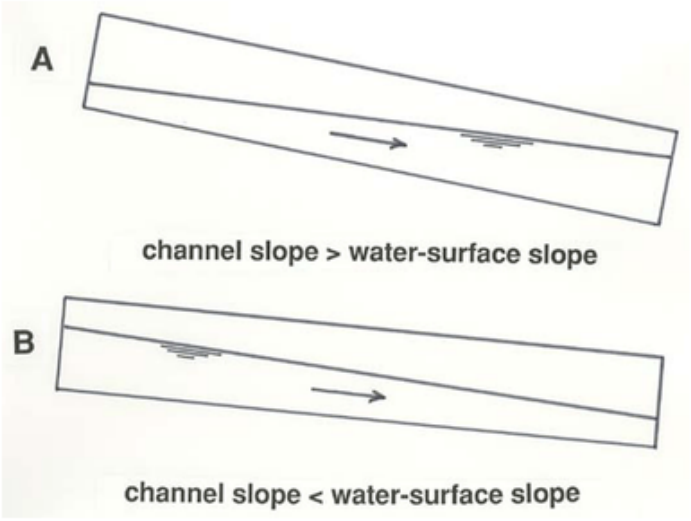


Figure 5.3.2: **A)** An open-channel flow for which the water-surface slope is less than the slope of the channel bottom. **B)** An open-channel flow for which the water-surface slope is greater than the slope of the channel bottom.

The key to the answer lies in flow resistance, which was addressed at length in Chapter 4. But there we analyzed the dynamics of flow resistance after assuming that the flow had already been adjusted for uniformity. Now we are asking how we can predict what the slope will be for uniform flow. This an important engineering problem: if you have to design a drainage culvert or an irrigation channel, you want to make sure that the flow is not grossly non-uniform, or it might end up overflowing its banks either upstream or downstream, and make you vulnerable to lawsuits.

The problem is fairly straightforward. First of all, you have at your disposal the basic resistance equation for open-channel flow (Equation 4.2.1, repeated here):

$$\tau_0 = \gamma d \sin \alpha \tag{5.3.1}$$

You also have an empirical equation for bed shear stress τ_o in terms of a resistance coefficient, which could be the friction factor f or the Chézy coefficient C (Equation 4.6.1, repeated here in slightly rearranged form):

$$\tau_0 = \frac{f}{8}\rho U^2 \tag{5.3.2}$$

You also know the mean velocity U, because you have chosen Q yourself and you already know d, so by the relation $Q = Udb$ (where b is the known width of the channel) you can solve for U. Compute the mean-flow Reynolds number Re, go to a diagram like that in Figure 4.7.7 (that diagram was found for flow in a circular pipe, but it is known to give fairly good results for open-channel flow, provided that you use the hydraulic radius both for the channel flow and for the pipe flow) to find f and thus, by Equation 5.3.2, τ_o. Then, knowing τ_o, you can use Equation 5.3.1 to find the slope angle α. You could adjust the channel slope by use of your scissors jack—and you would *have* to do that if the channel bottom is rigid rather than mantled with loose sediment—but with the full bed of sediment, the flow eventually adjusts the slope to the condition of uniform flow by eroding sediment and one end and depositing sediment at the other end.

Now for a further aspect of uniform flow, one that is more relevant to natural open-channel flows on the Earth's surface. Excavate a very long, straight channel, ending at the brink of a large, deep, open pit into which the flow will fall freely, on a gently and uniformly sloping area of the land surface. A length of many kilometers would be good. Arrange to pass a discharge Q of your choosing down the channel. You can readily appreciate that if the channel is sufficiently long the flow in the channel will be close to being uniform, although you can assist the approach to uniformity by fiddling a bit with the flow at the downstream end, by installing a sluice gate or a porous weir to prevent the decrease in upstream depth as the flow falls out of the channel. You will also have to be prepared to feed in some bed sediment at the upstream end, to replenish what is transported down the channel and out the end, if the flow turns out to be strong enough to move some of the sediment. Otherwise, you would be modeling the long-term behavior of a real river, whereby the river gradually wears down the land area on which it flows, thus decreasing the slope of the land over the long term.

The big question now is: what will the uniform flow depth be, given the imposed slope and discharge? Is the flow fast and shallow,

or is it slow and deep? You have the same hydraulic relationships available as in the previous situation, but now their application is not as straightforward. Think about what you know and what you do not know. What is given is the slope angle α, the discharge Q, the bed sediment size D, and the channel width b The unknowns are the mean flow velocity U, the flow depth d, the resistance coefficient or friction factor f, and the boundary shear stress τ_{o}. You have four relationships available that involve these knowns and unknowns:

- $\tau_{texto} = \gamma d \sin \alpha$ (the basic resistance equation for uniform channel flow)
- $Q = Udb$ (conservation of flow volume)
- $\tau_0 = (f/8)\rho U^2$ (the relationship between flow velocity and boundary shear stress)
- $f = f(\mathrm{Re}, D/d)$ (the dependence of the friction coefficient on flow velocity, flow depth, and bed roughness)

These are the same equations used in the earlier situation. The difference is that you cannot proceed step by step to find the answer: you need to deal with them all at once. The problem is well posed (four unknowns, four equations), but you cannot obtain the solution analytically, in closed form; you need to find the solution by some iterative numerical technique. The important point here, though, is that there *is* a unique solution: for any given combination of channel slope, bed sediment, and water discharge, there is a certain flow depth, mean flow velocity, and boundary shear stress. And your intuition tells you, correctly in this case, that the uniform flow depth increases with water discharge and also with bed roughness: the greater the discharge, and the rougher the bed (meaning more resistance to flow), the greater the flow depth for uniform flow. It is clear also that the flow depth depends on the slope: the greater the slope, the smaller the flow depth.

This page titled 5.3: Uniform Flow is shared under a CC BY-NC-SA 4.0 license and was authored, remixed, and/or curated by John Southard (MIT OpenCourseware) via source content that was edited to the style and standards of the LibreTexts platform.

5.4: Energy in Open-Channel Flow

To address the two channel-transition problems posed earlier, we need to have a closer look at mechanical energy in an open-channel flow, and at how the partitioning of the various components of that mechanical energy, kinetic and potential, are changed at the transition in question.

I noted back in Chapter 3 that the Bernoulli equation is an expression of the work–energy theorem: the work done by the fluid pressure is equal to the change in kinetic energy of the flow. Remember that, in cases like this, if the change in kinetic energy is reversible a quantity called potential energy is defined as minus the work done, and then the sum of kinetic energy and potential energy, often called mechanical energy, is unchanged or conserved. Forces for which this is true, like the fluid pressure in this case, are said to be *conservative* forces. Gravity is a good example: a ball thrown upward gains potential energy on its way up at the same rate it loses kinetic energy, if the frictional resistance of the air is ignored. Frictional forces, on the other hand, degrade mechanical energy into thermal energy (more commonly called heat or heat energy).

Review the derivation of the Bernoulli equation in Chapter 3 and you will see that fluid pressure is a conservative force: in the absence of friction, the change in pressure potential energy per unit volume between two points 1 and 2 down a streamline, which is minus the work per unit volume $-(p_2 - p_1)$ by the fluid pressure, is equal to the change in kinetic energy per unit volume, $(\rho/2)({v_2}^2 - {v_1}^2)$, so the two kinds of mechanical energy are interchangeable in this case also. It should therefore seem natural that when the fluid is in a gravity field a term for gravitational potential energy can be included in the Bernoulli equation as well. Because gravitational potential energy is mgh (where m is the mass of the body under consideration and h is the elevation relative to an arbitrary horizontal plane), the potential energy per unit volume is ρgh.

So in the expanded Bernoulli equation the mechanical energy per unit volume of fluid moving along a streamline, $v^2/2 + p + \rho gh$, is constant. This can be written a little more conveniently for our purposes as energy per unit weight of fluid E_w. Because weight equals volume multiplied by ρg,

$$E_W = \frac{v^2}{2g} + \frac{p}{\gamma} + h \tag{5.4.1}$$

Note that each term has the dimensions of length; E_w is called the **total head**, and the terms on the right are called the **velocity head**, the **pressure head**, and the **elevation head**, respectively. In a real fluid, friction degrades mechanical energy to heat as the fluid moves along a streamline. This decrease in mechanical energy from point to point, expressed per unit weight of fluid, is called the **head loss**. If you add up all three terms on the right in Equation 5.4.1 the sum decreases downstream, no matter how the values of the individual terms change.

It would be nice to generalize Equation 5.4.1 so that it applies to an entire open-channel flow, not just to each streamline in it. The problem in doing this is that velocity, elevation, and pressure are not constant from point to point on a cross section. But if there are no strong fluid accelerations normal to the flow direction, pressure is close to being hydrostatically distributed: $p = \gamma(d - y)$. Then the sum of the elevation head and the pressure head can be written

$$\begin{aligned} h + \frac{p}{\gamma} &= h_o + y + \frac{p}{\gamma} \\ &= h_o + y + \frac{\gamma(d-y)}{\gamma} \\ &= h_o + d \end{aligned} \tag{5.4.2}$$

where h_o is the elevation of the channel bottom. Variations in pressure and elevation over the cross section are thus taken into account in Equation 5.4.1. Variation in velocity is still a problem, but in turbulent flows the velocity profile is so flat over most of the section that only a small correction need be made in order to replace v by the cross-sectional mean velocity U. Equation 5.4.1 can then be written between two cross sections 1 and 2 in a channel flow that varies only slowly downstream as

$$\begin{aligned} \text{head loss} &= (E_w)_2 - (E_w)_1 \\ &= \frac{U_2^2}{2g} + h_{o2} + d_2 - \left(\frac{U_1^2}{2g} + h_{o1} + d_1 \right) \end{aligned} \tag{5.4.3}$$

A plot of E_w against downchannel position is called the **energy grade line**, and the slope of this line (or, generally, curve) is the **energy gradient** or **energy slope**.

In a *uniform* open-channel flow, for which both kinetic energy and potential energy are the same at every cross section but potential energy decreases downstream, the head loss is simply the rate of decrease of elevation head downstream, or in other words the slope of the water surface and bed surface, which is then also equal to the energy slope.

It is often useful to apply Equation 5.4.3 to an open-channel flow that varies rapidly enough that there is little head loss but slowly enough that the hydrostatic-pressure approximation is not too far wrong. Those conditions are not very restrictive: examples are a gentle rise or fall in the channel bed, as in the first "practical problem" posed earlier in this chapter (Figure 5.2.1) or a gentle expansion or contraction of the channel walls. The development in the rest of this section is meant to address such cases. Equation 5.4.3 becomes

$$\frac{U_2^2}{2g} + h_{o2} + d_2 = \frac{U_1^2}{2g} + h_{o1} + d_1 \tag{5.4.4}$$

A convenient quantity to substitute into Equation 5.4.4 is $d + U^2/2\mathrm{g}$, called the **specific head** H_o:

$$H_o = d + \frac{U^2}{2g} \tag{5.4.5}$$

Ho, also called the **specific energy**, is simply the head (i.e., flow energy per unit weight) relative to the channel bottom. Using H_o , Equation 5.4.4 becomes

$$H_{o2} + h_{o2} = H_{o1} + h_{o1} \tag{5.4.6}$$

or

$$H_{o2} = H_{o1} - (h_{o2} - h_{o1}) \tag{5.4.7}$$

Now look at a unit slice parallel to the flow direction in a two- dimensional flow. In other words, you do not have to worry about the sidewalls because they are far away relative to what is happening locally.) Discharge per unit width q is constant and equal to Ud. Substitution of $U = q/d$ into the definition for specific head eliminates U and provides a relation between d and H_o for each value of q:

$$H_o = \frac{q^2}{2gd^2} + d \tag{5.4.8}$$

The family of curves of H_o vs. d for various values of q is called the **specific-head diagram** or **specific-energy diagram** (Figure 5.4.1).

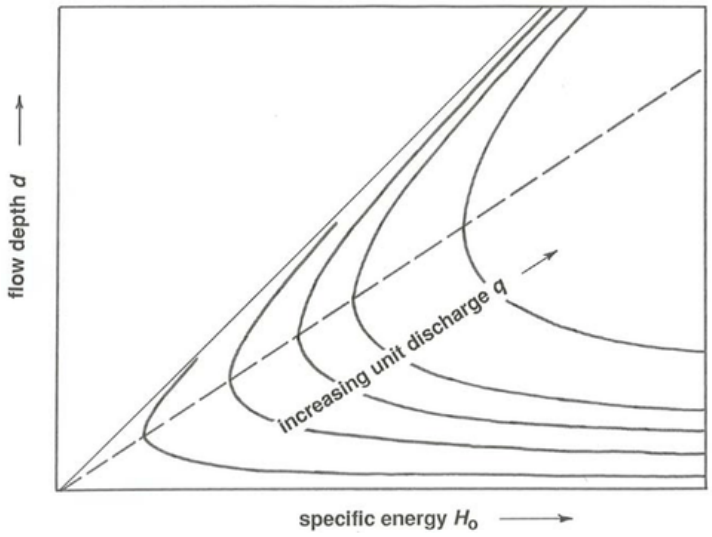


Figure 5.4.1: The specific-energy diagram. Each of the curves is for a given value of discharge per unit width, q.

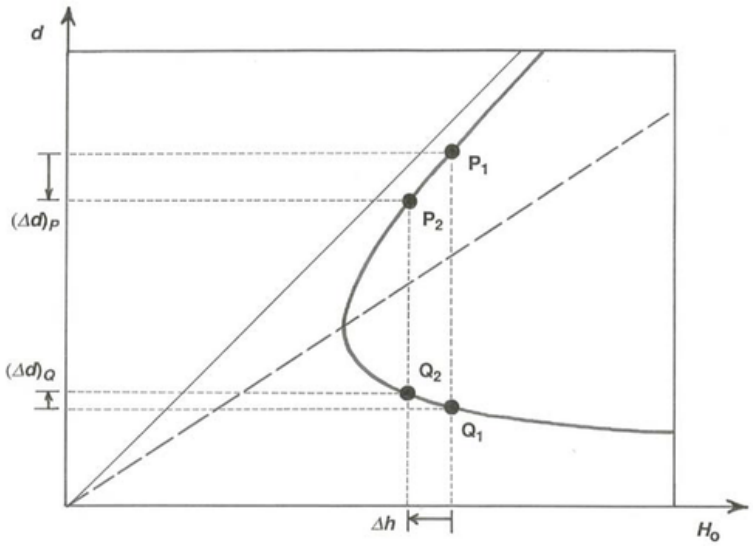


Figure 5.4.2: The specific-energy diagram for one particular value of q, to illustrate the effect of raising the channel bottom by a distance δh. See text for explanation.

To illustrate the usefulness of the specific-head diagram, suppose that the flow approaching the step shown in Figure 5.2.1 is characterized by values of q, d, and H_o (i.e.: discharge per unit channel width; depth; and flow energy) that plot at point P_1 in Figure 5.4.2, on the upper part of the curve for the given q. Because the bottom rises by a positive distance $\delta h = h_{o2} - h_{o1}$, by Equation 5.4.7 the specific head H_{o2} associated with the flow downstream of the transition lies a distance δh to the left of H_{o1} along the H_{o1} axis; P_2 is the corresponding point that represents the flow. Flow depth downstream of the step is therefore smaller by $(\Delta d)_P$ in Figure 5.4.2 than in the approaching flow, and by the relation $q = Ud$ the flow velocity is greater (Figure 5.4.3). Does that do damage to your intuition?

By virtue of the doubly branched form of the curves in Figure 5.4.1 there can also be an approaching flow, represented by point Q_1 on the lower part of the same curve, with exactly the same discharge and flow energy but with shallower depth and higher velocity. In this case the flow downstream of the transition, represented by the point Q_2 found by moving a distance δh leftward along the H_o axis as before, has depth greater by $(\delta d)Q$ than the approaching flow, and smaller velocity (Figure 5.4.4). Open-channel hydraulicians speak of *upper and lower alternate depths*.

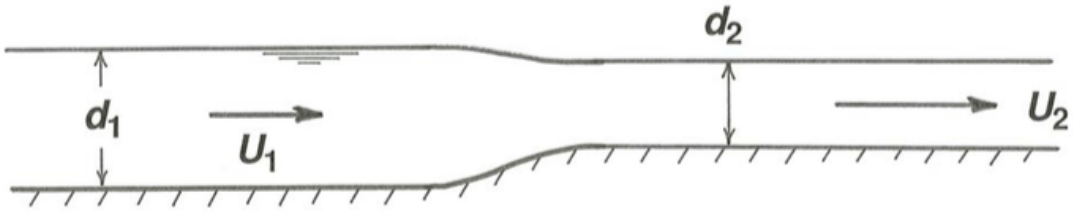


Figure 5.4.3: The effect of raising the channel bottom beneath a subcritical approaching flow. The depth decreases over the transition, and the mean flow velocity increases.

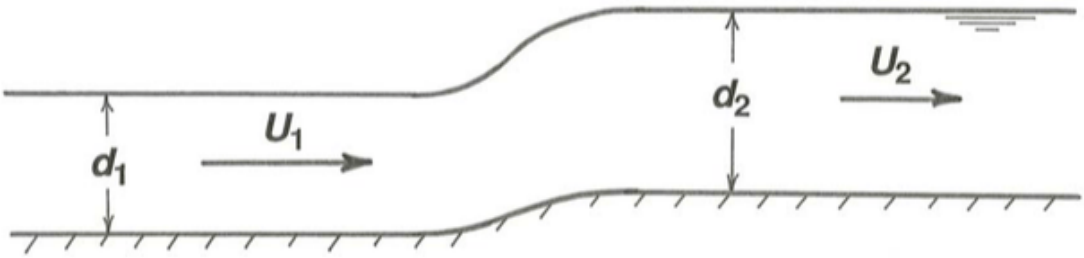


Figure 5.4.4: The effect of raising the channel bottom beneath a supercritical approaching flow. The depth increases over the transition, and the mean flow velocity decreases.

For points at which the curves of d vs. H_o have vertical tangents, depth and velocity do not change in the transition. Flows corresponding to these points are called critical flows. The equation for such points is found in two steps. First, differentiate the function in Equation 5.4.8 to find $dH_o/d(d)$, set this derivative equal to zero, and solve for q as a function of d. The result is

$$q_c^2 = gd_c^3 \tag{5.4.9}$$

where the subscript c indicates that the equation is for the critical condition of vertical tangency. Then substitute this expression for q_c^2 into Equation 5.4.8 to obtain

$$H_{oc} = \frac{3}{2}d_c \tag{5.4.10}$$

again with the subscript c denoting critical flow.

The locus of points in the specific-head diagram for which the flow is critical is thus a straight line with a slope of $2/3$. It is shown in Figure 5.4.1 as a dashed line extending upward and to the right from the origin. Flows corresponding to points above the line are **subcritical** (deeper depths and lower velocities), and flows corresponding to points below the line are **supercritical** (shallower depths and higher velocities).

Thus, to every combination of discharge per unit width q and flow energy (represented by H_o) there correspond two different possible flow states, with different depth and velocity given by the two intersections of the curve of d vs. H_o for that q and the vertical line associated with that H_o. In some kinds of transitions along the channel, the flow is forced all the way from one of these states to the other, thereby passing through the critical state during the transition. Any flow, whatever its origin and therefore whatever its depth and discharge, falls at some point on one of the curves in the specific-head diagram, and is therefore either supercritical or subcritical (or critical). The behavior of that flow in a transition is radically different depending on whether the flow is subcritical or supercritical. This difference in behavior is fundamentally a consequence of the requirement of conservation of flow energy expressed by Equation 5.4.4, together with the conservation-of-mass requirement that

$$q = \frac{U_1}{d_1} = \frac{U_2}{d_2} \tag{5.4.11}$$

For example, in the transition examined above, the variables U_1, d_1, h_{o1}, and h_{o2} are all given, and Equations 5.4.4 and 5.4.10 then specify exactly which combination of U_2 and d_2 must hold.

It happens that the condition for critical flow corresponds to a mean-flow Froude number $U/(gd)^{1/2}$ of unity. To verify this, simply substitute Equation 5.4.9, the condition for critical flow, into Equation 5.4.5, the definition for H_o, to obtain a relation between U and d for critical flow: $U^2 = gd$, or $\mathrm{Fr} = 1$. Subcritical flows are characterized by Froude numbers less than one, and supercritical flows are characterized by Froude numbers greater than one.

You will see in Chapter 6, on oscillatory flow, that the speed c of a gravity wave in shallow water is $(gd)^{1/2}$, where d is the water depth. If you substitute this wave speed c for the denominator $(gd)^{1/2}$ in the definition of the Froude number, you see that for a Froude number equal to one the mean flow velocity is equal to the speed of surface waves. A water-surface wave that is moving in the upstream direction appears to an observer on the channel bank to be standing still. This means that if the Froude number of the flow is greater than one, wavelike disturbances cannot propagate upstream: the flow coming from upstream cannot know what is in store for it at positions downstream. In subcritical flow, on the other hand, the upstream flow *can* be influenced, commonly for long distances, by conditions downstream.

That last point is well illustrated by one final consideration of the upward step shown in Figure 5.2.1. As the step height is gradually increased, the corresponding point on the upper branch of the specific head diagram moves leftward and downward from point P toward the point of vertical tangent, C. The farther along the curve the point shifts, the greater is the decrease in flow depth over the step. But there is a limit to this effect: the specific energy cannot decrease beyond that corresponding to the point C of vertical tangent, because the flow has to stay on the $q = \text{constant curve}$. So what happens as the step is raised even further? The flow over the step remains critical and the depth upstream of the step increases. Instead of having no effect on the upstream flow, as was the case for lower steps, the step now acts as a dam: its effect is felt far upstream.

You might be wondering at this point how the flow condition represented by the alternate point on the specific-head diagram can be attained. To see how that might happen, suppose that the geometry of the step in Figure 5.2.1 is changed a bit: after the crest of the step is reached, the channel bottom falls smoothly again to its original height. If now for the approaching subcritical flow with given q the step height is raised to the point where the flow over the step has just attained the critical condition, represented by point C on the curve for the given q in Figure 5.4.5, the passage of the flow downstream to the original level is manifested on the specific-head diagram as a shift from point P to point Q vertically below the original point P but on the lower (supercritical) limb of the q curve. The flow is now at the same elevation, and has the same energy (i.e., the same channel-bottom elevation and the same specific head), but it is now flowing at a greatly different combination of depth and velocity, corresponding to supercritical flow (Figure 5.4.6). What is happening, physically, in contrast to graphically, is that the critical flow at the crest of the step accelerates down the lee side of the step, to attain a supercritical velocity (and, by virtue of conservation of mass, a shallower depth). If the step is raised even beyond what is needed to attain the critical condition, then the flow upstream is dammed, and its depth increases, forcing point P upward to the right along the curve for the given q in the specific-energy diagram.

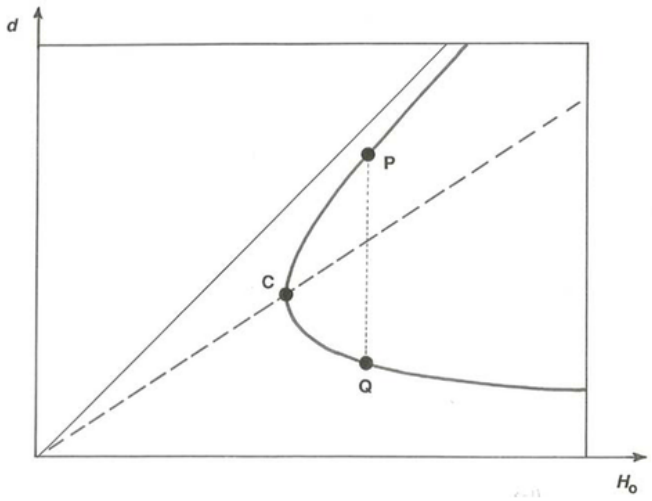


Figure 5.4.5: The specific-energy diagram for one particular value of q, to illustrate the effect of raising and then lowering the channel bottom to force the flow to pass from subcritical to supercritical.

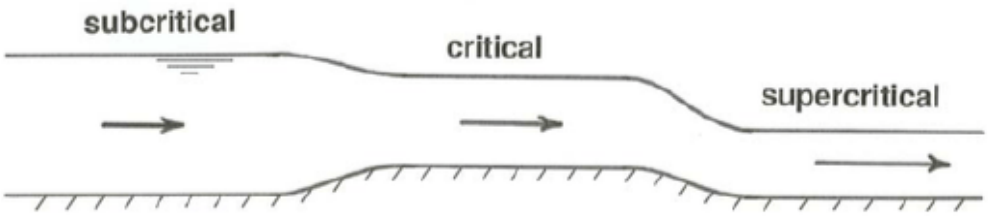


Figure 5.4.6: The behavior of the flow over a rise and then a fall of the channel bottom, when an approaching subcritical flow is forced to the critical condition by raising the step by a sufficiently large increment.

A final comment is that the supercritical flow downstream of the step does not stay supercritical for a very great distance, unless the slope of the bottom downstream of the step becomes much steeper. If the bottom retains its gentle slope, a hydraulic jump is likely to be formed at some point downstream, with the consequence that the flow reverts to its original subcritical condition; see the following section.

This page titled 5.4: Energy in Open-Channel Flow is shared under a CC BY-NC-SA 4.0 license and was authored, remixed, and/or curated by John Southard (MIT OpenCourseware) via source content that was edited to the style and standards of the LibreTexts platform.

5.5: The Hydraulic Jump

We still have not milked the positive-step example, as arranged in Figure 5.4.6, for all the insight it affords. We made the implicit assumption that the flow coming from upstream had a combination of depth and velocity corresponding to the given q that was the outcome of the particular gentle channel slope that exists for a long distance upstream; see the earlier section on uniform flow. The combination of slope, discharge per unit width, and bed roughness was such as to provide subcritical flow at that d and U. We should expect that the flow would like to settle back to that same subcritical condition, somewhere far downstream of the step. But you have just seen that for a sufficiently high step— just high enough for the flow to attain the condition of critical flow, but not so high as to change the upstream flow—the flow for some distance downstream of the step is supercritical. How, then, does the flow pass from being supercritical, just downstream of the step, to subcritical far downstream? The answer is that commonly in situations like this the change from supercritical to subcritical is abrupt, in the form of what is called a **hydraulic jump**, rather than gradual.

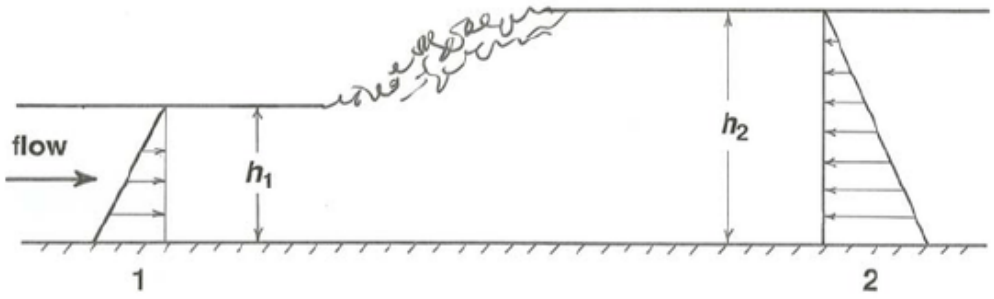


Figure 5.5.1: The hydraulic jump. The distribution of hydrostatic pressure is shown at section 1, upstream of the jump, and at section 2, downstream of the jump.

Hydraulic jumps are a striking feature of open-channel flow. You have all seen them, if only in your kitchen sink. You turn the faucet on full force, and the descending jet impinges on the bottom of the sink to form a thin, fast-moving sheet of water, with supercritical depth and velocity, that spreads out in all directions. But at a certain radius from the point of impact of the jet, which depends on the force of the down-flowing jet, the flow jumps up to a deeper and slower flow as it moves toward the drain. The jump is in the form of a steep and nearly stationary front accompanied by strong turbulence (Figure 5.5.1). Another situation in which a hydraulic jump commonly forms is downstream of a change from a relatively steep channel slope, with which supercritical flow is associated, to a relatively gentle channel slope, over which a uniform flow would be subcritical. If the change in slope is sufficiently rapid, the transition from supercritical flow to subcritical flow is in the form of a hydraulic jump rather than a smooth change in depth and velocity.

The nature of the hydraulic jump cannot be accounted for by use of the energy equation, because there is a substantial dissipation of energy owing to the turbulence associated with the jump; we need to appeal instead to conservation of momentum.

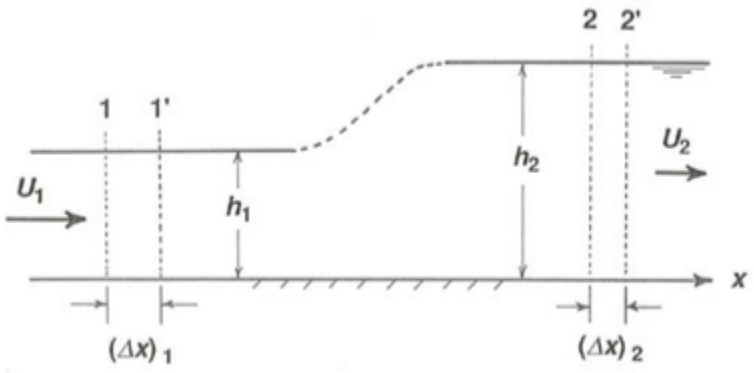


Figure 5.5.2: Definition sketch for deriving the moment diagram for flow through a hydraulic jump. The block of fluid contained between sections 1 and 2 at a given time is located between sections $1'$ and $2'$ a short time Δt later.

Figure 5.5.1 is a cross-section view of the flow from upstream of the hydraulic jump to downstream of it. Look at a block of the flow bounded by imaginary vertical planes at cross sections 1 and 2. The distributions of hydrostatic pressure forces are shown on the upstream and downstream faces of the block. You would have to locate section 2 quite a distance downstream of the jump, because it takes a long distance for the downstream flow to become organized. In the absence of any submerged obstacle to the flow between sections 1 and 2, the only streamwise forces on the fluid in the block are the pressure forces on the upstream and downstream faces; the hydraulic jump itself exerts no force on the flow. To see the effect of these forces, we need to do some momentum bookkeeping for use in Newton's second law, $F = ma$. For that purpose, look at Figure 5.5.2, a slight redrawing of Figure 5.5.1.

In a short time interval Δt, the block of fluid moves downstream from positions 1 and 2 to positions $1'$ and $2'$. In that time it has lost momentum equal to that of the fluid that was between sections 1 and $1'$. That momentum, written per unit flow width (remember that the channel is of the same width from upstream to downstream of the hydraulic jump) is $[\rho d_1 (\Delta x)_1] U_1$, where U_1 is the mean velocity at section 1. This can be expressed slightly differently, keeping in mind that $U_1 = (\Delta x)_1 / \Delta t$ and $q = Ud$, as $\rho d_1 U_1^2 \Delta t$, or $\rho q U_1 \Delta t$. This can be written in still another form by eliminating U_1 by use of the relationship $q = Ud$ again: $(q^2 \rho / d_1)\, \Delta t$. Likewise, during Δt the fluid block has gained momentum equal to that of the fluid that has moved in to occupy the volume between sections 2 and $2'$: $(q^2 \rho / d_2)\, \Delta t$. The change in momentum as the fluid block moves from position 1–2 to position $1'$–$2'$ is then

$$\left(\frac{q^2 \rho}{h_1}\right) \Delta t - \left(\frac{q^2 \rho}{h_2}\right) \Delta t \tag{5.5.1}$$

or

$$\left(\frac{q^2 \rho}{h_1} - \frac{q^2 \rho}{h_2}\right) \Delta t \tag{5.5.2}$$

The time rate of change of momentum of the fluid block is then obtained by dividing by the time interval Δt:

$$\frac{q^2 \rho}{h_1} - \frac{q^2 \rho}{h_2} \tag{5.5.3}$$

By Newton's second law, we can set this rate of change of momentum equal to the net streamwise force on the fluid block, F_1 (acting in the downstream direction) minus F_2 (acting in the upstream direction). The linear distribution of hydrostatic pressure forces on the upstream and downstream faces of the fluid block make it easy to find the resultant forces F_1 and F_2:

$$F_1 = \int_0^{h_1} \rho g y dy = \frac{1}{2} \rho g h_1^2 \tag{5.5.4}$$

and likewise $\mathrm{F}_2 = (1/2) \rho \mathrm{g} d_2^2$. The net force on the fluid block is then

$$F_1 - F_2 = \frac{\rho g h_1^2}{2} - \frac{\rho g h_2^2}{2} \tag{5.5.5}$$

Finally, setting this net force equal to the rate of change of momentum,

$$\frac{q^2 \rho}{h_1} - \frac{q^2 \rho}{h_2} = \frac{\rho g h_1^2}{2} - \frac{\rho g h_2^2}{2} \tag{5.5.6}$$

We can massage this a bit to put it into a form that is more convenient for our purposes by rearranging and dividing through by ρg:

$$\left(\frac{q^2}{g h_1} + \frac{h_1^2}{2}\right) - \left(\frac{q^2}{g h_2} + \frac{h_2^2}{2}\right) = 0 \tag{5.5.7}$$

What is commonly done is to define a quantity

$$M = \frac{q}{g d} + \frac{d^2}{2} \tag{5.5.8}$$

called the **momentum function**. Then Equation 5.5.7 boils down to $M_1 - M_2 = 0$, which says that the momentum function does

not change through the transition, provided that no streamwise forces other than the hydrostatic pressure forces (like resistance forces exerted by obstacles in the channel bottom) act on the fluid block.

Just as with the specific energy in an earlier section, we can plot a useful graph of the momentum function M against the flow depth d (Figure 5-15). And just as with the specific-energy diagram (Figure 5.2.1), you can verify the shape of the curve in Figure $5.5.3$ by assuming a value for q, choosing some values for d, and computing the corresponding values of M; in this case, however, there is no unrealistic limb of the function below the $d = 0$ axis. There is a family of curves, of the general shape shown in Figure $5.5.3$, one for each value of discharge per unit width q. As with the specific-energy diagram, all points on the upper limb of each curve, above the point of vertical tangent, represent supercritical flow, and all points on the lower limb, below the point of vertical tangent, represent subcritical flow.

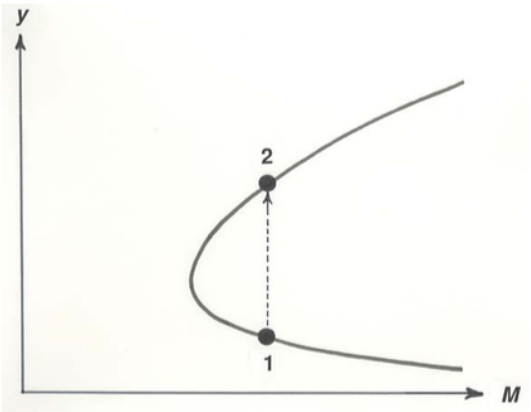


Figure $5.5.3$: The momentum diagram: a plot of the momentum function M vs. flow depth y, shown for one of a family of curves for values of discharge per unit width, q.

Now we have the tools to predict the height of the hydraulic jump. We start at point 1 on the lower, supercritical limb of the curve in Figure $5.5.3$, and jump up to point 2, at the same value of M but on the upper, subcritical limb, corresponding to the deeper, subcritical flow downstream of the hydraulic jump. You can see that the closer to the critical condition the upstream supercritical flow is, the smaller is the height of the hydraulic jump to subcritical flow, represented by the vertical distance between the respective points of intersection of the $M =$ constant vertical line with the two limbs of the curve in Figure $5.5.3$.

Note

Just as the shapes of the curves in the family of curves with q as the parameter in Figure $5.5.3$ differ from the shapes of the corresponding curves in Figure 5.2.1, the specific-head diagram, so do the equations for the condition of critical flow—but that need not concern us here. You yourself can take the one further step, the same as for the specific-head diagram, to find the shape of the curve for critical flows in Figure $5.5.2$, the momentum-function diagram.

Finally, one incidental note is in order. The subcritical flow downstream of the jump, which emerges from the considerations above, is not exactly of the same depth and velocity as the subcritical uniform flow that is ultimately attained far downstream of the step; there is some slow further adjustment to that condition.

This page titled 5.5: The Hydraulic Jump is shared under a CC BY-NC-SA 4.0 license and was authored, remixed, and/or curated by John Southard (MIT OpenCourseware) via source content that was edited to the style and standards of the LibreTexts platform.

5.6: Hydraulic Regimes of Open-Channel Flow

Now that you know about supercritical vs. subcritical flow as well as about laminar vs. turbulent flow, various phenomena of open-channel flow can be drawn together into a single graph, to give you an idea of the wide range of hydraulic regimes of flow that can exist. Figure $5.6.1$ is a graph of mean flow depth against mean flow velocity for steady uniform open-channel flow in a wide rectangular channel. If bed roughness is present, its height is assumed to be a small fraction of the flow depth. Both depth and velocity span several orders of magnitude, a far greater range than is found in the sediment-transporting flows encountered in natural flow environments.

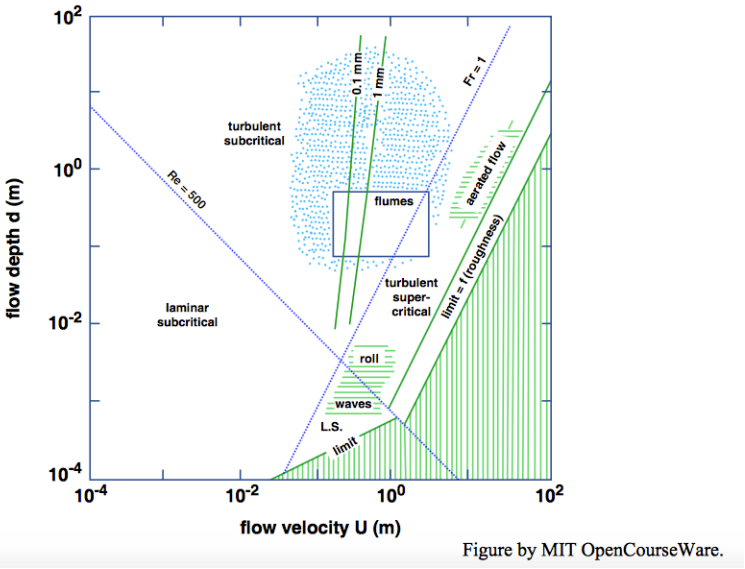


Figure $5.6.1$: Hydraulic regimes of open-channel flow in a graph of mean flow depth vs. mean flow velocity. See text for explanation of curves.

It is easy to plot curves in Figure $5.6.1$ corresponding to $\mathrm{Fr} = 1$, for the transition between subcritical flow and supercritical flow, and to $\mathrm{Re} = 500$ (Re based on flow depth), for the transition between laminar flow and turbulent flow. In a *log–log* plot like Figure $5.6.1$ both of these conditions plot as straight lines; the line for $\mathrm{Fr} = 1$ slopes upward to the right, and the line for $\mathrm{Re} = 500$ slopes downward to the right. These two lines partition the graph into four sectors: *turbulent subcritical* in the upper left (the most common in natural open-channel flows), *turbulent supercritical* in the upper right, *laminar subcritical* in the lower left, and *laminar supercritical* in the lower right.

The usefulness of a graph like Figure $5.6.1$ is that it helps to put into perspective the wide range of open-channel flows. The flow regimes shown in Figure 5.5.3 are just extensions of the concept of flow regimes introduced in the discussion of flow around a sphere in Chapter 3.

In the lower part of Figure $5.6.1$ are two curves (one for laminar flow and the other for turbulent flow) sloping upward to the right, below which steady, uniform open-channel flows cannot exist. These curves are defined by the condition that channel slope approaches the vertical, giving the greatest gravitational driving force possible. It is easy to get an exact solution for the curve that expresses this condition for laminar flow, by integrating Equation 4.7.6 to find the mean velocity U as a function of flow depth, fluid properties γ and μ, and channel slope angle ϕ, and then taking $\sin\phi = 1$, giving $U = d^2\gamma/3\mu$. This plots as a straight line in $5.6.1$. A sheet of rainwater running down a soapy windowpane is an example of flows represented by this line.

It is not as easy to obtain the limiting curve for turbulent flows, because we have to work with a resistance diagram like that in Figure 4.7.11. The curve shown in Figure $5.6.1$ was drawn in an approximate way by obtaining the friction factor f from the smooth-flow curve in Figure 4.7.7 and using that value together with $\tau_0 = \gamma d \sin\alpha$ in Equation 4.6.4. Figure 4.7.7 is for circular pipes, but it should be roughly applicable to open-channel flow provided that the pipe diameter is appropriately replaced. Four times the flow depth was used in place of pipe diameter in computing the Reynolds number in Figure 4.7.7, because as noted in Chapter 4 the hydraulic radius of a circular pipe is one-fourth the pipe diameter, whereas the hydraulic radius of a very wide open-channel flow is just about equal to the flow depth. For rough flows the limiting curve in Figure 5.5.3 would be displaced upward somewhat, because the friction factor is greater for a given Reynolds number.

This page titled 5.6: Hydraulic Regimes of Open-Channel Flow is shared under a CC BY-NC-SA 4.0 license and was authored, remixed, and/or curated by John Southard (MIT OpenCourseware) via source content that was edited to the style and standards of the LibreTexts platform.

5.7: Gradually Varied Flow

Nonuniform flows for which the changes in depth and velocity are so abrupt that radial accelerations distort the vertical distribution of fluid pressure from the hydrostatic condition are called **rapidly varied flows**. Flow over a sharp-crested dam or weir, and flow under a sluice gate, are good examples. Such flows are difficult to deal with analytically, and I will not pursue them here, although they are important in many engineering applications.

Nonuniform open-channel flows for which the changes in depth and velocity are slow enough in the downstream direction that the vertical distribution of fluid pressure from the free surface to the bottom is not much different from hydrostatic are called **gradually varied flows**. An example is the flow transition over a gentle step, introduced at the beginning of this chapter (Fig. 5.2.1). It is completed in a sufficiently short distance that loss of flow energy by friction can be neglected, but the fluid accelerations are still sufficiently small that the vertical distribution of fluid pressure is close to being hydrostatic. In most gradually varied flows, however, the change takes place over a distance sufficiently great that we cannot assume zero energy loss due to bottom friction. The second channel-transition example posed at the beginning of this chapter falls into that category.

To see what happens to the elevation of the water surface through a transition over such a long distance that bottom friction cannot be neglected, we need to start with the equation for the total head at a cross section of the flow and differentiate each term with respect to distance in the flow direction. (In what follows, I am going to write γ instead of d for the flow depth.) Start with Equation 5.4.1, written using the elevation of the channel bottom h_o (cf. Equation 5.4.2):

$$E_w = \frac{U^2}{2g} + y + h_o \tag{5.7.1}$$

Differentiate Equation 5.5.1 with respect to the flow direction x:

$$\frac{dE_w}{dx} = \frac{\mathrm{d}\left(U^2/2g\right)}{dx} + \frac{dy}{dx} + \frac{dh_o}{dx} \tag{5.7.2}$$

The term on the left side of Equation 5.7.2 is the rate of change in total energy in the downstream direction. This is always negative, because energy is inevitably lost by friction. Think in terms of the downward slope of the line formed by plotting E_w as a function of downstream distance. This slope, denoted by S_e, is what was called the **energy slope**, or the **energy gradient**, or the **slope of the energy line** earlier in this chapter. By convention, such a negative slope is considered to be positive S_e, so we replace dE_w/dx in Equation 5.7.2 by $-S_e$.

Friction loss in nonuniform flow is not well studied, but to get somewhere just in a qualitative way we can assume that the friction loss in slightly to moderately nonuniform flow is not greatly different from what it would be in uniform flow—and we have already dealt with that satisfactorily in Chapter 4. Remember the Chézy coefficient I introduced back then? According to Equation 4.6.3, repeated here as Equation 5.7.3,

$$U = C(y \sin \alpha)^{1/2} \tag{5.7.3}$$

Assuming that $\tan \alpha \approx \sin \alpha$, which is a very good approximation for the small angles we are dealing with here, and keeping in mind that the slope $\tan \alpha$ is just S_e, and solving for S_e,

$$S_e = \frac{U^2}{C^2 y} \tag{5.7.4}$$

This can be written a little more usefully by getting rid of U by use of the relation $q = Uy$; remember that the discharge per unit channel width q (which is constant along the channel) is related to the mean velocity U by this relation. Then Equation 5.7.4 can be written

$$S_e = \frac{q^2}{C^2 y^3} \tag{5.7.5}$$

Now for some manipulation of the right side of Equation 5.7.2. The first term on the right can be massaged in the following way to put it into a more useful form. In what follows, again keep in mind that the discharge per unit channel width q is related to the mean velocity U and the flow depth y by the equation $q = Uy$.

$$\frac{d}{dx}\left(\frac{U^2}{2g}\right) = \frac{d}{dx}\left(\frac{q^2}{2gy^2}\right)$$
$$= \frac{q^2}{2g}\frac{d}{dx}\left(\frac{1}{y^2}\right)$$
$$= \frac{q^2}{2g}\left(\frac{-2}{y^3}\right)\frac{dy}{dx}$$
$$= -\frac{q^2}{gy^3}\frac{dy}{dx} \tag{5.7.6}$$

For later convenience, one more thing needs to be done with this result. Go back to Equation 5.4.9, which gives the relationship between q and y that holds when the flow is critical, and write the depth as y instead of d (just a matter of notation, as explained above), and substitute that equation into Equation 5.7.6. What you get is

$$\frac{d}{dx}\left(\frac{U^2}{2g}\right) = -\frac{yc^3}{y^3}\frac{dy}{dx} \tag{5.7.7}$$

With regard to the second term on the right in Equation 5.7.2, we do not have to do anything further with it, because it just represents the rate of change of flow depth in the downstream direction.

The last term in Equation 5.7.2 represents the slope of the channel bottom (remember that h_o was defined as the elevation of the channel bottom), and because in the realm of channel flows the downward slope is arbitrarily defined as positive that last term can just be written $-S_o$, where $-S_o$ is the slope of the channel bottom. $-S_o$ can be written in a form that you will see is useful: think about the hypothetical uniform flow that could pass down the given bottom slope (which, remember, in reality has a nonuniform flow at some different depth passing over it). The depth of this hypothetical uniform flow over any given bottom slope is called the **normal depth**, y_n. Just as with S_e, you can express $-S_o$ in terms of the Chézy equation by using this normal depth y_n:

$$S_o = \frac{q^2}{C^2 y_n^3} \tag{5.7.8}$$

So now, upon substitution of all these reworked forms of the various terms into Equation 5.7.2, and then bringing the terms with dy/dx to the left and the other two to the right, the equation reads as follows:

$$\frac{dy}{dx}\left(1 - \frac{y_c^3}{y^3}\right) = \frac{q^2}{C^2 y_n^3} - \frac{q^2}{C^2 y^3} \tag{5.7.9}$$

Rewrite the second term on the right in the form

$$\frac{q^2}{C^2\left(\frac{y^3}{y_n^3}\right)y_n^3}$$

and apply to this term the expression for S_o given in Equation 5.7.8 to obtain

$$S_o\left(\frac{y_n^3}{y^3}\right)$$

and substitute that result into Equation 5.7.9, replacing the last term back with S_o also. Finally, solve for dy/dx to get the grand finale:

$$\frac{dy}{dx} = S_o\frac{1 - \left(\frac{y_n}{y}\right)^3}{1 - \left(\frac{y_c}{y}\right)^3} \tag{5.7.10}$$

To get you back on the ground after that tortuous (also torturous?) exercise in manipulation (see Figure 5.7.1 for a summary "road map"), what Equation 5.7.10 does is give, for a flow that is slowly changing its depth in the downstream direction, the rate of change of depth with downstream distance, as a function of

1. The bottom slope S_o
2. The critical depth y_c associated with the given discharge (that is, the flow depth you would see if a flow with that discharge per unit width were in the form of critical flow—which it is not), and

3. The normal depth y_n associated with the given discharge (that is, the flow depth you would see if a flow with that bottom slope and that discharge per unit width were uniform—which it is not).

The only thing that stands in the way of perfection is the assumption we made that the friction loss in nonuniform flow at a given depth and discharge is the same as would be seen in the corresponding uniform flow at the same depth and discharge.

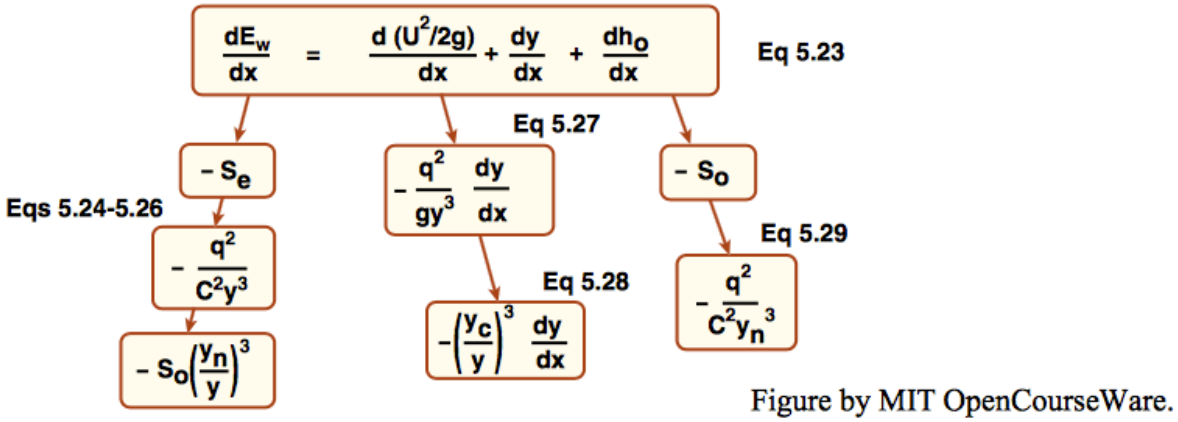


Figure 5.7.1: A "road map" to aid in following the analysis of backwater curves in the text.

People do numerical integrations of Equation 5.7.10 to get approximate but reasonable water-surface profiles in real gradually varied flows. But what is also commonly done is just to use Equation 5.7.10 as a qualitative guide to the profile shape to be expected. We will do a little of that here, so that we can finally address the problem of what the water surface looks like as the river runs into the deep reservoir—and that is just one of the many important problems that can be attacked by this approach.

What you need to think about is the sign of dy/dx on the left side of Equation 5.7.10, because if dy/dx is positive then the flow depth increases downstream, and if dy/dx is negative then the flow depth decreases downstream— and this is just the information we need in order to keep track of what the water surface does relative to the channel bottom.

The derivative dy/dx is *positive* (meaning that the depth increases downstream) if in Equation 5.7.10 both the numerator and the denominator are positive or if both the numerator and the denominator are *negative*. Conversely, dy/dx is negative, and the depth decreases downstream, if the numerator and the denominator have different sign.

Another thing we can do is think about the conditions under which

1. dy/dx *becomes zero*, meaning that the flow approaches the uniform condition, or
2. dy/dx *approaches infinity*, meaning that the water surface gets steeper and steeper (obviously, something has to happen before it gets to be vertical!), or
3. dy/dx *becomes equal to* S_o, meaning that the water surface approaches horizontality.

Suppose that our river flow is subcritical, as is usually the case for large rivers, meaning that the depth is greater than critical and the velocity is less than critical. We can express this by the condition $y > y_c$. So the *denominator* in the fraction in the right side of Equation 5.7.10, which in the following I will call F, is always *less than one*. With regard to the *numerator*, you know already that whatever the actual shape of the water-surface profile, the depth must ultimately increase when the reservoir is reached, so $y > y_n$ as well. Also, because we said that the approaching river is subcritical, you know that $y_n > y_c$. You can easily convince yourself that these three inequalities guarantee that the fraction F must be positive and less than one, so dy/dx is positive and less than S_o, meaning that the depth gradually increases downstream.

As y gets larger and larger in the process, both the numerator and the denominator of F go to one, meaning that dy/dx goes to S_o, which if you think about it a little bit is the same as saying that *the water surface itself becomes horizontal*. So our conclusion is that the water-surface profile is as shown in Figure 5.7.2A: it is asymptotic to the uniform-flow profile upstream, and to the horizontal water surface of the reservoir downstream. This kind of curve is called a **backwater curve**, for reasons I suppose are obvious.

To carry this analysis just a little further, what is the effect of assuming that the river upstream is flowing at conditions closer

to being critical? You can see by inspection of the fraction F that as $y_n \to y_c$, F itself stays closer and closer to one for $y > y_n$, meaning that the transition from the almost uniform flow upstream to the horizontal reservoir level downstream is sharper and sharper (that is, it takes place over a shorter and shorter distance), until, for critical flow upstream, the river meets the reservoir at a sharp angle (Figure $5.7.2$B)!

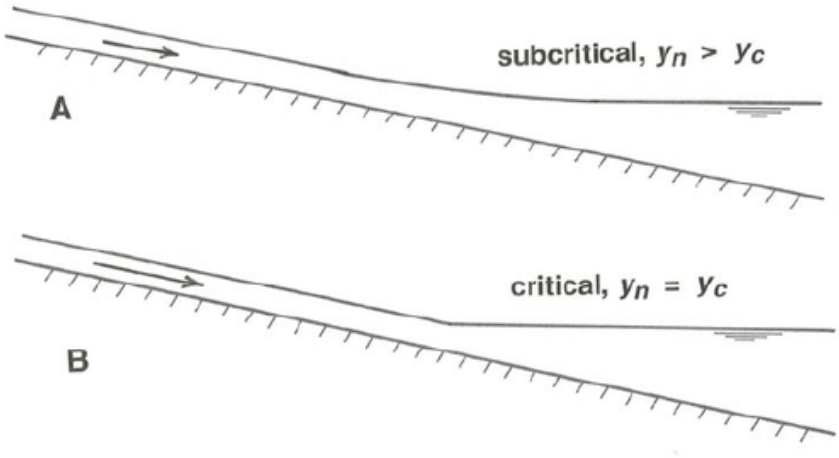


Figure $5.7.2$: Qualitative water-surface profiles when a river in **A)** subcritical flow and **B)** supercritical flow enters a lake or a reservoir.

For big rivers flowing well below the critical condition, the backwater effect is felt not just for kilometers but for tens of kilometers upstream, and the superelevation of the actual water surface above the hypothetical point of intersection between the uniform flow and the reservoir level can be many meters. You can imagine the importance of being able to predict the magnitude of this superelevation at all points upstream, when you are worrying about how many homes and farms and businesses you are going to be flooding when you build that dam.

I have just scratched the surface of the business of analyzing backwater effects. There are many qualitatively different kinds of backwater curves, depending upon whether the approaching flow is subcritical, critical, or supercritical, and upon whether

1. $y > y_n$ and $y > y_c$,
2. y is between y_n and y_c, or
3. $y < y_n$ and $y < y_c$.

This page titled 5.7: Gradually Varied Flow is shared under a CC BY-NC-SA 4.0 license and was authored, remixed, and/or curated by John Southard (MIT OpenCourseware) via source content that was edited to the style and standards of the LibreTexts platform.

6: OSCILLATORY FLOW

6.1: Introduction
6.2: The Nature of Waves
6.3: Water Motions Due to Waves
6.4: Wave Boundary Layers
6.5: Combined Flow (Waves plus Current)

This page titled 6: Oscillatory Flow is shared under a CC BY-NC-SA 4.0 license and was authored, remixed, and/or curated by John Southard (MIT OpenCourseware) via source content that was edited to the style and standards of the LibreTexts platform.

6.1: Introduction

The first thing that comes to your mind when I mention water waves are probably the waves that appear on the water surface when the wind blows. These range in size from tiny ripples to giants up to a few tens of meters high and up to a few thousands of meters long. But many other kinds of waves make their appearance on water surfaces in nature. Here are the important kinds:

- **Flood waves in rivers**: Very long and very low, these waves propagate downstream at a speed that is different from the speed of the flowing water itself. It is important to try to predict both the speed and the maximum height of the flood wave.
- **Seiches in lakes and estuaries**: These are standing waves that are set up in an elongated basin by a sudden change in water-surface elevation in part of the basin, for example by a sudden drop in atmospheric pressure or by transport of surface water by a sudden strong wind. They may have just one node or more than one node.
- **Tidal bores in estuaries**: These are waves of translation, in which the water moves along with the wave. They have steep turbulent fronts, which can be hazardous to small boats.
- **Tsunamis (seismic sea waves) in the ocean**: These are extremely long and low-amplitude waves with high propagation speeds that are generated by sudden large-scale movements of the sea floor, usually by movement on faults but also by volcanic eruptions or submarine landslides. Their extreme destructiveness comes about because their amplitude increases spectacularly, sometimes to several tens of meters, when they shoal.
- **Internal waves in the atmosphere and the ocean**: When a fluid is stratified by density, waves can develop within the layer through which the density varies. This is easiest to appreciate when the density change is compressed to a jump discontinuity at a well-defined surface, but internal waves can exist also in layers with only gradual change in density. Internal waves care common in many settings in the ocean, and water velocities associated with the waves are in some cases strong enough to move bottom sediment. They are also common in the atmosphere.

Water waves of these kinds are called **gravity waves**, because, as you will see in a minute, gravity is the important force involved. But another important kind of waves, pressure waves, are present also in fluids, both air and water.

This page titled 6.1: Introduction is shared under a CC BY-NC-SA 4.0 license and was authored, remixed, and/or curated by John Southard (MIT OpenCourseware) via source content that was edited to the style and standards of the LibreTexts platform.

6.2: The Nature of Waves

Introduction

In a very fundamental sense, the waves that are of interest to us here can be viewed as a manifestation of unsteady free-surface flow subjected to gravitational forces. That is, any unsteady flow with a deformable free surface can be considered to be a kind of wave.

Do not let it bother you that real water waves involve changes in the water-surface geometry even when you follow along with the waves. You know from Physics I that a function of the form $y = f(x - ct)$ represents a wave traveling with speed c in the positive x direction—and the shape of the wave does not change if you just travel along with the wave. And c could be a function of t, meaning that the speed of the wave changes everywhere with time but the shape of the wave train still stays the same. But now suppose that you took one additional step: let c be a function of x rather than t. Then the shape of the wave changes as it moves: there is no speed at which you can travel, along with the wave, to keep the wave shape looking the same. The best way to think about this situation is that each point on the wave (you could call such points **wavelets**) has its own speed, so that, as all of them move, the overall shape of the wave changes with time.

In terms of the forces involved in wave motion, the motions of the water in the interior and the geometry of the free surface are an outcome of the interaction between pressure forces and gravity forces. Although it may or may not help you any, one way of thinking about waves is to consider that gravity tries to even out some initial nonplanarity of the water surface, and in doing so produces a usually complex unsteady flow in which the water-surface geometry changes as a function of time, but the characteristic amplitude of the water-surface disturbance has no way of actually decreasing unless viscous forces act also.

Real waves do decrease in amplitude, of course, because of the slight shear and therefore viscous friction in the interior of the water. But unless the waves produce water motions at the bottom, the rate of viscous dissipation of the wave motion is very slight. Mathematically, this means that the viscous term in the equation of motion can be ignored. Only when an oscillatory boundary develops at the bottom is the viscous dissipation substantial.

The Equations of Motion

The equation of motion that describes water waves is just the Navier– Stokes equation without the viscous term but including a term for gravity. It turns out that this equation for inviscid flow affected by gravity can be put into the form of a wave equation, so you mathematically the existence of waves should not surprise you.

If you had never fooled around with waves before, your natural inclination upon reading the foregoing paragraph would probably be to try to solve the equations to account for the observed behavior of water waves. And people have been doing this since the middle of the 1800s. But there are two serious impediments to simple solutions:

1. The equation is nonlinear, because of the presence of the convective acceleration term, which as you know from Chapter 3 involves products of velocities and spatial derivative of velocities.
2. An even more serious problem is that one of the boundary conditions— the geometry of the free surface—is itself one of the unknowns in the problem!

So it is unfortunately true that there is no general solution to the problem. People have therefore tried to make various simplifying assumptions that allow some mathematical progress in certain ranges of conditions for water waves. Much mathematical effort has gone into developing these partial approaches and establishing their limits of approximate validity.

Classification of Water Waves

It is notoriously difficult to develop a rational classification of water waves, basically because of the mathematical complexity mentioned above. One way to classify water waves I already mentioned: does the water move with the waves (**translatory waves**), or does the water merely oscillate as the wave passes, to return to its original position after the wave has passed (**oscillatory waves**)? But I also mentioned a more fundamental approach: waves for which the convective inertia terms can be neglected are called **linear waves**, and those for which the convective inertia terms are at least in part included in the analysis are called

nonlinear waves.

Yet another fundamental approach to classification is on the basis of the relative magnitudes of the three important length scales in the problem: wave height H, wavelength L, and water depth d. Out of these three you can make three characteristic ratios: H/L, H/d, and L/d. In deep water, H/d and L/d are both small, and the most important parameter is H/L, called the **wave steepness**. In shallow water, on the other hand, neither H/d nor L/d is likely to be small, and the most important parameter is likely to be H/d, called the **relative height**. In an intermediate range of water depths, the situation is more complicated.

This page titled 6.2: The Nature of Waves is shared under a CC BY-NC-SA 4.0 license and was authored, remixed, and/or curated by John Southard (MIT OpenCourseware) via source content that was edited to the style and standards of the LibreTexts platform.

6.3: Water Motions Due to Waves

The aspect of surface gravity waves that is relevant to sediment movement lies largely in the back-and-forth movement of the water at the bottom: are those oscillatory currents strong enough to entrain bottom sediment? To get at the nature of bottom water motions under oscillatory waves, it is best to start with small-amplitude wave theory. The most far-reaching progress in theory of water waves came about by making the assumption that the wave steepness H/L is so small that the convective accelerations (like $u\partial u/\partial x$) in the equation of motion can be neglected compared to the local accelerations (like $\partial u/\partial t$). It turns out that this assumption simplifies the equation to such an extent that an exact solution can be obtained, by methods beyond the scope of these notes. Such waves are called **Airy waves**, after the person who first developed the solution.

It turns out that the small-amplitude solution holds to good approximation for values of wave steepness H/L well beyond what we have any right to expect. So we can get a good idea of the behavior of finite-amplitude waves just by relying on the small-amplitude solution.

What the solution gives us is the fluid velocity and fluid pressure at every point, and the geometry of the water surface, all a function of time. The water motions below the surface, and especially near the bottom, are of greatest interest in sediment transport.

As an oscillatory wave passes by, each little element or parcel of the water undergoes a closed-loop trajectory or orbit, making one traverse of that orbit as each wave form passes. As your intuition might tell you, the diameter of the orbits decreases with depth below the free surface. This makes sense, because the water-surface disturbance is generated and maintained at the surface by the forces of the wind on the water.

In deep-water waves, for which L/d is very small, the orbits are everywhere nearly circular, and the size of the orbits decreases sharply with increasing depth until they are negligible at depths equal to only one wavelength (Figure $6.3.1$). The orbits are perfectly circular only in the limit of vanishingly small H/L, but even for non-negligible H/L the orbits are very close to being circular. In shallower water the passage of the waves causes water motions all the way to the bottom, although except at the largest values of L/d the diameter of the orbits still decreases with depth. The orbits even at the surface are somewhat elliptical, flattened in the vertical, and they become more elliptical with depth, until at the bottom they are back-and forth straight lines (Figure $6.3.2$).

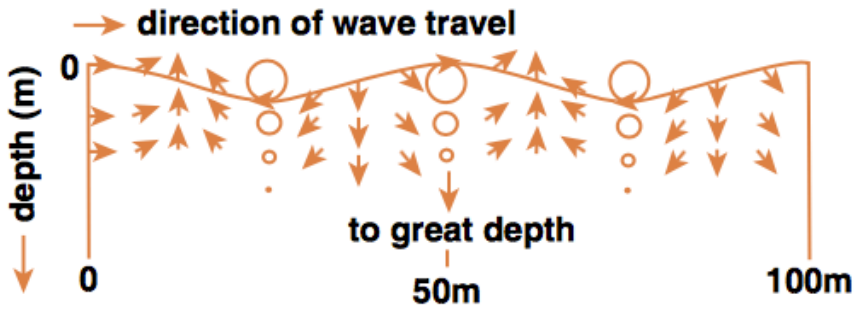


Figure by MIT OpenCourseWare.

Figure $6.3.1$: Instantaneous velocity vectors at a given time, and orbital paths of fluid particles over one complete cycle, in a wave motion in deep water. (From Neumann and Pierson, 1966.)

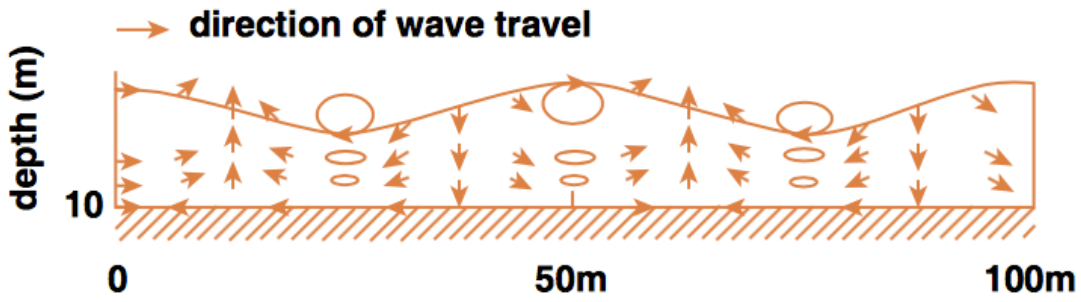


Figure by MIT OpenCourseWare.

Figure 6.3.2: Instantaneous velocity vectors at a given time, and orbital paths of fluid particles over one complete cycle, in a wave motion in water of constant shallow depth. Approximate conditions are shown for a wave with amplitude of $2.5\mathrm{m}$ and a wavelength of $50\mathrm{m}$ in water $10\mathrm{m}$ deep. (From Neumann and Pierson, 1966.)

The effect of finite wave steepness is to distort the wave form such that crests are sharper and troughs are broader, and to distort the orbits such that the speeds are greater when the water is moving in the direction of wave propagation than in the direction opposite wave propagation. (But the net transport remains nearly zero, because the time during which the higher forward speeds prevail are shorter than the times during which the lower reverse speeds prevail.)

The size of wind-generated surface gravity waves depends on three things: wind speed, duration, and fetch. It is obvious to even the most casual observer that wave size increases with wind speed. The reason is that the wind transfers some of its kinetic energy to the waves, both by shear stresses on the water surface and by the front-to-back pressure differences you learned about in Chapter 3, and this adds mechanical energy to the waves, in the form of kinetic energy of the water motions in the wave and potential energy associated with elevation differences of the undulatory water surface. But the waves are not created instantly by the wind: it takes time for the waves to build to a state of equilibrium with the wind. One or both of two processes eventually begin to dissipate the energy of the waves:

1. Breaking of the wave crests (called whitecapping), as the waves become steeper, which converts the organized mechanical energy of the waves to turbulence and thence to heat; and
2. If the wave are large enough relative to the water depth, bottom friction, which bleeds off energy at the bottom of the water column, in the oscillatory-flow boundary layer (more on that later) and converts it to heat.

The term **fetch** is used for the distance over which the wind can work on the waves. You know, from standing at the shore of the ocean or a lake with the wind blowing offshore, that the waves grow from little ripples to much larger waves in the offshore direction, ultimately to reach equilibrium with the wind if the fetch is long enough.

If you, as an otherwise knowledgeable sedimentationist, were approaching the problem of bottom water movement by waves for the first time, one of the first things that would occur to you would probably be to ask how to predict the nature of the bottom water motions as a function of the wind speed. The bottom water motions might be characterized by the oscillation period T, the size of the excursions of water elements near the bottom, called the orbital diameter d_o, or the maximum near-bottom water velocity during one oscillation period, which I will denote by U_m. These three quantities are not independent of one another: they are related by the equation $U_m T = \pi d_\mathrm{o}$. You might try your hand at deriving this simple relationship sometime, when you have some time to spare.

Unfortunately there is no simple way to make such a prediction, because it depends on the balance, mentioned above, between energy input from the wind and energy dissipation both at the surface, by whitecapping, and at the bottom, by bottom friction. One thing, albeit only qualitative, that can be said is that the shallower the water depth, the more important the bottom friction is in determining the balance. In very deep water its role is non-existent, whereas in very shallow water it becomes the dominant effect. Where the water is sufficiently shallow that a wind with effectively unlimited fetch has produced a fully developed wave state, such that energy loss by bottom friction does not allow the waves to grow any larger, the sea state has been called a **depth-limited sea**. Such wave states must be common in the shallow ocean during powerful storms, and much of the work of the waves on the sediment bottom takes place at those times.

It is easy to make a regular train of waves in a wave tank: all you need to do is put a wave generator of some kind in one end (a flap that is hinged at the bottom and moved back and forth in simple harmonic motion at the top does nicely) and energy-absorbing material at the other end, to prevent reflection of the incoming waves. You know, however, that waves that have attained

equilibrium with a wind, or are building toward equilibrium, are far less regular: the crests are not regular and straight-crested, and if you try to watch a single wave crest as it progresses, it soon disappears, to be replaced by other wave crests. The explanation is that the wave state actually is a combination, or superposition, of a set of "component" waves, each with a slightly different period, speed, and direction of propagation. The reality of these component waves is manifested not in the region of wave generation but along distant shores. You are at the beach, during a nice settled spell of summer weather, watching the waves come into shore and break on the beach. Close observation would reveal that these waves, called swell, come from a single direction and are very regular in their size and period. These are waves that were generated by some distant storm and have crossed a great expanse of open ocean to arrive at your beach. Deep-water waves are said to be *dispersive*: the Airy wave solution, mentioned above, for the speed of deep-water waves is $c^2 = gL/2\pi$, where c is the wave speed and L is the wavelength of the waves. That means that longer waves outrun shorter waves, to arrive at distant locations earlier. And the waves sort themselves out by direction as well. It is those two effects—dispersion and directionality—that make the incoming swell so regular.

In the midst of a storm at sea, however, matters are different: the sea state comprises a range of wave sizes and directions, making for a complicated surface topography. Such a wave state is usually represented by what is called a **two-dimensional wave spectrum**, and the waves are referred to as **spectral waves**. Think in terms of a joint frequency distribution of wave energy in terms of wave period (or wave frequency) and direction. The sea state generated by a wind that blows in one direction for a long time shows a very elongated distribution, with a wide range of periods but a much narrower range of directions, but if the wind direction is changing, as commonly happens during the passage of a storm, the wave state has to readjust, and while it does so the two-dimensional wave spectrum is likely to broad in direction as well as in period.

The relevance of the wave spectrum is that it translates to what the water motions are at depth, although the picture of motions at depth is mediated, or filtered, by the rapid decrease in amplitude of the component wave motions with depth. Because of this rapid decrease, the water column acts as a kind of low-pass filter, emphasizing the contribution of the larger wave components at the expense of the smaller, thus making the water motions at the bottom less variable, in both period and orientation, than at the surface. Even so, during strong but changing winds you might expect the water motions at the bottom to be not as simple as a regular back-and-forth motion with a single orientation.

This page titled 6.3: Water Motions Due to Waves is shared under a CC BY-NC-SA 4.0 license and was authored, remixed, and/or curated by John Southard (MIT OpenCourseware) via source content that was edited to the style and standards of the LibreTexts platform.

6.4: Wave Boundary Layers

The linearized small-amplitude solution for velocity mentioned in the previous section predicts spatially slowly varying velocities both at and below the water surface at any given time. In the case of waves in shallow to intermediate water depths (that is, for which the wavelength is not very small relative to the water depth), these velocities are predicted to be still appreciable even at the bottom—and when the wavelength is large relative to the water depth, the magnitudes of near-bottom velocities are about the same as the velocities at the surface. Remember that the assumption of inviscid flow means that these nonzero near-bottom velocities extend all the way to the bottom.

Viscosities of real fluids like water are small enough that the free- surface profile and the spatial and temporal distribution of velocities is well accounted for by the inviscid solutions, and viscous damping is small—so small that large waves can travel across wide ocean basins without great loss of energy. But the predicted nonzero velocities at the solid bottom boundary under the waves is clearly contrary to fact: just as in unidirectional flows of real fluids, the velocity must go to zero at the bottom boundary. This leads to the concept of *the bottom boundary layer in oscillatory flows*: this is commonly called the **wave boundary layer**.

Many of the physical effects associated with wave boundary layers are analogous to or parallel to those of unidirectional-flow boundary layers. Here is a mostly qualitative account of some of the important things about wave boundary layers. The first thing to note is that, just as with unidirectional flows, at relatively low values of a suitably defined Reynolds number the boundary layer is laminar, and at higher values of the Reynolds number the boundary layer is turbulent, even though the flow in the domain above the boundary layer, where the inviscid assumption holds, is effectively nonturbulent (provided that there is no coexisting unidirectional current; see a later section).

If the wave Reynolds number is defined as $\rho U_m d_o/\mu$, where U_m is the maximum bottom velocity predicted by the inviscid theory and d_o is orbital diameter given by the inviscid theory, then the critical value for the transition from laminar to turbulent flow in the wave boundary layer is known from observations in wave tanks and oscillatory flow ducts in the laboratory to be about 10^4.

An exact solution can be found for the velocity profile in the laminar boundary layer. The mathematics is straightforward but beyond the scope of these notes. The result, when expressed as the velocity deficit u_d, the difference between the inviscid bottom velocity (which in the context of the laminar boundary can be viewed as the velocity at the top of the boundary layer) and the actual velocity at some height z above the bottom, is

$$u_d = e^{\left(-\sqrt{\frac{\omega}{2v}}z\right)} \cos\left(kx - \omega t + \sqrt{\frac{\omega}{2v}}z\right) \tag{6.4.1}$$

where ω is the angular frequency of the oscillation (related to the period T by $\omega = 2\pi/T$), k is the wave number (related to the wavelength L by $k = 2\pi/L$), ν is the kinematic viscosity μ/ρ, and z is measured upward from the bottom.

The solution in Equation 6.4.1 has two factors, one expressing a negative exponential dependence and the other expressing a cosine dependence. The former causes u_d to drop off sharply with height above the bottom, and the latter just takes account of the time variation in the velocity—but it is important to note that there is a phase difference with the overlying inviscid flow, and the phase difference itself depends on z, ranging upward from zero at the bottom at the same time u_d is getting smaller.

The negative exponential dependence of u_d on z in Equation 6.4.1 means that the effective boundary-layer thickness is fairly well defined, although technically one has to take some arbitrary value like 0.01 for u_d in order to obtain a definite thickness for the boundary layer. It turns out that the value of z that corresponds to $u_d = 0.01$, which is usually denoted by δ_L, is

$$z = \delta_L = 5\sqrt{\frac{2v}{\omega}} \tag{6.4.2}$$

But most boundary layers under waves in the real ocean under conditions of interest in sediment transport are *turbulent* rather than laminar. Theoretical analyses of the turbulent wave boundary layer have been carried out by replacing the molecular viscosity by a turbulent eddy viscosity, making some assumption about how the eddy viscosity varies vertically, and obtaining an expression for the vertical velocity distribution. The velocity profile is found in this way to be logarithmic. Again there is the problem of how to define arbitrarily the boundary-layer thickness, but the height δ_T of the turbulent boundary layer is usually taken to be

$$\delta_T = \frac{2\kappa u_*}{\omega} \tag{6.4.3}$$

where κ is von Kármán's constant, the inverse of the constant A introduced in Chapter 4, and u_* is again the shear velocity (which could be taken as the maximum or the time average).

A significant aspect of wave boundary layers is that they do not keep growing upward into the interior of the flow indefinitely, the way unidirectional- flow boundary layers do, provided that density stratification does not inhibit their upward growth. The reason is that the thickness of the wave boundary layer is limited by the cessation and turnaround of the flow in each cycle. For turbulent wave boundary layers over rough beds, the thickness of the wave boundary layer is likely to be something less than one meter—far smaller than the typical boundary layer beneath currents in deep-water natural environments.

Just to give you a feel for the velocity structure in the oscillatory-flow boundary layer is like, Figure $6.4.1$ is a graph (admittedly somewhat complicated) that shows flow velocity in the laminar oscillatory boundary layer vs. height above the bottom for four equally spaced times during one complete oscillation cycle (0, $\pi/2$, π, $3\pi/2$, and 2π). The vertical coordinate is labeled with values of the length variable under the radical sign in Equation $6.4.2$ but with slightly different notation. The curves in Figure $6.4.1$ are labeled in two ways: 1–4 unprimed, and 1–4 primed. The unprimed numbers are for what the velocity of the bottom would look like to a neutrally buoyant observer riding with the oscillatory flow just outside the boundary layer. This corresponds to oscillating a flat plate in a tank of still water. The primed numbers are for the equivalent curves, more relevant to our interests here, that show the velocity profile of the fluid relative to an observer planted firmly on the bottom. You can see how, during each half cycle (for example, from curve $0'$ to curve $1'$ to curve $2'$) there is a considerable mismatch in phase between the upper part of the boundary layer and the lower part.

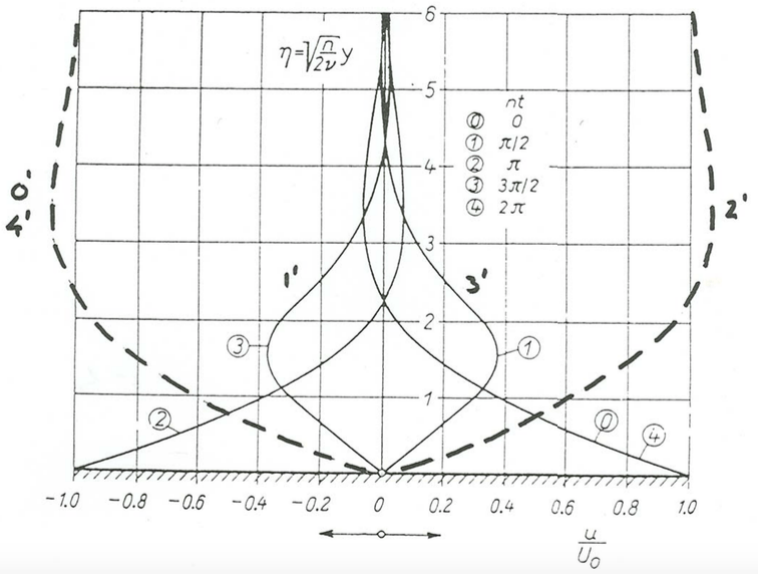


Figure $6.4.1$: Plot of fluid velocity u, normalized by dividing by the velocity U_o outside the laminar oscillatory boundary layer, vs. distance above the bottom, for one complete oscillation cycle. See text for explanation. See Equation $6.4.2$ for the nature of the vertical coordinate. The top of the graph corresponds approximately to the top of the boundary layer. (Modified from Schlichting, 1960, p. 76.)

Finally, the magnitude of the bottom shear stress is important both for its role in sediment transport and also for its effect on attenuation of wave energy by bottom friction, so a lot of effort has gone into developing ways to predict the bottom shear stress. Basically it boils down to dealing with a **wave friction factor** f_w, analogous to the unidirectional-flow friction factor, and working with an experimentally determined **wave friction-factor diagram** expressing the dependence of the wave friction factor on the Reynolds number and, for rough beds, a **relative roughness** d_o/D, where D is the size of the roughness elements.

One interesting aspect of the bed shear stress in oscillatory flow is that in laminar boundary layers the maximum shear stress leads the maximum velocity by a phase angle of $\pi/4$, meaning that the maximum shear stress acts on the bottom at a time equal to $T/8$ (where T is the period of the oscillation) before the velocity reaches its maximum at the top of the boundary layer. In turbulent boundary layers the same effect is present but the phase difference is somewhat smaller.

This page titled 6.4: Wave Boundary Layers is shared under a CC BY-NC-SA 4.0 license and was authored, remixed, and/or curated by John Southard (MIT OpenCourseware) via source content that was edited to the style and standards of the LibreTexts platform.

6.5: Combined Flow (Waves plus Current)

Introduction

It is common, in lakes and in the ocean, for currents and waves to coexist. Such a flow, involving both waves and a current, is called **combined flow**. In the interior of the current, far away from the bottom boundary, the waves superimpose upon the current a wholesale oscillatory motion of the water that does not affect in any substantial way the structure of turbulence in the current, because very little shear is introduced into the fluid. Near the bottom, however, in the bottom boundary layer, the oscillatory wave motion and the unidirectional current interact in complex ways, with important consequences for sediment entrainment and movement. Such a boundary layer is called a **combined-flow boundary layer** or a **wave-plus-current boundary layer**.

Varieties of Combined Flow

The simplest of combined flows are those involving a train of waves of the "wave tank" variety (with only one wave component, with a single period and a single direction) and the direction of wave propagation is the same as the direction of the current. Then you can imagine a range of combined flows, with one end member being a symmetrical purely oscillatory flow and the other end member being a current without superimposed waves (Figure 6.5.1). In the range for which the oscillatory flow speed is greater than the unidirectional flow speed, the water elements oscillate but undergo a net shift in position. In the range for which the unidirectional flow speed is greater than the oscillatory flow speed, the water elements move in one direction only but at time-varying speed. The "middle" case is that of a stop–start movement.

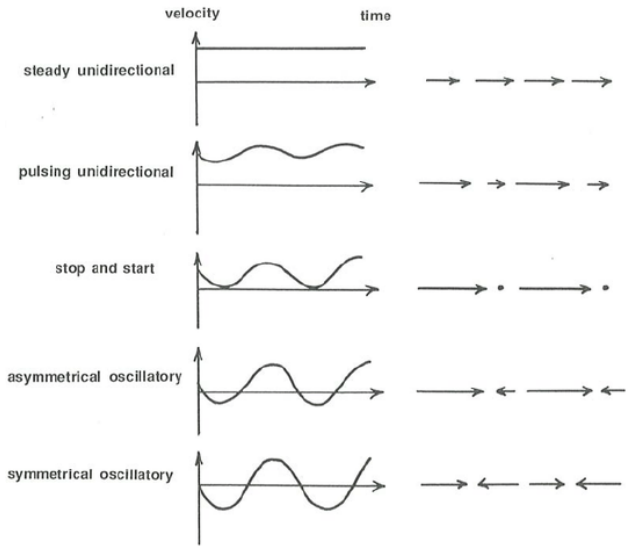


Figure 6.5.1: The range of combined flows, when the orientations of the unidirectional component and the oscillatory component are the same.

Just to complicate matters further, the asymmetry in the maximum forward and backward velocities in oscillation-dominated combined flow is not the only way that such a velocity asymmetry is produced: it can exist even in purely oscillatory flow for which the forward stroke is at a higher velocity but for a shorter time, and the backward stroke is at a lower velocity but for a longer time (Figure 6.5.2). the net water movement is still zero, but there is asymmetry in the velocities, and, if the waves are moving sediment, an even greater asymmetry in sediment transport. Such asymmetrical purely oscillatory flow develops when shallow-water waves are propagating into shallower water (that is called shoaling).

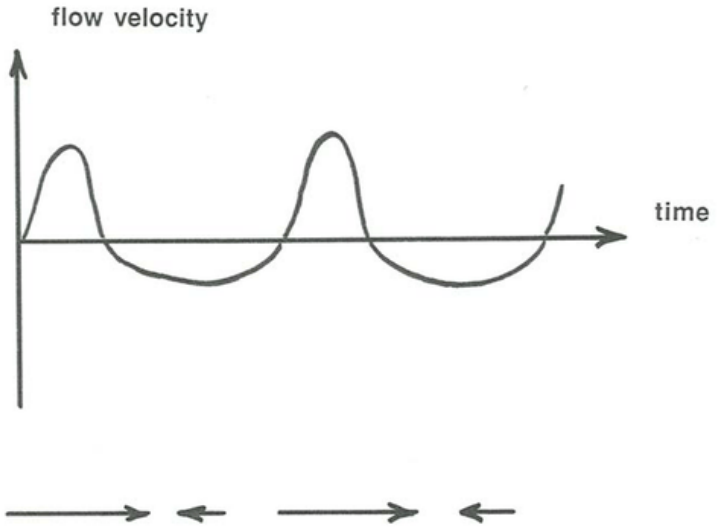


Figure 6.5.2: Time history of flow velocity in asymmetrical purely oscillatory flow.

Of course, the range of combined flow described above are a special case, because there can be any angle between the direction of wave propagation and the direction of the current, from zero degrees to ninety degrees. Most of the experimental work on combined flow has been done in the zero-degree case, because that is by far the easiest to set up in the laboratory. In the natural environment, however, the zero-degree case is the exception rather than the rule. Some thought on your part should convince you that the non-zero-degree case involves water movements that are either looping or zigzag, depending upon whether the flow is oscillation-dominated or current-dominated, respectively.

Matters are considerably more complicated when the waves are spectral waves, with more than one component. A bit of elementary physics might help here to guide your thinking. When two sinusoidal oscillations in a horizontal plane, with the same frequency, are combined, the resulting trajectories of material particles describe an ellipse. If, however, the frequencies are different, the trajectories acquire a more complicated, but infinitely repeating, pattern, called Lissajous figures These figures are complexly looping, but they are infinitely repeating, tracing out the same trajectory over and over again, always within the confines of a rectangular box defined by the amplitudes of the two oscillations. (Try googling “Lissajous figures” on the Internet to see some engaging animations.) Such figure simulate what the bottom water movements would be under the action of two wave components with different periods and amplitudes.

Matters become more complicated when there are three or more oscillatory components, with different orientations and frequencies. Then the particle trajectories appear totally irregular and non-repeating (see Figure 6.5.3, which is fake but it gives you the idea). Such would be the nature of bottom water movements in purely oscillatory flow produced by spectral waves for which more than one component contributes to the bottom water movement. Keep in mind that all of this is before a current is superimposed on the oscillatory motion.

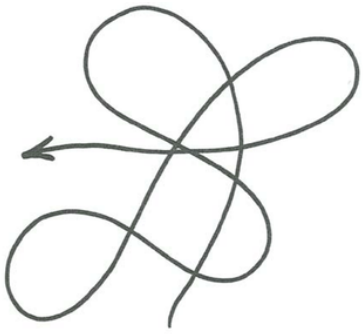


Figure 6.5.3: Cartoon to give you some idea of what the trajectories of near-bottom water elements would be in the case of three or more oscillatory components, with different orientations and frequencies.

The effects of this most general case of combined flow on sediment movement has, to my knowledge a least, been little studied

in the laboratory, owing to the great difficulty in arranging for such flows, but sediment movement under such flows in common natural environments like lakes and the shallow ocean must be more the rule than the exception.

What helps to save sedimentationists from this morass of complexity is the low-pass-filter effect of the water column, mentioned earlier: even in the case of a broadly two-dimensional wave spectrum, the bottom water movements are likely to be dominated by only the strongest component(s), thereby making the water movements more like the simpler cases discussed above. At times when the wave spectrum is undergoing major adjustments to the changing direction of strong winds, however, the more general case is likely to be important.

The Combined-Flow Boundary Layer

In combined flows, the boundary layer consists of a wave boundary layer, immediately adjacent to the bottom, commonly some tens of centimeters thick if the bottom is sufficiently rough as to cause the wave boundary layer to be turbulent, and a much thicker current boundary layer, extending upward for tens of meters (see Chapter 7 for more on current boundary layers in large-scale natural environments influenced by the Earth's rotation.) In other words, the wave boundary layer is embedded in the lowermost part of the current boundary layer. Such boundary layers are called **combined-flow boundary layers** or **wave–current boundary layers**. Such boundary layers are the rule during storms in the shallow ocean, over continental shelves, and as such they are a key aspect of continental-shelf sediment transport.

A simple-minded approach to the structure of wave–current boundary layers would be to simply add the time-varying velocity of a wave boundary layer to the unidirectional-flow velocity profile. The problem is that such an approach does not take into account a substantial element of nonlinearity, as follows. Within the wave boundary layer, the superimposition of the current causes the forward stroke of the oscillatory bottom water motion to be of greater velocity than the backward stroke. You learned back in Chapter 4 that, for fully developed turbulent flow (sufficiently large Reynolds number) the flow resistance goes approximately as the square of the velocity—so you should expect the time-average boundary shear stress beneath the wave–current boundary layer to be greater than what it would be for the given current without the accompanying waves. You should expect that the characteristics of the turbulence within the wave boundary layer would be much different from the purely oscillatory case. Above the wave boundary layer, however, the turbulence is unaffected by the presence of the wave boundary layer below: there, you can indeed think in terms of a bodily back-and-forth oscillatory motion being superimposed on the unidirectional current. One way of expressing this is that the wave boundary layer "sees" this region or layer of the flow—within the current boundary layer but above the wave boundary layer—as the interior of the flow. If you could observe the details of the flow in this layer while moving your head in orbits that match the oscillatory component of the flow, they would look the same as if there were no oscillatory component to the flow.

The velocity profile in the combined flow above the wave boundary layer is different from that of a purely unidirectional current, though, because the "anchoring" effect on the profile in the region of the flow nearest the bed is different. Do you recall from Chapter 4 (see Figure 4.8.1 in particular) how, at any given level above the bed in a unidirectional current the slope of the law-of-the-wall velocity profile is the same for dynamically rough flow as for dynamically smooth flow but the actual velocity is smaller, because of the greater boundary resistance in rough flow? In a wave–current boundary layer the presence of the wave boundary layer has an effect of the same kind: the slope of the velocity profile, a reflection of the turbulence structure of the current, is the same as for a purely unidirectional current, but the velocity is smaller because of the greater flow resistance at the bottom of the wave boundary layer. This is shown clearly in Figure 6.5.4: look at the two curves in the left-hand part of the graph, and you will see that at a given elevation the velocity is smaller for the combined flow than in the purely unidirectional flow.

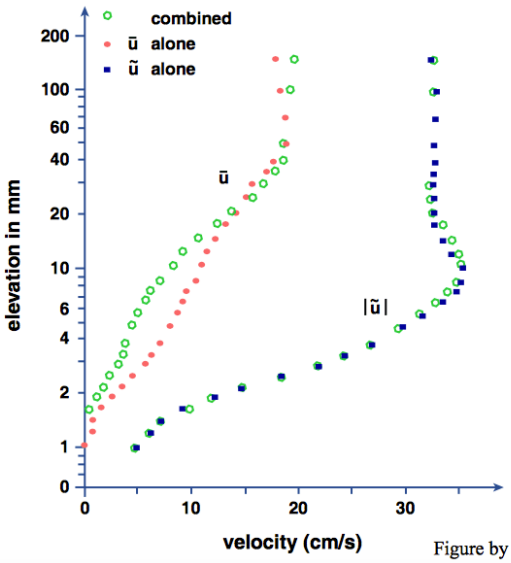


Figure by MIT OpenCourseWare.

Figure 6.5.4: Velocity profiles in purely unidirectional flow, purely oscillatory flow, and combined flow. The red dots are for purely unidirectional flow; the blue squares are for purely oscillatory flow; and the green circles are for combined flow. The two curves on the left show the unidirectional velocity component, and the curves on the right show the oscillatory velocity component. (From Nielsen, 1992, p. 62.)

It is also clear from Figure 6.5.4 that the oscillatory velocity in the wave boundary layer in a combined flow is not much different from the oscillatory velocity in the wave boundary layer of a purely oscillatory flow, at least for flows in which the oscillatory component is larger than the unidirectional component. The bottom line, therefore, is that the velocity profile in the wave boundary layer is not greatly changed by the addition of a current, but the velocity profile in the flow above the wave boundary layer is substantially different than in a purely unidirectional flow (Figure 6.5.5).

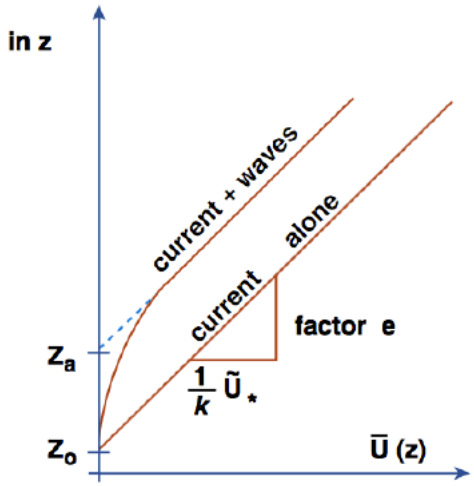


Figure by MIT OpenCourseWare.

Figure 6.5.5: How the addition of an oscillatory component of the flow changes the velocity profile of the unidirectional component of the flow. (From Nielsen, 1992, p. 79.)

References

- Nielsen, P., 1992, Sea Bed Mechanics.
- Schlichting, H., 1960, Boundary Layer Theory: New York, McGraw-Hill, 647 p.

This page titled 6.5: Combined Flow (Waves plus Current) is shared under a CC BY-NC-SA 4.0 license and was authored, remixed, and/or curated by John Southard (MIT OpenCourseware) via source content that was edited to the style and standards of the LibreTexts platform.

7: FLOW IN ROTATING ENVIRONMENTS

7.1: Playing on a Rotating Table

7.2: The Coriolis Effect on the Earth's Surface

7.3: The Rossby Number and Inertia Currents

7.4: The Ekman Spiral

7.5: Geostrophic Motion

7.6: Ekman Layers

7.7: Planetary Boundary Layers- The Ekman Layer, The Logarithmic Layer, and The Mixed Layer

This page titled 7: Flow in Rotating Environments is shared under a CC BY-NC-SA 4.0 license and was authored, remixed, and/or curated by John Southard (MIT OpenCourseware) via source content that was edited to the style and standards of the LibreTexts platform.

7.1: Playing on a Rotating Table

Introduction

In everything up to now in these notes, we have assumed that the flow environment is stationary. Just think back to flow around a sphere or flow down a channel. And even if the flow environment is in uniform motion, relative to you as the observer, you have already seen that you can convert the problem to that of a stationary flow environment just by moving with flow environment itself; think back to the problem of relative motion of a sphere and an ambient fluid.

But what if the flow environment is accelerating? That turns out to be quite a different matter. This chapter examines some of the effects of steady rotation of the flow environment. (Remember that rotation involves acceleration, of the radial rather than the tangential kind, even with a steady rotation rate.) The effects of rotation on the flow are striking, and I think not intuitive. These effects are of central importance in the study of what are called **geophysical flows**: the movements of the atmosphere and the oceans on scales of hundreds and thousands of kilometers. The boundaries of these flows are the rotating solid Earth, and we the observers are rotating with that solid Earth. Admittedly, the effects of rotation do not have a very direct bearing on the small-scale dynamics of sediment transport, but the indirect consequences are so far-reaching that I could not resist including this chapter in these notes.

Playing on a Rotating Table

In a large unobstructed indoor area (a gymnasium or a warehouse would be best, but a big room in your house would suffice), build a giant flat horizontal turntable—just a disk mounted at its center point on a vertical rotating shaft (Figure 7.1.1). You can rotate the whole disk at any desired constant rotation rate, described by its angular velocity γ, measured in radians per second. It would be best if you painted the surface of the disk a flat black, the better to observe the motions of the brilliantly white marker spheres you are going to roll around on the surface. To make things really exciting, be sure to coat the white marker spheres with a thick chalky coating of some sort that tracks off evenly onto the surface of the turntable as the spheres roll about.

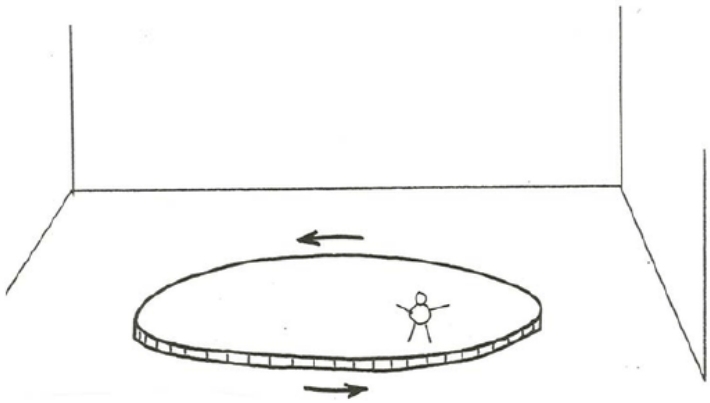


Figure 7.1.1: Playing on a rotating table.

To do things right, you are also going to need an observation perch above the turntable. This perch should be easily movable from place to place above the surface, but (and this is important) stationary relative to the floor of the room while it is in use. One of those mechanized cherry-picker seats, extending horizontally from the margin of the disk, would do nicely, if you can afford it.

Set the rotation rate, settle into your perch, occupy a point just over the turntable, and roll one of your marked spheres onto the table, just as if you were at a bowling alley. Here is the big question: What would the track of the sphere look like on the turntable? (You are going to have to assume that the turntable exerts no substantial force on the rolling ball. That is not really true, but the effects are small enough that you can safely ignore them for the purposes of this demonstration. If you are uncomfortable with that assumption, you can always imagine a magic air-hockey puck that scoots nearly frictionlessly over the turntable, leaving a powdery white trail behind it.)

The big jump that your powers of deduction or imagination have to take here is to see that the track left by the ball on the table

would be *curved* (Figure 7.1.2). And, once you are comfortable with that idea, it might naturally occur to you to think about whether that curved track is a circular arc. The answer turns out to be NO, although the reasons are a bit too intricate to deal with at the moment.

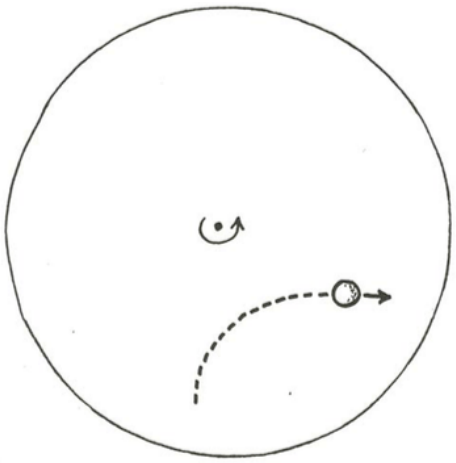


Figure 7.1.2: The track left by a ball rolling on a rotating table.

If you cannot afford the time and money to build the turntable but you still want to get some results, here is a simpler and much less expensive way of demonstrating the phenomenon (Figure 7.1.3). Pin a big piece of posterboard to the wall so that it can be rotated about its center point, and have an assistant stand to one side and rotate the posterboard in a hand-over-hand motion as steadily as possible. Stand on one side of the posterboard with a marker pen, and draw a line on the posterboard in such a way that the tip of the pen moves in uniform rectilinear motion *relative to the underlying wall*. That is not easy to do, because you need to try to ignore the surface of the posterboard, and the mark that is being made on it, and instead concentrate on the imaginary path of the pen point on the motionless wall behind. You would find (Figure 7.1.4) that no matter where you start on the posterboard, and no matter which direction you choose for your line, the mark on the posterboard will be an arc, not a straight line!

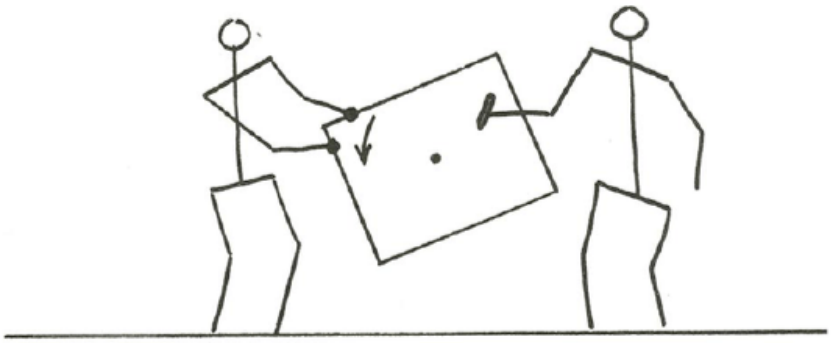


Figure 7.1.3: How to show that the track of an object moving in a straight line looks curved from the viewpoint of an observer in a rotating frame of reference.

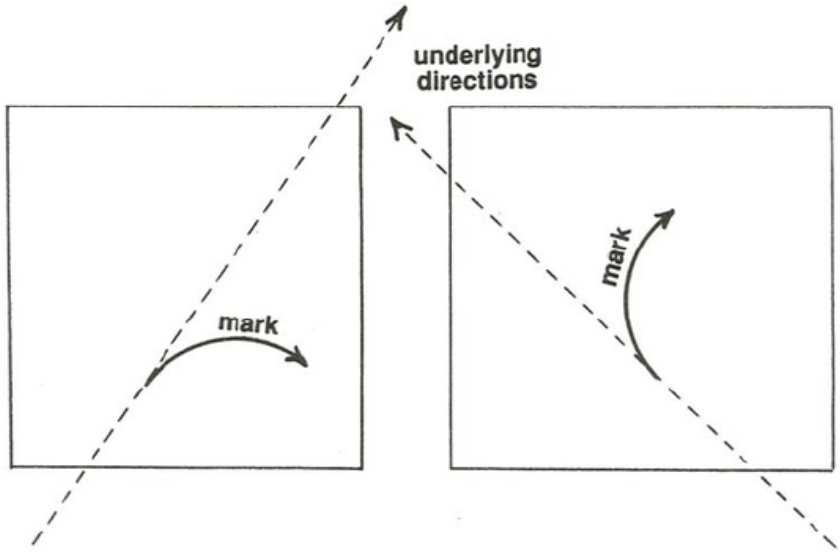


Figure 7.1.3.

You do not even need to rig up such a posterboard exercise, really; just think about your rapidly obsolescing phonograph. Pretend that the needle that passively follows the groove in the record is in fact constrained to move from the edge of the record to the center of the record in an almost straight line relative to the underlying stationary phonograph structure. The needle makes a spiral path on the record, with curvature as described in the two foregoing experiments.

And incidentally, this phonograph exercise shows conclusively that the curving arc is not exactly circular: the curvature is tighter along parts of the path located closer to the axis of rotation. That is basically because the velocity of the moving object (the needle) relative to the rotating surface (the record) decreases as the needle makes its way toward the center of the record. Why? Because the speed of the needle relative to the fixed stars is constant but the velocity of points on the record increases from zero at the center to a maximum at the outer edge.

But back to the big turntable: have your assistant roll a marker sphere onto the turntable while you are riding on the turntable. Watch the ball as it rolls and leaves its curving track. It will look to you as though some mysterious sideways force is continuously acting on the ball normal to its path to push it off its course. Something seems to be wrong with Newton's first law, which tells you that the ball should be moving in a straight line at constant speed. You know what the problem is, of course: the fictitious side force is an artifact of your observation of the ball from the standpoint of the rotating turntable. If you reoccupied your perch and rolled a clean, bright, chalkless ball onto the dimly lit black surface of the turntable, you would see the ball roll in a nice straight line! The fictitious side force that seems to act on moving bodies in a rotating environment is called the **Coriolis force**, after the nineteenth-century French mathematician who first analyzed the effect. And the apparent acceleration of the sphere (it is a radial acceleration, not a tangential acceleration, in that only the direction changes, not the speed) is called the **Coriolis acceleration**. The entire effect is called the **Coriolis effect**.

What is the relevance of this demonstration to the motion of fluids? You could produce all kinds of fluid flows right on the surface of that turntable, by using that surface as your fluid dynamics laboratory: flow in an open channel, a free-convective flow in a big dishpan, or even just a sheet of water flowing freely across the surface of the turntable. In each case, every tiny element of the flowing fluid is subjected to that same Coriolis force. For the right combinations of fluid speeds and rotation rates, the Coriolis effect would have profound consequences for the pattern of fluid movement.

This page titled 7.1: Playing on a Rotating Table is shared under a CC BY-NC-SA 4.0 license and was authored, remixed, and/or curated by John Southard (MIT OpenCourseware) via source content that was edited to the style and standards of the LibreTexts platform.

7.2: The Coriolis Effect on the Earth's Surface

Fluid flows you observe on the Earth's surface experience a Coriolis acceleration. That is because the Earth is rotating, and both you and the flowing fluid are rotating with it. The effects you discovered on your turntable show up in those flows as well. The only places this should seem really obvious to you are at the North Pole and the South Pole—where the Earth's surface is perpendicular to the axis of rotation. But the Coriolis acceleration affects fluid motions everywhere else on the Earth's surface also.

The complete mathematical development of the Coriolis effect, although straightforward, would take us too far off the path of these notes, so I will give you an abbreviated and incomplete picture, just for the flavor.

I mentioned above that the rate of rotation of a rotating body is denoted by ω. But to be specific about such a rotation, you need to describe the orientation and the sense of the rotation as well. The rotation of the Earth is described by its angular velocity—a vector, denoted by Ω, lying within the axis of rotation and with length equal to the rate of rotation ω. By convention, the angular velocity vector points north to express the sense of rotation of the Earth, which is counterclockwise when viewed from above the North Pole (Figure $7.2.1$). The angular velocity Ω thus specifies the orientation, sense, and rate of rotation of the Earth.

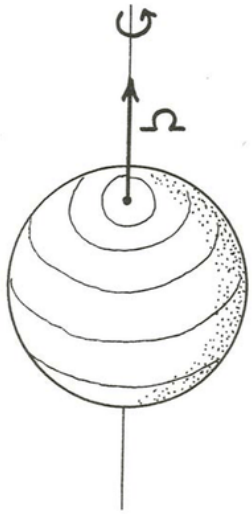


Figure $7.2.1$: The angular velocity vector of the rotating Earth.

Look at a point on the Earth's surface. The speed v of that point, relative to outer space, is equal to the angular velocity ω times the distance from the rotation axis to the point. Expressed in terms of the radius R of the Earth and the latitude angle ϕ, this can be written $R\omega \sin(90^\circ - \phi)$ (Figure $7.2.2$).

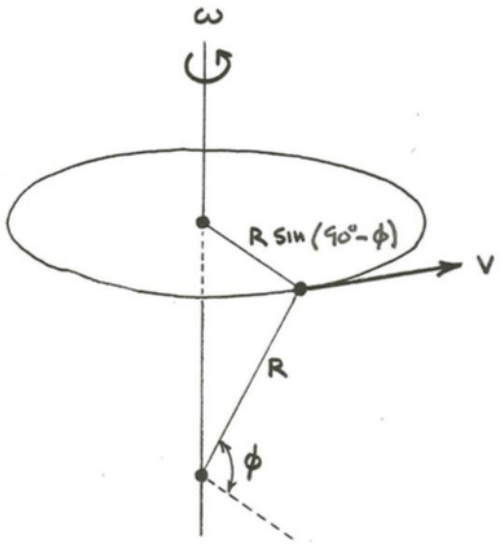


Figure 7.2.2: Definition sketch for writing the velocity of a point in or on the Earth in terms of the radius of the Earth, the angular velocity of the Earth, and the latitude of the point.

A more elegant way of looking at the movement of a point on the Earth's surface is to characterize the position of the point by a position vector r that stretches from the center of the Earth to the given point (Figure 7.2.3) and then express the velocity of the point as $v = \Omega \times r$. The product on the right side is a **cross product** of vectors, defined so that the result has a magnitude $r\omega \sin(90^\circ - \phi)$, which is the same as the result in the last paragraph, because $r = R$. Note that the vector product is itself a vector; the vector product is arranged so that its direction and sense correctly describe the velocity of the given point on the Earth's surface. Note also that v is normal to both Ω and r; that is one of the properties of the cross product.

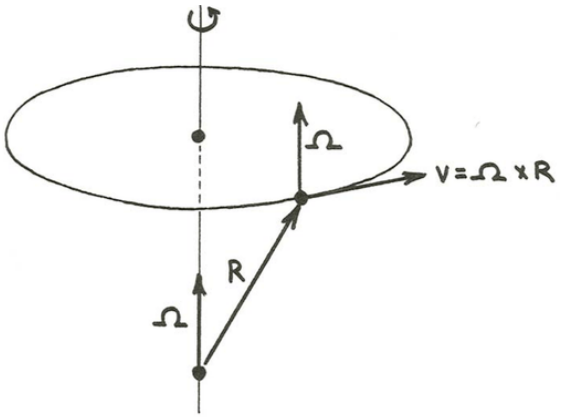


Figure 7.2.3: Another way of expressing the velocity of a point in or on the Earth.

Now look at a little marker particle moving along with the air of the atmosphere or the water of the ocean. That particle has its own velocity relative to the solid Earth; call that velocity v_R, where the subscript R is meant to suggest that the velocity is *relative* to the rotating Earth. The motion of the particle can also be viewed from outer space; call its velocity relative to that "fixed" frame of reference v_I, where the subscript I stands for *inertial*, an adjective that in physics is associated with a frame of reference that is not accelerating. It should make good sense to you that

$$v_I = v_R + \Omega \times r \tag{7.2.1}$$

Equation 7.2.1 just tells you that the absolute velocity of the moving particle is the sum of its velocity relative to the rotating Earth plus the rotational velocity of the point, stationary relative to the Earth, past which the particle happens to be moving at a given time.

The complications begin when we look at the *acceleration* of the marker particle, not just its velocity. The acceleration of the particle is the time rate of change of its velocity. To find the acceleration you have to differentiate the vector v_I with respect to time, and then, for use of the result in our rotating earthly frame of reference, express the result in terms of quantities like v_R that

are observed from within that rotating frame of reference. I will just cite the result for a_I, the acceleration of the particle relative to the outer-space reference frame:

$$\boldsymbol{a}_I = \boldsymbol{a}_R + 2\boldsymbol{\Omega} \times \boldsymbol{v}_R + \boldsymbol{\Omega} \times \boldsymbol{\Omega} \times \boldsymbol{r} + \frac{d\boldsymbol{\Omega}}{dt} \times \boldsymbol{r} \tag{7.2.2}$$

where a_R is the acceleration of the particle as observed from the rotating Earth. (For details, see Pedlosky, 1987, Chapter 1.)

There are four terms on the right side of Equation 7.2.2. The first, a_R, is easy to understand, but the other three need some explanation. The fourth expresses the effect of *time rate of change of the rotation rate*; it is something we need not worry about for geophysical flows. The third is the *centripetal acceleration*, with which you are all familiar in at least a qualitative way: if you tie a rope around a boulder and swing it around in a big circle, you are producing a centripetal ("center-seeking") acceleration of the boulder, arising from the inward-directed radial force you are exerting on the boulder to constrain it to travel in a circular arc rather than go off straight on its own. The second term is the one we are after in this exercise: it is the *Coriolis acceleration*.

Look more closely at the Coriolis acceleration term in Equation 7.2.2. First of all, it is a vector itself, because it is a cross product of two vectors. Its magnitude is a linear function of the magnitude of the velocity v_R: the faster the particle moves, the larger the Coriolis acceleration. Also, its magnitude depends not only on the magnitude of v_R but also on the direction of v_R relative to the Earth's axis. In every case, though, the direction of the Coriolis acceleration is normal to vR itself (remember the properties of the cross product), and that is consistent with what you learned about the Coriolis acceleration on your big turntable.

A good way to study the effects of the Coriolis acceleration on fluids moving at the Earth's surface is to look at a particular point on the Earth's surface at a particular latitude ϕ (Figure 7.2.4). To a local observer the situation there looks planar, so think about a plane that is tangent to the Earth's surface at the given point. I will call that the **horizontal plane**, because it is horizontal at the tangent point. The motions of both the atmosphere and the oceans most affected by the Coriolis acceleration are almost entirely horizontal flows: broad-scale vertical motions in the atmosphere and oceans are usually of far smaller velocity than horizontal motions, and locally strong vertical motions, as within cloud convection cells, are on space and time scales for which the Coriolis effect turns out to be unimportant.

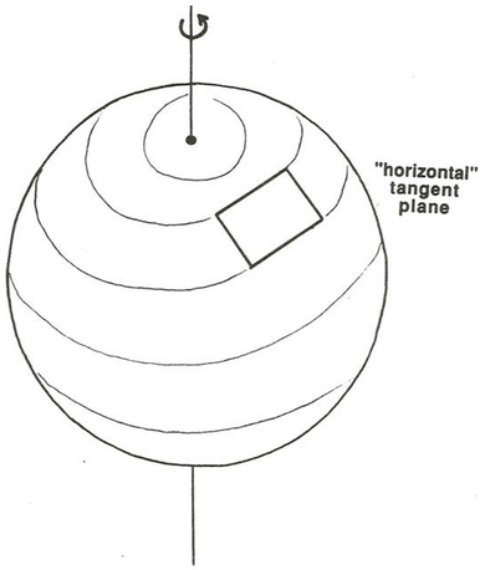


Figure 7.2.4: The "horizontal" tangent plane.

In the horizontal plane it is natural to set up a coordinate system with one axis vertical, one in the direction of movement of the particle, and the other horizontal and normal to the direction of movement (Figure 7.2.5). And the Coriolis acceleration itself can be resolved into components in those three directions (Figure 7.2.6). Think just about the horizontal components of the Coriolis acceleration, because they are what are important for the horizontal motions of fluids; it is easy to show that the vertical component of the Coriolis force in a vertical flow is swamped by the balance between the two large vertically acting forces—pressure and gravity—and is therefore negligible.

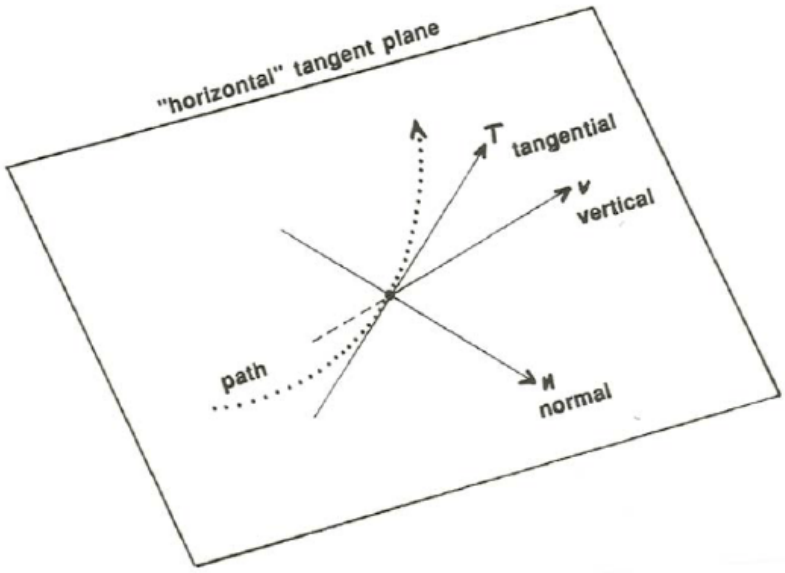


Figure 7.2.5: A useful coordinate system in the horizontal tangent plane.

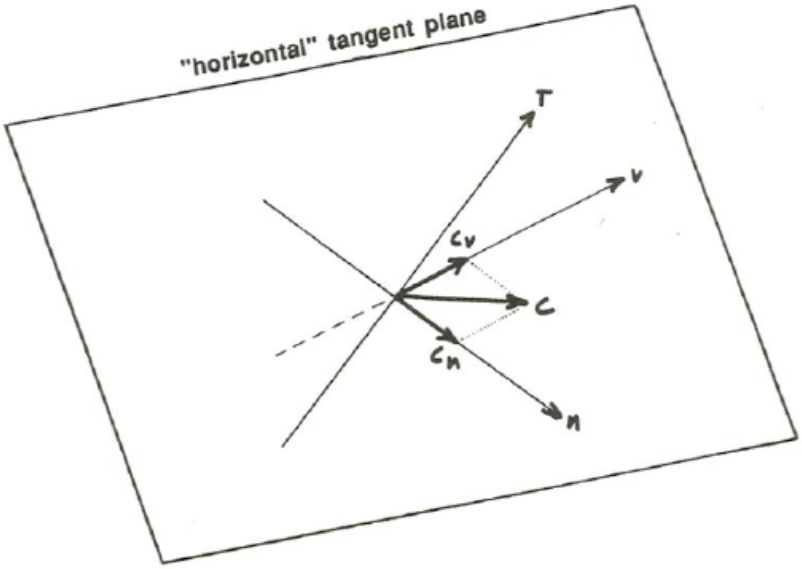


Figure 7.2.6: Resolving the Coriolis acceleration in the horizontal tangent plane.

You have already seen that the component of the Coriolis acceleration in the direction of movement, the t axis in Figure 7.2.6 , is always zero. What we need to worry about is the magnitude of the horizontal component of the Coriolis acceleration in the direction normal to the horizontal movement, and how it varies with both latitude and the direction of movement within the horizontal plane. I will do this in a shortcut way by looking at two special directions, north–south and east–west.

Look at the east–west orientation first. The Coriolis acceleration is directed normal to both v and Ω, which to an observer on the horizontal plane is a vector that sticks up into the sky toward the south and at an angle to the horizontal that is equal to 90° minus the latitude angle ϕ. By reference to Figure 7.2.7, if you resolve that vector into the horizontal plane the component has the magnitude $2v\omega \sin\phi$. Now look at the north–south orientation. To an observer on the horizontal plane the Coriolis acceleration vector is horizontal and points due east for a northward movement and due west for a southward movement. By reference to Figure 7.2.8, the magnitude of the Coriolis acceleration is again $2v\omega \sin\phi$. Although the mathematics is much more intricate, it turns out that the Coriolis acceleration has this same magnitude, $2v\omega \sin\phi$, for any direction of movement in the horizontal plane.

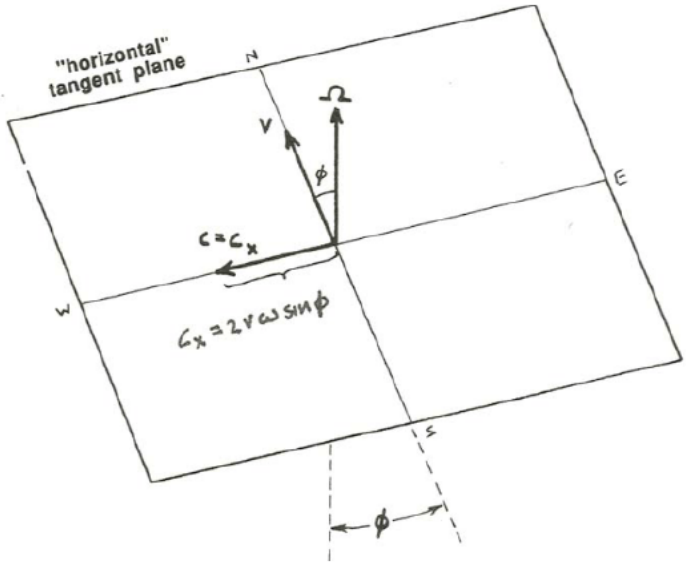


Figure 7.2.7: The component of the Coriolis acceleration in the east–west orientation in the horizontal tangent plane.

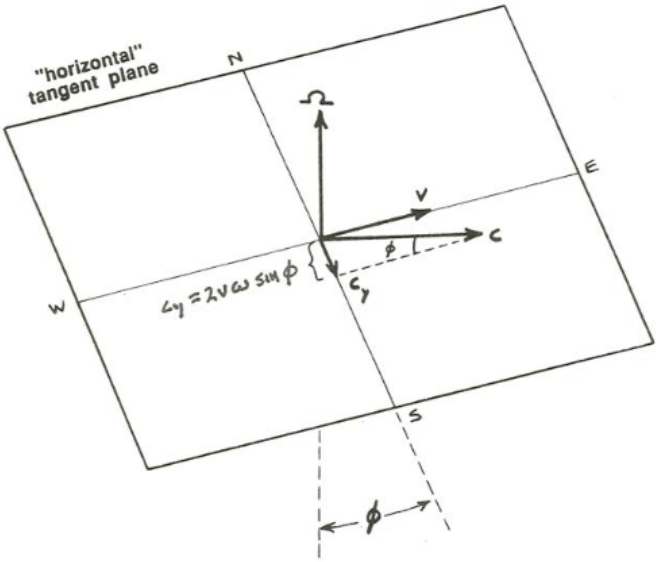


Figure 7.2.8: The component of the Coriolis acceleration in the north–south orientation in the horizontal tangent plane.

So the bottom line on the Coriolis acceleration for horizontal movements on the Earth's surface is this:

1. Its magnitude is directly proportional to the speed of the body,
2. Its horizontal component is always directed normal to the direction of movement (to the right in the Northern Hemisphere but to the left in the Southern Hemisphere), and
3. Its magnitude is always $2v\omega \sin \phi$.

So the Coriolis effect is largest at the poles and zero at the Equator. (It works just the opposite way for the *vertical* component of the Coriolis acceleration—largest at the Equator—but, as I said before, the vertical component is unimportant anyway.) What is usually done with this expression for the Coriolis acceleration is to extract the $2v\omega \sin \phi$ part and call it the **Coriolis parameter**, denoted by f.

Finally, I want to make sure that you do not confuse the separate effects of the centripetal acceleration and the Coriolis acceleration, both of which affect the motion of bodies on the Earth's surface as viewed by an observer on the Earth. The centripetal acceleration affects all bodies in and on the Earth, whether they are stationary or moving. To reveal its effect, go back to your turntable and place a big shallow pan of water on it. You know what happens when the table is rotated: the water banks up against the outer side of the pan, and the inward-sloping water surface sets up a horizontal component of the gravity force that

counterbalances the outward centrifugal force. After the initial adjustment in water-surface slope is made, the centrifugal force has no further direct effect on the movement of the water relative to an observer riding on the turntable. (Lakes and oceans on Earth adjust in this same way—as does the solid Earth itself. It is the reason why the Earth is an oblate spheroid, with equatorial diameter larger than pole-to-pole diameter, rather than a sphere.) Because the velocity of the water relative to the boundaries of the pan is zero, there is no Coriolis acceleration.

Now move your hand in the water to produce a gentle current in the interior of the water in the pan. Of course the pattern of flow will be modified by friction and eventually die away, but while the water is moving it experiences the Coriolis acceleration, and the configuration of the current is more or less strongly affected, depending upon the speed of the water and the rate of rotation of the turntable. It is these effects in the atmosphere and oceans that we are going to investigate in the rest of this chapter.

This page titled 7.2: The Coriolis Effect on the Earth's Surface is shared under a CC BY-NC-SA 4.0 license and was authored, remixed, and/or curated by John Southard (MIT OpenCourseware) via source content that was edited to the style and standards of the LibreTexts platform.

7.3: The Rossby Number and Inertia Currents

The Rossby Number

How can we gain a general idea about whether the motion of a fluid or a solid object on or near the Earth's surface would manifest non-negligibly the Coriolis effect? The answer lies in a dimensionless parameter called the Rossby number. Any such motion, whether it is a flow of a fluid or the flight of a bullet or an artillery shell or a rocket, has some characteristic speed U and moves over some characteristic distance L. Depending upon the latitude, there is some particular value of the Coriolis parameter, ranging from zero at the Equator to a maximum at the poles. The essential idea is this: how long does it take for the material to make its trip, in comparison to how much the Earth rotates under the material while it is making its trip?

The only way to combine the three variables U with dimensions of length/time), L (with dimensions of length), and f (with dimensions of 1/length) is U/fL, which is one form of what is called the **Rossby number**. You can think of the Rossby number as the ratio of two velocities, because the combination fL has the dimensions of a velocity. In the case of the ocean current, moving at a few centimeters per second over a distance of, say, a thousand kilometers, the Rossby number is very small; in the case of a speeding bullet, the velocity is very large and the distance of travel is no more than something like a thousand meters, the Rossby number is very large. In other words, the Earth rotates quite a lot in the time it takes for the ocean current to move from place to place, so the effect of the Earth's rotation on the movement of the fluid is great. By contrast, the Earth rotates very little in the time it takes the bullet to travel from the rifle to the target, so the Coriolis acceleration is negligible.

Inertia Currents

I mentioned earlier that you might generate a current in the interior of the big pan on your turntable and then study the effect of the Coriolis acceleration on that current. If the pan is broad enough and deep enough, the mass of water you set in motion can move for quite some time and distance just by its own inertia before being brought to a stop by friction forces exerted by the adjacent fluid. Currents of this kind are called **inertia currents**. In nature they might be produced by passage of a sudden squall or a fast-moving windstorm over a large body of water.

Consider a small parcel of water anywhere in your inertia current. Your first thought might be that, because no forces are acting on it, it would move in a straight line at constant speed—and that would be true, if your turntable were not rotating. But remember that, from the standpoint of an observer on the turntable, the rotation of the turntable results in a Coriolis acceleration, so you have to deal with a force per unit mass of fluid equal to fv, the Coriolis acceleration (v is the velocity and f is the Coriolis parameter), acting at right angles to the direction of movement. If the turntable is rotating counterclockwise as viewed from above, then the Coriolis force acts to the right of the direction of movement. That sense of rotation is the same as in the Northern Hemisphere on the Earth. If the turntable is rotating clockwise, then the Coriolis force acts to the left of the direction of movement, as in the Southern Hemisphere.

The dynamicist's approach to the problem of how the water in the inertia current moves as a function of time is to derive the governing equations of motion, including pressure forces, viscous forces, gravity forces, and Coriolis forces, and then specialize the equations for the particular flow, making any judicious simplifications necessary for good mathematical progress. We will not go through such an exercise here. For inertia currents the equations simplify very nicely, just because we are assuming that the only force we have to deal with is the Coriolis force.

When written in an xyz coordinate system with reference to the horizontal plane at some point on the Earth (z being vertical, x being east, and y being north), the two horizontal equations come out to be just

$$\begin{aligned} \tfrac{du}{dt} &= 2v\omega \sin\phi \\ \tfrac{dv}{dt} &= -2u\omega \sin\phi \end{aligned} \tag{7.3.1}$$

or, using the notation for the Coriolis parameter,

$$\begin{aligned} \tfrac{du}{dt} &= fv \\ \tfrac{dv}{dt} &= -fu \end{aligned} \tag{7.3.2}$$

where u and v are the x and y components, respectively, of velocity of the fluid relative to the horizontal plane defined above.

Do not worry about the signs in front of the Coriolis terms; they come about when the x and y components of the Coriolis acceleration are derived for the horizontal plane. This is a simple set of equations. Its solution, for an initial condition that $u = U$ and $v = 0$ at $t = 0$, is

$$\begin{aligned} u &= U \cos ft \\ v &= -U \sin ft \end{aligned} \tag{7.3.3}$$

If you go back to your storehouse of mathematical knowledge you can easily demonstrate to yourself that this solution represents motion around a circle at constant speed, with the time t as a parameter. For circular motion like this, the radius of the circle is just U/f, and the time it takes a particle to go all the way around the circle is $2\pi/f$. This circle is called an **inertia circle**, and the period is called the **inertia period**.

That the water in an inertia current in a rotating system moves in circles does not seem intuitively obvious (at least not to me!). Keep in mind here that the situation with the inertia current is not the same as with the rolling ball. The inertia current acts in a body of water that is moving around with the turntable, whereas the rolling ball moved in a straight line relative to the fixed stars and has no connection with the turntable itself.

At first thought you might guess that the inertia period is the same as the period of rotation of the turntable itself. But you would be wrong! Call the period of rotation T_r, and the inertia period T_I. I told you above that

$$\begin{aligned} T_I &= 2\pi/f \\ &= 2\pi/2\omega \sin \phi \end{aligned} \tag{7.3.4}$$

$$= \pi/\omega \sin \phi \tag{7.3.5}$$

Let me remind you that in any rotatory motion the relationship between the angular velocity and the period is $\omega Tr = 2\pi$, or $T_r = 2\pi/\omega$, or $\omega = 2\pi/Tr$. Substituting this into Equation 7.3.5,

$$T_I = \frac{T_r}{2 \sin \phi} \tag{7.3.6}$$

An interesting result, no? The inertia period is *not* the same as the rotation period. For your turntable, which acts like a horizontal plane at the North Pole, where the latitude is 90°, the inertia period is exactly *one-half* the rotation period.

Just to give you some feel for how large the inertia circle would be on your turntable and on the real Earth, here are some simple examples. Suppose your turntable is rotating with a period of 100 s—slow enough so that you would not have any trouble staying on board, and you probably would not develop motion sickness either. An inertia current of 1 cm/s in your big pan would have an inertia circle radius of 8 cm, and a current of 10 cm/s would have an inertia circle radius of 80 cm. A current of any speed would have an inertia period of 50 s. So you would actually be able to observe the inertia circles, if the pan is large enough and the current velocity is small enough.

At the North Pole the inertia period is 12 hours, and it increases (not linearly!) with decreasing latitude, going to infinity at the Equator. At latitude 45° it is about 17.5 hours, and at latitude 30° it is about 24 hours. At latitude 45° the radius of the inertia circle is about 1 km for an inertial current of 10 cm/s, and about 10 km for an inertial current of 1 m/s.

Figure 7.3.1 shows the track of a tracer in an inertia current that was measured over a period of about a week in the Baltic Sea (Gustafson and Kullenberg, 1933). The periods of the loops match the theoretical inertia period for that latitude very closely. There is net translation of the marker because the inertia current was superimposed on a larger-scale current of some other kind. Note that the size of the inertia circles decreases with time, presumably because the current slowed down because of friction.

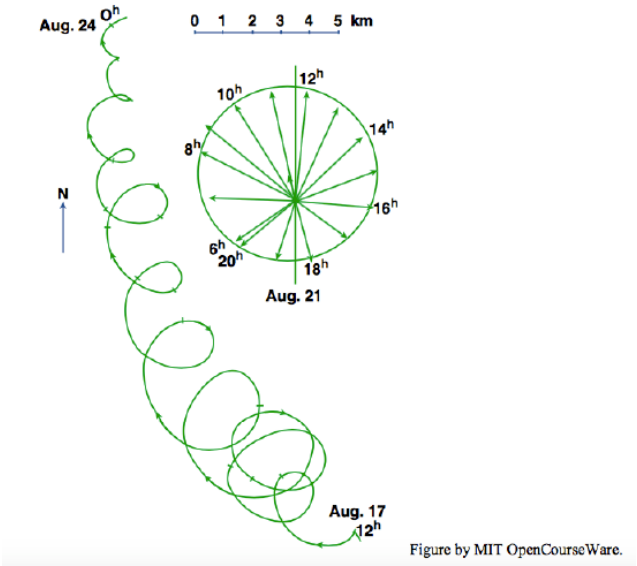


Figure 7.3.1: Inertia circles in the Baltic Sea. (From Neumann and Pierson, 1966.)

This page titled 7.3: The Rossby Number and Inertia Currents is shared under a CC BY-NC-SA 4.0 license and was authored, remixed, and/or curated by John Southard (MIT OpenCourseware) via source content that was edited to the style and standards of the LibreTexts platform.

7.4: The Ekman Spiral

A wind blowing over a water surface exerts a force on the surface, and that force tends to drag or push the water in the direction of the wind. Surface currents of this kind are called **pure drift currents**. This is in addition to the more readily observable effect of generation of surface waves, discussed in Chapter 6.

Your intuition tells you that the wind-driven current is in the direction of the wind, and that its effect decreases downward from the surface. In a nonrotating system both of these suppositions are true, but, from what has been said already above, you should suspect that the Coriolis acceleration complicates matters in a rotating system. This section deals briefly with some of the intricacies of the Coriolis effect on wind-driven currents.

What can we deduce about the current, without actually solving the equations of motion? First of all, it should be clear, even without worrying about change in direction with depth, that the speed of the current should decrease downward because of frictional retardation, for just the same reasons as did the fluid contained between a stationary lower plate and a moving upper plate considered way back in Chapter 1.

But what about the *direction* of the current? Think about the balance of forces on a small parcel of fluid at the water surface (Figure $7.4.1$). The surface water feels not only the wind force, in the direction of the wind, but also the Coriolis force, at right angles to the direction of water motion, and a friction force exerted by the slower water below, in the direction opposite to the surface water motion. Because the parcel of surface water is not accelerating, these three forces have to add up to zero. From Figure $7.4.1$ you can see that the only way you can balance these three forces is for the surface water to move at some angle between 0° and 90° to one side of the wind direction—to the right of the wind in the Northern Hemisphere and to the left of the wind in the Southern Hemisphere.

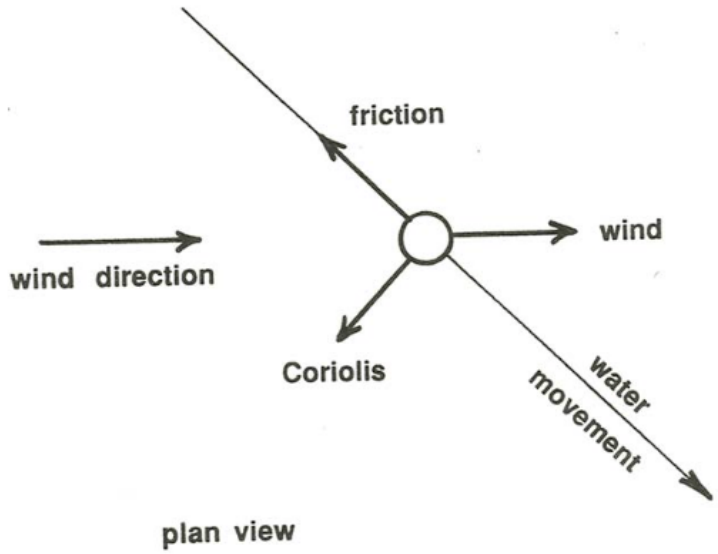


Figure $7.4.1$: Balance of forces on a surface water element under a wind.

Now look at a slightly lower layer of water. A frictional force is exerted on its upper surface by the overlying layer, and a frictional force is exerted on its lower surface by the underlying layer. The same line of reasoning we used in Chapter 1 for flow between parallel plates moving relative to each other suggests that these two frictional forces are of the same magnitude but in different directions. But there has to be some left-over net friction force, because that is the only force that is available to balance the Coriolis force. For there to be a friction force directed opposite to the Coriolis force, the velocity vector must be turning continuously away from the wind direction with depth! See Figure $7.4.2$ for how this works. And so on for each successively deeper layer: each lower layer of water moves in a direction farther to the right (or left) of the surface wind direction.

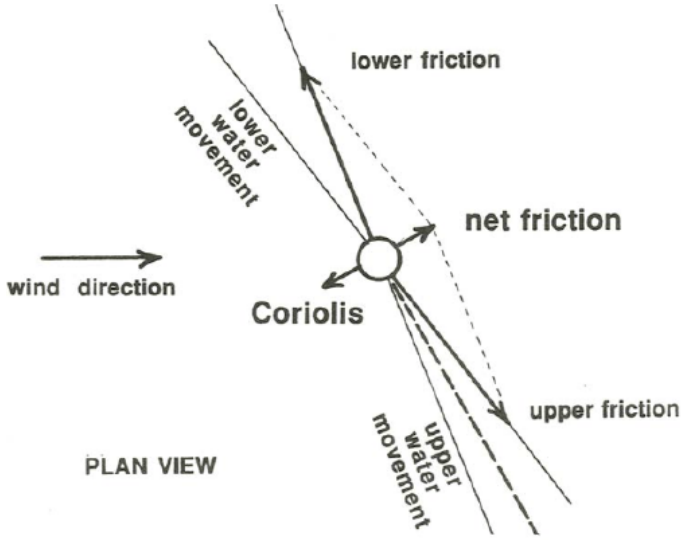


Figure 7.4.2: Balance of forces on a subsurface water element under a wind.

The only trouble with the argument in the last two paragraphs is that it is discrete rather than continuous. To solve the problem right, we would have to write the differential equations of motion, subject to the appropriate boundary conditions, and solve them for the vertical distribution of current speed and direction, both of which must of course vary continuously with depth. But the above argument gives you the qualitative physical essence of what is happening.

This problem was first solved analytically by Sven Ekman, a Norwegian physical oceanographer, in 1905. The assumptions behind the solution are that the surface wind is uniform in both speed and direction everywhere and that the ocean is of infinite extent horizontally, so that water does not get piled up in the downwind direction to create an extra force in the form of a horizontal pressure gradient and complicate matters, and also that the ocean is infinitely deep. In case you want to play around with the solution, here it is:

$$\begin{aligned} u &= U_o e^{-(\pi/D)z} \cos\left[(\pi/4) - (\pi/D)z\right] \\ v &= U_o e^{-(\pi/D)z} \sin\left[(\pi/4) - (\pi/D)z\right] \end{aligned} \tag{7.4.1}$$

where v is the velocity component at any depth in the wind direction, u is the velocity component to the right of the wind direction, z is depth below the water surface, U_o is the water speed at the surface, and D is a parameter that contains the water density ρ, the Coriolis parameter f, and a viscosity coefficient A:

$$D = \pi\sqrt{\frac{A}{\rho f}} \tag{7.4.2}$$

What Equations 7.4.1 tell you is that at the water surface the velocity is directed at exactly 45° to the right of the wind, and with depth the direction of the velocity swings farther and farther to the right while the speed falls off exponentially. Figures 7.4.3A and 7.4.3B show two graphical views of the velocity profile with depth. You can see from these figures why the solution is called the **Ekman spiral**!

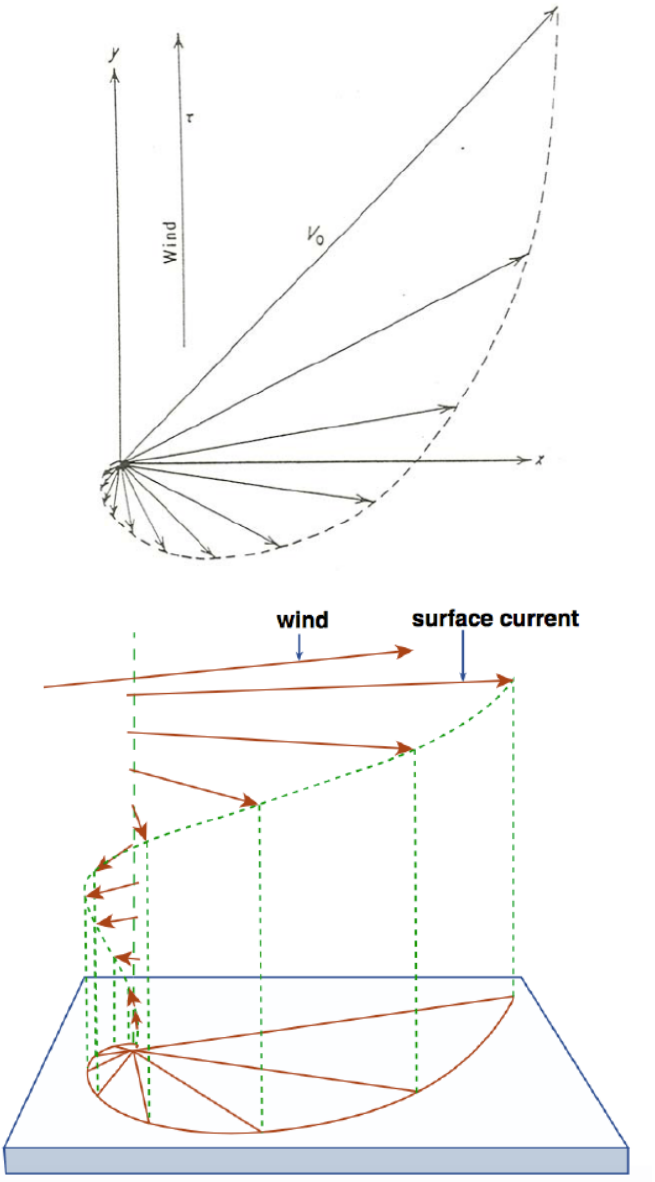


Figure 7.4.3: **A)** The Ekman spiral. (From Neumann and Pierson, 1966.) **B)** A three-dimensional view of the Ekman spiral. (From Gross, 1990.)

Here are some interesting properties of Equations 7.4.1. If you substitute $z = D$ into the equations, you find that at depth D the velocity components are

$$\begin{aligned} u &= U_0 e^{-\pi} \cos(\pi/4 - \pi) \\ v &= U_0 e^{-\pi} \sin(\pi/4 - \pi) \end{aligned} \tag{7.4.3}$$

which tell you that at depth D the speed has decreased to $e^{-\pi}$ times the surface velocity (which is less than five percent), and the direction is *opposite* to the surface current! One can also find the total mass transport of water involved in this Ekman-spiral current, by multiplying the velocity components u and v by the water density ρ and integrating Equations 7.4.1 over the depth from 0 to ∞. The result is spectacular: *the net transport of water is directed at exactly* 90° *to the surface wind!* I suppose that will seem counterintuitive, but such are the mysteries of the Coriolis effect.

This page titled 7.4: The Ekman Spiral is shared under a CC BY-NC-SA 4.0 license and was authored, remixed, and/or curated by John Southard (MIT OpenCourseware) via source content that was edited to the style and standards of the LibreTexts platform.

7.5: Geostrophic Motion

So far I have discussed some oceanic consequences of the Coriolis effect. Although important, these are on fairly local scales. But the Coriolis effect also plays a striking and fundamentally important role in the dynamics of the large-scale currents and circulations in both the oceans and the atmosphere.

Here is the background you need to know. All of the large-scale motions of the oceans and atmosphere, of the kind you would see on a weather map of North America or a chart of North Atlantic currents, owe their existence to *horizontal pressure gradients*: changes in pressure from place to place when viewed at the same altitude (in the atmosphere) or the same depth (in the oceans).

This is not the place to describe in much detail how these horizontal pressure gradients come about; I hope it will suffice to say that in the atmosphere they arise from differential heating and cooling and the resulting expansion and contraction of the atmosphere, and in the oceans they arise from a number of effects, including large-scale differences in temperature and salinity and also the horizontal movement and "piling up" of surface waters in response to winds.

Just to give you some feeling for the origin of horizontal pressure differences in the atmosphere, think about a hypothetical convection cell, one that is greatly oversimplified but fundamentally representative of what really happens in the atmosphere on a large scale. Unfortunately this is not something I can expect you to build in your back yard—although essentially the same thing happens in a big tank of differentially heated and cooled water. Figure 7.5.1 shows a gigantic north–south slice through a hypothetical atmosphere. Suppose that, before convection begins, the atmosphere is at the same temperature everywhere at any given altitude. Because air density is a function of temperature, and air pressure is a function of how the air density varies with altitude above the given altitude level, the pressure is the same everywhere at the given altitude, as shown by the horizontal lines in Figure 7.5.1, which represent the intersections of horizontal planes with surfaces of equal pressure (called **isobaric surfaces**).

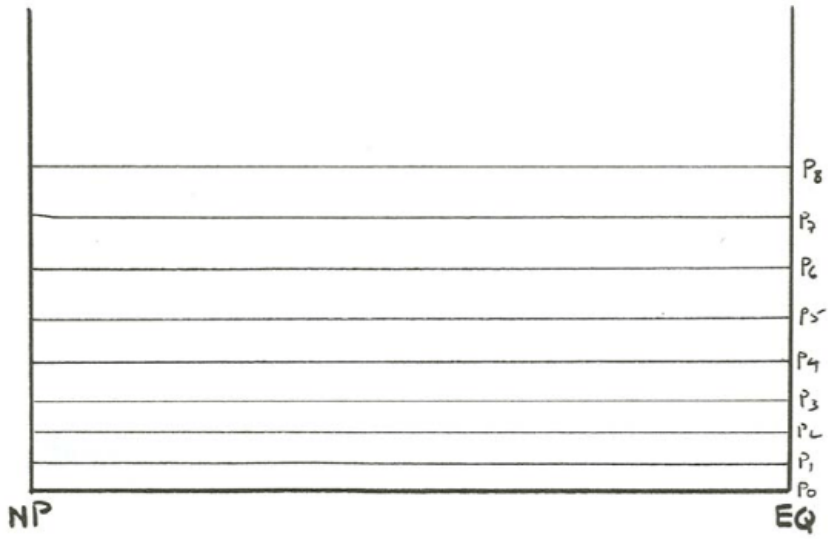


Figure 7.5.1: North–south slice through a hypothetical atmosphere, before the action. NP, North Pole; EQ, Equator.

To get the convection cell going, suppose that the atmosphere is heated at low latitudes, near the Equator, and cooled at high latitudes, near the North Pole. At low latitudes the entire column of the atmosphere expands upward, and at high latitudes the entire column of the atmosphere contracts downward, in response to the change in temperature and therefore in density. In response to this expansion and contraction, the isobaric surfaces everywhere above the ground surface take on a poleward slope, as shown in Figure 7.5.2. The effect is a movement of air from low latitudes to high latitudes, as can be seen by considering how the pressure varies across some arbitrary horizontal surface in the atmosphere, shown by the dashed line in Figure 7.5.2. Because of the way the isobaric surfaces cut the horizontal surface, there is a south-to-north decrease in pressure along the horizontal surface, and this pressure gradient causes south-to-north air movement.

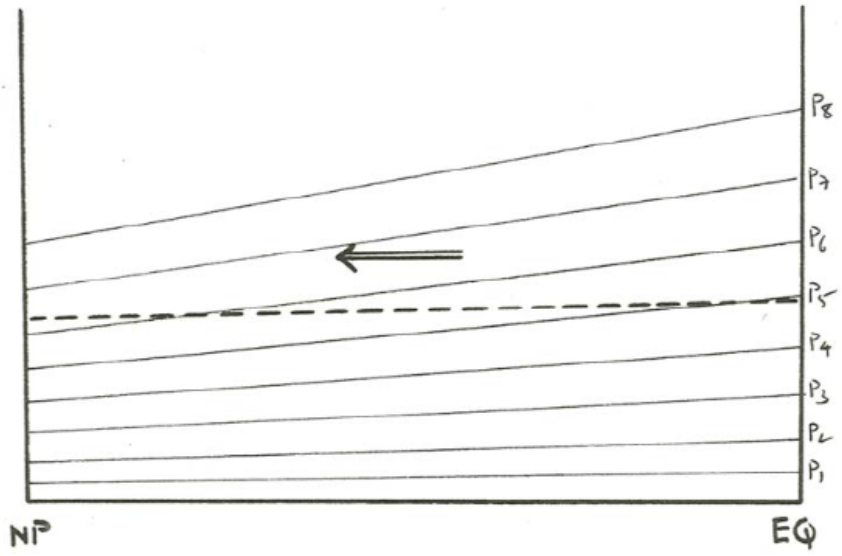


Figure 7.5.2: North–south slice through the hypothetical atmosphere, after heating and cooling begins.

The south-to-north air movement results in a greater total mass of air in an atmospheric column near the North Pole than in an atmospheric column near the Equator. At and near the Earth's surface, therefore, the atmospheric pressure is greater near the North Pole than near the Equator, so along some horizontal surface low in the atmosphere the horizontal pressure gradient is north-to-south rather than south-to-north. The equilibrium pattern of convective motion then shows (Figure 7.5.3) northward flow in the upper atmosphere, where the horizontal pressure gradient is to the north, and southward flow in the lower atmosphere, where the pressure gradient is to the south. At some intermediate level, the isobaric surfaces are horizontal, and there is no horizontal motion.

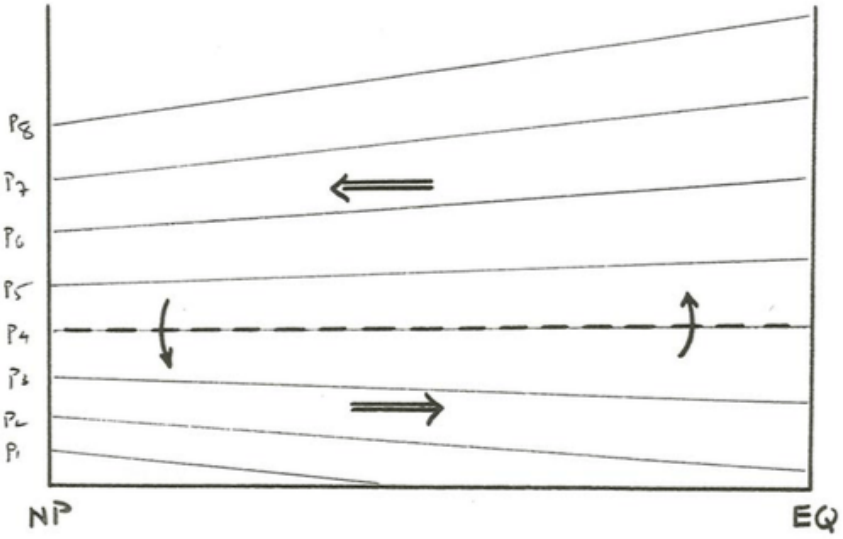


Figure 7.5.3: Circulation produced in the hypothetical atmosphere by heating and cooling.

The foregoing exercise is meant to show how the actual motions in familiar thermal convection cells are qualitatively understandable responses to horizontal pressure gradients set up by differential heating and cooling and consequent expansion and contraction. What I want you to carry away from this example is the idea that there are always going to be horizontal pressure gradients in the atmosphere, which tend to generate winds. (Currents in the deep ocean are generated by such pressure gradients as well.) Now we have to see how the Coriolis acceleration affects these pressure-gradient-generated winds.

I said in an earlier section that the motions of the atmosphere and oceans on the Earth's surface are dominantly horizontal on a large scale (keep in mind that the slopes of the isobaric surfaces in Figure 7.5.3 are greatly exaggerated) and that only the horizontal component of the Coriolis acceleration has to be considered in these horizontal motions. Think about the fundamental

balance of forces that govern these motions. To do a complete job of this we would have to pick apart the governing equations of motion in some detail, but the important effects should make good sense to you without that.

First of all, just as with flow in pipes and channels (Chapter 4), we can think about the balance of forces in the plane parallel to the solid boundary, to which the motions are parallel, and be content in the knowledge that in the normal-to-boundary direction the equation of motion boils down to a balance between the downward weight of the fluid and the upward pressure gradient, as a manifestation of what I called the *hydrostatic balance* in Chapter 1.

Which horizontal forces need we take into account? The candidates are five: *pressure*, *friction*, *gravity*, *Coriolis*, and (if the wind blows in a horizontally curved path) *centrifugal force*. By what was said in the last paragraph, gravity need not be included. And the centrifugal force is really important only in tightly curving winds, as in tornadoes; even around the eye of a hurricane it is not the dominant effect, although it is not negligible either. That leaves pressure, friction, and Coriolis.

I hope it will make sense to you when I claim that, well above the layer of the atmosphere that is in the immediate vicinity of the surface, frictional effects should be very small compared with the other forces. This is indeed the case, as you will see from the outcome of the present line of argument later, but it is not easy to justify. Then the dominant balance of forces is just between the pressure gradient and the Coriolis force. It is this force balance that has such far-reaching consequences for the nature of atmospheric and oceanic motions.

Think about the direction of the wind, relative to the pressure gradient, when the air is moving under the influence of a balance between the pressure- gradient force and the Coriolis force. Use Figure 7.5.4, which is a plan view of some large area over which a horizontal pressure gradient in the atmosphere acts, as a guide. In Figure 7.5.4 the light lines represent the intersections of the isobaric surfaces with a horizontal plane at some fixed altitude at which we are considering the atmospheric motion; these lines, called **isobars**, are exactly the same as the those they used to show on the weather maps in the newspapers and on television.

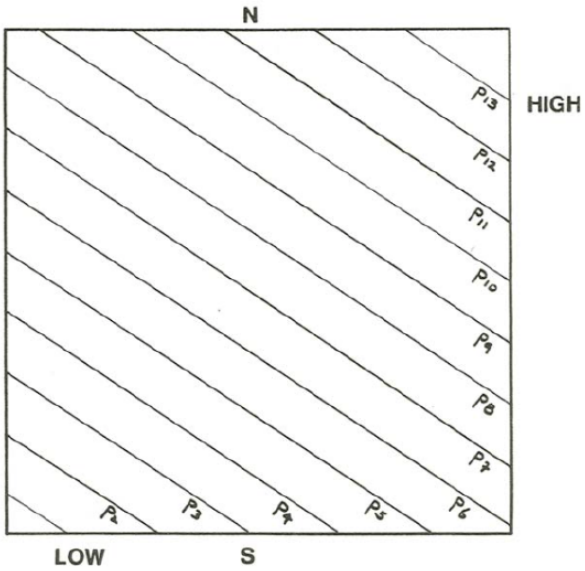


Figure 7.5.4: Plan view of a large area of the atmosphere in which there is a horizontal pressure gradient.

The pressure-gradient force acts at right angles to the isobars, in the direction of decreasing pressure. So (Figure 7.5.5) in the absence of Coriolis effects the wind should blow straight across the isobars. But on our rotating Earth (Figure 7.5.6), because the Coriolis force always acts at right angles to the direction of motion, the only way there can be a balance between the pressure gradient and the Coriolis is for the wind to blow *along* the isobars, not *across* them!

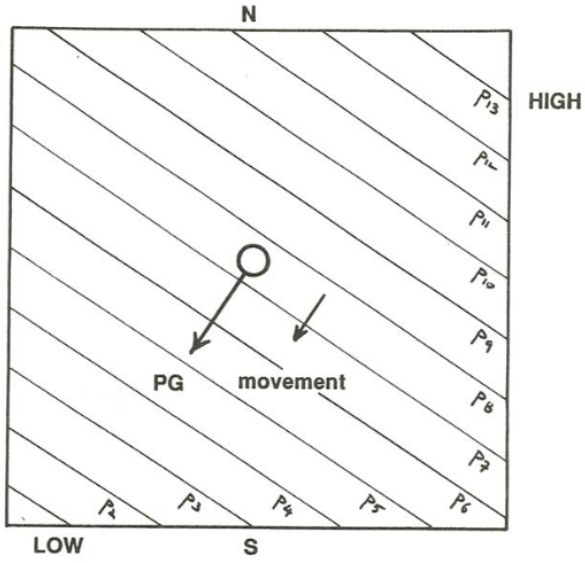


Figure 7.5.5: In the absence of Coriolis effects, the wind should blow across the isobars toward lower pressure.

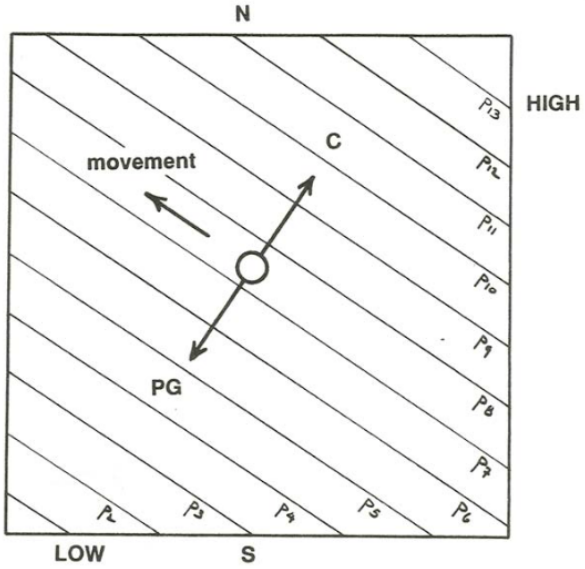


Figure 7.5.6: In the presence of Coriolis effects, the wind blows parallel to the isobars.

If the startling conclusion in the last paragraph seems fishy to you, or you do not fully understand what is going on, try drawing the balance of the two forces when a parcel of air is moving horizontally in some arbitrary direction other than parallel to the isobars (Figure 7.5.7). You would see that the resultant of the two forces always has a component off to one side of the assumed direction of motion, and the direction of that component is such as to swing the trajectory of the air lump closer to being along the isobars. There can be no balance until those two force vectors act in directions exactly opposite to each other, and that direction is parallel to the isobars.

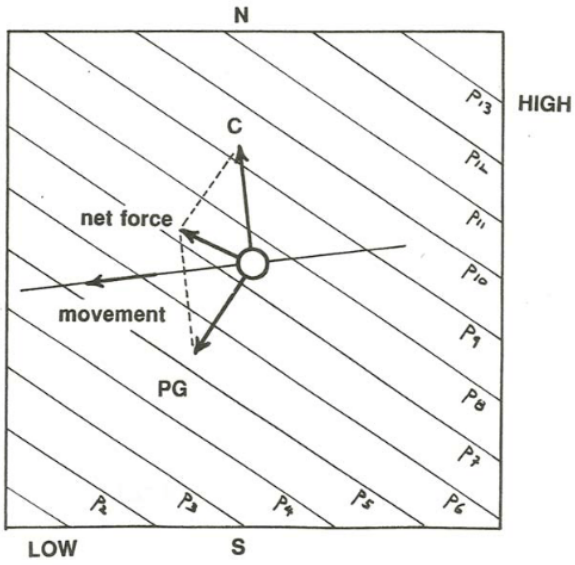


Figure 7.5.7: The net force on a parcel of air that is not moving parallel to the isobars is such as to cause its movement to become more nearly parallel to the isobars.

Planetary fluid motion of the kind analyzed above, for which the balance between the pressure-gradient force and the Coriolis force dictates a direction of movement along the isobars, is called **geostrophic motion**, and the balance of forces itself is called the **geostrophic balance**. It is of fundamental importance in both the atmosphere and the oceans. In fact, it seems safe to say that geostrophic motion is by far the most striking aspect of large-scale planetary fluid motions.

The reality of geostrophic motion is apparent from even a cursory glance at a "real" weather map (one that shows isobars): the winds are almost parallel to the isobars, and in such a sense that in the Northern Hemisphere if you look across the isobars down the pressure gradient, toward the region of low pressure, the wind blows from your left to your right. Another way of saying that is that (in the Northern Hemisphere) the winds move counterclockwise around areas of low pressure and clockwise around regions of high pressure (Figure 7.5.8).

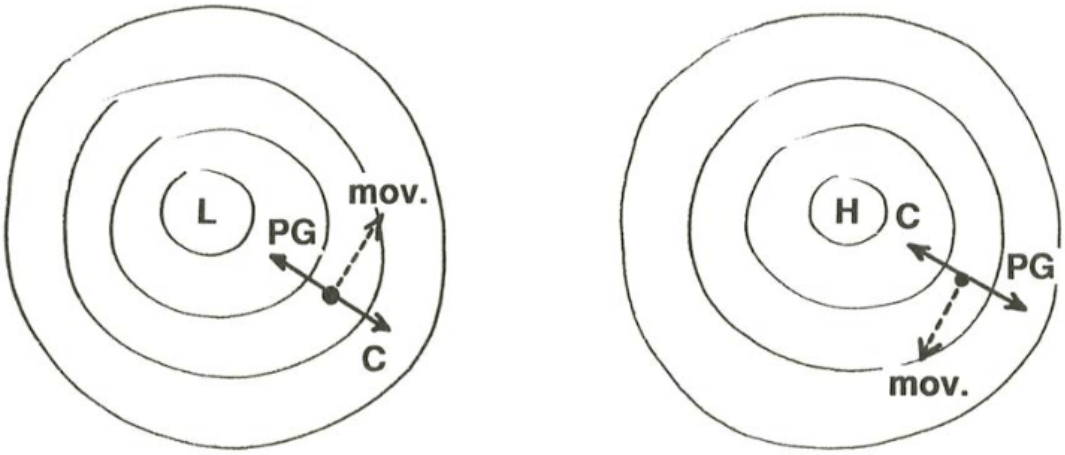


Figure 7.5.8: In the Northern Hemisphere, winds move counterclockwise around low-pressure area and clockwise around high-pressure areas.

This page titled 7.5: Geostrophic Motion is shared under a CC BY-NC-SA 4.0 license and was authored, remixed, and/or curated by John Southard (MIT OpenCourseware) via source content that was edited to the style and standards of the LibreTexts platform.

7.6: Ekman Layers

It might have occurred to you, the perceptive reader, that there has to be something more to the phenomenon of geostrophic motion than what I have shown above—because the air somehow has to get down the pressure gradient, or else the pressure gradients would keep on increasing. (Think back to the convection-cell example I presented earlier.) Somehow there has to be movement of the air across the isobars, as in the more direct flow that would be set up in the absence of rotation.

The way out of this dilemma is to include the effect of friction forces in the lowermost part of the atmosphere. Think about the friction forces on a small test parcel of air moving near the ground. The overlying and underlying layers of air exert friction forces on the top and bottom surfaces of the parcel, and these forces are in different directions: the lower layer exerts a force opposite to the direction of motion, and the upper layer exerts a force in the direction of motion. The key point (Figure 7.6.1) is that the upper of these shear forces is slightly smaller than the lower, because the shear stress decreases upward from a maximum at the ground, just as in open-channel flow we considered in Chapter 4. So the net friction force should act opposite to the direction of motion.

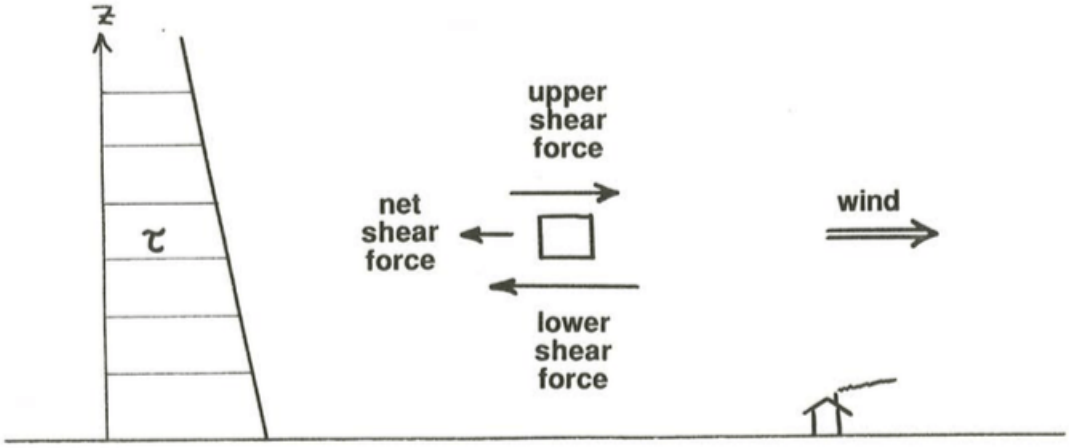


Figure 7.6.1: The net shear force on a parcel of air parcel moving near the Earth's surface or on a parcel of water moving near the ocean bottom. (The effect of the turning of the flow in the bottom Ekman layer is not taken into account in this approximate sketch; see the section on the bottom Ekman layer in the text for a more realistic account.)

Now a qualitative balance among the three forces (pressure gradient, large; Coriolis, large; friction, small but nonnegligible) shows (Figure 7.6.2) that the wind blows across the isobars at a small angle from high pressure to low pressure. This you can see clearly on any good weather map (of which the map in Figure 7.6.3 is a cartoon version) drawn for conditions at the surface, where the frictional influence is greatest: the air spirals inward toward the low-pressure area, there to have a small upward component to its motion and then flow outward at high altitudes in compensation for the inflow at low altitudes. The origin of the friction force shown in Figure 7.6.2 is of the same nature as was shown in Figure 7.4.2 for the surface Ekman layer: as the flow turns, the directions, as well as the magnitudes, of the friction forces on the top and on the bottom of a fluid element are slightly different, leading to a net friction force at a large angle to the direction of motion of the element.

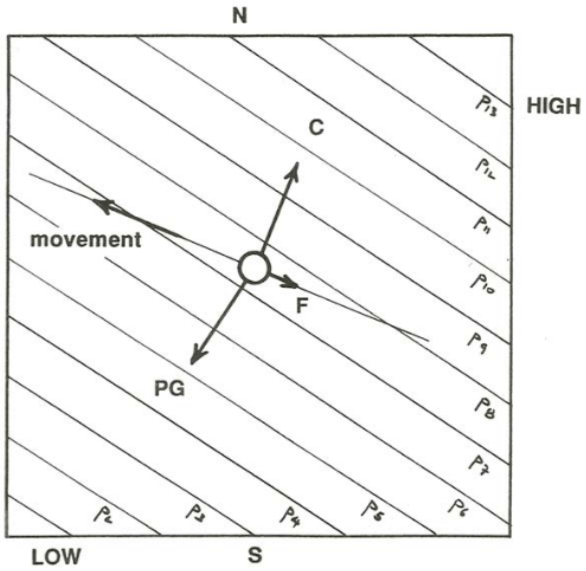


Figure 7.6.2: The effect of near-surface friction makes the wind blow across the isobars at a small angle toward lower pressure.

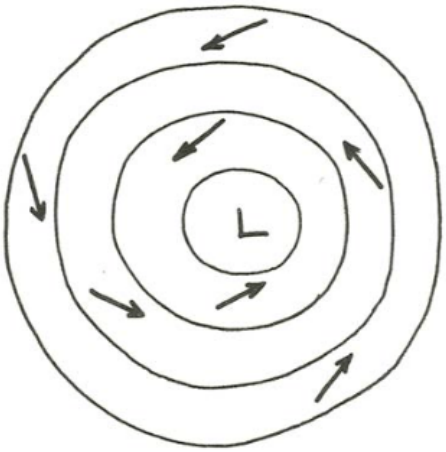


Figure 7.6.3: Cartoon weather map showing a low-pressure area, with winds blowing counterclockwise around the place of lower pressure but with a component spiraling inward across the isobars.

The lowermost layer of the atmosphere or the ocean, adjacent to the land surface in the case of the atmosphere or to the ocean bottom in the case of the ocean, in which the direction of flow turns gradually from the direction of the overlying geostrophic flow, is called the **Ekman layer** (or the bottom Ekman layer). The mathematical solution for the structure of the Ekman layer was developed by Ekman in 1905. (See Pedlosky, 1979, Chapter 4, for a lucid derivation.) The Ekman layer is the region of the flow in which the frictional effect of the bottom boundary is significant. Downward through the Ekman layer, the magnitude of the velocity decreases from its geostrophic value to zero, by the no-slip condition, at the bottom and the direction of the velocity turns from the geostrophic direction to its maximum deviation at the bottom, theoretically at 45 degrees to the geostrophic direction—to the left in the Northern Hemisphere and to the right in the Southern Hemisphere. Figures 7.6.4 and 7.6.5 show two views of the horizontal velocity vector within the Ekman layer. You can see from Figure 7.6.4 that the velocity vector executes a spiral, similar to the Ekman spiral at the ocean surface under a wind, but not the same. Figure 7.6.4, in particular, shows clearly that the magnitude of the velocity reaches a maximum near the top of the Ekman layer before settling into its geostrophic value farther upward.

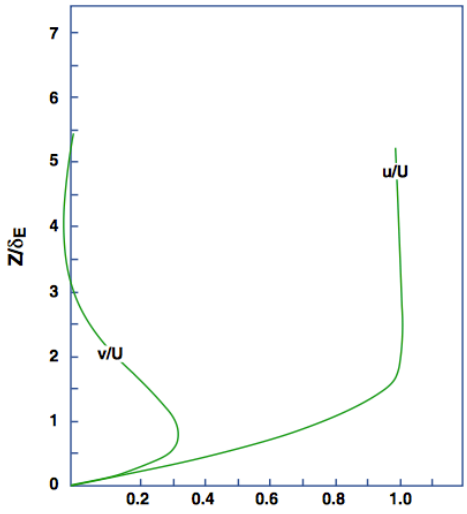


Figure by MIT OpenCourseWare.

Figure 7.6.4: The velocity in the bottom Ekman layer. The velocity u is the current speed in the direction of the overlying geostrophic flow, and the velocity v is the current speed in the direction normal to that. Both u and v are normalized by dividing by the geostrophic current speed U. The numbers associated with the velocity vectors are values of z/δ_E, where z is the height normal to the bottom and δ_E is the conventional Ekman-layer thickness. From Pedlosky (1979).

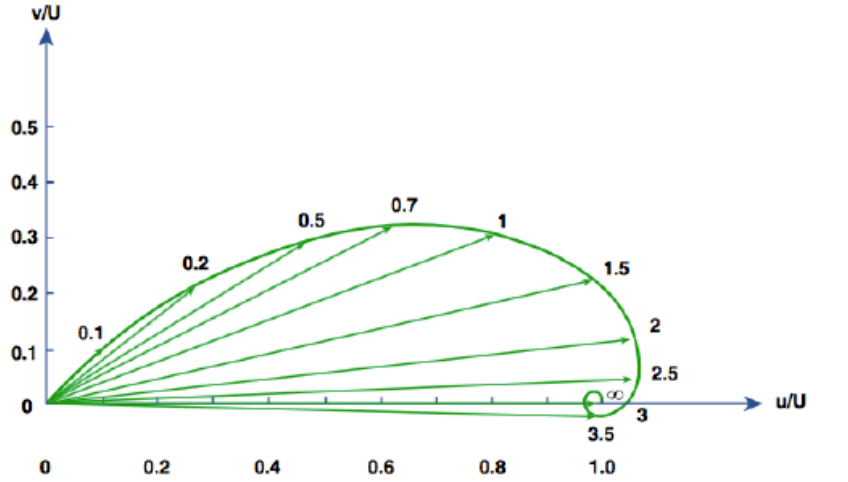


Figure by MIT OpenCourseWare.

Figure 7.6.5: Vertical profiles of u, the component of Ekman-layer velocity in the direction of the overlying geostrophic flow, and v, the component normal to the direction of the geostrophic flow. Both velocity components are nondimensionalized by dividing by the magnitude of the geostrophic velocity, U. The height above the boundary is nondimensionalized by dividing by the conventional Ekman-layer thickness δ_E. From Pedlosky (1979).

The thickness of the bottom Ekman layer should depend on the viscosity of the fluid and on the Coriolis parameter. These two factors work against one another: the greater the viscosity, the greater the thickness affected by friction, and the greater the Coriolis effect, as measured by the Coriolis parameter f, the less the thickness. The conventional measure of the Ekman-layer thickness is $[A_V(f/2)]^{1/2}$, conventionally denoted by δ_E. (Do not be concerned with the reasons for the factor 2 in the denominator.) Upward in the Ekman layer the effect of friction tails off rapidly, but keep in mind that the upper limit is indefinite: the velocity decreases upward as a negative exponential function of height above the bottom boundary. It is best to view δ_E as *representative* of the thickness of the Ekman layer; in the parlance of geophysical fluid dynamics, the Ekman-layer thickness is of order δ_E. Finally, it will probably seem counterintuitive to you that the thickness of the Ekman layer does *not* depend on the geostrophic velocity.

As is so often the case, the value to use for the kinematic viscosity in the theory for the bottom Ekman layer is a problem. The molecular kinematic viscosity ν could be used, and that gives an exact solution for a laminar Ekman layer. The problem is that the

mean-flow Reynolds numbers of large-scale flow in both the ocean and the atmosphere are so large that the Ekman layer must be turbulent rather than laminar. Alternatively, the eddy viscosity A_V can be used, but you have seen earlier that the eddy viscosity is itself a function of the flow, rather than a property of the fluid, and it might be expected to vary with height above the bottom boundary. With what seem to be reasonable values of eddy viscosity, the Ekman-layer thickness is on the order of some tens of meters, which is about what has been observed in the atmosphere and oceans.

This page titled 7.6: Ekman Layers is shared under a CC BY-NC-SA 4.0 license and was authored, remixed, and/or curated by John Southard (MIT OpenCourseware) via source content that was edited to the style and standards of the LibreTexts platform.

7.7: Planetary Boundary Layers- The Ekman Layer, The Logarithmic Layer, and The Mixed Layer

Introduction

I am now going to subject you to a further set of flow layers, one of which, the Ekman layer, you have already encountered. You can think of this concluding section as a continuation of the material on boundary layers in Chapter 4, in the context of the large-scale bottom boundary layers in the atmosphere and in the oceans—which are called **planetary boundary layers**. (Note on terminology: in the atmosphere, it is called the atmospheric boundary layer; in flow in the shallow ocean, on continental shelves, for example, it is often called the bottom boundary layer; in the deep ocean, it is commonly called the benthic boundary layer. They are all the same, in essential dynamics).

Given that the winds and the ocean bottom currents flow over a solid boundary, it is understandable that there must be a bottom boundary layer in those settings. All of what was said about boundary layers in Chapter 4 can be applied to these planetary boundary layers—but with the important additional effect of the Earth's rotation. In the previous section you learned about the Ekman layer, which, as a part of the planetary boundary layer, is an additional boundary-layer element brought about by the Coriolis effect.

The Mixed Layer

Stable stratification is ubiquitous in the atmosphere and the oceans. By stable stratification I mean that the vertical profile of fluid density in the medium is such that if you were to capture a small parcel of the fluid and move it bodily upward, without allowing any exchange of thermal energy between the parcel and its surroundings (in thermodynamics that is called an *adiabatic process*), it would arrive with density greater than its surroundings, and if you moved it downward, it would arrive with density less than its surroundings. That means that there is no tendency for convective vertical mixing: the density stratification is such that the parcel would always be pushed back toward the place where it started.

The atmosphere and the oceans are fundamentally different in respect to the origin of stable stratification. The main reason is that the atmosphere is heated at its base: the sun warms the ground surface, and the lowermost layer of the atmosphere is in turn warmed by the ground—during the day, that is, and not at all times and places even then. By contrast, the heating of the lowermost layer of the ocean by heat flow from the substrate is not very important in the dynamics of near-bottom flow.

You learned back in Chapters 3 and 4 that shear produces turbulence, and the stronger the shearing, the more likely it is that turbulence is produced. You also learned that, in flow of a viscous fluid past a boundary, the shear is strongest near the boundary and decreases way from the boundary. Here you need to think in terms of a *competition*: one the one hand, stratification tends to damp turbulence, whereas on the other hand, shear tends to produce turbulence. That leads to the concept that under the right conditions a turbulent layer develops adjacent to the boundary, in which turbulence produced by shear causes vertical mixing, as you learned about in Chapter 4. Such a layer is called the **mixed layer**. So the thickness of the mixed layer depends upon the competition between the intensity of the near-boundary shear and the strength of the stratification. Figure 7.7.1 shows a striking example of a mixed layer in the ocean.

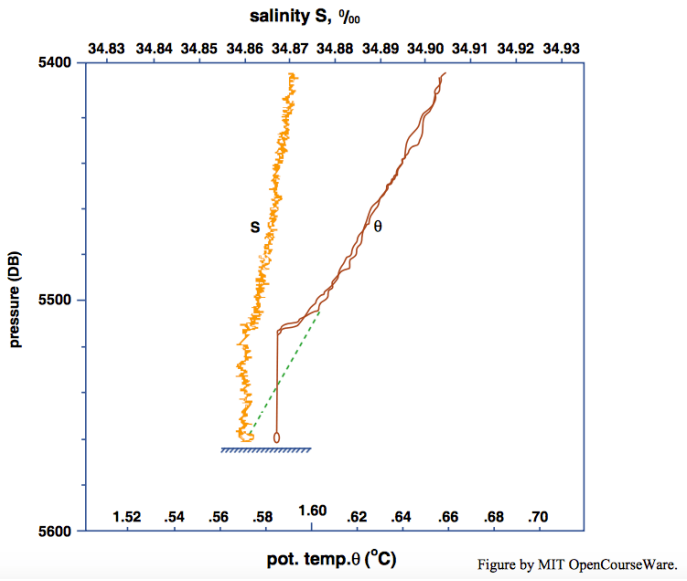


Figure 7.7.1: An example of the mixed layer in the deep ocean. The most natural way of explaining why the potential temperature in the lowermost layer shows no variation with depth is that this layer is thoroughly mixed by shear turbulence. (The potential temperature is what the temperature of an element of the fluid medium would be if the element were transported to some reference level without exchange of thermal energy with its surroundings. A constant potential temperature means neutrally stable stratification: neither stable nor unstable. Mechanical mixing tends to produce such neutrally stable stratification.) (From Armi and Millard, 1976.)

Things are different in the atmosphere, because of the tendency for diurnal (day to night) difference in heating of the ground by solar radiation during the day and cooling of the ground by long-wave radiation to space during the night. The tendency for development of a mixed layer by shear turbulence is present in the atmosphere as well as the ocean, but the other effect, strong convection by ground heating, is even more important. The two processes act together to produce a well-defined mixed layer, even when the atmosphere is overall stably stratified (as is true most of the time, except in the vicinity of low- pressure areas, where uprise of air through a deep layer is caused by other effects). At times when the convectively uprising air reaches the local condensation level, puffy cumulus clouds form, and mark the top of the mixed layer nicely. You probably have experienced the structure of the atmospheric mixed layer yourself: as you gain altitude in your jetliner on a nice sunny day, the ride is bumpy until you reach the tops of the cumulus clouds, whereafter you have a much smoother ride.

What is the relationship between the mixed layer, on the one hand, and the Ekman layer, which you learned about earlier in this chapter, on the other hand? Commonly, the thickness of the mixed layer in the ocean is the greater part of a hundred meters, and that of the mixed layer in the atmosphere is on the order of a thousand meters. That's several times the thickness of the Ekman layer. So you can think of the Ekman layer as typically being embedded deeply in the mixed layer. The flow is turbulent at heights above the bottom well above the turning of the flow velocity in the Ekman layer.

A grand large-scale mental experiment might not be out of place here. Suppose that you could somehow set up a gigantic tank, as large as an ocean basin, on a rotating platform. To a depth of a few thousands of meters, fill the tank with water that is at the same temperature (and salinity) throughout, so that there is no density stratification whatsoever. Somehow, produce a broad current in the medium, on a scale of thousands of kilometers on both the along-flow and cross-flow directions. In the parlance of geophysical fluid dynamics, what we are aiming for is a flow with a very small Rossby number.

What would you observe? A vertical profile of velocity that is the same, in essential respects, as the fully developed boundary-layer flow, akin to what is shown in Figure 3.6.5, back in Chapter 3 on boundary layers. The boundary layer would have grown to occupy the full depth of the flow, and the flow would be turbulent throughout. The Ekman layer, however, would be there, immediately above the bottom: that's the fundamental difference between a deep uniform flow in a nonrotating system and one in a rotating system. The fundamental reason why such a flow is never observed in the deep ocean is the ubiquitous stable stratification, described above: the thickness of the turbulent boundary-layer flow is severely limited by that stratification.

The Logarithmic Layer

You might be wondering, at this point, about the relevance of the large body of material on flow resistance and velocity profiles in turbulent shear flows past a solid boundary, treated in much detail in Chapter 4, to planetary boundary-layer flow. The essential

point is easy to state: everything developed in Chapter 4 is relevant to the planetary boundary layer. Very near the bottom boundary, deep in the mixed layer (and at the base of the Ekman layer) the same arguments used in Chapter 4 to deal with the inner layer and the outer layer of the flow hold equally well in the case of the planetary boundary layer: there may or may not be a viscous sublayer, depending upon the particular the value of the boundary Reynolds number, but in any case there is a part of the inner layer that is described by the law of the wall. Also, there is an outer layer, where a "velocity defect law" must hold, and there is an overlap layer, which (as mentioned in Chapter 4 but not developed in detail) requires that both the law of the wall and the velocity defect law be logarithmic. In the context of the planetary boundary layer, this lowermost layer, in which the velocity profile is logarithmic, is called the **logarithmic layer**. In the ocean, the logarithmic layer is typically only few meters thick—but it is what the bottom sediment feels! It is thicker in the atmosphere, but still not nearly as thick as the entire Ekman layer.

References Cited for Chapter 7

Armi, L., and Millard, R.C., Jr., 1976, The bottom boundary layer of the deep ocean: Journal of Physical Oceanography, v. 81, p. 4983-4990.

Gross, M.G., 19090, Oceanography; A View of the Earth, Fifth Edition: Englewood Cliffs, New Jersey, Prentice-Hall, 441 p.

Gustafson, T., and Kullenberg, B., 1933, Trägheitsströmungen in deer Ostsee: Medd. Göteborgs Oceanogr. Inst., no. 5.

Neumann, G, and Pierson, W..J., Jr., 1966, Principles of Physical Oceanography: Englewood Cliffs, New Jersey, Prentice-Hall, 545 p.

Pedlosky, J, 1987, Geophysical Fluid Dynamics, 2nd Edition: New York, Springer-Verlag.

This page titled 7.7: Planetary Boundary Layers- The Ekman Layer, The Logarithmic Layer, and The Mixed Layer is shared under a CC BY-NC-SA 4.0 license and was authored, remixed, and/or curated by John Southard (MIT OpenCourseware) via source content that was edited to the style and standards of the LibreTexts platform.

8: SEDIMENTS, VARIABLES, AND FLUMES

8.1: Introduction to Sediments, Variables, and Flumes
8.2: Hydrodynamic Perspective
8.3: Particle Motions vs. Turbulence
8.4: Observing Sediment Transport
8.5: Variables
8.6: Flumes

This page titled 8: Sediments, Variables, and Flumes is shared under a CC BY-NC-SA 4.0 license and was authored, remixed, and/or curated by John Southard (MIT OpenCourseware) via source content that was edited to the style and standards of the LibreTexts platform.

8.1: Introduction to Sediments, Variables, and Flumes

Introduction

In the natural sciences, the word **sediment** is used for loose particulate material at the Earth's surface that has been produced by weathering of rocks and then transported by wind or water or ice. Because weathering acts everywhere to some degree, and the Earth is enveloped by moving air and water, it should not surprise you that sediment is ubiquitous. In engineering applications, the word "sediment" is used to refer not only to natural sediment but also to particulate material, of whatever origin, that is transported (or just potentially transportable) in some flow device or system.

The dynamics of sediment transport is a large field, which is of interest in a wide variety of disciplines in the Earth sciences and engineering: geology, geomorphology, geography, oceanography, environmental science and engineering, civil engineering, mechanical engineering, and chemical engineering. Civil engineering has probably had more impact on the development of ideas and techniques in sediment transport mechanics than any other single discipline.

In Part 2 of these notes I will deal with some of the most important phenomena and problems connected with the transport of denser solid particles by turbulent flow of a less dense fluid, which in most cases of interest is water or air. Emphasis will be on

- the *forces exerted on the sediment particles* by the flowing fluid
- the *modes of movement of the particles* by the flow, and
- the *shaping of a loose sediment bed* by the flow.

The greatest emphasis will be on flows in which the concentration of transported sediment is low enough that the turbulence structure of the flow—and the approach we can take to the dynamics of the flow itself—is not grossly different from flows without sediment. Flows with greater concentrations, sometimes approaching the limiting concentration of close packing of the sediment particles, are important in both natural sciences and engineering, but the limited scope of these notes precludes treatment here—they should be the topic of an entire additional set of notes.

Sediment

Before we get started on sediment movement, I will point out some useful things to know about the sediment itself. These have to do with the *size, shape, and density* of the material.

The picture I want you to have is of what might be called a "gravity bed" of loose sediment particles: the particles are denser than the fluid, and they form a bottom boundary to the flow, below which the mass of particles rests packed together in a framework that is stable against the pull of gravity (Figure 8.1.1). We will be dealing with the uppermost part of this bed, where the particles are accessible to the flow—by which I mean that if not actually in motion at a given time, they are resting on the bed surface, or are located at a depth below the sediment–fluid interface small enough that the flow can (and presumably will, at some time) erode to that depth, given enough time even without any change in the overall or average flow conditions. This uppermost layer of potentially movable sediment is usually called the **active layer**.

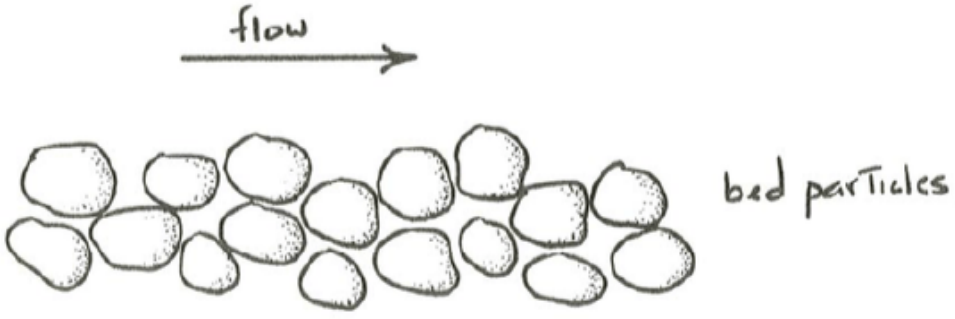


Figure 8.1.1: A "gravity bed" of loose sediment particles.

Each bed particle is characterized by a size, a shape, and a density. Density is the simplest to deal with: the **mean density** of a particle is just the ratio of its mass to its volume. Size and shape are more difficult to deal with.

Size would be a straightforward concept only if the particle had the shape of a regular geometric solid. Some particles approach spherical shape, but most are irregular in shape. A theoretically satisfying measure of the size of an irregular particle is its **nominal diameter**: the diameter of a sphere with the same volume as the given particle. You can imagine, however, the difficulty you would have in measuring the nominal diameter of a sand grain! What is done is to define and measure size *operationally*: the meaning of size lies in how we actually measure it. The size of sediment coarser than about $0.1\ \mathrm{mm}$ is usually measured by passing it though a sieve with nearly square openings formed by a grid of (usually) metal wire. Approximately speaking, a sieve discriminates size by passing all particles whose longest dimension in the smallest cross-sectional area is about that of the size of the sieve opening.

All natural sediments have a range of particle sizes. The spread of sizes around the average size is called the **sorting**: a well sorted sediment shows a narrow spread of sizes, and a poorly sorted sediment shows a wide spread of sizes (Figure $8.1.2$). (In civil engineering practice, the terminology is just the opposite: a well sorted sediment is poorly graded, and a poorly sorted sediment is well graded.) The effect of sorting on sediment transport is a rapidly advancing area of research nowadays.

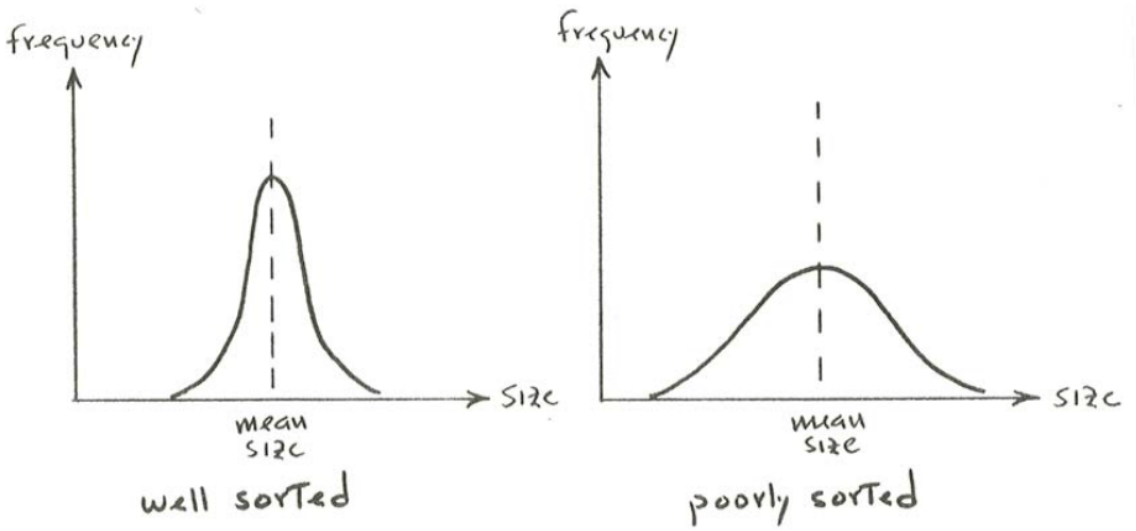


Figure $8.1.2$: Sorting: the spread of sizes around the mean.

Shape is even more difficult to deal with than size. Clearly, natural sediment particles with their irregular shapes would require an enormous number of separate and independent variables to describe the shape: a hopeless situation. Fairly well-rounded sediment particles are often approximated by triaxial ellipsoids, which need only two ratios among three independent variables (longest axis, intermediate axis, and shortest axis) to characterize the shape.

Even though we will not be dealing with anything but a single sediment density and an average sediment size in the following, it does not hurt to keep in mind always that a natural sediment has a three-dimensional joint distribution of size, shape, and density, which always has to be approximated in some way, and always very crudely. That joint distribution has too many axes for me to draw, but Figure $8.1.3$ shows a simpler two-dimensional joint frequency distribution of size and density, with shape ignored. We can do better than Figure $8.1.3$, though: most natural sediments have a dominant density fraction associated with quartz, feldspar, rock fragments, and carbonate particles, and a subordinate fraction consisting of a variety of heavy minerals with much greater density (Figure $8.1.4$).

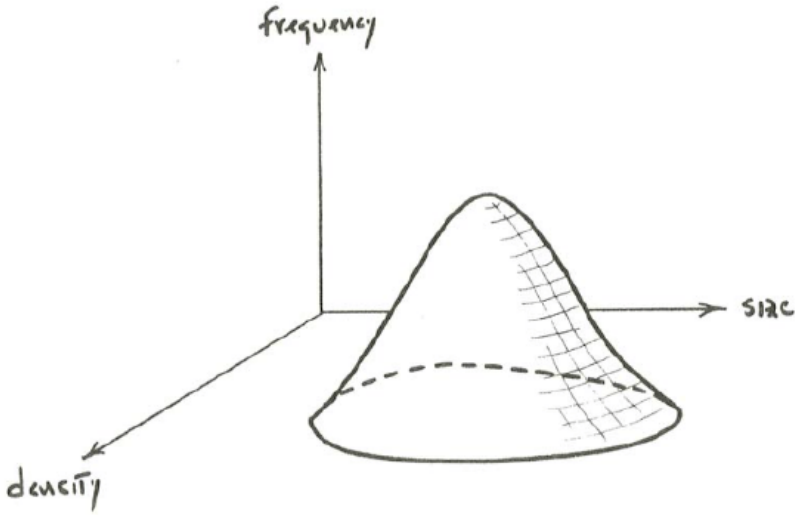


Figure 8.1.3: A joint frequency distribution of sediment size and sediment density.

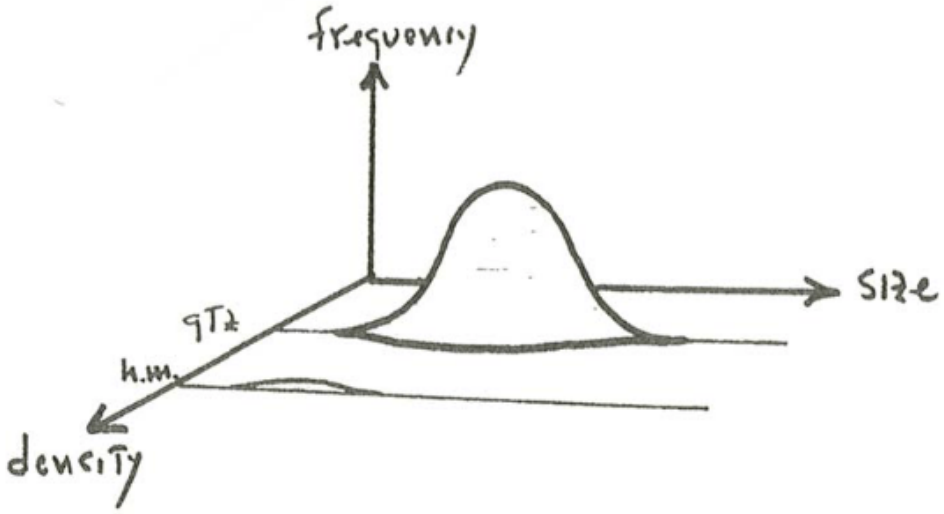


Figure 8.1.4: What the joint size–density frequency distribution looks like for many natural sediments.

The ratio of particle density to fluid density ranges enormously in natural sediment-transporting flows, from winds on Mars to water flows on Earth (Figure 8.1.5). The important points along this spectrum for us earthling sedimentologists are for quartz-density and heavy-mineral sediments in water and air. But we must not be presumptuous: think of all the places there must be in the universe where sediment is being moved, at this very moment, for which the density ratio is greatly different from these few particular cases of greatest interest to us. It is wise for sediment dynamicists to keep a broad perspective, because otherwise, in concentrating on just a few cases some important general effects might be misinterpreted, or even missed.

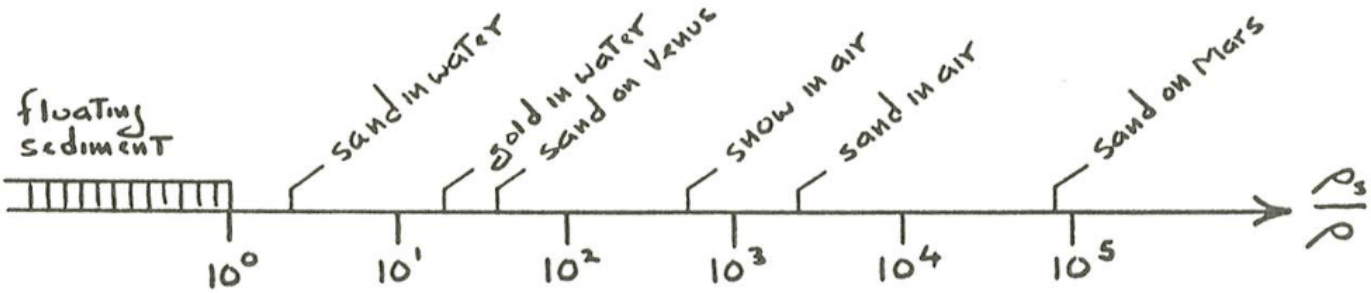


Figure 8.1.5: The spectrums of density ratios ρ

This page titled 8.1: Introduction to Sediments, Variables, and Flumes is shared under a CC BY-NC-SA 4.0 license and was authored, remixed, and/or curated by John Southard (MIT OpenCourseware) via source content that was edited to the style and standards of the LibreTexts platform.

8.2: Hydrodynamic Perspective

The dynamics of sediment transport could be viewed as part of the field of **two-phase flows**: flows of a fluid that contains within it discrete particles of some solid or even of some other immiscible fluid. Accordingly, there are liquid flows with solid particles, liquid flows with liquid particles (drops), liquid flows with gas particles (bubbles), gas flows with solid particles, and gas flows with liquid drops. (The nature of gases precludes the existence of gas flows with gas bubbles!) The included phase may be either more dense or less dense than the including phase.

Turbulent sediment-transporting flows are far more important than laminar sediment-transporting flows, although some laminar flows do transport sediment. Turbulent sediment-transporting flows represent one of the most difficult problems in all of fluid mechanics, partly because the presence of the included phase alters the turbulence structure of the including phase, and partly because in many cases the flow boundary consists of the sediment particles themselves, and then the flow can shape its own boundary but is in turn affected by that shaped boundary. It is the feedback or mutual interaction between a sediment-moving flow and its deformable sediment boundary that lies at the heart of so many flows that move solid particles.

Figure 8.2.1 may be useful in giving you some perspective on the complexity of sediment-transporting flows. Figure 8.2.1 shows the changes in the essential nature of the flow, starting with turbulent flow in a closed conduit and ending up in sediment-transporting flow over a loose sediment bed. The step from a circular pipe to a rectangular duct adds the presence of a weak but non- negligible secondary circulation, while the structure of the shear-flow turbulence is not greatly different. In the next step, to an open rectangular channel, the turbulence structure is again only slightly different, as are the secondary circulations, but the deformable free surface makes for rather different effects in unsteady flows, as you have seen in Chapter 5. The next step, to a rectangular channel with a loose sediment bed, is the big one: because the flow can mold the bed, and the bed in turn has a strong effect on the flow, the turbulence structure and the free-surface geometry are significantly different in certain ranges of flow. The last step, to a channel with erodible banks, makes for greatly different bed geometry, at least in certain ranges of flow.

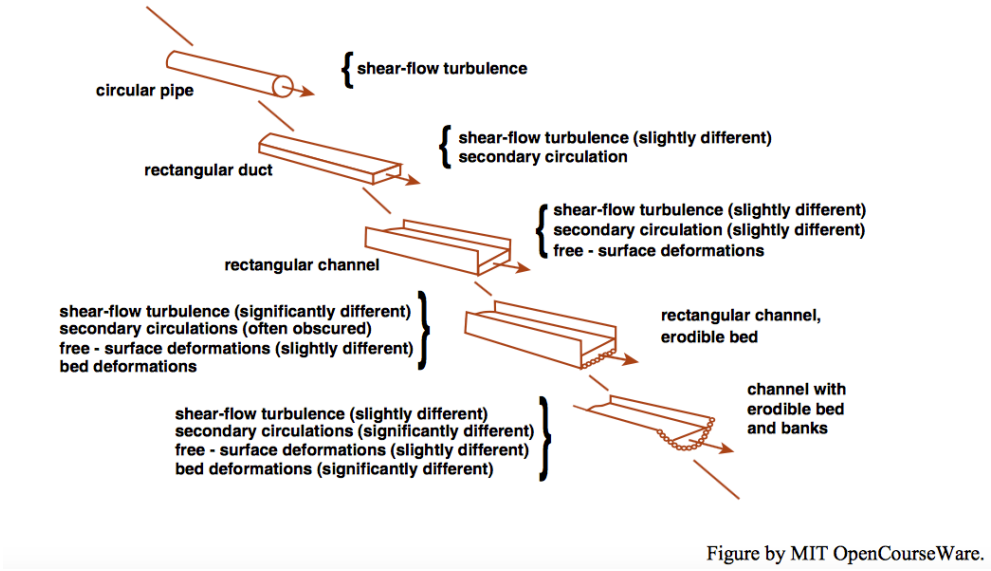


Figure by MIT OpenCourseWare.

Figure 8.2.1: Perspective on the complexity of sediment-transporting flows.

This page titled 8.2: Hydrodynamic Perspective is shared under a CC BY-NC-SA 4.0 license and was authored, remixed, and/or curated by John Southard (MIT OpenCourseware) via source content that was edited to the style and standards of the LibreTexts platform.

8.3: Particle Motions vs. Turbulence

A few qualitative observations on the effect of a turbulent flow field on the motions of suspended particles might be useful here, to set the stage for later chapters.

Think about a sediment particle in a turbulent fluid. Clearly, its trajectory will be sinuous rather than straight, and its velocity will be irregular rather than constant. The particle undergoes two kinds of accelerations at the same time:

1. *temporal accelerations*, because the velocity varies with time at points the particle happens to occupy; and
2. *spatial accelerations*, because the particle falls through regions with different fluid velocity.

Physical effects, partly related, that we have to consider are the following. Details on some of these effects are given in later paragraphs.

- Relative inertia
- Particle size relative to eddy size
- Turbulent velocity fluctuations relative to particle velocity
- The effect of acceleration on the drag force

The effect of *relative inertia* is expressed by the ratio ρ_s/ρ. For $\rho_s/\rho >> 1$, the much greater inertia of the particle causes its trajectory to be relatively little affected by the turbulence (Figure $8.3.1$A). For $\rho_s/\rho \approx 1$, on the other hand, the approximately equal inertia of the particle and the fluid causes the trajectory of the particle to be strongly affected by the turbulence (Figure $8.3.1$B). This effect is independent of the weight of the particle: in an extraterrestrial place with very small g, a particle can have a small immersed specific weight γ' but large ρ_s/ρ, whereas in an extraterrestrial place with very large g, a particle can have a large γ' but small ρ_s/ρ. On the Earth, however, weight and relative inertia are unavoidably linked.

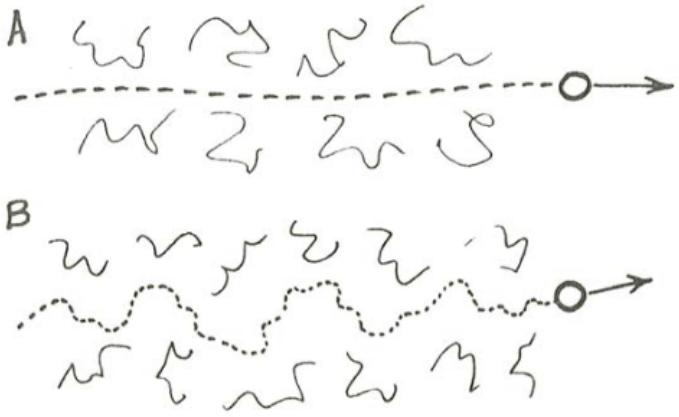


Figure $8.3.1$: The effect of relative particle inertia when a particle moves through a turbulent fluid. **A)** Relative inertia is high; **B)** relative inertia is low.

If the sediment particle is much larger than the turbulent eddies, then small eddies distort the local velocity field near the surface of the particle and affect the drag force on the particle, but the motion of the particle is not much affected (Figure $8.3.2$A). If the particle is much smaller than the surrounding eddies, however, the particle senses a nearly uniform but unsteady fluid acceleration in its vicinity; the curvature of the particle trajectory is large relative to particle size (Figure $8.3.2$B).

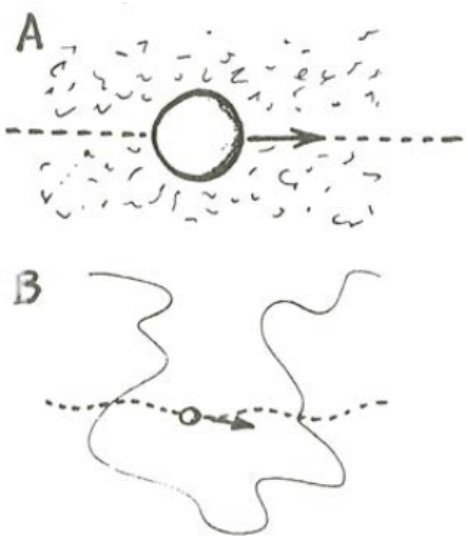


Figure 8.3.2: The effect of particle size relative to eddy size. **A)** The particles are much larger than the eddies. **B)** The particles are smaller than the maximum eddy size.

The effect of turbulent velocity fluctuations relative to particle velocity is especially relevant to settling particles. If the vertical turbulent velocity fluctuations are much greater than the settling velocity of the particle, then the particle has a highly sinuous trajectory, with frequent reversals of its vertical velocity component (Figure 8.3.3A). If the vertical turbulent velocity fluctuations are much less than the settling velocity of the particle, however, then the settling velocity is little affected by turbulence: the fall is always downward, the speed of the particle relative to the bottom varies only slightly, and the path of settling is only slightly sinuous (Figure 8.3.3B).

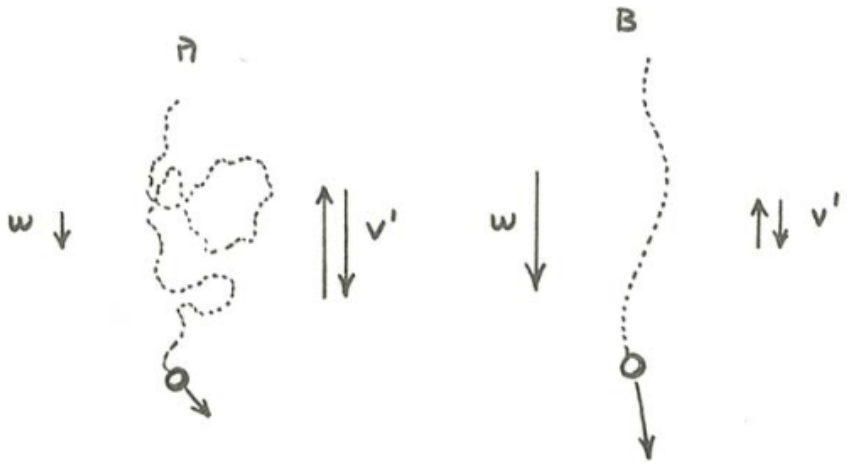


Figure 8.3.3: Effect of particle settling velocity relative to turbulent velocity fluctuations. **A)** The particle settles slowly relative to the vertical velocity fluctuations. **B)** The particle settles rapidly relative to the vertical velocity fluctuations.

What was done in Chapters 2 and 3 in Part 1 on the drag force on a sphere was predicated upon steady flow. When the local fluid velocity around the sphere is changing, the drag force is in general different from that predicted for a uniform relative velocity of the same value, because the local patterns of velocity and fluid pressure lag behind the changing free-stream flow velocity.

This page titled 8.3: Particle Motions vs. Turbulence is shared under a CC BY-NC-SA 4.0 license and was authored, remixed, and/or curated by John Southard (MIT OpenCourseware) via source content that was edited to the style and standards of the LibreTexts platform.

8.4: Observing Sediment Transport

What are the main things about sediment transport you might want to observe? Here are four of them, and some comments on the ways those observations might be carried out.

Particle Movement. The eye is an excellent instrument for perceiving the details of movement of sediment particles, but you need techniques like cinematography (high-speed or slow-motion) or video for a record, and also for speeding up or slowing down the process so that the eye can better perceive the nature of the movement. Various other optical methods for tracing particle movement have also been developed.

Bed Geometry. Visual observation and photography are the main ways of dealing with the bed configuration in still life. Time-lapse cinematography is especially useful for gaining information on the kinematics of individual bed forms: they generally move too slowly for you to see what they are doing in real time. When the bed is obscured by moving sediment, as is so often the case, you have to resort to mechanical profiling or sonic profiling.

Sediment Load. The sediment load can be sampled with traps or samplers of various kinds that purport to catch a representative volume sample of the sediment–water mixture. Indirect methods that involve the effect of the sediment–water mixture on a beam of light or sound are common: these can be as simple as attenuation along a line, or by focusing separate beams they can examine the sediment load in small regions that approximate points.

Sediment Transport Rate. It is notoriously, and frustratingly, difficult to make good measurements of the sediment transport rate without serious disruption of the flow. Local volume sampling of the load along with simultaneous measurements of local time-average velocity, integrated over the cross section of the flow, is the most common way. For bed load, traps of a great many kinds have been devised, and if they are calibrated well they can be quite reliable. I will have more to say on the intricacies of measuring the sediment load and the sediment transport rate in a later chapter.

Here is a list of most of the aspects of sediment transport you might want to observe, measure, or think about, along with some brief comments.

- **Entrainment**. The flow exerts sufficient force on a bed particle to set it into motion.
- **Traction**. Particles are moved in contact with or close to the bed by fluid forces.
- **Saltation**. Particle undergo near-bed ballistic movement, largely unaffected by turbulence.
- **Suspension**. The flow lifts particles away from the bed after entrainment.
- **Turbulence**. The particles distort the local fluid velocity field, alter the structure of the turbulence, and themselves undergo turbulent accelerations.
- **Settling**. Particles settle toward the bed through the surrounding fluid.Hindered settling. The proximity of other settling particles hinders the settling of each particle.
- **Collisions**. Differing velocities plus inertia leads to collisions (or close encounters) between particles.
- **Diffusion**. Suspended sediment undergoes upward turbulent diffusion against the concentration gradient.
- **Distrainment**. Particles come to rest on the bed.
- **Liquefaction**. Rearrangement of packing in the bed leads to reduction in particle contact, partial or total support of particles by pore fluid, then refreezing of the texture by dewatering.
- **Bed configuration**. Bed-load transport plus complex dynamic bed instabilities lead to various characteristic bed geometries.

This page titled 8.4: Observing Sediment Transport is shared under a CC BY-NC-SA 4.0 license and was authored, remixed, and/or curated by John Southard (MIT OpenCourseware) via source content that was edited to the style and standards of the LibreTexts platform.

8.5: Variables

It seems like a good idea at this point to think in a very general way about which variables are likely to be important in problems of sediment transport, and to organize those variables into a set of dimensionless variables that is likely to be useful as a framework from which to simplify or (complexify or specialize!) in any particular problem we deal with later. This is your chance to think about the phenomenon of sediment transport in its broadest aspects.

This endeavor involves some assumptions about what might be called the *target flow*. For the sake of definiteness, we will look at the movement of cohesionless sediment by steady uniform flows in straight rectangular channels of effectively infinite width in a nonrotating system. We thereby ignore the effects of channel width, cross-section shape, channel curvature, and the Earth's rotation, and we restrict ourselves to equilibrium sediment transport. The first three restrictions are especially serious in fluvial sediment transport, but our target flow is a good start, from which these other effects can be evaluated. Ignoring the Earth's rotation is not as serious as it might seem, because most aspects of sediment transport are tied up with the local near-bottom structure of turbulent shear flows, which, as you saw in Chapter 7, are about the same in geophysical flows as in actually or effectively nonrotating flows. Time-dependent problems in sediment transport are also of great importance, but again our target case represents a good reference. Finally, the assumption of cohesionless flows shuts us out of the complex, frustrating, and extremely important world of fine cohesive sediments—another topic that deserves its own separate set of notes.

The most important sediment-transport effects we will deal with in later chapters are easy to list:

- modes of grain movement
- speeds of grain movement
- sediment load
- sediment transport rate
- bed configuration

Variables

Which variables might have a role in influencing or determining these effects? The possibilities form a long list (and there probably are others I have not thought of):

Sediment:

- joint size–shape–density distribution
- elastic properties

Fluid:

- density ρ
- viscosity μ
- specific weight (weight per unit volume) γ
- elastic properties
- thermal properties
- surface tension

Flow:

- mean depth d
- mean velocity U
- discharge (per unit width) q
- boundary shear stress τ_o
- slope S
- power P

System:

- acceleration of gravity g

Clearly this list is too long: some items can safely be neglected, and some items are actually redundant.

First, here are some comments on the variables that characterize the sediment. There are no redundancies in the items for the sediment in the above list, but they are effectively non-quantifiable because of grain shape. And even if grain shape is neglected, the size–density distribution has to be characterized by a two-variable joint frequency distribution (see Figure 8.1.3). As mentioned earlier, a good approximation in practice might be to assume one dominant blade-shaped spike in the distribution corresponding to crudely quartz-density sediment, and one or more subsidiary spikes for heavy minerals (Figure 8.1.4). It is common practice in work on sediment transport to assume that all grains have the same density, so that the sediment can be characterized by the mean or median size D and the density ρ_s. Adding the standard deviation σ of the size distribution makes for *three variables* describing the sediment.

With regard to variables characterizing the flow, there is a serious redundancy in the foregoing list: only two variables are needed to specify the bulk flow, one of them being the flow depth and the other a flow-strength variable. The two most logical candidates for the flow-strength variable are the boundary shear stress τ_o and the mean velocity U (or the surface velocity U_s). (Some might take exception to that statement, however, and claim that the flow power P is the most fundamental flow-strength variable.)

In choosing the flow-strength variable, we could address three considerations:

- Which variables *specify* or *characterize* the state of sediment transport, in the sense that specification of those variables unambiguously corresponds to or identifies the state of sediment movement, whether those variables are imposed upon the system or are themselves fixed by the operation of the system?
- Which variables are truly *independent*, in the sense that they are imposed on the system and are unaffected by its operation?
- Which variables *govern* the state of sediment transport, in the sense that they are dynamically most directly responsible for particle transport and bed- configuration development, whether or not they are independent?

One of the important goals in studying the phenomena of sediment transport is to show as clearly and unambiguously as possible the hydraulic relationships among those phenomena. It would be good to have a one-to-one correlation between sediment-transport states and combinations of variables, because that would represent the clearest start on knowing what we have to deal with or explain.

In terms of unambiguous characterization, U and d (or q and d) are the most appropriate variables to describe the flow because, for a given fluid, for each combination of U and d in steady uniform flow there is one and only one average state of the flow, in terms of velocity structure and boundary forces. This is not the case, however, if τ_o or P is used in place of U or q: if τ_o or P is used, there is an element of ambiguity in that for certain variables values of τ_o or P more than one bed state at a given flow depth is possible. Although I am getting ahead of myself in bringing up this matter before the chapter on bed configurations, I will point out here that this has to do with the substantial decrease in form resistance in the transition from ripples or dunes to plane bed with increasing U or q at constant d. You can see from the cartoon graph in Figure $8.5.1$ that because of this effect there is a non-negligible range of τ_o for which three different values of U are possible. But you can see from the graph that if you specify U, you thereby uniquely specify τ_o. An alternative approach would be to use only the part of τ_o, called the **skin friction**, that represents the local shear forces on the bed, and leave out of consideration the part of τ_o, called the **form drag**, that arises from large-scale pressure differences on the fore and aft sides of roughness elements. The ambiguity noted above would thereby be circumvented. The problem is that although there are several published procedures for such a **drag partition**, none works remarkably well (yet).

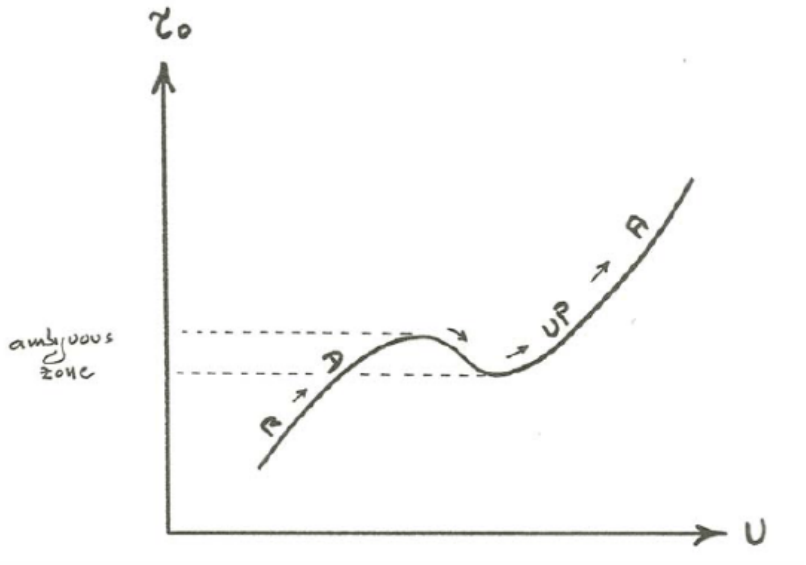


Figure 8.5.1: Graph of bed shear stress τ_o vs. mean flow velocity U for a flow that is transporting sediment generating rugged bed configurations. R, ripples; D, dunes; UP, upper-regime plane bed; A, antidunes. The two horizontal dashed lines show the range of τ_o for which a given value of τ_o can be associated with three different values of U.

Independence need not be a criterion in choice of variables to describe the state of sediment transport, because a given set of variables can equally well describe the state of sediment transport whether any given variable in the set is dependent or independent: the state of sediment transport is a function of the nature of the flow but not of how the flow is arranged or established, provided that the flow is strong enough at the outset to produce general sediment movement on the bed.

Independence of variables depends to a great extent upon the nature of the sediment-transporting system. For an example of this, think about an extremely long channel (tens of kilometers, say) with bottom slope S, straight vertical sidewalls, and an erodible sediment bed, into which a constant water discharge Q is introduced at the upstream end (Figure 8.5.2). Assume that after a transient period of flow adjustment a steady state is maintained by introducing sediment at the upstream end at a rate equal to the sediment discharge Q_s at the downstream end. The imposed variables here are Q and S; Q_s, U, and d are adjusted by the flow. Because of the great channel length, flow and sediment transport are virtually uniform along most of the channel except near the upstream and downstream ends. Even though the flow might prefer a different S for the given Q, adjustment in S is so slow that, on time scales that are short in terms of geologic time but long in terms of bed-form movement, S can be considered fixed. Hence Q and S are independent variables, and U and d along with all variables that express the details of flow structure and sediment transport are dependent upon Q and S.

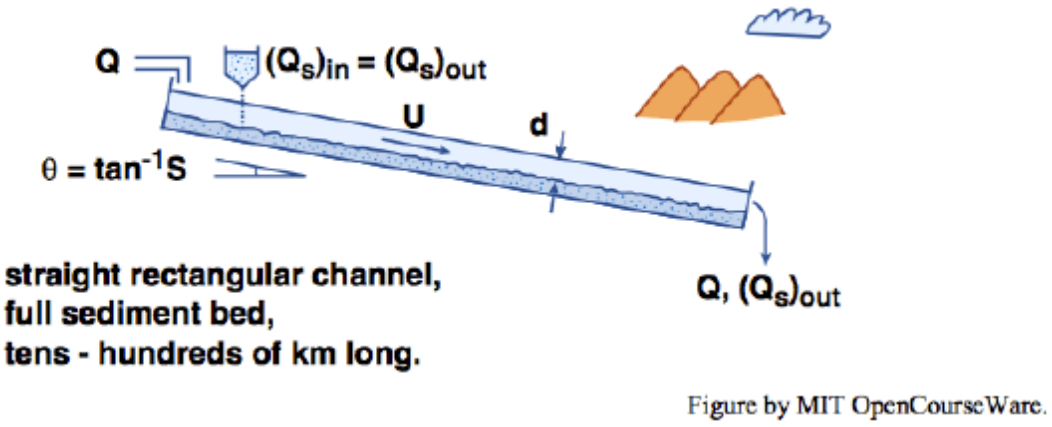


Figure 8.5.2: A sediment-feed flume experiment in a very long channel.

In a similar but much shorter channel, tens of meters, say (Figure \PageInded3), S can change so rapidly by erosion and deposition along the channel that the flow cannot be considered uniform until S has reached a state of adjustment to the imposed Q; Q is an independent variable, but S is now dependent, in the sense that it cannot be preset except approximately by manipulation of

d by means of a gate or weir at an overfall at the downstream end of the channel. And in constant-volume recirculating channels, in which there is no overfall, d is truly independent and S is truly dependent.

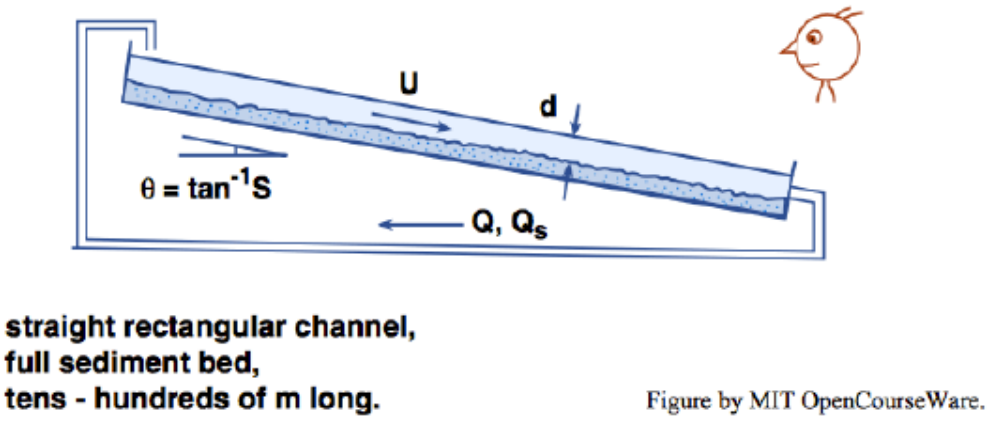


Figure \PageInded3: A sediment-feed flume experiment in a very short channel.

With regard to *governing* variables, at first thought τ_o is a more logical choice than U for characterizing the effect of the flow on the bed, because the force exerted by the flow on the bed is what causes the sediment transport in the first place. And for transport over planar bed surfaces, that is certainly true. But you will see in a later chapter that, over a wide range of flow and sediment conditions, the flow molds the bed into rugged flow-transverse ridges called bed forms. On beds covered with such bed forms, only a small part of τ_o represents the boundary friction that is directly responsible for grain transport, the rest being form drag on the main roughness elements (Figure 8.5.4). In such situations, therefore, τ_o is as much a surrogate variable as U, in the sense that it is not directly responsible for particle transport and bed-form development, as are near-bed flow structure and distribution of boundary skin friction in space and time. These latter, however, are themselves uniquely characterized by U and d.

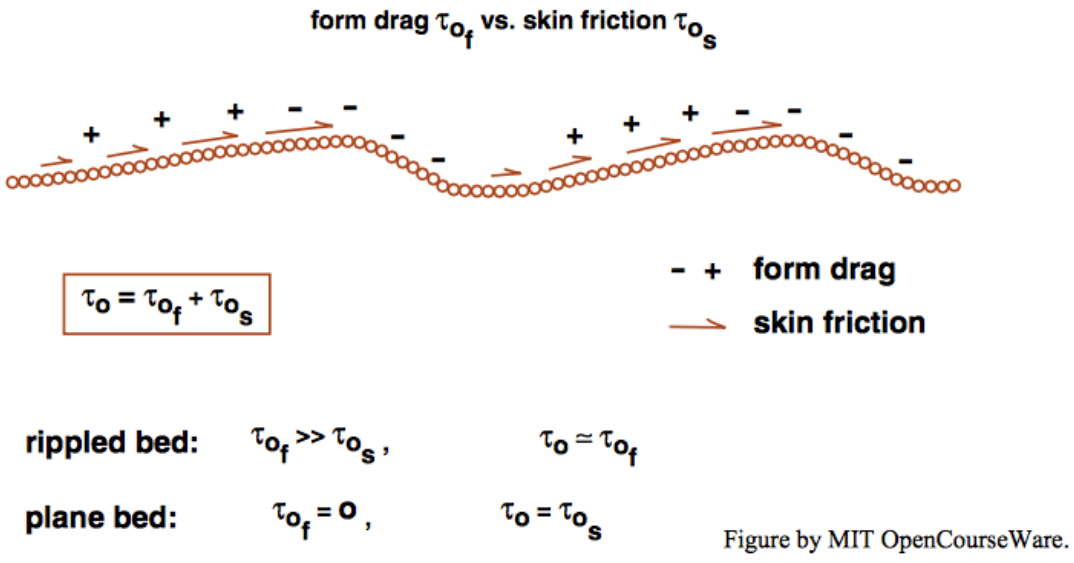


Figure 8.5.4: Form drag and skin friction on a sediment bed with ripple or dune bed forms.

When bed forms are present, the spatially and temporally averaged local skin friction would seem to be a better variable than τ_o in characterizing the state of sediment transport, because it is free from the ambiguity mentioned above but at the same time is more directly responsible for the sediment movement. The trouble is that it cannot be measured, and it can be estimated only with considerable uncertainty using presently available drag-partition approaches.

Several variables on the list are of minor or negligible importance in most sediment-transport problems: the elastic and thermal properties of the fluid and the sediment, and the surface tension of the fluid.

So the final minimal list of variables that describe sediment transport in our target flow is as follows:

- Mean flow velocity U or boundary shear stress τ_o
- Mean flow depth d
- Fluid density ρ
- Fluid viscosity μ
- Median sediment diameter D
- Sediment sorting σ
- Sediment density ρ_s
- Acceleration of gravity g or submerged sediment specific weight γ'

There are eight variables on the list, so we should expect to have an equivalent set of *five dimensionless variables* that describe the state of sediment transport equally well. A great many different sets are possible: you can choose a variety of sets of three repeating variables, and then you could manipulate those sets further by multiplying and dividing the various individual dimensionless variables in those sets.

In general, we could move in one (or both) of two directions at this point. We could try to develop a set that has the greatest relevance to the physical effects involved in the sediment transport, or we could try to develop a set that has the sedimentologically most relevant or interesting variables segregated into different dimensionless variables.

With regard to sets of dimensionless variables that are relevant to the physical effects of sediment transport, I will mention just two possibilities:

$\frac{\tau_o}{\gamma' D}$	Shields parameter, a dimensionless τ_o
$\frac{\rho u_* D}{\mu}$	roughness Reynolds number, Re_*
d/D	relative roughness
$\frac{\rho_s}{\rho}$	density ratio
$\frac{\sigma}{D}$	sorting-to-size ratio

You could construct this set by using τ_o, ρ, and D as repeaters. The physical significance of the roughness Reynolds number was discussed back in Chapter 4. The Shields parameter also has a clear physical significance. The fluid force on bed particles is approximately proportional to $\tau_o D^2$, whereas the weight of the bed particles is proportional to $\gamma' D^3$. The ratio of these two quantities is the Shields parameter, so the Shields parameter is proportional to the ratio of the fluid force on particles to the weight of the particles. For that reason it could also be called a *mobility number*.

Another dynamically meaningful set of dimensionless variables can be formed using U as the flow-strength variable:

$\frac{\rho U d}{\mu}$	Reynolds number based on depth and velocity
$\frac{U}{(gd)^{1/2}}$	Froude number based on depth and velocity
d/D	relative roughness
$\frac{\rho_s}{\rho}$	density ratio
$\frac{\sigma}{D}$	sorting-to-size ratio

The repeaters in this set are ρ, U, and d. The mean-flow Reynolds number describes the structure of the mean flow, and the mean-flow Froude number is relevant to the energy state of the flow, as discussed in Chapter 5.

Probably the most useful set of dimensionless variables for the purpose of unambiguous description of the state of flow and sediment transport is one in which the sedimentologically interesting variables U, d, and D are segregated into separate dimensionless variables:

$\left(\frac{\rho\gamma'}{\mu^2}\right)^{1/3} d$	dimensionless flow depth d^o
$\left(\frac{\rho^2}{\mu\gamma'}\right)^{1/3} U$	dimensionless flow velocity U^o
$\left(\frac{\rho\gamma'}{\mu^2}\right)^{1/3} D$	dimensionless sediment size D^o
$\frac{\rho_s}{\rho}$	density ratio
$\frac{\sigma}{D}$	sorting-to-size ratio

The repeaters for this set are ρ, μ, and γ'.

This page titled 8.5: Variables is shared under a CC BY-NC-SA 4.0 license and was authored, remixed, and/or curated by John Southard (MIT OpenCourseware) via source content that was edited to the style and standards of the LibreTexts platform.

8.6: Flumes

Out beyond the edge of official terminology, sedimentologists often refer to **flumology**—presumably meaning the science and art of gaining knowledge and understanding of physical sedimentary processes by passing water and sediment through laboratory open channels, called flumes. I thought that it might be useful to include this brief section on flumes before launching upon chapters dealing with sediment transport, because much of our understanding of sediment transport has been developed by watching and measuring the movement of sediment in flumes (and oscillatory-flow channels and tanks as well). I will be referring to flume experiments often in coming chapters.

Dictionaries define flumes as artificial channels for transporting water. That is really not restrictive enough for our purposes, though: flumes designed for nonscientific uses are usually fairly steep and crude in structure. In the context of scientific and engineering studies, I might define a flume as *a laboratory channel through which liquid is passed in order to study hydraulic processes and phenomena under controlled conditions*.

Flumes are built both indoors and outdoors. One of the most famous flumes—among geologists, at least—was G.K. Gilbert's flume, outdoors on the campus of the University of California at Berkeley. Around the turn of the twentieth century Gilbert made a pioneering study of modes and processes of sediment transport by currents, which stands to this day as a valuable source of data and ideas. But hydraulic engineers had been using flumes for decades before that.

Flumes are built of wood, metal, glass, or plastic. Each material has its advantages and disadvantages. The cross section is usually but not always rectangular. Widths usually are from several centimeters to a few meters, and lengths range from a few meters to well over a hundred meters. The largest recirculating flume in the world is at the University of Tsukuba, in Japan; it is 160 m long and 4 m wide, and it can recirculate both water and sediment. I am sure that any objective observer would consider it to be an impressive structure. (I certainly did, when I was first shown it.) I am not sure where the largest tilting flume is.

The technology of construction of all but the largest flumes is straightforward, and the problems were for the most part solved long ago. In sediment-recirculating flumes, the most critical design decision revolves around the kind of pump used and/or the arrangement for extracting sediment from the flow and delivering it to the head of the channel.

Flumes are only one kind of large-scale hydraulic equipment used for studying sediment movement. Flumes, carrying unidirectional gravity-driven free-surface flow, are distinct from *closed ducts and conduits*, also widely used for hydraulic studies, which have pressure-gradient-driven flow without a free surface. Closed ducts may be used for unidirectional, oscillatory, or combined flow. Also widely used are simple *tanks or basins* arranged mainly for oscillatory flows under surface gravity waves.

Advantages of flumes:

- sediment transport is relatively easy to watch and measure
- particular processes can be isolated for study

Disadvantages of flumes:

- flow and sedimentation can be oversimplified
- the physical scale of the flow and sediment movement is usually too small

The slope of the flume may be fixed or adjustable; most flumes, except the very largest, are *tilting*. But when you are working with sediment transport, your flume does not really need to be tilting, because the flow itself redistributes the sediment to produce a sediment bed with slope equal to the energy slope as uniform flow is established. If you prepare a planar and uniform bed of sediment and then set up a flow over it, if the flume slope is too steep there will be erosion near the upstream end and deposition near the downstream end until a uniform flow is attained over a sediment bed that tapers upstream (Figure 8.6.1A). Conversely, if you start with a flume slope that is too gentle, the result is a bed that tapers downstream (Figure 8.6.1B). You just have to make sure that the flume slope you start with is near enough the slope for uniform flow that you have a full bed of sediment everywhere in the flume once the flow stops adjusting to uniformity.

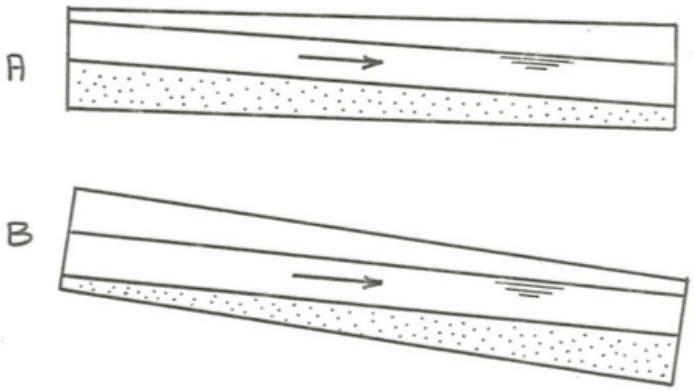


Figure 8.6.1: **A)** A uniform sediment-transporting flow in a flume with a floor that is less steep than the slope of the bed surface and the water surface. **B)** A uniform sediment-transporting flow in a flume with a floor steeper than the slope of the bed surface and the water surface.

Flumes vary in their arrangements for recirculation of water and sediment. Logically there are four possible combinations of recirculation; see Figure 2.

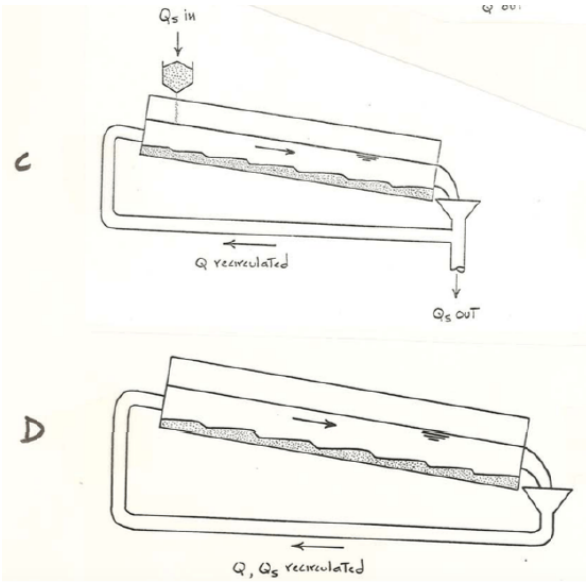


Figure 2: Differing arrangements for recirculation of water and sediment in flumes.

Water no, sediment no (Figure 2A). This arrangement is uncommon, because it is limited by water supply. Only laboratories located near dams on large rivers can afford to run large discharges of water through flumes without recirculation. Also, water temperature cannot be controlled independently. And if you do not catch the sediment, you lose it.

Water no, sediment yes (Figure 2B). The same comments apply as in the preceding case, except that you do not lose the sediment.

Water yes, sediment no (Figure 2C). This arrangement is more common. Its advantages are that the sediment discharge is imposed independently upon the flow. But it can be a technical challenge to separate all the sediment from the water and then feed new sediment at the upstream end.

Water yes, sediment yes (Figure 2D). This arrangement is simplest and also common. Here the flow establishes its own sediment discharge; you cannot impose sediment discharge on the system. Provided that the sediment is not too coarse, this is the easiest arrangement technologically. But it is difficult to arrange for gravels.

There are two different arrangement for water-recirculating flumes:

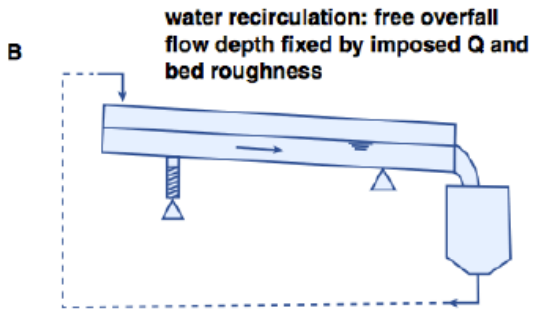


Figure by MIT OpenCourseWare.

Figure 8.6.3: **A)** A closed-circuit recirculating flume. **B)** A free-overfall recirculating flume.

Overfall flumes (Figure 8.6.3A). In some flumes, which I will call overfall flumes, there is a free overfall at the downstream end of the channel into a separate tailbox, from which water (and in many cases also the sediment) is pumped to the head of the channel. In such flumes, the flow depth in uniform flow is fixed by the imposed water discharge and bed roughness. You can set or adjust the slope only by fiddling with a weir or gate of some kind at the downstream end of the channel, to change the water depth and therefore the mean velocity.

Closed-circuit flumes (Figure 8.6.3B). In other flumes, which I will call closed-circuit flumes, there is no overfall at the downstream end; the flow passes continuously into the tailbox, to be pumped back to the head of the channel. In closed-circuit flumes, the flow depth is fixed by the volume of water in the system. You impose the water discharge and flow depth and thereby the mean velocity, which in turn determines all aspects of the sediment transport as well as the slope.

Both overfall flumes and closed-circuit flumes are in wide use. Each has advantages and disadvantages. They are used for slightly different purposes, which I will touch upon in passing in later chapters.

You will see, in Chapter 13, on mixed-size sediment, that the differences between sediment-feed flumes and sediment-recirculating flumes has significant implications (Parker and Wilcock, 1993). In a sediment-feed flume, the sediment discharge is imposed upon the flow and the flow must become adjusted to accomplish the necessary transport of all of the size fractions in the feed mix. In sediment-recirculating flumes, there is no such constraint: the flow is free to adjust its sediment-transporting behavior without any external constraint imposed except for water discharge and bed material.

References Cited Chapter 8

Parker, G., and Wilcock, P.R., 1993, Sediment feed and recirculating flumes: A fundamental difference: Journal of Hydraulic Engineering, v. 119, p. 1192- 1204.

This page titled 8.6: Flumes is shared under a CC BY-NC-SA 4.0 license and was authored, remixed, and/or curated by John Southard (MIT OpenCourseware) via source content that was edited to the style and standards of the LibreTexts platform.

9: THRESHOLD OF MOVEMENT

9.1: Introduction to Threshold of Movement
9.2: Forces on Bed Particles
9.3: Balance of Forces and Dimensional Analysis
9.4: Movement Threshold
9.5: Recasting the Shields Diagram
9.6: The Effect of Density Ratio

This page titled 9: Threshold of Movement is shared under a CC BY-NC-SA 4.0 license and was authored, remixed, and/or curated by John Southard (MIT OpenCourseware) via source content that was edited to the style and standards of the LibreTexts platform.

9.1: Introduction to Threshold of Movement

One of the classic problems in sediment transport is to predict the flow strength at which sediment movement first begins. This condition for incipient movement is usually expressed in terms of a **critical shear stress** or **threshold shear stress**, which I will denote by τ_{oc}. The problem can be viewed either as the minimum shear stress needed to move a given particle, or as the largest grain size that can be moved by a given shear stress. The latter is termed **competence** by geologists.

Incipient movement should be one of the simplest problems in sediment transport, because at that point the flow has not yet become a two-phase flow, and all the principles and techniques of sediment-free flow—what is called *rigid-boundary hydraulics*—should still apply. Even in this simplest of problems, however, understanding is far from complete, which should put you on your guard about the great many approaches and formulas in the literature that are supposed to deal with established sediment movement.

This page titled 9.1: Introduction to Threshold of Movement is shared under a CC BY-NC-SA 4.0 license and was authored, remixed, and/or curated by John Southard (MIT OpenCourseware) via source content that was edited to the style and standards of the LibreTexts platform.

9.2: Forces on Bed Particles

Introduction

Look at a representative sediment particle resting on the surface of a cohesionless sediment bed at the bottom of a flowing fluid (Figure 9.2.1). If the fluid is not moving fast enough to move the particle, then the particle is motionless, therefore not accelerating, so all the forces acting on it must be in balance. What are those forces? They are of three kinds: *particle weight*, particle-to-particle *contact forces*, and *fluid forces*.

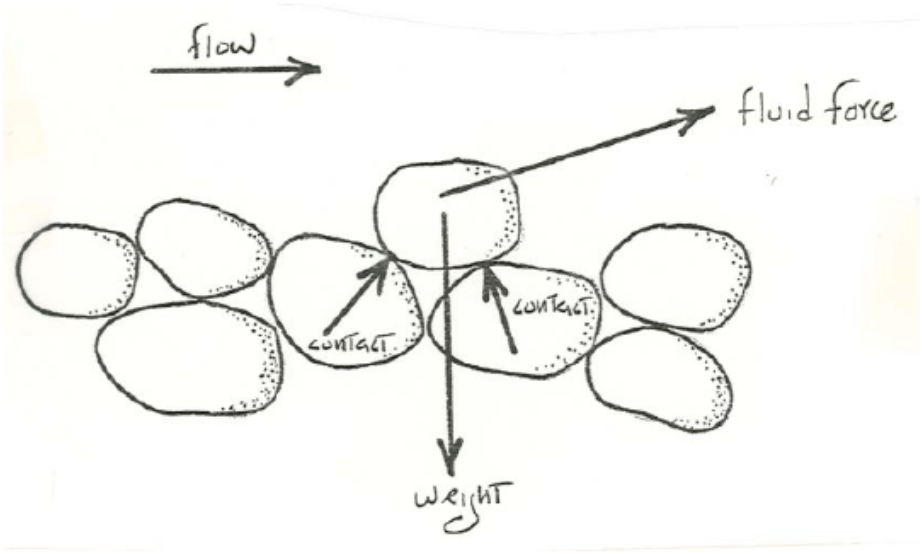


Figure 9.2.1: Forces on a sediment particle resting on a bed of similar particles.

The particle weight is easy to deal with: it is just the submerged weight per unit volume of the sediment material, γ', times the volume of the particle. It acts vertically downward through the center of mass of the particle. The contact forces, exerted upward on the given particle by the underlying particles (usually three) on which it rests, become adjusted in light of the contact geometry, the particle weight, and the fluid forces so that the particle is motionless.

The fluid forces are much more difficult to deal with. First we need a little more background on the nature of flow very near the bed in a turbulent shear flow.

Fluid Forces

Because there is locally a flow around the bed particle, you should expect there to be both viscous shear stresses and pressure acting at every point of the surface of the particle (Figure 9.2.2). It is those viscous and pressure forces, summed over the entire surface of the particle, that give rise to the resultant fluid force on the particle. This resultant force is specified by its *magnitude, direction, and line of action through the particle*.

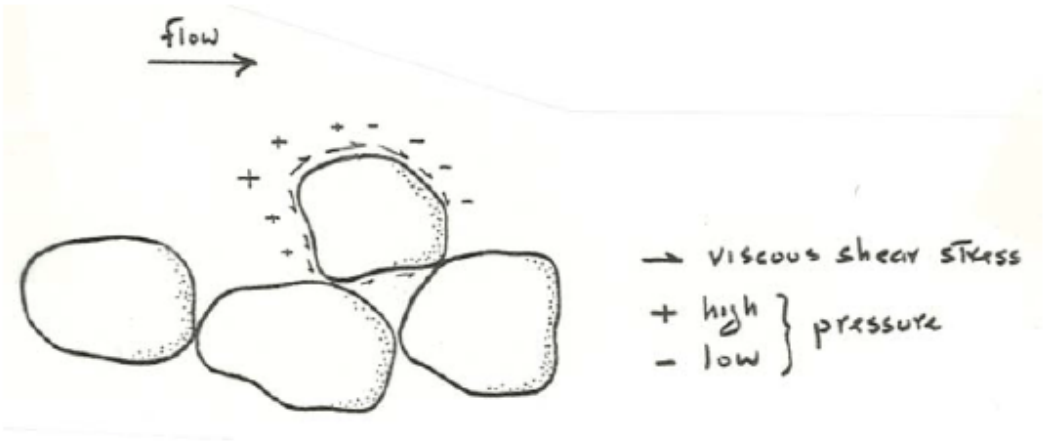


Figure 9.2.2: Viscous shear stress and pressure acting at all points of a sediment particle resting on a bed of similar particles.

Keep in mind that if the flow is turbulent, which is almost always the case in problems of sedimentological interest, the resultant force varies strongly with time, on time scales ranging from small fractions of a second to many minutes (in the case of very large-scale flows, in which the maximum eddy size can be very large), even if the flow is steady in the time-average sense. And this is true even if the particle is within the viscous sublayer. Remember that the viscous sublayer is not really nonturbulent: the local velocity fluctuates substantially within it. The important point is that the turbulence is unimportant in contributing turbulent shear stress to the total shear stress in the viscous sublayer. You can readily understand the existence of velocity fluctuations in the viscous sublayer in the context of the burst–sweep cycle described in Chapter 4: the viscous sublayer is thinned and accelerated as masses of high-speed fluid impinge on the bed, and then it thickens and decelerates again.

What determines the magnitude, distribution, and relative importance of the viscous and pressure forces? Think about the variables that govern the fluid force on a bed particle. Some should come to mind readily: the diameter D of the particle (which determines the surface area of the particle, and also how far up into the flow the particle projects), the fluid viscosity μ (viscous stresses are important); the fluid density ρ (fluid is accelerating in the vicinity of the particle); the boundary shear stress τ_0 (that is the variable that best characterizes the strength of the flow around the particle); and the geometry of the particle itself and its relationship to underlying particles. The geometry varies widely—it is different for each particle—but, for any given particle, the other variables lead naturally to a single dimensionless variable $\rho u_* D/\mu$, which you have already seen in Chapter 4 as the boundary Reynolds number.

A further comment about the boundary shear stress is in order here. It is not the boundary shear stress, as carefully defined in Chapter 4 as the time-average force per unit area on the bed, averaged over an area of the bed that is large enough to guarantee a representative spatial average, that is directly relevant to threshold of movement; it is the picture of local fluid forces on individual bed particles and how those forces vary with time. Nonetheless, τ_0 is a good *descriptor* of the threshold condition for movement, because it represents the average of the forces on the bed particles. There is an important qualification to that statement, however: the bed has to be planar in the large, without any features like bed forms that are much larger than the particles themselves, or otherwise much or most of the bed shear stress is associated with form drag rather than with the skin friction, which is what actually moves the particles.

Figure 9.2.3 shows in a qualitative way how the fluid force on a given particle should vary with the boundary Reynolds number Re_*.

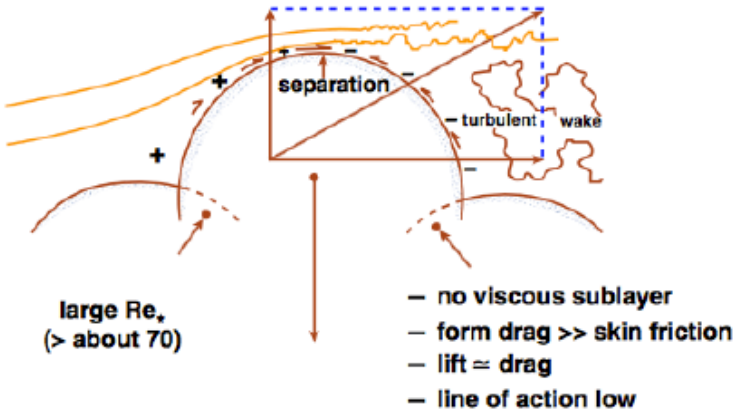


Figure by MIT OpenCourseWare.

Figure 9.2.3: Fluid forces on a particle resting on a sediment bed, for **A)** small values and **B)** large values f the particle Reynolds number Re_*.

- For **small** Re_* (which corresponds to relatively small values of a Reynolds number based on local flow velocity around the particle) there is no well defined boundary layer along the top surface of the particle, and there is no flow separation behind the particle (Figure 9.2.3A). Both viscous forces and pressure forces are important. The line of action of the resultant force lies well above the center of mass of the particle, because the viscous forces are strongest on the uppermost surface of the particle.
- For **large** Re_* (which corresponds to relatively large values of a Reynolds number based on local flow velocity) there is a well defined local boundary layer on the surface of the particle, and pronounced flow separation, with a turbulent wake behind the particle (Figure 9.2.3B). Pressure forces far outweigh viscous forces, and because the net pressure force comes about mainly by the difference in pressure from front to back the line of action of the resultant force is closer to the center of mass of the particle.

There is no reason to expect the resultant force to be parallel to the overall surface of the bed; this leads to the idea of resolving the resultant force into a component parallel to the bed, called the **drag**, and a component normal to the bed, called the **lift** (Figure 9.2.4). Several investigators, using sometimes ingenious experimental methods, have attempted to make direct measurements of the lift and drag forces on bed particles (or surrogates, like regularly spaced hemispheres on a planar boundary); see Einstein and El-Samni (1949), Chepil (1958, 1961), Coleman (1967), and Coleman and Ellis (1976).

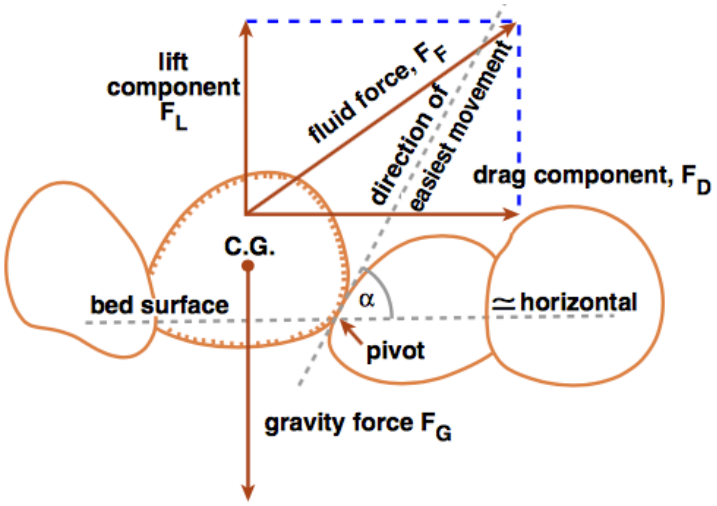


Figure by MIT OpenCourseWare.

Figure by G.V. Middleton.)

A lift force on the particle is to be expected because the pressure is high around the base of the particle (the front stagnation point is located low on the front surface of the particle), and relatively low over the top surface of the particle, as well as in the rear; to see that, all you have to do is apply the Bernoulli equation qualitatively. People have made ingenious experiments to measure

the lift force, and the lift force has been found to be almost equal to the drag force at high boundary Reynolds numbers. There is some evidence that at very low Reynolds numbers the lift force actually becomes weakly negative, for reasons no one seems to understand very well yet.

Another important thing you should expect about the fluid force is that it is extremely unsteady, because of fluctuations in velocity associated with the passage of fairly large eddies just outside the near-boundary layer of the flow. Actual measurements have shown fluctuations by as much as a factor of four in the instantaneous fluid forces on bed particles.

This page titled 9.2: Forces on Bed Particles is shared under a CC BY-NC-SA 4.0 license and was authored, remixed, and/or curated by John Southard (MIT OpenCourseware) via source content that was edited to the style and standards of the LibreTexts platform.

9.3: Balance of Forces and Dimensional Analysis

We could take either of two approaches at this point: make a dimensional analysis to develop a graphical framework for expressing and rationally organizing observational results, or try to develop an analytical solution. First I will outline the classical analytical approach, to see where it leads. That approach involves assuming that the particle is pivoted out of its position, around its two downstream contact points, when the moment due to the fluid force finally becomes larger than the opposing moment due to the weight of the particle. Unfortunately this analytical approach turns out to be of little more help than a simple dimensional analysis, for two reasons: irregularity of geometry, and complexities of the fluid force itself.

Balance of Forces

Particles begin to move on the bed when the combined lift and drag forces produced by the fluid become large enough to counteract the gravity and frictional forces that hold the particle in place. It is impossible to define the balance of forces or moments acting on particles uniquely for all grains: some particles lie in positions from which they are more easily lifted, slid, or rolled than others. It is equally impossible to define a single fluid force that applies to all particles: some particles are more exposed to the flow and subjected to larger fluid forces than other particles, and the fluid forces at the bed fluctuate with time because of turbulence in the flow.

We will begin by considering an average particle, in an average position on the bed, subjected to an average fluid force; we will return later to the problem of an appropriate definition of these averages. To simplify matters further, assume that friction prevents sliding of one particle past another and that the moving particle simply pivots about an axis normal to the flow direction. The condition for the beginning of motion then is that the moments tending to rotate the particle downstream are just balanced by the moments (in the opposite sense) that tend to hold the grain in place (Figure 9.2.4).

To determine the fluid-force moment exactly, we would have to sum all the products of the forces times their normal distances from the lines of action to the pivot axis. We can simplify further by assuming that the bed is horizontal and by considering, at first, only drag forces. Then it is convenient to consider only those components of the gravity and drag forces that act normal to the line joining the pivot to the center of gravity of the particle.

The total moment produced by summing body forces (like the gravity forces acting on each element of volume making up the particle) is the same as the total force times the distance of the center of gravity from the pivot. You can readily see that if we divide the gravity force into two components, normal to and parallel to the line joining the pivot to the center of gravity, then the moment due to the second of these components must be equal to zero, because that component has a line of action passing through the pivot itself. So we can write the condition for the beginning of movement as

$$a_1 \left(F_G \sin \alpha\right) = a_2 (F_D \cos \alpha) \tag{9.3.1}$$

The left side of Equation 9.3.1 is the total moment due to gravity, which tends to rotate the grain upstream about the pivot or to hold it in place against the moment due to fluid drag forces tending to rotate the particle downstream. The right side represents this fluid-drag moment in a purely conventional way. The drag moment must actually be calculated as the integral of all the products of the drag forces acting on each element of the surface, times the normal distance of each of these forces from the pivot. But because we do not know the distribution of the drag forces over the surface of the particle, there is no way we can actually evaluate that integral, so it is represented conventionally simply as a product of the total component of drag, $F_D \cos \alpha$, which opposes the total component of gravity, $F_G \sin \alpha$, times a normal distance a_2. The value of a_2 cannot be determined analytically, so a_2 is actually a “fudge factor” that is chosen to make the equation balance.

The gravity force F_G can be written

$$F_G = c_1 D^3 \gamma' \tag{9.3.2}$$

where c_1 is a coefficient that takes account of the particle shape. The fluid drag force F_D can be assumed equal to the average boundary shear stress to times the area of the grain, and can be written

$$F_D = c_2 D^2 \tau_o \tag{9.3.3}$$

where the coefficient c_2 takes into account not only the geometry and packing of the grains (which determines the “area of the

grain") but also the variation of the drag coefficient. Thus c_2 can be expected to vary with boundary Reynolds number. Substituting Equations 9.3.2 and 9.3.3 for F_G and F_D into Equation 9.3.1 and writing $\tau_o = \tau_c$ for the critical condition gives

$$a_1 c_1 D^3 \gamma' \sin\alpha = a_2 c_2 D^2 \tau_c \cos\alpha label 9.4 \tag{9.3.4}$$

or, solving for τ_c,

$$\tau_c = \frac{a_1 c_1}{a_2 c_2} \gamma' D \tan\alpha \tag{9.3.5}$$

Equation 9.3.5 can be made dimensionless by dividing both sides by $\gamma' D$:

$$\beta_c = \frac{\tau_c}{\gamma' D} = \frac{a_1 c_1}{a_2 c_2} \tan\alpha \tag{9.3.6}$$

where β_c, the critical value of a dimensionless variable $\tau_0/\gamma' D$, called **Shields' β** or the **Shields' parameter**, should be expected to be a function of grain geometry and boundary Reynolds number. (The Shields parameter is named after an American engineer who first put the study of incipient movement on a rational basis in the 1930s while working at a hydraulics laboratory in Germany.)

What Equation 9.3.6 tells us is that the Shields parameter is a function of a term that itself depends on various effects, both geometrical and dynamical.
The quantities a_1, c_1, and $\tan\alpha$ are geometrical, and depend on the grain shape and grain packing. The quantities a_2 and c_2 are partly also geometrical, but they also include a dependence on the details of flow around the grains and the resulting distributions of pressure forces and viscous forces, and they are therefore a function of the boundary Reynolds number. We cannot proceed any further than Equation 9.3.6 without knowing more about the details of this Re_* dependence, to say nothing of the problem of taking account of particle shape and packing.

The foregoing analysis is not much different if lift is considered as well as drag, because there should be a proportionality between the two forces which also depends only on grain geometry and boundary Reynolds number.

In deriving Equation 9.3.6 it was assumed that the bed slope is negligibly small. If this is not the case, then it is easily shown that $\sin\alpha$ in the Equation 9.3.6 should be replaced by $\sin(\alpha - \phi)$, where ϕ is the slope angle (positive in the downstream direction). So, if other conditions remain the same, increasing bed slope decreases the critical value of β.

Many other theoretical approaches to incipient motion, along the same lines as that above but taking other effects, like lift forces and bed slope, into consideration as well, have appeared in the literature. None takes us much further than the foregoing simplified analysis.

Dimensional Analysis

The list of variables that should describe the condition of incipient movement is fairly straightforward (Figure 9.3.1): τ_o, D, ρ, μ, ρ_s, and γ'. Flow depth should not be important, because the particles are in the inner layer of a turbulent boundary layer (see Chapter 4 of Part I), in which only the local structure of the flow governs the forces felt by the bed particles.

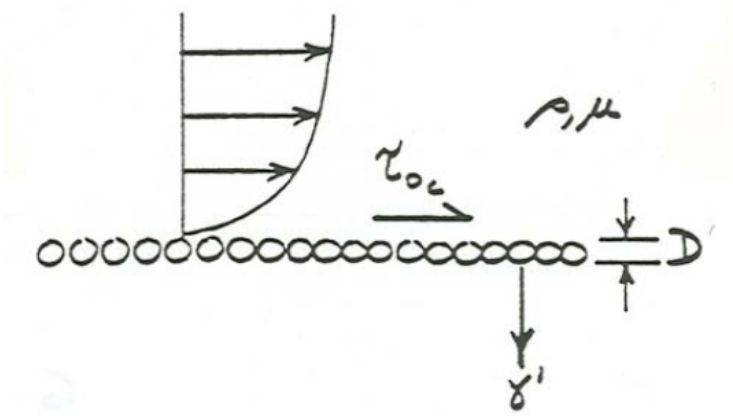


Figure 9.3.1: Variables that characterize the threshold of particle movement.

You might think that the sediment density ρ_s has no business here, because the sediment is not moving (by definition). In reality it might be important, however, because it affects the time scale of the response of the particle to a sudden acceleration of the flow: other things being equal, the denser the particle the less rapidly it would accelerate in response to a sudden increase in resultant fluid force to a value large enough to move the particle. And that is important for incipient movement, because the particle might be rocked out of its position of rest by a passing unusually strong eddy, only to fall back to it and undergo no permanent displacement.

Two points about the list of variables above deserve further comment. The first has to do with the choice of τ_o as the variable that characterizes the strength of the flow. Because in the material in earlier chapters on flow around a sphere the drag force was related to a velocity, you might reasonably ask why not use a velocity rather than τ_o. One answer is that, after all, what is moving the grains is basically a force acting on the bed, so the boundary shear stress is a more logical choice than any velocity. (You might reasonably respond that the force itself is caused by the local velocity of flow around the grains.) Another answer is that it is difficult to specify exactly which velocity should be used. The most easily measured velocities (the mean velocity of flow U or the surface velocity U_s) are not, in any clear or straightforward way, related to the velocity measured near the bed, which is what determines the force that tends to move the grains. If we were to use the mean velocity we would have to add another variable, the depth of flow, because the same mean velocities may give rise to different near-bed velocities, or shear stresses, if the flow depth is different. To get around these problems it has always seemed most natural to use τ_o instead of a velocity—but remember that a graph or criterion for incipient movement in terms of τ_o (like the famous Shields diagram, introduced below) can always be recast into a form that involves flow velocity and flow depth, if it is velocity that you are most interested in.

The second point is that in listing the variables I have chosen to combine the gravity g and the sediment density ρ_s into a single variable with the fluid density: $\gamma' = g(\rho_s - \rho)$. This is equivalent to assuming that the only important effect of both gravity and particle density is in controlling the submerged weight of the particle. We assume that surface gravity waves in the fluid are not important—which is equivalent to assuming that the flow is not shallow enough so that the motion of the fluid over the grains affects the free surface. This is clearly an invalid assumption for very shallow, gravel-bed rivers.

So you should expect to deal with three independent dimensionless variables, and therefore to be able to express the condition for incipient movement as a surface in a three-dimensional graph. One of these can be the density ratio ρ_S/ρ. The other two then have to involve τ_o, D, μ, and γ'. The traditional variables have been the boundary Reynolds number $\rho u_* D/\mu$ and the Shields parameter $\tau_0/\gamma' D$, already introduced above.

$$\text{threshold} = f(\rho, \mu, \gamma, D, \tau_0) \tag{9.3.7}$$

and, nondimensionalizing,

$$\frac{\tau_c}{\gamma' D} = f\left(\frac{\rho u_* D}{\mu}\right) \tag{9.3.8}$$

where τ_c is the threshold value of the bed shear stress.

You already know about the hydraulic significance of the boundary Reynolds number: it characterizes the nature or structure of the flow near the bed. And recall from Chapter 8 that the Shields parameter also has a real physical meaning: by multiplying the top and bottom of the Shields parameter by D^2 you can see that it is proportional to the ratio of fluid force on the particle to the weight of the particle. The effect of the density ratio ρ_s/ρ is still unclear, but is known not to be large, and anyway most sediment problems involve quartz-density sediment in water.

So just by looking at the dimensional structure of the problem of incipient movement, we have arrived at the same conclusion as from the force-balance analysis, expressed by Equation 9.3.6, in the preceding section.

This page titled 9.3: Balance of Forces and Dimensional Analysis is shared under a CC BY-NC-SA 4.0 license and was authored, remixed, and/or curated by John Southard (MIT OpenCourseware) via source content that was edited to the style and standards of the LibreTexts platform.

9.4: Movement Threshold

How is the Threshold for Movement Identified?

At this point, as a prelude to looking at the various diagrams that are in common use for incipient movement, it seems appropriate to pose the following fundamental question: *How is the condition of incipient movement identified?* An untutored outside observer might naturally assume that the answer is to watch the sediment bed to determine when, under conditions of slowly increasing flow strength, the sediment begins to move. But there is a serious problem with such a procedure, as can easily be demonstrated by a simple flume experiment: even for bed shear stresses (or flow velocities) that are well below what would conventionally be considered to represent the threshold or critical condition for sediment movement, some bed particles are moved by the flow. It is easy to understand why this is so. Recall from the material on turbulence in Chapter 3 that because of the impingement of turbulent eddies on the sediment bed the instantaneous fluid forces on sediment particles varies widely. The consequence is that even in weak flows a particularly strong turbulent eddy would occasionally cause one or more particles to move. There is thus a wide range of flow conditions that cause weak sediment movement. Put another way, the question becomes: How long should one wait to detect movement of a particle on the sediment bed? A minute? An hour? A day?

The wide range of bed shear stresses for which there is weak particle motion brings forth an additional question: *Does a threshold bed shear stresses for incipient movement really exist?* Some would contend that the range of bed shear stresses for weak particle motion is *indefinitely* wide, and that because of that there is a conceptual flaw in the assumption that a definite threshold condition can be defined. It is true that the weaker the flow, the smaller the number of bed particles that are moved by the flow (per unit time and per unit area of the bed), but the lower limit for any particle motion is indefinite. For a cogent exposition of the impossibility of assigning a definite threshold condition, see the paper by Lavelle and Mofjeld (1987).

This difficulty in defining the condition of incipient movement is largely because incipient movement is stochastic, in that the instantaneous resultant force on a bed particle varies irregularly through time just as does, say, a turbulent velocity component. One conceptually satisfying way of looking at the threshold of sediment movement is in terms of the relationship between two different probability frequency distributions: the distribution of instantaneous local τ_o needed to move the set of particles occupying some area of the bed surface, and the distribution of instantaneous local τo that acts on any small area of the bed, of about the size of the particles, through time (Figure $9.4.1$; after Grass 1970). When the two distributions do not overlap (Figure $9.4.1$A), the flow is never strong enough to move any of the particles on the bed, whereas when the two distributions overlap somewhat (Figure $9.4.1$B), there is a subset of particles on the bed surface which can be, and therefore are, moved by the flow. With increasing flow strength the distributions come to overlap entirely (Figure $9.4.1$C), meaning that all the particles on the bed surface are susceptible to movement. When the condition for movement threshold is viewed in this way, it is easy to identify the basis for the skeptics' view that it is not possible to define the condition of incipient movement: they would argue that the right-hand (high flow strength) tail of the frequency distribution of instantaneous local τ_o extends indefinitely far to the right, toward higher bed shear stresses. One could argue, of course, that if the time average of the instantaneous shear stress is sufficiently small, none of the bed particles would ever move, but that condition is so far from the conventional view of the movement threshold as to be irrelevant to the problem, in a practical sense.

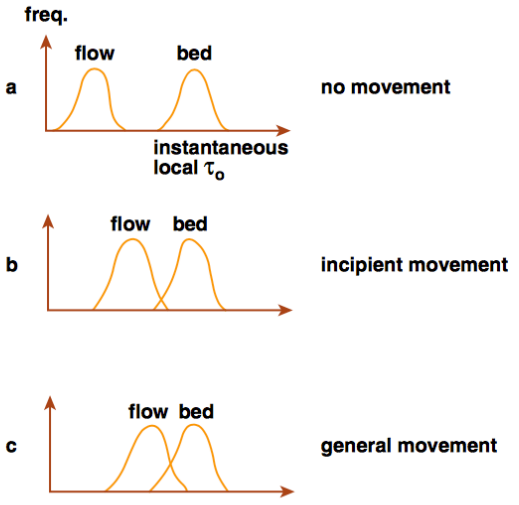


Figure by MIT OpenCourseWare.

Figure 9.4.1: Threshold of movement, viewed in terms of the relationship between frequency distribution of instantaneous fluid forces exerted on bed particles and frequency distribution of fluid forces needed to move the particles. (Schematic; modified from Grass, 1970.)

Here we take the approach, in common with most sedimentationists, that the concept of a threshold for sediment movement has a certain physical reality, despite the uncertainty described above, and that techniques must be available to identify the threshold condition. There are two ways to attempt to identify the threshold condition, which might be termed, unofficially, the watch- the-bed technique and the reference-transport-rate method.

The watch-the-bed method: as mentioned at the beginning of this section, this is in a sense the most natural way of defining the threshold condition. The problem of the wide range of conditions of weak sediment movement might be circumvented by general agreement, by convention, about where in this range of weak movement the threshold condition is situated. As you can imagine, much of the scatter in data on movement threshold is the result of differing views in this respect.

There have been attempts at quantifying the conditions for incipient movement. Neill (1968) and Yalin (1977) argued that kinematic similarity of movement of grains implies identity of the dimensionless parameter $N = nD^3/u_*$, where n is the number of grains in motion per unit area and unit time. They suggested adopting 10^{-6} as a practical critical value of N, and pointed out that, for equal values of the Shields parameter must be 30 times greater in air than in water, so that for equal N, n must be 30 times greater. Such attempts at quantification have never come into general use.

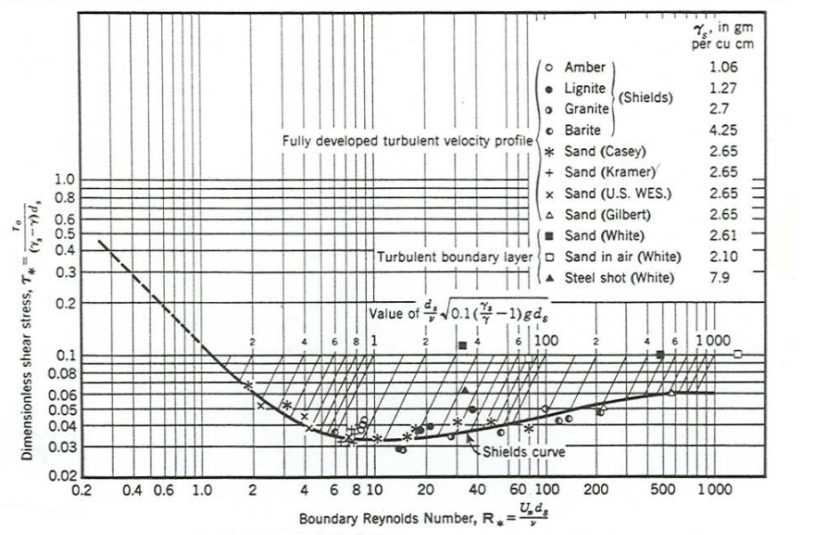
The *reference-transport-rate method*: A second way of defining the threshold condition is to circumvent the uncertainty about when movement begins by defining some small value of the dimensionless unit sediment transport rate that seems to correspond most closely to what the consensus view of the threshold condition is, and assume, for practical purposes, that that value represents the threshold condition. There will be more on the reference-transport-rate method in the later chapter on mixed-size sediments.

In practice, what has to be done is to make a fairly large number of measurements of the dimensionless unit sediment transport rate at a number of flow strengths above the threshold, plot the results, fit a curve to the results in some way, either as an analytical function of just “by eye”, and then extrapolate (or interpolate, if at least one of the data points lies below the reference condition) to find the value of bed shear stress associated with the reference transport rate.

There is a potential inconsistency between the two methods described in the preceding paragraphs. In the watch-the-bed method, a flume run is usually set up with an initially planar bed, and the bed is watched for signs of particle movement on that planar bed. In the reference-transport method, the measurements are usually made after the sediment transport has come into equilibrium with the flow, and there is the possibility that bed forms, especially ripples, have formed on the bed. The sediment transport rate over a rippled bed is in general different from that over a planar bed of the same sediment experiencing the same flow conditions—so the threshold condition is identified in a fundamentally different situation.

Representations of the Movement Threshold

What has traditionally been done, in studies of incipient movement, is to plot experimental results in a graph with the axis variables arranged in such a way that a unique curve in the graph separates conditions of established movement from conditions of no movement. The earliest such work is that of Shields (1936), who plotted initial-movement data from flume experiments on a graph of boundary shear stress nondimensionalized by dividing by the submerged specific weight and the mean size of the sediment (the resulting dimensionless variable is now called the Shields parameter; see the section on variables in Chapter 8) against the boundary Reynolds number. The result was not the first such attempt, but it became firmly established, especially in the field of hydraulic engineering, by virtue of its rational basis in fluid dynamics.



Courtesy of American Society of Civil Engineers. Used with permission.

Figure 9.4.2: The Shields diagram. (From Vanoni, 1975.)

The experimental results obtained by Shields himself, together with some earlier data. The threshold is called the **Shields curve**. There are two striking things about Figure 9.4.2:

- There is considerable scatter in the points.
- Shields had no data for Re_* less than about 2 or greater than 600.

It helps to evaluate the significance of the Shields diagram if you understand more clearly how the data were obtained. Shields made his experiments in flumes 0.8 m and 0.4 m wide, with beds composed of granite fragments 0.85 mm to 2.4 mm in diameter, coal ($\rho_s = 1.27$ g/cm^3) 1.8 mm to 2.5 mm in diameter, amber ($\rho_s = 1.06$ g/cm^3) 1.6 mm in diameter, and barite ($\rho_s = 4.2$ g/cm^3) 0.36 mm to 3.4 mm in diameter. Bed shear stress was determined from the resistance equation, $\tau_o = \gamma d \sin\phi$ (Chapter 4 in PartI). The bed was carefully leveled before each run. Discharge and therefore mean velocity were increased in steps, and the slope was adjusted to maintain uniform flow. After grains began to move on the bed, bed load was collected in a trap at the end of the flume so that the rate of sediment transport for a given condition could be determined. For each bed material several observations were made at different discharges and rates of sediment transport, and the beginning of grain movement was determined not so much by direct observation as by plotting the measured rates of transport and extrapolating to the value of τ_o that corresponded to zero rate of transport. (Shields did not report exactly how he made the extrapolation.) Shields observed that this corresponded to what other workers had described as “weak movement” of particles.

Shields himself noted that small ripples tend to form on the bed as soon as particles start to move. The presence of these ripples affects the rate of bed-load movement, so there is some question about exactly what was being determined when Shields extrapolated the measured rates to zero: initiation of movement on a plane bed, or initiation of movement on a rippled bed?

It has been observed by other workers that the critical shear stress for initiation of particle movement on a rippled bed is greater than for that on a plane bed, although the mean velocity of flow is less. The explanation is that ripples create form resistance, which contributes most of the measured average bottom shear stress. If the depth does not change, the slope of the flume has to be increased to produce the shear stress needed to balance this form resistance and produce the same velocity. It is observed, however, that the slope and velocity needed to move particles on a rippled bed can be reduced below that necessary to move

particles on a plane bed, because the phenomenon of flow separation over the ripples produces locally high and widely fluctuating shear stresses on the bed, which are large enough to move grains even at mean flow velocities lower than those required to move grains on a plane bed.

To make this more explicit, imagine setting up two series of flume experiments, side by side, with exactly the same flow depth and flow velocity, one with a planar sediment bed and one with a rippled bed. Start at a velocity so low that there is no particle movement in either flume. Because of the large form drag on the rippled bed, slope and therefore boundary shear stress is much greater than for the planar bed. Now gradually increase flow velocity in both flumes while keeping flow depth constant but increasing the slope to maintain uniform flow. Boundary shear stress thus increases in both flumes, but at all times it is greater on the rippled bed than on the planar bed. Particle movement starts first on the rippled bed; eventually, at a substantially higher flow velocity, particles begin to be moved on the planar bed also, but boundary shear stress on the planar bed at that point turns out to be lower than that for which particle movement began on the rippled bed.

The original Shields diagram has been used with little modification right up to the present, especially by hydraulic engineers. Miller et al. (1977) updated the Shields diagram, by drawing upon various more recent data to replot the diagram and redraw the curve; see Figure 9.4.3. The Miller et al. diagram is also in wide use. More recently, Buffington and Montgomery (1997) made an exhaustive and systematic compilation and analysis of studies on movement threshold. They were able to identify a systematic difference in the position of the Shields curve in the Shields diagram between data obtained by the watch-the- bed method and the reference-transport-rate method (Figure 9.4.4). They found a systematic difference in the location of the Shields curve, such that the curve based on the reference-transport-rate method lies above the curve based on the watch-the-bed method.

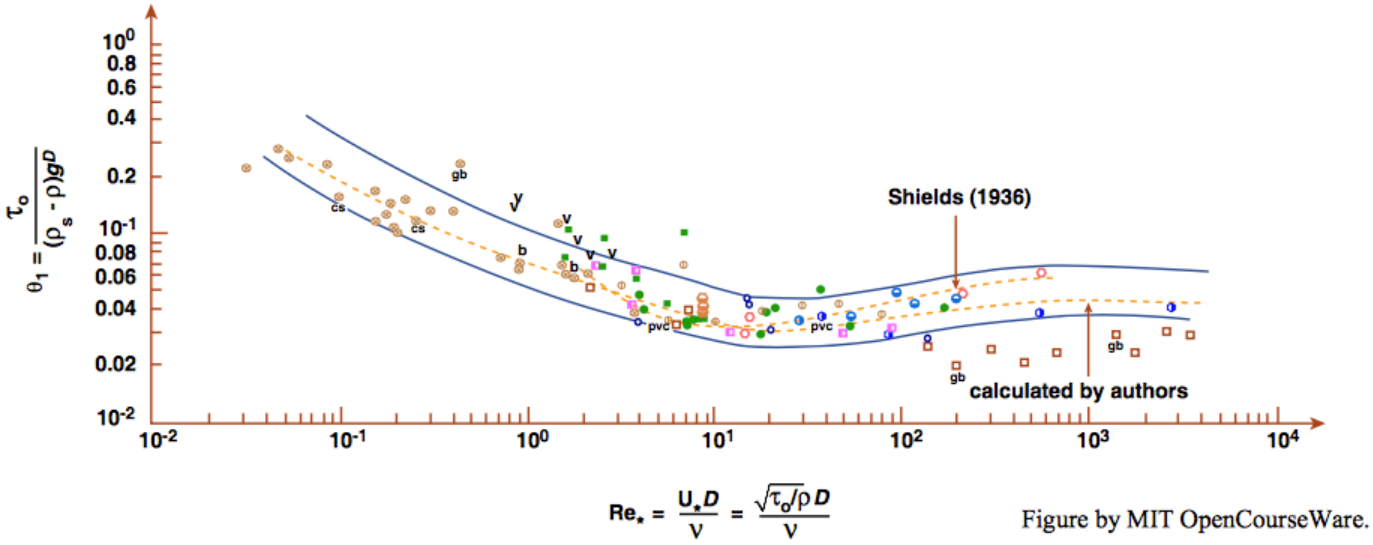


Figure 9.4.3: A modified and updated version of the Shields diagram. (From Miller et al., 1977.)

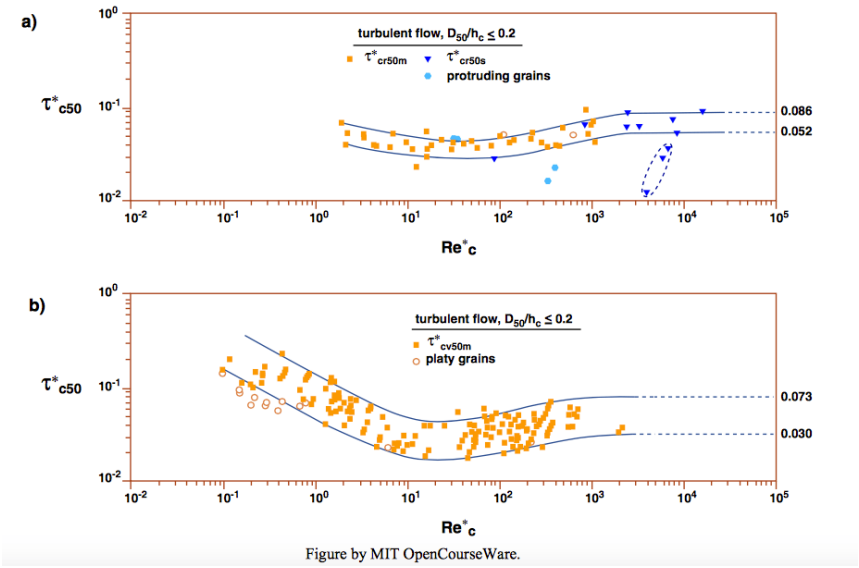


Figure by MIT OpenCourseWare.

Figure 9.4.4: Comparison of data on threshold boundary shear stress (expressed as Shields parameter based on median sediment size; \(\tau^{*}_{c 50}=\tau_{\text{o}} / \gamma^{\prime} D_{50}\) for **A)** the reference-transport-rate method and **B)** the watch-the-bed method. (From Buffington and Montgomery, 1997.)

This page titled 9.4: Movement Threshold is shared under a CC BY-NC-SA 4.0 license and was authored, remixed, and/or curated by John Southard (MIT OpenCourseware) via source content that was edited to the style and standards of the LibreTexts platform.

9.5: Recasting the Shields Diagram

The Shields diagram has a satisfying underlying physical significance, but it is awkward to use to find the threshold shear stress that corresponds to a given sediment diameter, or to find the largest sediment diameter that is moved by a given shear stress, because both τ_o and D appear in both of the axis variables. (This exemplifies the difference between two contrasting goals, both of them laudatory but often in conflict: expressing results in a form that most directly reveals the underlying processes, or in a form that is most useful in practical work.) To get around this problem the Shields parameter and the boundary Reynolds number can easily be recast into two equivalent dimensionless variables, one with D but not τ_o and the other with τ_o but not D. You can verify for yourself that these are $\tau_o \left(\rho/\gamma'^2\mu^2\right)^{1/3}$ and $D\left(\rho\gamma'/\mu^2\right)^{1/3}$. Figure $9.5.1$ shows a recast version of the Shields diagram, From Miller et al. (1977). The axes in Figure $9.5.1$ are labeled with u_* and D, so the graph does not look dimensionless, but those values are for a water temperature of $20°\text{C}$; the compilers just took the dimensionless graph, substituted in the $20°$ values of ρ and μ into the axis variables, and ended up with the $20°$ values of u_* and D. In effect, the graph is still really dimensionless.

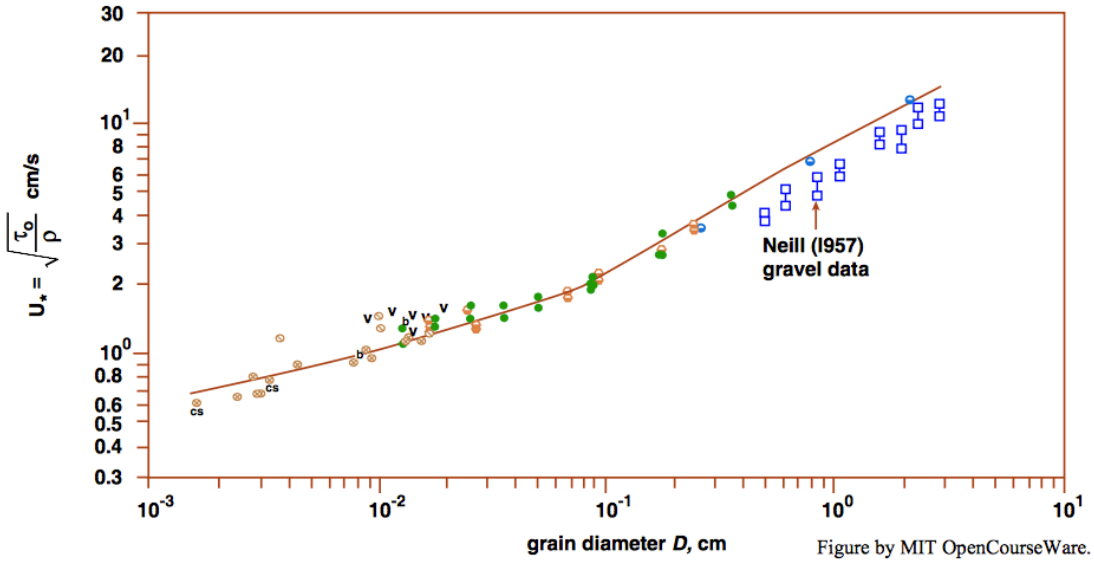


Figure $9.5.1$: A version of the updated Shields diagram, recast in terms of shear velocity u_* and particle diameter D, and standardized to temperature 20°C. (From Miller et al., 1977.)

One of the problems about the movement threshold is that there is a wide range of flow conditions for which there's weak but noticeable sediment movement. That leads to the problem of how to define the condition of incipient movement in the first place. Quantitative criteria have been proposed, but they have not yet become firmly established. Nonetheless, the Shields diagram continues to be used, because it gives good ballpark results for both engineering and sedimentological purposes. Various investigators have tried to establish arbitrary but experimentally reproducible definitions of the beginning of movement.

By observation of the bed through a microscope, Vanoni (1964) found that movement was intermittent on any small area of the bed, and, when it did occur, it took place in local gusts with several grains moving at once. He defined the critical stage of movement in terms of four gust frequencies (Figure $9.5.2$):

- **negligible** ($< 0.1\ \text{s}^{-1}$)
- **small** (0.1–$0.33\ \text{s}^{-1}$)
- **critical** (0.33–$1\ \text{s}^{-1}$)
- **general** ($> 1\ \text{s}^{-1}$)

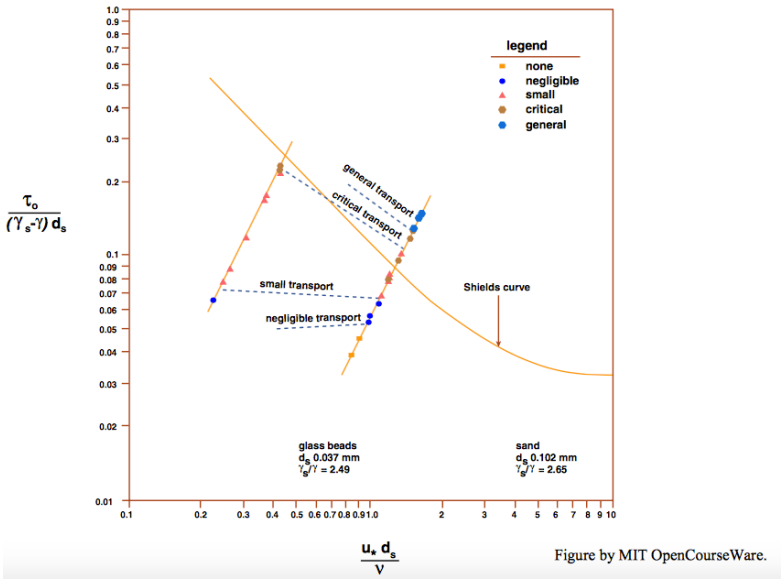


Figure 9.5.2: Graph of Shields parameter vs. particle Reynolds number for conditions near threshold, for runs with two sediments in a turbulent shear flow. (From Vanoni, 1964.)

Figure 9.5.2 makes clear how wide the range of condition is for which an objective observer, unschooled in the intricacies or defining incipient movement, might judge where to locate the threshold condition. As you have seen, this effect has even led some observers to question whether a criterion for inception of movement can even be formulated at all: movement tails off so gradually with decreasing flow strength that even in very weak flows, if one waits long enough one might see a particle moved by an instantaneous local fluid force on the bed, that is at the very extreme of the frequency distribution of such forces.

The Hjulström Diagram

No account of the threshold of sediment movement would be complete without mention of the famous graph proposed long ago by Hjulström (1939) (reproduced without change here as Figure 9.5.3), which has been used, or at least cited, by generations of sedimentationists. Hjulström undertook to represent the boundaries among erosion, transportation, and deposition in a graph of flow velocity vs. particle size. He acknowledged that use of the mean velocity to characterize the flow is inadequate, and viewed it as only “a temporary substitute until more data are available” (Hjulström, 1939, p. 9). The heavy bands between transportation and erosion, labeled “A”, were meant to represent the uncertainty of the data used to define the boundary. It is clear that Hjulström intended that band to represent the threshold of bed-load transport as the flow velocity is gradually increased. The word “erosion” in the graph is better read as “traction transport”: the former is best reserved for net removal of sediment from a given area of a sediment bed by the action of the fluid flow. (There can be transportation without erosion, if the sediment transport rate does not increase in the downstream direction and the local concentration of sediment in transport does not change with time.) The curve labeled “B” was meant to show cessation of transportation as the flow velocity gradually decreases; Hjulström relied upon some earlier flume observations that indicated that for sediments coarser than about medium sand the flow velocity for cessation of sediment movement about two-thirds that for inception of movement (see comments in the following paragraph). Hjulström showed the part of Curve B for fine sediments as a dashed line presumably because no data were available in that range. The widening gap between curves A and B is a consequence of the effect of cohesion increasing the velocities needed for initiation of movement. It seems likely that if the effects of cohesion in fine sediments could somehow be eliminated, the gap between curves A and B would be narrow for the entire range of sediment sizes.

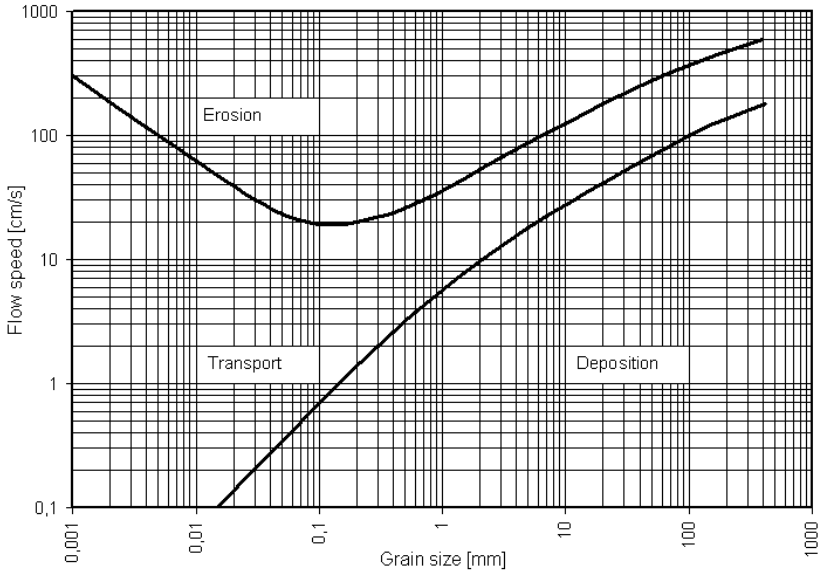


Figure 9.5.3: The Hjulström *Curve. by Wikipedia. Is licensed under CC BY-SA 3.0*

The idea that the flow strength for cessation of movement is less than, rather than equal to, the flow strength for initiation of movement may have to do with a kind of hysteresis effect: as weak transport continues on a granular bed at about threshold conditions, the bed becomes partly armored, in the sense that most of the bed particles have found stable positions, and a small number of particles, not having found such positions and thus being the very most mobile, continue to pick their way across the immobile bed surface at flow strengths slightly lower than that for which inception of movement was judged to have begun. In any case, the range of flow velocities represented by the gap between Hjulström's curves A and B lies within the rather wide range, noted in an earlier section, for which there is at least some weak transport, so the difference between the two curves seems not to be of great consequence.

The Hjulström diagram was later modified by Sundborg (1956). Figure 9.5.4 shows Sundborg's version, taken directly from the original. Sundborg's graph shows separate curves for the movement threshold corresponding to several water depths, as is necessary if the flow velocity rather than the boundary shear stress (as in the Shields diagram) is used for the flow strength. The purpose of the lightly shaded band that includes these specific curves for the various flow velocities was not explicitly described, but it was probably meant to represent uncertainty in the data. Sundborg made note of Hjulström's lower curve, for cessation of movement, but did not include it in his version.

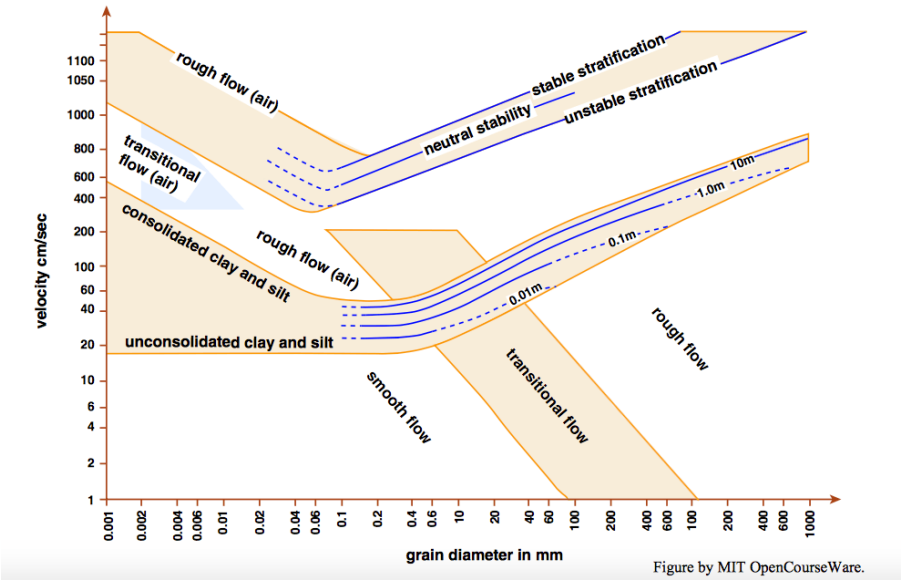


Figure 9.5.4: Sundborg's modification of the Hjulström diagram. (After Sundborg, 1956.)

Such are the origins of what might be called the Hjulström–Sundborg diagram. A diagram like Sundborg's version, showing a

family of threshold curves as a function of flow depth, with the curves based on the same data as the Shields diagram or its successors, has much potential for use by sedimentary geologists, despite the engineers' aversion to using velocity rather than boundary shear stress for this purpose. Various versions of the Hjulström diagram have appeared in a great many textbooks and monographs since Sundborg's contribution, but often in deplorably corrupted form: the curve for cessation of transportation is usually shown far lower than in the Hjulström original, with velocities lower than the curve for incipient movement by a factor of more than five!

This page titled 9.5: Recasting the Shields Diagram is shared under a CC BY-NC-SA 4.0 license and was authored, remixed, and/or curated by John Southard (MIT OpenCourseware) via source content that was edited to the style and standards of the LibreTexts platform.

9.6: The Effect of Density Ratio

It was mentioned in Paragraph 27 above that the density ratio ρ_s/ρ might be important in governing the motion threshold. In that case, the dimensional analysis put forth in the earlier section should be extended in order to include the effect of relative density:

$$\text{threshold} = f\left(\rho, \rho_s, \mu, \gamma', D, \tau_o\right) \tag{9.6.1}$$

and, nondimensionalizing in the same way as before,

$$\frac{\tau_c}{\gamma' D} = f\left(\frac{\rho u_* D}{\mu}, \frac{\rho_s}{\rho}\right) \tag{9.6.2}$$

where τ_c is the threshold value of the bed shear stress.

To my knowledge, little consideration has been given to that possibility in the literature on threshold. Shields himself plotted data not just for quartz-density sand in water but for amber (specific gravity 1.06), lignite (specific gravity 1.27), and barite (specific gravity 4.25). The points for amber and lignite lie slightly above the curve, and the points for barite lie slightly below the curve, suggesting that ρ_s/ρ has at least a slight effect. A later study by Ward (1969) showed the same results, although with greater range of difference in threshold with density ratio. I am not aware of any more recent studies of the effect of density ratio on thresholds in water flows. A potential pitfall in interpreting these results, however, is that the experiments were not controlled for possible effects of particle shape, and in the case of plastic beads (styrene, specific gravity 1.18; polyethylene, specific gravity 1.06) in oil, the possibility of subtle particle- to-particle forces were not considered.

The results seem counterintuitive, at least to this observer: should it not be the case that the particles with greater density, and thus greater inertia, would be less likely to be set into motion by suddenly greater fluid force on the particle than a particle with lesser density? A specific set of experiments in which a criterion for threshold is applied uniformly, and in which particle sorting and shape are adjusted to be the same for the various sediment batches with different density, might bring some clarity to the issue.

If the decrease in Shields parameter (the dimensionless threshold shear stress) with increasing density ratio is indeed real, then it should be even greater for the case of quartz particles under the wind, for which the density ratio is far greater than for even the densest solid particles under water flows. Extensive observations of the threshold bed shear stresses for several particle compositions, sizes, and densities under wind (Iversen et al., 1976) gave results of about 0.1 for the threshold Shields parameter over a range of boundary Reynolds numbers from about 5 to about 50, and their results were generally consistent with earlier wind-tunnel studies of threshold (see Chapter 11 for more on eolian thresholds). Thresholds under water flows in this range of Re_* average around 0.6, judging from the modified Shields plots presented by Buffington et al. (1997) (see Figure 9.5.1 above). The increase in dimensionless threshold with increasing density ratio does therefore seem to be real.

In a later study by Iversen et al. (1987), in which they synthesized earlier results on threshold over a wide range of density ratios, they purport to show that the dimensionless threshold decreases systematically with increasing density ratio from that characteristic of mineral particles in water to that of mineral particles in the extremely low atmospheric density of Mars; see Figures $9.6.1$ and $9.6.2$. Be on your guard here, however: their dimensionless coefficient A uses ρ_s instead of $(\rho_s - \rho)$ in the variable $(\rho_s - \rho)\, g$, called γ' in these notes, in the denominator, so the results for the threshold in water, shown on the left-hand side of Figure $9.6.1$, cannot be compared directly with the conventional Shields curve. The decrease in their threshold coefficient A from the Venus-wind-tunnel case to the Mars-wind-tunnel case seems to support their position, but even so the values for the Venus wind tunnel, for which the density ratio is not greatly different from that of sand in water, is significantly higher than the generally accepted values shown on the Shields diagram and its later modifications, discussed above. the matter seems (at least to this writer) not be settled.

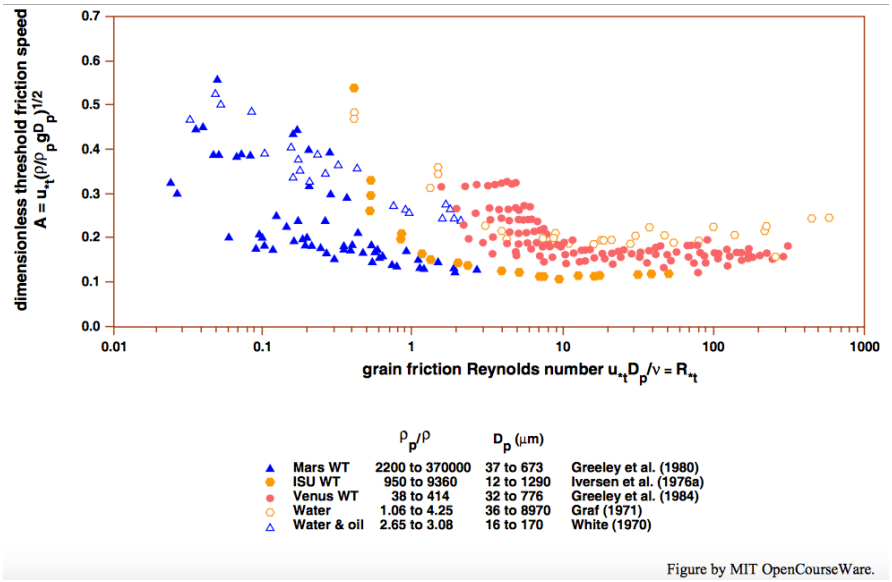


Figure 9.6.1: Threshold graph from Iversen et al. (1987).

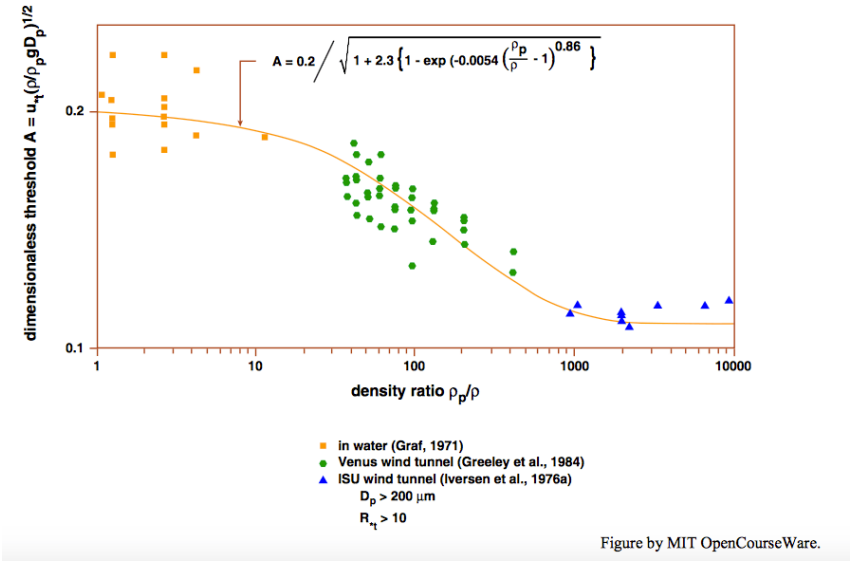


Figure 9.6.2: Effect of density ratio on threshold, for particles larger than 0.2 mm and particle Reynolds numbers greater than 10. (From Iversen et al. 1987.)

References Cited Chapter 9

Buffington, J.M., and Montgomery, D.R., 1997, A systematic analysis of eight decades of incipient motion studies, with special reference to gravel-bedded rivers: Water Resources Research, v. 33, p. 1993-2029.

Chepil, W.S., 1958, The use of evenly spaced hemispheres to evaluate aerodynamic forces on a soil surface: American Geophysical Union, Transactions, v. 39, p. 397- 404.

Chepil, W.S., 1961, The use of spheres to measure lift and drag on wind-eroded soil grains: Soil Science Society of America, Proceedings, v. 25, p. 343-345.

Coleman, N.L.,1967, A theoretical and experimental study of drag and lift forces acting on a sphere resting on a hypothetical stream bed: International Association for Hydraulic Research, 12th Congress, proceedings, v. 3, p. 185-192.

Coleman, N.L., and Ellis, W.M., 1976, Model study of the drag coefficient of a streambed particle: Third Federal Interagency Sedimentation Conference, Denver, Colorado, Proceedings, p. 4-12.

Einstein, H.A., and El-Samni, E.A., 1949, Hydrodynamic forces on a rough wall: reviews of Modern Physics, v. 21, p. 520-524.

Grass, A.J., 1970, Initial instability of fine bed sand: American Society of Civil Engineers, Proceedings, Journal of the Hydraulics Division, v. 96, p. 619- 632.

Hjulstrøm, F., 1939, Transportation of debris by moving water, in Trask, P.D., ed., Recent Marine Sediments; A Symposium: Tulsa, Oklahoma, American Association of Petroleum Geologists, p. 5-31.

Iversen, J.D., Pollack, J.B., Greeley, R., and White, B.R., 1976, Saltation threshold on Mars: the effect of interparticle force, surface roughness, and low atmospheric density: Icarus, v. 29, p. 381-393.

Iversen, J.D., Greeley, R., Marshall, J.R., and Pollack, J.B., 1987, Aeolian saltation threshold: the effect of density ratio: Sedimentology, v. 34, p. 699-706.

Lavelle, J.W., and Mofjeld, H.O., 1987, Do critical stresses for incipient motion and erosion really exist?: Journal of Hydraulic Engineering, v. 113, p. 370- 385.

Miller, M.C., McCave, I.N., and Komar, P.D., 1977, Threshold of sediment motion under uinidirectional currents: Sedimentology, v. 24, p. 507-527.

Neill, C.R., 1968, Note on initial movement of coarse uniform bed-material: Journal of Hydraulic Research, v. 6, p. 173-176.

Shields, A., 1936, Anwendung der Ähnlichkeitsmechanik auf die Geschiebebewegung: Berlin, Preussische Versuchanstalt für Wasserbau und Schiffbau, Mitteilungen, no. 26, 25 p.

Sundborg, A., 1956, The River Klarålven: Chapter 2. The morphological activity of flowing water—erosion of the stream bed: Geografiska Annaler, v. 38, p. 165-221.

Vanoni, V.A., ed., 1975, Sedimentation Engineering: American Society of Civil Engineers, Manuals and Reports on Engineering Practice, No. 54, 745 p.

Ward, B.D., 1969, relative density effects on incipient bed movement: Water Resources research, v. 5, p. 1090-1096.

Yalin, M.S., 1977, Mechanics of Sediment Transport, 2nd Edition: Oxford, U.K., Pergamon, 298 p.

This page titled 9.6: The Effect of Density Ratio is shared under a CC BY-NC-SA 4.0 license and was authored, remixed, and/or curated by John Southard (MIT OpenCourseware) via source content that was edited to the style and standards of the LibreTexts platform.

10: MOVEMENT OF SEDIMENT BY WATER FLOWS

10.1: Introduction to the Movement of Sediment by Water Flows
10.2: The Bed, the Flow, and the Load
10.3: Transport Mode Versus Flow Intensity
10.4: Bed Load
10.5: Suspension in a Shear Flow- The Diffusional Theory of Suspension

This page titled 10: Movement of Sediment by Water Flows is shared under a CC BY-NC-SA 4.0 license and was authored, remixed, and/or curated by John Southard (MIT OpenCourseware) via source content that was edited to the style and standards of the LibreTexts platform.

10.1: Introduction to the Movement of Sediment by Water Flows

A simple flume experiment on sediment movement by a unidirectional current of water in a flume serves to introduce the material in this chapter. Place a layer of sediment in the flume, level it to have a planar surface, and establish a uniform flow at a certain depth and velocity. Gradually, in steps, increase the strength of the flow beyond the condition for incipient movement. The magnitude of the flow strength relative to what is required for incipient movement of the bed sediment is conventionally called the **flow intensity**, and is usually taken to be the ratio τ_o/τ_{oc} (or, what is the same, u_*/u_{*c}), where the subscript c denotes the threshold ("critical") condition.

At first the particles move as **bed load**, by hopping, rolling, and/or sliding. Particle movement is neither continuous nor uniform over the bed: brief gusts or pulses of movement affect groups of particles locally, and seemingly randomly, on the bed. Particles move a short distance, stop, and then move again. Even when they are moving, they are generally not moving as fast as the fluid near the bed surface.

As the flow becomes stronger, some of the particles moving near the bed are lifted upward by upward-moving turbulent eddies and travel for more or less long distances downstream as **suspended load**. The stronger the flow and/or the finer the sediment, the greater is the concentration of suspended sediment, the higher it can travel in the flow, and the longer it moves downstream before returning to the bed. Of course, the particles are not really suspended in the way that a picture is suspended on the wall by a nail; they are continuously settling through the surrounding fluid, and eventually they return to the bed. If the sediment is fine and the flow is strong, however, the particles are likely to travel for the entire length of the flume.

If you introduce a small quantity of very fine clay-size sediment into the flow, you would find that it too travels in suspension, but the essential difference between this part of the suspended load and the coarser part you observed before is that even if you add large quantities of it to the flow, it would not be represented in the bed. Fine sediment of this kind is called **wash load**. Extremely fine particles, in the size range of small fractions of a micrometer, can be kept in effectively permanent suspension, because their mass is so small that they can be moved about by the random bombardments of the molecules constituting the fluid itself. These random motions are a manifestation of Brownian motion.

For flow intensities not much above threshold, it is fairly easy to observe the particle motions in the bed load, provided that you have clear water, good lighting, and sharp eyes (close-up slow-motion vision would be a big help), but as the flow intensity increases, the concentration of particles in motion as bed load increases, and it becomes difficult or impossible to observe the motions of individual particles. Unfortunately, no one yet seems to have devised a good way to see into the dense layer of moving bed-load particles at high flow intensities to study its characteristics. This important aspect of sediment transport remains contentious and inadequately studied.

To gain an appreciation of a rather different mode of sediment movement, you need to resort to a wind tunnel. It is not difficult to build one: all you need to do is construct a rectangular duct resting on the floor, leading from a flared entrance at the upwind end to a large empty chamber at the downwind end, with an exhaust fan in the side of the chamber to create a wind through the duct. A louver just downwind of the fan lets you adjust the wind velocity. Especially when the ratio of sediment density to fluid density is very large, as with quartz sand in a wind tunnel, sediment particles are entrained impulsively by the flow at middling to steep take-off angles and move downstream in long arching trajectories little affected by the fluid turbulence to make impact with the bed at low angles. This characteristic mode of movement, known as **saltation**, is especially important in the transport of sand by wind. Its manifestation in transport of particles that are not much denser than the transporting fluid, however, is much less striking or distinctive.

This page titled 10.1: Introduction to the Movement of Sediment by Water Flows is shared under a CC BY-NC-SA 4.0 license and was authored, remixed, and/or curated by John Southard (MIT OpenCourseware) via source content that was edited to the style and standards of the LibreTexts platform.

10.2: The Bed, the Flow, and the Load

The aggregate of sediment particles being transported by a flow at a given time is called the **load**. At the very outset, it seems appropriate to define what is meant by the bed, the flow, and the bed load (Figure 10.2.1). (I am not sure that the following definitions, intuitive as they seem to me, would be approved by all specialists in sediment transport.) The *bed* comprises all of the particles that at a given time are motionless and in direct contact with the substrate, and the *load* comprises all of the particles that are in motion in a given flow, whether or not they are in contact with the bed. That leaves the less certain definition of the *flow*: all the material, fluid and solid, that at a given time are in motion above the bed.

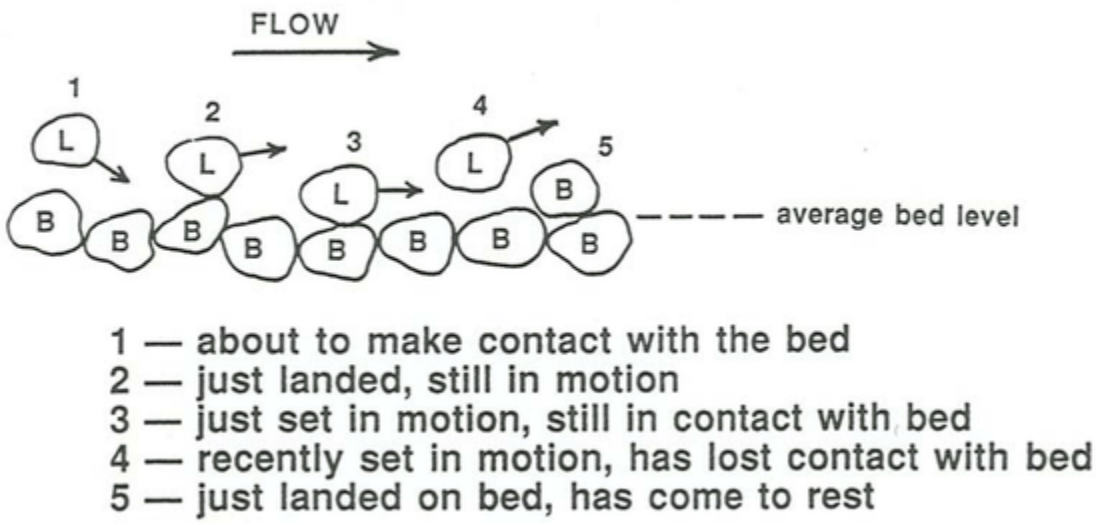


Figure 10.2.1: The flow, the bed, and the load.

The load can further be subdivided in two different ways. On the one hand, the load can be divided into **bed-material load**, which is that part of the load whose sizes are represented in the bed, and **wash load**, which is that part of the load whose sizes are not present in the bed in appreciable percentages. The wash load, which if present is always the finest fraction of the load, is carried through a reach of the flow without any exchange of sediment between the bed and the flow. On the other hand, the load can also be divided into **bed load**, which travels in direct contact with the bed or so close to the bed as not to be substantially affected by the fluid turbulence, and **suspended load**, which is maintained in temporary suspension above the bed by the action of upward-moving turbulent eddies. I hope that it is clear from these definitions that bed load is always bed-material load, and suspended load is likely to be partly bed-material load and partly wash load, although in particular cases it could be all wash load, or all bed-material load. Confused? Figure 10.2.2 may or may not be of help.

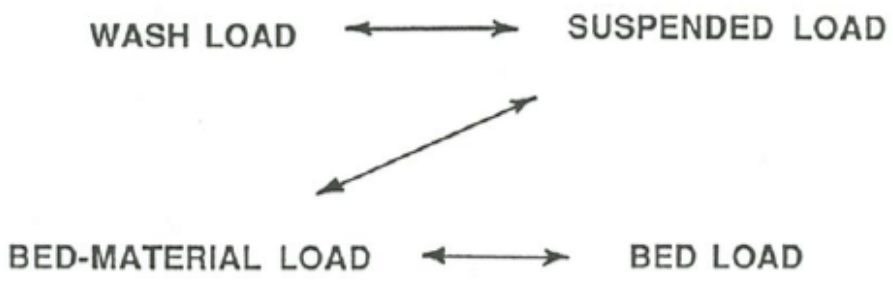


Figure 10.2.2: Relationships among the various kinds of sediment load.

The movement of bed load is sometimes called **traction**. Bed-load movement can be by rolling, sliding, or hopping. Words like those three are not entirely adequate for the task of describing the nature of bed-load movement, however, because the moving

particles commonly partake of all three “modes”, which vary in importance from movement event to movement event, and from instant to instant during a movement event. It is not easy to observe bed-load movement in great detail, but when you have the chance to watch a carefully made high-speed close-up motion picture of bed load (in flows where the load is not yet so abundant as to obscure one’s view) you see that the particles characteristically take occasional excursions downstream, by rolling and hopping along irregularly, and then come to rest for some time before being moved again.

Particle shape has a substantial influence on mode of bed-load movement: disk-shaped particles have a much greater tendency to slide or bulldoze, whereas equant or spheroidal particles have a much greater tendency to roll or hop. Discoidal particles can under some conditions be seen to roll like cartwheels!

There is clearly a problem in distinguishing between bed load and suspended load: how far can a particle move up into the flow and still be considered bed load? The standard criterion is whether or not fluid turbulence has a substantial effect on the time and distance involved in the excursion. It is important to keep in mind that there is no sharp break between bed load and suspended load: a given particle can be part of the bed load at one moment and part of the suspended load at another moment, and not moving at all at still another moment. The consequence of this is that at any given time there is an appreciable overlap in the size distributions of the bed load and the suspended load, although obviously the suspended load tends to be finer than the bed load. Moreover, there seems to be no sharp break, or jump discontinuity, in the volume concentration of sediment upward from the bed-load layer into the suspended-load layer (although accurate observations are not easy to make). That is to be expected, because in a sense the bed-load layer acts as the “lower boundary condition” for the suspended-load concentration; see the later section on suspension.

The relative proportions of the bed material that moves as bed load and as suspended load depend upon the characteristics of the bed material, especially its size, and on the flow conditions. Very coarse bed material in rivers (gravel) generally moves as bed load, whereas fine to medium sands move predominantly as suspended load. The mode of movement of the coarser sand sizes generally varies depending on the hydraulic conditions: at low flow intensities the coarser sand fractions move predominantly as bed load, whereas at high flow intensities they are taken into suspension. Even at the same average discharge, sand of a given size may alternate between suspension and traction, as it is caught up by powerful eddies (for example, the separation eddies formed on the lee sides of major bed forms) or returns to the bed in less turbulent parts of the flow. Most sand sizes do not travel in continuous suspension; the very fact that these sizes constitute a major part of the bed material in most rivers indicates that they are taken into suspension only intermittently. To distinguish this mode of transport from the almost continuous suspension typical of wash load, which is generally composed of particles finer than fine sand, we could call the coarser part of the suspended load the **intermittent suspension load**.

The distinction between bed load and suspended load can be made either on a practical observational basis or on a more theoretical basis with reference to support mechanisms. The practical definitions, those given above, are based on the observation that the bed load is carried in direct contact with the bed or very close to the bed whereas the suspended load is carried far above the bed. The more theoretical definitions are based on the concept (not easily applied, in practice!) that the suspended load is the part of the load that is supported entirely by fluid turbulence, and the bed load is the part of the load that is supported in one way or another by the bed itself, not by fluid turbulence. Bed-load particles that are moving in direct contact with the bed are supported, at least in part, directly by the bed, if the possible contribution of fluid lift forces is left out of account. By this definition, bed-load particles that are temporarily not in direct contact with the bed are either following a path that is largely unaffected by fluid turbulence, in consequence of having parted contact with the bed by a momentarily stronger fluid force (saltating particles fall naturally into this category) or are maintained in motion above the bed, perhaps at a distance of many particle diameters, by collisions with other particles that are part of a thick bed-load layer at high flow intensities. There will be more to say about the existence and nature of these latter bed-load layers later in this chapter.

Finally, here are a few words about how sediment concentration might be measured. Measuring the concentration of suspended sediment is fairly straightforward: you could imagine capturing a volume of the flow, in a snap- close bottle of some kind that does not disrupt the flow very much, and measuring the volume or mass of sediment per unit volume of the fluid–solid mixture. Provided that the measured volume is small relative to the characteristic spatial rate of change of “average” concentration (for example, you would not want your sample to integrate over a large fraction of the flow depth) but large enough relative to small-scale variations in sediment concentration related to the details of local eddy structure, your sample should provide a representative measure of the local average sediment concentration. Measuring the concentration of bed load, however, is a different matter. The bed-load layer is by its very nature thin. People attempt to measure the transport rate of the bed load (that is not a trivial matter either; see the later chapter on transport rates) but ordinarily not the bed- load concentration. Conceptually, however, it is reasonable to think about a kind of “area concentration” of bed load: the volume or mass of bed load, per unit bed area and as a time average, above a small area of the sediment bed. But I cannot provide any helpful ideas about how to measure such a quantity.

This page titled 10.2: The Bed, the Flow, and the Load is shared under a CC BY-NC-SA 4.0 license and was authored, remixed, and/or curated by John Southard (MIT OpenCourseware) via source content that was edited to the style and standards of the LibreTexts platform.

10.3: Transport Mode Versus Flow Intensity

Before we go into more detail about how sediment particles move, as bed load or in suspension or in saltation, it is worth developing a rational framework for relating the various modes of movement to one another. As with so many aspects of sediment transport, it is valuable to think in terms of *regimes*: distinctive ranges of the phenomenon, characterized by modes of particle movement that differ from other ranges. In this case, such regimes have been called transport stages. To develop a good framework for visualizing and assessing the results of experiments on **transport stages**, start by making a list of the variables that are likely to be important in determining the transport stage. The flow strength is best defined by the bed shear stress, just as it is for the threshold of movement. In contrast to the problem of movement threshold, however, the flow depth, which reflects the possible effects of outer-layer flow phenomena like large-scale turbulence (see Chapter 4), might not be ignorable, but as a first approximation suppose that the flow is characterized only by τ_o. Both particle size D and particle density ρ_s need to be included. The submerged specific weight of the particles, γ', must be included as well as the particle density ρ_s, because of the effect of particle weight in settling, aside from the effect of particle inertia when the particles experience accelerations caused by fluid turbulence. The fluid properties ρ and μ have to be included for the usual reasons. Then

$$\text{transport stage} = f\left(\tau_o, D, \rho, \mu, \rho_s, \gamma'\right) \tag{10.3.1}$$

and we should expect that everything about the transport stage, expressed in dimensionless form, should be expressible in terms of three dimensionless variables. Examples of such things are: the positions of boundaries or boundary zones between qualitatively different transport stages; lengths or heights of particle trajectories, nondimensionalized by dividing by the particle diameter D; or particle velocities, nondimensionalized by dividing by the shear velocity u_*.

One such set of dimensionless variables might be:

- $(\tau_o)^o = \left(\rho/\gamma'\mu^2\right)^{1/3}\tau_o$, a dimensionless form of τ_o
- $\mathrm{D}^o = \left(\rho\gamma'/\mu^2\right)^{1/3} D$, a dimensionless form of the particle diameter D
- ρ_s/ρ

The advantage of this set is that the leading variables, τ_o and D, are segregated into different dimensionless variables. An alternative would be to replace the dimensionless boundary shear stress with the flow intensity, u_*/u_{*c}. In either case, one could attempt to plot experimental or theoretical results in two-dimensional graphs for certain values of ρ_s/ρ (most importantly, quartz-density sediment in water-density fluid).

Figure $10.3.1$, a very generalized version of a graph of boundary shear stress vs. particle size, makes a start at representing transport stages. In Figure $10.3.1$, the axes are labeled in two ways: the dimensionless versions of τ_o and D mentioned above, and also actual values of τ_o and D at a water temperature of $10°\mathrm{C}$, to give a more concrete appreciation of conditions. We know at the outset that one boundary has to be present in the graph: the curve for threshold of particle motion. That is readily obtained by transforming the Shields curve (see Chapter 9) into these coordinates. Another boundary, which we consider next, is the curve for the onset of suspension in addition to bed-load movement.

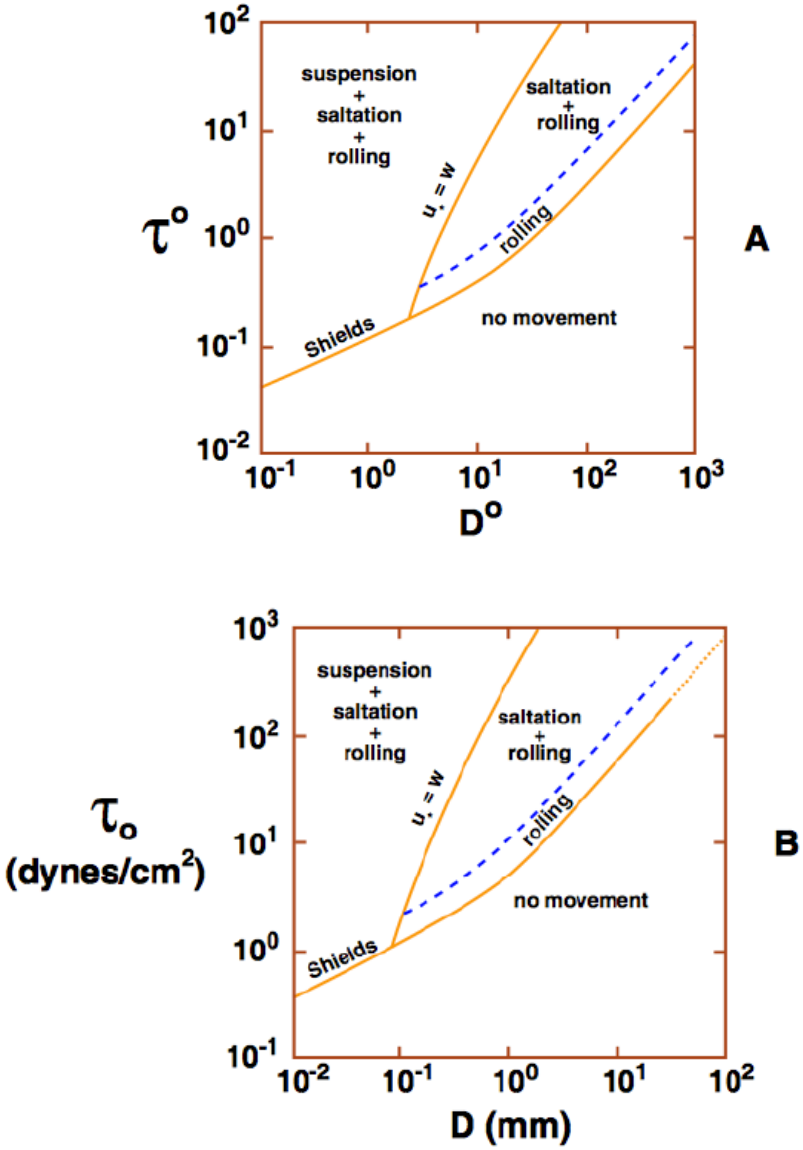


Figure 10.3.1: Transport stages in **A)** a dimensionless graph of boundary shear stress vs. particle size and **B)** the same graph, but with actual values of boundary shear stress and particle size standardized to a water temperature of $10^{\circ}\mathrm{C}$.

The natural criterion for suspension is that the vertical turbulent velocities are at least as large as the settling velocities of the sediment particles; otherwise, particles could never be carried any higher above the bed than the entraining forces permit. The problem is that although for a given sediment size the settling velocity is fairly well defined (if effects of sorting and particle shape are ignored), the vertical turbulent velocities are distributed over a wide range of values. Should we use the very largest but very uncommon values, or smaller but more frequent values? What has commonly been done is to assume that the root-mean-square (rms) value of the vertical turbulent velocities is a good measure to use. Measurements in turbulent boundary-layer flows past both smooth and rough boundaries have shown that there is a maximum close to the bed and that the maximum values reached are proportional to the shear velocity u_* (Blinco and Patheniades, 1971). The data of McQuivey and Richardson (1969) and Antonia and Luxton (1971) show that the maximum value of $(\mathrm{rms}\ v)/u_*$ is approximately equal to one and that the value does not depend strongly on the type of roughness. An approximate criterion for the onset of suspension is then

$$u_* = w \tag{10.3.2}$$

For values of u_* less than w, there should be no suspension, and for values of u_* greater than w, some of the sediment should be traveling as suspended load. There is no reason to expect, however, that the coefficient of proportionality in Equation 10.3.2 is exactly equal to one; the coefficient would presumably need to be adjusted somewhat in light of actual observations on the onset of suspension. Middleton (1976) has argued that the criterion $u_* > w$ is also supported by a comparison of hydraulic

measurements with the settling velocity of the largest particle sizes present in the suspended load of several rivers.

What remains is to convert the suspension criterion in Equation 10.3.2 to a corresponding curve in Figure 10.3.1. To do this, first write Equation 10.3.2 as

$$[(\tau_o)^o]^{1/2} = w^o \tag{10.3.3}$$

by use of the definition of u_*. Then use the definition of the dimensionless boundary shear stress $(\tau_o)^o$, given above, and a corresponding definition of dimensionless settling velocity, $w^o = (\rho^2/\gamma'\mu)^{1/3} w$ (see Chapter 2) to obtain an expression for τ_o in terms of $(\tau_o)^o$ and an expression for w in terms of w^o:

$$\begin{aligned} \tau_o &= \left(\frac{\gamma'^2\mu^2}{\rho}\right)^{1/3} (\tau_o)^o \\ w &= \left(\frac{\gamma'\mu}{\rho^2}\right) w^o \end{aligned} \tag{10.3.4}$$

Now substitute the expressions for τ_o and w in Equation 10.3.4 into Equation 10.3.3:

$$\left[\left(\frac{\gamma'^2\mu^2}{\rho}\right)(\tau_0)^0\right]^{1/3} = \rho^{1/2}\left[\left(\frac{\gamma'\mu}{\rho^2}\right)^{1/3} w_0\right] \tag{10.3.5}$$

and simplify to obtain

$$\tau_o^{1/2} = \rho^{1/2} w \tag{10.3.6}$$

The final step is to use the curve for w_o as a function of D_o (Figure 3.9.3 in Chapter 3) to obtain the relationship between $(\tau_o)^o$ and D_o corresponding to the criterion for suspension:

$$\left[(\tau_0)^0\right]^{1/2} = f\left(D^0\right) \tag{10.3.7}$$

Keep in mind that over most of its range, for settling-velocity Reynolds numbers greater than the Stokes range, the function in Equation 10.3.7 has to be determined by observation.

We see that the curve that represents the suspension criterion slopes more steeply than the curve for incipient movement. This is just a manifestation of the fact that, qualitatively, the shear stress needed to make $\mathrm{rms}\ v$ equal to the settling velocity with increasing particle size increases more rapidly than does the shear stress needed for incipient movement with increasing particle size. The consequence is that the two curves intersect at a certain small value of dimensionless particle size. (The suspension-inception curve does not extend downward below the movement-inception curve, because the flow there is not strong enough to move any sediment in the first place.) To the left of the intersection point, the fall velocity of the sediment particles is exceeded by the magnitude of the turbulent velocity fluctuations in the flow even at flow strengths just sufficient for sediment movement, so that sediment particles can be put into suspension as soon as they begin to be moved. Keep in mind, however, that at this and even finer sediment sizes, some of the sediment moves as bed load as well as suspended load. The existence of current ripples in sediments effectively at least as fine as medium silt is a good indication of this, inasmuch as ripples owe their existence to bed-load transport; see Chapter 12.

Finally, Figure 10.3.2, which shows transport stages in a graph of u_*/w, the ratio of to shear velocity u_* to settling velocity w vs. flow intensity u_*/u_{*c} is an equivalent form of Figure 10.3.1; it is just a rubber-sheeted $D^o - \tau^o$ diagram. It is neater and more synthetic than Figure 10.3.1, although perhaps less useful. Because $w = f(D)$ and $w \neq f(u_*/u_{*c})$, there is a one-to-one correspondence between sediment diameter D and points on a vertical line in this graph. The movement-inception curve becomes the left-hand vertical axis $(u_* = u_{*c})$, and the suspension-inception criterion, $u_* = w$, becomes a horizontal line. The area below the line for the suspension-inception criterion represents only bed-load transport, and the area above the line represents bed-load and suspended-load transport together.

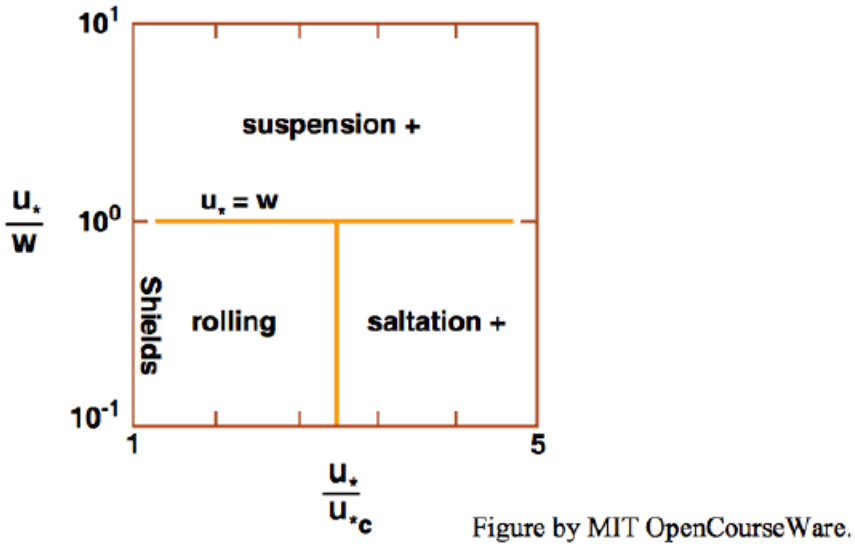


Figure by MIT OpenCourseWare.

Figure 10.3.2: Transport stages in a graph of u_*, the ratio of shear velocity to particle settling velocity, vs. flow intensity u_*/u_{*c}.

This page titled 10.3: Transport Mode Versus Flow Intensity is shared under a CC BY-NC-SA 4.0 license and was authored, remixed, and/or curated by John Southard (MIT OpenCourseware) via source content that was edited to the style and standards of the LibreTexts platform.

10.4: Bed Load

Styles of Bed-Load Movement at Low Flow Intensities

Transport of the surficial particles on a locally planar bed produces a distinctive microtopography, consisting of small-scale irregular and discontinuous ridges and depressions oriented approximately parallel to the flow. The spacing of these features on a sand bed is of the order of several millimeters, and the relief is very small, generally only a few particle diameters. This lineated relief is a characteristic feature of transport, for particles ranging from silt sizes (Mantz, 1977) up to at least very coarse sand, and for hydraulic conditions ranging from just above the threshold of particle movement to high flow intensities that produce upper-regime, plane-bed conditions. It is the manifestation of the low-speeds streaks associated with the burst–sweep cycle, described in Chapter 4.

It does not take special experimental conditions to see manifestations of this lineated microtopography. Here are two everyday (well, almost) examples. It is a cold, gray day, and the snow has just begun to fall. Before the paved surface of the road is completely whitened, you see distinctive, shifting white streaks of snow aligned with the wind blowing across the road. Or you are standing at the kitchen sink, washing root vegetables fresh from the garden. The fine fraction of the loosened sediment is carried in suspension down the drain, never to be seen again, but the coarser fraction is immediately formed into small- scale streaks on the surface of the sink, beneath the fast-flowing water headed for the drain. Go back to the final section in Chapter 4, on coherent structures in turbulent flow, for the dynamics behind these bed-load streaks.

The ridges and depressions are produced by the action of small but strong turbulent eddies on the bed. Exactly how this takes place is becoming clearer as the structure of turbulence close to the bed becomes better understood as a result of numerous laboratory studies. The relevance of these observations to sediment movement has been discussed more thoroughly by Grass (1971, 1974), Karcz (1973), Jackson (1976), Sumer and Oguz (1978), Bridge (1978), Sumer and Deigaard (1981), and Leeder (1983a).

Most experimental observations have been made on boundaries that are dynamically smooth or transitionally rough, i.e., on boundaries characterized by a viscous sublayer that is at least poorly developed. But observations of dynamically rough boundaries (e.g., by Grass, 1971) show that even for flows without a viscous sublayer there exists a region close to the boundary, which Grass called the “inner zone”, for $y^+ < 40$, characterized by distinctive low-speed longitudinal streaks and a quasi-cyclic alternation of events that has come to be known as the burst–sweep cycle (see Chapter 4). As strong vortices with axes transverse to the flow approach the boundary, they produce pressure gradients that tend to lift up the streaks and eject them into the turbulent boundary layer. This “burst” of slow-moving fluid is capable of carrying small particles away from the bed to distances a few centimeters above the bed. Sumer and Oguz (1978) found that particles whose settling velocity was of the order of $0.5u_*$ were carried “in a single continuous motion” up to dimensionless elevations y^+ of 100–200. The slow-moving fluid in the burst then mixes with, and is accelerated by, the fluid in the outer zone, and some returns to the bed as a fast-moving vortex or “sweep”, which in turn creates a new burst, and so on. The process is not strictly periodic, although on the average it displays a period and scale controlled mainly by the velocity and thickness of the turbulent boundary layer. If the period of bursts is T and the velocity far from the bed is U, then $UT/\delta = 5$, where δ is the thickness of the boundary layer (in an open-channel flow, the depth of the flow).

The existence of the burst–sweep cycle suggests an explanation of the phenomena of particle movement described above. The gusts of movement of particles along the bed described by many workers since Vanoni (1964) probably correspond to fluid sweeps in the burst-sweep cycle, when velocity gradients close to the bed, and therefore shear stresses, are locally high. Particles tend to be swept to one side or the other of fast-moving fluid streaks to gather under slow- moving streaks and produce the characteristic current lineation observed on plane beds.

For sand finer than about $0.6\ \mathrm{mm}$, movement of particles over a plane bed eventually results in minor accumulations of particles that grow to form ripples (Chapter 11). The ripples then change the pattern of flow at the bed, and therefore also the interaction of the flow and the moving sediment particles. Separation of flow takes place at the ripple crest, and the boundary layer is reestablished downstream of where the flow reattaches to the bed, on the stoss side of the next ripple downstream. Although the bed surface is now much more irregular, the same lineated surface seen on a plane bed can generally be observed on the upper stoss sides of ripples or larger bed forms, if the water is clear and there is good low-angle lighting.

Perhaps the least difficult way of observing how bed-load particles move as the flow intensity increases beyond the threshold of movement is to study the movement of a single particle over a bed composed of similar particles that are held in place by an

adhesive. The only problem with such experiments, although not a serious one, that is that there is no exchange between moving particles and the sediment bed: while not in motion, the test particle always rest high, in a very exposed position, and can never move into a low position (often called a **pocket**) recently vacated by another entrained particle. Such experiments have been reported by Meland and Norrman (1966), Francis (1973), Abbott and Francis (1977), and Nakagawa et al. (1980). Valuable as these single-particle studies are, however, there is no substitute for watching the motion of bed-load particles on real sediment beds. The observational difficulties are formidable: one needs clear water (no suspended load to obscure the view), a magnified close-up view, and, ideally, high-speed filming or video recording, because the rapidity with which the state of particle motion changes makes it not very productive to watch particle motions in real time.

Meland and Norrman (1966) distinguished three stages of particle motion:

1. In the stage of **"stop-and-go" movement**, the particle is for a part of the time trapped between other particles on the bed. This stage follows initiation of motion and is especially typical of particles smaller than the average bed material. At this stage a very small increase in u_* above the critical value produces a marked increase in the average rate of particle movement, which however is controlled mainly by the bed and particle size.
2. In the stage of **continuous movement in contact with the bed**, the particle rolls or skims over the surface of the bed.
3. In the highest stage, particles begin to be **lifted up above the bed level or to make long jumps**. Increases in particle velocity are roughly proportional to increases in shear velocity.

Francis (1973) also distinguished three modes of movement, although they do not correspond exactly with the stages described by Meland and Norrman:

1. **rolling** of particles in contact with the bed (roughly equivalent to stages 1 and 2 of Meland and Norrman);
2. **saltation**, with particles rising up to heights of about two to four particle diameters above the bed and then falling back along "ballistic" paths, as illustrated in Figure 10.4.1; and
3. **suspension**, in which at first particles move in "leaps" that are distinguished from saltation by their length and sinuous trajectories (Figure 10.4.1), but as suspension becomes better developed the particles rise farther above the bed and return to it less often.

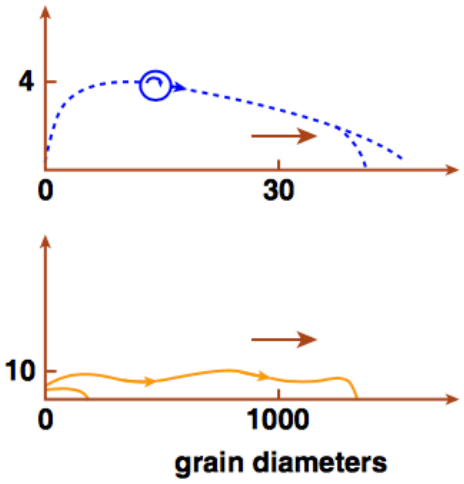


Figure by MIT OpenCourseWare.

Figure 10.4.1: Sketches of typical particle trajectories observed by Francis (1973). Above: saltation trajectory. Below: suspension trajectory (wavy line, with saltation trajectory shown to same scale for comparison. (From Francis, 1973.)

Francis (1973) distinguished saltation from suspension on the basis of a qualitative assessment of the particle trajectory. Abbott and Francis (1977, p. 229) suggested a more rigorous definition: a particle is in saltation when it "jumps away from the bed and follows such a trajectory that its vertical acceleration is always directed downwards between the upward impulses sustained while in contact with the bed." If at any time the vertical acceleration is directed upwards, then the particle is regarded as being in suspension. According to this definition, whether or not a particle is in suspension cannot be determined simply from qualitative observation: a detailed analysis of the vertical component of its acceleration, based on high-speed photography of its trajectory, is needed. Further discussion of the nature of saltation (which is better developed in air than in water) will be deferred until we have examined some of the experimental results on the relation between flow intensity and rate of sediment movement. The mode of movement at shear velocities just above the threshold value u_{*c} predicted by the Shields diagram was investigated by Abbott and Francis (1977), with the results shown in Figure 10.4.2.

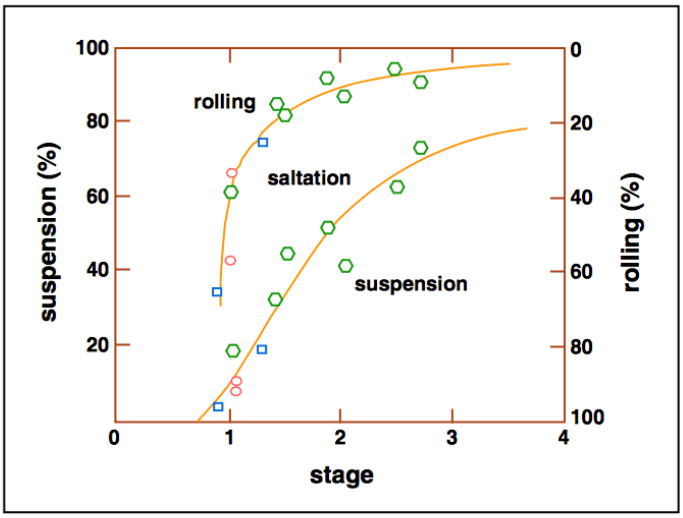


Figure by MIT OpenCourseWare.

Figure $10.4.2$: Trajectories of a saltating glass sphere calculated for the case of drag only (non-rotating sphere) and drag plus lift (a sphere rotating 275 times per second) compared with the observed trajectory. It can be seen that spinning produced a large effect both on the shape of the trajectory and on the maximum height of rise. (From White and Schultz, 1977.)

The earliest particle movements, at u_*/u_{*c} of about 1 (corresponding to u_*/w about 0.15), are by rolling, but as the flow intensity increases, saltation rapidly becomes the dominant mode of particle movement. By the time u_*/w has reached values of only about 0.3, about 50% of the particle trajectories are classified as being in the suspension mode, using the strict definition of Abbott and Francis (1977), but the particles follow paths that are still very close to the bed, and the average speed of the particles, U_G, is roughly proportional to the shear velocity. (U_G/u_* is about 6 to 8, indicating that the speed of the particle is almost equal to that of the flow close to the bed) At $u_*/w = 0.5$ most trajectories would be classified by Abbott and Francis (1977) as in the suspension mode, but the particles are still moving mainly close to the bed in a mode that might be subjectively described by most observers as being more like saltation than true suspension.

As flow intensities are increased further, particle trajectories become longer and more irregular and the particles are carried higher into the flow. At these higher intensities it seems more reasonable to normalize the average speed of particle movement by dividing by mean flow velocity U (a property of the main flow) than by dividing by shear velocity u_* (a property of the flow just above the bed). Abbott and Francis (1977, and see Francis, 1973) found that for particles of equal density U_G/U was directly related to w/u_*, the reciprocal of u_*/w (Figure $10.4.3$). At u_*/w greater than 0.5 the average particle speed was actually higher than the mean flow velocity, because most trajectories carried the particles up into the higher and therefore more rapidly moving parts of the flow. (Earlier experiments reported by Francis, 1973, suggest that in most cases U_G/U does not approach 1 until u_*/w approaches 1.) This is consistent with the suspension criterion, $u_* > w$, introduced in an earlier section.

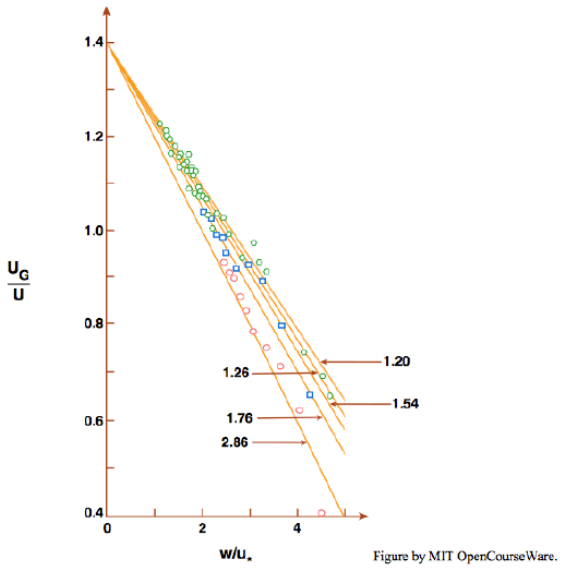


Figure $10.4.3$: Plot of dimensionless particle speed U_G/U vs. the ratio of particle settling velocity to shear velocity, w/u_*. Different symbols and lines refer to experimental particles of different specific gravities. (From Abbott and Francis, 1977.)

In his pioneer stochastic model for particle movement, Einstein (1950) postulated that the average distance traveled by a particle moving as bed load does not depend upon the flow intensity. Fernandez Luque (1974; see also Fernandez Luque and van Beek, 1976), in observations of particles moving over a loose planar bed at shear stresses only slightly larger than critical, found from direct observation that the average length of individual particle "steps" (or saltation jumps) was a constant equal to 16 times the particle diameter. Particles accelerated slightly at the beginning of each jump and decelerated upon returning to the bed but generally did not come to rest. On the average a particle jumped about 18 times, for a total step length of 288 particle diameters, before coming to rest. The average velocity while moving was reduced by collisions with the bed surface to about 85% of the maximum velocity achieved in each jump.

There have been few observational studies of the motions of bed-load particles in flows over loose rather than immobilized, sediment beds. Drake et al. (1988), in a study that shows how much information about particle motions can be obtained by carefully arranged observation, recorded the movements of bed-load particles on the bed of a clear-water stream by means of high-speed cinematography. The stream was $6.45\ \mathrm{m}$ wide and $0.35\ \mathrm{m}$ deep, and the bed consisted of moderately sorted sand and gravel with a median size of $4\ \mathrm{mm}$. During filming, the bed shear stress was about $6\ \mathrm{Pa}$, which was about twice the threshold for movement. There was active bed-load movement, but the concentration of bed load was not so great as to obscure the motions of the particles. The particles moved mainly by rolling, although the finest moved by saltation, and large, angular particles moved by brief sliding, pushing smaller particles out of the way. Displacement times for individual particles, which lasted for a few tenths of a second, were much shorter than repose times. Figure $10.4.4$ shows representative trajectories of four particles, of various sizes, as seen in side view, taken from the motion-picture frames.

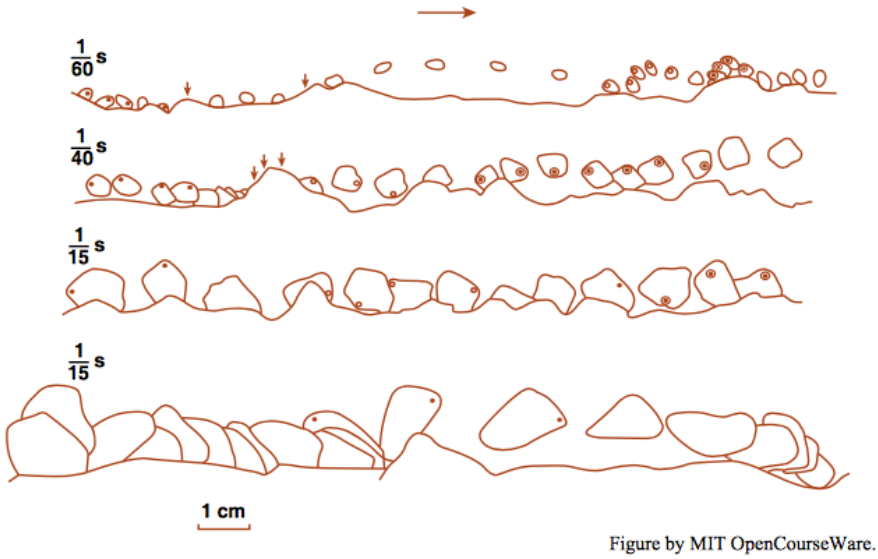


Figure by MIT OpenCourseWare.

Figure 10.4.4: Typical bed-load trajectories of four particles of differing sizes, traced from side-view high-speed motion pictures in a stream with median bed- material size of 4 mm. The filming speed, in frames per second, is given for each trajectory. (From Drake et al., 1988.)

Effect of Shape

The movement of particles on the bed is strongly affected by their shape. Particles tend to become oriented on the bed by pivoting around other particles or resting against them, and they do not necessarily orient themselves with their maximum projection area normal to the flow, as they generally do during settling. Certain shapes—notably prolate forms (rollers) but also disks— roll more easily than others.

An early experimental study of the effect of shape was made by Krumbein (1942) using artificial ellipsoidal particles, all with the same nominal diameter, in a flume with a smooth bed. Depth was held constant at 0.3 m and velocity was varied by changing the slope. Krumbein found that, for a given fluid velocity, spheres and rollers moved fastest. Within any one shape class (e.g., rollers), particles velocity increased with increasing sphericity; the shape effect was greatest at low fluid velocities and particle velocities, and was less important as particles tended to be taken into suspension.

Lane and Carlson (1954) found that pebbles lining the beds of Colorado drainage canals were sorted by both size and shape. In a given sample of bed pebbles the disk-shaped pebbles had substantially smaller volumes than the more spherical pebbles—the opposite of what would be the case if the pebbles had the same settling velocity—indicating that spherical pebbles rolled more easily and were more easily set in motion than disk-shaped pebbles, which tended to assume more stable, imbricated orientations on the bed.

Bradley et al. (1972) studied the effect of shape both in the field (Knik River, Alaska) and in the laboratory. They detected downstream sorting of shapes, with platy pebbles being the most easily transported, then elongate pebbles (rollers), and more equant pebbles being the least easily transported. They recognized that the anomalies in the shape effects observed in different field and laboratory investigations are probably caused by the different shape-sorting effects of particles moving by traction and by suspension. The readier transport of bladed pebbles can probably be explained by their observed “erratic saltation” type of motion, which tends to lift the bladed particles up into the flow, so that at sufficiently high fluid velocities their low settling velocity is more important than their poor rollability.

Bed Loading Movement at High Flow Intensities

As the flow intensity increases, and bed load becomes more abundant, the bed-load layer becomes thicker and the separation distance between bed-load particles becomes smaller. The difficulties of observing the details of particle motions in such thick, high-concentration bed-load layers become formidable— one might even say insurmountable. It seems fair to say that the ratio of hard observational data to theoretical deduction is probably lower in this area of sediment transport than in any other. The literature is replete with speculation about the forces and motions involved.

We start with the classic work of Bagnold (1954, 1956), which has played such an important role in subsequent thinking. Bagnold made pioneering experiments on interparticle forces in a strongly sheared mixture of water and solid particles. The experiments were made in a small, table-top apparatus that consisted of two concentric cylinders, with a thin annular space between. The inner cylinder was held stationary and the outer cylinder was rotated, giving almost uniform shear in the annular space, much like the hypothetical kitchen-table experiment described in Chapter 1. The annular space was filled with water containing a certain concentration of neutrally buoyant solid spherical particles. For a range of particle concentrations and rotation rates, Bagnold measured both the shear stress and the normal stress on the wall of the inner cylinder. He observed that both the normal stress and the shear stress were in excess of those for zero particle concentration, and he attributed these stresses, which he called dispersive stresses, to the intuitively reasonable effect of lateral forces engendered by particle interactions in the sheared mixture. Such interactions might be actual ballistic collisions, albeit cushioned to a greater or lesser degree by the ambient fluid, or they might only involve lateral particle motions caused by distortions of the local flow field by the presence of nearby particles moving at different speeds in the sheared medium.

It is easy to develop a dimensionless framework in which to evaluate the results of Bagnold's experiments. Imagine that you are weightless, high above the Earth in a space station. You are equipped, somehow, to do the experiment described in Chapter 1, shearing a fluid between parallel plates, but without having to worry about leakage of fluid around the edges. You are at liberty to use particles of any density, because you do not have to be concerned that the particles will settle under their own weight or be centrifuged in a rotating device.

Which variables would govern the dispersive normal stress and dispersive shear stress of the kind that Bagnold observed in his experiments (Figure 10-9)? Plate spacing L and relative plate velocity V are not important by themselves but only in combination to give the shear rate V/L; call that R. The others are straightforward: density and viscosity of the fluid, and density, size, and concentration of the particles. You can nondimensionalize the stresses in a way similar to a particle Reynolds number: $(T/\rho)^{1/2}D/\mu$, and $(P/\rho)^{1/2}D/\mu$. One obvious independent dimensionless variable is ρ_s/ρ , the density ratio, and another is the concentration C itself, if it is taken to be a volume concentration. The third dimensionless variable needs to involve the shear rate; it is most natural to construct a variable in the form of a Reynolds number, $\rho RD^2/\mu$.

Bagnold's experiments were more restricted than your space-station experiment, because to avoid centrifugation he had to use neutrally buoyant particles. The implication of that is that the dispersive effects he found would have been even greater if ρ_s/ρ could have been greater, as with natural sediment in water.

The dispersive stresses Bagnold observed are now known to be important in a wide range of what are called **grain flows**: flows of loose solid particles caused by the direct force of gravity, without the necessary involvement of a fluid medium. Grain flows are important in certain natural environments, as in snow avalanches, certain kinds of landslides, and, on small scales, sand flows down the lee faces of eolian sand dunes, and in technology as well.

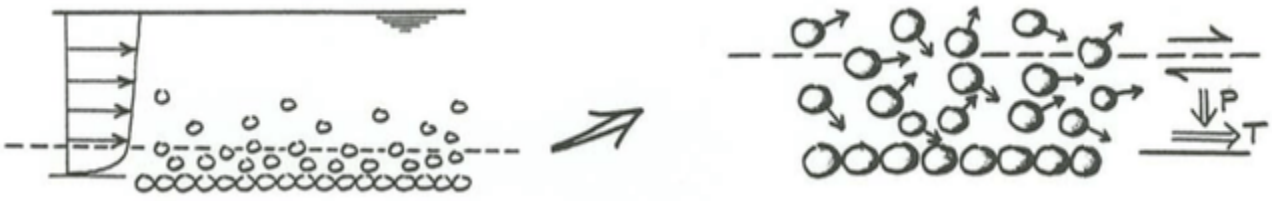


Figure $10.4.5$: The "gravity-bed case": a turbulent shear flow in a gravity field, transporting sediment particles denser than the fluid medium.

Bagnold (1956) took the further step of applying the concept of dispersive stresses to what he called the "gravity-bed case": a flow of fluid in a channel or conduit in a gravitational field, transporting denser particles near the bed, as what we would call, in the context of this chapter, bed load (Figure $10.4.5$). The idea is that if the flow is strong enough there can be a lowermost layer of transported sediment, with a thickness of many particle diameters, in which the shear is sufficiently strong that a dispersive normal stress makes its appearance and acts to maintain the bed-load layer in a dispersed state. Bagnold theorized that within this sheared and dispersed bed-load layer the fluid turbulence is unimportant, in the sense that it is not the principal agent that maintains the particles in the dispersed state. These ideas were later elaborated by Dzulynski and Sanders (1962), who applied the term **traction carpet** (which is in common use to this day; see, for example, Hiscott, 1994, 1995, and Sohn, 1995) to the concept, and by Moss (1972), who introduced the term **rheological layer** for essentially the same concept. A quotation from Moss (1972, p. 162) captures the essence of the phenomenon well:

> As bed-load motion becomes more intense in sand-sized materials, a stage is reached wherein collisions between particles become inevitable and thereafter the load proceeds as a dense mass of colliding particles, buoyed up by the dispersive

> pressure thus generated.... This moving mass of particles behaves like a viscous fluid, but has a remarkably sharp boundary with the flow above and maintains almost constant thickness over quite large bed areas.... (It) will be called the "rheological layer."

The problem is that although the concept of a dispersion layer is consistent with the well-established importance of dispersive stresses in certain ranges of shearing of particle–fluid mixtures, no one has ever seen inside one, owing to the obvious experimental difficulties. (One investigator—the writer of these notes!—once tried to overcome the observational difficulties by means of the seemingly ingenious technique of using monochromatic illumination of transparent sediment particles being transported in a concentrated bed-load layer by a transparent liquid with exactly the same index of refraction as the particles, in order to have a clear and unobstructed view of a few opaque fluid and sediment marker particles and record details of particle motions in the interior of the bed- load layer using high-speed cinematography. He could never get it to work well enough, though.) Until the importance of dispersive stress in concentrated bed- load layers is established by observation, rather than merely deduced, the concept is best regarded as hypothetical rather than as proven. Of course, traction carpets or rheological layers can still exist; it is just a matter of whether dispersive stresses or other effects like small-scale fluid turbulence are the more important factor in their dynamics.

Saltation in Water

In Chapter 11 you will learn that in the wind, saltation is the principal, and very characteristic, mode of particle movement. In saltation, particles take long, arching trajectories above the bed, little influenced by the turbulence in the flow. Here we address the question: What is the nature and relative importance of saltation in water? The importance of saltation in air is clear, but there is much less agreement on its importance in water. Saltating particle rise much higher above the bed in air (commonly a large fraction of a meter) than in water (only a few millimeters) because of the much greater effect of fluid drag and the reduced effect of particle inertia in water. Kalinske (1943) calculated that the height to which saltating particles would rise, for given particle size and shear velocity, should be inversely proportional to the fluid density, i.e., particles should rise 800 times higher in air than in water. Also, the criterion for suspension developed in a previous section, $u_* = w$, implies that particles should be relatively easily taken into suspension in water, because of the much lower settling velocity of particles in water than in air. Therefore most engineering writers (Einstein, 1950; Einstein and Chien, 1955; Ippen, 1971; Vanoni, 1975) have assumed that suspension by turbulence is a much more important mechanism of sediment transport in rivers than saltation, even quite close to the bed. In contrast to this view, Bagnold (1956, 1973) has argued that true saltation is independent of turbulence, and that high concentrations of particles close to the bed tend to suppress turbulence and make saltation (and particle collisions) the dominant mechanism of sediment transport.

Certain observations by Gordon et al. (1972), Fernandez Luque (1974), Fernandez Luque and van Beek (1976), and Abbott and Francis (1977) suggest that simple ballistic movement of particles, and movement by particles impacting on the bottom, may not be as important in water as some authors have held. Gordon et al. (1972) studied the saltation of spheres of diameter $6.6\ \mathrm{mm}$ and specific gravity 1.3 in a flow of water. Particle movement was made essentially two-dimensional by confining the flow within a flume only $7.9\ \mathrm{mm}$ wide. Observed trajectories were typical of saltation except that take-off angles were rather low, generally in the range of 10° to 35°. One reason for the low lift-off angle was that a saltating particle did not simply bounce off the loose particles on the bed; instead the moving particle rolled around the particle on the bed before lifting off to make another saltatory jump. There was a clear correlation between the fractional loss of kinetic energy and the angle of incidence in the collision, but the collisions were not simple elastic collisions; it seems clear that a combination of particle inertia and fluid drag forces was involved. Both Fernandez Luque (1974) and Abbott and Francis (1977), studying saltation in water, found that very few apparent saltations could be explained entirely as simple ballistic trajectories; some other kind of lift force was involved in most trajectories. These authors did not investigate Magnus effects, but it seems probable (particularly for the data reported by Francis) that the main lift was provided by turbulence. Abbott and Francis (1977, p. 253) found that "there appears to be an effective elastic rebound between the bed and a moving grain impinging on it." Very few observed saltations immediately followed the return of a particle to the bed; most were preceded by some rolling. Furthermore, there seemed to be no difference in take- off velocity between particles rebounding from the bed and particles beginning a saltation from rest or rolling.

Murphy and Hooshiari (1982) studied the saltation of marbles $15.7\ \mathrm{mm}$ in diameter on a bed of similar but fixed marbles. The settling velocity, about $0.8\ \mathrm{m/s}$, was much higher than the shear velocities needed to produce continuous saltation (0.08–$0.11\ \mathrm{m/s}$), so there is no doubt that saltation rather than suspension was the dominant mode of movement. In this case, particles appeared to be rebounding directly from the bed, though the exact mechanism of initial rise from the bed could not be studied by the stroboscopic technique used. Analysis of the trajectories indicated that they could be satisfactorily accounted for by a model that took into account gravity (and buoyancy), horizontal and vertical components of drag, and the added-mass effect that is produced by accelerating a solid through a fluid (Hamilton and Courtney, 1977). Magnus effects were not significant for particles of this size and shape in water. The observations suggest that bed impact forces are sufficient to produce the upward rise, and that lift forces

are not necessary. If this is true (and it is not proven, because the bed was rigid in the model, not loose as it would be in nature) then there is the possibility that saltation of larger (gravel-size) particles in water may be different from that of sand in water. It may be that the saltation of gravel in water is more like that of sand in air than that of sand in water.

All of the observations described above were made on flows in which very few particles were in saltation. Possibly fluid drag and lift play a much reduced role in initiating and maintaining saltation in a “traction carpet”, but the observations certainly suggest severe limitations on a simple impact hypothesis for saltation at low concentrations in water, and they indicate a very significant role for turbulence in transport of sand as bed load.

This page titled 10.4: Bed Load is shared under a CC BY-NC-SA 4.0 license and was authored, remixed, and/or curated by John Southard (MIT OpenCourseware) via source content that was edited to the style and standards of the LibreTexts platform.

10.5: Suspension in a Shear Flow- The Diffusional Theory of Suspension

Suspended particles are held up above the bed by the turbulent motion of the fluid. The weight of the particle is transmitted directly to the fluid, by way of the drag force exerted by the particles as they fall through the surrounding fluid, and increases the hydrostatic fluid pressure at the bed, in much the same way an airplane in flight increases the atmospheric pressure in an ill-defined circular area on the ground below. Suspended particles thus exert a force on the bed, albeit indirectly, in contrast to the direct forces exerted on the bed by moving bed-load particles.

It is theoretically possible for particles to move through the fluid close to the bed without actually being in contact with the bed, and yet not be in suspension. This happens in true saltation: the ballistic motion of the particles results from fluid lift forces and/or particles striking the bed, but it is not at all dependent on turbulence—and in fact Francis (1973) has described saltation of particles in a laminar flow. It has also been postulated that particles may be held in a dispersed state close to the bed by actual collisions between particles or by near-misses that produce viscous forces with vertical components that hold the particles above the bed. This is the "dispersive pressure" of Bagnold (1956), the effectiveness of which is still a matter for debate.

It was noted earlier in this chapter that particles first begin to travel in suspension when the vertical component of turbulence (or, more precisely, the normal-to-the-bed component of the turbulence) becomes about equal to the settling velocity of the particles (Equation 10.3.2). As noted earlier, there is no natural way to characterize the magnitude of this fluctuating component of the vertical fluid velocity, because it fluctuates over a wide range of values; the rms value is usually used to characterize its magnitude for this purpose. Contrary to a view that has sometimes been expressed in the literature, suspension does not depend on asymmetry in the frequency distribution of the vertical fluctuating velocities: provided that at least some of the vertical fluctuations are greater than the settling velocities of the particles, some of the particles experience suspension, even if the frequency distribution of fluctuating velocities is asymmetrical, because the conditions would still be conducive to diffusion (see Chapter 1): random motions of the medium, in combination with an upward gradient in sediment concentration, from nonzero in the bed-load layer to some smaller value, perhaps even zero, at some greater height above the bed. Such an asymmetry in the frequency distribution of vertical velocities might, however, affect the details of the concentration distribution.

Before dealing with the more important but more complicated case of suspension in a turbulent shear flow, we will look at suspension by homogeneous and isotropic turbulence. The characteristics of the turbulence do not vary from place to place within a certain region of the fluid, and neither do they vary with direction at any point within that region. Rouse (1939), the first to study sediment suspension in this way, produced a close approximation to isotropic turbulence by vertically oscillating an array of square grids in a large-diameter vertical cylinder ("turbulence jar").

The downward volume flux of particles by settling, from a region in the fluid having a concentration C of uniform-size particles, is $-wC$. It is reasonable to assume that the upward vertical diffusion of particles follows a Fickian diffusion law, like many other diffusion processes (see Chapter 1), so that the upward volume flux of particles by diffusion is $\varepsilon_S dC/dy$, where ε_S is a diffusion coefficient, which should be constant in a field of isotropic turbulence of any particular type and strength, and the positive y direction is upward. Equating the two fluxes gives an expression for the vertical distribution of the concentration of suspended particles:

$$wC + \varepsilon_S \frac{dC}{dy} = 0 \tag{10.5.1}$$

The resulting expression for suspended sediment concentration as a function of height y above the bed, developed below, is sometimes called the diffusional theory of suspended-sediment concentration. It also seems reasonable that the diffusion coefficient ε_S is proportional to, if not actually equal to, the corresponding coefficient for the diffusion of fluid momentum, i.e., the kinematic eddy viscosity, and therefore in a turbulence jar it should be proportional to the frequency of vertical oscillation of the grid. Rouse verified that this is the case, thus confirming the validity of the diffusion equation (see also experimental results reported by Antsyferov and Kos'yan, 1980).

In nature, homogeneous and isotropic turbulence is the exception; we have to deal with turbulence that typically varies in its characteristics with distance from the boundary, and at least to some extent with direction, mainly normal to the boundary at any point. In a turbulent shear flow, as for example, in a river, a tidal current, or a strong wind, where turbulence is not even approximately homogeneous and isotropic except perhaps at large distances from the bed, we should expect that the diffusion

coefficient varies in the direction y normal to the bed, so we need an expression that tells us how it varies with y before we can make use of Equation 10.5.1 to predict how the sediment concentration varies with y.

To find such an expression we assume the sediment diffusion coefficient ε_S to be proportional to the eddy viscosity ε, given by

$$\tau = \rho\varepsilon\frac{du}{dy} \tag{10.5.2}$$

Assuming that $\varepsilon_S = \beta\varepsilon$, then

$$\tau = \frac{\varepsilon_S\rho}{\beta}\frac{du}{dy} \tag{10.5.3}$$

where β is a coefficient that is likely to be close to one. You already know that τ varies linearly with y in uniform open channel flow,

$$\tau = \tau_o\left(1-\frac{y}{d}\right) \tag{10.5.4}$$

(see Chapter 4), so

$$\begin{aligned}\varepsilon_S &= \frac{\frac{\beta\tau_o}{\rho}\left(1-\frac{y}{d}\right)}{\frac{du}{dy}} \\ &= \frac{\beta u_*^2\left(1-\frac{y}{d}\right)}{\frac{du}{dy}}\end{aligned} \tag{10.5.5}$$

Using the law of the wall in differential form (Chapter 4),

$$\frac{du}{dy} = \frac{u_*}{\kappa y} \tag{10.5.6}$$

we have

$$\varepsilon_S = \beta u_*\left(1-\frac{y}{d}\right)\kappa y \tag{10.5.7}$$

Equation 10.5.7 is the relationship between ε_S and y that we need in order to solve Equation 10.5.3. Combining Equations 10.5.1 and 10.5.7 gives

$$\frac{dC}{C} = \frac{-wdy}{\beta\kappa u_*\left(1-\frac{y}{d}\right)y}label10.15 \tag{10.5.8}$$

which can be integrated to give the equation first derived by Rouse (1937):

$$\ln C = \frac{w}{\beta\kappa u_*}\int_a^d \frac{dy}{\left(1-\frac{y}{d}\right)y}label10.16 \tag{10.5.9}$$

or

$$\frac{C}{C_a} = \left(\frac{d-y}{y}\frac{a}{d-a}\right)^z \tag{10.5.10}$$

where

$$z = \frac{w}{\beta\kappa u_*} \tag{10.5.11}$$

The exponent z is sometimes called the **Rouse number**.

You can see from Equations 10.5.10 and 10.5.11 that the larger the value of z, the more rapidly the suspended-sediment concentration decreases with height above the reference level a. Equation 10.5.10, graphed in Figure 10.5.1, gives the concentration of suspended sediment of a given settling velocity w at a height y above the bed relative to its concentration C_a at an arbitrarily chosen "reference level" $y = a$ above the bed.

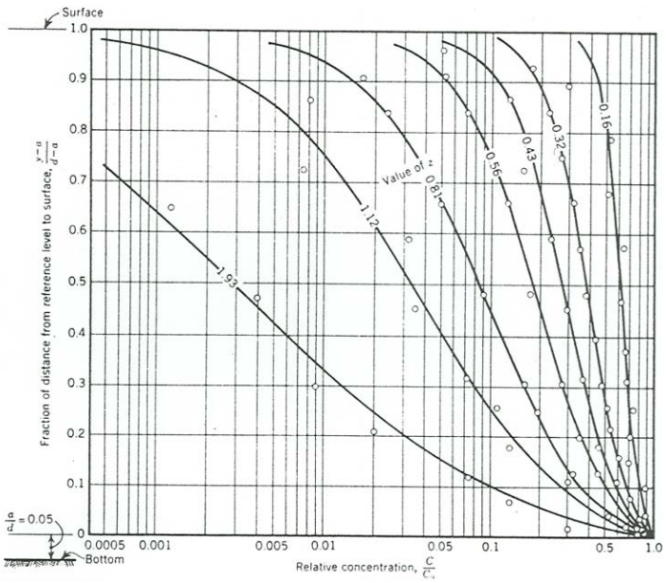


Figure 10.5.1: Courtesy of American Society of Civil Engineers. Used with permission. *Distribution of the relative concentrations of suspended sediment with relative depth above the datum* $y = 0.011 - 3711 - 485d$. *(From Vanoni, 1975.)*

Ideally, the reference concentration C_a would be taken to be as close to the bed as possible but still far enough above the bed that a balance between downward settling and upward turbulent diffusion of suspended sediment is physically reasonable. The theory fails very close to the bed, because a balance between passive upward turbulent diffusion and downward settling is not applicable there: particle movements at and very near the bed are controlled by fluid lift and drag forces, and if concentrations are high these movements may be significantly affected by collisions or interactions between particles. The reference height a above the bed is most naturally just above the bed-load layer. This is consistent with the idea that the sediment concentration at the top of the bed-load layer acts as a lower boundary condition for the distribution of suspended sediment higher in the flow. This points up the problem of specifying the suspended-sediment concentration in absolute rather than relative terms: no successful theory has been developed yet for the bed-load concentration as a function of flow and sediment conditions. Because the structure of the flow and the dynamics of bed-load movement are so complex in the near-bed layer when the flow is strong enough to move sediment in suspension, no elegant way has been developed to put this appealing idea, that the bed load forms the lower boundary condition for the suspended load, into useful practice.

Experiments to test Equation ??? were reported by Vanoni (1946). These experiments were mostly made at relatively high velocities over a planar bed (either a sand bed or the rigid floor of the flume) and at varying concentrations of sand. Vanoni found a general agreement between predicted and observed sediment concentrations (Figure 10.5.1).

Because both β and κ are supposed to be constants, the main factor that determines the distribution of suspended sediment with height y above the bed should be the ratio of the settling velocity w to the shear velocity u_*. It was suggested in an earlier section of this chapter that a critical ratio of about one determines whether any particles will go into suspension: since $\beta \approx 1$ and $\kappa \approx 0.4$, w/u_* less than one corresponds to z less than 2.5. We can see from Figure 10.5.1 that at values of z greater than 2.5 any sediment in suspension would be concentrated in a zone very close to the bed—and this tends to confirm the choice of w/u_* as a suitable criterion for suspension.

Two factors in open-channel flows have a direct effect on the ratio w/u_* and therefore on the vertical profile of suspended-sediment concentration: viscosity, and friction. First the viscosity: for a given particle size and shape, w is reduced by an increase in the viscosity sensed by the settling particles. That can be brought about in two ways: a reduction in the temperature of the fluid, which increases the viscosity of the fluid itself, or an increase in the wash-load concentration. In the latter case, the viscosity of the fluid remains the same but the effective viscosity of the deformable medium (the fluid charged with wash load) that is sensed by the particles of the suspended bed-material load, which are much larger than the particles of the wash load, is greater. Both of these effects act to reduce the ratio w/u_*, and hence the Rouse number z, and make sediment more uniformly distributed in the vertical (Equation ???). The fluid-viscosity effect diminishes with increasing settling-velocity Reynolds number, however, and becomes unimportant when the range of Reynolds numbers for which the drag coefficient is approximately constant is reached; see Chapter 2.

Now for the effect of friction: for a given mean flow velocity, an increase in the coefficient of bottom friction causes an increase in bottom shear stress, and therefore in shear velocity. To see why, go back to the definition of the friction factor f (Equation

4.7.7 in Chapter 4): $\tau_o = (f/8)\rho U^2$, or $U/u_* = (8/f)^{1/2}$. So an increase in the shear velocity also results in a more uniform vertical distribution of suspended sediment, by decreasing the ratio w/u_*. In sand-bed rivers, changes in f are produced mainly by changes in the relative roughness, which depends mainly on the nature and size of the bed forms. Large bed forms, like dunes, produce large values of f, and therefore cause suspended bed-material sediment to be distributed more uniformly in the vertical than if the bed were planar. In fact, it is been observed in flume studies that the vertically averaged suspended-sediment concentration actually decreases somewhat in the transition from a dune-covered sand bed to an upper-regime plane bed, with its accompanying decrease in flow resistance, as the flow velocity increases.

The theory of suspension by turbulent flows outlined above is based on the assumption that the flow is steady. This is be a reasonable approximation for most rivers, but tidal currents change quite rapidly in both depth and speed over the tidal cycle. It has been shown that in experimental turbulent shear flows, decelerating flows have larger turbulence intensities, and produce larger shear stresses on the bed, than steady flows. Decelerating flows therefore might be expected to be more erosive, and to have a higher capacity for suspended sediment, than steady or accelerating flows. Wimbush and Munk (1970), Gordon and Dohne (1973), Gordon (1975), Bohlen (1977), and McCave (1979) have reported measurements suggesting that turbulence intensities are higher than normal during deceleration of flows on both flood and ebb tides. Gordon (1975) and Bohlen (1977) have commented on the implications for transport of suspended sediment by tidal currents, but convincing direct evidence of the effect of deceleration on sediment transport by tidal currents is still lacking.

The diffusional theory of suspension presented above is based on the assumption that turbulence diffuses sediment according to a simple (“Fickian”) diffusion law. This assumption is in reasonably good accord with experiment, but it is not the only possible basis for a theory of sediment suspension. Alternative theories, based on different assumptions, are described by Nordin and McQuivey 1971), Drew (1975; see also Drew and Kogelman, 1975), Willis (1979), Herczynski and Pienkovska (1980), and McTigue (1981), among others.

Although the diffusional theory of sediment suspension has been described as “the brightest analytical achievement to date in the field of river hydraulics” (Hsu et al., 1980; see also Kennedy, 1984, p. 1257), in that it represents an elegant and rational theoretical approach, based on reasonably well understood physical effects, that does quite well in its predictions without relying upon any suspicious “fudge factors”, it is subject to a number of criticisms:

- The theory takes no account of the details of how the sediment particles are actually handled by the eddies in the turbulent flow field. There are two different aspects to this. One has to do with the interesting and counterintuitive effect of the tendency of eddies to trap sediment particles (Tooby et al. 1977; Nielsen, 1984), discussed briefly in Chapter 3. The other is that the theory assumes turbulence that is isotropic in its vertical motions, i.e., that the frequency distribution of the vertical velocity is symmetrical. There is good reason to believe, however, that close to the bed the vertical component is anisotropic (Leeder 1983a, 1983b): the less common upward motions are stronger than the more common downward motions in this region, as would be expected from the semicoherent burst–sweep structure of the near-bed turbulence (Chapter 4). As first proposed by Bagnold (1966), and further developed by Leeder (1983a, 1983b), the anisotropy in vertical turbulent velocities is what maintains sediment in suspension—with the implication that without this anisotropy the concentration of sediment in suspension would be much less. The flaw in this concept is that, to maintain balance of fluid masses passing upward and downward in the turbulence field, the downward-moving eddies must cover a greater area, in any plane through the flow that is parallel to the bottom boundary, than the upward-moving eddies, thus maintaining a balanced exchange of sediment even in the face of the vertical anisotropy of turbulence. Despite some assertions in the literature to the contrary, such anisotropy is only a minor distorting effect on the diffusional theory, and is not a necessary condition for the maintenance of bed-material sediment in suspension.
- Vanoni (1946, and many subsequent investigations reported and analyzed in Vanoni, 1975) found that in some experiments, particularly those in which there was a high concentration of coarse sediment close to the bed, the value of the supposedly universal von Kármán constant decreased from its accepted value of 0.38 to values as low as 0.2. He interpreted this as indicating that the presence of sand moving close to the boundary changed the structure of turbulence in the flow. The von Kármán constant κ plays a fundamental role in the diffusional theory of suspended sediment, by virtue of its effect on the gradient of time-average flow velocity in the law of the wall (Equation ???); if κ is itself affected nonnegligibly by the presence of suspended sediment, then it becomes part of the problem rather than an independent input to the problem, and the theory would become much more complicated.
- Besides the uncertainty about κ, several authors have reported large deviations of β from the expected value close to unity. There are reasons to expect that solid particles are not diffused at the same rate as fluid momentum, and that the ratio of the two rates of diffusion is not a constant but varies with the properties of both the sediment and the fluid turbulence. At present there is no satisfactory way to predict the value of β. Prediction presumably will become possible only when there is a better understanding of the mechanism of diffusion.
- In the usual theory the sediment diffusion coefficient is assumed to be proportional to the eddy viscosity and the distribution with depth to be given by Equation 10.5.11. This equation predicts that ε_S (and ε) drop slowly to zero as the free surface is

approached. Because sediment cannot diffuse through the free surface, ε_S must be equal to zero there. Coleman (1970) has, however, calculatedεs directly from observed values of C and dC/dy using Equation 10.5.1. He found that there is a strong dependence on depth only near the bed; over most of the flow, and even quite close to the free surface, ε_S appears to be independent of depth.

For all of these reasons, the diffusional theory of sediment suspension, though it is a better theory than that available for most aspects of sediment transport, must still be regarded as somewhat less than completely satisfactory.

A Note on the Effect of Acceleration of Gravity on Sediment Movement

It is worthwhile to consider how sediment movement and bed configurations in water flows might differ where the acceleration of gravity is different. Back in Chapter 8, in the section on dimensionless variables), a set of dimensionless variables was developed in which the leading variables in a sediment-transport system,—variables with dimensions of length, like particle size, or variables with dimensions of velocity—can be organized in such a way that each of the leading variables in sequestered in its own dimensionless version. In each such variable, the acceleration of gravity enters as well. If gravity is different, any length or velocity variable in a dynamically similar system must then also be different. Southard and Boguchwal (1990) show that, in the case of Mars, for which the acceleration of gravity is only about 0.4 times that of Earth, a length variable on Mars would be about 1.36 times that on Earth, and a velocity variable on Mars would be about 0.74 times that on earth, for a dynamically similar system.

References Cited Chapter 10

Abbott, J.E., and Francis, J.R.D., 1977, Saltation and suspension trajectories of solid grains in a water stream: Royal Society [London], Philosophical Transactions, v, 284, p. 225-254.

Antonia, R.A., and Luxton, R.E., 1971, The response of a turbulent boundary layer to a step change in surface roughness, Part 1, smooth to rough: Journal of Fluid Mechanics, v. 48, p. 721-761.

Antsyferov, S.M., and Kos'yan, R.D., 1980, Sediments suspended in stream flow: American Society of Civil Engineers, Proceedings, Journal of the Hydraulics Division, v. 106, p. 313-330.

Bagnold, R.A., 1954, Experiments on a gravity-free dispersion of large solid spheres in a Newtonian fluid under shear: Royal Society [London], Proceedings, v. A225, p. 49-63.

Bagnold, R.A., 1956, The flow of cohesionless grains in fluids: Royal Society [London], Philosophical Transactions, v. A249, p. 235-297.

Bagnold, R.A., 1966, An approach to the sediment transport problem from general physics: U.S. Geological Survey, Professional Paper 422-I, 37 p.

Bagnold, R.A., 1973, The nature of saltation and of “bed load” transport in water: Royal Society [London], Proceedings, v. A332, p. 473-504.

Blinco, P.H., and Partheniades. E., 1971, Turbulence characteristics in free surface flows over smooth and rough boundaries: Journal of Hydraulic Research v. 9, no. 8, p. 43-69.

Bohlen. W.F., 1977, Shear stress and sediment transport in unsteady turbulent flows: in Wiley, M., ed., Estuarine Processes. Vol. I. Uses, Stresses, and Adaptation to the Estuary, p. 109-123: New York, Academic Press, Vol. 2, 541 p

Bradley. W.C.. Fahnestock, R.K., and Rowekamp, E.T., 1972, Coarse sediment transport by flood flows, Knik River, Alaska: Geological Society of America, Bulletin, v. 83, p. 1261-1284.

Bridge, J.S., 1978, Origin of horizontal lamination under turbulent boundary layers: Sedimentary Geology, v. 20, p. 1-16.

Coleman, N.L., 1970, Flume studies of the sediment transfer coefficient: Water Resources Research, v. 6, p. 801-809.

Drake, T.G., Shreve, R.L., Dietrich, W.E., Whiting, P.J., and Leopold, L.J., 1988, Bedload transport of fine gravel observed by motion-

picture photography: Journal of Fluid Mechanics, v. 192, p. 193-217.

Drew, D.A., 1975, Turbulent sediment transport over a flat bottom using momentum balance: Journal of Applied Mechanics, v. 42, p. 38-44.

Drew, D.A., and Kogelman, S., 1975, Turbulent sediment transport using momentum balance—the strong turbulence approximation: Applied Science Research, v. 30, p. 279-290.

Dzulynski, S., and Sanders, J.E., 1962, Current marks on firm mud bottoms: Connecticut Academy of Arts and Sciences, Transactions, v. 42, p. 57-96.

Einstein, H.A., 1950, The bed-loan function for sediment transportation in open channel flows: U.S. Department of Agriculture, Technical Bulletin 1026, 70 p. (reprinted as Appendix B in Shen, H.W., ed. 1972, Sedimentation, Fort Collins, Colorado).

Einstein, H.A., and Chien, N., 1955, Effects of heavy sediment concentration near the bed on velocity and sediment distribution: U.S. Army Corps of Engineers, Missouri River Division, M.R.D. Sediment Series no. 8, 76 p.

Fernandez Luque, R., 1974, Erosion and Transport of Bed-Load Sediment: Ph.D. Thesis, Technical Highschool, Delft, Holland, Krips. Repro. B.V., Meppel, 65 p. plus tables and figs.

Fernandez Luque, R., and Van Beek, R., 1976, Erosion and transport of bed-load sediment: Journal of Hydraulic Research, v. 14, p. 127-144.

Francis, J.R.D., 1973, Experiments on the motion of solitary grains along the bed of a water-stream: Royal Society [London], Proceedings, v. A332, p. 443-471.

Gordon, C.M., 1975, Sediment entrainment and suspension in a turbulent tidal flow: Marine Geology, v. 18, p. M57-M64.

Gordon, C.M., and Dohne, C.F., 1973, Some observations on turbulent flows in a tidal estuary: Journal of Geophysical Research, v. 78, p. 1971-1978.

Gordon, R., Carmichael, J.B., and Isackson, F.J., 1972, Saltation of plastic balls in a “one- dimensional” flume: Water Resources Research, v. 8, p. 444-459

Grass, A.J., 1971, Structural features of turbulent flow over smooth and rough boundaries: Journal of Fluid Mechanics, v. 4, p. 149-190.

Grass, A.J.. 1974, Transport of fine sand on a flat bed: turbulence and suspension mechanics: Technical University of Denmark, Proceedings Euromech 48, p. 33- 34.

Hamilton, W.S., and Courtney, G.L., 1977, Added mass of sphere starting upward near floor: American Society of Civil Engineers, Proceedings, Journal of the Engineering Mechanics Division, v. 103, p. 79-97.

Herczynski, R., and Pienkovska, I., 1980, Toward a statistical theory of suspension: Annual Review of Fluid Mechanics, v. 12, p. 237-269.

Hiscott, R.N., 1994, Traction-carpet stratification in turbidites—Fact or fiction?: Journal of Sedimentary Research, v. A64, p. 204-208.

Hiscott, R.N., 1995, Traction-carpet stratification in turbidites—Fact or fiction?—Reply: Journal of Sedimentary Research, v. A65, p. 704-705.

Hsu, S.T., van der Beken, A., Landweber, L., and Kennedy, J.F., 1980, Sediment suspension in turbulent pipe flow: American Society of Civil Engineers, Proceedings, Journal of the Hydraulics Division, v. 106, p. 1783-1793.

Ippen, A.T., 1971, A new look at sedimentation in turbulent streams: Boston Society of Civil Engineers, Proceedings, v. 58, p. 131-161.

Jackson, R.G., 1976, Sedimentological and fluid dynamic implications of the turbulent bursting phenomenon in geophysical flows: Journal of Fluid Mechanics, v. 77, p. 531-560.

Kalinske, A.A., 1943, Turbulence and the transport of sand and silt by wind: New York Academy of Science, Annals, v. 44, p. 41-54.

Karcz, I., 1973, Reflections on the origin of some small-scale longitudinal streambed scours in Morisawa, M., ed., Fluvial Geomorphology: 4th Annual Geomorphology Symposium, Proceedings, State University of New York at Binghamton, Publications in Geomorphology, p. 149-173.

Kennedy, J.F., 1984, Reflections on rivers, research and Rouse: Journal of Hydraulic Engineering, v. 109, p. 1254-1271.

Krumbein, W.C., 1942, Settling velocity and flume-behavior of non-spherical particles: American Geophysical Union, Transactions v. 23, p. 621-632.

Lane, E.W., and Carlson, E.J., 1954, Some observations on the effect of particle shape on the movement of coarse sediments: American Geophysical Union, Transactions, v. 35, p. 453-462.

Leeder, M.R., 1983a, On the interactions between turbulent flow, sediment transport and bedform mechanics in channelized flow: International Association of Sedimentologists, Special Publication 6, p. 5-18.

Leeder, M.R., 1983b, On the dynamics of sediment suspension by residual Reynolds stresses—confirmation of Bagnold's theory: Sedimentology, v. 30, p. 485-491.

Mantz, P.A., 1977, Incipient transport of fine grains and flakes by fluids—extended shields diagram: American Society of Civil Engineers, Proceedings, Journal of the Hydraulics Division, v. 103, p. 601-615.

McCave, I.N., 1979, Tidal currents at the North Hines Lightship, southern North Sea: Flow directions and turbulence in relation to maintenance of sand bars: Marine Geology, v. 31, p. 101-113.

McQuivey, R.S., and Richardson, E.V., 1969, Some turbulence measurements in open- channel flows: American Society of Civil Engineers, Proceedings, Journal of the Hydraulics Division, v. 95, p. 209-223.

McTigue, D.F., 1981, Mixture theory for suspended sediment transport: American Society of Civil Engineers, Proceedings, Journal of the Hydraulics Division, v. 107, p. 659- 673.

Meland, N., and Norrman, J.O., 1966, Transport velocities of single particles in bed-load motion: Geografiska Annaler, v. A48, p. 165-182.

Middleton, G.V., 1976, Hydraulic interpretation of sand size distributions: Journal of Geology, v. 84, p. 405-426.

Moss, A.J., 1972, Bed-load sediments: Sedimentology, 18, p. 159-219.

Murphy, P.J., and Hooshiari, H., 1982, Saltation in water dynamics: American Society of Civil Engineers, Proceedings, Journal of the Hydraulics Division, v. 108, p. 1251- 1267.

Nakagawa, H., and Tsujimoto, T., 1980, Statistical analysis of sediment motions on dunes—discussion: American Society of Civil Engineers, Proceedings, Journal of the Hydraulics Division, v. 106, p. 221-226.

Nielsen, P., 1984, On the motion of suspended sand particles: Journal of Geophysical Research, v. 89, p. 616-626.

Nordin, C.F., and McQuivey, R.S., 1971, Suspended load, in Shen, H.W., ed., River Mechanics, Vol 1, p. 12-1–12-30.

Rouse, H., 1937, Modern conceptions of the mechanics of turbulence: American Society of Civil Engineers, Transactions, v. 102, p. 436-505.

Rouse, H., 1939, Experiments on the mechanics of sediment suspension: 5th International Congress on Applied Mechanics, Cambridge, Mass., p. 550-554.

Sohn, Y.K., 1995, Traction-carpet stratification in turbidites—fact or fiction?— Discussion: Journal of Sedimentary Research, v. A65, p. 703-705.

Southard, J.B., and Boguchwal, L.A., 1990, Bed configurations in steady unidirectional water flows. Part 3. Effects of temperature and gravity: Journal of Sedimentary Petrology, v. 60, p. 680-686.

Sumer, B.M., and Deigaard, R., 1981, Particle motions near the bottom in turbulent flow in an open channel, Part 2: Journal of Fluid Mechanics, v. 109, p. 311-337.

Sumer, B.M., and Oguz, B., 1978, Particle motions near the bottom in turbulent flow in an open channel: Journal of Fluid Mechanics, v. 86, p. 109-128.

Tooby, P.F., Wick, G.L., and Isaacs, J.D., 1977, The motion of a small sphere in a rotating velocity field: a possible mechanism for suspending particles in turbulence: Journal of Geophysical Research, v. 82, p. 2096-2100.

Vanoni, V.A., 1946, Transportation of sediment in suspension: American Society of Civil Engineers, Transactions, v. 111, p. 67-133,

Vanoni, V.A., 1964, Measurements of critical shear stress for entraining fine sediments in a boundary layer: California Institute of Technology, W. M. Keck Laboratory of Hydraulics and Water Resources, Report KH-R-7, 47 p.

Vanoni, V.A., ed., 1975, Sedimentation Engineering: American Society of Civil Engineers, Manuals and Reports on Engineering Practice, No. 54, 745 p.

Willetts, B., 1998, Aeolian and fluvial grain transport: Royal Society (London), Philosophical Transactions, v. A356, p. 2497-2513.

Williams, G., 1964, Some aspects of the eolian saltation load: Sedimentology, v. 3, p. 257-287.

Willis, J.C., 1979, Suspended load from error-function models: American Society of Civil Engineers, Proceedings, Journal of the Hydraulics Division, v. 105, p. 801-816.

Wimbush, M., and Munk, W., 1970, The benthic boundary layer, in Maxwell, A. E., ed., The Sea, Vol. 4, Part 1, Ch. 19, p. 31-758: New York, Wiley-Interscience, 791 p.

This page titled 10.5: Suspension in a Shear Flow- The Diffusional Theory of Suspension is shared under a CC BY-NC-SA 4.0 license and was authored, remixed, and/or curated by John Southard (MIT OpenCourseware) via source content that was edited to the style and standards of the LibreTexts platform.

11: MOVEMENT OF SEDIMENT BY THE WIND

Research in the field of eolian sediment transport, over the past several decades, has fallen fairly naturally into three overlapping areas: soil erosion; transport of sand by saltation; and the nature and dynamics of eolian bed forms (wind ripples and eolian dunes). (The adjective *eolian*, meaning *produced*, *eroded*, *carried*, or deposited by *the wind*, and spelled *aeolian* in British-style English, comes from the name of a minor Greek god, Aeolos, who was the keeper of the four winds; see the Encyclopedia Mythica or the Wikipedia on the Internet for more information.) This chapter deals with the second of those areas. Loess—deposits of windblown silt that is carried in suspension far from its source, for tens or even hundreds of kilometers—covers a far larger percentage of the Earth's surface than eolian sand, and it is important for agriculture in many parts of the world, but the topic of loess deposition is beyond the scope of these notes.

11.1: Introduction

11.2: Saltation I

11.3: Saltation II

This page titled 11: Movement of Sediment by the Wind is shared under a CC BY-NC-SA 4.0 license and was authored, remixed, and/or curated by John Southard (MIT OpenCourseware) via source content that was edited to the style and standards of the LibreTexts platform.

11.1: Introduction

Everyone knows that winds on the Earth are commonly strong enough to erode, transport, and deposit sediment. What is perhaps less obvious is that the modes of sediment transport by the wind are greatly different from those of sediment transport by water flows. This great difference does not arise from any great difference in the structure of the wind at the lowermost levels in the atmosphere: you saw in Chapter 7 that low in the atmospheric boundary layer the dynamics of flow are the same in all essential respects as in turbulent shear flows above a solid boundary in water. The difference lies in the greatly different ratio of sediment density to fluid density, which is almost eight hundred times greater in air than in water; go back and look at Figure 8.1.5 in Chapter 8 to see where the point for ρ_s/ρ lies for quartz-density particles in air, relative to the point for quartz-density particles in water. This difference has profound effects on the nature of particle movement in the two fluid media. As discussed briefly in Chapter 8, the very large ratio of particle density to air density means that the trajectories of particles that are in transport by the wind are largely independent of the fluid turbulence, except for fine particles, in the silt and clay size range.

Another important difference between sediment transport by wind and sediment transport by water is that the wind is a more efficient size-sorting agent. For transport by water, it is broadly true that larger particles are more difficult to move than finer particles—silts are moved much more readily than gravels, for example—but the weakness of this effect is highlighted by the nearly equal mobility of a wide range of sand to gravel sizes in many flow settings, as discussed in Chapter 14. By contrast, the wind entrains dust and silt much more readily than sand, provided that the sediment is not bound to the substrate by cohesive forces, and gravel is much more difficult to move than sand. Except in the very strongest winds, all but the finest gravel sizes are invariably immobile, whereas water flows, even leaving rheological flows like debris flows out of account, can move even large boulders if the flow is sufficiently strong.

It is not an exaggeration for me to say that the modern era of study of sand movement by the wind started with R.A. Bagnold's work in the deserts of North Africa in the 1930s, which culminated in the publication of his little book (literally "little": 265 pages in a book measuring 22 cm by 14 cm) *The Physics of Blown Sand and Desert Dunes* in 1941. It is a classic, in the fullest sense of the term: it is an outstanding example of a magisterial work that sets the course of future work in a field of science for many decades. It is by far the most widely cited work on eolian sediment movement, and it remains essential reading for anyone who is seriously interested in the topic. Also, several extensive early wind-tunnel studies of eolian sand transport, with results that are still valuable today, are worthy of mention (Kawamura, 1951; Zingg, 1952, 1953; Horikawa and Shen, 1960; Belly, 1964). Chepil, in a long series of papers, (see especially Chepil, 1945, 1958, 1959), was the pioneer in modern studies of wind erosion of soils; some of his work bears directly upon the transport of loose sand by wind. After the appearance of a multitude of papers on saltation from the mid-1970s to the mid-1990s, in large part from just a few groups of researchers (Greeley and co-workers; Willetts and co-workers; Anderson, Haff, and co-workers; see the list of references at the end of the chapter), the frequency of published works on saltation has decreased somewhat. You are likely to get that impression if you scan the list of references. For clear reviews of the eolian sediment movement, see Greeley and Iversen (1985), Anderson (1989), Anderson et al. (1991), and Willetts (1998).

Research in the field of eolian sediment transport, over the past several decades, has fallen fairly naturally into three overlapping areas: soil erosion; transport of sand by saltation; and the nature and dynamics of eolian bed forms (wind ripples and eolian dunes). (The adjective *eolian*, meaning *produced*, *eroded*, *carried*, or deposited by *the wind*, and spelled *aeolian* in British-style English, comes from the name of a minor Greek god, Aeolos, who was the keeper of the four winds; see the Encyclopedia Mythica or the Wikipedia on the Internet for more information.) This chapter deals with the second of those areas. Loess—deposits of windblown silt that is carried in suspension far from its source, for tens or even hundreds of kilometers—covers a far larger percentage of the Earth's surface than eolian sand, and it is important for agriculture in many parts of the world, but the topic of loess deposition is beyond the scope of these notes.

This page titled 11.1: Introduction is shared under a CC BY-NC-SA 4.0 license and was authored, remixed, and/or curated by John Southard (MIT OpenCourseware) via source content that was edited to the style and standards of the LibreTexts platform.

11.2: Saltation I

Introduction

The characteristic mode of motion of sand particles in air is **saltation**: particles are launched from the bed, take arching trajectories of widely varying heights and lengths, and splash down onto the bed at low angles, commonly rebounding and/or putting other particles into motion. The term, introduced into geology by McGee (1908, p. 199), is derived from the Latin verb *saltare*, meaning to jump or leap. Movement by saltation has also been invoked for water transport of particles near the bed (see chapter 10), although the distinctiveness of saltation in water is not nearly as clear as in air.

Saltation in air became well known through the early experimental studies by Bagnold (1941), Chepil (1945), Zingg (1952), and others. In recent years there has been much attention to eolian saltation, in part because of the growing concern over desertification, and also in part because of the interest in how sediment is transported by wind on other planets—most especially, Mars. Early studies of saltation dealt in large part with the nature and dynamics of saltation trajectories. Later, especially during the late 1980s and early 1990s, emphasis tended to shift to a more unified consideration of the overall saltation system produced by a steady wind. In more recent years, this has extended to study of saltation in the unsteady winds characteristic of natural environments. Also, as computational power has grown it has become possible to develop increasingly sophisticated numerical models of saltation.

The study of saltation can be viewed as falling into several related areas:

- threshold for motion
- forces causing liftoff
- the geometry and dynamics of particle trajectories, including the distributions of jump height and jump distance
- the effects of wind velocity and of sediment size, sorting, and particle shape on mode of saltation and on saltation transport rates
- the effect of unsteadiness of the wind on saltation
- the effect of the saltation cloud on the structure of the near-surface wind

To some extent it is artificial to treat these topics separately, but nonetheless it seems helpful in developing clear understanding. Accordingly, each of these topics treated in sections below, after some comments about observing saltation.

Saltating particles are highly abrasive, because of their very large relative inertia—much greater than for water-borne particles. Both natural and artificial solid materials at heights within the saltation cloud, even hard rocks, are gradually abraded. Saltating sand also sculpts distinctive eolian landforms. Such topics are not within the scope of these notes.

As the size of particles in saltation decreases toward the silt range, the decrease in particle mass means an increasing effect of turbulence on particle trajectories. Wind speed is important in this respect as well, inasmuch as the characteristic magnitude of velocity fluctuations from eddy to eddy increases with mean wind speed. At sufficiently fine particle sizes, and for sufficiently strong winds, the particles are carried in suspension rather than in saltation; see Figure 11.2.1 (in the same spirit as Figure 10.3.1 in Chapter 10), showing in cartoon form the regions of distinctive modes of eolian particle movement as a function of sediment size and wind speed. What is known about the transition from saltation to suspension is described in a later section of this chapter.

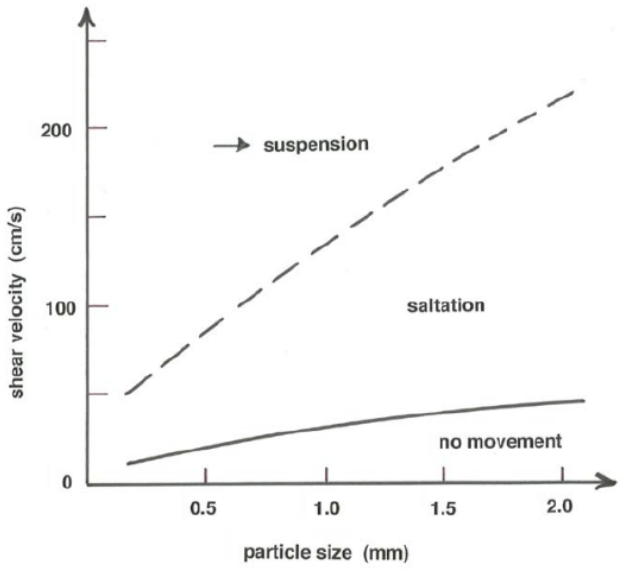


Figure 2 of Owen, 1964.)

A distinction is commonly made between saltation, whereby particles take ballistic excursions well above the bed, and **surface creep** (also called **impact creep** or **reptation**), whereby particles are moved for short distances without losing contact with the bed surface. Particles that are too large to be moved in saltation (but not so large as to be immovable by the given wind) characteristically engage in surface creep. Particles of sizes susceptible to saltation can also move as creep, however, if a saltation impact is sufficient only to impart slight movement to a given particle on the bed surface. Even in very well sorted sediments, surface creep as well as saltation is an important mode of transport.

Observing Saltation

The very best way to appreciate saltation is to observe it for yourself. Imagine yourself out on the surface of a sand dune on a windy day. If you get your eye level down to within a few decimeters of the surface—you risk getting sand in your eyes, ears, nose, and mouth—and sight horizontally across the wind, you see a blurry layer of saltating sand, with concentration tailing off upward for as much as a meter above the surface. You are seeing the characteristic saltation cloud. Unfortunately, your eye cannot easily follow the trajectories of individual particles.

To see saltation trajectories clearly, you need to build your own wind tunnel (Figure 11.2.2). That's not a difficult matter, even if you are on a limited budget and have no more space than an ordinarily large spare room. A classic "Bagnold" wind tunnel consists of a horizontal rectangular duct, wider than high and with a flared entrance, emptying into a large box equipped with a fan mounted high in the wall opposite the downwind end of the duct. If you fabricate the roof of the duct in the form of several removable segments, it is easy to gain access to the sand bed. Because fans with continuously variable speed are not easy to obtain or arrange, it would be helpful to mount an adjustable louver just outside the fan, in order to set the wind velocity in the duct to any desired value. Lay in a planar bed of medium sand in the duct, turn on the fan, and gradually increase the wind velocity until saltation is established. The only significant difference between saltation in your wind tunnel and the saltation you observed on the sand dune is that the range of eddy sizes in the duct is much smaller, the consequence being that the wind is not nearly as gusty: the saltation is much closer to being steady (unchanging with time).

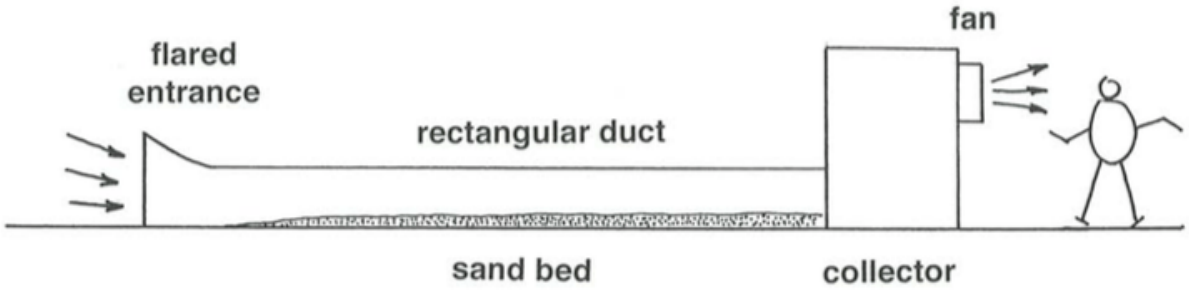


Figure 11.2.2: A simple but effective wind tunnel.

To see saltation trajectories (Figure 11.2.3), cut a thin slit along the centerline of the tunnel roof, not far from the downwind end, and mount a strong light source above the slit, with a second slit between the strobe and the roof, for good collimation. With that arrangement you can illuminate a thin streamwise slice of the flow. Trajectories of saltating particles that move in this illuminated slice show up well as curving bright streaks. It would be even better to use a stroboscope as the light source. Then the trajectories show up as series of closely spaced illuminated dots. If the concentration of saltating particle is not too high, so that individual trajectories can be discriminated, then by making sufficiently careful measurements of a photographic image you could compute velocities and accelerations of individual saltating particles along their trajectories.

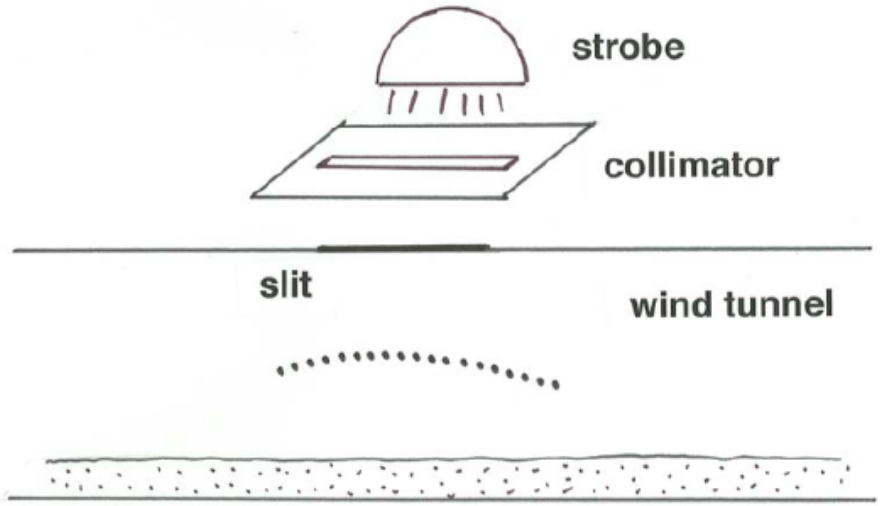


Figure 11.2.3: A lighting arrangement to see saltation trajectories.

Saltation Trajectories

The general nature of the trajectories of saltating particles is known from early descriptions by many investigators, most notably Bagnold (1941) and Zingg (1953), but also in several later studies. Figure 11.2.4, from Maegley (1976), is a representation of a typical saltation trajectory from the early literature on saltation. After launch, the subsequent path of the particle is the outcome of the constant downward force of gravity (that is, the weight of the particle), on the one hand, and the fluid drag force occasioned by the motion of the particle relative to the surrounding air, which evolves as the particle traverses its path.

Although some authors have described the saltation trajectory as parabolic, what is immediately apparent about the trajectory in Figure 11.2.4 is that it is *asymmetrical*: the angle of takeoff is much larger than the angle of impact. You could make two other significant observations about saltation trajectories: they are convex upward all along their courses, from takeoff to landing; and their length, from takeoff to landing, is much greater than the maximum height they reach.

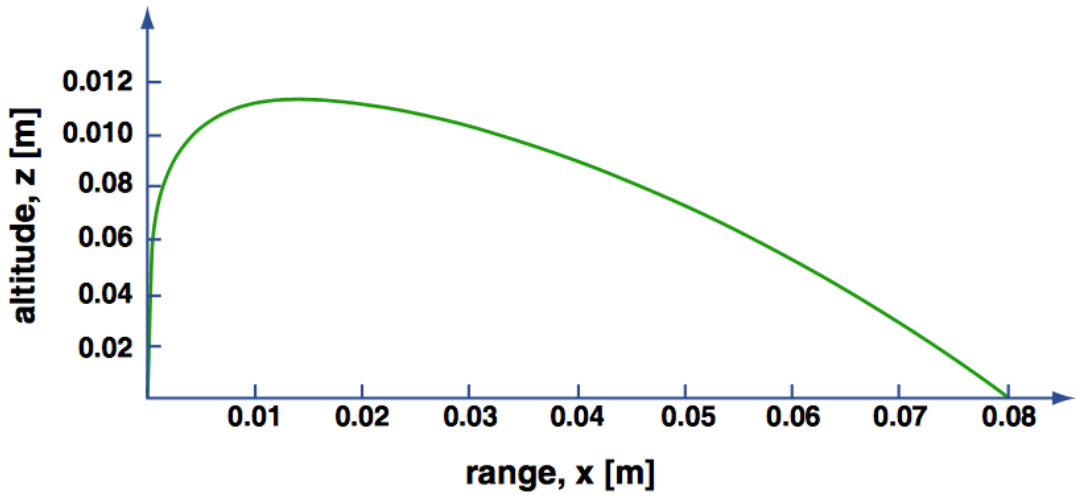


Figure by MIT OpenCourseWare.

Figure 11.2.4: A typical saltation trajectory. (From Maegley, 1976.)

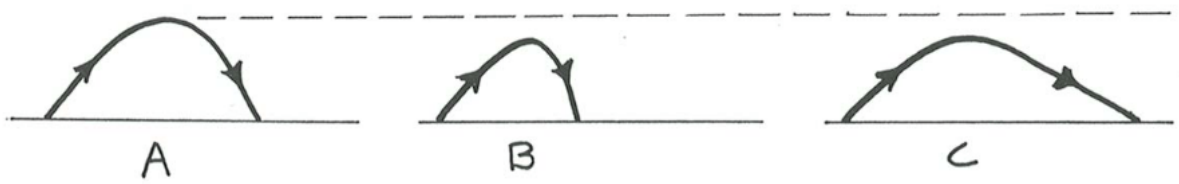


Figure 11.2.5: Qualitative trajectories of particles launched at a fixed angle from a horizontal surface: **A)** in a vacuum; **B)** into air at rest; **C)** into a wind stream with speed greater than the initial horizontal component of particle velocity.

You can gain some qualitative insight into the asymmetry and upward convexity of saltation trajectories noted above by means of simple thought experiment on particle accelerations. Suppose that a particle is somehow launched into the air at some representative angle, say forty to fifty degrees, at some initial speed (Figure 11.2.5). If the medium is a vacuum, you know from elementary physics that the trajectory of the particle, from takeoff to landing, would be a perfect parabola (Figure 11.2.5A). If the medium is air at rest, then the height of the trajectory would be slightly smaller, because air drag adds to the downward force of gravity and makes the vertical component of deceleration during ascent smaller. Air drag also acts to decrease the horizontal component of velocity throughout the course of the trajectory, so the descent of the particle is at a steeper angle than the ascent (Figure 11.2.5B).

Now suppose that the particle is launched at the same angle and initial speed into a wind stream. There are two cases to consider:

1. the initial speed of the particle is less than that of the wind stream, and
2. the initial speed of the particle is greater than the wind speed. (Here we assume, for simplicity, that because of the logarithmic shape of the velocity profile the particle traverses only a very thin layer of low wind velocity in the immediate proximity to the surface and thereafter finds itself, for most of its path, in a region in which the wind velocity is nearly constant with height. This does not do damage to our first-order thought experiment.)

If the initial speed of the particle is *greater* than the wind speed, the wind causes horizontal deceleration, just as in the case of launch into still air. Qualitatively, the shape of the trajectory is the same as in the case of launch into still air (Figure 11.2.5 B). If, however, the initial speed of the particle is *smaller* than the wind speed, the wind causes horizontal acceleration, and the steepness of the ascending part of the trajectory is smaller (Figure 11.2.5C). The steepness and the shape of the descending part of the trajectory depends on the relative importance of the downward pull of gravity and the remaining horizontal acceleration, but in any case the downward path is less steep than the ascending part. What we can conclude from this simple exercise is that, by comparison of Figure 11.2.5C with Figure 11.2.4, in typical saltation the particle is launched into the wind with a smaller horizontal component of velocity than the speed of the wind in the region well above the surface.

Following the early observations of saltation trajectories by Bagnold (1941) and Chepil (1945), many authors have assumed that the particles typically leave the bed at a steep, nearly vertical angle. Careful measurements of frequency distribution of takeoff

angles by White and Schulz (1977), by use of the technique described above for viewing saltation trajectories in a wind tunnel, together with high-speed cinematography, showed that the average takeoff angle was 50°, and less than 10% of the particles observed had takeoff angles of more than 80° (Figure $11.2.6$A). A notable feature of the distribution shown in Figure $11.2.6$A is that the distribution is strongly skewed: the mode lies in the range 20–40°, and the distribution tails off steadily toward steeper angles, but no angles less than 20° were measured. White and Schulz also found that the average angle of impact at the end of a saltation trajectory was 14° (Figure $11.2.6$B), and the distribution was much more nearly symmetrical.

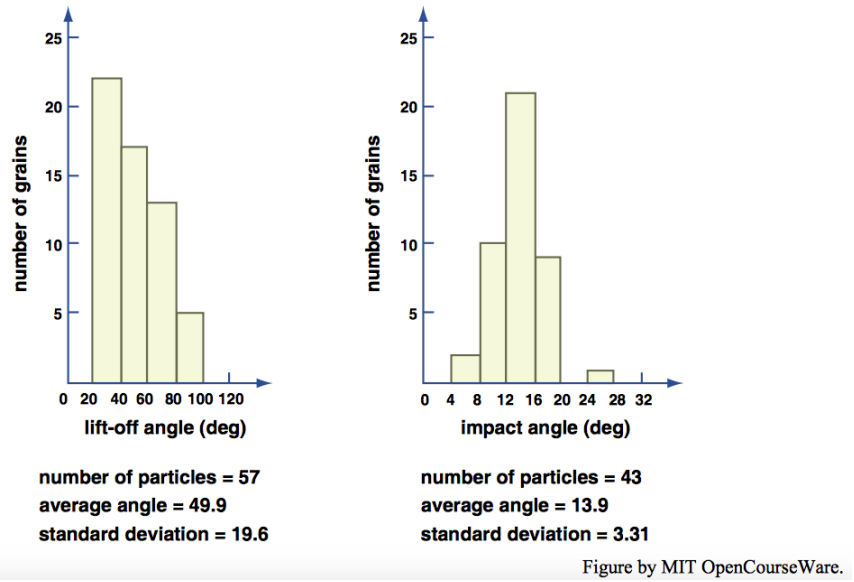


Figure $11.2.6$: Frequency distribution of A) takeoff angle and B) impact angle for $0.5\ \mathrm{mm}$ glass spheres saltating in a wind tunnel (From White and Schulz, 1977.)

The results obtained by White and Schulz might be questioned because they were obtained from single-size glass spheres. More recent studies have found lower launch angles. Willetts and Rice (1985), using natural sands, measured average takeoff angles of 52–54° for particles ejected from rest by impacts of already saltating particles but considerably smaller average angles of 21–33° for rebounds of already saltating particles. Nalpanis et al. (1993) measured takeoff angles of 35–41°, for natural sands, and Nishimura and Hunt (2000) measured even lower takeoff angles of 21–25° for ice spheres and for spherical mustard seeds. If large and immovable particles are present on the bed surface, finer particles in saltation are observed to rebound from them upon impact at sometimes very steep angles, in some cases even with a component in the direction opposite to the wind.

Saltation Lengths

Why are the lengths of saltation trajectories so much greater than the heights? It was noted at the beginning of this chapter that the relative inertia of sand particles in air is extremely large, but nonetheless the air at all times exerts a drag force on the particles, because there is always a difference between the velocity of the particle and the velocity of the wind. Only for very fine dust particles in suspension does this velocity difference become negligible.

White and Schulz (1977) also measured takeoff speeds and impact speeds of saltating particles (Figure $11.2.7$). Takeoff speeds averaged about $70\ \mathrm{cm/s}$, not much more than the friction velocity u_*—but keep in mind that such a value of u_* corresponds to wind speeds of several meters per second only some centimeters above the bed. Suppose that a sand particle is launched vertically into a wind stream at such a speed. The rising particle almost immediately encounters much higher wind speeds. At any given instant, the velocity of the particle relative to the air is the vector difference between the velocity of the particle relative to the ground and the horizontal velocity of the wind relative to the ground (Figure $11.2.8$). In the initial, rising part of the trajectory, this vector velocity is directed upward and upwind.

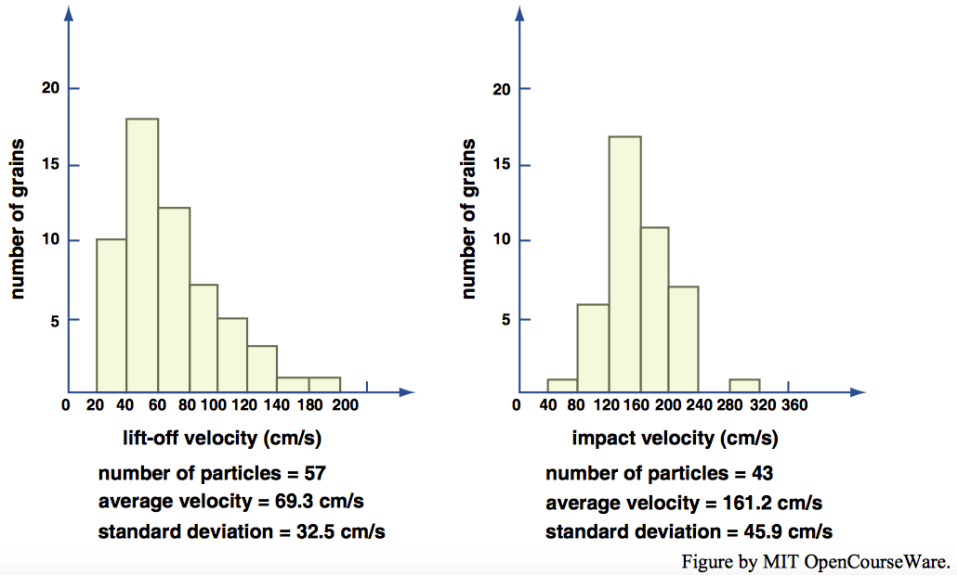


Figure $11.2.7$: Frequency distribution of **A)** takeoff speed and **B)** impact speed for $0.5\ \mathrm{mm}$ glass spheres saltating in a wind tunnel (From White and Schulz, 1977.)

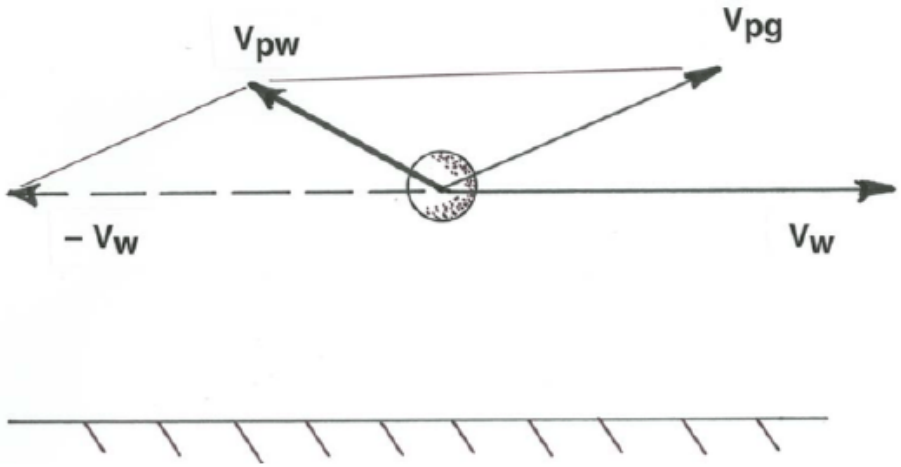


Figure $11.2.8$: The speed of a saltating particle relative to the surrounding air. $\mathrm{V_w}$ = the velocity of the wind; $\mathrm{V_{pg}}$ = the velocity of the particle relative to the ground; $\mathrm{V_{pw}}$ = the velocity of the particle relative to the wind.

Bagnold (1941) supposed that the importance of the effect of particle speed relative to the air can be characterized by the ratio of fluid drag force to particle weight, a quantity he termed the **susceptibility** (although that useful term has not subsequently propagated itself through the literature on saltation). Figure $11.2.9$, from Bagnold (1941), shows the susceptibility of several sand sizes as a function of wind speed. You can see from Figure $11.2.9$ that for relative speeds of several meters per second the susceptibility of sizes between $0.3\ \mathrm{mm}$ and $1.0\ \mathrm{mm}$—which largely span the range of sizes of saltating particle—lies between about one and ten: the air drag is greater than the particle weight, but not far greater. The implication is that the air drag does not much affect the details of the saltation trajectory but is important in determining the overall course of the trajectory. If the fluid drag were much less, the saltation length would be reduced. A further implication then seems to be that for saltation trajectories on Mars, where the density ratio ρ_s/ρ is even greater than on Earth, saltation height should be greater, relative to saltation length, than on Earth.

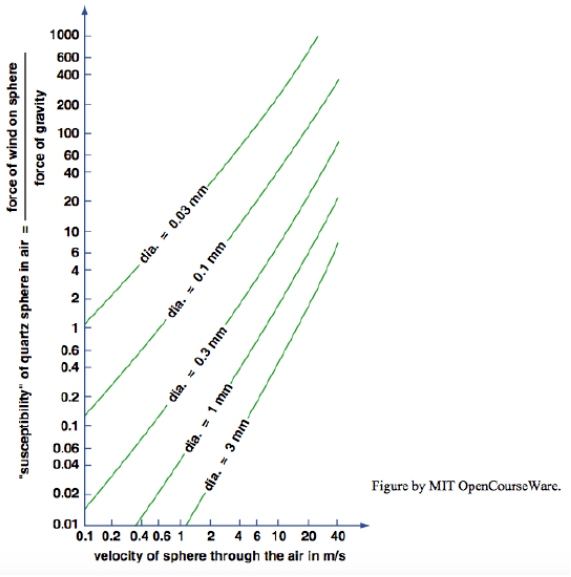


Figure 11.2.9: The susceptibility of two particle sizes as a function of wind speed. (From Bagnold, 1941.)

The average impact speeds of about $160\ \mathrm{cm/s}$ measured by White and Schulz (Fig. 11.2.7) are much less than the wind speed at heights traversed by the particles near the tops of their saltation trajectories. Given that wind speeds are greater than that down to heights of only a few centimeters, those values of impact speed tell us that the wind has not nearly "finished the job" of accelerating the particle to the prevailing wind speed before the particle descends to splash down again onto the bed.

The foregoing material is only the briefest qualitative introduction to saltation trajectories. Several authors, beginning with Bagnold, have developed methods for computing saltation trajectories; see, for example, Owen (1964) and White and Schulz (1977). As Bagnold notes, it is essentially the same problem as the practical computation of the trajectories of cannonballs and artillery shells. The basic computational problem is that neither the velocity nor the fluid drag on the particle can be assumed independently: the two evolve together.

Saltation Heights and the Magnus (Robins) Effect

It seems to be a common belief that the near-surface zone of saltation (the saltation cloud) has a well-defined upper limit. This might in part be because of the statement in Bagnold's influential 1941 book that the saltation cloud has "a clearly marked upper surface" (p. 19). Also, Owen, in his classic 1964 paper, illustrates a series of saltation trajectories all with the same shape, height, and length (his Figure 1), which a casual reader might assume was intended to represent real saltation—but Owen in fact took care to point out that the figure was meant only to illustrate the simplifying assumptions he made in his study, and that the saltation "in reality must be endowed with a certain randomness" (Owen, 1964, p. 226).

It is clear, from later observational studies, that for a given sand and wind there is a considerable variation in the height to which saltating particles rise. This shown perhaps most clearly by results of measurements of sand transport rate as a function of height above the bed. Using beds of moderately well sorted sand, both Zingg (1953) and Williams (1964) found that the sediment transport rate, per unit width across the wind and for unit height above the bed, varied as a negative exponential function of the height above the bed. Several later studies have shown similar results. (For more on sand transport rates in saltation, see the later section.)

If you go back to what you learned in Physics I, you can easily compute the theoretical height to which a saltating particle would rise in the contrary-to-fact case of no air drag on the particle. The particle has some initial kinetic energy, $mv^2/2$, where m is the mass of the particle and v is the initial speed of the particle. As the particle rises, against the pull of gravity, its kinetic energy is converted to potential energy of height, mgh, where g is the acceleration due to gravity and h is height above the bed. To find the maximum height of rise, at the top of the parabolic trajectory, set the kinetic energy equal to the potential energy and solve for h : $h = v^2/2g$.

The value of the no-air-drag result is that it serves as a standard for comparison of actual saltation trajectories. In light of what was said in the earlier sections on saltation trajectories, we might conclude that real trajectories should always have a lesser maximum height of rise, owing to air drag. We would, however, be mistaken: experiments (e.g., by White and Schulz, 1977) slow

clearly that saltation heights are even greater than the no-air-drag value (Figure 11.2.10). The reason seems to lie in the spin of the saltating particles.

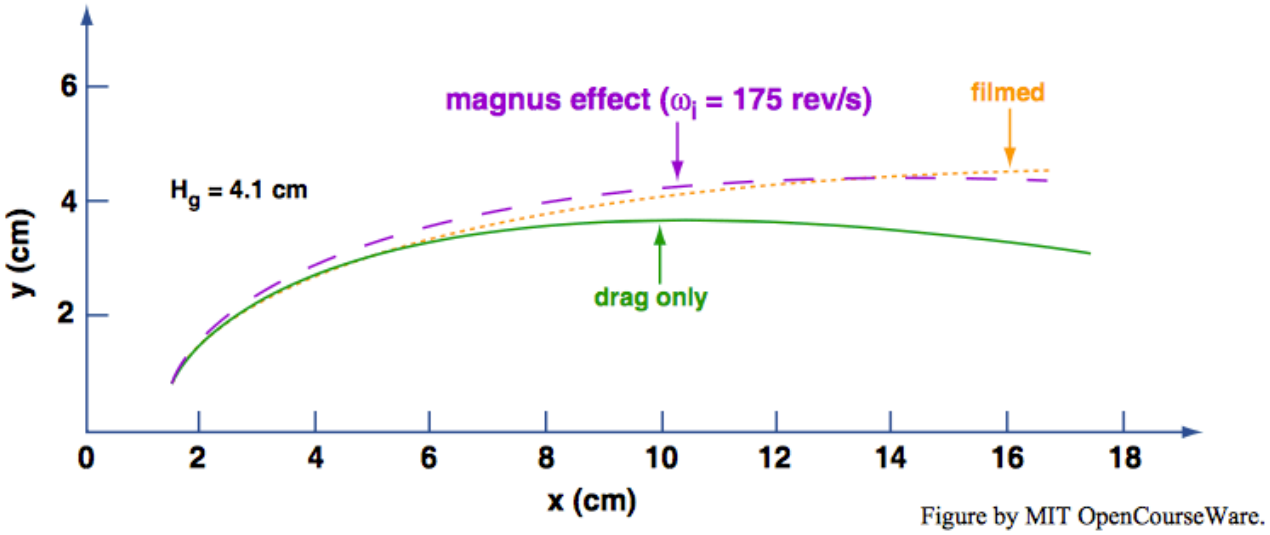


Figure 11.2.10: Trajectories of a saltating glass sphere calculated for the case of drag only (non-rotating sphere; dashed curve) and drag plus lift (a sphere with a rotation rate of 275 per second; semi-dashed curve) compared with the observed trajectory (solid curve). (From White and Schulz, 1977.)

As observed early on by Chepil (1945), particles in saltation have spectacularly high spin rates of hundreds of revolutions per second. The spinning must somehow be imparted to the particles at, and/or soon after, takeoff into the wind stream. Spinning generates a lift force that acts while the particle is in flight. This effect of spinning is generally called the Magnus effect for cylinders and the Robins effect for spheres (Figure 11.2.11). Rotation of the particle changes the streamlines so that they are no longer symmetrical about the particle: streamlines are closer together above the particle, implying that velocities are greater there than they are below the particle (Figure 11.2.11). From the Bernoulli equation (Chapter 3) it follows that the pressure is less above the particle than below, and the particle experiences a lift force. The variation in lift coefficient with rate of spinning is known, so the lift force can be calculated. White and Schulz (1977) could account for the observed saltation trajectories only by taking this effect into account. For most observed trajectories the rate of spinning could not be observed directly, but a good fit of observed trajectories to theoretical calculations could be made by assuming a rate of spin of several hundred revolutions per second. This is known from photographic studies to be about the right value for the spin.

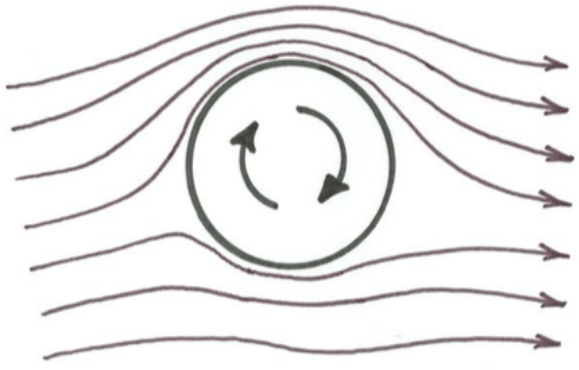


Figure 11.2.11: Vertical streamwise cross section through a spinning sphere immersed in a flowing fluid, to illustrate the Robins effect. See text for explanation.

Threshold of Motion for Eolian Sand Transport and the Question of the Forces that Cause Saltation

Clearly, no particles at rest on a broad horizontal surface of sand are set in motion until the wind reaches a certain strength. At

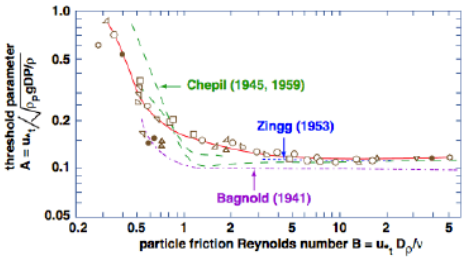
wind speeds below the threshold for movement, the forces on the sand particles are the same as was discussed in Chapter 9 for water flows, because the fluid dynamics of the wind very near the ground is the same for air as for water. As in water flows, the nature of the fluid forces on the bed-surface particles—pressure forces and viscous forces, which can be resolved into a drag component, parallel to the bed, and a lift component normal to the bed—are a function of the particle Reynolds number. In fact, much of what is known about lift and drag forces as a function of particle Reynolds number has been learned from experiments in wind tunnels, beginning with Einstein and El-Samni (1949) and Chepil (1958, 1961).

The difficulties in defining the onset (or even the existence) of a definite threshold flow strength as discussed in Chapter 9 for sediment under water flows exist for sediment under air flows as well, although with certain important differences. As you saw in Chapter 9, in water flows the sediment transport rate in the range of flow strengths for which the threshold might be located is wide, and the mode of movement (bed load) is the same over that range. In contrast, in air flows a different mode of sediment movement—saltation—sets in soon after movement begins, and transport rates increase far more rapidly once sediment movement begins than in water flows.

As the wind speed increases, particles are set in motion by the fluid forces. Beginning with Bagnold, this has been called the **fluid threshold** or the **aerodynamic threshold**. Soon after particle motion starts—in just a few seconds—saltation sets in, in a kind of cascade whereby the concentration of saltating particles increases rapidly to its equilibrium state. Then, if the wind speed decreases, the saltation eventually ceases. The condition of cessation of saltation is called the **impact threshold**. One of the first-order facts about saltation is that the fluid threshold is at a wind speed less than the fluid threshold, as first remarked by Bagnold (1941) and confirmed observationally many times since. There is thus a strong hysteresis effect in saltation.

There has been a long-standing controversy about whether bed particles hop and roll for a brief time before cascading into fully developed saltation, as first proposed by Bagnold (1941), or whether they vibrate in place, in response to the rapidly fluctuating fluid forces they feel, before finally being launched into movement above the bed surface, as reported by soil scientists studying entrainment of soil particles by the wind. The consensus seems to be that, in the case of sand particles, the sand particles undergo some brief movement as bed load for a brief time before saltation develops.

Observations of movement threshold under air flows have been made since the early days of the modern era of research on sand movement by the wind. Following on early studies by Bagnold (1941), Chepil (1945, 1959), and Zingg (1952, 1953), Iversen et al. (1976a) made extensive observations of eolian thresholds by use of sediments of varying size, density; their results (Figure 11.2.12) show a nearly constant value of threshold Shields parameter for boundary Reynolds numbers down to about five, and then increasing threshold Shields parameter with further decrease in boundary Reynolds number. As mentioned in Chapter 9, the Shields parameter for threshold under air is somewhat greater than for under water, for the same values of boundary Reynolds number.



material	density, gm/cm³	diameter, μm
instant tea	0.21	719
silica gel	0.89	17; 169
nut shell	1.1	40 to 359
clover seed	1.3	1290
sugar	1.59	393
glass	2.42	31 to 48
glass	2.5	38 to 586
sand	2.65	526
aluminum	2.7	36 to 204
glass	3.99	55 to 519
copper oxide	6.0	10
bronze	7.8	616
copper	8.94	12; 37
lead	11.35	8; 720

Figure by MIT OpenCourseWare.

Figure 11.2.12: Plot of threshold Shields parameter against boundary Reynolds number for observations of threshold conditions for a number of sediments under air. From Iversen et al. (1976a); their threshold parameter A is the same as the Shields parameter except that ρ_s is used in the denominator instead of $(\rho_s - \rho)$ in the variable $(\rho_s - \rho)g$, called γ' in these notes.

Nickling (1988) devised an experiment in which particles newly set into motion at near-threshold conditions were observed by

means of a horizontal laser beam directed horizontally across the flow one millimeter above an originally intact planar sand bed. Sediments with a range of size and sorting were used. Nickling's results showed (Figure 11.2.13) that for the relatively poorly sorted sediments there is a range of flow strengths (as measured by the shear velocity) for which small number of particles are moved before flow strengths become great enough for saltation to begin, whereupon the number of particles in motion increases sharply. For the relatively well-sorted sediments, however, that range of flow strengths effectively vanishes: saltation begins immediately upon attainment of motion brought about by the fluid forces.

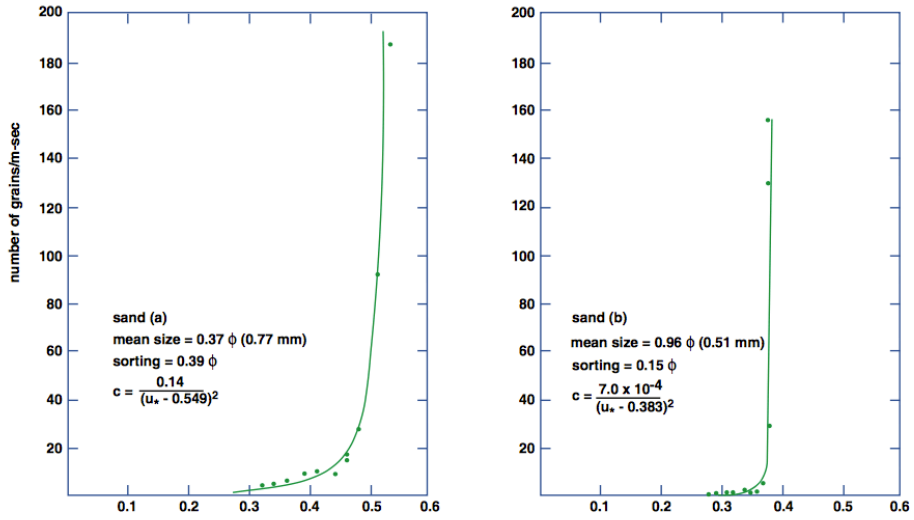


Figure by MIT OpenCourseWare.

Figure 11.2.13: Plots of numbers of particles in motion, per unit time and per unit width normal to the wind, versus shear velocity, for two sediments: **A)** a relatively poorly sorted sand, with mean size $0.77\ \mathrm{mm}$ and with a sorting value of 0.39 phi units, and **B)** a relatively well sorted sand, with mean size $0.51\ \mathrm{mm}$ and sorting of 0.15 phi units. (From Nickling, 1988.)

Most studies of threshold of eolian transport have been made in wind tunnels, in which nearly steady winds can be arranged. In the field, observations of threshold are far more difficult, in large part because winds across natural sand surface are much gustier, owing to the much larger scale of eddies in the lower atmosphere. In small wind tunnels, fluctuations in bed shear stress with time at a point are short relative to the time scales of saltation of individual particles, whereas in the field they are typically far longer. Such considerations point toward a later section of this chapter, on saltation in unsteady winds.

The forces that cause a particle to be launched into a saltation jump in the wind have been controversial. There are two candidates: aerodynamic forces of lift and drag, and impacts by other saltating particles as they splash down onto the bed. (Of course, the two could, and probably do, act in concert; the question is which is the more important.) The moderate to large takeoff angles of saltating particles do not in themselves indicate the relative importance of the two kinds of forces: it might be supposed that strong aerodynamic lift forces should be responsible for steep takeoff angles, but it is clear also that similarly steep angles can be the result of rebounds upon splashdown. The controversy dates back to the early days of the modern era of study of eolian sand movement: Chepil (1945, 1961) considered aerodynamic forces to be dominant, whereas Bagnold (1941) believed saltation impacts to be principally responsible for saltation takeoff.

It seems clear that the presence of the saltating particles extracts momentum from the wind within the saltation layer, as discussed in a later section, so the fluid shear stress on the bed must be much less than would be the case with the same sand bed and with the same overlying wind but with the bed particle immovable. Owen (1964) went so far as to hypothesize that the shear stress exerted by the wind on the sand bed is just sufficient to maintain the surface particles in a mobile state. The implication of that hypothesis is that the aerodynamic forces of lift and drag should be much less important in maintaining saltation than rebound of particles, as well as mobilization of other particles, at the point of collision.

Theoretical models of continuous saltation, beginning with Tsuchiya (1969, 1970) and Reizes (1978), demonstrate that saltation can continue once started, without the necessity of any fluid lift or drag forces acting on particles resting on the bed, but they do not lead to any predictions about particle trajectories that can distinguish this hypothesis conclusively from the fluid-force hypothesis.

This page titled 11.2: Saltation I is shared under a CC BY-NC-SA 4.0 license and was authored, remixed, and/or curated by John Southard (MIT OpenCourseware) via source content that was edited to the style and standards of the LibreTexts platform.

11.3: Saltation II

The Effect of Saltation on the Velocity Profile of the Wind

You have seen that the air exerts a drag force on the saltating particles as they rise from the bed. Conversely, the equal and opposite force exerted by the particles on the wind tends to slow the wind. Given the commonly substantial concentration of particles in the saltation layer, you should expect the structure of the wind in the saltation layer to be different from that in the absence of saltation. At first thought, you might assume that there is a kind of symmetry at work here: perhaps the particles tend accordingly to speed up the wind as they descend from the tops of their trajectories down into region of lower wind speed. If, however, our earlier deduction to the effect that the particles have not yet been fully accelerated by the wind even when they reach the ends of their trajectories is true, then the saltating particles must be responsible for a net decrease in wind velocity. You will see below that this is indeed the case.

As with so many aspects of eolian saltation, Bagnold was the first to give systematic attention to the effect of saltation on wind velocity. Bagnold (1941), and many later researchers, have measured wind-velocity profiles in the presence of saltation. Figure 11.3.1, taken directly from Bagnold's book, shows actual measurements.

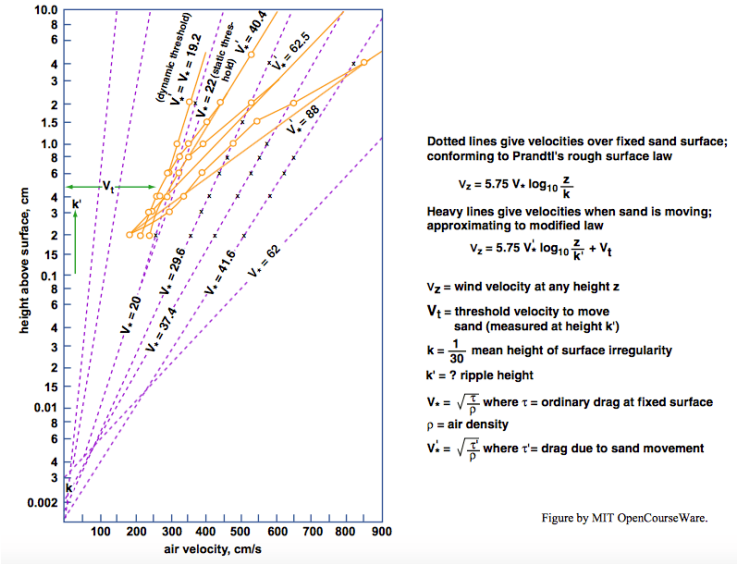


Figure 11.3.1: Profiles of wind velocity in saltation. (From Bagnold, 1941.)

Recall from Chapter 4 that the air speed over a fixed rough bed varies logarithmically with height above the bed, according to the law of the wall for rough boundaries (Equation 4.7.22, reproduced here as Equation 11.3.1, for your convenience):

$$\frac{\overline{u}}{u_*} = A \ln \frac{y}{y_0} \tag{11.3.1}$$

where y_0, the roughness length, is nothing more than a convenience variable to put the law of the wall as expressed in the form of Equation 4.7.20 into a neater form. The roughness length y_0 has the property that when the profile expressed by Equation 11.3.1 is extrapolated downward, its intercept with the $\overline{u}/u_*$ axis (nominally, zero wind velocity) is at a value of y, the height above the bed, of $D/30$ for close-packed granular roughness—but in reality Equation 11.3.1 ceases to hold at heights above the bed not much greater than the particle diameter, as discussed in Chapter 4.

In a dimensional plot of wind speed u against height y above the sand bed, if u_* is changed, the slope of the velocity profile varies, but the intercept y_0 does not, according to Equation 11.3.1 (see Figure 11.3.2, an idealization of Figure 11.3.1). What Figure 11.3.2 shows is that when a saltation layer is present the profile of wind speed in the region above the saltation layer is still logarithmic, but with a significant modification: profiles for different shear velocities no longer converge on the point $(0, y_0)$ located on the y axis (where $u = 0$) but, approximately, on a point (u_o', y_0'), where u_0' is not equal to zero and y_0' is much larger than y_0. The effect

on the velocity profile above the saltation layer is the same as if the roughness of the bed had been increased— as if, in Equation 4.7.20 or 4.7.21 the size of the roughness elements, D, had been increased. The saltation layer thus adds resistance to the wind, as we deduced at the beginning of this section.

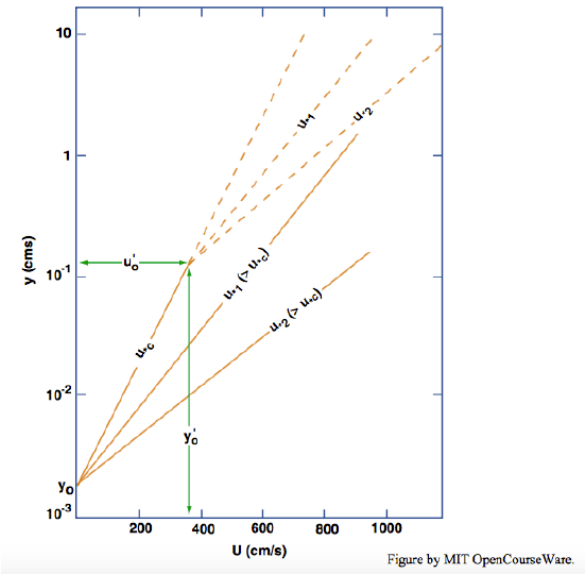


Figure by G.V. Middleton.)

The question then arises: how low does the wind speed become, deep in the saltation layer, just above the tops of the bed particles? Owen (1964) offered the following hypothesis, noted in an earlier section: the shear stress exerted by the wind on the sand bed is just sufficient to maintain the surface particles in a mobile state—which is much lower than would be the case with the same sand bed and with the same overlying wind but with the bed particle immovable.

Jump-Distance Distribution

The downwind distance traversed by saltating particles ranges from very short, perhaps of the order of a few millimeters (the minimum saltation distance is partly a matter of semantics, hinging upon one's view of the transition from particle movement in surface creep to particle movement in saltation) to very long, as much as several meters in strong winds under which the saltation layer extends upward by more than a meter. When the flights of a large number of saltating particles in a uniform wind are considered, there is some well defined probability distribution of jump distances.

Measuring the jump-distance frequency distribution is not straightforward. Direct measurement of jump distances, by means of tracking trajectories photographically, is likely to be biased toward the longer trajectories, owing to the greater particle concentrations at lower levels, which tend to obscure the individual trajectories, and the slower particle speeds, which makes measurements of speeds from photographic images more difficult. The few attempts at measurement have exploited the indirect method of measuring the catch of particles in long bed-level traps of various designs (Kawamura, 1951; Horikawa and Shen, 1960; Belly, 1964).

It is not difficult to show that the jump-distance distribution is related to the distribution of catch in a horizontal sand trap by

$$f(\eta) = \frac{1}{Go}\frac{dG}{dx} \tag{11.3.2}$$

(Kawamura, 1951), where $f(\eta)$ is the frequency distribution of saltation jump distances η, G is the saltation catch (mass per unit area and unit time) in a horizontal trap with leading edge at $x = 0$ and extending downwind in the positive x direction, and G_O is the total mass launched into saltation from a unit area in unit time.

The few measurements of jump-distance distribution show three significant features:

- The frequency of jump distances increases monotonically with decreasing jump distance, apparently right up to the transition to surface creep; in other words, the maximum of the curve is at very small, or even zero, jump distance.
- The mean jump distance is significantly greater than the spacing of the wind ripples over which the saltation takes place.

- There is no well-defined maximum jump distance, as is to be expected, given the gradually decreasing concentration of saltating particles with height, but the frequency of jump distances several meters long is not negligible.

Mass-balance considerations in the context of jump-distance distributions are enlightening. Think about saltation that is uniform, in the sense that the picture of saltation is exactly the same at every point along the wind direction. Uniform saltation is very closely approximated where a sand-moving wind blows steadily over a level sand surface of great extent. In uniform saltation, the mass of particles launched from a small unit area of the bed must be equal to the mass of particles arriving onto that area—and, more specifically, the jump-distance distributions of both the incoming and outgoing particles must be identical, or the saltation would not be uniform. This is a demanding requirement, because each incoming particle gives rise to zero, one, or more outgoing particle motions with jump distances not likely to be identical to its own. Nature somehow manages to adjust the jump-distance distribution of outgoing particles to be the same as that of the incoming particles. There must be a self-regulating mechanism at work: if not enough downwind transport is engendered from the unit area by the incoming particles, the intensity of saltation falls off downwind until what leaves matches what arrives, and if the incoming particles cause an even greater transport rate out of the area, the saltation transport rate increases until the rate becomes uniform. This transformation of incoming saltation to outgoing saltation can be described in terms of what Werner (1990) calls the **splash function**. The following makes these matters more concrete.

In eolian saltation the mass of moving particles that make contact with a small reference area on the bed includes particles launched into saltation from a range of distances upwind, from only a fraction of a particle diameter, in the case of the surface creep, to as much as a few meters, in the case of the highest-flying particles in saltation. With x as incoming jump length, let the function $g_{in}(x)$ represent the jump-distance distribution of this incoming mass of particles, expressed as mass per unit bed area per unit time. Similarly, with y as outgoing jump length the function $g_{out}(y)$ represents the corresponding jump-distance distribution of the outgoing mass of particles. In uniform saltation, incoming and outgoing mass must be the same for any given jump length, so g_{out} and g_{in} are identical distributions. Mathematically this can be expressed as

$$\int_0^\infty g(x)F(x,y)dx = g(y) \tag{11.3.3}$$

Where $F(x,y)$ is the splash function of Werner (1990). Equation 11.3.3 is an integral equation—one that contains an integral. A function with the form of F in Equation 11.3.3 is said to be the kernel of the equation. In this case, a mathematician might call F a self-replicating kernel function, because it has the remarkable property of transforming the other factor in the integral on the left, $g(x)$, into an identical function, $g(y)$, on the right.

The requirement, mentioned above, that in uniform saltation the jump-distance distributions become adjusted so that the incoming and outgoing jump-distance distributions, g_{in} and g_{out}, are identical and a function of the wind strength can be expressed in the context of Equation 11.3.3 as follows. For each value of incoming jump distance x, the splash function acts on the incoming mass of saltating particles to give a contribution to the mass distribution of outgoing jump distance, and the sum of all of these contributions is the outgoing mass distribution of jump distances.

What can we say, qualitatively, about the nature of the splash function F?

- The momentum of incoming particles, and therefore their ability to set particles in motion at any given outgoing jump distance, increases with increasing incoming jump distance, so F should be a monotonically increasing function of x at constant y for all y, including $y = 0$.
- The mass of particles set in motion by arrival of particles with a given jump distance x should be greater for smaller outgoing jump distances than for larger, so F should be a monotonically decreasing function of y for constant x.
- Incoming particles with very small jump distances can give rise to only a narrow range of jump distances, and therefore relatively small momentum, not much larger than their own, whereas incoming particles with very large jump distances, and therefore relatively large momentum, can give rise to a wide range of outgoing jump distances from very small to even larger than their own, so the overall rate of decrease of F with increasing y at constant x should be sharpest for very small x and become gentler with increasing x.
- F must approach zero as x approaches zero, because the mass of particles mobilized must go to zero as the incoming jump distance, and therefore the momentum of the incoming particles, goes to zero.

Figure 11.3.3 shows, qualitatively, what the splash function F might actually look like.

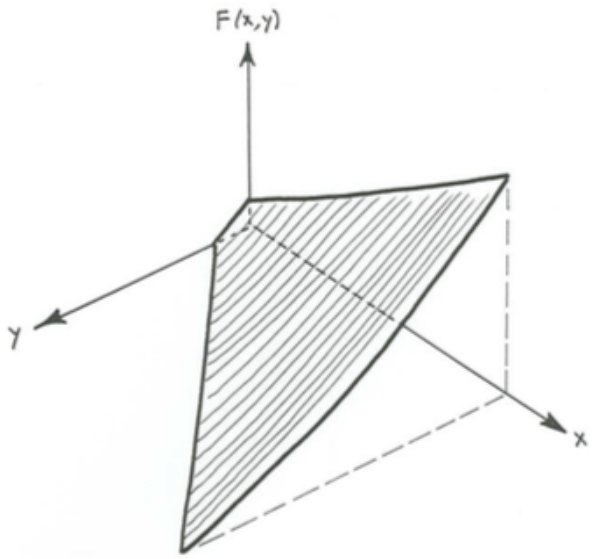


Figure 11.3.3: A qualitative representation of the splash function.

Saltation Transport Rates

It was mentioned in the section on saltation heights that the concentration of saltating particles tails off gradually upward. This is known from sampling to measure the transport rate of saltating particles. Such measurement is simple in principle but somewhat troublesome in actual practice. The common procedure is to install, on a vertical shaft or frame in the sand, a series of particle-catching devices, which are uncovered for a fixed time and then the mass of particles caught in each is measured. A curve of catch versus height is plotted, and the total transport rate is the integral of that curve from the bed to a level above the highest saltation heights. Once the transport at any given level is known, the concentration of the saltating particles at that level can be found if the time-average wind speed is measured at the same level at the same time, inasmuch as the transport rate must equal the concentration times the speed of passage of the parcel of air that contains the particles. Systematic measurements of transport rate date from the time of Bagnold (1941); see also the early and widely cited work of Williams (1964).

One practical problem is that any such catching devices, no matter how well designed, inevitably disturb the passing wind to some extent, and even aside from that, measurements near the sand bed, where the mass flux of particle is greatest, is difficult to arrange. In recent years, high-resolution measurements using non-intrusive optical sensors have been developed (e.g., Butterfield, 1999), thus mitigating some of the problems. Another problem is that it is not easy to measure the transport rate of sediment moved as surface creep.

A more general problem, however, has to do with what is actually being measured. The wind is gusty on natural sand surfaces. Even on a broad, horizontal sand- coved plain, the large-scale eddy structure in the lowermost atmosphere means that the saltation catch varies with time on periods of seconds to many minutes. The problem is exacerbated on the upwind flanks of sand dunes, owing to the strong wake produced by an upwind dune. A catch averaged over many minutes may be very different from an “instantaneous” measurement, taken over a number of seconds. This problem could be circumvented in a wind tunnel, but the tunnel would have to be large enough that the saltation profile is fully developed vertically even in very strong winds. Few wind tunnels are of such a size.

Saltation in Unsteady Winds

In recent years, increasing attention has been given to how the saltation cloud adjusts to changing wind conditions, given that winds in the outdoors are characteristically highly variable, on time scales of minutes to hours. The problem can be posed as follows. A surface of loose sand lies susceptible to saltation. A strong gust of wind initiates saltation. How do the conditions of saltation respond? The saltating cloud responds rapidly. The response of the saltation to the changing wind speed has been studied in wind tunnels and in the field (e.g., Butterfield, 1991, 1998) (Figure 11.3.4), and several numerical models have been developed to account for the observations (e.g., Anderson and Haff, 1991; McEwan and Willetts, 1991; Spies and McEwan, 2000; Spies et al., 2000). In numerical simulations by Spies and McEwan (2000), you can see how the transport rate develops in time and space: at a given time after onset of the wind, the transport rate reaches a maximum near the upstream edge of the sand

bed, and the maximum in transport rate moves downstream with time.

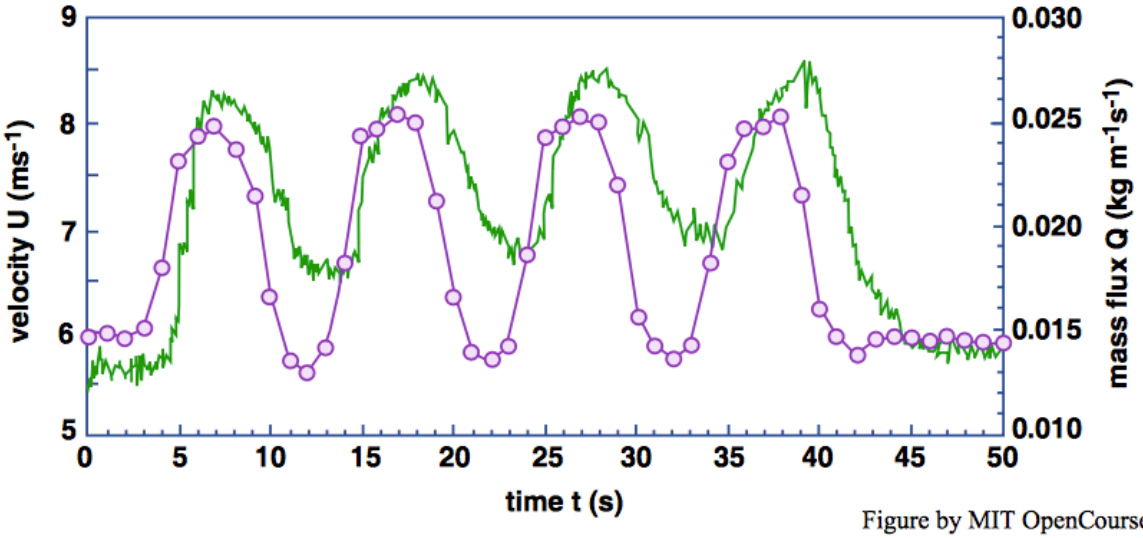


Figure by MIT OpenCourseWare.

Figure 11.3.4: Synchronized measurements of transport rate (grams per centimeter width per second) and shear velocity (meters per second) versus time for a sinusoidally varying wind velocity. The open squares are for wind velocity, and the heavy curve is for transport rate. (From Butterfield, 1998.)

One significant aspect of the response of saltation to a sudden increase in wind speed, from below threshold to well above, is that the saltation transport rate first increases but then decreases somewhat before settling into equilibrium with the wind. The reason is easy to understand: it takes some time for the effect of theft of fluid momentum on the part of the saltating particles to develop—so there is a brief period of time during which the aerodynamic forces on bed particles has not decreased significantly, while the impact forces exerted by saltating particles on the bed have already become significant. As the wind adjusts in such a way as to exert a smaller bed shear stress (see the earlier section), the saltation cloud settles down to a state of somewhat less vigorous saltation. There is thus a transient maximum in saltation transport at the outset of a transport event. Spies et al. (2000) have done numerical simulations of this effect.

The Transition from Saltation to Suspension

You learned way back in Chapter 3 that the characteristic fluctuations in velocity in a turbulent flow are a certain small percentage of the mean velocity. Because of that, the characteristic vertical fluctuating velocity in near-surface winds should increase with wind speed. If those vertical velocities are sufficiently large, even saltating sand particles are affected in the trajectories by the fluctuations. Likewise, in a wind with a given speed, the effect of the velocity fluctuations on particle trajectories increases with decreasing particle size.

The transition from classic saltation trajectories to trajectories that are non-negligibly affected by turbulence is an area of study in eolian sedimentation that has less attention than the study of saltation. A distinction needs to be made here between

1. fine particles (usually referred to in the eolian literature as *dust*), which are raised either directly by the wind or indirectly by the impact of saltating larger particles on exposed surfaces of sediment or bedrock, and which go directly into true suspension even at wind speeds for which vertical fluctuating turbulent velocities are much lower than the settling velocities of the coarser saltating particles, and
2. sand particles moved by winds so strong that the vertical fluctuating velocities become comparable to the settling velocities of the particles, causing particle trajectories to show at least some influence of turbulence.

Nishimura and Hunt (2000) found, in a wind-tunnel study of particle trajectories, that the transition from saltation to suspension begins to be noticeable when the shear velocity is still as low as one-tenth the particle settling velocity. As wind speeds increase beyond that, particle trajectories show greater and greater irregularity due to interaction with turbulent eddies (Figure 11.3.5).

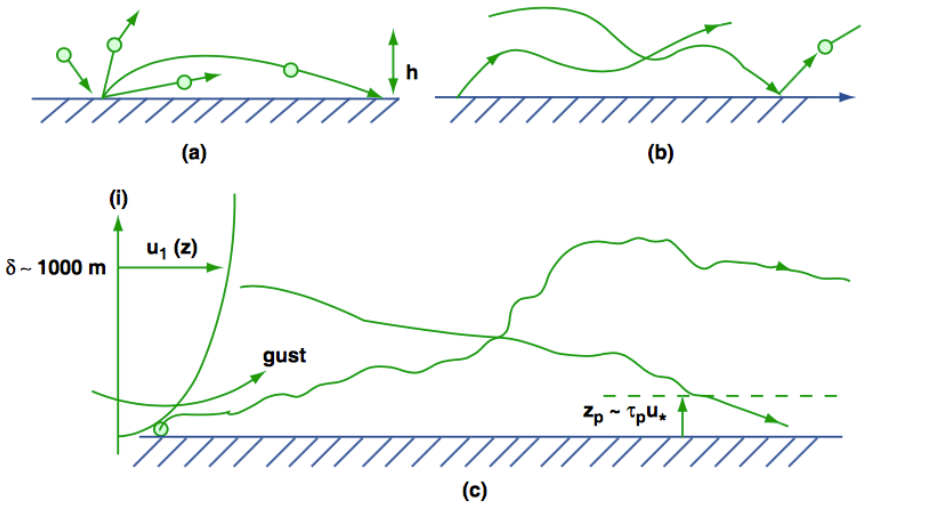


Figure 11.3.5: Cartoon of the transition from saltation to suspension. **A)** Saltating particles are unaffected by fluid turbulence; **B)** saltating particles are slightly affected by fluid turbulence; **C)** particle trajectories are strongly affected by fluid turbulence. (From Nishimura and Hunt, 2000.)

Models of Eolian Saltation

After the early work of Reizes (1978), and concurrently with the development and elaboration of the concept of the splash function by Werner and co-workers, the focus of studies of eolian saltation began to shift toward modeling of eolian sediment transport as a unified phenomenon with saltation dynamics as the basis (e.g., Anderson and Hallet, 1986; Ungar and Haff, 1987; Anderson and Haff, 1988; Werner and Haff, 1988; Werner, 1990; Haff and Anderson, 1993). As time has gone on since the late 1980s, with the development of ever greater computing power, numerical models of eolian transport have become more and more able to simulate the physics of saltation and the consequences for eolian sediment flux.

Models at first aimed at simulating saltation transport in steady and fully developed winds, of the kind that can be produced without difficulty in a long wind tunnel (e.g., McEwan and Willets, 1991, 1993a, 1993b; Willetts, 1998). More recent models have moved on to simulation of unsteady winds—for example, a saltation event in which a sudden strong wind gust generates a cloud of saltating particles, which develops in time and with downwind distance, as described in an earlier section (e.g., Spies and McEwan, 2000; Spies et al, 2000).

Sand Movement on Mars and Venus

Look back at Figure 8.1.5, in Chapter 8, to remind yourself that the case of sand transport by wind on the Earth's surface is only one point in the wide range of density ratios for which solid particles are transported by fluid flows. The density ratio for sand movement on Mars (if we assume that the mineral particles available on the Martian surface are not greatly different in density from those on the surface of the Earth) lies even farther to the right along the ρ_s/ρ axis than the density ratio for eolian sediment transport on Earth. In contrast, the Venus case lies not much farther to the right than the case of transport of ultra-heavy minerals (gold being the obviously important example) by water flows on the Earth's surface! It seems fair to say that the great bulk of the research so far on transport of loose particulate sediment on Mars and Venus has come from the research group headed by R. Greeley, and especially on the part of J.D. Iversen and of B.R. White (Greeley et al., 1974; Greeley et al., 1976; Iversen et al., 1975; Iversen et al. 1976a; Iversen et al. 1976b; Iversen et al. 1976c; White, 1979; Iversen and White, 1982; White et al., 1987) as well as more recent contributions (e.g., Fenton and Bandfield, 2003; Bourke et al., 2004). Much of the data and conclusions from the work of Greeley's group is presented in the book by Greeley and Iversen (1985). The emphasis in these notes is on eolian sand movement on Mars, in light of the spectacular recent advances in our understanding, and the much enhanced interest, that have arisen from the Rover results.

A first-order and seemingly unassailable deduction we can make at the outset is that saltation should be the dominant mode of movement of sand-size particles on Mars—because the relative inertia of the particles is even greater than in eolian transport on Earth. In the case of Venus, for which the density ratio is greater than for sand in water on Earth by not much more than one order

of magnitude, particle trajectories are much more likely to be affected by the turbulence in the wind than is the case for saltation on Mars.

Look back to the discussion of the effect of density ratio on thresholds, in Chapter 9, to see that in terms of the Shields diagram, in which the threshold for sediment motion is expressed in terms of the Shields parameter and the particle Reynolds number, the difference between dimensionless threshold for mineral particles in water and for mineral particles in air is not entirely clear (to me, at least). Given the great differences in atmospheric density between Earth and Mars, as well as the difference in gravity, you should expect that when expressed in dimensional terms the thresholds should be quite different. Figure 11.3.6 shows a comparison of motion thresholds expressed in terms of the shear velocity of the wind.

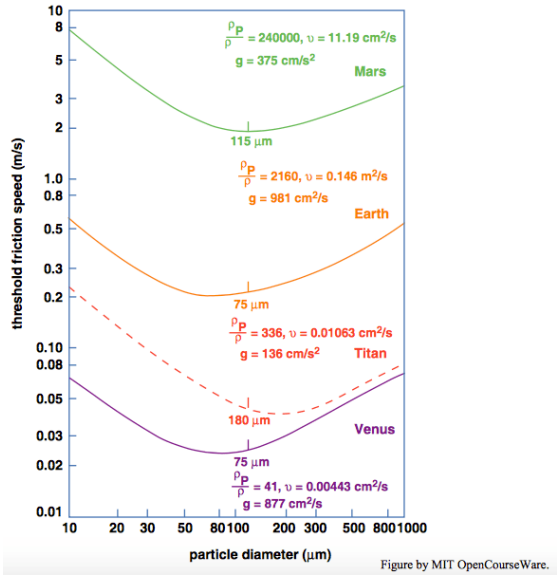


Figure 11.3.6: Predicted threshold shear velocity versus particle diameter for Earth, Mars, and Venus. (From Greeley and Iversen, 1985.)

It seems clear that saltation jump heights and lengths must be much greater on Mars than on Earth, owing to the greater wind speeds and lesser gravity. Another significant deduction we can make is that because of the much greater wind speeds on Mars, together with the even greater relative inertia of the particles, the destructive effects of impacts of saltating mineral particles on rock surfaces should be even greater on Mars than on Earth.

References Cited Chapter 11

Anderson, R.S., 1989, Saltation of sand: a qualitative review with biological analogy: Royal Society (London), Proceedings, v. B96, p. 149-165.

Anderson, R.S, and Haff, P.K., 1988, Simulation of eolian saltation: Science, v. 241, p. 820-823.

Anderson, R.S., and Haff, P.K., 1991, Wind modification and bed response during saltation of sand in air, in Barndorff-Nielsen O.E., and Willetts, B.B., eds., Aeolian Grain Transport 1; Mechanics: Acta Mechanica, Supplementum 1, Springer-Verlag, p. 21-51.

Anderson, R.S., and Hallet, B., 1986, Sediment transport by wind: Toward a general model: Geological Society of America, Bulletin, v. 97, p. 523-535.

Anderson, R.S., Sørensen, M., and Willetts, B.B., 1991, A review of recent progress in our understanding of aeolian sediment transport, in Barndorff-Nielsen O.E., and Willetts, B.B., eds., Aeolian Grain Transport 1; Mechanics: Acta Mechanica, Supplementum 1, Springer-Verlag, p. 1-19.

Bagnold, R.A., 1941, The Physics of Blown Sand and Desert Dunes: Chapman & Hall, 265 p.

Belly, P.Y., 1964, Sand Movement by Wind: US Army, Corps of Engineers, Coastal Engineering Research center, Technical Memorandum 1, 38 p.

Bourke, M.C., Bullard, J.E., and Barnouin-Jha, O.S., 2004, Aeolian sediment transport pathways and aerodynamics at troughs on Mars: Journal of Geophysical research, v. 109, E07005, 16 p.

Butterfield, G.R., 1991, Grain transport rates in steady and unsteady turbulent airflows, inBarndorff-Nielsen OE, Willetts BB, eds, Aeolian Grain Transport 1; Mechanics: Acta Mechanica Supplementum 1, Springer-Verlag, p. 97-122.

Butterfield, G.R., 1998, Transitional behaviour of saltation: wind tunnel observations of unsteady winds: Journal of Arid Environments, v. 39, p. 377-394.

Butterfield, G.R., 1999, Near-bed mass flux profiles in aeolian sand transport: high-resolution measurements in a wind tunnel: Earth Surface Processes and Landforms, v. 24, p. 393- 412.

Chepil, W.S., 1945, Dynamics of wind erosion I, Nature of movement of soil by wind: Soil Science, v. 60, p. 305-320.

Chepil, W.S., 1958, The use of evenly spaced hemispheres to evaluate aerodynamic forces on a soil surface: American Geophysical Union, Transactions, v. 39, p. 397-404.

Chepil, W.S., 1959, Equilibrium of soil grains at the threshold of movement by wind: Soil Science Society of America, Proceedings, v. 23, p. 422-428.

Chepil, W.S., 1961, The use of spheres to measure lift and drag on wind-eroded soil grains: Soil Science Society of America, Proceedings, v. 25, p. 343-345.

Einstein, H.A., and El-Samni, E.A. 1949, Hydrodynamic forces on a rough wall: Reviews of Modern Physics, v. 21, p. 520-524.

Fenton, L.K., and Bandfield, J.L., 2003, Aeolian processes in Proctor Crater on Mars: Sedimentary history as analyzed from multiple data sets: Journal of Geophysical research, v. 108 (E12), 5129, 39 p.

Greeley, R., and Iversen, J.D., 1985, Wind As a Geological Process on Earth, Mars, Venus and Titan: Cambridge University Press, 333 p.

Greeley, R., Iversen J.D., Pollack, J.B., Udovich, N., and White, B., 1974, Wind tunnel studies of Martian aeolian processes: Royal Society (London), Proceedings, v. A341, p. 331-360.

Greeley, R., White, B., Leach, R., Iversen, J., and Pollack, J., 1976, Mars: wind friction speeds for particle movement: Geophysical Research Letters, v. 3, p. 417-420.

Haff, P.K., and Anderson, R.S., 1993, Grain scale simulations of loose sedimentary beds: the example of grain–bed impacts in aeolian saltation: Sedimentology, v. 40, p. 175-198.

Horikawa, K., and Shen, H.W., 1960, Sand movement by wind action: US Army, Corps of Engineers, Beach Erosion Board, Technical Memorandum 119, 51 p.

Iversen, J.D., and White, B.R., 1982, Saltation threshold on Earth, Mars and Venus: Sedimentology, v. 29, p. 111-119.

Iversen, J.D., Greeley, R., White, B.R., and Pollack, J.B., 1975, Eolian erosion of the Martian surface, Part 1: erosion rate similitude: Icarus, v. 26, p. 321-331.

Iversen, J.D., Pollack, J.B., Greeley, R., and White, B.R., 1976a, Saltation threshold on Mars: the effect of interparticle force, surface roughness, and low atmospheric density: Icarus, v. 29, p. 381-393.

Iversen, J.D., Greeley, R., and Pollack, J.B., 1976b, Windblown dust on Earth, Mars and Venus: Journal of the Atmospheric Sciences, v. 33, p. 2425-2429.

Iversen, J.D., Greeley, R., White, B.R., and Pollack, J.B., 1976c, The effect of vertical distortion in the modeling of sedimentation phenomena: Martian crater wake streaks: Journal of Geophysical Research, v. 81, p. 4846-4856.

Kawamura, R., 1951, Study of sand movement by wind: University of California, Berkeley, Institute of Engineering Research, Technical Report HEL-2-8, 40 p.

Maegley, W.J., 1976, Saltation and Martian sandstorms: Reviews of Geophysics and Space Physics, v. 14, p. 135-132.

McEwan, I.K., and Willetts, B.B., 1991, Numerical model of the saltation cloud, in Barndorff- Nielsen, O.E., and Willetts, B.B., eds., Aeolian Grain Transport 1; Mechanics: Acta Mechanica, Supplementum 1, Springer-Verlag, p. 53-66.

McEwan, I.K., and Willetts, B.B., 1993a, Sand transport by wind: a review of the current conceptual model, in Pye, K., ed., The Dynamics and Environmental Context of Aeolian Sedimentary Systems: Geological Society of London, Special Publication 72, p. 7-16.

McEwan, I.K., and Willetts, B.B., 1993b, Adaptation of the near-surface wind to the development of sand transport: Journal of Fluid Mechanics, v. 252, p. 99-115.

McGee, W.J., 1908, Outlines of hydrology: Geological Society of America, Bulletin, v. 19, p. 193-220.

Nalpanis, P., Hunt, J.C.R., and Barrett, C.F., 1993, Saltating particles over flat beds: Journal of Fluid Mechanics, v. 251, p. 661-685.

Nickling, W.G., 1988, The initiation of particle movement by wind: Sedimentology, v. 35, p. 499-511.

Nishimura, K., and Hunt, J.C.R., 2000, Saltation and incipient suspension above a flat particle bed below a turbulent boundary layer: Journal of Fluid Mechanics, v. 417, p. 77-102.

Owen, P.R., 1964, Saltation of uniform grains in air: Journal of Fluid Mechanics, v. 20, p. 225- 242.

Reizes, J.A., 1978, Numerical study of continuous saltation: American Society of Civil Engineers, Proceedings, Journal of the Hydraulics Division, v. 104, p. 1305-1321.

Spies, P.J., and McEwan, I.K., 2000, Equilibration of saltation: Earth Surface Processes and Landforms, v. 25, p. 437-453.

Spies, P.J., McEwan, I.K., and Butterfield, G.R., 2000, One-dimensional transitional behaviour in saltation: Earth Surface Processes and Landforms, v. 25, p. 505-518.

Tsuchiya, Y., 1969, Mechanics of the successive saltation of a sand particle on a granular bed in a turbulent stream: Kyoto University, Disaster Prevention Research Institute, Bulletin, v. 19, Part 1, no. 152, p. 31-44.

Tsuchiya, Y., 1970, On the mechanics of saltation of a spherical sand particle in a turbulent stream: Kyoto University, Disaster Prevention Research Institute, Bulletin, v. 19, no. 5, p. 52-57.

Ungar, J.E., and Haff, P.K. 1987, Steady state saltation in air: Sedimentology, v. 34, p. 289-299. Werner, B.T., 1990, A steady-state model of wind-blown sand transport: Journal of Geology, v. 98, p. 1-17.

Werner, B.T., and Haff, P.K., 1988, The impact process in aeolian saltation: two-dimensional simulation: Sedimentology, v. 35, p. 189-196.

White, B.R., 1979, Soil transport by winds on Mars: Journal of Geophysical Research, v. 84, p. 4643-4651.

White, B.R., and Schulz, J.C., 1977, Magnus effect in saltation: Journal of Fluid Mechanics, v. 81, p. 497-512.

White, B.R., Leach, R.N., Greeley, R., and Iversen, J.D., 1987, Saltation threshold experiments conducted under reduced gravity conditions: AIAA, 25th Aerospace Sciences Meeting, 12-15 January, Reno, Nevada, Paper AIAA-87-0621, 9 p.

Willetts, B.B., 1998, Aeolian and fluvial transport: Royal Society (London), Philosophical Transactions, Series A, v. 356, p. 2497-2513.

Willetts, B.B., and Rice, M.A., 1985, Intersaltation collisions, in Barndorff-Nielsen, O.E., ed., Proceedings of the International Workshop on the Physics of Blown Sand: Demark, University of Aarhus, Department of Theoretical Statistics, Memoir 8, p. 83-100.

Williams, G., 1964, Some aspects of the eolian saltation load: Sedimentology, v. 3, p. 257-287.

Zingg, A.W., 1952, A study of the characteristics of sand movement by wind: M.S. thesis, Kansas State College, 79 p.

Zingg, A.W., 1953, Wind tunnel studies of the movement of sedimentary material: State University of Iowa, Iowa Institute of Hydraulic Research, Fifth Hydraulics Conference, Proceedings, McNown, J.S., and Boyer, M.C., eds., p. 111-136.

This page titled 11.3: Saltation II is shared under a CC BY-NC-SA 4.0 license and was authored, remixed, and/or curated by John Southard (MIT OpenCourseware) via source content that was edited to the style and standards of the LibreTexts platform.

12: BED CONFIGURATIONS GENERATED BY WATER FLOWS AND THE WIND

12.1: Introduction to Bed Configurations
12.2: Unidirectional-Flow Bed Configurations
12.3: Velocity Profiles over Ripples
12.4: Movement of Ripples and Dunes
12.5: 2D Dunes and 3D Dunes
12.6: Oscillatory-Flow and Combined-Flow Bed Configurations
12.7: Wind Ripples and Eolian Dunes
12.8: Works Cited and Reading List

This page titled 12: Bed Configurations Generated by Water Flows and the Wind is shared under a CC BY-NC-SA 4.0 license and was authored, remixed, and/or curated by John Southard (MIT OpenCourseware) via source content that was edited to the style and standards of the LibreTexts platform.

12.1: Introduction to Bed Configurations

A striking characteristic of the transport of granular sediment over a bed of the same material by a turbulent flow of fluid is that in a wide range of conditions the bed is molded into topographic features, called bed forms, on a scale that is orders of magnitude larger than the grains. Little ripples at one's feet at the seashore, or on a dry river bed, or in the desert, and gigantic dunes in the desert and (even more common, but not apparent to the casual observer) in large rivers and the shallow ocean—all of these are examples of bed forms. Generations of scientists and engineers have marveled at the rich and confusing variety of these features.

First I will introduce some terminology. The overall bed geometry that exists at a given time in response to the flow (the **bed configuration**) is composed of individual topographic elements (**bed forms**). The aggregate or ensemble of similar bed configurations that can be produced by a given mean flow over a given sediment bed is the **bed state**: The bed configuration differs in detail from time to time, and the bed state can be considered to be the average over the infinity of configurations that are possible under those conditions. The term **bed phase** can be used for recognizably or qualitatively different kinds of bed configurations which are produced over some range of flow and sediment conditions and which are closely related in geometry and dynamics. Finally, the term **bedform** (one word) is widely used, indiscriminately, for all four of the foregoing aspects of the bed geometry.

Bed configurations that are common in natural flow environments can be generated by purely unidirectional flows, combined flows, and purely oscillatory flows. I pointed out in Chapter 6 that even purely oscillatory flows in natural flow environments can be more complex than those with only one oscillatory flow component, and that a wide range of oscillatory flows can be superimposed on a unidirectional current. (This would be a good point at which to go back and review the nature of oscillatory and combined flows.)

You can well imagine, then, how wide a range of bed configurations we should expect to have to deal with if we endeavor to make an inclusive survey of bed configurations. The enormous range of flows that can generate bed configurations, together with the complex dynamics of the response of the bed, makes for highly varied geometry of the resulting bed configurations. In one sense, though, this is fortunate for sedimentologists, because it provides a great variety of different sedimentary structures which can be used in attempting to make paleoflow interpretations!

Both engineers and geologists have been making laboratory experiments on bed forms for over one hundred years, as well as watching their movement in natural flow environments. Understanding of unidirectional-flow bed configurations is fairly good by now, although by no means perfect. Work on oscillatory-flow bed configurations is less well advanced, I think owing to the difficulty of arranging oscillatory flows with long oscillation periods in the laboratory. Finally, combined-flow bed configurations have still not been much studied.

If the flow changes with time, the bed configuration adjusts in response. In natural flows, equilibrium between the bed and the flow is the exception rather than the rule: usually the bed configuration lags behind the change in the flow. Such disequilibrium is a major element of complexity that makes relationships among bed phases much more difficult to decipher, but its effects are very important in natural flow environments.

In the natural environment most bed forms are seen in sands, but they are produced in silts and gravels as well. Of greatest interest to geologists, oceanographers, and hydraulic engineers are bed forms produced by flows of air or water over mineral sediments with equant grain shape, but a far wider range, important in many engineering applications, can be produced by flows of other fluids with other densities and viscosities over sediments less dense or more dense than the common mineral sediments.

Many natural scientists believe (and I am among them) that there must be enormous numbers of Earth-like planets throughout the universe. The field of extraterrestrial planets is a rapidly growing field nowadays, and it would not surprise me to learn, in the not too distant future, that such Earth-like planets are being discovered. In studying a physical phenomenon like bed configurations, there is an element of danger in restricting our consideration only to the few points in the spectrum of density ratios with which we have at hand: sand in water on Earth; sand in air on Earth; sand in the Martian atmosphere of the Venusian atmosphere; see Figure 8.1.5, in Chapter 8). In a sense, there is nothing special about those particular points in the spectrum!

Apart from their intrinsic scientific interest, bed forms are important in both geology and engineering. Large subaqueous bed forms many meters high can be obstacles to navigation, and their movement can be a threat to submarine structures. Engineers are interested in bed configurations partly because they play an important role in determining the sediment transport rate, but perhaps mainly because of their importance in determining the resistance which a channel presents to a flow. For example,

predicting the depth of flow in a channel built with a given slope and designed to carry a given water discharge necessitates knowing the bed configuration to be expected. Sedimentologists have given attention to bed configurations mostly because of their role in the development of stratification in sedimentary deposits; bed forms are one of the most useful tools available for interpreting ancient sedimentary environments.

The status of observations on bed configurations is good, but there is much room for further improvement. It is easy to observe bed configurations in steady unidirectional and simple bidirectional oscillatory flows in laboratory channels and tanks. But there is still a great need for further laboratory work, in part because the usually small width-to-depth ratios of tanks and flumes tend to inhibit full development of the three-dimensional aspects of the bed geometry, but also, and more importantly, because not much work has been done with multidirectional oscillatory flows, and, especially, combined flows. And even the largest of laboratory experiments are restricted to flow depths at the lower end of the range of natural flow depths. In nature, on the other hand, observations on bed configurations are limited by practical and technical difficulties, and the flows that produce them are usually more complicated.

This page titled 12.1: Introduction to Bed Configurations is shared under a CC BY-NC-SA 4.0 license and was authored, remixed, and/or curated by John Southard (MIT OpenCourseware) via source content that was edited to the style and standards of the LibreTexts platform.

12.2: Unidirectional-Flow Bed Configurations

Introduction

Bed configurations made by unidirectional flows have been studied more than those made by oscillatory flows and combined flows. They are formed in rivers and in shallow marine environments with strong currents, and also in engineering flows like outdoor canals and channels of various kinds, as well as in pipes and conduits carrying granular materials.

In shallow marine environments, even symmetrically reversing tidal currents produce bed forms that look much like those in truly unidirectional flows, presumably because the current in each direction flows for a long enough time for the bed to respond to what it feels as a unidirectional flow. In asymmetrical tidal currents, the bed forms show net movement and asymmetry in the direction of the stronger flow, but they suffer interesting modifications by the weaker flow in the other direction.

A Flume Experiment on Unidirectional-Flow Bed Configurations

To get an idea of the bed configurations produced by a steady uniform flow of water over a sand bed, and the succession of different kinds of bed configurations that appear as the flow strength is increased, imagine making a series of exploratory flume experiments on sand with a mean size between $0.2\ \mathrm{mm}$ and $0.5\ \mathrm{mm}$.

Build a large open channel consisting of wood or metal, with a rectangular cross section (Figure $12.2.1$). The channel might be about one meter wide and a few tens of meters long. Install a pump and some piping to take the water from the downstream end and recirculate it to the upstream end of the channel. You might mount the whole channel on a set of screw jacks near the upstream end, so that you can change the slope of the channel easily, but this is not really necessary. It would also be nice to make at least one sidewall of the channel out of glass or transparent plastic, for good viewing of the bed configurations.

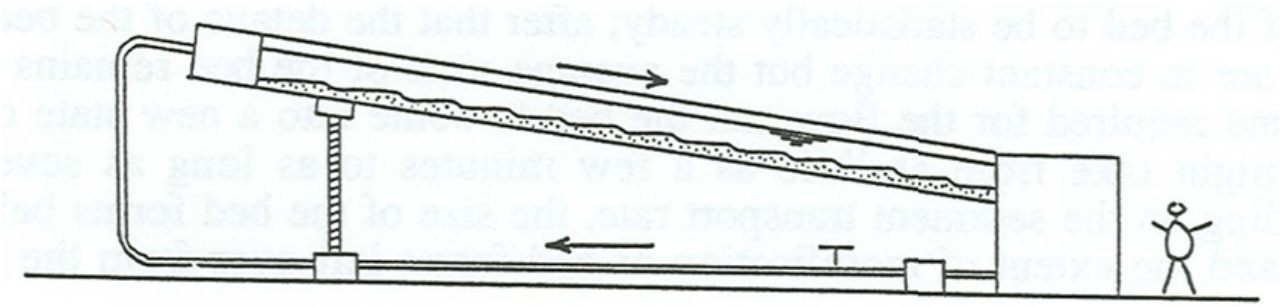


Figure $12.2.1$: A home-made flume for studying bed configurations in unidirectional flow.

Place a thick layer of sand on the bottom of the channel and then pass a series of steady and uniform flows over it. Arrange each run to have the same mean flow depth (as great as the flume will allow, ideally at least a large fraction of a meter, but a decimeter or two would suffice) and increase the mean flow velocity slightly from run to run.

In each run, let the flow interact with the bed long enough for the state of the bed to be statistically steady or unchanging. After that time the details of the bed configuration change constantly but the average state of the bed remains the same. The time required for the flow and the bed to come into a new state of equilibrium might be as little as a few minutes or as long as several days, depending on the sediment transport rate, the size of the bed forms that develop, and the extent of modification of bed forms that remained from the preceding run.

You could speed the attainment of equilibrium somewhat by continually adjusting the slope of the channel to maintain uniform flow as the bed roughness changes (the rougher the bed, the steeper the water-surface slope for a given water discharge), but these adjustments are not necessary, because the flow itself adjusts the bed for uniform flow by erosion at one end and deposition at the other.

If you are impatient for results, the way to make bed forms develop most rapidly is to start with an irregular sediment bed, but it is more instructive to start with a planar bed. (You can easily arrange a planar bed by passing a straight horizontal scraper blade along the bed. If you mount the blade on a carriage that slides on the straight upper edges of the flume walls, with a little care you obtain a beautifully planar bed.) Now turn the pump on and gradually increase the flow velocity.

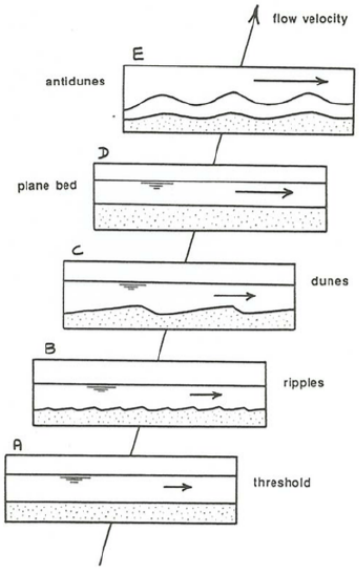


Figure 12.2.2: The sequence of bed phases with increasing flow velocity at a given flow depth, for medium sand.

Ripples:

After you exceed threshold conditions (Figure 12.2.2A), wait for a short time, and the flow will build very small irregularities at random points on the bed, not more than several grain diameters high, from which small ripples develop spontaneously.

You can help bed forms to develop on the planar bed by poking your finger into the bed at some point to localize the first appearance of bed forms. The flow soon transforms the little mound you made with your finger into a flow-molded bed form. The flow disturbance caused by this bed form scours the bed just downstream, and piles up enough sediment for another bed form to be produced, and so on until a beautiful widening train of downstream-growing bed forms is formed (Figure 12.2.3). Trains of bed forms like this, starting from various points on the bed, soon join together and pass through a complicated stage of development, finally to become a fully developed bed configuration (Figure 12.2.2B). The stronger the grain transport, the sooner the bed forms appear, and the faster they approach equilibrium. These bed forms, which I will later classify as **ripples**, show generally triangular shapes in cross sections parallel to the flow.

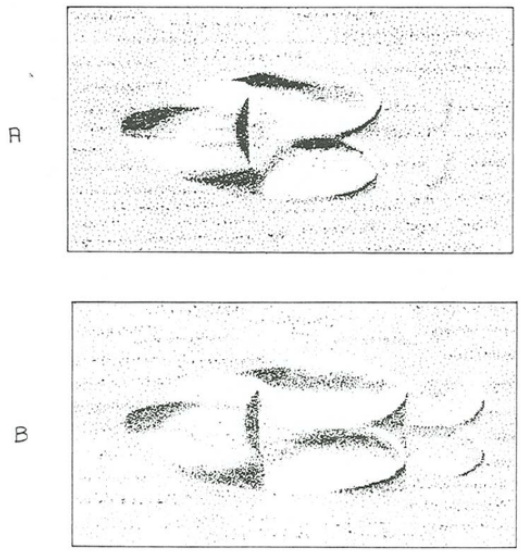


Figure 12.2.3: Two stages in the development of a train of ripples from a planar sand bed. Flow is from left to right, and light is from the upper left. The view is straight down on the sand bed. The depression in the left part of the pictures was made by dragging a rod along the bed. The mound thus produced was modified by the flow to become a ripple. (From photographs similar to those shown in Southard and Dingler, 1971.)

At this point I should introduce some terms for the geometry of ripples and other bed forms of similar shape; see Figure 12.2.4 . The region around the highest point on the ripple profile is the **crest**, and the region around the lowest point is the **trough**. The upstream-facing surface of the ripple, extending from a trough to the next crest downstream, is the **stoss surface**, and the downstream- facing surface, extending from a crest to the next trough downstream, is the **lee surface**. A well defined and nearly planar segment of the lee surface, called the **slip face**, is usually a prominent part of the profile. The top of the slip face is marked by a sharp break in slope called the **brink**. There is often but not always a break in slope at the base of the slip face also. The top of the slip face is not always the highest point on the profile, and the base of the slip face is not always the lowest point on the profile.

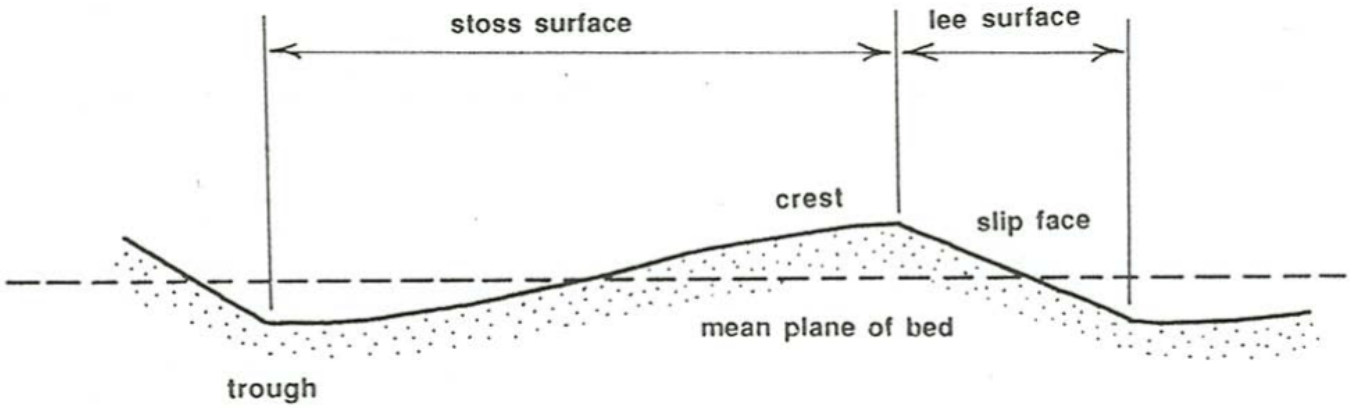


Figure 12.2.4: Terminology for ripple geometry in flow-parallel profile.

The stoss surfaces of ripples are gently sloping, usually less than about $10'$ relative to the mean plane of the bed, and their lee surfaces are steeper, usually at or not much less than the angle of repose of the granular material in water. Crests and troughs are oriented dominantly transverse to the mean flow but are irregular in detail in height and arrangement. The average spacing of ripples is of the order of $10–20$ cm, and the average height is a few centimeters. The ripples move downstream, at speeds orders of magnitude slower than the flow itself, by erosion of sediment from the stoss surface and deposition of sediment on the lee surface.

The field of ripples is commonly *three-dimensional*, rather than *two-dimensional* as it would be if the ripples were regular and straight-crested. (This terminology has the potential to be confusing. It is common in fluid dynamics to apply the term *two-*

dimensional to any feature that looks the same in all flow- parallel cross sections. That is true for perfectly regular ripples, with straight, flow-normal crests and troughs that are of the same height all along the ripple.) Most current ripples show great variability in their pattern of crests and troughs, as well as in crest heights and trough depths.

Dunes:

At a flow velocity that is a moderate fraction of a meter per second, ripples are replaced by larger bed forms usually called **dunes** (Figure $12.2.2$C). Dunes are fairly similar to ripples in geometry and movement, but they are at least an order of magnitude larger. The transition from ripples to dunes is complete over a narrow range of only a few centimeters per second in flow velocity. Within this transition the bed geometry is complicated: the ripples become slightly larger, with poorly defined larger forms intermingled, and then abruptly the larger forms become better organized and dominate the smaller forms. With increasing flow velocity, more and more sediment is transported over the dunes as suspended load. If your flume is large enough, the dunes become large enough under some conditions of sand size and flow velocity for smaller dunes to be superimposed on larger dunes.

Plane Bed:

With further increase in flow velocity the dunes become lower and more rounded, over a fairly wide interval of flow velocity, until finally they disappear entirely, giving way to a **planar bed surface** over which abundant suspended load as well as bed load is transported (Figure $12.2.2$D). Judging from the appearance of the bed after the flow is abruptly brought to a stop, the transport surface is very nearly planar, with relief no greater than a few grain diameters, although this subtle relief, reflecting the existence and movement of very low-relief bed forms, is thought by some to be responsible for the generation of planar lamination under conditions of net aggradation of the bed (see Chapter 16). Because the bed is obscured by abundant bed load and suspended load, it is difficult to observe the mode of grain transport over the planar bed except through the sidewall of the flume.

Antidunes:

As the flow velocity is increased still further, subdued standing waves appear on the water surface, and the resulting pattern of higher and lower near-bed flow velocity causes the bed to be molded correspondingly into a train of waves that are in phase with the water-surface waves. Under certain conditions these coupled bed waves and surface waves increase in amplitude and become unstable: they move slowly upstream and at the same time grow in amplitude, until they become so steep that they break abruptly, throwing much sediment into suspension (Figure $12.2.2$E). The bed and the water surface then revert to a planar or nearly planar condition, whereupon the waves build again and the cycle is repeated. Because of their upstream movement these forms are called **antidunes**, so named by G.K. Gilbert (1914) in his pioneering flume experiments on sediment transport and bed configurations.

In an approximate way, the condition for development of antidunes is that the upstream speed of propagation of surface water waves is about the same as the mean velocity of flow, so that the surface water waves have only a small speed relative to the channel bottom. The speed of shallow-water surface waves is well known to be $(gd)^{1/2}$ (see Chapter 6), where g is the acceleration of gravity and d is the water depth. The condition for development of antidunes is therefore

$$U \approx (gd)^{1/2} \tag{12.2.1}$$

or, dividing both sides by the right side to make the terms dimensionless,

$$\frac{U}{(gd)^{1/2}} \approx 1 \tag{12.2.2}$$

So conditions are favorable for the development of antidunes when the mean-flow Froude number approaches one. Of course, there must be an underlying instability in the first place to make the antidunes grow in amplitude when in- phase bed waves develop under the water-surface waves.

An instructive variation on your exploratory flume experiment is to increase the flow depth by a factor of two and cover the entire flow with a rigid planar sheet parallel to the mean plane of the bed. The flow structure in the lower half of the closed duct formed in this way is very nearly the same as that in the original open-channel flow (before surface waves set in), except for some differences in the largest-scale eddies in the outer layer owing to the possibility of large eddies making their way across the center plane of the flow, in the case of the closed duct. Now make the same sequence of runs with the top cover in place. You would find the same succession of bed configurations (Figure $12.2.5$) except for one major difference: standing waves and antidunes would not

appear, and plane-bed transport would be observed up to indefinitely high flow velocities. This demonstrates that the dynamics of antidunes is unrelated to the dynamics of ripples, dunes, and plane bed: antidunes are dependent upon the presence of the free surface, whereas ripples and dunes are independent of the presence of the free surface.

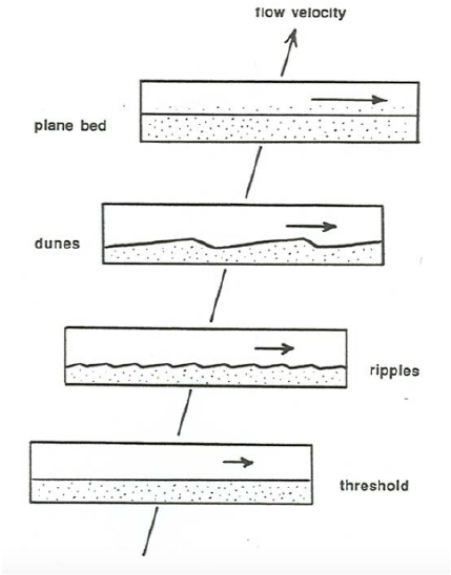


Figure 12.2.5: Sequence of bed phases as a function of flow velocity over medium sand in a closed conduit.

Dimensional Analysis

Now for a list of the most important variables associated with the fluid, the sediment, and the flow that define the bed state. Once we know the important variables, we can then develop a useful corresponding set of dimensionless variables and plot the positions of bed states observed in the laboratory and in natural flows in a graph with these dimensionless variables along the axes, to identify the fields or regions of existence or stability of the various bed phases. Although that does not address the dynamics behind the various bed phases—a fascinating and complicated matter, about which the last word is nowhere near having been said (see a later section in this chapter)—it provides a useful basis for paleoflow interpretations on the part of sedimentary geologists who work with the ancient sedimentary record, because the various bed configurations are commonly preserved in the record at least partly intact.

As is usual for work with real sediments in nature, even for equilibrium bed states in steady flows the number of variables is depressingly infinite, because an infinite number of variables are needed to describe the joint probability distribution of sediment density, grain size, and grain shape that is associated with any natural sediment. To obtain useful results we have to make some simplifying assumptions. We will assume that the sediment has only a single density and fairly equant particle shape, is subangular to subrounded rather than highly angular or perfectly well rounded, and is moderately well sorted but not unisize. Those assumptions might seem overly restrictive, but they describe most natural sands and fine gravels rather well: most natural sediments have densities not much different from that of quartz and are of approximately equant grain shape. Then the sediment can be characterized fairly well by just the average size D and the density ρ_s. Ignoring the size distribution is not as good an assumption; we should include the sorting σ in the analysis, but few studies have been made on the effect of sorting on bed configuration. The submerged weight per unit volume γ' of the sediment must be included in addition to ρ_s to take account of particle weight as well as particle inertia.

As usual, ρ and μ are needed to characterize the fluid. Two variables are needed to describe the flow: a flow-strength variable, and the flow depth d. Keeping in mind the discussion of flow variables in Chapter 8, we will first use U, which will lead to an unambiguous description in a three-dimensional graph, and then τ_o, which will lead to a two-dimensional graph with considerable overlapping of phase fields, although we will see that with an appropriate method for drag partition, to separate the skin friction from the total bed shear stress, a much better two-dimensional representation is possible.

Using first U as the flow-strength variable,

$$\text{bed state} = f\left(U, d, D, \rho, \mu, \gamma', \rho_s\right) \tag{12.2.3}$$

By dimensional analysis the seven variables chosen in an earlier section as being the most natural in characterizing the bed state can be grouped into four dimensionless variables that equally well characterize the bed state, in the sense that to every combination of the four dimensionless variables there is one and only one dimensionless bed state. Many such sets of dimensionless variables, all equivalent, are possible. Perhaps the simplest set, and certainly the most meaningful in terms of the physics of the flow, is the mean-flow Reynolds number $\rho U d/\mu$, a mean-flow Froude number $\rho^{1/2}U/\left(\gamma' d\right)^{1/2}$ written using γ', the relative roughness d/D, and the density ratio ρ_s/ρ. Another set, more useful sedimentologically in that it segregates U, d, and D into separate variables (Southard 1971; Harms et al. 1982; Southard and Boguchwal 1990), is

Illegal pream-token (\)

For a given density ratio ρ_s/ρ, data on bed states obtained for equilibrium flume runs in steady uniform flow and for field observations in flows thought to be reasonable approximations to steady uniform flow can be plotted in a three-dimensional graph with d^o, U^o, and D^o along the axes (Figure $12.2.6$). I will call this three-dimensional graph the *dimensionless depth–velocity–size diagram*. Each bed state that is observed in a flume or in a natural flow can be viewed as one of an infinite number of realizations of a single dimensionless bed state. The corresponding dimensionless depth d^o, dimensionless velocity U^o, and dimensionless sediment size D^o for that dimensionless bed state can be computed from the given data on d, U, D, ρ, and μ and plotted in the graph. The stability fields for the various bed phases occupy certain volumes (three-dimensional regions) in this graph, and the volumes should fill space exhaustively and non-overlappingly. Boundaries between bed phases are three-dimensional surfaces or transitional zones. The graph has to be in three dimensions, but you can see its nature fairly well by making two-dimensional sections through it. Such a graph is loosely analogous to the phase diagrams that petrologists use to represent the thermodynamic equilibrium of mineral phases. Bed-phase stability graphs are a good way of systematizing and unifying disparate data on bed states in a wide variety of flows and sediments.

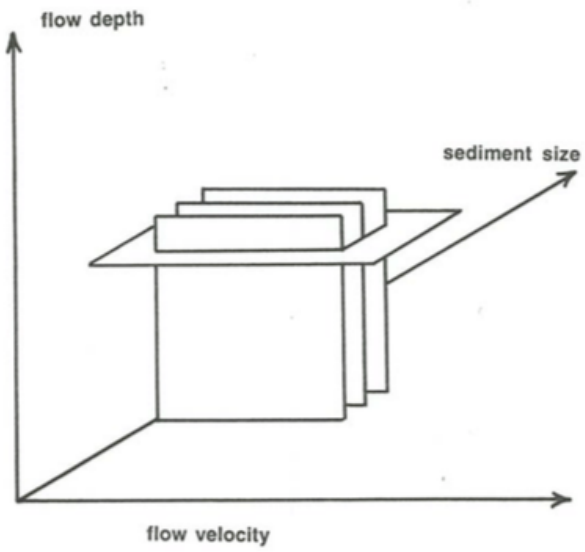


Figure $12.2.6$: The depth–velocity–size diagram for unidirectional-flow bed phases, showing three depth–velocity sections and one velocity–size section.

By virtue of the role of fluid density and fluid viscosity in the dimensional analysis on which the dimensionless variables in Equations ??? are based, the dimensionless depth–velocity–size diagram is implicitly standardized for water temperature. It is therefore possible to label the axes of the graph in an alternative way by using depths, velocities, and sizes referred to some arbitrary hypothetical water temperature. In compiling literature data for a depth-velocity-size diagram, I chose a reference temperature of $10^{\circ}\mathrm{C}$ as being reasonably representative of a wide range of natural subaqueous environments with flow- generated bed configurations in sands; otherwise there is nothing special about it. Using Equations ??? I computed from the original data the values of the $10^{\circ}\mathrm{C}$ depth d_{10}, the $10^{\circ}\mathrm{C}$ velocity U_{10}, and the $10^{\circ}\mathrm{C}$ size D10 for a flow of $10^{\circ}\mathrm{C}$ water dynamically equivalent to the actual flow, in the sense that it corresponds to the same set of values of d^o, U^o, and D^o. This is easily done (Southard and Boguchwal, 1990) for each variable by formulating the dimensionless value both from the given conditions and from the $10^{\circ}\mathrm{C}$ conditions, setting the two equal,

Illegal pream-token (\)

and then solving for the $10^{\circ}\mathrm{C}$ value on the assumption that the slight variation of ρ with temperature can be neglected (the error

being by a factor of only 1.003 even for $30'$ water):

Illegal pream-token (\)

In the rest of this chapter, depth, velocity, and sediment size referred to $10°\mathrm{C}$ water temperature in this way are called $10°\mathrm{C}$ -equivalent depth, velocity, and sediment size. Note in Equations ??? and ??? that because the factor in parentheses on the right side of the equations is raised to the $2/3$ power for d and D but to the $1/3$ power for U, a change in water temperature and therefore μ/ρ produces a greater change in effective flow depth and sediment size than in effective flow velocity.

The dimensionless depth–velocity–size diagram presented in a later section from literature data was drawn by computing d^o, U^o, and D^o for all the data points and plotting those points in a three-dimensional graph with d^o, U^o, and D^o along the axes. But then the three axes were converted to the $10°\mathrm{C}$-equivalent quantities d_{10}, U_{10}, and D_{10} by the procedure outlined above. The interior of the graph remains unchanged, but the graph becomes more useful by providing a concrete representation of depths, velocities, and sediment sizes. The values of d^o, U^o, and D^o associated with any point in the graph can be obtained using Equations ??? . Figure $12.2.7$ allows easy conversion between actual values of depth, velocity, and sediment size and dimensionless depth, velocity, and sediment size for two water temperatures, $0'\mathrm{C}$ and $30'\mathrm{C}$.

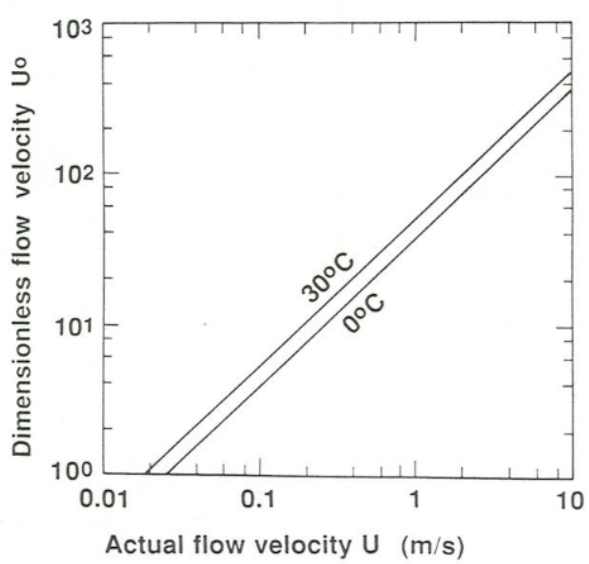


Figure $12.2.7$: Graph for converting between actual flow depth, flow velocity, and particle size, and dimensionless flow depth, flow velocity, and particle size.

If you want to use the dimensionless depth–velocity–size diagram to find the depth, velocity, and size of a bed state at some water temperature other than $10'\mathrm{C}$ that corresponds to a certain point (i.e., a certain dimensionless bed state) in the diagram, you have to use Equations ??? in reverse:

Illegal pream-token (\)

Because the particular bed state and the corresponding hypothetical (10^{\prime}\mathrm{C}\) bed state are rigorously similar (geometrically, kinematically, and dynamically), dependent variables with the dimensions of length, like bed-form height or spacing, are in the same ratio between the two states as d/d_{10} or D/D_{10}, found from Equations ???, ???, or ??? to be

$$\frac{d}{d_{10}} = \left(\frac{\mu}{\mu_{10}}\right)^{2/3} \tag{12.2.4}$$

and dependent variables with the dimensions of velocity, like the speed of bed-form movement, are in the same ratio between the two states as U/U_{10}, found likewise from Equations ???, ???, or ??? to be

$$\frac{U}{U_{10}} = \left(\frac{\mu}{\mu_{10}}\right)^{1/3} \tag{12.2.5}$$

It is difficult for the mind to translate values for dimensionless flow depth, flow velocity, and sediment size into real combinations of flow and sediment. In water flows on the Earth's surface, with water temperatures from $0°\mathrm{C}$ to $30°\mathrm{C}$ and a range of actual flow

depths from $0.01\ \mathrm{m}$ to $10\ \mathrm{m}$, dimensionless flow depth ranges from about 102 to almost 106. Likewise, in the same range of water temperature, for actual flow velocities from $0.1\ \mathrm{m/s}$ to a few meters per second, dimensionless flow velocity ranges from about 5 to about 150, and for actual sediment sizes from a few hundredths of a millimeter to a few centimeters, dimensionless sediment size ranges from about 0.5 to about 750.

Hydraulic Relationships

Depth-Velocity-Size Diagram

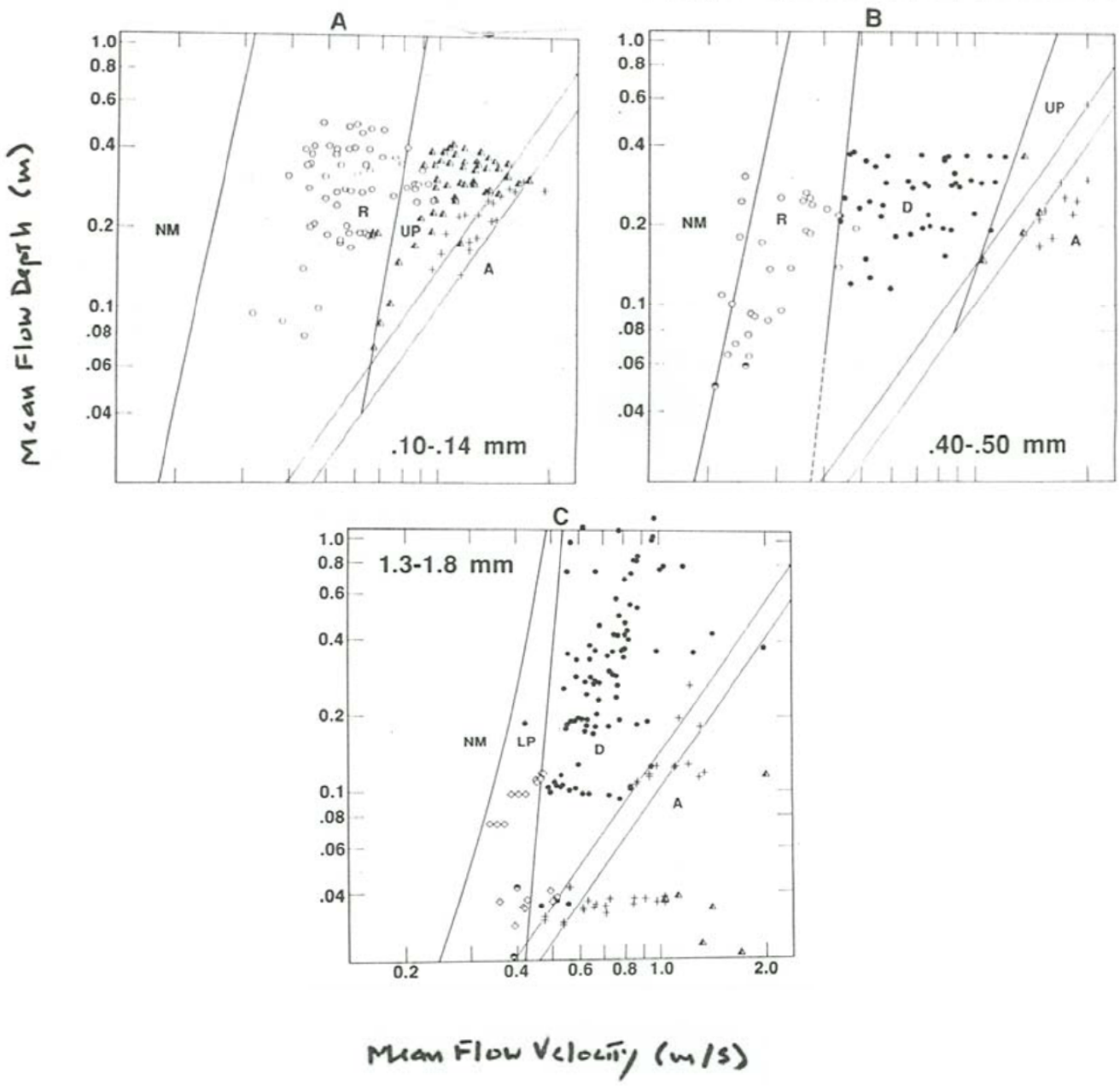


Figure 12.2.8: Bed phases in graphs of mean flow depth vs. mean flow

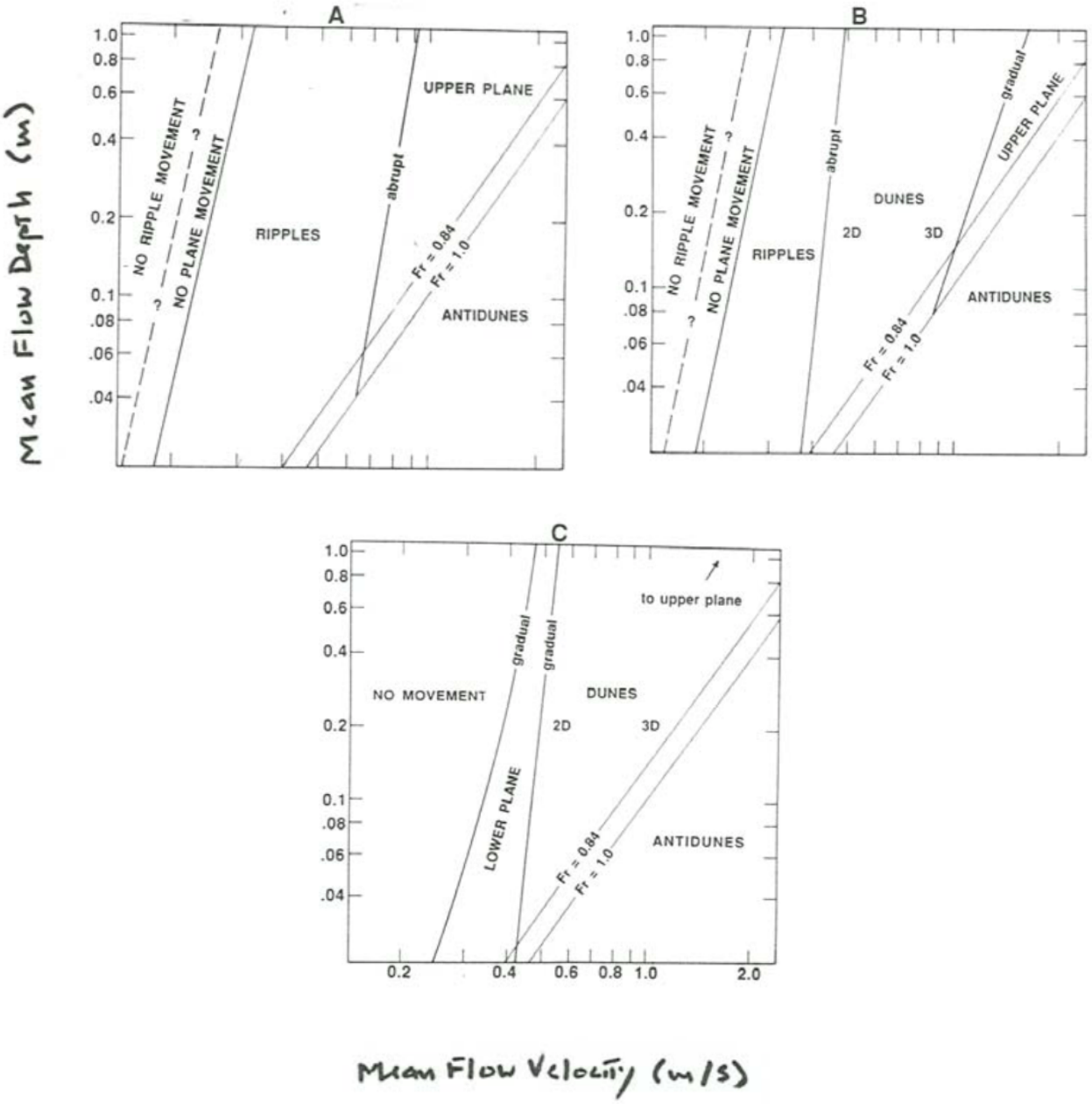

A
B
C
Mean Flow Depth (m)
1.0
0.8
0.6
0.4
0.2
0.1
.08
.06
.04
NO RIPPLE MOVEMENT
?
NO PLANE MOVEMENT
RIPPLES
abrupt
UPPER PLANE
Fr = 0.84
Fr = 1.0
ANTIDUNES
gradual
DUNES
2D
3D
NO MOVEMENT
LOWER PLANE
to upper plane
0.2
0.4
0.6
0.8
1.0
2.0
Mean Flow Velocity (m/s)

Figure 12.2.8.

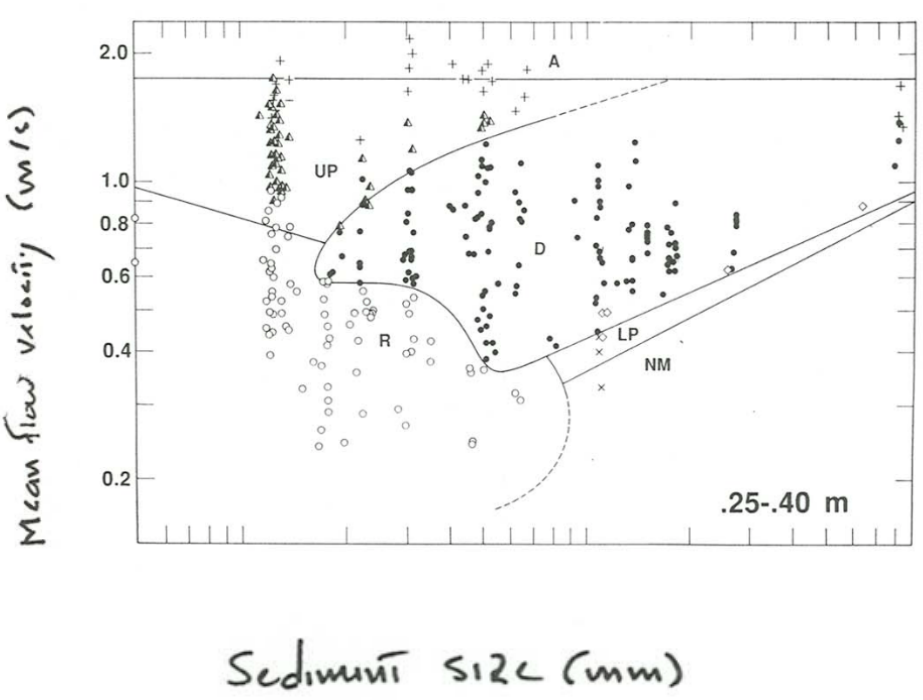


Figure 12.2.10: Bed phases in a graph of mean flow velocity vs. mean sediment size, for a mean flow depth of 0.25–0.40 m.

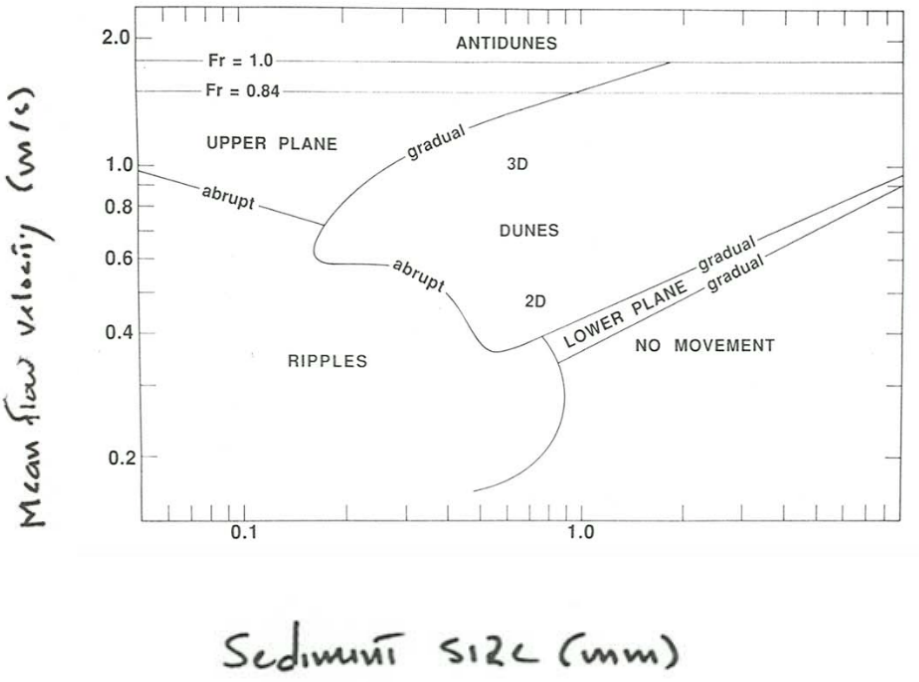


Figure 12.2.10.

Figures 12.2.8, 12.2.9, 12.2.10, and 12.2.11 show what the depth–velocity–size diagram for quartz sand in water looks like, on the basis of laboratory experiments made by many investigators. The experiments have been made mainly at flow depths less than a meter. It is much more difficult to obtain data points from deeper natural flows, and none are included in these figures; see below for further discussion of bed configurations in deeper flow depths.

I have labeled the axes in Figures 12.2.8 through 12.2.11 not with the dimensionless variables but with the actual values of flow velocity U, flow depth d, and sediment size D that correspond to the respective dimensionless variables for an arbitrary reference

water temperature of $10°C$. This provides a concrete feeling for flow and sediment conditions while preserving the interior features of the dimensionless graph. Ignoring the water temperature would lead to considerable scatter in the data points, and would obscure the strong regularities shown by the dimensionless diagram.

Figures 12.2.8 and 12.2.9 show three depth–velocity sections for sediment sizes of $0.10–0.14$ mm, $0.40–0.50$ mm, and $1.30–1.80$ mm. Figure 12.2.8 shows data points from many experimental studies, and Figure 12.2.9 is a schematic version of Figure 12.2.8. Figures 12.2.10 and 12.2.11 show a velocity–size section for a flow depth of $0.25–0.40$ m. Figure 12.2.10 shows data points, and Figure 12.2.11 is a schematic version. Figures 12.2.8 through 12.2.11 are from Boguchwal and Southard (1990).

The section for $0.10–0.14$ mm sand (Figures 12.2.8A, 12.2.9A) shows fields only for ripples, upper-regime plane bed, and antidunes. All the boundaries here and in the other two graphs in Figures 12.2.8 and 12.2.9 slope upward to the right. The boundary between ripples and plane bed slopes in that sense because the deeper the flow the greater the velocity needed for a given bed shear stress. The boundary between plane bed and antidunes slopes in that sense because it is well represented by the condition that the Froude number $U/(gd)^{1/2}$ is equal to one, as discussed above. The latter boundary is shown to truncate the former, because (though data are scanty) as the Froude number approaches one, antidunes develop irrespective of the preexisting configuration. This relation holds true also, and more clearly, for coarser sediments (Figures 12.2.8B, 12.2.8C, 12.2.9B, 12.2.10C).

Figure 12.2.8A (and Figure 12.2.8B, for medium sands, as well) show two kinds of boundary between movement and no movement. To the right is the curve for incipient movement on a plane bed, and to the left is the boundary that defines the minimum velocity needed to maintain preexisting ripples at equilibrium. It is clear that the latter boundary lies to the left of the former, but the existing data are not good enough to define the positions of these boundaries well. (Only the former boundary is shown in Figures 12.2.8A and 12.2.9B.)

The section for $0.40–0.50$ mm sand (Figures 12.2.8B, 12.2.9B) shows an additional field for dunes between the fields for ripples and for plane bed. The boundary between dunes and plane bed clearly slopes less steeply than the boundary between ripples and dunes. For depths less than about 0.05 m it is difficult to differentiate between ripples and dunes, because dunes become severely limited in size by the shallow flow depth. The appearance and expansion of the dune field with increasing sediment size pushes the lower termination of the plane-bed field to greater depths and velocities, nearly out of the range of most flume work. The antidune field truncates not only the ripple field, as with finer sands, but the dune field as well.

In the section for $1.30–1.80$ mm sand (Figures 12.2.8C, 12.2.9C), a lower- regime plane bed replaces ripples at low flow velocities. Upper-regime plane bed is still present in the upper right, but few flume data are available. Upper-regime plane beds succeed antidunes with increasing velocity and decreasing depth in the lower right; apparently the bed becomes planar once again as the Froude number becomes sufficiently greater than one. The left-hand boundary in Figures 12.2.8C and 12.2.9C represents the threshold for sediment movement on a plane bed. Sections for even greater sediment size are qualitatively similar to the section shown in Figures 12.2.8C and 12.2.9C.

In the velocity–size section for flow depths of $0.25–0.40$ m (Figures 12.2.10, 12.2.11), ripples are the stable bed phase for sediment sizes finer than about 0.8 mm. The range of flow velocity for ripples becomes narrower with increasing sediment size, and the ripple field finally ends against the fields for plane beds with or without sediment movement. Relationships in this region are difficult to study because in these sand sizes and flow velocities a long time is needed for the bed to attain equilibrium. In medium sands ripples give way abruptly to dunes with increasing flow velocity, but, in finer sediment, ripples give way (also abruptly) to plane bed. Although not well constrained, the ripple–plane boundary rises to higher velocities with decreasing sediment size.

Dunes are stable over a wide range of flow velocities in sediments from medium sand to indefinitely coarse gravel. Both the lower and upper boundaries of the dune field rise with increasing flow velocity, and both are gradual transitions rather than sharp breaks. For sediments coarser than about 0.8 mm there is a narrow field below the dune field for lower-regime plane bed; the lower boundary of this field is represented by the curve for threshold of sediment movement on a plane bed.

There is one *triple point* among ripples, dunes, and upper plane bed at a sediment size of about 0.2 mm, and another among ripples, dunes and lower plane bed at a sediment size of about 0.8 mm. The coverage of data around these two triple points constrains the bed-phase relationships fairly closely. Between these two triple points the dune field forms a kind of indented salient pointing toward finer sediment sizes. The boundary between ripples and upper plane bed seems to pass beneath the dune field at the upper left triple point to emerge again at coarser sediment size and lower flow velocity as the boundary between ripples and lower plane bed at the lower right triple point.

Other velocity–size sections, for other flow depths, show the same qualitative relationships as Figures 12.2.10 and 12.2.11. With increasing flow depth the lower boundary of the antidune field rises very rapidly, and antidunes are unimportant in flows greater

than a few meters deep. All the other boundaries rise more slowly with increasing flow depth. There is also some change in the shape of the dune field with increasing flow depth.

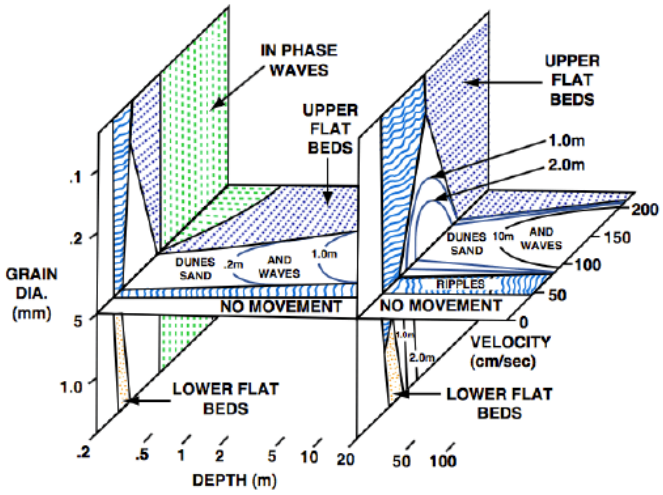
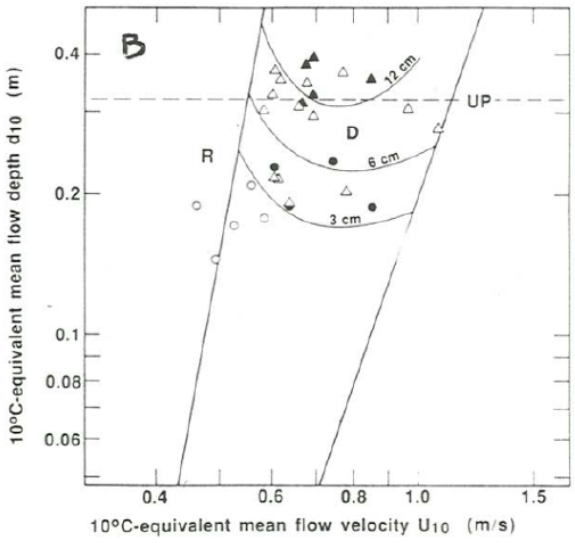


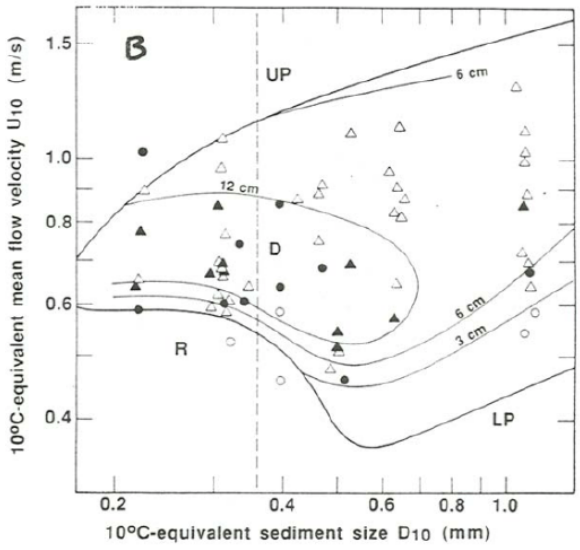
Figure by MIT OpenCourseWare.

Figure 12.2.12: Schematic depth–velocity–size diagram showing bed-phase stability field for bed phases in steady unidirectional water flows with a wide range of flow depths in flumes and natural environments. (From Rubin and McCulloch, 1980.)

Numerous observations of bed configurations in natural environments in which sands are subjected to fairly steady unidirectional flows indicate that the stability relationships of bed configurations in deeper flows are a straightforward extrapolation of the depth–velocity–size diagram discussed above. Ripples are almost the same in shallow flows and deep flows, but dunes in deep flows are much larger than dunes in shallow flows. Figure 12.2.12, after Rubin and McCulloch (1980), shows an extrapolation of the depth–velocity–size diagram to much greater flow depths based on data from several studies in natural flow environments.



Figures 12.2.8 *and* 12.2.10 *in the depth–velocity–size diagram.*



Figures $12.2.8$ *and* $12.2.10$ *in the depth–velocity–size diagram.*

There must be a definite average dune height and spacing associated with each point in the existence field for dunes in the depth–velocity–size diagram. Unfortunately, few experimental studies have reported dune dimensions systematically. Figures $12.2.13$ and $12.2.14$ make use of data on dune spacings and heights from the best data set, that of Guy et al. (1966), in a crude attempt to contour dune spacings and heights in the depth–velocity–size diagram. Figures $12.2.13$A and $12.2.13$B show contours of dune spacing and height in a depth–velocity section for a sediment size of 0.30–0.40 mm, and Figures $12.2.14$A and $12.2.14$B show contours of dune spacing and height in a velocity–size section for a flow depth of 0.25–0.40 m.

In the depth-velocity section (Fig. $12.2.13$A), dune spacing increases from lower left to upper right, with increasing depth and velocity. In the velocity-size section (Fig. $12.2.14$A), dune spacing increases from lower right to upper left with increasing velocity and decreasing sediment size; the greatest spacings are at the upper-plane-bed boundary and a sediment size of between 0.2 and 0.3 mm. Dune height shows a different and more complicated behavior. In the depth–velocity section (Fig. $12.2.13$B), dune height increases monotonically with increasing depth but shows an increase and then a decrease with increasing flow velocity at constant depth. In the velocity–size section (Fig. $12.2.14$B), there is an elongated core of greatest heights extending from near the left-hand extremity of the dune field, at the finest sizes of about 0.2 mm, rightward to sizes of 0.5 to 0.6 mm. Heights seem to decrease in all directions from that core, most rapidly with decreasing flow velocity.

The sections in Figures $12.2.13$ and $12.2.14$ intersect each other at right angles at the dashed line shown on both sections. You have to imagine the contours as cuts through a family of curved surfaces in three dimensions filling the dune field in the depth–velocity–size diagram.

Diagrams with Bed Shear Stress

So far we have looked at the hydraulic relationships of bed phases using the mean flow velocity U as the flow-strength variable. Most investigators have chosen to use the bed shear stress τ_o rather than U. What do the same relationships look like in graphs using the bed shear stress τ_o? One thing we can say right away about such graphs is that the effect of flow depth is much less: the effect of the substantial change in velocity with flow depth for a given bed shear stress is no longer relevant, and all that is left is the smaller effect on the bed shear stress of changes in bed-form geometry with flow depth. A single suitably nondimensionalized two-dimensional graph of bed shear stress against sediment size should therefore be expected to represent bed states reasonably well. Simons and Richardson (1966) seem to have been the first to use such a plot, although in the dimensional form of τ_o vs. D. A later and more comprehensive of plots of this kind was given by Allen (1982, Vol. 1, p. 339–340), who plots Shields parameter and dimensionless (temperature-standardized) stream power against dimensionless (temperature-standardized) sediment size.

Boundary shear stress can be nondimensionalized in various ways. The conventional way is to form a dimensionless variable containing τ_o and D, namely $\tau_o/\gamma' D$, usually called the Shields parameter (see Chapter 9). One can also work with a dimensionless form of the stream power $\tau_o U$, on the theory that the sediment transport depends most fundamentally upon stream power. Another alternative is $\tau_o \left(\rho/\gamma'^2 \mu^2\right)^{1/3}$, which I call here the dimensionless boundary shear stress T^o. The disadvantage with T^o is that it

does not embody the physics of the phenomenon nearly as well as the Shields parameter, but the advantage is that, when T° is used with D°, $\tau_{\circ}$ and D do not appear together in the same dimensionless variable. We will work with this last alternative, because it lends itself more directly to temperature standardization, which is important in the range of conditions for which Reynolds-number effects cannot be neglected, and also because sediment-size effects are thereby manifested entirely through the dimensionless sediment size $D\left(\rho\gamma'/\mu^2\right)^{1/3}$.

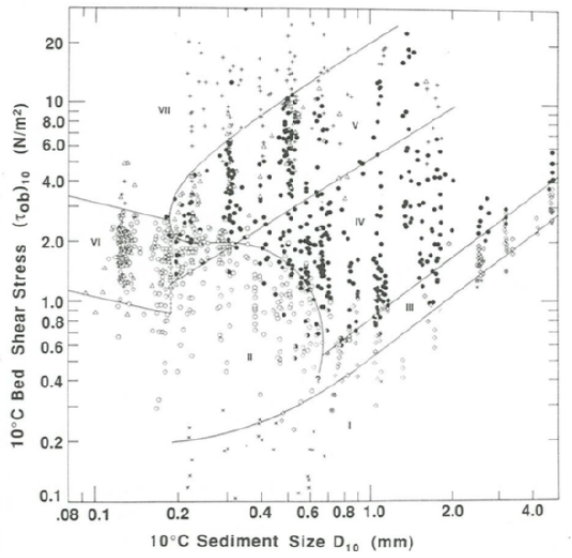


Figure 12.2.15: Bed phases in a dimensionless (temperature-standardized) plot of sidewall-corrected bed shear stress vs. sediment size for bed phases. labels for regions: I, no movement on plane bed; II, ripples; III, lower plane bed; IV, dunes; V overlap region of dunes, upper plane bed, and antidunes; VI, overlap region of ripples, upper plane bed, and antidunes; VII overlap region of upper plane bed and antidunes.

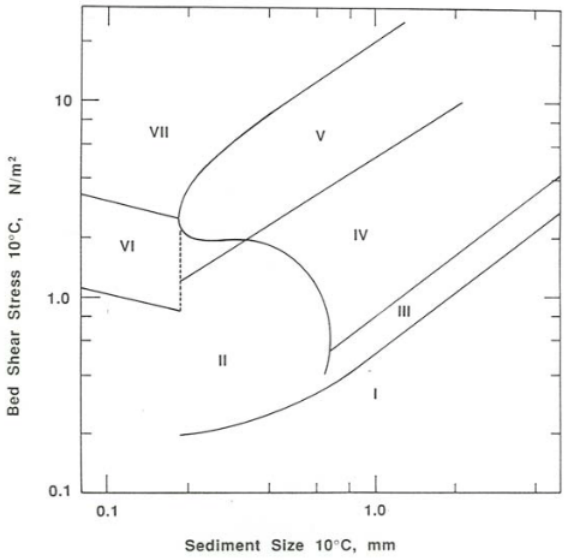


Figure 12.2.15.

Figure 12.2.15 is a plot of T° vs. D° showing the stability fields for the various bed phases. The same data sources were used as for the depth–velocity– size graph discussed above, except that fewer studies were used because some studies that reported the mean flow velocity did not report the energy slope, so $\tau_{\circ}$ could not be computed. Only runs made at depths greater than 0.06 m were used. In all, 1204 runs were used. $10^{\circ}\mathrm{C}$-equivalent flow depths d_{10} range from 0.06 m up to the deepest reported in the sources used, a little greater than 1 m (by Nordin 1976). Figure 12.2.16 is a schematic version of Figure 12.2.15.

The value of τo for each run was corrected for sidewall effects by the method proposed by Vanoni and Brooks (1957). (For a summary of this method, see Vanoni 1975, p. 152–154.) The result is an estimate of the shear stress τ_{ob} acting on the sediment bed only. Because the bed is always rougher than the sidewalls (except for dynamically smooth flow over a planar granular bed),

and the width/depth ratio is never infinite, this estimate of τ_{ob} is always greater than the boundary shear stress averaged over the wetted perimeter of the flow, which is found from the experimental data by use of the resistance equation for steady uniform flow in an open channel, $\tau_o = \rho g A S/p$, where A is the cross-sectional area of the flow and p is the wetted perimeter of the flow. For bed states with rugged flow-transverse bed forms in flows with small width/depth ratios, τ_{ob} can be almost half again as large as τ_o.

The axes of the graph in Figure $12.2.15$ are not labeled with T^o and T^o but with D_{10} and $(\tau_{ob})_{10}$, the sidewall-corrected bed shear stress standardized to a water temperature of $10°C$. As with depth, velocity, and size in an earlier section, (\left(\tau_{\mathrm{o}b\right)_{10}\) is related to (\tau_{\mathrm{o}b}\) by the equation

$$(\tau_{ob})_{10} = \tau_{ob}\left(\frac{\mu_{10}}{\mu}\right)^{2/3} \tag{12.2.6}$$

obtained by equating values of T^o for $10°C$ and for the given conditions and solving for $(\tau_{ob})_{10}$ on the assumption that ρ and γ' do not vary with temperature.

Scatter or overlapping of points for different bed phases is much greater in Figure $12.2.15$ than in the various sections through the dimensionless depth– velocity–size diagram, for two main reasons:

1. It is well known that because the form resistance, which is the dominant contribution to the total bed shear stress over rugged flow-transverse bed forms, disappears in the transition from ripples to upper plane bed or from dunes to upper plane bed, the total bed shear stress actually decreases with increasing mean flow velocity in these transitions before it increases again. For that reason, there is a certain range of τ_{ob} for which three different values of U are possible; see Figure 8.5.1, back in Chapter 8. In a plot of τ_{ob} against D, this means that there is an approximately horizontal band across the graph in which values of U, and thus also their associated bed phases, overlap or fold onto one another. In Figure $12.2.15$ this is shown as a field of overlapping dunes, upper plane bed, and antidunes, labeled V, and a field of overlapping ripples, upper plane bed, and antidunes, labeled VI.
2. Accurate measurement of water-surface slope S, and therefore τ_o, is understandably less accurate than measurement of U : water-surface slopes are small, so long channels and careful surveying are needed, and in any case the slope varies with time around some long-term average as the details of the bed configuration fluctuate, so long time series of S are needed for good accuracy. These problems with the slope presumably affect all of Figure $12.2.15$, but they are noticeable only at bed-phase boundaries that should not be affected by the shear-stress ambiguity noted above, like the boundary between ripples and dunes or the boundary between lower plane bed and dunes.

The effects of data scatter and phase-field overlap make partitioning Figure $12.2.15$ into existence fields for the various bed phases not a straightforward matter. The more straightforward results for the depth–velocity–size diagram were used as a guide in developing a rational partition.

Because of the moderate degree of scatter of ripple and dune points, the boundary between ripples (Region II) and dunes (Region IV) can be located only in a general way. The overall shape of the boundary was made qualitatively similar to that in the depth–velocity–size diagram (Figures $12.2.8$ through $12.2.11$). It is reasonable to suppose that this boundary continues downward past the question mark and then leftward to define the minimum shear stress for existence of ripples, as in Figures $12.2.10$ and $12.2.11$. Because few investigators have attempted to identify the weakest flows for which preexisting ripples are maintained as flow strength is very gradually decreased while equilibrium is maintained, existing data are inadequate to define the position of this extension. Either the plane-bed threshold curve is eclipsed by the lower part of the ripple field, as in Figures $12.2.10$ and $12.2.11$, or the lower boundary of the ripple field is at bed shear stresses entirely above those for the plane-bed threshold curve. The threshold curve itself is not extended leftward because of this uncertainty.

Interpretation of the remaining boundaries is based upon the existence of a minimum sediment size of about $0.15–0.20\ \mathrm{mm}$ for existence of dunes, as shown clearly by left-pointing “nose” of the dune field in the velocity–size sections through the depth–velocity–size diagram together with the effect of the \(\tau_{\text{o}}\) ambiguity on the relations among ripples, dunes, and plane beds. As in the velocity–size sections through the depth–velocity–size diagram, the ripple–dune boundary in Figure $12.2.16$ is interpreted to pass leftward through an inflection point and then curve upward and again rightward, passing through the sediment-size minimum for dunes, to become the upper limit of dune stability (between Regions V and VII).

Owing to the shear-stress ambiguity there is a substantial range of shear stresses below this upper boundary for dunes for which either dunes or plane bed can exist. The lower limit of this overlap region (Region V) is shown as a straight line sloping downward to the left. Neither the shape nor the position of this line is well constrained by the data. By its nature, this boundary must end leftward at the minimum sediment size for the existence of dunes; it is therefore connected upward to the point of minimum sediment size by a vertical dashed line. In the small unlabeled region with approximately triangular shape (bounded below by this

lower limit of upper-plane-bed stability, above by the upper limit of ripple stability, and to the left by the leftward limit of dune stability), ripple and dune points overlap.

To the left of the minimum sediment size for dunes, ripple pass directly into upper plane bed with increasing flow strength, and again there is a broad region of overlap of ripples and upper plane bed (Region VI). In this region the vertical span of the overlap region is about as great as the span of available data, so the two boundaries sloping downward to the right here (the upper showing the maximum shear stresses for existence of ripples, and the lower showing the minimum shear stresses for existence of plane beds) are poorly constrained. The slopes of these lines were chosen only by analogy with that of the boundary between ripples and upper plane bed in the velocity–depth sections of the depth–velocity–size diagram; both their slope and their parallelism are arbitrary.

The upper of these two boundaries, giving the upper limit for ripples, is shown to end at the sediment-size minimum for dunes (i.e., the point of vertical tangent at the leftward extremity of the dune field), although this is not a necessity: the intersection could just as well lie somewhat above or somewhat below that point. In any case, the second of these boundaries, representing the lower limit for existence of upper plane beds, must terminate rightward at the same sediment size—hence the vertical dashed line connecting the two boundaries. Because the intersection should not be expected to be exactly at the minimum sediment size for dunes, this vertical dashed line should actually be at a slightly different and greater sediment size from the vertical dashed line, mentioned above, that connects the two analogous curves for dunes at greater sediment sizes. So there must really be *two* vertical dashed lines, very close together. Existing data, extensive as they are, are inadequate to locate the two corresponding sediment sizes with certainty, and they are shown as a single vertical dashed line in Figure $12.2.15$.

Points for antidunes appear throughout Regions VI and VII and in the upper part of Region V in Figure $12.2.15$. Presumably the reason there is no boundary between upper plane bed and antidunes in what is labeled as Region VII in Figure $12.2.15$ is that the transition from upper plane bed to antidunes with increasing flow velocity at the flow depths characteristic of many flume experiments takes place at bed shear stresses well below those of Region VII.

The consequences of lumping all flow depths into the single plot represented by Figure $12.2.15$ are substantial only for antidunes, because the onset of antidunes depends upon the mean-flow Froude number. Plots of $(\tau_{ob})_{10}$ vs. D_{10} for the individual depth categories used in plotting the depth–velocity–size diagram show a systematic, although still scattered, rise in the position of the minimum shear stresses for antidunes as flow depth increases. Other effects of flow depth on the positions of the various boundaries in $(\tau_{ob})_{10}$–D_{10} plots are so minor as to be swamped by the data scatter.

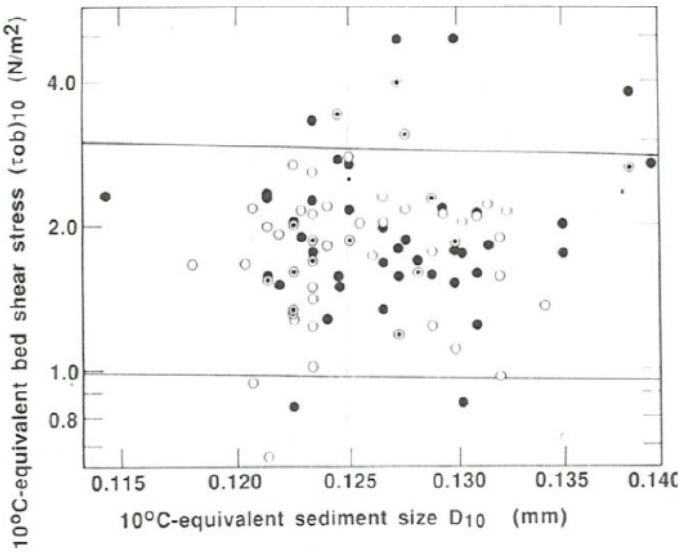


Figure $12.2.15$. *Symbols: solid circles, upper plane bed; bull's-eye circles, antidunes; open circles, ripples.*

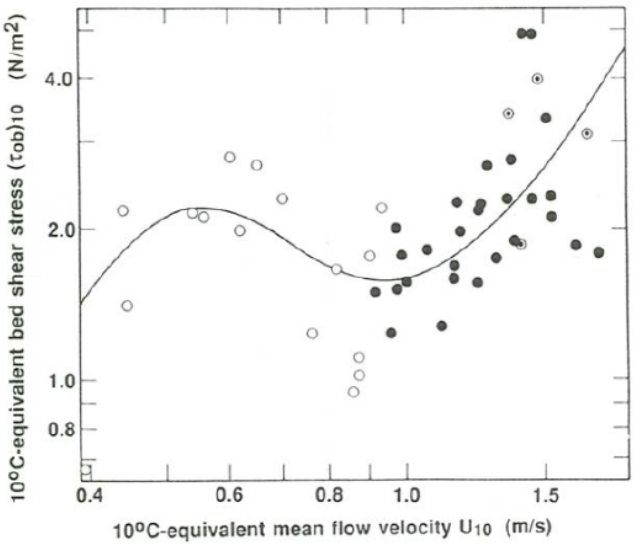


Figure 12.2.17.

The welter of overlapped points for ripples, upper plane bed, and antidunes for sediment sizes around $0.12\ \mathrm{mm}$, mostly from the work of Willis et al. (1972), is difficult to distinguish in Figure $12.2.15$, so all the runs made in that study for which slope was reported are replotted in Figure $12.2.17$ with the sediment-size axis stretched relative to the shear-stress axis. The straight lines represent the minimum shear stresses for ripples and the minimum shear stresses for upper plane beds, taken from Figure $12.2.15$. The thorough blending of points for the three phases is clear. Figure $12.2.18$, a plot of $10^{\circ}\mathrm{C}$-equivalent bed shear stress against $10^{\circ}\mathrm{C}$-equivalent mean flow velocity for those same points, shows why the points in Figure ({12{.}2{.}\eatSpaces{17} \endSpaces}\) are so scrambled. Despite the considerable scatter, there clearly is first an increase, then a decrease, and then again an increase in shear stress with increasing velocity, as shown by the curve that represents very approximately the trend of the data points. The range in shear stress between the local minimum and the local maximum in that curve, together with the inevitable scatter in the shear stresses themselves, is sufficient for substantial mixing of the points.

The plot in Figure $12.2.15$ could be transformed into a plot of Shields parameter against dimensionless sediment size, or into a plot of dimensionless flow power against dimensionless sediment size (neither of which is shown here), but with no obvious advantages for sedimentological interpretation. These plots would be qualitatively different in certain ways from those presented by Allen (1982) because of the influence of the results from the depth–velocity–size diagram on our method of partitioning Figure $12.2.15$.

Van den Berg and van Gelder (1993) introduced a bed-phase stability diagram (Figure $12.2.19$) based on boundary shear stress that in large part removes the difficulties discussed above. The horizontal axis is the dimensionless sediment size used above, and the vertical axis is a Shields parameter modified in such a way that the bed shear stress is represented by the part generated by the particle roughness rather than the form drag associated with bed forms. The strategy is to express the bed shear stress in terms of a Chézy coefficient (see Chapter 4) that is a function of the ratio of water depth to D_{90}, the ninetieth-percentile particle size. This largely circumvents the dominance of form drag in the presence of rugged bed forms. You can see from the diagram that there is much less ambiguity in partitioning of existence fields than in Figure $12.2.15$, but there is still considerable overlap between dunes and upper plane bed, suggesting that the method for drag partitioning is still less than perfect. Nonetheless, Figure $12.2.19$ is a great improvement over earlier existence diagrams based on bed shear stress.

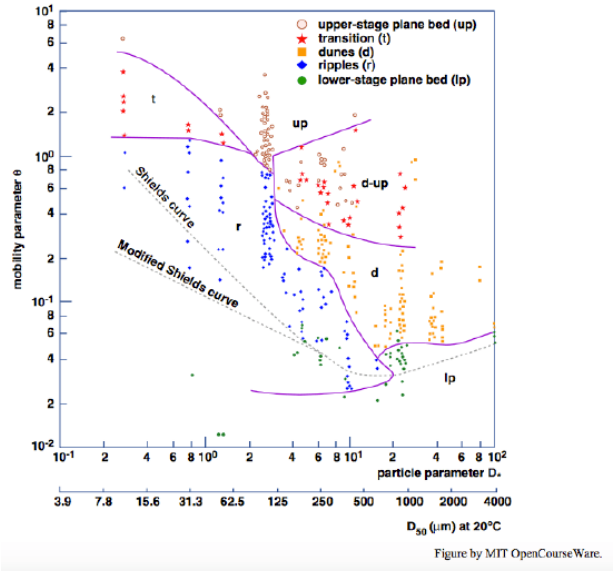


Figure 12.2.19: Existence fields for bed phases in a dimensionless plot of modified Shields parameter vs. dimensionless sediment size. (From van den Berg and van Gelder, 1993.)

Flow Regimes

This is the place to be more specific about the terms **lower flow regime** and **upper flow regime** I have used a few times already. Simons and Richardson (1963) proposed that bed phases be classified into a lower flow regime and an upper flow regime on the basis of the transition from the rugged ripple-like bed phases (ripples and dunes) formed at relatively low flow strengths and the less rugged bed phases (upper plane bed and antidunes) formed at high flow strengths (Figure 12.2.20A). The motivation for this classification was not so much the sharp distinction in bed geometry in itself as the great decrease in flow resistance in passing from the lower flow regime to the upper flow regime. Geologists have found the distinction useful not only in terms of the differing bed geometry but also in terms of the consequent great difference in sedimentary structures produced: with the minor exception of lower-regime plane beds, lower-regime conditions give rise to cross-stratified structures, whereas upper-regime conditions give rise mostly to planar lamination—although antidunes produce cross-stratification as well: see Chapter 15.

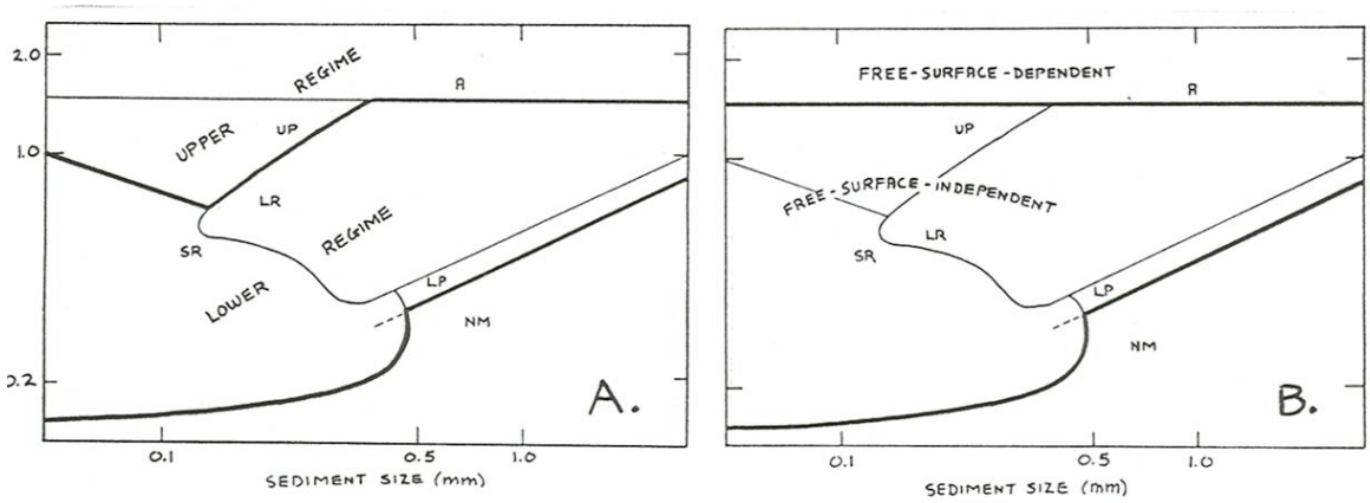


Figure 12.2.10*) showing the customary division into an upper flow regime and a lower flow regime based on the transition from ripple and dune bed phases to upper plane bed or antidunes.* ***B)*** *The same velocity–size diagram showing an alternative division into a lower group of bed phases (lower plane bed ripples, dunes, and upper plane bed) whose dynamics are independent of the presence of a free surface and an upper bed phase (antidunes) whose dynamics are dependent upon the presence of a free surface.*

In terms of bed-configuration dynamics, it is also natural to divide bed phases into two groups in a different way on the basis of the importance of a free surface (Figure 12.2.20B). Ripples, dunes, and plane bed are bed phases whose occurrence is independent of the existence of a free surface: recall that in the exploratory flume experiments described earlier in this chapter

the existence of ripples was not affected by placing a board over the water surface. These bed phases could therefore be termed *free-surface-independent* bed phases. Antidunes, on the other hand, are dependent upon the existence of a free surface, and could therefore be termed a *free-surface-dependent* bed phase.

Flow Over Ripples and Dunes

Flow over ripples and dunes is dominated by **flow separation**, a phenomenon whereby the flow separates from the solid boundary in the region where the boundary curves away from the general upstream flow direction. The general picture of separated flow over a ripple or a dune is shown in Figure 12.2.21, and in more cartoonlike form in Figure 12.2.22. When the flow reaches the crest it continues to move in the same direction rather than bending downward to follow the contour of the bed. Strong turbulence develops along the surface of strong shear, called the **shear layer**, which represents the contrast between the high velocity in the separated flow and the low velocity in the shelter of the bed form. This turbulence expands both upward and downward, and at some position downstream of the crest the turbulent shear layer meets the sediment bed. The flow is said to **reattach** to the bed at that point. Downstream of reattachment, the flow near the bed is directed downstream once again. Upstream of reattachment, in what is called the **separation vortex**, the bed feels a weak flow in the reverse direction.

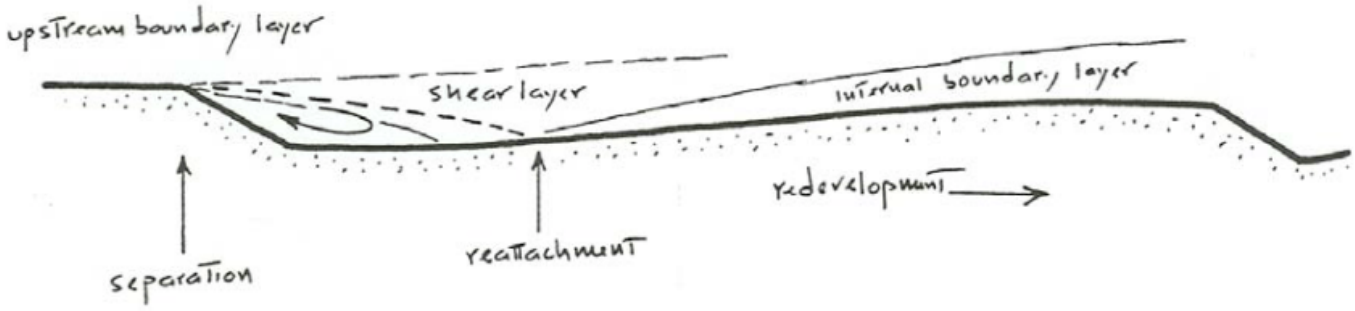


Figure 12.2.21: Flow structure over ripple or dune bed forms. (Schematic, but not much vertical exaggeration.)

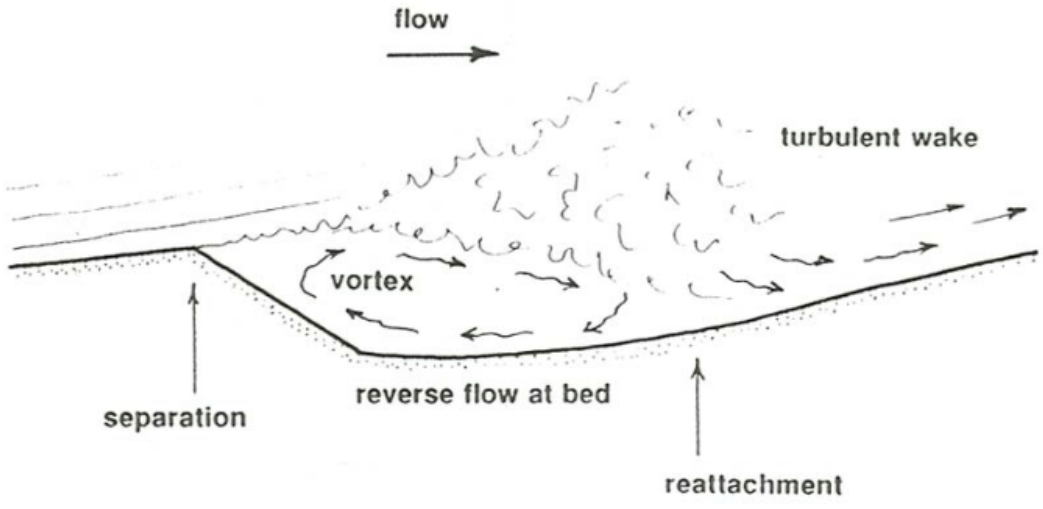


Figure 12.2.21 *that is less schematic but has some vertical exaggeration.*

Take a tour of a ripple or dune profile by starting at a crest, sliding down the slip face, and then walking across the trough and up the stoss surface of the next bed form downstream (Figure 12.2.23). The flow you would feel differs greatly along the profile. With the appropriate equipment you could actually do this on a large dune in a river or a tidal current, or more easily on a subaerial dune when the wind is blowing. Refer to Figures 12.2.21 and 12.2.22 as you read the next paragraph.

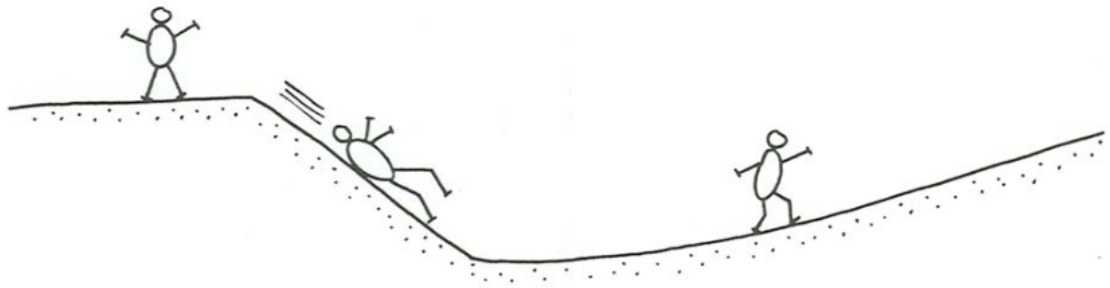


Figure 12.2.23: A field trip on a dune.

As you move down the slip face and into the trough you would feel a weak, irregular, eddying current in the opposite direction. Near the reattachment line you would feel the full effect of the turbulence in the shear layer. In the reattachment zone the strong eddies generated in the shear layer impinge upon the bed and flatten out against it to cause temporarily very high local shear stresses. You would feel strong puffs or gusts of flow trying to push you this way and that. But even though the shear stress is high at certain points and certain times, it is nearly zero on the average. As you continue to walk up the slope toward the next crest, the flow velocity and therefore the boundary shear stress would gradually increase, because the flow is crowded upward, but the intensity of the turbulence would lessen.

This page titled 12.2: Unidirectional-Flow Bed Configurations is shared under a CC BY-NC-SA 4.0 license and was authored, remixed, and/or curated by John Southard (MIT OpenCourseware) via source content that was edited to the style and standards of the LibreTexts platform.

12.3: Velocity Profiles over Ripples

The material in the latter part of Chapter 4 on velocity profiles over rough beds is useful here in dealing with vertical profiles of time-average velocity over fields of ripple-shaped bed forms, large or small. It is natural to think about such profiles in two different ranges of height above the bed: well above the ripples, and close to the bed.

Think first about the velocity profile above a plane parallel to the mean bed level and one to two ripple heights above the ripple crests. Unless the ripple height is such a large fraction of the flow depth that the whole flow accelerates and decelerates as it passes over the ripples, such a velocity profile is almost the same wherever it is taken, because at this height the upward-diffusing wake turbulence generated by flow separation at ripple crests is well blended spatially. In the following paragraphs we will use the adjective *integrated* for such profiles (cf. Paola, 1983). These profiles characterize layers of the flow that blanket entire fields of bed forms without varying at the scale of those bed forms.

First we need to do a little more with velocity profiles near the bed in dynamically rough flows, as a continuation of Chapter 4. This additional material deals with the inner layer not far above the tops of the particles, which we skipped in Chapter 4.

For sand-size bed roughness the lowermost part of the inner layer, not far above the tops of the grains, is not much more than a few millimeters thick, but for water flowing over gravels or for wind blowing over large ground-surface roughness it may be decimeters or even meters thick, and no sophisticated, miniaturized velocity meters are needed to include it in measured velocity profiles. At positions this close to the bed there is a troublesome problem that we have avoided up to now: where is the origin for y? It seems reasonable to suppose that the $y = 0$ level lies somewhere between the bases and the tops of the surface particles. A natural choice would be the average surface elevation—the spatial average of the heights, normal to the mean plane of the bed, at which a solid surface is first encountered in descending onto the bed. You will see, however, that this does not produce the best fit of velocity to Equations 4.7.20 or 4.7.21 of Chapter 4. And it is not a very practical choice anyway. With close-packed granular roughness, the plane through the tops of the grains (which itself is not very well defined) is usually taken as the $y = 0$ level for velocity measurements.

For a given dimensionless distance y^+ from the boundary, u/u_* is not the same in rough and smooth flow, because the second term on the right side of Equation 4.7.13 always has a value different from B in Equation 4.7.14. But the shape and slope of the velocity profile are the same: if you differentiate Equation 4.7.13 for the rough-flow velocity profile with respect to y, you get

$$\frac{du}{dy} = \frac{Au_*}{y} \tag{12.3.1}$$

which is exactly the same as Equation 4.7.12 for flow over a smooth bottom. You might expect, however, that, at positions closer down to the tops of the grains, the grains have some effect on the shape as well as the position of the velocity profile, making the shape different from the smooth-flow case. In other words, when y is not much greater than D, the velocity gradient depends not only on τ_o, ρ, and y but also on D:

$$\frac{du}{dy} = f\left(\tau_o, \rho, y, D\right) \tag{12.3.2}$$

or in dimensionless form,

$$\frac{u}{u_*}\frac{du}{dy} = f\left(\frac{D}{y}\right) \tag{12.3.3}$$

It is convenient to extract the same constant A from the function on the right in Equation 12.3.3, so that the effect of proximity to the bed grains can be viewed as a correction function by which the right side of Equation 12.3.1 must be multiplied:

$$\frac{du}{dy} = \frac{Au_*}{y} f\left(\frac{D}{y}\right) \tag{12.3.4}$$

There is no simple way of dealing with the physics behind the correction function $f(D/y)$ in Equation 12.3.4. The only thing we can say with certainty is that as y gets smaller (and D/y gets larger) the correction gets larger. To investigate the correction function further we can expand it as a power series in D/y (Monin and Yaglom, 1971; remember that any function can be approximated in this way by an appropriate power series.) Equation 12.3.4 can then be written

$$\frac{du}{dy} = \frac{Au_*}{y}\left[1 + a\frac{D}{y} + b\left(\frac{D}{y}\right)^2 + ...\right] \tag{12.3.5}$$

As the boundary is approached from above, and the correction gets larger, the term $a(D/y)$, the dominant term while the correction is still small, gets less important relative to terms of higher order in D/y. In the following we will consider only positions higher than one to two diameters above the tops of the roughness elements. Measurements are seldom made closer to the bed anyway, because to get a representative value for the mean velocity a large number of profiles must be taken at different places relative to the roughness elements and then spatially averaged.) To conform to the usual practice in dealing with the grain-proximity correction, we will recast Equation 12.3.5 into a slightly different form by introducing a new variable $y - y_1$ for the vertical coordinate, where y_1 is a small constant that's in the same ballpark as D itself. We also need the following algebraic identity:

$$\frac{1}{y} = \left(\frac{1}{y-c}\right)\left(\frac{y-c}{y}\right) = \left(\frac{1}{y-c}\right)\left(1 - \frac{c}{y}\right) \tag{12.3.6}$$

where y is some variable and c is a constant. Then, replacing $1/y$ in Equation 12.3.5 with the right side of the identity above and letting the constant be y_1,

$$\begin{aligned}\tfrac{du}{dy} &= \tfrac{Au_*}{y-y_1}\left(1 - \tfrac{y}{y_1}\right)\left[1 + \mathrm{a}\tfrac{D}{y} + \mathrm{b}\left(\tfrac{D}{y}\right)^2 + ...\right] \\ &= \frac{Au_*}{y-y_1}\left(1 - \frac{y_1}{y} + a_y^D + \text{terms in}\frac{1}{y^2}\text{ etc.}\right)\end{aligned} \tag{12.3.7}$$

Neglecting terms of order higher than $1/y$ on the right side, Equation 12.3.7 becomes

$$\frac{du}{dy} = \frac{Au_*}{y-y_1}\left(1 + \frac{aD - y_1}{y}\right) \tag{12.3.8}$$

We are at liberty to adjust the definition of y_1 at the outset in such a way that $y_1 = aD$; then Equation 12.3.8 becomes

$$\frac{du}{dy} = \frac{Au_*}{y-y_1} \tag{12.3.9}$$

Equation 12.3.9 can be integrated in the same way as the rough-flow equivalent of Equation 4.7.12 in Chapter 4 to be in the same form as Equation 4.7.14,

$$\frac{u}{u_*} = A\ln\frac{y-y_1}{D} + B' \tag{12.3.10}$$

and Equation 12.3.10 can be manipulated into the same form as Equation 4.7.22 in Chapter 4, with y_o and no separate constant of integration,

$$\frac{u}{u_*} = A\ln\frac{y-y_1}{y_o} \tag{12.3.11}$$

Equations 12.3.10 and 12.3.11 are the conventional way of dealing with the correction function $f(D/y)$ that appears in Equation 12.3.4. Shifting the origin of the y coordinate by the small quantity y_1 usually straightens out the velocity profile in a semilog plot down to positions not far above the tops of the roughness elements. What is commonly done with wind-velocity profiles above the land surface is to take $y = 0$ at the base of the roughness elements—the ground on which the observer is standing—and then find the value of y_1 which when subtracted from y gives the best straight-line fit of data to Equation 12.3.11. The distance y_1 (often denoted by d) is called the **displacement height** or the **zero-plane displacement**. The situation is a little different with close-packed granular roughness, which is of greater interest here: usually the velocity profile is measured with respect to the tops of the grains, and then the apparent origin for y is lowered to produce the best straight-line fit to Equation 12.3.11. (The plane through the tops of the grains is not ideally well defined, but it is impossible to define a dynamically natural plane that represents the bases of the grains in a full bed of loose sediment.) So the value of y_1 depends not only on the physics of the problem but also on the y origin chosen at the outset. For a wide variety of roughness geometries, the distance y_1 has been found to be between 0.2 and 0.4 roughness diameters below the tops of the roughness elements (Jackson, 1981).

The physical significance of the displacement height y_1 has never been clear. There is some experimental evidence that the height y_1 above the origin is the level in the flow at which the boundary shear stress τ_o appears to act (Thom, 1971). The horizontal component of the force per unit area the flow exerts on its bed has not only a magnitude but also a line of action. In other words, if we could measure τo with enough accuracy and detail we would find that it appears to act on some plane parallel to the bed.

(Presumably this plane would lie somewhere between the bases and tops of the roughness elements.) Choose an arbitrary plane above or below the bed and find the moment M per unit bed area associated with the force τ_o per unit bed area. Dividing M by τ_o gives a quantity with the dimensions of length, and this length is just the distance above or below the arbitrary plane at which τ_o acts. Jackson (1981) reasons that this distance is none other than the displacement height y_1.

Now, finally, back to velocity profiles over bed forms. In the following, the subscript t denotes variables associated with the total bed shear stress, and the subscript s denotes variables associated with the skin friction. If the flow depth is large relative to the ripple height the lower part of the integrated profile (and with little error the upper part also) is well described by Equation 12.3.11 , the law of the wall for rough boundaries written here using the subscript t,

$$\frac{u}{(u_*)_t} = A \ln \frac{y - (y_1)_t}{(y_o)_t} \tag{12.3.12}$$

The boundary shear stress $(\tau_o)_t$ concealed in $(u_*)_t$ in Equation 12.3.12 is the total shear stress the flow exerts on the rippled bed. If you were to invent a good way of measuring pressure and viscous shear stress at every point on the bed, you would have to average over an area much larger than the scale of the ripples to get a representative value for $(\tau_o)_t$. Most of $(\tau_o)_t$ is from drag exerted on the ripples, not local stress exerted on the granular bed surface—called skin friction. This latter skin-friction component of the total drag would be largely viscous drag, if flow in the immediate vicinity of the bed is dynamically smooth, or it may itself be largely form drag, if the flow in the vicinity of the bed is dynamically rough. By analogy with the results in Chapter 4 for granular roughness, the roughness length $(y_o)_t$ associated with the integrated velocity profile in Equation 12.3.12 is proportional to the height of the ripples and is a small fraction thereof, the exact value depending on the shape (and most importantly the steepness) of the ripples. The displacement height $(y_1)_t$ is such that the origin for the velocity profile lies somewhat below the ripple crests. As the ratio of flow depth to ripple height decreases (but not to the point where there is no longer an integrated profile) it becomes more difficult to distinguish between inner and outer layers of the flow, but the wall-law representation is still a good approximation.

Now look at the velocity profile near the bed at points on the stoss surface of a given ripple. At points well downstream from reattachment the velocity profile near the bed follows the law of the wall also, because of the upward development of the internal boundary layer at the expense of the turbulent wake downstream of separation. If the boundary Reynolds number based on the skin friction $(\tau_o)_s$ and the local granular roughness height is larger than about 10 the flow in the internal boundary layer is dynamically rough, and the velocity profile is given by

$$\frac{u}{(u_*)_s} = A \ln \frac{y - (y_1)_s}{(y_o)_s} \tag{12.3.13}$$

where $(\tau_o)_s$ in the shear velocity $(u_*)_s$ is a local boundary shear stress that can be viewed as averaged over an area that is large compared with the granular roughness but small compared with the ripples themselves. We will use the adjective local for profiles of this kind, because they apply only to particular points on the ripple. The profile in Equation 12.3.13 is characterized by values of roughness length $(y_o)_s$ and displacement height $(y_1)_s$ associated with the granular roughness, and both of these are smaller than the corresponding values associated with the integrated wall-law profile in Equation 12.3.12.

If the local boundary Reynolds number is much smaller, less than about 5, the local velocity profile is represented instead by the law of the wall for smooth flow, Equation 4.7.6 in Chapter 4,

$$\frac{u}{(u_*)_S} = A \ln \frac{\rho (u_*)_S y}{\mu} + B \tag{12.3.14}$$

where B has a value of about 5.1, as noted in Chapter 4. In this case the skin friction on the stoss surface of the ripple is mostly viscous drag rather than granular form drag. At intermediate boundary Reynolds numbers the velocity profile is represented by the law of the wall for transitionally rough flow. This can be put into the same form as the rough-flow profile, Equation 12.3.13, but with y_n then a function of the local boundary Reynolds number as well as the roughness height, and the skin friction is partly viscous drag and partly form drag. Whether the local flow in the growing boundary layer is smooth or rough, however, $(u_*)_s$ in Equations 12.3.13 or 12.3.14 is much smaller than $(u_*)_t$ in Equation 12.3.12, because whatever its nature the skin friction on the ripple surface is much smaller than the form drag on the ripples.

The local wall-law profile varies with distance up the stoss surface: as the flow in the internal boundary layer accelerates up the slope, the skin friction $(\tau_o)_s$ increases, as does the height to which the profile is applicable. You can be sure, however, that in a simple dimensional semilog plot with $\log y$ on the vertical axis and u on the horizontal axis the slopes of the straight lines that represent the local wall-law profile are always much greater than the slope of the single straight line for the integrated wall-law

profile that holds well above the level of the crests of the ripples, because $(u_*)_t$ is much larger than $(u_*)_s$; see Figure 12.3.1, which summarizes the relationship between the integrated profile and the local profile above a given point on the stoss surface of a ripple. In between the regions of applicability of the local wall-law profile near the bed and the integrated wall-law profile well above the ripples is a complicated region of the flow in which the velocity grades from one profile to the other. This region thins downstream along the stoss surface but is not consumed completely even when the flow reaches the next ripple crest downstream.

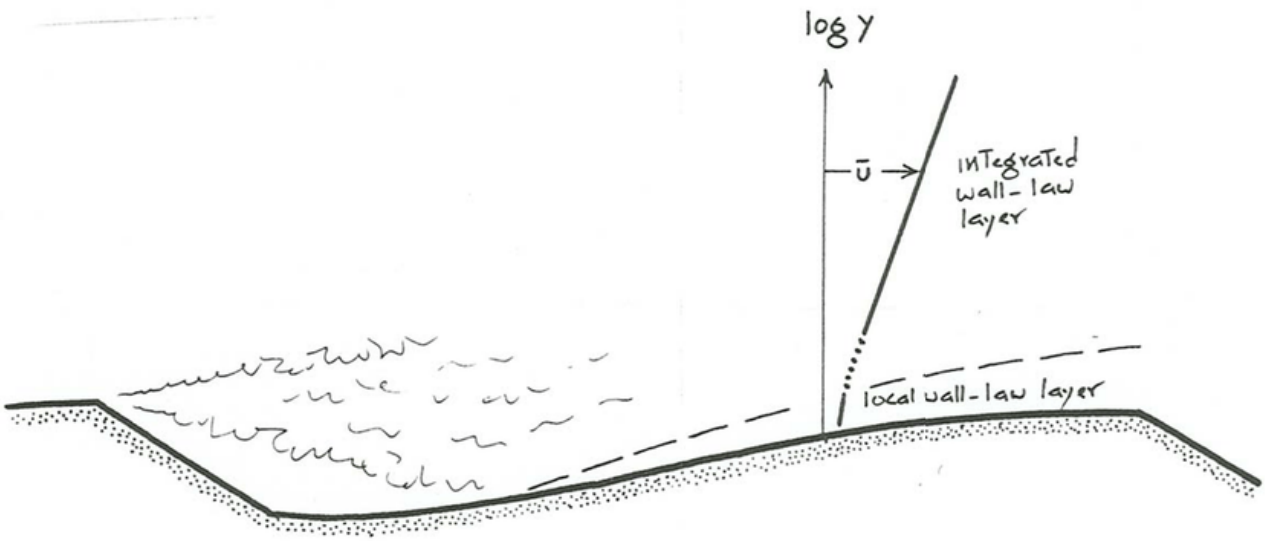


Figure 12.3.1: Relationship between the integrated wall-law layer and the local wall-law layer developed over a dune bed.

Where small dunes are superimposed on much larger dunes, the foregoing line of reasoning can be taken a step further. Large internal boundary layers develop on the stoss surfaces of the larger dunes in just the same way that small internal boundary layers develop on the smaller dunes. The smaller dunes, of which there presumably are a great number on the stoss face of each larger dune, act as local roughness beneath the internal boundary layer that develops up the stoss surface of each larger dune. There is therefore a layer of the flow well above the crests of the smaller dunes but still well below the crests of the larger dunes in which the velocity follows an intermediate wall-law profile (Figure 12.3.2). This intermediate profile looks simultaneously like an integrated (although slowly varying) profile to a small observer stationed on one of the smaller dunes but like a local profile to a large observer stationed on one of the larger dunes. This profile is characterized by values of u_*, y_o, and y_1 intermediate between those of the integrated profile over the large dunes and those of the local profile over the smaller dunes. From the standpoint of the large dunes the intermediate value of u_* represents a local boundary shear stress, so in a sense it is skin friction even though form drag predominates over viscous drag. At the same time, the viscous drag and smaller-scale form drag associated with the sediment grains on the surfaces of the smaller dunes represent skin friction relative to the smaller dunes.

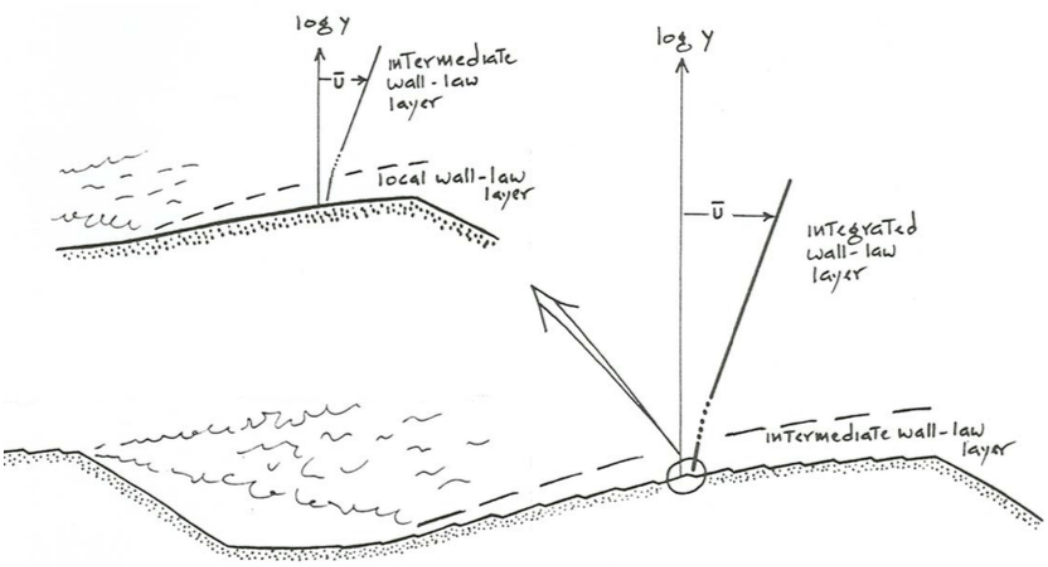


Figure 12.3.2: Intermediate wall-law layer developed over a dune bed on which smaller dunes are superimposed on larger dunes. The intermediate layer acts as an integrated layer with respect to the smaller dunes but as a local layer with respect to the larger dunes.

The same ideas can even be extended to very large dunes (which many would call sand waves) on which two orders of smaller dunes with two greatly different scales are superimposed. There are then two different intermediate layers of the flow, of the kind just described, each with its own wall-law profile characterized by its own set of values of u_*, y_o, and y_1: one that is local relative to the largest dunes (the sand waves themselves) but integrated relative to the larger superimposed dunes and one that is local relative to the larger superimposed dunes but integrated relative to the smaller superimposed dunes.

You could take velocity profiles at a large number of points along the profile of one or more of the largest dunes present on the bed and average them all together to obtain a spatially averaged velocity profile. In a sense this spatially averaged profile represents the entire flow. Such averaging is not entirely satisfactory, for two reasons:

1. Owing to growth of the internal boundary layer, the near-bed part of the velocity profile varies with position along the dune profile (even aside from the gross changes caused by separation and reattachment in the vicinity of the trough).
2. Because the origin plane for the integrated wall-law region associated with dunes of a given order is parallel to the mean plane of the bed in the vicinity of those dunes, whereas the origin for the individual profiles is naturally taken at the bed surface itself, the base of the integrated wall-law profile is encountered at different heights in different places. The latter problem is not as serious as it seems, however, because at the height of even the lowest of such integrated wall- law regions, points at rather different heights plot close to each other on a logarithmic vertical axis. Provided that the ratio of spacing to height of the dunes of each order is large, so that separation bubbles occupy only a small fraction of the area of the bed, the spatially averaged profile in a semilog plot of height against velocity shows a series of straight-line segments connected by smooth transitions, just like the individual profiles—although the transitions are likely to be more gradual, for the two reasons noted above. The values for boundary shear stress obtained from these straight-line segments in the spatially averaged profile represent the spatial averages of the boundary shear stresses associated with each order of bed form present, ranging upward in scale from the grain roughness itself. For further details on such spatially averaged velocity profiles over dunes, see Smith and McLean (1977).

This page titled 12.3: Velocity Profiles over Ripples is shared under a CC BY-NC-SA 4.0 license and was authored, remixed, and/or curated by John Southard (MIT OpenCourseware) via source content that was edited to the style and standards of the LibreTexts platform.

12.4: Movement of Ripples and Dunes

Sediment Movement over Ripples and Dunes

The mode of sediment transport varies greatly from place to place over the ripple or dune profile. A repetition of your traverse, this time to watch the sediment movement, would be instructive. See Figure 12.4.1 for a key to the material discussed below. Start at the reattachment zone, where the time-average bed-load transport rate is near zero. Strong eddies in the reattaching shear layer impinge upon the bed to cause strong but sporadic grain transport. At low mean- flow velocities, sediment is shifted this way and that on the bed in local pulses that strike seemingly at random. This is the site of first suspension of sediment as flow velocity gradually increases: swirls of sediment are put into suspension in puffs and gusts, and then the grains either settle directly back to the bed or are dispersed up into the flow.

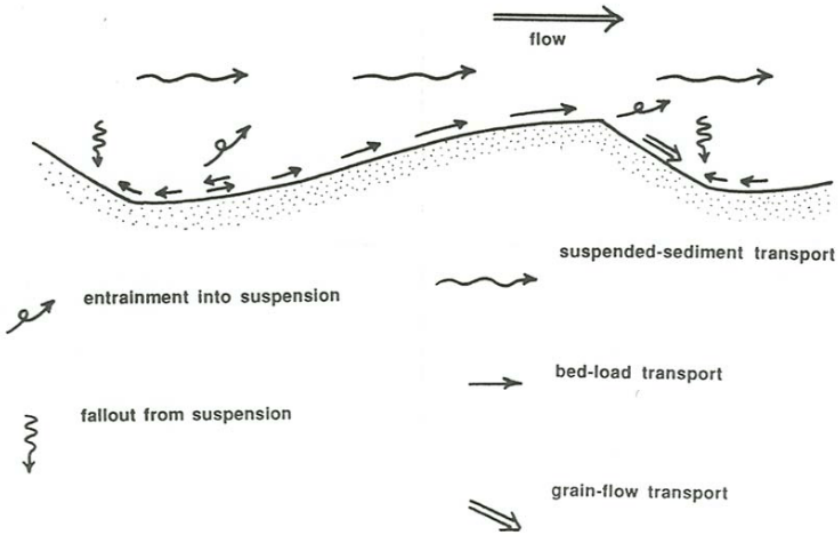


Figure 12.4.1: Modes of sediment movement over ripples or dunes.

Downchannel from reattachment the pulses of movement are directed more and more consistently downchannel and gradually give way to more uniform grain movement up the stoss slope. In the other direction they cease to be important just a short distance upchannel from reattachment, because flow in the separation vortex behind the bed form is relatively weak.

Particle movement up the stoss surface is much like that on a planar sediment bed: it is in the form of isolated puffs at low mean-flow velocities, and in the form of a continuous sheet at higher velocities. With increasing velocity the bed-load movement is obscured by sediment suspended from the trough or from upstream ripples. Dunes often have ripples or even smaller dunes superimposed on their stoss slopes; this should not surprise you, because such bed forms develop wherever they have sufficient space and suitable flow conditions.

At low flow velocities all of the sediment that is transported as bed load to the brink is deposited there. This sediment tends to build the stoss surface forward over the top of the lee surface. The sediment slips down the lee surface as a kind of grain flow to try to restore a stable angle of repose. Grain flow is localized and sporadic when the rate of delivery is slow but widespread and continuous at higher flow velocities. The result is a nearly planar slip face, with a break in slope not only at the top but also at the base, where the slip face builds forward onto the surface of the trough downstream.

At higher flow velocities some fraction of the transported grains are carried beyond the crest above the separation surface, to settle through the complicated turbulent flow field in the wake of the ripple and land at various points (Figure 12.4.2): on the slip face, in the trough, on the stoss surface of the next ripple downstream, or even on some ripple much farther downstream. Where the grains land depends on several factors: the flow velocity, the settling velocity, the height of the grains above the bed as they pass over the brink, and which eddies the grains happen to fall through.

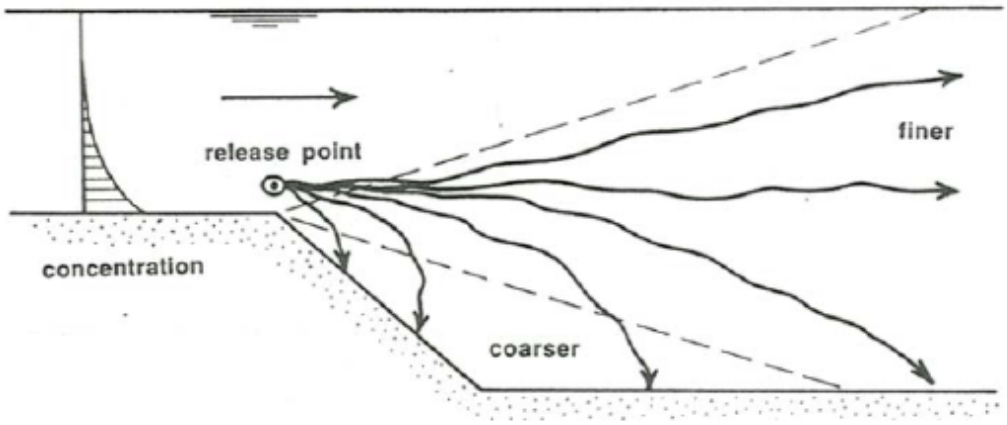


Figure 12.4.2: Trajectories of sediment particles passing through a given point (the “release point”) above the crest or a ripple or a dune.

When the ripple geometry is three-dimensional, many troughs show no well defined separation vortex, and patterns of flow and sediment transport are not as simple as outlined above. The bed surface near the base of the lee slope nonetheless usually feels flows that are much weaker than over the stoss slope, although these flows may have a substantial cross-stream component. Transverse flow in the lee of the dunes often makes ripples in troughs and on lee slopes, with crests oriented at a large and variable angle to the dune crests.

Movement of Ripples and Dunes

Ripples and dunes move downstream, at speeds that are orders of magnitude slower than the flow speed, by erosion on the stoss surface and deposition on the lee surface. It is surprisingly difficult to characterize this downstream movement, partly because the bed forms change their profiles with time but even more importantly because any given bed form has a finite lifetime: it is born, it moves, and it eventually dies, usually within a travel distance equal to only a small multiple of the bed-form spacing, something like 5–10 spacings. The moderately regular arrangement of ripples in a still photograph is deceiving. This section says some things about the nature and analysis of movement of ripples and dunes.

A fundamental characteristic of ripples is that they move downstream at some velocity U_B, by erosion on the stoss surface and deposition on the lee surface. This velocity is of interest because

- it is an index of bed-load transport rate, because we have seen that most of the bed load moving on a ripple bed is cycled within the same ripple, and
- it is one of the determinants of the stratification geometry produced by ripple movement.

This section addresses the measurement of U_B, along with some results, and also its use in estimating sediment transport rates. A discussion of its role in the geometry of sedimentary structures would take us too far afield; see papers by Allen (1970), Ashley et al. (1982), Rubin and Hunter (1982), and Harms et al. (1982, Chapter 3).

It is surprisingly difficult to characterize the downstream movement of ripples. If each ripple had an unchanging streamwise profile, U_B would be both well defined and readily measurable. Because most ripples have a fairly sharp break in slope at the brink, it is usually no problem to follow a distinguishable point on the profile as the ripple moves. But the profile shape changes as the pattern of sediment transport over the ripple changes, even if the profile area stays the same. This usually causes the position of the brink to change relative to the center of area of the ripple over just a short distance of movement, so even the position of a well defined point on the profile does not necessarily represent well the position of the ripple. Moreover, the profile area of a ripple itself is changed by several processes, which can act concurrently:

- intensification of scour in a trough and deposition of the eroded sediment on the stoss surface or farther downstream;
- transfer of sediment from one ripple to another by either bed-load transport or suspended-load transport;
- overriding of one ripple by the next ripple upstream;
- division of one ripple into two, as a new trough develops on the stoss surface of a ripple as a result of some change in upstream flow pattern.

The last two processes imply that ripples do not live forever: they come into being, move for some distance that is usually a small

number of ripple spacings, and then disappear.

A good way to apprehend the transitory existence of individual ripples is to generate a train of ripples in your flume and photograph them with a time- lapse movie camera as they move downstream. When you viewed the film at normal speed you would see the ripples doing all sorts of crazy things that are hard to appreciate by real-time viewing; the moderately regular succession of ripples when viewed in a still picture is deceiving. Two other instructive things you could do are described in the following paragraphs.

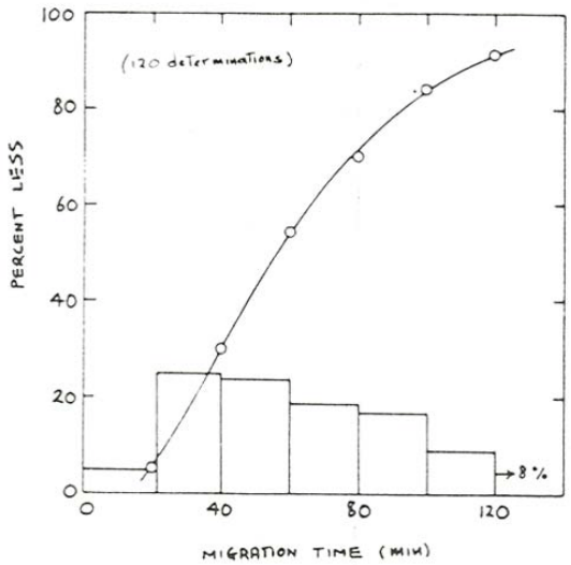


Figure 12.4.3: Histogram and cumulative curve of times for passage of two successive ripple crests past a fixed point, for $0.38\ \mathrm{mm}$ sand in a flow with mean flow depth $0.3\ \mathrm{cm}$ and mean flow velocity $29.2\ \mathrm{cm/s}$. (Data are from Southard et al., 1980.)

You might stock up on sandwiches and caffeine, occupy a station somewhere along the channel, and for a large number of ripples measure the time T_r needed for two successive ripple crests to pass the station. After getting some rest you could then plot a cumulative distribution of T_r. (When multiplied by the spacing of the passing ripple, the inverse of T_r is a good representation of U_B.) Figure 12.4.3, measured by Southard et al. (1980), is such a curve. Note the wide range in passage times. It was found that hundreds of ripples would have had to be measured to obtain a stable cumulative curve, although substantially fewer were sufficient for a stable mean value.

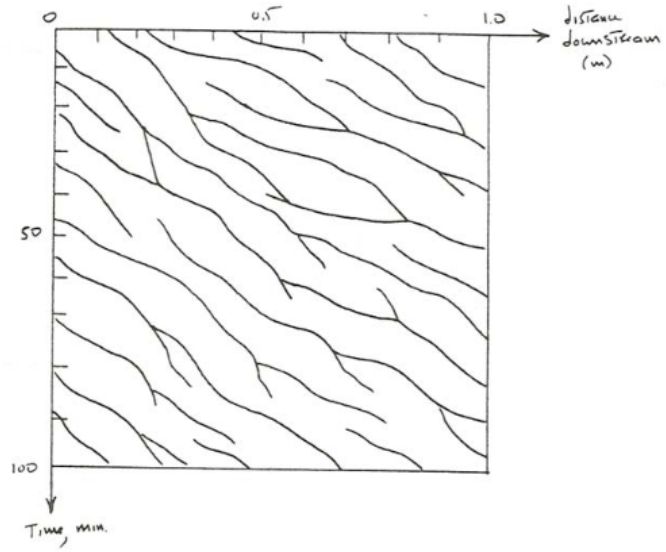


Figure 12.4.4: Positions of ripples in a space–time plot. The curves show positions of ripple crests as a function of time and downstream position. The flow is steady and uniform, and the bed state is unchanging on average. (Schematic.)

To quantify the variability in ripple movement you might enlist a large number of volunteers to stand along the transparent sidewall and be responsible for keeping track of the positions of the ripples as a function of time. A plot of position vs. time would look like Figure 12.4.4, from which you can see that

- for a given ripple U_B varies widely and irregularly with time;
- a given ripple exists for a distance of movement that is only a few ripple spacings;
- ripples usually are born by division of one large ripple into two smaller ones, and usually die by becoming smaller and slower and then being overridden by a faster-moving ripple (on the average, deaths equal births).

Despite all of this variability, when considered as an aggregate the lines in the graph have a definite average slope, which is probably the best measure of U_B.

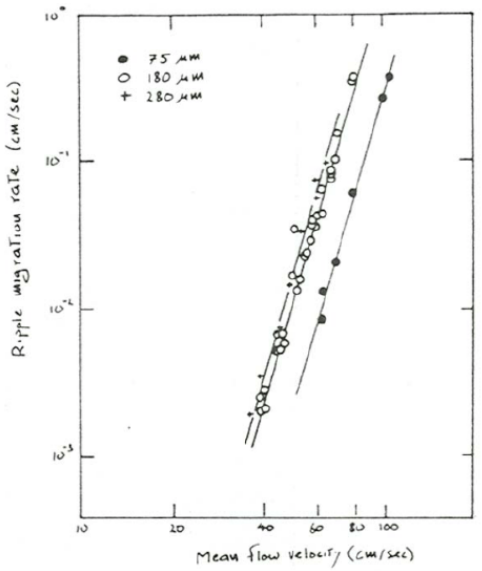


Figure 12.4.3: Plot of bed-form speed U_B vs. mean flow velocity U in uniform flow for three sand sizes. (Data are from Dillo, 1960.)

You should expect U_B to increase steeply with mean flow velocity U for a given sand, because, as you will learn in Chapter 12, bed-load transport rate increases steeply with flow strength and most of the bed load remains within individual ripples. The magnitude of this increase depends, however, on the concurrent change in ripple size, because the larger the ripple, the slower it moves for a given bed-load transport rate. The effect should therefore be most pronounced for ripples, which vary little in size with flow conditions and sediment size. Systematic data on bed-form velocity as a function of flow strength and sediment size are surprisingly scarce, presumably owing to the difficulty of accurate measurement. Figure 12.4.3, a plot of U_B vs. U for three different sand sizes (Dillo, 1960), shows that U_B increases sharply with U for a given sand size, as expected. Note, however, that ripples in coarser sands move faster than ripples in finer sands. The reason for this seemingly anomalous behavior is unclear. There seem to be two possibilities:

1. The volume transport of sand as traction load in the accelerating flow over the stoss face of the ripple might be greater in coarser sand than in finer sand at a given mean flow velocity.
2. The ripples in the coarser sand may have been smaller than in the finer sand, so that U_B is greater even though bed-load transport rate might have been smaller.

In the absence of suspension, particles are cycled through individual bed forms. Think about a particle in the interior of a moving bed form (a ripple or a dune). The particle is of course stationary relative to the substrate. As the bed forms moves, the particle finds itself closer and closer to the stoss surface. When it become exposed at the surface, it is entrained, moves up to the brink as part of the bed load, and then slumps or slides down the lee slope, stopping at some point on the slope (or at its base), there to be buried by later lee-side deposition to become entombed again, temporarily, within the body of the bed form.

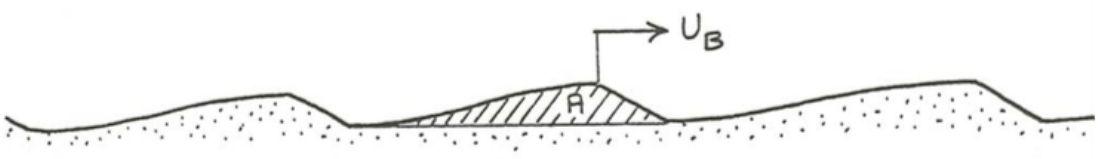


Figure 12.4.4: Definition sketch for derivation of a relationship for bed-form transport rate.

To the extent that the moving sediment is cycled within bed forms, the bed-load transport rate can be expressed in terms of the speed of movement of the bed forms. For ripples this is a good approximation, because bed-load transport rate is usually zero or nearly so at some point in the trough. Only if bed-load transport rate is nowhere zero over the bed-form profile, as is generally the case with antidunes, is this not true. To derive an expression for the bed-load transport rate associated with bed-form movements, consider a train of identical bed forms in which bed-load transport rate is zero in the troughs (Figure 12.4.4). The ripples have cross-sectional area A and spacing (i.e., repeat distance of cross-section geometry) L. The time needed for passage of a bed form past a given point is T_r. The rate q_f, expressed per unit width normal to the flow, at which volume of sediment is moved downstream by bed-load transport within the ripples (remember that this involves stripping of sediment from the stoss surface, dumping at the crest, and slumping down the lee surface) is the same as the rate of downstream shift of the ripple cross section, except for a correction factor discussed below. A good way of thinking about this is to consider that the entire cross-sectional area of the ripple passes a given point on the bed in time $T_r = L/U_B$, so the average rate of passage of cross-sectional area past the point during this time is A/T_r, or, eliminating T_r, AU_B/L. So

$$q_f = K_1 \frac{AU_B}{L} \tag{12.4.1}$$

For a more elegant derivation of this result, see Simons et al. (1965).

The correction factor K_1 is needed because the transport rate is expressed as solids volume whereas bed volume is expressed as bulk volume, solids plus void space. It is easy to derive a relationship between solids volume V_s and bulk volume V_b in a sediment sample. Because voids volume and solids volume add up to total volume in a sediment,

$$V_v + V_s = V_b \tag{12.4.2}$$

where V_v is voids volume. Also, the porosity k is defined as

$$\lambda = \frac{V_v}{V_b} \tag{12.4.3}$$

Combining Equations 12.4.2 and 12.4.3 to eliminate V_v gives the relationship between solids volume and bulk volume:

$$V_b = \frac{1}{1-\lambda} V_s \tag{12.4.4}$$

Because λ in equant and fairly well sorted sediments is on the order of 0.2–0.4, depending on both sorting and packing, the porosity correction factor $1/(1-\lambda)$ is always positive and a little larger than one. Using Equation 12.4.4, Equation 12.4.1 becomes

$$q_f = \frac{1}{1-\lambda} \frac{AU_B}{L} \tag{12.4.5}$$

In the rest of this chapter $1/(1-\lambda)$ will be written K_1 for convenience. If the bed forms have the shape of end-to-end triangles with height H, then $A = HL/2$ and Equation 12.4.5 becomes

$$q_f = K_I \frac{HU_B}{2} \tag{12.4.6}$$

Rubin and Hunter (1982) proposed that q_f be called the **bed-form transport rate** and that the remainder of the bed-load transport rate, the part that bypasses the bed forms rather than being cycled within the same bed form, be called the **throughgoing transport rate**.

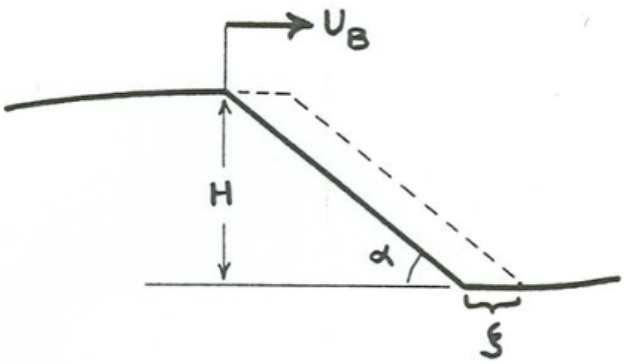


Figure 12.4.5: Definition sketch for derivation of a relationship for bed-load transport rate at the crest of a ripple or dune.

The bed-load transport rate (call it q_{sb}) is greatest at the crests of ripples. An expression for q_{sb} at a ripple crest can be derived on the assumption that all the bed load arriving at the crest is dumped there to slump down the lee face and build it forward (Figure 12.4.5). The slip-face angle is α and the horizontal distance of slip-face outbuilding is ζ. As before, ripple velocity is U_B and ripple height is H. The principle is that q_{sb} at the crest is equal to the time rate of addition of bulk sediment volume on the slip face. Because the increment in volume of the slip-face deposit is just the thickness of the slip-face deposit, $\zeta \sin\alpha$, times the length down the slip face, $H/\sin\alpha$,

$$\begin{aligned} q_{sb} &= K_1 \frac{d}{dt}\left[\left(\zeta \sin\alpha \frac{H}{\sin\alpha}\right)\right] \\ &= K_1 \frac{d(\zeta H)}{dt} \\ &= K_1 H \frac{d\zeta}{dt} \\ &= K_1 H U_B \end{aligned} \tag{12.4.7}$$

By comparison of Equations 12.4.6 and 12.4.7 we have the neat result that, for ripples with triangular cross-section, bed-load transport at the crests is exactly twice the average value. This result seems first to have been derived by Bagnold (1941).

This page titled 12.4: Movement of Ripples and Dunes is shared under a CC BY-NC-SA 4.0 license and was authored, remixed, and/or curated by John Southard (MIT OpenCourseware) via source content that was edited to the style and standards of the LibreTexts platform.

12.5: 2D Dunes and 3D Dunes

It has become widely stated, in the literature on unidirectional-flow dunes, that at low flow strengths in the dune range the dunes tend to be straight- crested, with fairly even crest elevations and trough elevations. Such bed forms are referred to as *two-dimensional* (2D), in the accepted hydrodynamic sense that the geometry of the features can be represented by a single flow parallel cross section extending unchanged across the width of the flow. In contrast, at high flow strengths in the dune range the dunes show much greater crest curvature, much less crest continuity, and much greater variability in trough depths. Such bed forms are said to be *three-dimensional* (3D). Correspondingly, large-scale cross stratification produced by the movement of dunes is recognized as either two-dimensional, interpreted as representing relatively low flow strengths in the dune regime, or three-dimensional, interpreted as representing relatively high flow strengths—as you will see in Chapter 15. Recently, however, Venditti et al. (2005), on the basis of a systematic set of flume experiments using well sorted half-millimeter sand, claim that at low flow strengths in the dune regime initially 2D dunes eventually evolve into 3D dunes—a finding that is inconsistent with much of the earlier flume studies on dunes. The issue is not yet settled.

Dynamics of Unidirectional-Flow Bed Configurations

Introduction

How is it that a turbulent flow molds a bed of loose sediment into stable bed forms? The subject of bed-configuration dynamics has long been one of frustration and controversy. The fundamental difficulty is easy to state: it has to do with the difficulty of specifying adequately how sediment transport rate varies from place to place over a geometrically irregular transport surface. Before elaborating, I should make clear what I mean by the sediment transport rate at a point. I will address more fully in the following chapter the rate at which sediment is transported past a given cross section of the flow, in solids volume per unit width of the flow; it is usually denoted by q_s. Here we need to think about how the "point" value of the volumetric transport rate, which you can view as the sediment transport rate over an arbitrarily small local area of the bed (again expressed per unit width of flow), varies from point to point on a nonplanar sediment bed. I will denote this by q_s also.

The velocity profile and the local bed shear stress (i.e., the skin friction) at some point on a nonplanar sediment bed, and their time variation, are not likely to be the same as at a point on a featureless planar bed with the same discharge and depth above it. This is because the details of forces and motions in accelerating and decelerating boundary layers are substantially different than in non-accelerating boundary layers. You have already seen this for the grossly non-uniform flows around bluff bodies like spheres and cylinders, but the effect is substantial even when much smaller accelerations or decelerations are caused by mild streamwise gradients in fluid pressure. The structure of the flow above any point tends to be inherited from upstream as the flow adjusts toward new conditions, so the flow at the given point depends in a complicated way on the shape of the bed for a long distance upstream. So even if q_s could be assumed to be in local equilibrium with the spatially varying flow, it could not be specified in any simple way as a function of position. Furthermore, q_s is likely not to be in equilibrium with local flow conditions, because a finite distance is needed for load to be dropped out or picked up as transport capacity changes. This distance should be expected to be greater for suspended load than for bed load, but it cannot be assumed to be negligible even for the latter.

The development of bed forms depends on the variation in q_s over the bed-form profile. In turn, q_s depends on the flow, and if an adequate expression for q_s as a function of position could be found it could be combined with the kinematic constraint imposed by conservation of sediment volume to give an equation that could be solved for the evolution of any initial bed geometry to a steady equilibrium geometry. But q_s cannot be specified so simply: as you have seen, the local sediment transport rate is itself a function of the bed configuration for which we are trying to solve.

In the face of this depressing prospect, many investigators have attempted with some limited success to glean physical understanding of the dynamics of bed configurations by making various simplifying assumptions that allow q_s to be expressed in a form that leads to mathematically tractable equations. Not many of these attempts have led to greatly improved understanding of the problem. This is a field of endeavor marked by an understandable scarcity of satisfying or useful results.

In this section I will concentrate not so much on a detailed review of the literature on bed-configuration dynamics as on the physical effects related to the existence, shape, size, and movement of bed forms. I will deal with each of these four aspects of dynamics in the following sections. The aim is to give you some appreciation of the potential and limitations of the various approaches to the problem of bed-configuration dynamics. It turns out to be easier to account qualitatively for shape and

movement than for existence and size. As a necessary preliminary I will first derive the sediment conservation equation, a kinematic relation expressing conservation of sediment volume (or mass) that has to hold in any sediment-transporting system.

Sediment Conservation Equation

In any flow that transports sediment, the volume or mass of transported sediment must be conserved. This requirement leads to a purely kinematic relationship that has to hold irrespective of the dynamics of sediment transport. I will concentrate on a two-dimensional flow (one that varies in two dimensions only, downstream and upward from the bed but not in the cross- stream direction), but the principle is the same for a flow that varies in all three directions.

Consider a small rectangular region R of the sediment bed, with unit width normal to the flow and with length Δx in the flow direction (Figure 12.5.1). The area of R is Δx because of the unit width. Denote by h the elevation of the bed above some arbitrary horizontal datum plane. Transport of sediment at any cross section can be expressed by q_s, the volumetric sediment transport rate per unit width of flow; this may include sediment moving as bed load or in suspension. (In Chapter 12, the symbol q_s is used for the unit transport rate expressed as mass rather than as volume.) Let the depth-averaged volume concentration of the load be C. (Strictly, C includes the concentration of bed load as well as suspended load.) The difference between q_s at the downstream boundary of R, $(q_s)_{out}$, and at the upstream boundary of R, $(q_s)_{in}$, is Δq_s:

$$(q_s)_{out} - (q_s)_{in} = \Delta q_s \tag{12.5.1}$$

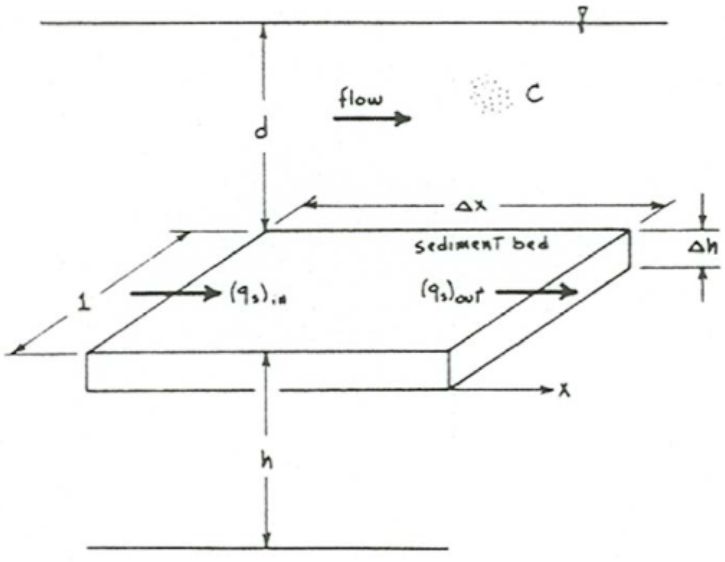


Figure 12.5.1: Definition sketch for derivation of the sediment conservation equation.

Any change Δh in bed elevation during some time interval Δt is caused by storage of sediment in R (deposition, or aggradation) or removal of sediment from R (erosion, or degradation). This change can be viewed as the sum of two contributions. One of these, Δh_s, is caused by downstream change in q_s: if q_s is greater across the upstream face than across the downstream face of R, then sediment must be stored in R, but if q_s is smaller, then sediment must be removed from storage in R. The other contribution, Δh_t, is caused by temporal change in C: if the concentration of transported sediment is decreasing with time, then there must be deposition on all areas of the bed, but if the concentration is increasing, then there must be erosion (assuming that sediment is not being added to the flow from above). The bulk volume $\Delta h_s \Delta x$ of aggraded or degraded bed in R due to downstream variation in q_s is equal to Δt times $(q_s)_{in} - (q_s)_{out}$, the rate of sediment storage due to the difference in transport rates across the upstream and downstream boundaries of R, with a correction for the porosity effect (Equation 12.4.4):

$$h_s \Delta x = \Delta t \left[(q_s)_{in} - (q_s)_{out} \right] = -K_1 \Delta q_s \Delta t \tag{12.5.2}$$

The porosity correction factor $1/(1-\lambda)$, again denoted by K_1, is needed because the volume of transported sediment is measured in solids volume whereas volume of bed sediment is measured in bulk volume, solids plus void space. The bulk volume of aggraded bed in R due to temporal variation in C is equal to minus the total change in volume of suspended sediment above R, again corrected for the porosity effect:

$$\Delta h_t \Delta x = -K_I d \Delta C \Delta x \tag{12.5.3}$$

where d is flow depth. Using Equations 12.5.2 and 12.5.3, the average rate of change of bed elevation with time over R, $\Delta h/\Delta t$, can now be written

$$\begin{aligned}\frac{\Delta h}{\Delta t} &= \frac{\Delta h_S}{\Delta t} + \frac{\Delta h_t}{\Delta t} \\ &= -K_1\left(\frac{\Delta q_s}{\Delta x} + d\frac{\Delta C}{\Delta t}\right)\end{aligned} \tag{12.5.4}$$

In the limit, as $\Delta x \to 0$, Equation 12.5.4 becomes

$$\frac{\Delta h}{\partial t} = -K_I\left(\frac{\partial q_s}{\partial x} + d\frac{\partial C}{\partial t}\right) \tag{12.5.5}$$

The differential equation (Equation 12.5.5) is a volume-balance relationship that must hold at every point on the bed regardless of the sediment-transport dynamics. It relates the time rate of change of bed elevation at a point, $\partial h/\partial t$, to the downstream rate of change of sediment transport rate at that point, $\partial q_s/\partial x$, and the time rate of change of total suspended-sediment concentration in the flow, $\partial C/\partial t$. It is usually called the sediment conservation equation, or the sediment continuity equation. Its use is essential in thinking about the temporal changes in bed geometry consequent upon spatial changes in transport rate. If C does not change with time, Equation 12.5.5 becomes

$$\frac{\partial h}{\partial t} = -K_1\frac{\partial q_s}{\partial x} \tag{12.5.6}$$

Rate of change of bed elevation is thus directly proportional to minus the downstream rate of change of sediment transport rate. If q_s decreases downstream for any reason, the bed is aggraded; if q_s increases downstream, the bed is degraded.

Movement of Bed Forms

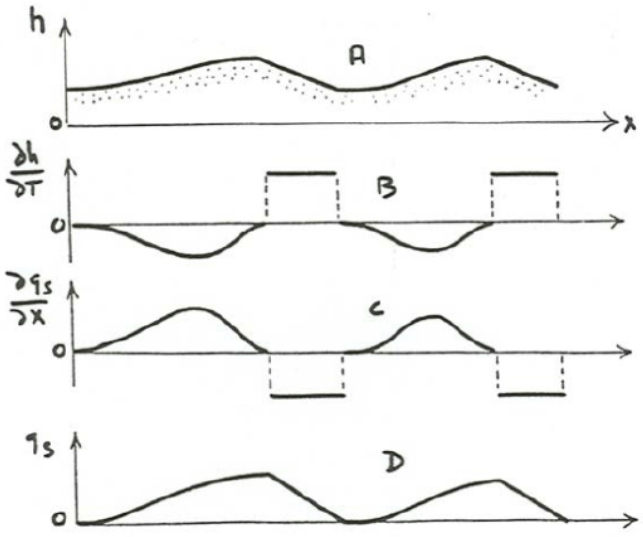


Figure 12.5.2: Variation of **A)** h, **B)** $\partial h/\partial t$, **C)** $\partial q_s/\partial x$, and **D)** q_s over a hypothetical unchanging bed form in a low-Froude-number flow.

Armed with the sediment conservation equation and all that has been said about flow and sediment transport in turbulent boundary layers, what can we do about accounting for the existence, size, shape, and movement of loose-sediment bed forms? Look first at *movement*, because that is the most straightforward. Consider a hypothetical bed form like that in Figure 12.5.2A, one element in a train of similar bed forms. Assume that the bed is in equilibrium with a steady sediment-transporting flow, and that the bed form moves downstream with unchanging size and shape. Equation 12.5.6 associates with the movement of the bed form a particular pattern of variation of q_s over the bed-form profile in the following way. For the bed form to move downstream it is a kinematic necessity that $\partial h/\partial t$ be negative on the upstream side of the bed form and positive on the downstream side (Figure 12.5.2B). Note that $\partial h/\partial t$ is zero at the crest and trough and has its greatest absolute value at points of steepest slope on the bed-form profile. By Equation 12.5.2, $\partial q_s/\partial x$ must vary with x in a sense just opposite to the variation in $\partial h/\partial t$ (Figure 12.5.2C), and therefore q_s itself must be greatest at the bed-form crest and least in the trough (Figure 12.5.2D). No zero point is shown on the q_s axis in Figure 12.5.2D, because any position of the curve is consistent with that of the curve for $\partial q_s/\partial x$ in Figure 12.5.2C.

On ripple bed forms, q_s is zero or nearly so in the trough, and it may even be negative if the reverse flow in the separation zone is strong enough. Over antidunes, on the other hand, there may not be much relative variation in q_s over the bed-form profile. If the bed form is to move downstream q_s must increase up the stoss surface from the trough to the crest and must decrease down the lee surface from the crest to the next trough.

In any flow of a low-viscosity fluid like air or water with a velocity large enough to transport sediment, Reynolds numbers of flow over even small ridges or mounds on the bed are large enough for substantial front-to-back asymmetry in local bed shear stress. Recall that beginning at Reynolds numbers of about 10 the spacing of streamlines is closer, and therefore the skin friction is greater, on the front side of a cylinder or a sphere than on the back. This becomes more pronounced with increasing Reynolds number, and when flow separation eventually develops, the skin friction on the back is negligible. The effects are qualitatively the same for any ridge or mound on a sediment bed. So provided that the free surface remains approximately planar above the bed form, any bed form—even one whose height is only a few grain diameters—should have larger q_s on the upstream side than on the downstream side, with a maximum near the crest and a minimum somewhere in the trough. From Figure $12.5.2$D it is clear that this distribution of q_s guarantees downstream movement. This distribution of q_s is not likely to be exactly the one needed for maintenance of bed-form shape, but that is a matter for the next section; the bed form always moves downstream even if its shape tends to change at the same time.

If the mean-flow Froude number is close to one, surface gravity waves interact with the bed to produce stationary or slowly shifting bed waves that are in phase or almost in phase with the water-surface waves. For these upstream- shifting bed forms, which in an earlier section were called antidunes, the interaction of the free-surface wave and the bed-surface wave is such that q_s decreases up the upstream slope and increases down the downstream slope, resulting in upstream movement. No capsule statement can be made at this point that elucidates the dynamical reasons for this variation of q_s.

Up to this point, it has been shown:

- what the variation in q_s has to be over a bed-form profile for the bed form to move, and
- that in the case of ripples the expected variations in q_s are in accord with the bed-form movement actually observed.

This may seem like a self-evident or trivial exercise, but it shows how we can obtain some insight into the behavior of bed forms by combining ideas about sediment transport with the sediment conservation equation, and it points the way toward other problems that are not as easy to deal with.

Shape of Bed Forms

Introduction

A striking characteristic of ripples and dunes is their asymmetrical profile, with a gently sloping upstream surface and a steeper, nearly angle-of-repose slip face on the downstream surface. Typically the bed profile shows a sharp angle at the top and bottom of the slip face—although reverse flow in the separation eddy can smooth out the slope break at the base. If the breaks in bed slope at the top and base of the slip face are ideally sharp, they represent jumps or discontinuities in $\partial h/\partial t$ and therefore by Equation $12.5.6$ in $\partial q_s/\partial x$ as well. Both h and q_s show kinks in their profiles at these points.

The Profile Shapes of Ripples and Dunes

In this section it is shown how the asymmetrical profile shape of ripples or dunes can be accounted for by combining the sediment conservation equation with a very general assumption about the physics of the sediment transport, namely that q_s increases with increasing flow strength. As in the preceding section, look at a hypothetical bed form in a train of identical bed forms (Figure $12.5.3$). In this section we start with a symmetrical bed form and consider how its profile changes with time. Consideration is restricted to flows with low Froude number, so that the water surface remains nearly planar whatever the bed geometry. The following line of reasoning was first presented by Exner (1925).

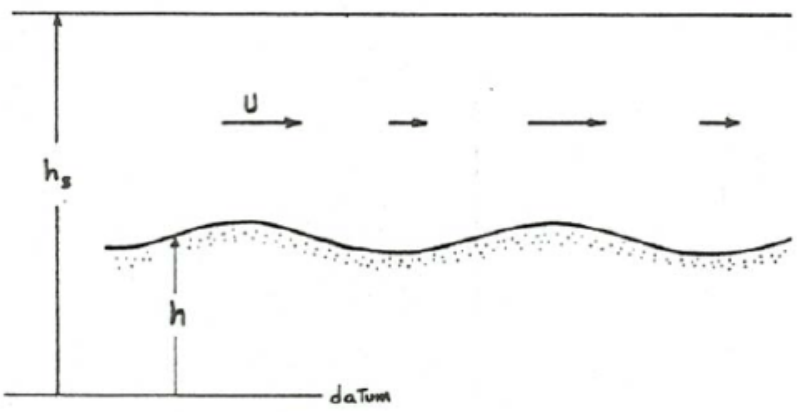


Figure 12.5.3: Definition sketch for analysis of the evolution of bed-form shape.

The strategy is to develop a relationship between bed elevation h and sediment transport rate q_s, in order to put the sediment conservation equation into a form that can be solved for bed elevation as a function of position and time. As discussed above, ultimately we would like to be able to supply enough physics for this approach to lead to insights about how bed forms grow. For now we have to be content with very simple assumptions about q_s that will lead to understanding of bed-form shape but not bed-form growth.

The mathematically simplest assumption we can make about q_s is that it is directly proportional to some variable that describes the flow strength above the point at which q_s is measured. Using mean flow velocity U as this flow-strength variable,

$$q_s = K_2 U \tag{12.5.7}$$

where K_2 is some constant. This has some serious shortcomings:

- there is a finite U for which q_s becomes nonzero, and at smaller U no sediment is moved;
- q_s does not vary linearly with U even when U is strong enough to move sediment; and
- if U rather than the skin friction is to be used to characterize q_s, the flow depth d must also be specified in the function.

Notwithstanding these difficulties, this is a workable assumption for the task at hand, because it contains a large element of truth and it permits insight into how the bed evolves. More sophisticated assumptions would lead to the same qualitative results on the evolution of bed-form shape but would necessitate working with equations that are much more difficult to solve. Furthermore, the fact that even such an oversimplified assumption about qs accounts well for the evolution of bed-form shape is revealing in itself.

Using Equation 12.5.7, the sediment conservation equation (Equation 12.5.6) can be written

$$\frac{\partial h}{\partial t} = -K_1 K_2 \frac{\partial U}{\partial x} \tag{12.5.8}$$

where K_1 is again the porosity correction factor $1/(1-\lambda)$. Conservation of fluid volume in the flow requires that, per unit width,

$$Ud = U(h_s - h) = K_3 \tag{12.5.9}$$

where h_s is water-surface elevation above the same arbitrary datum as for h, and K_3 is another constant. Equation 12.5.9 tells you that where the flow is deeper over some two-dimensional bed configuration the velocity is smaller, and where the flow is shallower the velocity is greater, so by Equation 12.5.5 there is deposition or erosion depending on the sign of $\partial U/\partial x$. Combining Equations 12.5.8 and 12.5.9,

$$\frac{\partial h}{\partial t} = \frac{K_1 K_2 K_3}{(h_s - h)^2} \frac{\partial (h_s - h)}{\partial x} \tag{12.5.10}$$

Assuming h_s to be constant (a reasonable assumption for flows at low Froude numbers) and writing K for the constant $K_1 K_2 K_3$, Equation 12.5.10 becomes

$$\frac{\partial h}{\partial t} = \frac{K}{(h_s - h)^2} \frac{\partial h}{\partial x} \tag{12.5.11}$$

You can verify for yourself that the solution to the fairly simple partial differential equation 12.5.11 is

$$h_s - h = f\left[\frac{Kt}{(h_s - h)^2} - x\right] \tag{12.5.12}$$

where f is an arbitrary function. To investigate the change in bed geometry with time, Exner (1925) assumed an initial bed topography given by a cosine function:

$$h = A_o + A_1 \cos\frac{2\pi}{L}\left[x - \frac{K_1 K_2 t}{(h_s - h)^2}\right] \tag{12.5.13}$$

where L is the spacing of the sinusoidal bed forms, and A_o and A_1 are constants. This is what the bed profile at time $t = 0$ would be if Equation 12.5.12 is specialized in such a way that the bed profile as a function of x and t is

$$h = A_o + A_1 \cos\frac{2\pi}{L}\left[x - \frac{K_1 K_2 t}{(h_s - h)^2}\right] \tag{12.5.14}$$

Figure 12.5.4 shows how the initial sinusoidal bed profile is modified with time according to Equation 12.5.14. The upstream slope of the bed form becomes gentler and the downstream slope becomes steeper, until finally the downstream slope passes through the vertical and an overhang develops. If this were a real bed form, a slip face would develop when the slope angle of the downstream side reaches the angle of repose. What is less clear from Figure 12.5.4 is that the bed form does not change in height as it changes in shape—but you can see from Equation 12.5.14 that the highest point on the bed form always has a height $h = A_o + A_1$, because the maximum value of the cosine function is one. This just means that the oversimplified assumption about q_s is inadequate to address the problem of bed-term growth.

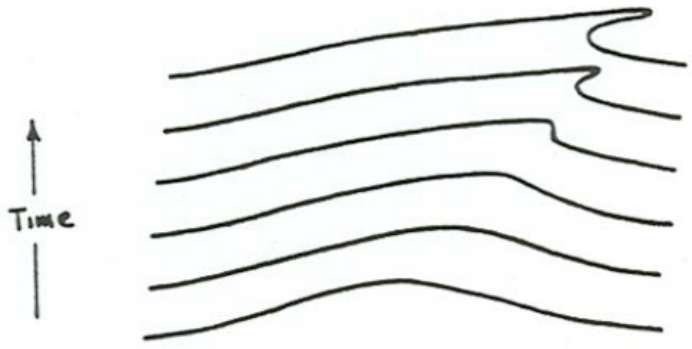


Figure 12.5.4: Evolution of an initially sinusoidal bed form with time. (After Exner, 1925.)

So even a very simple assumption about the dependence of q_s on the flow accounts for the tendency for an originally symmetrical bed-form profile to evolve into the markedly asymmetrical profile characteristic of ripples. If we use a different function in Equations 12.5.13 and 12.5.14 to represent a different symmetrical or nearly symmetrical initial profile, the end result is just about the same. It is easy to observe just this kind of profile development in the laboratory: mold a long and low symmetrical ridge transverse to the flow on the sand bed of your flume, turn up the discharge until the sand moves, and then watch the profile as it is transformed gradually into a ripple, just as in Figure 12.5.4.

Growth of Bed Forms

Introduction

It is more difficult to account for the growth of bed forms than for their movement and shape. Here I will follow the same approach as before, that of combining sediment-transport dynamics with the sediment conservation equation, but it will not lead to results that are as satisfying. This is because bed-form growth and decay, or more generally the stability of bed configurations, depends on the interaction of flow and sediment transport in ways too complicated to be expressed or parameterized by local conditions like flow velocity, boundary shear stress, bed elevation, or bed slope: it involves the entire bed configuration, not just

local variations in h and q_s.

After describing a hypothetical flume experiment to examine some of the physical effects that have to be explained, I will again examine the qualitative kinematic constraints imposed on q_s during bed-form growth and then review some of the attempts that have been made to account for the existence of bed forms by deriving and solving equations for bed-form growth based on various assumptions about transport dynamics.

Hypothetical Flume Experiment

Make a long series of low transverse ridges on a sand bed in your flume (Figure 12.5.5). It makes no difference whether these are initially symmetrical or asymmetrical, because you have already seen that the flow soon gives the profile of a transverse ridge a ripple shape, whatever its initial shape. It helps if you give the ridges an initial spacing that's is not greatly different from what you know beforehand about equilibrium ripple spacing (if any) corresponding to the conditions of flow and sediment size you are going to use, because then you maximize the duration of your experiment by reducing the tendency for the bed forms to change their spacing by dividing and merging. If you make the train of initial ridges very regular, the ripples stay very much alike for a long time as they evolve. Eventually the inevitable irregularities in initial bed geometry (together with the stochastic nature of the grain transport itself) lead to the irregular geometry characteristic of real bed forms, but this irregularity is not essential to the existence of the bed forms. I emphasize that this experiment is a valid way of thinking about the physics of growth and decay of ripples within the context of the initial spacing you choose, although in general you cannot expect these ripples to be happy with the given spacing forever, even if at first they grow rather than decay.

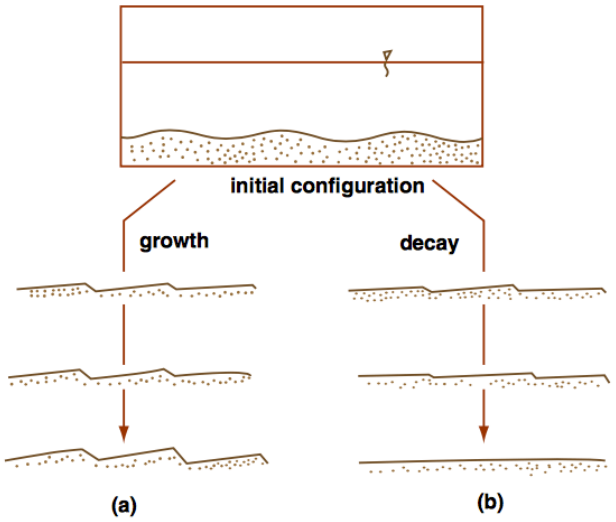


Figure 12.5.5: *Hypothetical flume experiment on growth and decay of a train of artificially constructed bed forms.*

Pass a sand-moving current over the ridges, and keep track of the elevations of crests and troughs. Under some conditions (Figure 12.5.5A) bed-form height increases as the troughs become deeper and the crests become higher. Stoss surfaces become steeper as well, because bed form spacing is strongly locked in to the original value and does not change, at least not until after a long running time. The lee surface is likely to become a slip face almost from the beginning, as you have already seen, and then stay that way. Associated with the increase in crest elevation and decrease in trough elevation is an increase in the volume of sand contained in the ripple per unit width (volume being measured upward from a plane coincident with the bed-form troughs). Time-lapse motion-picture photography of the ripples as they move is a good way of appreciating the changes in bed-form height and stoss-surface steepness. If you know something beforehand about equilibrium height of ripples as a function of flow conditions and sediment size, you could first generate a set of low ripples under one set of flow conditions and then change the flow conditions to what you know will make higher ripples, and then sit back and watch.

Now make a second run in which you start out with a train of initially high and steep ridges (Figure 12.5.5B). The bed forms rapidly become asymmetrical as before, and sediment transport and ripple movement are qualitatively the same as before, but the bed forms are degraded as they move downstream: there is a gradual increase in trough elevation and decrease in crest elevation, and a corresponding gradual decrease in bed-form volume and also in the steepness of the stoss surface. Depending on sediment size and flow conditions, the ripples may stabilize at some equilibrium height, shape, and velocity, or they may become more and

more like fast-moving sediment sheets with small downstream steps until ultimately the bed is transformed into a planar transport surface.

Both kinds of run are an approximate simulation of what happens when an equilibrium ripple bed configuration is subjected to a change in flow conditions. They leave out the effects of adjustment in ripple spacing by gradual accentuation of inevitable small irregularities in the profile and then division of one ripple into two, or fusion of two ripples into one. But they illustrate an important principle of bed-configuration stability: if very small disturbances grow larger, then some nonplanar bed configuration is the stable one under those conditions of flow and sediment, whereas if a preexisting nonplanar bed configuration is degraded to a planar transport surface, then upper-regime plane bed or lower-regime plane bed is the stable configuration. An analysis of how the ripple trains grow or decay in experiments like this should therefore provide insight into the dynamics of bed-form stability.

Conditions for Growth and Decay of Bed Forms

In this section I will reason as far as possible about the conditions for growth and decay of bed-form trains, like those in the hypothetical experiment described above. Take the x direction downstream and measure bed height from some plane parallel to the plane representing the mean bed surface and lying well below it. We will restrict ourselves to indefinitely long trains of two-dimensional flow-transverse bed forms in a transport system that's uniform in the large, in the sense that q_s averaged over an entire bed form does not change in the downstream direction (Figure $12.5.6$).

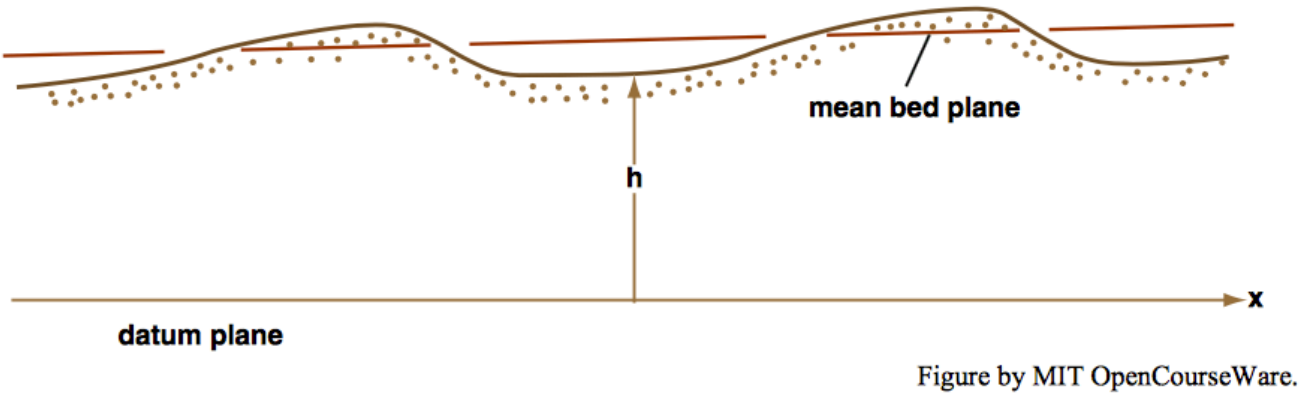


Figure by MIT OpenCourseWare.

Figure $12.5.6$: Definition sketch for analysis of growth and decay of bed-form trains in steady uniform flow.

The bed-form profile may or may not be changing. In either case, $\int h dx$ evaluated between two equivalent points on successive bed forms is constant. This expresses the condition that the bed is not aggrading or degrading on the average. If crests become higher, troughs have to become deeper in such a way that the mean bed elevation stays the same.

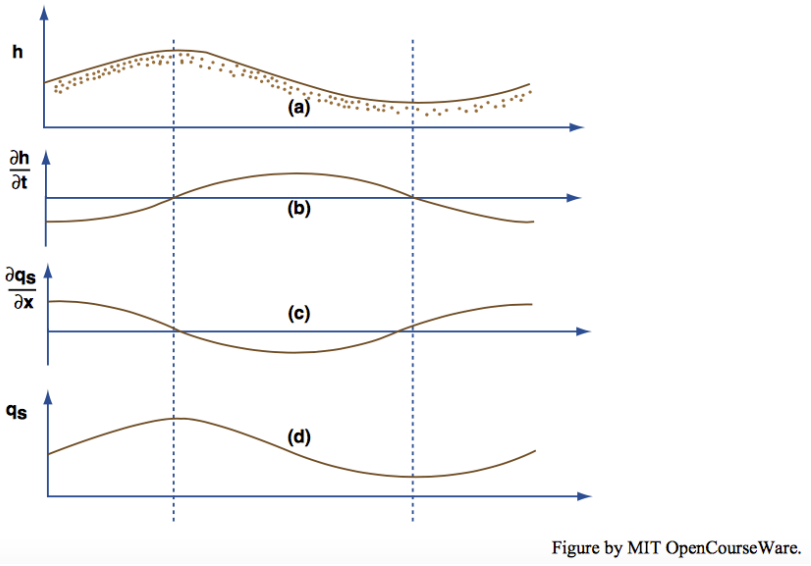


Figure 12.5.7: Profiles of **A)** h, **B)** $\partial h/\partial t$, **C)** $\partial q_s/\partial x$, and **D)** q_s, for an unchanging ripple train in steady uniform flow. For simplicity, the bed-elevation profile is shown as a sine curve; the results are qualitatively the same for any periodic bed profile.

It is instructive to consider first the reference case of an unchanging profile. In the following, refer to Figure 12.5.7 (which is fundamentally the same as Figure 12.5.2). The kinematic condition for an unchanging profile is that

$$h = f(x - U_B t) \tag{12.5.15}$$

where U_B is a constant and f is some periodic function that represents the bed profile at a given time. The argument $x - U_B t$ in the function implies that the profile propagates or shifts downstream at speed U_B as an unchanging wave form; U_B is therefore basically the same as the bed-form velocity used earlier in this chapter. To see the consequences of this condition, assume for now that the bed profile is a sine wave:

$$H = \sin(x - U_B t) \tag{12.5.16}$$

There is really no loss of generality in doing this, because any periodic bed profile can be represented as a Fourier sum of sinusoidal components; at the end of this paragraph we will revert to a general periodic function f.

Differentiating Equation 12.5.16 with respect to t,

$$\begin{aligned} \frac{\partial h}{\partial t} &= \frac{\partial}{\partial t}\sin(x - U_B t) \\ &= \frac{d[\sin(x - U_B t)]}{d(x - U_B t)} \frac{\partial (x - U_B t)}{\partial t} \\ &= U_B \cos(x - U_B t) \end{aligned} \tag{12.5.17}$$

by use of the chain rule for partial differentiation. Note that $\partial h/\partial t$ in Equation 12.5.17 is 90° out of phase with h in Equation 12.5.15, if the phase angle is measured in the downstream direction. In other words, the peak of the function in Equation 12.5.17 is offset downstream from that of the function in Equation 12.5.15 by one-quarter of a wavelength. (If you are not sure about the phase relationships, plot the four curves $y = \cos x$, $y = \sin x$, $y = -\cos x$, and $y = -\sin x$ and watch the sine wave shift along the x axis by 90°, i.e., one-quarter of a wavelength, each time.) Now, to find $\partial q_s/\partial x$ substitute Equation 12.5.17 into the sediment conservation equation, Equation 12.5.6:

$$\begin{aligned} \frac{\partial q_s}{\partial x} &= -\frac{1}{K_1}\frac{\partial h}{\partial t} \\ &= -\frac{U_B}{K_1}\cos(x - U_B t) \end{aligned} \tag{12.5.18}$$

Note that $\partial q_s/\partial x$ in Equation 12.5.18 is 270° out of phase with h in Equation 12.5.15 because of the minus sign, i.e., the crest of the $\partial q_s/\partial x$ profile is one-quarter of a wavelength upstream of the crest of the bed-elevation profile. Integrating $\partial q_s/\partial x$ in Equation 12.5.18 with respect to x,

$$\begin{aligned} q_s(x,t) &= \int \cos(x - U_B t)dx \\ &= \frac{U_B}{K_1}\int \cos(x - U_B t)dx \\ &= \frac{U_B}{K_1}\sin(x - U_B t) + c_1(t) \end{aligned} \tag{12.5.19}$$

where $c_1(t)$ is a constant of integration that in general could be a function of t, but is not in this case because we are assuming steady flow. (The constant of integration has to be a function of t because the integration is a "partial integration" of a function of two variables with respect to just one of those variables. while holding $U_B t$ constant.) Note that q_s is in phase with the bed profile and differs only by a multiplicative constant U_B/K_1 and an additive constant c_1.

$$h(x,t) = f(x - ct) \tag{12.5.20}$$

and,

$$q_s(x,t) = \frac{U_B}{K_1}f(x - U_B t) + c_1 \tag{12.5.21}$$

where c_1 is just a constant that relates the average bed elevation to the average sediment transport rate. The variation of q_s is in phase with the bed profile and has the same shape except for the constant factor U_B/K_1. Remember that this is all just a kinematic necessity; we have not specified anything about how q_s and h interact dynamically to produce the particular patterns observed.

From here on I will concentrate on lower-flow-regime ripple or dune bed forms. You have seen that if suspended-load transport is unimportant, lower-regime bed forms are dominated by slip faces that represent shock discontinuities. These discontinuities are associated with major flow separation over the bed form, but in a sense they are independent of the flow separation, in that they are a consequence of the steep increase in q_s with flow strength. Disregarding minor reverse flow in the lee eddy, q_s is zero from the toe of the slip face downstream to the reattachment point. If the profile is unchanging with time, this stretch of bed must be horizontal: within it q_s is independent of both x and t because it is identically zero there, so h, which differs from q_s only by a multiplicative and an additive constant (compare Equations 12.5.15 and 12.5.19), is constant in x and t there. This stretch of bed with $q_s = 0$ may not be quite the lowest in the profile. because of some upchannel-directed sediment transport just upchannel of the reattachment zone, but it can safely be assumed so without affecting the conclusions of this section. Likewise, there is no dynamical requirement that the brink at the top of the slip face is the highest point on the profile, even if the profile is unchanging with time, but, because there is such a strong tendency for flow separation to develop upstream of a negatively sloping surface, the brink should be just about the highest point on the profile. It is therefore convenient to let the slip face represent the bed-form height H, and it is also convenient to let the rate of downstream advance of the brink represent the velocity U_B of the ripple.

The presence of the shock discontinuity represented by the slip face imposes a further kinematic relationship that must hold among bed-form height, bed-form velocity, and the value of q_s at the brink:

$$(q_s)_{brink} = K_1 H U_B \tag{12.5.22}$$

This is exactly the same as Equation ???; if you go back and review the derivation of that equation, you will see that it holds for the present situation as well, provided that all of the load is dumped at the break in slope at the brink to build the slip face forward. Equation 12.5.22 holds generally, not just for an unchanging profile. Note that the slip-face angle drops out of the expression. This is consistent with the idea that the slip face is just the physical manifestation of a shock discontinuity in q_s. The sediment delivered to the crest could just as well be falling off a cliff, in terms of the kinematics of the phenomenon!

In the light of all this bed-form kinematics, what can be done about accounting for the results of the hypothetical experiment? In the first run the bed forms started out too low and grew to some stable greater height, and they changed their shape in the process. After the bed forms reached equilibrium, the distributions of h, $\partial h/\partial t$, $\partial q_s/\partial x$, and q_s must have been as shown in Figure 12.5.8B, which is qualitatively the same as Figure 12.5.2. Note the discontinuities in $\partial h/\partial t$ and $\partial q_s/\partial x$, reflecting the sharp kinks in bed elevation and transport rate at the top and bottom of the slip face. While the ripple train was adjusting, these curves must have been as shown in Figure 12.5.8A. The differences between Figure 12.5.8A and Figure 12.5.8B look minor, but they are very significant for ripple growth. Large differences should not be expected anyway, because change in ripple shape and height is slow relative to ripple movement. The maximum in q_s on the stoss slope is located a little upstream of the brink rather than right at it. This leads to upward growth of the upper stoss surface during migration. Also, there is a downchannel slope to the bed between the base of the slip face and the low point on the profile. These two differences reflect stronger-than-equilibrium scour in the reattachment zone and just downstream, leading to a temporal lowering of bed elevation in the trough. The extra sediment

produced by this scour is transported up the stoss surface to steepen the upper part. The slip face lengthens as it builds into the deepening trough, making ripple height greater. By Equation 12.5.22, U_B tends to decrease as the slip face lengthens, and this augments the tendency for increased trough scour, because the reattachment zone passes more slowly along the bed in the trough as it is driven downstream by the next ripple coming along. Eventually the geometry and sediment transport adjust to the new flow, and a picture qualitatively like that of Figure 12.5.8B is reestablished with a greater ripple height and a different ripple shape.

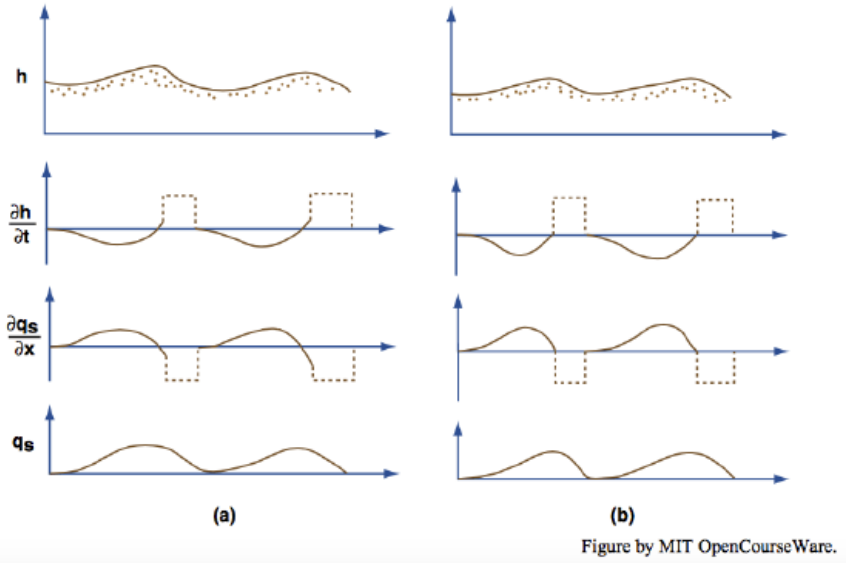


Figure 12.5.8: Profiles of **A)** h, **B)** $\partial h/\partial t$, **C)** $\partial q_s/\partial x$, and **D)** q_s, for a train of ripples increasing in height. **A)** Ripples are adjusting in height; **B)** ripples have reached equilibrium. See text for explanation.

In the second run, the bed forms started out too large and shrank either to some stable smaller height or were degraded completely. Figure 12.5.9 shows the distributions of h, $\partial h/\partial t$, $\partial q_s/\partial x$, and q_s as the ripples were changing. If the ripples reached equilibrium in the run, Figure 12.5.9A can be compared with Figure 12.5.9B for the stable smaller ripples. If not, then Figure 12.5.9A evolves into an uninteresting graph, not shown, in which h and q_s are positive and constant, and $\partial h/\partial t$ and $\partial q_s/\backslash \mathrm{parital} x$ are zero. Note in Figure 12.5.9A that q_s is increasing at all points up the stoss surface from reattachment. Because $\partial q_s/\partial x$ is still positive at the brink, $\partial h/\partial t$ is negative there, so the crest elevation is decreasing with time. Scour in the trough is weaker than needed to maintain trough depth, so the bed slopes upward at all points downchannel of the base of the slip face, although no sediment is moved on the stretch of bed from there to the reattachment point. Trough elevation increases as the slip face becomes shorter by building onto the upsloping trough surface, so both ripple height and ripple volume decrease. By Equation 12.5.22, U_B tends to increase as the slip face becomes shorter, and this augments the weakening of scour in the trough because it causes the reattachment zone to sweep more rapidly downchannel.

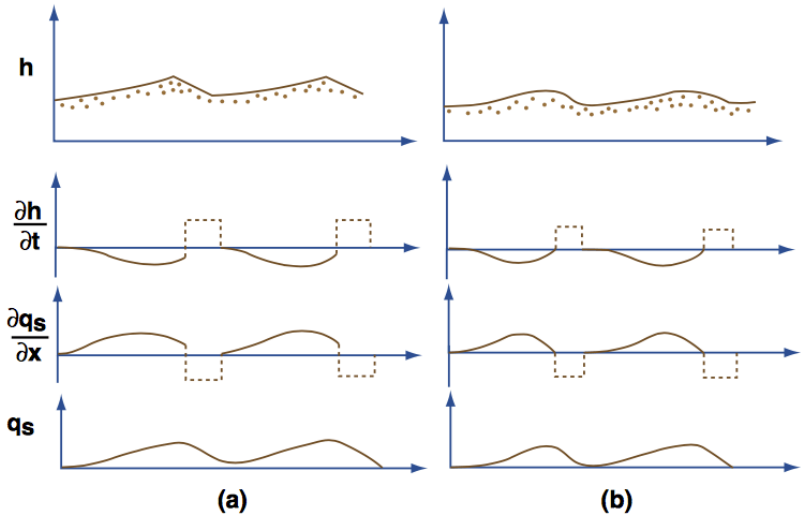


Figure by MIT OpenCourseWare.

Figure 12.5.9: Profiles of **A)** h, **B)** $\partial h/\partial t$, **C)** $\partial q_s/\partial x$, and **D)** q_s, for a train of ripples decreasing in height. **A)** Ripples are adjusting in height; **B)** ripples have reached equilibrium. See text for explanation.

In summary, changes in ripple height, shape, and velocity can be viewed in terms of the interaction among three related but distinguishable factors:

1. The dependence of q_s on flow structure along the reach of bed extending from the reattachment point up the stoss surface to the brink;
2. The rate at which the zones of differing flow structure downstream of the point of flow separation are swept along the bed surface by the advancing crest upstream, as specified by the relation expressed by Equation 12.5.22 among slip-face height, ripple velocity, and sediment transport rate at the brink; and
3. The slope of the trough surface onto which the slip face builds.

We have not solved any problems of bed-form stability here; we have only shown what factors are involved. Nonetheless, this line of approach is nonetheless useful, in that it aids in an understanding of the problem.

Stability Analyses

In order to understand the existence of bed forms, various investigators have resorted to stability analysis, a mathematical technique, useful in many areas of applied mathematics, whereby a partial differential equation is somehow developed that gives the rate of growth of a periodic disturbance or perturbation introduced onto the bed surface. The assumption is that if the rate of growth of the perturbation is positive the perturbation is amplified with time, and bed forms eventually develop. If, on the other hand, the perturbation is damped, then a plane bed should be the only stable bed configuration. The differential equation is of the same kind as used in the preceding sections. It comes about by supplying a relationship for q_s as a function of flow, which can be used to put the sediment conservation equation into a solvable form. This equation has to go beyond the oversimplified assumptions made in the section on shape of ripples, because we saw that those assumptions account only for change in ripple shape, not in ripple volume.

The great advantage of the stability approach is that it can be developed for perturbations with amplitude very small compared to wavelength, so that bed slopes are very small. It is then more likely that relationships for sediment transport that are not grossly unrealistic can be specified. By the same token, however, without further analysis this approach gives no information on the nature of the resulting bed configuration when the perturbation is amplified to the extent that that the small-amplitude assumption is no longer valid. There is the possibility, however, that an estimate of the spacing of the resulting bed forms can be obtained by determining the wavelength of the perturbation that shows the fastest rate of growth.

It is worth mentioning several attempts, along the above lines to account for observed bed configurations: those by Kennedy (1963, 1969), Smith (1970), Engelund (1970; see also Engelund and Fredsøe, 1974), Richards (1980), McLean (1990), Ji and Mendoza (1997), and Jerolmack et al. (2006). (You can see, from that list, that the pursuit of the fundamental dynamics by means of stability analysis has had a long history. The last word has not been spoken on that topic—a manifestation of the enduring

obstacles to a unified and generally accepted theory.)

Kennedy's analysis, which is most relevant to bed configurations at mean-flow Froude numbers close to one, assumes inviscid flow with a wavy free surface over a wavy boundary. By making simple assumptions about sediment transport rate as a function of near-bed velocity, Kennedy developed a framework that accounts well for the occurrence of antidunes—bed forms whose behavior is dependent upon the presence of the free surface. The theory does not so much predict the bed configuration as provide a rational framework in which to account for it: as do many later analyses by others, the analysis involves a parameter called the lag distance (the distance by which local sediment transport rate lags behind the local velocity at the bed) that would have to be supplied by either experiment or additional theory. For the stability of antidunes, the theory works well with physically realistic assumptions about the lag distance in that it succeeds in accounting for the observed spacing of antidunes. As might be expected from the essential role of the presence of the wavy free surface in the analysis, the theory is less successful in accounting for dunes. Kennedy's work stimulated many subsequent attempts along the same lines.

Smith (1970) developed a stability analysis to deal specifically with flow at Froude numbers low enough that free-surface effects are negligible. Making suitable assumptions about nature of the flow (eddy-viscous flow of real fluid) and about sediment transport rate as a function of flow, Smith developed an equation that, when linearized by retaining only the most significant terms, is amenable to stability analysis. The result is that, for these not grossly unrealistic assumptions about flow and sediment transport, a positive growth rate, and therefore development of ripple-like bed configurations, is predicted for all flows strong enough to transport sediment. This is a rather fundamental and satisfying way to account for the existence of ripple-like bed configurations under reasonably realistic assumptions about flow and sediment transport. Even aside from the usual problem of not being able to take finite-amplitude effects into account without further theory, however, the analysis does not account for the existence of plane-bed stability at the higher flow strengths.

Engelund (1970; see also Fredsøe, 1974, and Engelund and Fredsøe, 1974), in a somewhat different approach also involving an eddy-viscous fluid, but taking account of the distinction between suspended-load transport and bed-load transport, was able to account well for the transition from dunes to plane bed as a function of both grain size and flow strength. Richards (1980), using a more realistic description of the structure of turbulence near the bed, was able to account for the separate existence of ripples and dunes by predicting the occurrence of two separate modes of instability, one (for ripples) dependent on the bed roughness and the other (for dunes) dependent on the flow depth. More recently, McLean (1990) and Li and Mendoza (1997) have gone beyond linear stability analysis to account also for nonlinear finite-amplitude effects. Even more recently, Jerolmack et al. (2006) have developed a model of bed-form development that unifies the dynamics of ripples and dunes.

Are Ripples and Dunes Different?

Of course, the answer is "yes": dunes are larger than ripples. I should rephrase the question: Are the dynamics of ripples and dunes different? Most investigators have assumed that the answer to that question is also "yes". Those who have attempted to account for the existence of ripples and dunes by means of a stability analysis (see the preceding section) have invoked a short-wavelength instability that leads to the development of ripples and a long-wavelength instability that leads to the development of dunes. In that approach, the key to the development of ripples is a spatial (downstream) lag between bed shear stress and sediment transport rate (that is, the sedimentary transport rate lags the bed shear stress) in the case of ripples, and a spatial lag between bed shear stress that also involves suspended-load transport, in the case of dunes.

It has commonly been believed that there is a gap in spacing between what are considered to be ripples and what are considered to be dunes. In reporting a consensus among the "experts", Ashley (1990) chose a cutoff of $0.6\ \mathrm{m}$ spacing for the boundary between ripples and dunes. There indeed seems to be a paucity of bed forms with spacings in the range between a few decimeters and one meter (Figure $12.5.10$).

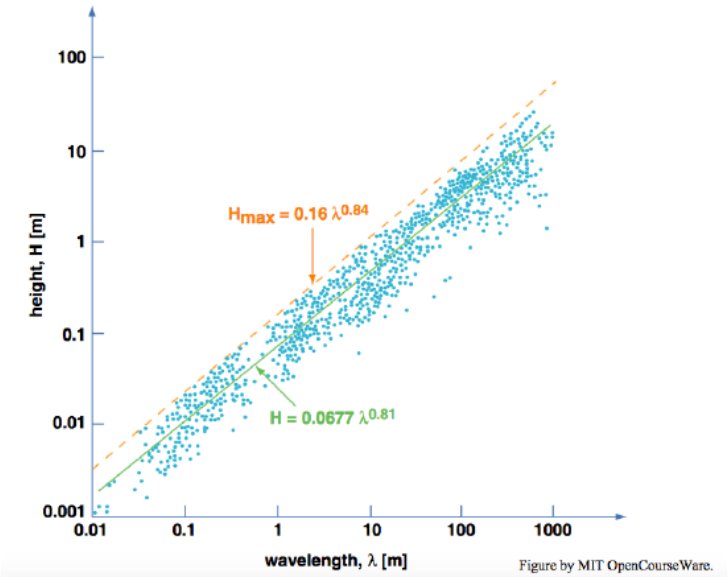


Figure 12.5.10: Plot of bed-form height vs. bed-form spacing. The dashed line is the maximum best-fit power-law relationship, and the solid line is the mean best- fit power-law relationship. (From Jerolmack et al., 2006, based on the work of B.W. Flemming.)

Clearly there is not a complete absence of ripple or dune bed forms in that range—but it is still uncertain whether there is a continuum in spacing between undoubted ripples and undoubted dunes, or whether those intermediate cases are stunted dunes (in very shallow flow) or newly developing dunes. The matter has not yet reached the stage of a general consensus. There have been only a few studies aimed particularly at describing the transition between ripples and dunes (Boguchwal and Southard, 1990; Bennett and Best, 1996; Lopez et al., 2000; Robert and Uhlman, 2001). The range of mean flow velocity, for a given flow depth, over which the transition is completed is rather narrow. Within that narrow range, there is a large change in bed-form geometry as well as the associated flow characteristics. What all of these studies seem to agree upon is that there is a real dynamical distinction between ripples and dunes.

This page titled 12.5: 2D Dunes and 3D Dunes is shared under a CC BY-NC-SA 4.0 license and was authored, remixed, and/or curated by John Southard (MIT OpenCourseware) via source content that was edited to the style and standards of the LibreTexts platform.

12.6: Oscillatory-Flow and Combined-Flow Bed Configurations

Introduction

As described in Chapter 6, water-surface waves propagating in water much shallower than the wavelength cause a back-and-forth motion of the water at the bottom. If the maximum speed of the water (which is attained in the middle of the oscillation) exceeds the threshold for sediment movement, oscillatory-flow bed forms develop. This is common in the shallow ocean. Swell from distant storms causes bottom oscillatory motion even though the weather is fine and calm locally. More importantly, bottom-water motions under large storm waves cause bed forms also. In that situation there is likely to be a non-negligible unidirectional current as well, resulting in a combined flow.

A Tank Experiment on Oscillatory-Flow Bed Configurations

There are three ways to make oscillatory-flow bed configurations in the laboratory. One is to build a big long tank and make waves in it by putting a wave generator at one end and a wave absorber at the other end (Figure 12.6.1). The generator does not need to be anything more than a flap hinged at the bottom and rocked back and forth in the direction of the tank axis at the desired period. This arrangement makes nice bed forms, but the trouble is that you are limited to short oscillation periods.

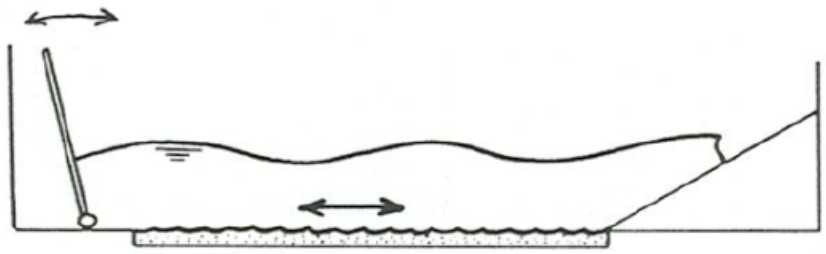


Figure 12.6.1: Making an oscillatory-flow bed configuration in a wave tank.

Another good way to make oscillatory-flow bed configurations is to build a horizontal closed duct that connects smoothly with reservoir tanks at both ends, fill the whole apparatus with water, and then put a piston in contact with the water surface in one of the reservoir tanks and oscillate it up and down at the desired period (Figure 12.6.2). This allows you to work with much longer-period oscillations, but there is the practical problem that the apparatus has its own natural oscillation period, and if you try to make oscillations at a much different period you have to fight against what the duct wants to do, and that means large forces.

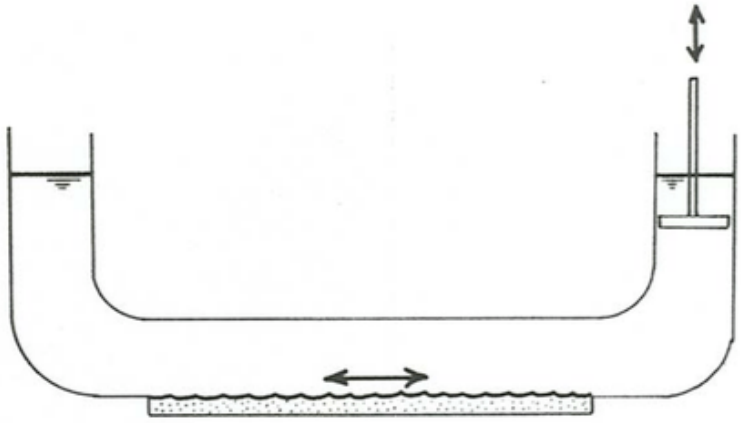


Figure 12.6.2: Making an oscillatory-flow bed configuration in an oscillatory-flow duct.

The third way should seem elegant and ingenious to you: place a sand-covered horizontal tray at the bottom of a large tank of water, and oscillate the tray back and forth underneath the water (Figure 12.6.3). The problem is that the details of particle and fluid accelerations are subtly different from the other two devices, and it turns out that the bed configurations produced in this kind of apparatus do not correspond well with those produced in the other two kinds of apparatus.

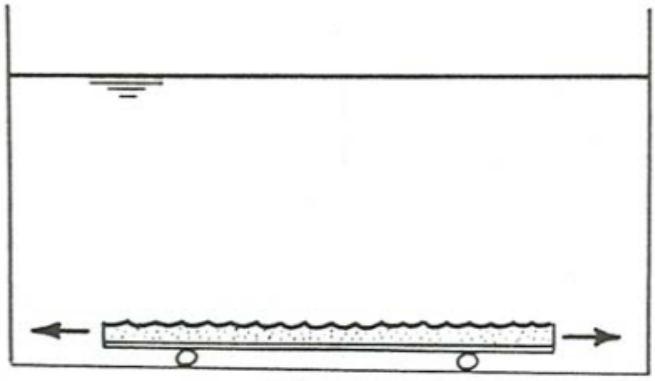


Figure 12.6.3: Making an oscillatory-flow bed configuration in an oscillatory bed beneath still fluid.

Imagine making an exploratory series of runs in an oscillatory-flow duct of the kind shown in Figure 12.6.2 to obtain a general idea of the nature of oscillatory-flow bed configurations. Work at just one oscillation period, in the range from three to five seconds. Start at a low maximum oscillation velocity and increase it in steps. Figure 12.6.4 shows the sequence of bed configurations you would observe.

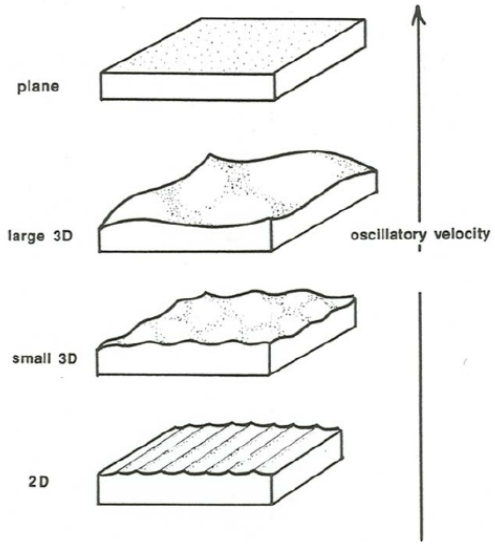


Figure 12.6.4: Sequence of oscillatory-flow bed configurations sin fine sands with increasing oscillation velocity, for an oscillation period of several seconds.

Once the movement threshold is reached, a pattern of extremely regular and straight-crested ripples develops on a previously planar bed. The ripples are symmetrical in cross section, with sharp crests and broad troughs. In striking contrast to unidirectional-flow bed configurations, the plan pattern is strikingly regular: ripple size varies little from ripple to ripple, and the ripples are straight and regular. At fairly low velocities the ripples are relatively small, withspacings of no more than several centimeters, but with increasing velocity the become larger and larger.

In a certain range of moderate velocities, the ripples become noticeably less regular and more three-dimensional, although they are still oriented dominantly transverse to the oscillatory flow. These three-dimensional ripples continue to grow in size with increasing velocity, until eventually they become flattened and are finally washed out to a planar bed. Therefore, just as in unidirectional flows, rugged bed configurations pass over into a stable plane-bed mode of transport with increasing velocity.

Oscillatory-flow bed configurations at longer oscillation periods are much less well studied, especially at high oscillatory velocities. Some comments on bed configurations produced under those conditions, which are very important in natural environments, are given in a later section.

Dimensional Analysis

Assume again, as we did earlier with unidirectional flow bed configurations, that the sediment is described well enough by its density ρ_s and average size D. The oscillatory flow is specified by any two of the following three variables: oscillation period T , orbital diameter d_o (the distance traveled by water particles during one-half of an oscillation), and maximum orbital velocity U_m; I'll use T and U_m here. As with unidirectional-flow bed configurations, we also need to include ρ, μ, and γ'. The number of independent variables is seven, so we should expect a set of four equivalent dimensionless variables.

One dimensionless variable can again be the density ratio ρ_s/ρ, and the other three have to include U_m, T, and D as well as ρ , μ, and γ'. Adopting the same strategy as for unidirectional flow, we can form a dimensionless maximum oscillation velocity, a dimensionless oscillation period, and a dimensionless sediment size:

$$\left(\frac{\rho^2}{\mu\gamma'}\right)^{1/3} U_m, \left(\frac{\gamma'^2}{\rho\mu}\right)^{1/3} T, \left(\frac{\gamma'\rho}{\mu^2}\right)^{1/3} D$$

Then we can plot another three-dimensional graph to show the stability fields of oscillatory-flow bed phases, just as for unidirectional-flow bed phases (Figure $12.6.5$). Relationships are best revealed by looking at a series of velocity–period sections through the graph for various values of sediment size (Figure $12.6.5$). Figure $12.6.6$ shows three such sections, one for very fine sands, 0.1–0.2 mm (Figure $12.6.6$A), one for medium sands, 0.3–0.4 mm (Figure $12.6.6$B), and one for coarse sands (0.5–0.6 mm (Figure $12.6.6$C). As with the graphs for unidirectional flows presented earlier, the axes are labeled with the $\backslash 10^{\circ}\mathrm{C}$ values of velocity and period corresponding to the actual dimensionless variables. The data shown in Figure $12.6.6$ are from laboratory experiments on oscillatory-flow bed configurations, made in both wave tanks and oscillatory-flow ducts, by several different investigators.

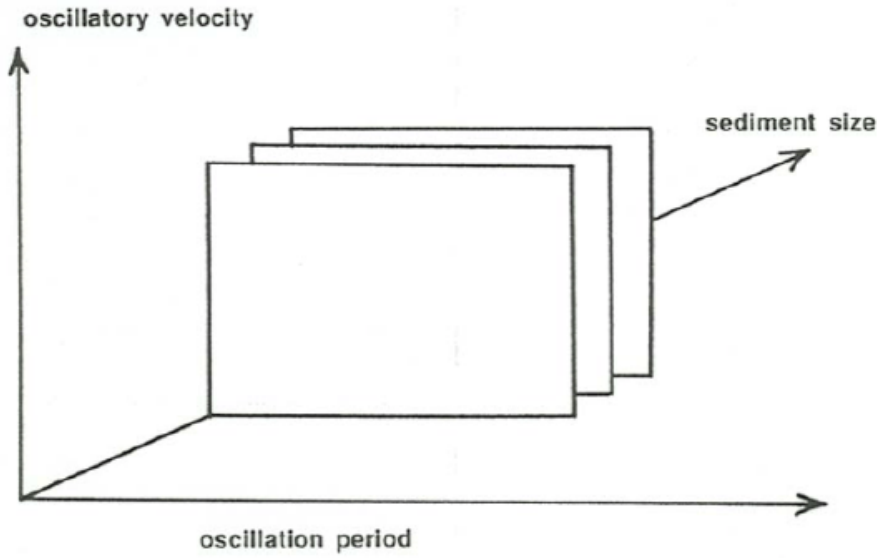


Figure $12.6.5$: The velocity–period–size diagram, showing velocity–period sections for three sediment sizes.

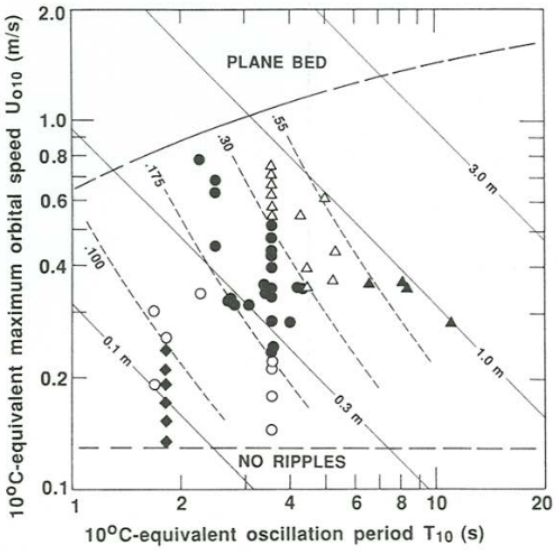


Figure 12.6.6: Velocity–period sections for sand sizes of **A)** 0.01–0.02 mm and **B)** 0.50–0.65 mm sand. Symbols for spacing: solid diamonds, < 0.100 mm; open circles, 0.100–0.175 mm; solid circles, 0.175–0.30 mm; open triangles, 0.30–0.55 mm; solid triangles, 0.55–1.00 mm; open squares, 1.00–1.75 mm; solid squares, > 1.75 mm. Horizontal tick marks indicate a three-dimensional configuration. Symbols without tick marks indicate a two-dimensional configuration, except that circles with enclosed X's represent a three-dimensional configuration for which a characteristic ripple spacing was not measured. Vertical tick marks indicate ripples whose spacing is much greater than duct width, so that the three-dimensional geometry of the ripples could not be observed. (From Southard, 1991.)

In each section in Figure 12.6.6, there is no movement at low velocities and a plane-bed mode of transport at high velocities. The intervening stability region for oscillation ripples narrows with decreasing oscillation period. As with ripples in unidirectional flows, there really are two different kinds of lower boundary of the stability field for oscillation ripples: one represents the threshold for sediment movement on a preexisting planar bed, and the other represents the minimum oscillation velocity needed to maintain the equilibrium of a preexisting ripple configuration. Existing data are not extensive enough to define the exact nature of these boundaries.

The most prominent feature of each of the sections in Figure 12.6.6 is the regular increase in ripple spacing from lower left to upper right, with increasing velocity and period. The contours of ripple spacing are close to being parallel to the lines of equal orbital diameter except near the transition to plane bed.

An important feature of the section for fine sands is a transition from extremely regular straight-crested ripples (which I will call two-dimensional ripples) at relatively low oscillation velocities to rather irregular ripples (which I will call three-dimensional ripples) with short and sinuous crest lines at relatively high oscillation velocities. The most three-dimensional bed configurations show only a weak tendency for flow-transverse orientation, and it is difficult or impossible to measure an average ripple spacing. In medium sands (Figure 12.6.6B) the transition from two-dimensional ripples to three-dimensional ripples takes place at velocities closer to the transition to plane bed, and the tendency for three-dimensionality is not as marked as in fine sands.

Superimposed smaller ripples are prominent in the troughs and on the flanks of the larger ripples formed at long oscillation periods and high oscillation velocities in fine sands. These small superimposed ripples have spacings of about 7 cm, and they seem to dynamically related to ripples in unidirectional flows. The one-way flow during each half of the oscillation lasts long enough and transports enough sediment so that a pattern of current ripples becomes established in local areas on the bed. The flow in the other direction reverses the asymmetry of these small ripples but does not destroy them.

Experimental data are least abundant for long periods and high velocities, but preliminary data show the existence of three-dimensional rounded bed forms with spacings of well over a meter in fine sands under these conditions. In contrast to the smaller two-dimensional ripples, these large ripples are not static but show a tendency to change their shape and shift their position with time, even after the bed configuration has stopped changing on the average.

In coarse sands (Figure 12.6.6C), no experiments have been made at the longest periods and highest velocities, but evidence from observations in modern shallow marine environments, and also from the ancient sedimentary record, suggests that ripples in coarse sands are two-dimensional over the entire range of periods and velocities characteristic of natural flow environments.

The flow over oscillation ripples is characteristic (Figure 12.6.7). During half of the oscillation cycle, the flow separates over the sharp crest of the ripple, putting abundant suspended sediment in suspension in the separation vortex over the downflow side. As the flow reverses, the vortex is abruptly carried over the crest of the ripple and deposits its suspended sediment. Flow separation is then rapidly reestablished on the other side of the ripple, and a new vortex develops. For this reason, these ripples have been called **vortex ripples**.

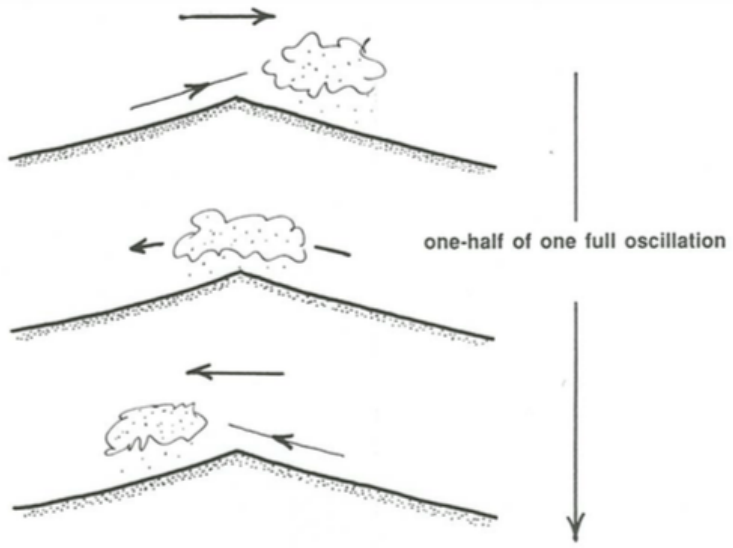


Figure 12.6.7: Sediment transport in suspension over the crest of an oscillation ripple.

Purely oscillatory flows that involve a discrete or continuous range of oscillatory components with different directions, periods, and velocities must be common in the shallow ocean. For example, when a storm passes a given area, strong winds tend to blow from different directions at different times. Some time is needed for the sea state to adjust itself to the changing wind directions, and during those times the sea state is complicated, with superimposed waves running in different directions. The nature of bed configurations under even simple combinations of two different wave trains is little known. Much more observational work needs to be done on this topic.

Combined-Flow Bed Configurations

So far we have considered only the two “end-member cases” of flows that make bed configurations. Even aside from the importance of time-varying unidirectional and oscillatory flows, and of purely oscillatory flows with more than just one oscillatory component, there is an entire range of combined flows that generate distinctive bed configurations. Observations in the natural environment are scarce, and systematic laboratory work (Arnott and Southard, 1990; Yokokawa, 1995; Dumas et al., 2005) has so far explored only a small part of the wide range of relevant conditions. This section is therefore necessarily shorter than the previous sections. Up to now, systematic observations have been made only for combined flows in which a single oscillatory component is superimposed on a current flowing with the same orientation as the oscillation. There is therefore still a major gap in our knowledge of combined-flow bed configurations.

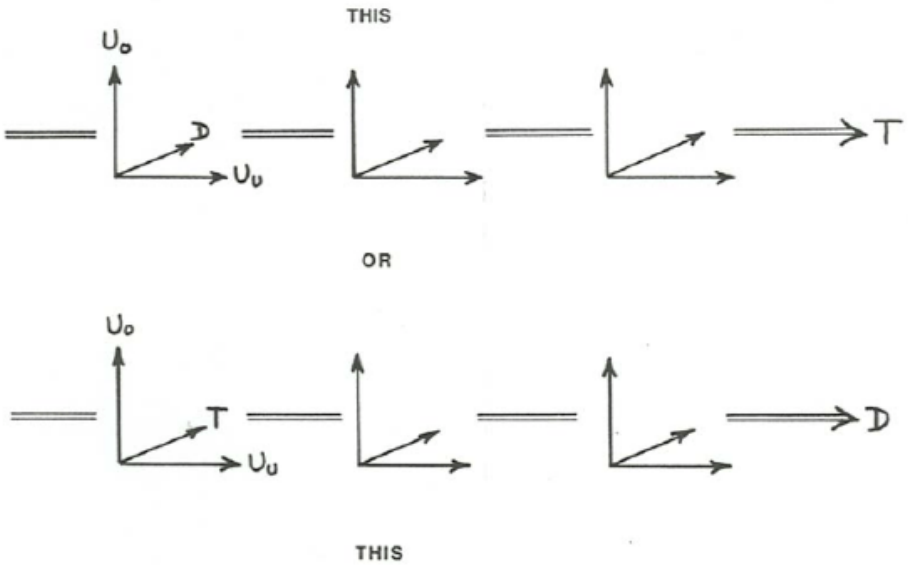


Figure 12.6.8: Ways of representing combined-flow bed configurations graphically.

Figure 12.6.8 is an inadequate attempt to provide a conceptual framework for thinking about combined-flow bed configurations. Ideally we would like to be able to plot observational data on combined-flow bed configurations on a graph with axes representing the four important independent variables: oscillatory velocity, unidirectional velocity, oscillation period, and sediment size. Unfortunately it is impossible for human beings to visualize four-dimensional graphs. A substitute approach (Figure 12.6.8) is to imagine one or the other of two equivalent kinds of graphs:

- a continuous series of three-dimensional graphs with the two velocity components and sediment size along the axes, one such graph for each value of oscillation period; or
- a continuous series of three-dimensional graphs with the two velocity components and oscillation period along the axes, one such graph for each value of sediment size.

Systematic laboratory experiments on combined-flow configurations have been carried out by Arnott and Southard and, more recently, covering wider range of flow and sediment conditions, by Dumas et al. (2005). The experiments by Dumas et al. (2005) were done in large oscillatory-flow ducts with oscillation periods ranging from about 8 s to 11 s (scaled to 10°C water temperature), with well-sorted sediments ranging in size from 0.10 to 0.23 mm (scaled to 10°C water temperature). Figure 12.6.9 shows three phase diagrams, for three combinations of oscillation period and sediment size, showing data points and phase boundaries. The boundaries within the field for ripples are gradual rather than abrupt. Bear in mind, when looking at these diagrams, that they are still an extremely “thin” representation of the graphic framework shown in Figure 12.6.8.

Image removed due to copyright restrictions.
Dumas, S., R. W. C. Arnott, and J. B. Southard. "Experiments on Oscillatory-flow and Combined-flow Bed Forms: Implications for Interpreting Parts of the Shallow-marine Sedimentary Record."
Journal of Sedimentary Research 75 (2005): 501-513.

Figure 12.6.9: Bed-phase diagrams for combined-flow bed phases, with oscillatory velocity component on the vertical axis and unidirectional velocity component on the horizontal axis. **A)** sediment size 0.14 mm, oscillation period 10.5 s; **B)** sediment size 0.14 mm, oscillation period 8.0 s; **C)** sediment size 0.22 mm; oscillation period 10.5 s.

Here are some of the features of Figure 12.6.9. At combinations of low oscillatory velocities and low unidirectional velocities, there is no sediment movement. At combinations of high oscillatory velocities and high unidirectional velocities, a planar bed with strong sediment movement is the stable bed configuration. Note that when even a small unidirectional component is present, the oscillatory velocity for the transition from ripples to plane bed is substantially lower than in purely oscillatory flow.

In the lower part of the region of ripple stability, the ripples are relatively small. Only a small unidirectional component is needed to make the small ripples fairly asymmetrical. Except when the unidirectional component is very weak, small combined-flow ripples are not greatly different in geometry from ripples in purely unidirectional flow.

In the upper part of the region of ripple stability, the ripples are relatively large. Only a small unidirectional flow component is needed to make the large three-dimensional oscillatory-flow bed forms produced at these oscillation periods and sediment sizes noticeably asymmetrical. For relatively large oscillatory velocities, especially in the finer sand size, the bed forms acquire a three-dimensional hummocky appearance; this region is shown by the shading in Figures 12.6.9A, B, and C; it is a feature that seems to become superimposed on the symmetrical to symmetrical large combined-flow ripples under those values of the velocity components.

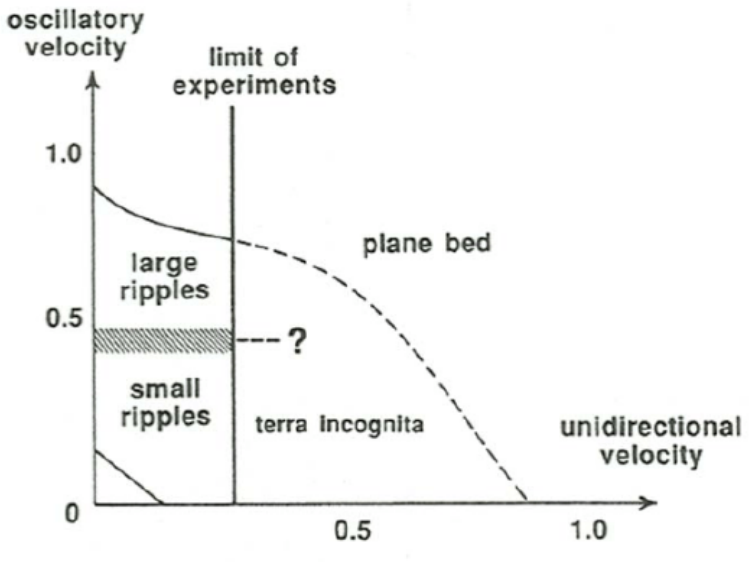


Figure 12.6.9 *to a wider range of combined-flow conditions. (From Southard, 1991.)*

At unidirectional velocities greater than are shown in this graph, the field for large combined-flow ripples must pinch out, because small ripples are known to be the only stable bed configuration in purely unidirectional flows in these fine sand sizes. Figure 12.6.10 shows a speculative extrapolation of Figure 12.6.9 to higher unidirectional velocities. The effect of an increasingly strong oscillatory velocity component on unidirectional-flow dunes in medium and coarse sands is an intriguing problem for which no experimental data are yet available.

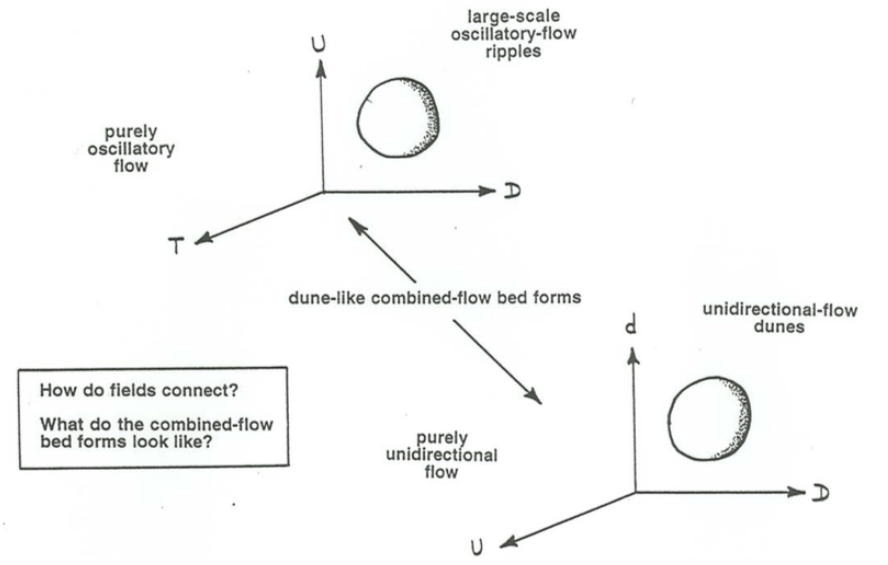


Figure 12.6.11: Relationship between large-sale ripples in purely oscillatory flow and dunes in purely unidirectional flow.

When the oscillation period is large, medium to high oscillation velocities produce large symmetrical ripples. Even a slight unidirectional component is known (e.g., Arnott and Southard, 1990; Dumas et al., 2005) to make these large ripples noticeably asymmetrical, to the point where they are not greatly different in geometry and internal stratification from unidirectional-flow dunes. That leads to an important question: *what do the large-scale bed forms in the intermediate range of flow conditions and sediment sizes look like?* There has been almost no systematic study of such bed forms, and yet deductively it seems that they should be important, and that a lot of the cross stratification we see in the ancient sedimentary record must have been produced under such conditions. Figure 12.6.11.

This page titled 12.6: Oscillatory-Flow and Combined-Flow Bed Configurations is shared under a CC BY-NC-SA 4.0 license and was authored, remixed, and/or curated by John Southard (MIT OpenCourseware) via source content that was edited to the style and standards of the LibreTexts platform.

12.7: Wind Ripples and Eolian Dunes

Wind Ripples

Introduction

When a sand-moving wind lows across a surface of loose sand, wind ripples soon make their appearance. In their classic manifestation, wind ripples are almost perfectly straight-crested low ridges extending for long distance transverse to the wind. In places, a wind ripple ends abruptly, and in other places there are “tuning fork” junctions at which a single ripple branches into two. Ripple spacing range mostly between a few centimeters and ten centimeters—although in coarser particle sizes the spacing increases up to a few meters and the ripple become much less regular in their geometry. Such ripples have been called **granule ripples**. Upwind (stoss) surfaces of common wind ripples have slope angles of X, and downwind(lee surface have slopes of X, much less than the angle of repose for loose sand. Crests as well as troughs are rounded. As with subaqueous current ripples, wind ripples move downwind at speeds orders of magnitude slower than the driving wind. In contrast to subaqueous current ripples, particle size at the crests of the ripples are coarser than in the troughs. It is in the troughs that finer particles—of very fine sand size down into silt size—find resting places, sheltered from the wind.

As with so many aspects of eolian sedimentation, modern study of wind ripples began with Bagnold (1941), who studied them both in the field and in laboratory wind tunnel. (It is especially easy to make wind ripples even in a short wind tunnel.) A later classic paper is that by Sharp (1963). Two of the most extensive wind-tunnel studies of wind ripples are those of Seppälä and Lindé (1978) and Walker (1981). In what to my knowledge is the most extensive and systematic wind-tunnel study of wind ripples to date, Walker (1981) found that ripple spacing increases with both mean particle size and wind velocity, and, for a given particle size, ripple spacing increases as the sorting become less good.

The dynamics of wind ripples has had a long history of controversy. Bagnold theorized that the spacing of wind ripples was set by a certain “characteristic” saltation jump length. Later workers, beginning with Sharp (1963), rejected Bagnold’s concept and emphasized the role of surface creep, driven by saltation impacts, in forming and maintaining the ripples. This line of thought culminated in a stability analysis of ripple development by Anderson (1987). A rather different approach to wind ripples was taken by Werner and Gillespie (1993) and by Landry and Werner (1994).

In recent years, physicists and applied mathematicians have been attracted to the dynamics of wind ripples, perhaps in part because it is such an intriguing example of dynamical self-organization, and perhaps in part because it lends itself to theoretical and numerical modeling in which the messiness of turbulence does not have a direct effect on the process. This interest has resulted in numerous papers, published mainly in physics periodicals; see, in particular, papers by Nishimori and Ouchi (1993), Ouchi and Nishimori (1995), Prigozhin (1995), Stam (1996), Hoyle and Woods (1997), Hoyle and Mehta (1999), Valance and Rioual (1999), Terzidis et al. (1998), Kurtze et al. (2000), Valdewalle and Galam (2000) Miao et al. (2001), Niño et al. (2002), and Yizhaq et al. (2004). In contrast, observational studies of wind ripples seem to have been scarce in recent times; see Andreotti et al. (2006).

Eolian Dunes

Introduction

In areas covered widely by movable sand, the wind shapes the sand into large-scale features called **dunes**. In contrast to the subaqueous case, for which there is controversy about the dynamical distinction between ripples and dunes, it is clear that there is a fundamental dynamical distinction between wind ripples and eolian dunes.This was first made explicit in a widely cited paper by Wilson (1972) (Figure 12.7.1). Eolian dunes range in spacing from many meters, at a minimum, to thousands of meters. There seems to be no upper limit to dune size, given sufficient sand and a sufficient reach on which the wind can do its work. For a thorough exposition of eolian dune types, see Pye and Tsoar (1990).

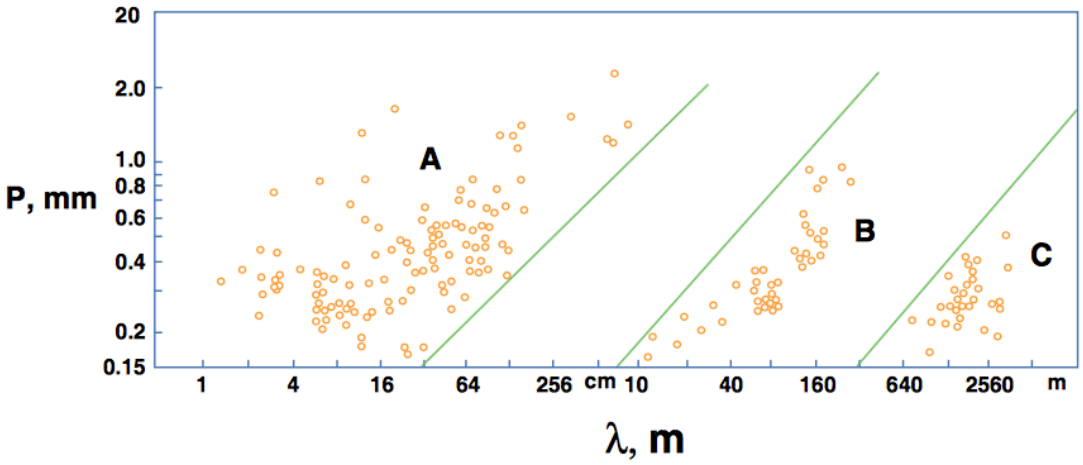


Figure by MIT OpenCourseWare.

Figure 12.7.1: Bed-form spacing λ against P_{20}, the coarse-twentieth-percentile particle diameter. \(**A** =\) wind ripples, \(**B** =\) dunes, \(**C** =\) draas. (From Wilson, 1972.)

In sharp contrast to subaqueous dunes, the shapes of eolian dunes, and their orientation elative to the sand-moving wind, range very widely. Features that are classified under the term *dune* range from those that are strictly transverse to the wind, to those that are extremely regular in geometry and are closely parallel to the wind—hence the distinction between transverse dunes and longitudinal dunes. In regions where the winds are highly variable in direction, star dunes, with arms oriented in various directions, form. Smaller dunes can be superimposed upon larger dunes.

A thought experiment seems in order here. In the case of subaqueous dunes, much of what we know comes from studies of dunes generated by unidirectional flows of water under equilibrium conditions in flumes. In the case of eolian dunes, no experimental programs of that sort have ever been conducted, to my knowledge at least. The basic problem is that because of the minimum size of dunes is so large, it would take an extraordinarily large wind tunnel to make experiments on the equilibrium characteristics of eolian dunes. And even then, of course, the presence of the roof in the wind tunnel would make the results less applicable to the natural environment, in which, in the context of eolian dunes, is effectively unlimited in height.

What would we find if we built a long quonset-hut-like building, perhaps a large fraction of a kilometer long, with a roof a few tens of meters high, over a deep bed of loose sand, and passed a controlled, steady wind through the tunnel, perhaps by means of a propeller driven by an old-fashioned airplane engine mounted at the downwind end of the tunnel, while at the same time adding new sand at the upwind end of the tunnel? Presumably, dunes would develop; how would their spacing depend on wind velocity and sand size? Would they grow to the point of constriction by the height of the tunnel for all wind speeds, or would their spacing increase with wind speed? Would dune size vary with sand size? The answers to those questions, which are fairly clear for subaqueous dunes, are not known.

Nature provides us with much less controlled conditions: everywhere on Earth, even in the least variable climatic conditions, the wind varies in both speed and direction. That variability makes any conclusions about how dune geometry depends on wind conditions fraught with uncertainty.

In areas where the availability of movable sand is limited, eolian dunes take the form of **barchans**: crescent-shaped dunes, with horns pointing downwind, that move across a non-moveable surface. Sand is supplied to the barchans from upwind; the barchans lose sediment, at about the same rate, from the downwind tips of the horns. Barchans are not restricted to eolian environments: it is easy to make miniature barchans in water flows in a flume in which limited quantities of fine sand or silt move across a the rigid floor of the flume.

Are eolian dunes and subaqueous dunes identical, in terms of the fundamental dynamics? This question is not explicitly addressed in the literature, to my knowledge, but I would speculate that the specialists, if asked, would say that they indeed are. The only way to know for sure would be to make a systematic series of observations over the range of intermediate ratios of particle density to fluid density—and that has never been done and is unlikely ever to happen.

This page titled 12.7: Wind Ripples and Eolian Dunes is shared under a CC BY-NC-SA 4.0 license and was authored, remixed, and/or curated by John Southard (MIT OpenCourseware) via source content that was edited to the style and standards of the LibreTexts platform.

12.8: Works Cited and Reading List

Works Cited

Allen, J.R.L., 1970, A quantitative model of climbing ripples and their cross-laminated deposits: Sedimentology, v. 14, p. 5-26.

Anderson, R.S., 1987, A theoretical model for aeolian impact ripples: Sedimentollgy, v. 34, p. 943-956.

Andreotti, B., Claudin, P., and Pouliquen, O., 2006, Aeolian sand ripples: experimental study of fully developed states: Physical Review Letters, v. 96, 028001, 4 p.

Arnott, R.W., and Southard, J.B., 1990, Exploratory flow-duct experiments on combined-flow bed configurations, and some implications for interpreting storm-even stratification: Journal of Sedimentary Petrology, v. 60, p. 211-219.

Ashley, G.M., 1990, Classification of large-scale subaqueous bed forms: a new look at an old problem: Journal of Sedimentary Petrology, v. 60, p. 160-172.

Ashley, G.M., Southard, J.B., and Boothroyd, J.C., 1982, Deposition of climbing-ripple beds: A flume simulation: Sedimentology, v. 29, p. 67-79.

Bagnold, R.A., 1941, The Physics of Blown Sand and Desert Dunes: London, Methuen, 265 p.

Bagnold, R.A., 1941, The Physics of Blown Sand and desert Dunes: Chapman & Hall, 265 p.

Bennett, S.J., and Best, J.L., 1996, Mean flow and turbulence strcture over fixed ripples and the ripple–dune transition, in Ashworth, P.J., Bennett, S.J., Best, J.L., and McLelland, S.J., Coherent Flow Structures in Open Channels: Wiley, p. 281-304.

Boguchwal, L.A., and Southard, J.B., 1990, Bed configurations in steady unidirectional water flows. Part 3. Effects of temperature and gravity: Journal of Sedimentary Petrology, v. 60, p. 680-686.

Dillo, H.G., 1960, Sandwanderungen in Tideflussen: Technische Hochschule Hannover, Franzius-Institut für Grund- und Wsserbau, Mitteilungen, v. 17, p. 135-253.

Dumas, S., Arnott, R.W.C., and Southard, J.B., 2005, Experiments on oscillatory-flow and combined-flow bed forms: implications for interpreting parts of the shallow-marine sedimentary record: Journal of Sedimentary Research, v. 75, p. 501-513.

Engelund, F., 1970, Instability of erodible beds: Journal of Fluid Mechanics, v. 42, p. 225-244.

Engelund, F., and Fredsøe, J., 1974, Transition from dunes to plane bed in alluvial channels: Technical University of Denmark, Institute of Hydraulic Engineering, Series Paper 4.

Exner, F.M., 1925, Über die Wechselwirkung zwischen Wasser und Geschiebe in Flussen: Vienna, Austria, Akademie der Wissenschaften, Sitzungsberichte, Mathematisch- Naturwissenschaftliche Klasse, Abteilung IIa, v. 134, p. 166-204.

Fredsøe, J, 1974, On the development of dunes in erodible channels: Journal of Fluid Mechanics, v. 64, p. 1-16.

Gilbert, G.K., 1914, The transportation of debris by running water: U.S. Geological Survey, Professional paper 86, 263 p.

Guy, H.P., Simons, D.B., and Richardson, E.V., 1966, Summary of alluvial channel data from flume experiments: U.S. Geological Survey, Professional paper 462-I, 96 p.

Harms, J.C., Southard, J.B., and Walker, R.G., 1982, Structures and Sequences in Clastic Rocks: Society of Economic Paleontologists and Mineralogists, Short Course 9, variously paged.

Hoyle, R.B., and Mehta, A, 1999, Two-species continuum model for aeolian sand ripples: Physical Review Letters, v. 83, p. 5170-5173.

Hoyle, R.B., and Woods, A.W., 1997, Analytical model of propagating sand ripples: Physical Review E, v. 56, p. 6861-6868.

Jackson, P.S., 1981, On the displacement height in the logarithmic velocity profile: Journal of Fluid Mechanics, v. 111, p. 15-25.

Jerolmack, D.J., Mohrig, D., and McElroy, B., 2006, A unified description of ripples and dunes in rivers, in Parker, G., and García, M.H., eds., River, Coastal and Estuarine Morphodynamics: London, Taylor & Francis Group, p. 843-851.

Ji, Z.G., and Mendoza, C., 1997, Weakly nonlinear stability anaoysis for dune formation: Journal of Hydraulic Engineering, v, 123, p. 979-985.

Kennedy, J.F., 1963, The mechanics of dunes and antidunes in erodible channels: Journal of Fluid Mechanics, v. 16, p. 521-544.

Kennedy, J.F., 1969, The formation of sediment ripples, dunes, and antidunes: Annual Review of Fluid Mechanics, v. 16, p. 147-168.

Kurtze, D.A., Both, J.A., and Hong, D.C., 2000, Surface instability in windblown sand: Physical Review E, v. 61, p. 6750-6758.

Landry, W., and Werner, B.T., 1994, Computer simulations of self-organized wind ripple patterns: Physica D, v. X, p. X-X.

Lopez, F., Fernandez, R., and Best, J., 2000, Turbulence and coherent flow structure associated with bedform amalgamation: an experimental study of the ripple–dune transition: American Society of Civil Engineers, Joint Conference on Water Resources Engineering and Water Resources Planning and Management, Minneapolis, Minnesota.

McLean, S.R., 1990, The stability of ripples and dunes: Earth-Science Reviews, v. 129, p. 131- 144.

Miao, T.D., Mu, Q.S., and Wu, S.Z., 2001, Computer simulation of aeolian sand ripples and dunes: Physics Letters A, v. 288, p. 16-22.

Middleton, G.V., and Southard, J.B., 1984, Mechanics of Sediment Movement, Second Edition: SEPM (Society for Sedimentary Geology), variously paged.

Monin, A.S., and Yaglom, A.M., 1971, Statistical Fluid Mechanics, Volume 1: Cambridge, Massachusetts, MIT Press, 769 p.

Niño, Y., Atala, A., Barahona, M., and Aracena, D., 2002, Discrete particle model for analyzing bedform development: Journal of Hydraulic Engineering, v. 128, p. 381-389.

Nishimori, H., and Ouchi, N., 1993, Formation of ripple patterns and dunes by wind-blown sand: Physical Review Letters, v. 71, p. 197-201.

Nordin, C.F., 1976, Flume studies with fine and coarse sands: U.S. Geological Survey, Open- File Report 76-762.

Ouchi, N.B., and Nishimori, H., 1995, Modeling of wind-blown sand using cellular automata: Physical Review E, v. 52, p. 5877-5880.

Paola, C., 1983, Flow and skin friction over natural rough beds: Cambridge, Massachusetts, Massachusetts Institute of Technology, Department of Earth and Planetary Sciences, Ph.D. dissertation, 347 p.

Prigozhin, L. 1995, Nonlinear dynamics of aeolian ripples: Physical review E, v. 60, 041302, 6 p.

Pye, K., and Tsoar, H., 1990, Aeolian Sand and Sand Dunes: Unwin Hyman, 396 p/

Richards, K.J., 1980, The formation of ripples and dunes on an erodible bed: Journal of Fluid Mechanics, v. 99, p. 597-618.

Robert, A, and Uhlman, W., 2001, An experimental study on the ripple–dune transition: Earth Surface Processes and Landforms, v. 26, p. 615-629.

Rubin, D.M., and Hunter, R.S., 1982, Bedform climbing in theory and nature: Sedimentology, v. 29, p. 121-138.

Rubin, D.M., and McCulloch, D.S., 1980, Single and superimposed bedforms: A synthesis of San Francisco Bay and flume observations: Sedimentary Geology, v. 26, p. 207-231.

Seppälä, M., and Lindé, K., 1978, Wind tunnel studies of ripple formation: Geografiska Annaler, v. A60, p. 29-42.

Sharp, R.P., 1963, Wind ripples: Journal of Geology, v. 71, p. 617-636.

Simons, D.B., and Richardson, E.V., 1966, Resistance to flow in alluvial channels: U.S. Geological Survey, Professional paper 422-J, 61 p.

Simons, D.B., and Richardson, E.V.,1963, Forms of bed roughness in alluvial channels: American Society of Civil Engineers, Transactions, v. 128, Part I, p. 284-302.

Simons, D.B., Richardson, E.V., and Nordin, C.F., Jr., 1965, Bedload equation for ripples and dunes: U.S. Geological Survey, Professional paper 462-H.

Smith, J.D., 1970, Stability of a sand bed subjected to a shear flow of low Froude number: Journal of Geophysical Research, v. 75, p. 5928-5939.

Smith, J.D., and McLean, S.R., 1977, Spatially averaged flow over a wavy surface: Journal of Geophysical research, v. 82, p. 1735-1746.

Southard, J.B., 1971, Representation of bed configurations in depth-velocity-size diagrams: Journal of Sedimentary petrology, v. 41, p. 903-915.

Southard, J.B., 1991, Experimental determination of bed-form stability: Annual Review of Fluid Mechanics, v. 19, p. 423-455.

Southard, J.B., and Boguchwal, L.A., 1990, Bed configurations in steady unidirectional water flows. Part 2. Synthesis of flume data: Journal of Sedimentary Petrology, v. 60, p. 658-679.

Southard, J.B., and Dingler, J.R., 1971, Flume study of ripple propagation behind mounds on flat sand beds: Sedimentology, v. 16, p. 251-263.

Southard, J.B., Boguchwal, L.A., and Romea, R.D., 1980, Test of scale modeling of sediment transport in steady unidirectional flow: Earth Surface Processes, v. 5, p. 17-23.

Stam, J.M.T., 1996, Migration and growth of aeolian bedforms: Mathematical Geology, v. 28, p. 519-536.

Terzidis, O., Claudin, P., and Bouchaud, J.P., 1998, A model for ripple instabilities in granular media: European Physical Journal B, v. 5, p. 245-249.

Thom, A.S., 1971, Momentum absorption by vegetation: Royal Meteorological Society, Journal, v. 97, p. 414-428.

Valance, A., and Rioual, F., 1999, A nonlinear model for aeolian sand ripples: European Physical Journal B, v. 10, p. 543-548.

Valdewalle, N., and Galam, S., 2000, A 1D Ising model for ripple formation: Journal of Physics A, v. 33, p. 4955-4962.

van den Berg, J.H., and van Gelder, A., 1993, A new bedform stability diagram, with emphasis on the transition of ripples to plane bed over fine and ssilt, in Marzo, M., and Puigdefàbregas, C., eds., Alluvial Sediments: International Association of Sedimentologists, Special Publication 17, p. 11-21.

Vanoni, V.A., and Brooks, N.H., 1957, Laboratory studies of the roughness and suspended load of alluvial streams: California Institute of Technology, Sedimentation Laboratory, Report E-68, MRD Sediment Series no. 11.

Vanoni, V.A., ed., 1975, Sedimentation Engineering: American Society of Civil Engineers, Manuals and Reports on Engineering Practice, no. 54, 745 p.

Walker, J.D., 1981, An experimental study of wind ripples: M.S., thesis, Massachusetts Institute of Technology, Cambridge, Massachusetts, USA, 145 p.

Werner, B.T., and Gillespie, D.T., 1993, Fundamentally discrete stochastic model for wind ripple dynamics: Physical review Letters, v. 71, p. 3230-3233.

Willis, J.C., Coleman, N.L., and Ellis, W.M., 1972, Laboratory study of transport of fine sand: American Society of Civil Engineers, Proceedings, Journal of the Hydraulics Division, v. 98, p. 489-502.

Yizhaq, H., Balmforth, N.J., and Provenzale, A., 2004, Blown by wind: nonlinear dynamics of aeolian sand ripples: Physica D, v. 195, p. 207-228.

Yokokawa, M., 1995, Combined-flow ripples: genetic experiments and applications for geologic records: Kyushu University, Faculty of Science, Memoirs, v. 29, no. 1, p. 1-38.

Recent Papers on Bed Configurations, not cited:

Alexander, J., Bridge, J.S., Cheel, R.J., and Leclair, S.F., 2001, Bedforms and associated sedimentary structures formed under supercritical water flows over aggrading sand beds: Sedimentology, v. 48, p. 133-152.

Arnott, R.W.C., and Hand, B.M., 1989, Bedforms, primary structures and grain fabric in the presence of suspended sediment rain: Journal of Sedimentary Petrology, v. 59, p. 1062- 1069.

American Society of Civil Engineers Task Committee, 2002, Flow and transport over dunes: Journal of Hydraulic Engineering, v. 128, p. 726-728.

Baas, J.H., 1999, An empirical model for the development and equilibrium morphology of current ripples in fine sand: Sedimentology, v. 46, p. 123-138.

Bartholdy, J., Bartholomae, A., and Flemming, B.W., 2002, Grain-size control of large compound flow-transverse bedforms in a tidal inlet of the Danish Wadden Sea: Marine Geology, v. 188, p. 391-413.

Bartholdy, J., Flemming, B.W., Bartholomä, A., and Ernstsen, V.B., 2005, Flow and grain size control of depth-independent simple subaqueous dunes: Journal of Geophysical Research, v. 110, F04S16, 12 p.

Bennett, S.J,, and Best, J.L., 1995, Mean flow and turbulence structure over fixed, two- dimensional dunes: implications for sediment transport and bedform stability: Sedimentology, v. 42, p. 491-513.

Besio, G., Blondeaux, P., Brocchini, M., and Vittori, G., 2004, On the modeling of sand wave migration: Journal of Geophysical Research, v 109, C04018, 13 p.

Best, J., 2005, The fluid dynamics of river dunes: A review of some future research directions: Journal of Geophysical Research, v. 110, F04S02, 21 p.

Best, J., and Bridge, J., 1992, The morphology and dynamics of low amplitude bedwaves upon upper stage plane beds and the preservation of planar laminae: Sedimentology, v. 39, p. 737-752.

Best, J.L., and Kostaschuk, R., 2002, An experimental study of turbulent flow over a low-angle dune: Journal of Geophysical Research, v. 107(C9), 3135, 19 p.

Blom, A., 2006, The impact of variability in dune dimensions on sediment sorting and morphodynamics, in Parker, G., and García, M.H., eds., River, Coastal and Estuarine Morphodynamics: London, Taylor & Francis Group, p. 873-881.

Blom, A., and Parker, G., 2004, Vertical sorting and the morphodynamics of bed form–dominated rivers: A modeling framework: Journal of Geophysical Research, v. 109, F02007, 15 p.

Blom, A., Ribberink, J.S., and de Vriend, H.J., 2003, Vertical sorting in bed forms: Flume experiments with a natural and a trimodal sediment mixture: Water Resources Research, v. 39 (2), 1025, ESG 1, 13 p.

Bridge, J.S., and Best, J.L., 1988 Flow, sediment transport and bedform dynamics over the transition from dunes to upper-stage plane beds: implications for the formation of planar laminae: Sedimentology, v. 35, p. 753-763.

Cacchione, D.A., Wiberg, P.L., Lynch, J., Irish, J., and Traykovski, P., 1999, Estimates of suspended-sediment flux and bedform activity on the inner portion of the Eel continental shelf: Marine Geology, v. 154, p. 83-97.

Carling, P.A., 1999, Subaqueous gravel dunes: Journal of Sedimentary Research, v. 69, p. 534- 545.

Carling, P.A., and Shvidchenko, A.B., 2002, A consideration of the dune:antidune transition in fine gravel: Sedimentology, v. 49, p.

1269-1282.

Carling, P.A., Gölz, E., Orr, H.G., and Radecki-Pawlik, A., 2000, The morphodynamics of fluvial sand dunes in the River Rhine, near Mainz, Germany. I. Sedimentology and morphology: Sedimentology, v. 47, p. 227-252.

Carling, P.A., Williams, J.J., Gölz, E., and Kelsey, A.D., 2000, The morphodynamics of fluvial sand dunes in the River Rhine, near Mainz, Germany. II. Hydrodynamics and sediment transport: Sedimentology, v. 47, p. 253-278.

Cataño-Lopera, Y.A., and García, M.H., 2006, Geometric and migrating characteristics of amalgamated bedforms under oscillatory flows, in Parker G, and García M, eds., River, Coastal and Estuarine Morphodynamics: London, Taylor & Francis Group, p. 1017-1026.

Chang, Y.S., and Hanes, D.M., 2004, Suspended sediment and hydrodynamics above mildly sloped long wave ripples: Journal of Geophysical Research, v. 109, C07022, 16 p.

Chang, Y.S., and Scotti, A., 2004, Modeling unsteady turbulent flows over ripples: Reynolds- averaged Navier-Stokes equations (RANS) versus large-eddy simulation (LES): Journal of Geophysical Research, v. 109, C09012, 16 p.

Cheel, R.J., 1990, Horizontal lamination and the sequence of bed phases and stratification under upper-flow-regime conditions: Sedimentology, v. 37, p. 517-529.

Clarke, L.B., and Werner, B.T., 2004, Tidally modulated occurrence of megaripples in a saturated surf zone: Journal of Geophysical Research, v. 109, C01012, 15 p.

Coleman, S.E., Fedele, J.J., and Garcia, M.H., 2003, Closed-conduit bed-form initiation and development: Journal of Hydraulic Engineering, v. 129, p. 956-965.

Coleman, S.E., Schlicke, E., and Blackbourn, S., 2006, Growth of wave-induced ripples, in Parker, G., and García, M.H., eds., River, Coastal and Estuarine Morphodynamics: London, Taylor & Francis Group, p. 963-971.

Crawford, A.M., and Hay, A.E., 2001, Linear transition ripple migration and wave orbital velocity skewness: Observations: Journal of Geophysical Research, v. 106, p. 14,113-14,128.

Damgaard, J., Soulsby, R., Peet, A., and Wright, S., 2003, Sand transport on steeply sloping plane and rippled beds: Journal of Hydraulic Engineering, v. 129, p. 706-719.

Davis, J.P., Walker, D.J., Townsend, M., and Young, I.R., 2004, Wave-formed sediment ripples: Transient analysis of ripple spectral development: Journal of Geophysical Research, v. 109, C07020, 15 p.

Dinehart, R.L., 1992, Evolution of coarse gravel bed forms: field measurements at flood stage: Water Resources Research, v. 28, p. 2667-2689.

Doucette, J.S., 2000, The distribution of nearshore bedforms and effects on sand suspension on low-energy, micro-tidal beaches in Southwestern Australia: Marine Geology, v. 165, p. 41-61.

Doucette, J.S., 2002, Geometry and grain-size sorting of ripples on low-energy sand beaches: field observations and model predictions: Sedimentology, v. 49, p. 483-503.

Duffy, G.P., and Hughes-Clarke, J.E., 2005, Applications of spatial cross correlation to detection of migration of submarine sand dunes: Journal of Geophysical Research, v. 110, F04S12.

Elhakeem, M., and Imran, J., 2006, A bedload model for uniform sediment derived from the movement of bed forms, in Parker, G., and García, M.H., eds., River, Coastal and Estuarine Morphodynamics: London, Taylor & Francis Group, p. 853-860.

Ernstsen, V.B., Noormets, R., Winter, C., Hebbeln, D., Bartholomä, A., Flemming, B.W., and Bartholdy, J., 2005, Development of subaqueous barchanoid-shaped dunes due to lateral grain size variability in a tidal inlet channel of the Danish Wadden Sea: Journal of Geophysical Research, v. 110,F04S08, 13 p.

Flemming, B.W., 1992, Bed phases in bioclastic sands exposed to unsteady, non-equilibrated flows: an experimental flume study: Senckenbergiana Maritima, v. 22. p. 95-108.

Giménez-Curto, L.A., and Corniero, M.A., 2003, Highest natural bed forms: Journal of Geophysical Research, v.108(C2), 3046, 7 p.

Gonzalez, R., and Eberli, G., 1997, Sediment transport and bedforms in a carbonate tidal inlet; Lee Stocking Island, Exumas, Bahamas: Sedimentology, v. 44, p. 1015-1030.

Ha, H.K., and Chough, S.K., 2003, Intermittent turbulent events over sandy current ripples: a motion-picture analysis of flume experiments: Sedimentary Geology, v. 161, p. 295- 308.

Harbor, D.J., 1998, Dynamics of bedforms in the lower Mississippi River: Journal of Sedimentary Research, v. 68 , p. 750-762.

Héquette, A., and Hill, P.R., 1995, Response of the seabed to storm-generated combined flows on a sandy Arctic shoreface, Canadian Beaufort Sea: Journal of Sedimentary Research, v. A65, p. 461-471.

Hersen, P., 2005, Flow effects on the morphology and dynamics of aeolian and subaqueous barchan dunes: Journal of Geophysical Research, v. 110, F04S07, 10 p.

Hoekstra, P., Bell, P., van Santen, P., Roode, N., Levoy, F., and Whitehouse, R., 2004, Bedform migration and bedload transport on an intertidal shoal: Continental Shelf Research, v. 24, p. 1249-1269.

Hulscher, S.J.M.H., 1996, Tidal-induced large-scale regular bed form patterns in a three- dimensional shallow water model: Journal of Geophysical Research, v. 101, p. 20,727- 20,744.

Hulscher, S.J.M.H., and Dohmen-Janssen, C.M., 2005, Introduction to special section on Marine Sand Wave and River Dune Dynamics: Journal of Geophysical Research, v. 110, F04S01, 6 p.

Jerolmack, D., and Mohrig, D., 2005, Interactions between bed forms: Topography, turbulence, and transport: Journal of Geophysical Research, v. 110, F02014, 13 p.

Kleinhans, M.G., 2001, The key role of fluvial dunes in transport and deposition of sand–gravel mixtures, a preliminary note: Sedimentary Geology, v. 143, p. 7-13.

Kleinhans, M.G., 2005, Upstream sediment input effects on experimental dune trough scour in sediment mixtures: Journal of Geophysical Research, v. 110, F04S06, 8 p.

Kleinhans, M.G., Wilbers, A.W.E., de Swaaf, A., and van den Berg, J.H., 2002, Sediment supply– limited bedforms in sand–gravel bed rivers: Journal of Sedimentary Research, v. 72, p. 629-640.

Kostaschuk, R., 2000, A field study of turbulence and sediment dynamics over subaqueous dunes with flow separation: Sedimentology, v. 47, p. 519-531.

Kostaschuk, R., 2006, Sediment transport mechanics and subaqueous dune morphology, in Parker G,, and García M., eds, River, Coastal and Estuarine Morphodynamics: London, Taylor & Francis Group, p. 795-801.

Kostaschuk, R., and Best, J., 2005, Response of sand dunes to variation in tidal flow: Fraser Estuary, Canada: Journal of Geophysical Research, v. 110, F04S04, 10 p.

Langlois, V., and Valance, A., 2005, Three-dimensionality of sand ripples under steady laminar shear flow: Journal of Geophysical Research, v. 110, F04S09, 12 p.

Larcombe, P., and Jago, C.F., 1996, The morphological dynamics of intertidal megaripples in the Mawddach Estuary, North Wales, and the implications for palaeoflow reconstructions: Sedimentology, v. 43, p. 541-559.

Lawless, M., and Robert, A., 2001, Three-dimensional flow structure around small-scale bedforms in a simulated gravel-bed environment: Earth Surface Processes and Landforms, v. 26, p.507-522.

Leclair, S.F., 2002, Preservation of cross-strata due to the migration of subaqueous dunes: an experimental investigation: Sedimentology, v. 49, p. 1157-1180.

Leclair, S.F., and Bridge, J.S., 2001, Qualitative interpretation of sedimentary structures formed by river dunes: Journal of Sedimentary Research, v. 71, p. 713-716.

Leclair, S.F., and Miller, J.Z., 2006, Time variation of probability distributions of dune-bed elevation in a large river, in Parker, G., and García, M.H., eds., River, Coastal and Estuarine Morphodynamics: London, Taylor & Francis Group, p. 803-812.

Lee, H.J., Jo, H.R., and Chu, Y.S., 2006, Dune migration on macrotidal flats under symmetrical tidal flows: Garolim Bay, Korea : Journal of Sedimentary Research, v. 76, p. 284-291.

Li, M.Z., 1994, Direct skin friction measurements and stress partitioning over movable sand ripples: Journal of Geophysical Research, v. 99, p. 791-799.

Li, M.Z., and Amos, C.L., 1998 Predicting ripple geometry aned bed roughness under combined waves and currents in a continental shelf environment Continental Shelf Research 18 941-970 .

Li, M.Z., and Amos, C.L., 1999a, Field observations of bedforms and sediment transport thresholds of fine sand under combined waves and currents: Marine Geology, v. 158, p. 147-160.

Li, M.Z., and Amos, C.L., 1999b, Sheet flow and large wave ripples under combined waves and currents: field observations, model prediction and effects on boundary layer dynamics: Continental Shelf Research, v. 19, p. 637-663.

Maddux, T.B., McLean, S.R., and Nelson, J.M., 2003a, Turbulent flow over three-dimensional dunes: 2. Fluid and bed stress: Journal of Geophysical Research, v.108 (F1), 6010, 11, 17 p.

Maddux, T.B., Nelson, J.M., and McLean, S.R., 2003b, Turbulent flow over three-dimensional dunes: 1. Free surface and flow response: Journal of Geophysical Research, v. 108, F1, 6009, 20 p.

Malarkey, J., and Davies, A.G., 2004, An eddy viscosity formulation for oscillatory flow over vortex ripples: Journal of Geophysical Research, v. 109, C12016, 13 p.

Mantz, P.A., 1992, Cohesionless fine-sediment bed forms in shallow flows: Journal of Hydraulic Engineering, v. 118, p. 743-764.

Marin, F., Abcha, N., Brossard, J., and Ezersky, A.B., 2005, Laboratory study of sand bed forms induced by solitary waves in shallow water: Journal of Geophysical Research, v. 110, F04S17.

Mazumder, R., 2000, Turbulence–particle interactions and their implications for sediment transport and bedform mechanics under unidirectional current: some recent developments: Earth-Science Reviews, v. 50, p. 113-124.

Mazumder, R., 2003, Sediment transport, aqueous bedform stability and morphodynamics under unidirectional current: a brief overview: Journal of African Earth Sciences, v. 36, p. 1- 14.

McLean, S.R., and Nelson, J.M., 2006, Sediment transport over ripples and dunes, in Parker, G., and García, M.H., eds., River, Coastal and Estuarine Morphodynamics: London, Taylor & Francis Group, 821-829.

McLean, S.R., Nelson, J.M., and Wolfe, S.R., 1994, Turbulence structure over two-dimensional bed forms: Implications for sediment transport: Journal of Geophysical Research, v. 99, p. 12,729-12,747.

McLean, S.R., Wolfe, S.R., and Nelson, J.M., 1999, Predicting boundary shear stress and sediment transport over bed forms: Journal of Hydraulic Engineering, v. 125, p. 725-736.

Morris, S.A., Kenyon, N.H., Limonov, A.F., and Alexander, J., 1998, Downstream changes of large-scale bedforms in turbidites around the Valencia channel mouth, north-west Mediterranean: implications for palaeoflow reconstruction: Sedimentology, v. 45, p. 365-377.

Murray, A.B., Coco, G., Green, M., Hume, T., and Thieler, R., 2006, Different approaches to modeling inner-shelf 'sorted bedforms', in Parker, G., and García, M.H., eds., River, Coastal and Estuarine Morphodynamics: London, Taylor & Francis Group, p. 1009- 1015.

Narteau, C., Lajeunesse, E., Métivier, F., and Rozier, O., 2006, Modelling of dune patterns by short range interactions, in Parker, G,, and García, M., eds., River, Coastal and Estuarine Morphodynamics: London, Taylor & Francis Group, p. 1035-1046.

Nelson, J.M., Shreve, R.L., McLean, S.R., and Drake, T.G., 1995, Role of near-bed turbulence structure in bed load transport and bed form mechanics: Water Resources Research, v. 31, p. 2071-2086.

Nelson, J.M., Burman, A.R., Shimizu, Y., McLean, S.R., Shreve, R.L., and Schmeeckle, M., 2006, Computing flow and sediment transport over bedforms, in Parker, G., and García, M.H., eds., River, Coastal and Estuarine Morphodynamics: London, Taylor & Francis Group, p. 861-872.

Németh, A.A., Hulscher, S.J.M.H., and van Damme, R.M.J., 2006, Simulating offshore sand waves: Coastal Engineering, v. 53, p. 265-275.

Ngusaru, A.S., and Hay, A.E., 2004, Cross-shore migration of lunate megaripples during Duck94: Journal of Geophysical Research, v. 109, C02006, 16 p.

Oost, A.P., and Baas, J.H., 1994, The development of small scale bedforms in tidal environments: an empirical model for unsteady flow and its applications: Sedimentology, v. 41, p. 883- 903.

Paarlberg, A.J., Dohmen-Janssen, C.M., and Hulscher, S.J.M.H., 2006, A parameterization for flow separation in a river dune development model, in Parker, G., and García, M.H., eds., River, Coastal and Estuarine Morphodynamics: London, Taylor & Francis Group, p. 883-895.

Parsons, D.R., Best, J.L., Orfeo, O., Hardy, R.J., Kostaschuk, R., and Lane, S.N., 2005, Morphology and flow fields of three-dimensional dunes, Rio Paraná, Argentina: Results from simultaneous multibeam echo sounding and acoustic Doppler current profiling: Journal of Geophysical Research, v. 110, F04S03, 9 p.

Passchier, S., and Kleinhans, M.G., 2005, Observations of sand waves, megaripples, and hummocks in the Dutch coastal area and their relation to currents and combined flow conditions: Journal of Geophysical Research, v. 110, F04S15, 15 p.

Ramsay, P.J., Smith, A.M., and Mason, T.R., 1996, Geostrophic sand ridge, dune fields and associated bedforms from the Northern KwaZulu–Natal shelf, south-east Africa: Sedimentology, v. 43, p. 407-419.

Robert, A., and Uhlman, W., 2001, An experimental study on the ripple–dune transition: Earth Surfsce Processes and Landforms, v. 26, p. 615-629

Schindler, R.J., and Robert, A., 2004, Suspended sediment concentration and the ripple–dune transition: Hydrological Processes, v. 18, p. 3215-3227.

Schindler, R.J., and Robert, A., 2005, Flow and turbulence structure across the ripple–dune transition: an experiment under mobile bed conditions: Sedimentology, v. 52, p. 627- 649.

Serra, S.G., and Vionnet, C.A., 2006, Migration of large dunes during extreme floods of the Paraná River, Argentina, in Parker, G., and García, M.H., eds., River, Coastal and Estuarine Morphodynamics: London, Taylor & Francis Group, p. 897-908.

Smyth, C.E., and Li, M.Z., 2005, Wave-current bedform scales, orientation, and migration on Sable Island Bank: Journal of Geophysical Research, v. 110, C02023, 12 p.

Smyth, C., Hay, A.E., and Zedel, L., 2002, Coherent Doppler Profiler measurements of near-bed suspended sediment fluxes and the influence of bed forms: Journal of Geophysical Research, v. 107(C8), 3105, 20 p.

Storms, J.E.A., van Dam, R.L., and Leclair, S.F., 1999, Preservation of cross-sets due to migration of current ripples over aggrading and non-aggrading beds: comparison of experimental data with theory: Sedimentology, v. 46, p. 189-200.

Tjerry, S., and Fredsøe, J., 2005, Calculation of dune morphology: Journal of Geophysical Research, v. 110, F04013, 13 p.

Trouw, K., Williams, J.J., and Rose, C.P., 2000, Modelling sand resuspension by waves over a rippled bed: Estuarine, Coastal and Shelf Science, v. 50, p. 143-151.

van den Berg, J.H., and van Gelder, A., 1998, Flow and sediment transport over large subaqueous dunes: Fraser River, Canada: Sedimentology, v. 45, p. 217-221.

van der Mark, C.F., Blom, A., and Hulscher, S.J.M.H., 2006, On modeling the variability of bedform dimensions, in Parker, G., and García, M.H., eds., River, Coastal and Estuarine Morphodynamics: London, Taylor & Francis Group, p. 831-841.

van Dijk, T.A.G.P., and Kleinhans, M.G., 2005, Processes controlling the dynamics of compound sand waves in the North Sea,

Netherlands: Journal of Geophysical Research, v. 110, F04S10, 15 p.

Vanwesenbeeck, V., and Lanckneus, J., 2000, Residual sediment transport paths on a tidal sand bank: a comparison between the modified McLaren model and bedform analysis: Journal of Sedimentary Research, v. 70, p. 470-477.

Venditti, J.G., and Bauer, B.O., 2005, Turbulent flow over a dune: Green River, Colorado: Earth Surface Processes and Landforms, v. 30, p. 289-304.

Venditti, J.G., Church, M., and Bennett, S.J., 2005a, On the transition between 2D and 3D dunes: Sedimentology, v. 52, p. 1343-1359.

Venditti, J.G., Church, M.A., and Bennett, S.J., 2005b, Bed form initiation from a flat sand bed: Journal of Geophysical Research, v. 110, F01009, 19 p .

Villard, P.V., and Church, M., 2005, Bar and dune development during a freshet: Fraser River Estuary, British Columbia, Canada: Sedimentology, v. 52 , p. 737-756.

Villard, P., and Kostaschuk, R., 1998, The relation between shear velocity and suspended sediment concentration over dunes: Fraser Estuary, Canada: Marine Geology, v. 148, p. 71-81.

Villard, P.V., and Osborne, P.D., 2002, Visualization of wave-induced suspension patterns over two-dimensional bedforms: Sedimentology, v. 49, p. 363-378.

Walgreen, M., Calvete, D., and de Swart, H.E., 2002, Growth of large-scale bed forms due to storm-driven and tidal currents: a model approach: Continental Shelf Research, v. 22, p. 2777-2793.

Werner, S.R., Beardsley, R.C., and Williams, A.J., III, 2003, Bottom friction and bed forms on the southern flank of Georges Bank: Journal of Geophysical Research, v. 108(C11), 8004, 21 p.

Whitehouse, R.J.S., Bassoullet, P., Dyer, K.R., Mitchener, H.J., and Roberts, W., 2000, The influence of bedforms on flow and sediment transport over intertidal mudflats: Continental Shelf Research, v. 20, p. 1099-1124.

Williams, J.J., Bell, P.S., and Thorne, P.D., 2003, Field measurements of flow fields and sediment transport above mobile bed forms: Journal of Geophysical Research, v. 108(C4), 3109, 36 p.

Williams, J.J., Bell, P.S., and Thorne, P.D., 2005, Unifying large and small wave-generated ripples: Journal of Geophysical Research, v. 110, C02008, 18 p.

Wilson, I.G., 1972, Universal discontinuities in bedforrms produced by the wind: Journal of Sedimentary Petrology, v. 42, p. 667-669.

Yamaguchi, S., and Izumi, N., 2006, Weakly nonlinear analysis of dunes by the use of a sediment transport formula incorporating the pressure gradient, in Parker, G., and García, M.H., eds., River, Coastal and Estuarine Morphodynamics: London, Taylor & Francis Group, p. 813-820.

Zedler E.A,, and Street, R.L., 2002, Large-eddy simulation of sediment transport: currents over ripples: Journal of Hydraulic Engineering, v. 127, p. 444-452.

Zedler, E.A., and Street, R.L., 2006, Sediment transport over ripples in oscillatory flow: Journal of Hydraulic Engineering, v. 132, p. 180-193.

This page titled 12.8: Works Cited and Reading List is shared under a CC BY-NC-SA 4.0 license and was authored, remixed, and/or curated by John Southard (MIT OpenCourseware) via source content that was edited to the style and standards of the LibreTexts platform.

13: THE SEDIMENT TRANSPORT RATE

In this brief chapter we focus on the concept of the sediment transport rate more than on the procedures by which it might be predicted. it would take a lot of additional space in these course notes to do justice to the details of even the small number of sediment-discharge formulas that are in common use.

13.1: Introduction to Sediment Transport Rates

13.2: The Sediment Load and the Sediment Transport Rate

13.3: Predicting the Sediment Transport Rate

This page titled 13: The Sediment Transport Rate is shared under a CC BY-NC-SA 4.0 license and was authored, remixed, and/or curated by John Southard (MIT OpenCourseware) via source content that was edited to the style and standards of the LibreTexts platform.

13.1: Introduction to Sediment Transport Rates

By the **sediment transport rate**, also called the **sediment discharge**, I mean the mass of sedimentary material, both particulate and dissolved, that passes across a given flow-transverse cross section of a given flow in unit time. (Sometimes the sediment transport rate is expressed in terms of weight or in terms of volume rather than in terms of mass.) The flow might be a unidirectional flow in a river or a tidal current, but it might also be the net unidirectional component of a combined flow, even one that is oscillation-dominated. Only in a purely oscillatory flow in which the back-and-forth phases of the flow are exactly symmetrical is there no net transport of sediment. Here we focus on the particulate sediment load of the flow, leaving aside the dissolved load, which is important in its own right but outside the scope of these physics-based notes.

Over the past hundred-plus years, much effort has been devoted to accounting for, or predicting, the sediment transport rate. Numerous procedures, usually involving one or more equations or formulas, have been proposed for prediction of the sediment transport rate. These are commonly called “sediment- discharge formulas”. (The term “formula” here is in some cases a bit misleading: some of the procedures involve the use of reference graphs in addition to mathematical equations.) No single formula or procedure has gained universal acceptance, and only a few have been in wide use. None of them does anywhere near a perfect job in predicting the sediment transport rate—which is understandable, given the complexity of turbulent two-phase sediment- transporting flow and the wider range of joint size–shape frequency distributions that are common in natural sediments. Prediction of the sediment transport rate is one of the most frustrating endeavors in the entire field of sediment dynamics.

This page titled 13.1: Introduction to Sediment Transport Rates is shared under a CC BY-NC-SA 4.0 license and was authored, remixed, and/or curated by John Southard (MIT OpenCourseware) via source content that was edited to the style and standards of the LibreTexts platform.

13.2: The Sediment Load and the Sediment Transport Rate

The Sediment Load

First you must be clear on the distinction between the sediment load and the sediment transport rate. Recall from Chapter 10 that the load is all of the sediment that is being moved by the flow at a given time. Figure 13.2.1 shows how to conceptualize the sediment load. In Figure 13.2.1, you can imagine somehow freezing a block of the flow that contains both water and particulate sediment, and then melting the block to collect the sediment in the block. That sediment is the load. You can think of the sediment load as the depth-integrated sediment mass above a unit area of the sediment bed:

$$L = \text{sediment load} = \int_0^d c(y)dy \tag{13.2.1}$$

where c is the local time-average sediment concentration. Then the average concentration of transported sediment, C, is equal to L/d.

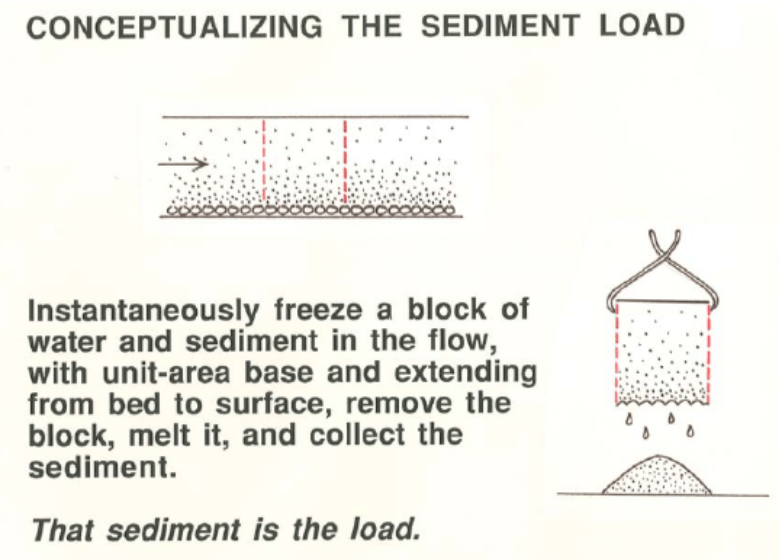


Figure 13.2.1: Conceptualizing the sediment load.

Just as a review of what was said about the sediment load back in Chapter 10, here are some points or comments about the sediment load:

- There is no fundamental break between the bed load and the suspended load.
- For a given particle that is susceptible to suspension in a given flow, the particle at various times might be traveling as either bed load or as suspended load, or it might temporarily be at rest on the bed surface or within the active layer.
- The ranges of particle size for the bed load and the suspended load in a given flow overlap.
- The suspended bed-material load is not really “suspended”; it is merely traveling, temporarily, in the turbulent flow above the bed.
- The bed-load layer is thin relative to the suspended-load layer.
- The bed-load layer is the lower boundary condition of the suspended-load layer.
- The sediment concentration in the bed-load layer is ordinarily much greater than that in the suspended-load layer.

The Sediment Transport Rate

The sediment transport rate is commonly denoted by Q_s. What is more useful, however, and what you are likely to encounter if you have to deal with sediment transport, is the sediment transport rate *per unit width of the flow*. That is called the **unit sediment**

transport rate; it is often denoted by q_s. Think in terms of a vertical slice of the flow, with unit width and oriented parallel to the flow. Which you use depends upon whether you are interested in how much sediment the entire flow carries (Q_s) or in the inherent intensity of the sediment transport (q_s).

Below are descriptions of three ways of conceptualizing the sediment transport rate. Each represents, in principle although not necessarily in practice, a way of measuring the sediment transport rate.

The magic screen: Obtain a magic screen, which, when installed across the flow, allows you to measure the mass m_i of each of the n particles that pass across the screen in unit time (Figure $13.2.2$). Then

$$q_s = \frac{\sum_1^n m_i}{\text{width of flow}} \tag{13.2.2}$$

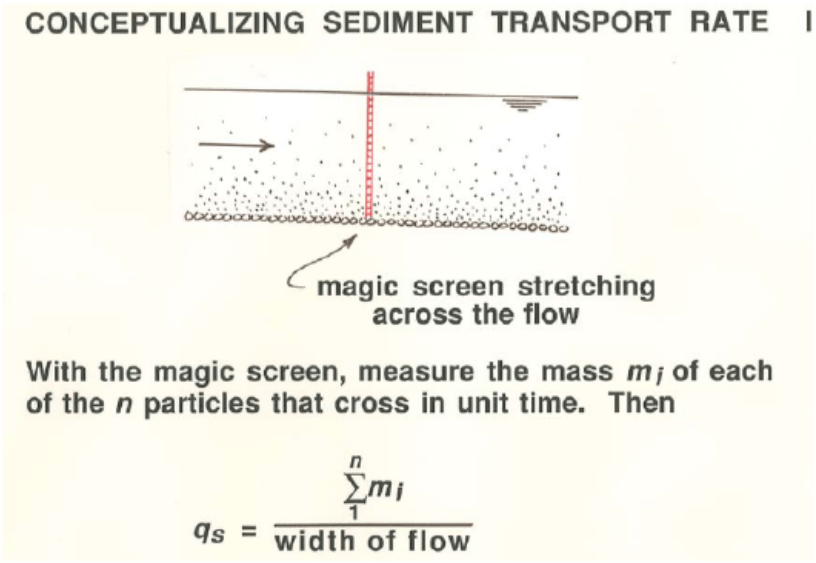


Figure $13.2.2$: *Conceptualizing the measurement of the sediment transport rate by use of a magic screen.*

The magic vacuum suction trap: Install a slot, across the entire width of the flow, that allows you to remove all of the particles, both bed load and suspended load, that pass across the cross section of the flow above the slot (Figure $13.2.3$). Think in terms of a magic vacuum cleaner that sucks all of the sediment particles out of the flow and into the trap. (In real life, that would not be extraordinarily difficult for the bed load but virtually impossible for the suspended load.) Suppose that you thereby extract a mass M of sediment that would have been transported across the location of the cross section in an interval of time T. Then the unit sediment transport rate q_s would be equal to M/T divided by the width of the flow.

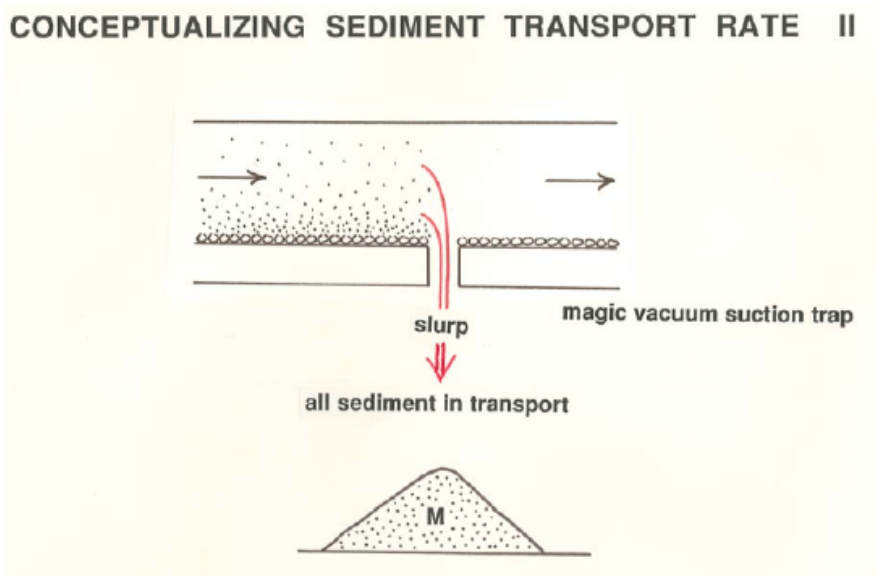


Figure 13.2.3: Conceptualizing the measurement of the sediment transport rate by use of a magic vacuum suction trap.

Depth-integrated sampling: (Figure 13.2.4) Along a vertical in the flow, measure the downstream component of velocity v_i of all of the particles in a tiny imaginary cube in the flow, with volume V, at a given instant. Then multiply v_i by the mass m_i of the particle, and sum over all n particles found. Divide the result by V to obtain the transport rate per unit area, and integrate the result over flow depth on a vertical traverse. That give you q_s for that cross-stream position in the flow.

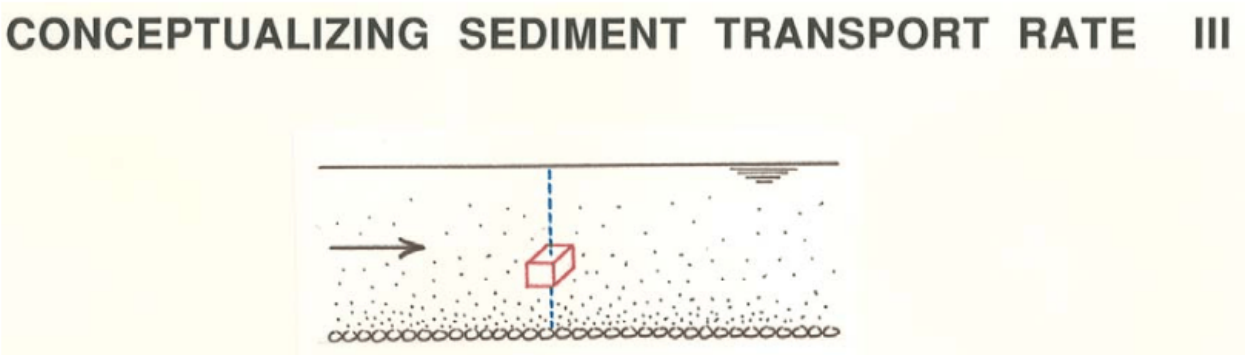


Figure 13.2.4: Conceptualizing the measurement of the sediment transport rate by use of depth-integrated sampling.

It is notoriously difficult to measure the sediment transport rate, even in controlled settings in laboratory flumes. In a flume, if only bed load is being transported, you can arrange a sediment trap in the form of a narrow slot extending across the entire channel, transverse to the flow direction. Provided that the width of the trap is at least as great as the longest excursions of bed-load particles, all of the bed load falls into the trap, to be collected and weighed. A warning is in order, however: the sampling time must short enough that the deficit in transport does not propagate, by recirculation of the sediment, back to the trap.

In a small stream you can catch the passing bed load by building a dam across the flow, and catch the load in a basket under the overfall across the dam. the problem is that in building the dam you are changing the nature of the stream and its sediment transport for some distance upstream of the dam.

Various kinds of portable bed-load traps have been devised and are in common use. Generally they consist of a receptacle that is open to the flow on the upstream side and screened to pass the water, but catch the sediment, on the downstream side. They are placed on the sediment bed for a time sufficient to catch a measurable quantity of the passing bed load. No matter how well designed, however, such traps distort the flow in their vicinity to a certain extent, and also, if there are rugged bed forms like ripple or dunes on the bed, then the catch depends strongly upon where the trap is placed relative to the crests and troughs of the bed forms.

Measuring the suspended load is a simpler matter, at least in principle. What is commonly done is to trap a volume of passing

flow, which contains the suspended load at that particular height above the bed, and combine that with the mean flow velocity at the given level to obtain the proportion of the entire sediment transport rate associated with a narrow interval of the flow depth. If that is done at a large number of heights above the bed, the combined result is a good measure of the suspended-load transport rate. (This is akin to the procedure outlined in the section on depth-integrated sampling, above.)

What is the Relationship between the Sediment Load and the Sediment Transport Rate?

Here is a question for you to ponder. Look back at Figure $13.2.1$ and think about the particle size distribution you would find in the pile of sediment that you obtained by melting that instantaneously frozen block of the flow. Now look back at Figure $13.2.3$ and think about the particle size distribution you would measure in the pile of sediment you obtained by magically vacuuming out all of the sediment passing by the location of the slot trap. *Would those two size distributions be the same or different?*

Just a moment's reflection should convince you that the two distributions would be the same if and only if the transport velocities of each of the particle size fractions in the sediment are the same. If they are not the same— and in general they are not the same, because, at least to a certain extent (we will look at that in more detail in Chapter 3), the coarser fractions tend to move more slowly than the finer fractions—then the particle size distributions will be different in the two cases. That highlights the fundamental difference between the sediment load and the sediment transport rate.

This page titled 13.2: The Sediment Load and the Sediment Transport Rate is shared under a CC BY-NC-SA 4.0 license and was authored, remixed, and/or curated by John Southard (MIT OpenCourseware) via source content that was edited to the style and standards of the LibreTexts platform.

13.3: Predicting the Sediment Transport Rate

The Variables that Govern the Unit Sediment Transport Rate

It should seem natural to you to make a list of all of the important variables and physical effects that govern the sediment transport rate. Once we have such a list, we can frame our consideration of the sediment transport rate by expressing the sediment transport rate, in dimensionless form, in terms of a natural or convenient set of governing dimensionless variables. Even if for no other reason, such a functional relationship should guide your thinking about the various sediment-discharge formulas you might encounter in the literature on sediment transport.

Here is a list of the important physical effects on sediment transport rate, together with the variables associated with those physical effects; see Figure 13.3.1.

- Fluid forces on bed-surface particles: This is what moves the sediment. These fluid forces involve the bed shear stress τ_o, the fluid properties ρ and μ, and the particle size D.
- The submerged weight of the particles is what resists the forces that tend to cause particle movement. It depends on the submerged specific weight of the particles, γ' , and the particle size D.
- The relative inertia of the sediment particles might have an effect on the sediment transport rate. It depends on the density of the sediment, ρ_s, and the density of the fluid, ρ.
- Turbulent diffusion of particles is important by virtue of its role in distribution sediment in suspension upward in the turbulent flow. It depends on a number of variables (Figure 13.3.1).
- Fluid forces on particles in motion also depends upon a number of variables (Figure 13.3.1).
- The presence of bed forms has an important effect on the sediment transport rate. As you saw in Chapter 11, that depends on a long list of variables (Figure 13.3.1).

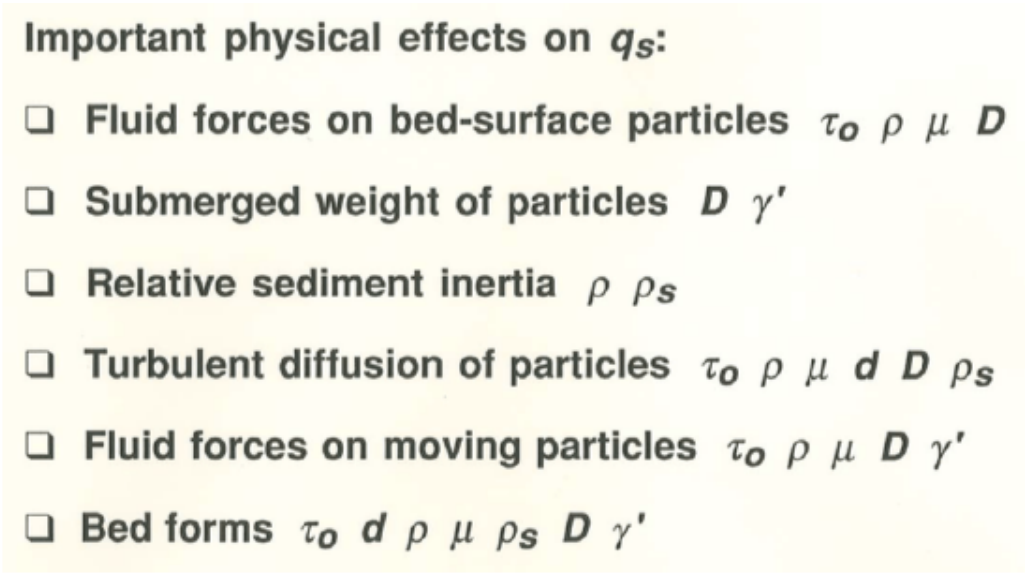


Figure 13.3.1: Important physical effects governing the unit sediment transport rate q_s.

If we collect all of the variables in the above list, we see that each of the seven variables τ_o, d, ρ, μ, ρ_s, D, and γ' appears somewhere in the list. Additionally, the effects of the joint size–shape–density ("SSD") frequency distribution of the sediment are not taken into account by these seven variables. So we can express the dependence of q_s on these variables as

$$q_s = f(\tau_o, d, \rho, \mu, \rho_s, D, \gamma', \text{SSD distribution}) \tag{13.3.1}$$

If we make the simplifying assumption that the SSD distribution is adequately represented by the mean or median size D and the standard deviation σ, then q_s is a function of no fewer than eight governing variables:

$$q_s = f(\tau_o, d, \rho, \mu, \rho_s, D, \sigma, \gamma') \tag{13.3.2}$$

Then, nondimensionalizing in a physically revealing way, an appropriate nondimensionalized sediment transport rate can be expressed as a function of five governing dimensionless variables:

$$\frac{q_s}{(\rho\gamma' D)^{1/2}} = f\left(\frac{\tau_o}{\gamma' D}, \frac{\rho u_* D}{\mu}, \frac{d}{D}, \frac{\sigma}{D}, \frac{\rho_s}{\rho}\right) \tag{13.3.3}$$

Here we have chosen to nondimensionalize the unit sediment transport rate by use of D rather than τ_o, although it is more common, in the literature on sediment transport, to do the latter. The most important governing independent dimensionless variable (which might be called the "leading variable", is the first, the Shields parameter; see Chapter 9. The next two, the boundary Reynolds number and the relative roughness, express the turbulent structure of the flow. An alternative nondimensionalization might segregate the boundary shear stress and the median particle size into separate dimensionless variables.

Clearly, the list of governing dimensionless variables is unworkably long. It can be simplified in the following ways. If we restrict consideration to quartz-density sand in water, the density ratio becomes irrelevant, and if we restrict consideration to well-sorted sediments, the dimensionless sorting becomes unimportant. If we consider only flows for which the particle size is much smaller than the flow depth (that leaves out all white-water mountain streams), then we can safely omit the relative roughness from the list. That leaves two important variables, expressing the importance of the boundary shear stress and the median particle size. (Our intuition would have told us, in the first place, that the sediment transport rate should depend mainly on the force that moves the particles, and the size, and thus the weight, of the particles!) Most, if not all, of the various sediment-discharge formulas that have been proposed make use of one or both of the boundary shear stress and the particle size, in one or another form.

Sediment-Discharge Formulas

To an untutored observer, the most natural way of developing a sediment-discharge formula would be to start from the equations of motion (the Navier-Stokes equations) for turbulent sediment-transporting flow. There are two severe problems in that, however:

1. The turbulence closure problem (see Chapter 4) makes it impossible to work from first principles without making certain assumptions, and
2. The complexity of the physics of particle transport in turbulent shear flows means that the physics of the sediment transport cannot be supplied in a fundamental way.

What is commonly done, in the face of these difficulties, is first to attempt to adduce a rational dynamical basis for the sediment-transport process as a kind of framework, which results in one or more equations with certain adjustable parameters, and then use judiciously chosen data sets on measured sediment transport rates, from laboratory or field studies, to fit the equations to the data. (The ideal, of course, would be to have an equation with *no* adjustable parameters; a function with three or more adjustable parameters could be fitted to almost any data set!) The problem is that there is then no guarantee that the given sediment-discharge formula will work particularly well outside the range of data on which it was based.

The first modern attempt to develop a sediment discharge formula dates way back to DuBoys, in 1879. In the course of the twentieth century, a great many sediment-discharge formulas were proposed. Several of those have been widely used. If you go into the literature on sediment-transport rates, you will repeatedly encounter the names of certain workers, mainly hydraulic engineers, whose names are associated with sediment-discharge formulas: Einstein (Hans Albert, not the more famous father, Albert); Meyer–Peter and Müller; Bagnold; Engelund and Hansen.

These course notes are not the place to describe the various widely used sediment-discharge formulas. Vanoni (1975) gives brief descriptions of several such formulas. Here I will concentrate only upon comparisons among those formulas. Three useful comparison studies have appeared in the literature: Vanoni (1975), Gomez and Church (1989), and Nakato (1990).

Comparison of the Various Sediment-Discharge Formulas

First, what do the data on sediment transport rate look like? Figure 13.3.2 is a plot of dimensionless unit sediment transport rate, nondimensionalized by use of sediment size D, fluid density ρ, and submerged specific weight of the sediment, γ', against a dimensionless measure of the boundary shear stress, the Shields parameter $\tau_o/\gamma' D$. The data are from both laboratory studies and measurements in rivers. In this undistorted log–log plot, you can see clearly the following:

- The sediment transport rate is a very steeply increasing function of the boundary shear stress. From the slope of the best-fit

line in the graph, *the unit sediment transport rate goes approximately as the cube of the boundary shear stress.*

- Over five orders of magnitude of the unit sediment transport rate, the data fall along a fairly well-defined trend.
- Nonetheless there is considerable scatter in the data: if you pick one value of the dimensionless boundary shear stress, then, even if you ignore outlying points, there is an approximately order-of magnitude (factor of ten) spread in the data points.

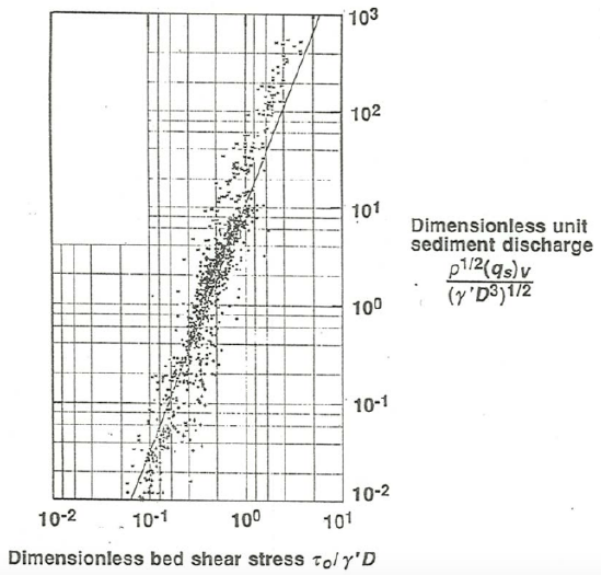
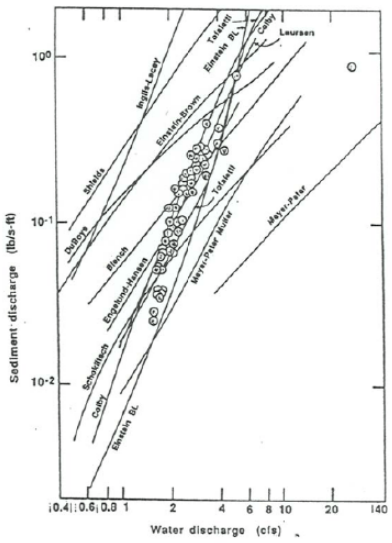


Figure 13.3.2: Plot of dimensionless unit sediment transport rate (expressed as volume, not mass) against dimensionless boundary shear stress (in the form of the Shields parameter) for various sets of measurement data. (Modified from Vanoni, 1975.)

This large spread in values should not surprise you, when you consider that

1. The effects of particle size distribution and of the variable presence of bed forms is not taken into account, and
2. As you saw above, it is difficult to make accurate measurements of the sediment transport rate.

Figure 13.3.3 shows a comparison of the performance of several sediment-discharge formulas in accounting for a single high-quality set of measurements of unit sediment discharge. You can see that the various formulas vary greatly in how well they match the actual data. In fairness, however, I could point out that the conditions represented by this data set are far from the conditions for which some of the discharge formulas were derived. For example, the widely used Meyer–Peter formula was derived for coarse sediments, whereas the data set shown in the figure is for sand that falls just barely within the medium-sand range. The lesson here, I suppose, is that you cannot expect any sediment-discharge formula to work well outside the range for which it was conceived.



Courtesy of American Society of Civil Engineers. Used with permission.

Figure 13.3.3: Sediment discharge against water discharge for the Niobrara River near Cody, Wyoming, U.S.A. obtained from observations (data points) and calculations on the basis of several sediment-discharge formulas (solid curves). (From Vanoni, 1975.)

Chapter 13 References Cited

Vanoni, V.A., ed., 1975, Sedimentation Engineering: American Society of Civil Engineers, Manuals and Reports on Engineering Practice, no. 54, 745 p.

Gomez, B., and Church, M., 1989, An assessment of bed load sediment transport: formulae for gravel bed rivers: Water Resources Research, v. 25, p. 1161- 1186.

Nakato, T., 1990, Tests of selected sediment-transport formulas: Journal of Hydraulic Engineering, v. 116, p. 362-379.

This page titled 13.3: Predicting the Sediment Transport Rate is shared under a CC BY-NC-SA 4.0 license and was authored, remixed, and/or curated by John Southard (MIT OpenCourseware) via source content that was edited to the style and standards of the LibreTexts platform.

14: MIXED-SIZE SEDIMENTS

14.1: Introduction
14.2: Several Consequences of Size
14.3: A Look at Some Real Data on Fractional Transport Rates, From the Flume and From the Field
14.4: Movement Threshold in Mixed-Sized Sediments
14.5: Deviations from the Condition of Equal Mobility

This page titled 14: Mixed-Size Sediments is shared under a CC BY-NC-SA 4.0 license and was authored, remixed, and/or curated by John Southard (MIT OpenCourseware) via source content that was edited to the style and standards of the LibreTexts platform.

14.1: Introduction

In a certain sense, this is the most significant chapter in Part 2 of these course notes—inasmuch as virtually all natural sediments comprise a range of particle sizes, not just a single size. Most of what was said in earlier chapters, on threshold, transport mode, and transport rate, involve an implicit assumption that the sediment is effectively of a single size (hence the term “unisize” sediment), in the sense that the effect of the spread of sizes around the mean (that is, the **sorting**) is sufficiently small that it can be ignored, at least for very well sorted sediments. All sedimentationists know, however, that such an assumption cannot be valid even for moderately sorted sediments, to say nothing of poorly sorted sediments, with a wide spread of particle sizes, like the sand–gravel mixtures that are so common in rivers.

I will probably be insulting your intelligence when I explain the meaning of “size fraction”. A **size fraction** in a natural sediment or an artificial mixture of sediments is a specified range of sizes within the size distribution of the sediment. Such size fractions are usually perceived or chosen to be very narrow relative to the overall range of sizes in the sediment. The choice of lower and upper size limits of the fraction are basically arbitrary—in practice, usually governed by the subdivisions of the conventional powers-of-two grade scale for sediment size. Keep in mind, however, that the size varies, perhaps non-negligibly, even within a narrowly defined size fraction. A size fraction is *not* a single size.

If, for definiteness, we assume a certain definite size-distribution shape for mixed-size sediments, like a log-normal distribution, then the relative size of a given size fraction is specified by three things: the sorting of the distribution, the mean or median size of the distribution, and the position of the given size fraction within the distribution (which is most naturally described by D_i/D_m, where D_m is the mean or median size and D_i is the size of the given fraction). Beyond this, of course, matters become much more complex (hopelessly so?) when we allow the shape of the size distribution to vary, as it does greatly, even to the point of bimodal and trimodal distributions, in natural sediments. (A great many natural sediments, particularly sand–gravel mixtures, are strongly bimodal.) You can see that the task of addressing the problem of threshold and transport of mixed-size sediments is a daunting one.

A final note seems in order here. The focus of this chapter is on sediment size. As you saw in Chapter 8, sediments in general have a joint frequency distribution of size, shape, and density. The study of mixed-shape and mixed-density sediment has not progressed as far as study of mixed-size sediment. It seems fair to say that the effect of mixed shapes is not as significant as the effect of mixed sizes—except, perhaps, for uncommon sediments with extremely nonspherical shapes. The effect of mixed-density sediments is important, for example, in understanding the development of placers. For completeness, these notes should have additional sections on mixed-shape and mixed-density sediments.

A Useful Thought Experiment

To get your thinking started, imagine a planar bed of mixed-size sediment, with a wide range of sizes from sand to gravel, over which a uniform flow is arranged to be passed. Assume that the particle-size distribution is unimodal. Suppose that the flow extends uniformly so far upstream and downstream as to be effectively infinite in extent. Clearly this is an idealization of the flow in real streams and rivers—but there is an essential element of reality to it, inasmuch as during a period of strong flow in a river the flow for the most part works on a bed of sediment that was lying there, waiting to be worked on before the event, and the flow picks up and moves what it wants to, without an externally constrained supply of sediment. A sediment-recirculating flume (see Chapter 8) works the same way, and in that sense is a good model for fluvial sediment transport.

You could attempt to measure three significant aspects of the transport of the mixed-size sediment in such an experiment. One is the relationship among the load (the sediment in transport at a given time), the bed surface (the sediment that is exposed to the flow at any given time), and the substrate (the bulk sediment from which the flow entrains, transports, and deposits sediment particles of various sizes). A second question has to do with movement thresholds: how do the thresholds for the various size fractions in the sediment mixture differ from one another? A third aspect is the relationship among the rates of transport of the various size fractions (usually called fractional transport rates; see below) of the sediment mixture. These three aspects are considered in some detail in the following sections.

This page titled 14.1: Introduction is shared under a CC BY-NC-SA 4.0 license and was authored, remixed, and/or curated by John Southard (MIT OpenCourseware) via source content that was edited to the style and standards of the LibreTexts platform.

14.2: Several Consequences of Size

The Bed-Surface Size Distribution

If the flow is sufficiently strong, it moves some of the sediment that is resting on the bed surface. The question now arises: after the sediment transport reaches an equilibrium state, *is the size distribution of the sediment on the bed surface the same as that of the sediment in the substrate?* An unsophisticated observer might suppose, beforehand, that it would be the same. In general, however, it is *not*: it is *coarser* than the substrate. In part this develops because the flow selectively entrains the finer fractions in preference to the coarser fractions. In the sediment-transport literature, this has been termed **selective entrainment**. That should seem natural to you in light of what was said in Chapter 9, on movement threshold: it takes a stronger flow to move coarser sediment than it does to move finer sediment, so at first thought it might seem that in a mixed-size sediment the coarser fractions should be more difficult to move than the finer fractions.

There is another effect as well: the flow "develops" the bed surface as it works on it, in such a way that finer particles find their way down beneath coarser particles, leaving a bed-surface layer that is coarser than the underlying layers. Such a coarser surface layer, beneath a flow that is transporting the bed-material sediment in equilibrium, is called **pavement** (Parker and Klingeman, 1982; Parker et al., 1982a; Parker et al., 1982b). Pavement is similar to, but different from, **armor**, which is a coarse surface layer that develops as a flow winnows finer sediment to the point where no more sediment can be entrained by the flow. In other words, armor is a coarse bed-surface layer which, once it is formed, never moves, under ordinary circumstances (it could, of course, be disrupted by a rare, catastrophic event), whereas pavement is a coarse surface layer which, if not in equilibrium with the flow, is moved, at least in part, under ordinary circumstances. (By "ordinary circumstances" here I mean strong flow events that might occur during some number of time periods, small or large, in a typical year.)

Another way of thinking about the development of a coarse surface layer during bed-material transport is that, if the coarser fractions are more difficult to transport than the finer fractions, the concentration of those coarser fractions on the bed surface must increase, in order for the flow to transport the sediment it is given to transport. That is true to the extent that the sediment-transporting system is like a sediment-feed flume (See Chapter 8), for which the flow and the bed must become adjusted to transport the sediment that is fed, independently, into the flow at the upstream end of the flume.

Fractional Transport Rates

Suppose, now, that you measured the unit transport rate (that is, transport rate, in mass per unit time, per unit cross-stream width of the flow) of each size fraction in the mixture of transported sediment. These transport rates are called **fractional transport rates**, often denoted by q_{bi}, where q represents the unit transport rate, the subscript i denotes the ith fraction in the mixture, and the subscript b stands for bed load or bed-material load. (In natural flow environments, of course, the size distribution is continuous, so you need to divide the size continuum, arbitrarily, into a large number of narrow fractions.)

You might measure the fractional transport rates in the following way—without great difficulty in a laboratory flume, but not without great difficulty, if not impossible, in a real stream or river! Build a slot trap of some kind across the flow at some station and extract all of the passing sediment during some interval of time. That might be called the "transport catch" (an unofficial term). If you divide the mass of the transport catch by the time interval and the width of the trap, you have the total unit transport rate, q_b. Then sieve the transport catch into the various size fractions, to find the proportion p_i of each of the fractions in the catch, and multiply each of the p_i by the total transport rate q_b to find the fractional transport rates q_{bi}. (That works well for the bed load, but much, if not most, of the suspended bed-material load is likely to pass over the trap. But the problem lies in practice, not in concept.)

Gradation Independence Versus Equal Mobility

For the relationships among the various fractional transport rates, you can think in terms of two end members. At one extreme, you might suppose that *the transport of each size fraction is entirely independent of the presence of all of the other size fractions*. Then the transport rate of each fraction could, in principle at least, be found by appeal to the same considerations that were described in the Chapter 13, on sediment transport rates. Such a situation might be called **gradation independence**. At the other extreme, you might suppose that, if you normalize the fractional transport rates by dividing them by the proportion f_i of the given

fraction in the sediment bed *all of the various fractions have the same normalized fractional transport rate*; in other words, the ratio of the fractional transport rate of a given size fraction to the proportion of the given size fraction in the bed sediment is the same for all of the size fractions. Such a condition has been termed **equal mobility**.

The condition of equal mobility might strike you as counterintuitive: should it not be more difficult for a flow to transport the coarser fractions than to transport the finer fractions? You might call this the **particle-weight effect**: larger particles are more difficult to move because they are heavier (Figure 14.2.1). Two important countervailing effects tend to offset the particle-weight effect, though: (1) the **hiding–sheltering effect**, whereby larger particles are more exposed to the flow and thus have exerted on them a greater fluid force, but smaller particles tend to be sheltered from the forces of the flow by the larger particles (Figure 14.2.2); and (2) the **rollability effect**, whereby larger particles can roll easily over a bed of smaller particles, but smaller particles cannot roll easily over a bed of larger particles (Figure 14.2.3). The relative importance of the particle-weight effect, on the one hand, and the combination of the hiding– sheltering effect and the rollability effect, on the other hand, is an essential element in mixed-size sediment transport.

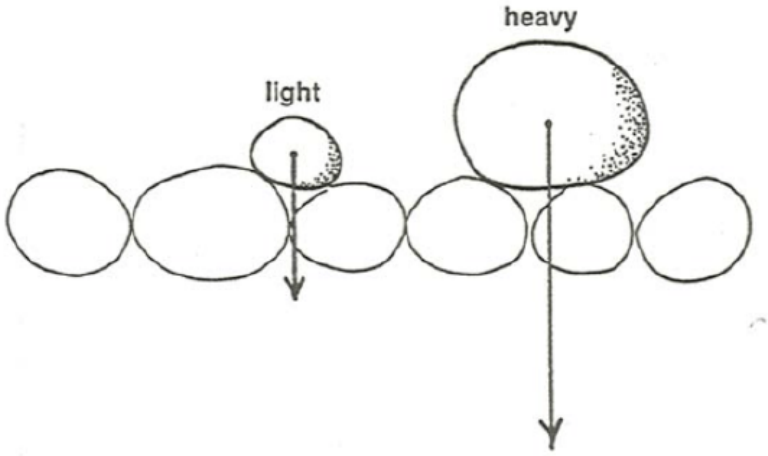


Figure 14.2.1: The particle-weight effect: larger particles are harder to move because they are heavier.

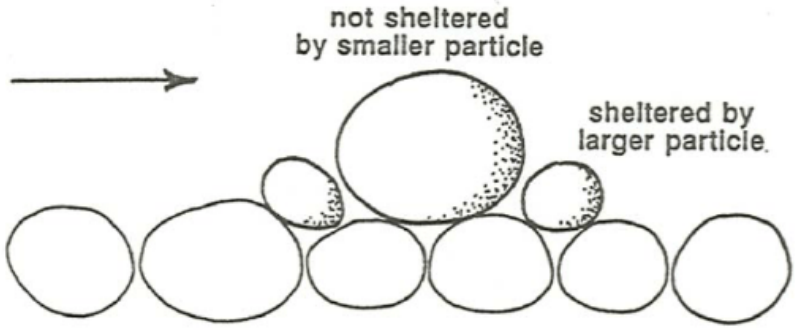


Figure 14.2.2: The hiding–sheltering effect: larger particles are more exposed to the flow, and smaller particles tend to be sheltered by larger particles.

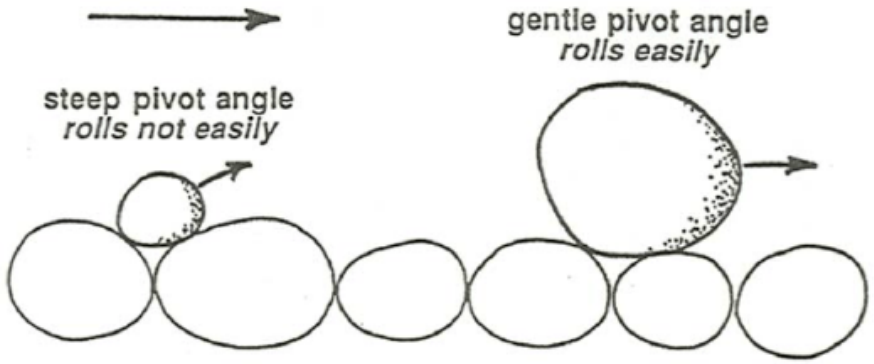


Figure 14.2.3: The rollability effect: larger particles can roll easily over a bed of smaller particles, but smaller particle cannot easily roll over a bed of larger particles.

In the case of a sediment-feed flume (see Chapter 8), in which a bed of sediment is laid down and then a flow is passed over that bed while sediment that is identical to the bed sediment is fed at some rate at the upstream end of the flume, to be caught and discarded at the downstream end, the condition of equal mobility is *forced upon the system*, simply because the flow must transport all of the sediment it is given. Otherwise, the flow and sediment transport could never attain an equilibrium state. In order to transport the inherently more difficultly transportable fractions—the coarser fractions, presumably—the size distribution of the bed surface must become adjusted in such a way that the proportion of those difficultly transportable fractions on the bed surface are in greater proportion than they are in the underlying sediment bed. In a sediment- recirculating flume, by contrast, there is no such constraint: the flow is free to adjust its transport of the various size fractions in accordance with their inherent transportability. A fundamental question thus arises: to what extent does transport of mixed-size sediment in a sediment-recirculating flume approach the condition of equal mobility, even though that condition is not forced upon it? The reasons for the importance of that question is that natural rivers and streams, at least over short scales of space and time, seem to behave more like sediment- recirculating flumes than like sediment-feed flumes. The answer to that question will become apparent in a later section of this chapter.

A Thought Experiment to Demonstrate the Difference Between Gradation Dependence and Equal Mobility

Here is a hypothetical laboratory experiment to reveal more clearly for you the distinction between gradation independence and equal mobility. It would not be dauntingly difficult to do in an appropriately equipped sedimentation laboratory. Obtain or prepare three batches of sediment with nearly perfect sorting: classic “unisize” sediments. Their sizes might range from medium sand to fine gravel. Use each, in turn, for a series of flume runs to measure the unit sediment transport rate q_b (transport rate per unit width of flow), where the subscript b signifies bed-material load, over a wide range of boundary shear stresses τ_o, from only slightly above the threshold shear stress to a very large boundary shear stress, several times the threshold value. Plot graphs of q_b against τ_o for each of the three sediments on a single graph (Figure 14.2.4).

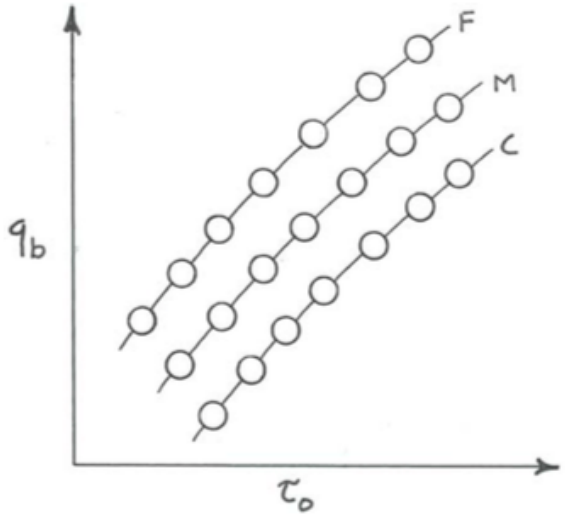


Figure $14.2.4$: Plot of q_b vs. τ_o for the three unisize sediment batches.

You know, beforehand, from the material in Chapter 12, what the graphs would look like, in an approximate way at least: for each sediment, the data points for the runs would fall on an approximately straight line in a $\log - \log$ plot, with q_b increasing steeply with τ_o. The curve for the finest sediment would lie above that for the middle sediment, and the curve for the coarsest sediment would lie below that for the middle sediment—because the flow moves finer sediment more easily than coarser sediment.

Another way of viewing the results graphically is to plot the results in a three-dimensional graph, by adding a third axis, the particle size (Figure $14.2.5$). Each of the three curves lies in its own plane, corresponding to position on the D axis. The earlier graph then is just a projection of the curves in those three separate planes onto the q_b–τ_o axis plane.

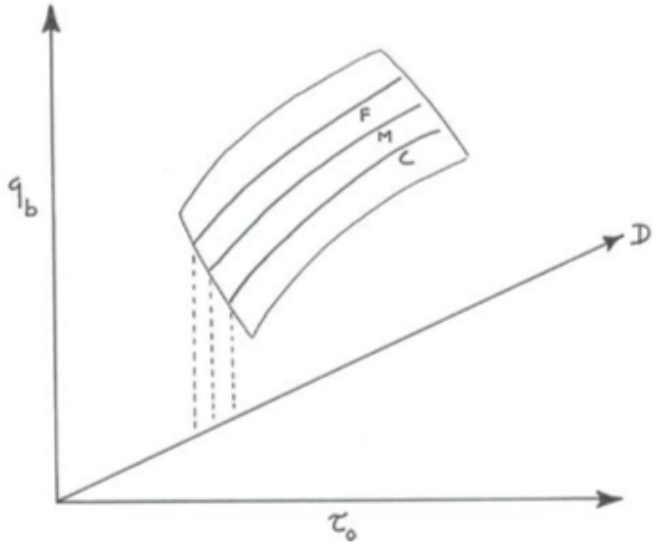


Figure $14.2.5$: Three-dimensional plot of q_b versus τ_o and D for the three unisize sediment batches.

Now mix the three unisize sediments together, to form a single starkly trimodal sediment mixture. Make a similar series of runs, with similar values of τ_o. For each value of τ_o, you need to compute the fractional transport rate of each of the three size fractions: $q_{bi} = (p_i/f_i)q_b$, where q_b is the total transport rate measured, p_i is the proportion of the transport rate (that is, the "transport catch"; see an earlier section) for the ith size fraction $(i = 1, 2, 3, \text{remember})$, and f_i is the proportion of the ith size fraction in the bulk sediment mixture you placed in the flume. Here we have normalized the q_{bi} by dividing by f_i, to make clearest sense of the results. Again you can plot the results of q_{bi} in a three-dimensional graph, analogous to that in Figure $14.2.5$, of q_{bi} vs. τ_o and D_i (with D_i taking on three values—those of the modes of the trimodal particle-size distribution you created by mixing the three separate unisize batches).

Now the question is: what would the graph look like for the end- member cases of complete gradation independence, on the one hand, and perfect equal mobility, on the other hand?

(1) *Gradation independence*: In the case of gradation independence, if the (p_i/f_i) for the three fractions are what they would be in the absence of the other fractions—that is, each fraction behaves in transport without any interaction with the other size fractions—then the results would plot as three curves in the q_b–τ_o–D_i graph, one curve in each of three $D_i = \text{constant}$ planes just as with the graph for the separate batches, and the curves would be the same as before, after the change from q_b to $(p_i/f_i)q_b$ is taken into account (Figure $14.2.6$).

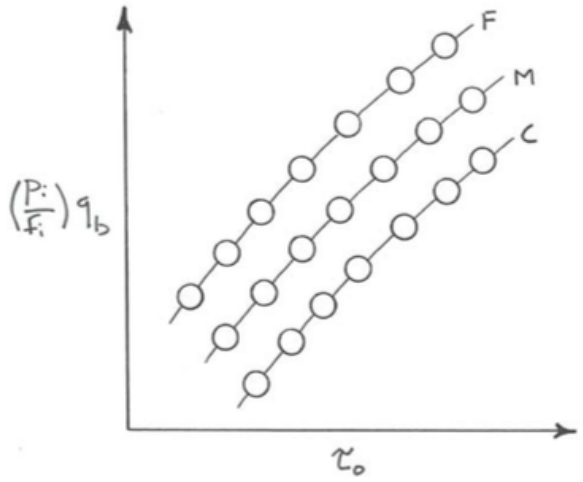


Figure $14.2.6$: **(Left)** Three-dimensional graph of normalized fractional transport rate $(p_i/f_i)q_b$ *vs.* τ_o *and* D_i *for the three-size sediment mixture, for the case of perfect gradation independence.* ***(right)*** *The graph in Part A projected onto the* q_b–τ_o *plane.*

(2) *Perfect equal mobility*: In the case of perfect equal mobility, all of the normalized fractional transport rates are the same for a given value of τ_o: the transport dynamics of the various fractions are so closely interdependent that the transport rates of the various fractions are all the same, when adjusted for their proportions in the sediment mixture. In a graph of normalized fractional transport rate $(p_i/f_i)q_b$ vs. τ_o and D_i (Figure $14.2.7$), again there are three steeply rising curves, one for each value of D_i, but now all three curves are the same, and when they are projected onto the $(p_i/f_i)q_b$–τ_o plane, *they fall on a single curve*.

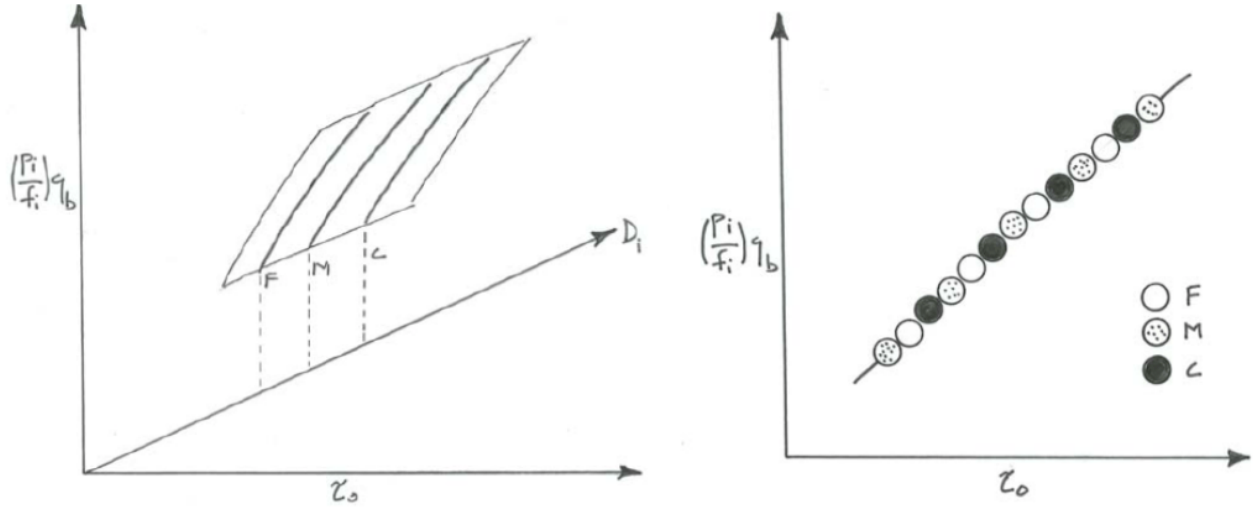


Figure $14.2.7$: **(Left)** Three-dimensional graph of normalized fractional transport rate $(p_i/f_i)q_b$ vs. τ_o and D_i for the three-size sediment mixture, for the case of perfect equal mobility. **(Right)** The graph in Part A projected onto the q_b–τ_o plane.

It is instructive to look also at how the three curves project onto the $(p_i/f_i)q_b$ vs. D_i axis plane of the three-dimensional graph: with each value of τ_o is associated a series of three points, and each of those sets of three points lies on a horizontal line, parallel

to the D_i axis (Figure 14.2.8). If the condition of equal mobility is not fulfilled, however, the curve would not be a horizontal line: if the fractional transport rates decrease with increasing sediment size, the curve would slope downward toward the coarser sizes (Figure 14.2.9A) and if the fractional transport rates increase with increasing sediment size, the curve would slope upward toward the coarser sizes (Figure 14.2.9B).

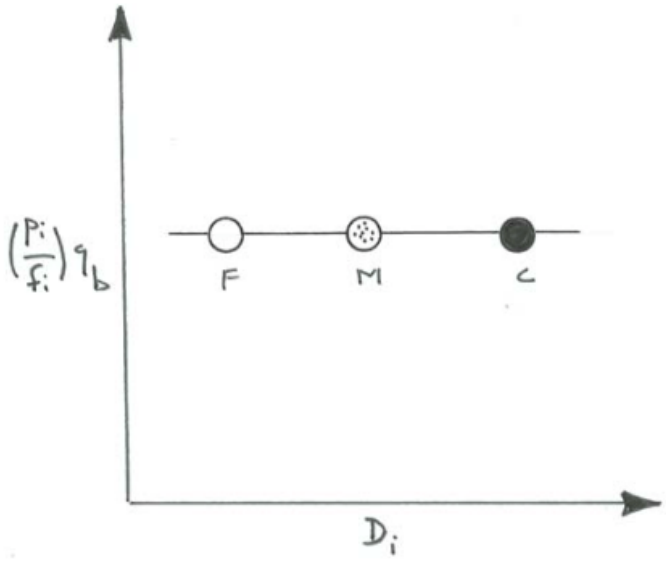


Figure 14.2.8: Graph of normalized fractional transport rate $(p_i/f_i)q_b$ *vs.* D_i *for the condition of perfect equal mobility of all of the size fractions.*

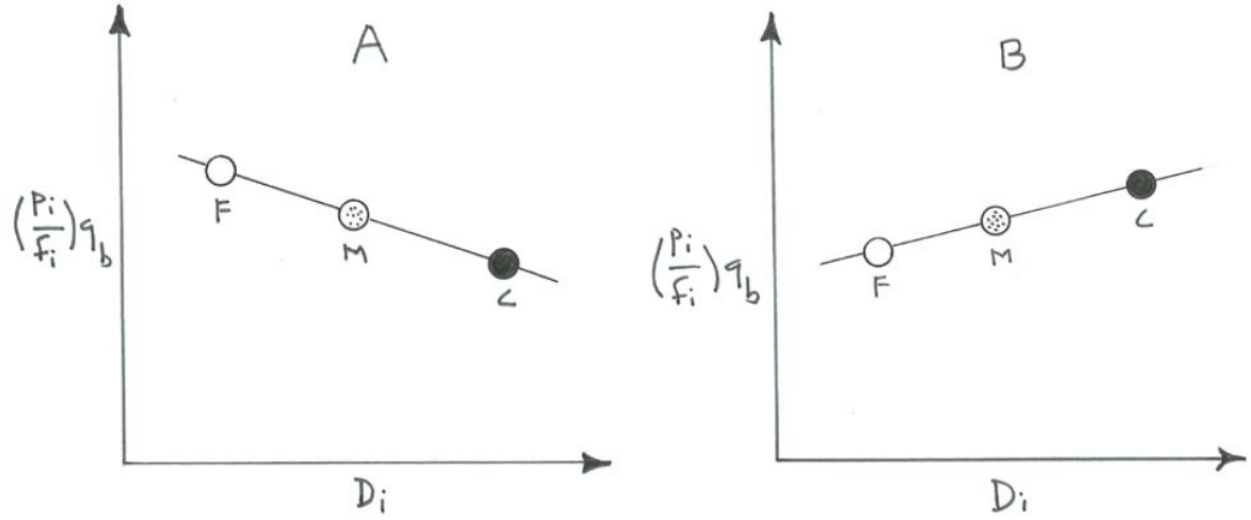


Figure 14.2.9: ***A)*** *Graph of normalized fractional transport rate* $(p_i/f_i)q_b$ *vs.* D_i *if the fractional transport rates decrease with increasing sediment size.* ***B)*** *Graph of normalized fractional transport rate* $(p_i/f_i)q_b$ *vs.* D_i *if the fractional transport rates increase with increasing sediment size. The shapes of the curves here are not meant to be significant: they are meant only to show the upward or downward trend of the data.*

This page titled 14.2: Several Consequences of Size is shared under a CC BY-NC-SA 4.0 license and was authored, remixed, and/or curated by John Southard (MIT OpenCourseware) via source content that was edited to the style and standards of the LibreTexts platform.

14.3: A Look at Some Real Data on Fractional Transport Rates, From the Flume and From the Field

There has been a long-standing controversy over the reality or importance of equal mobility since the concept was first proposed by Parker et al. (1982b). Some sets of measurements, in flumes and in streams, have shown a close approach to equal mobility, whereas other studies have shown strong deviations from equal mobility.

First we look at the results of the most revealing flume studies of fractional transport rates in unimodal sediment made up to now. Wilcock and Southard (1989) made a flume study of fractional transport rates in a sediment-recirculating flume. The sediment was of mixed size, with a mean size of $1.83\ \mathrm{mm}$ and a unimodal distribution. In seven runs with increasing bed shear stress, the fractional bed-load transport rates of several size fractions, ranging in size from $0.5\ \mathrm{mm}$ to $6\ \mathrm{mm}$, were measured by use of a slot trap that extended across the width of the flume. Once weighed, the samples were returned to the system. Sampling was done at two times during a run: while the bed was still initially planar, and at a later time when the bed and the flow had reached equilibrium. In the runs at lower bed shear stress, the bed remained planar for the entire run, but at higher bed shear stresses, dunes developed on the bed.

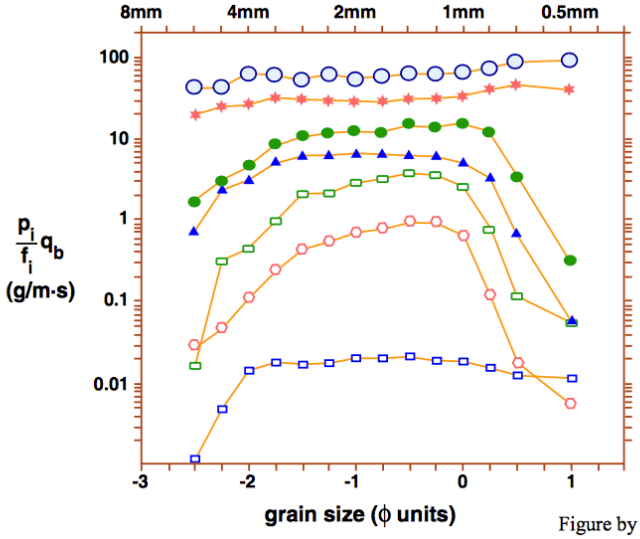


Figure by MIT OpenCourseWare.

Figure $14.3.1$: Fractional transport rate $(p_i/f_i)q_b$ vs. particle size for seven runs with increasing bed shear stress. Each curve represents one value of the bed shear stress (not given here). These data were taken at the end of each run, after the flow and the bed had come into equilibrium with the flow. (From Wilcock and Southard, 1988.)

You can see from Figure $14.3.1$ (compare this figure with Figures 14.2.8 and 14.2.9) that for a wide range of size fractions in the middle part of the size distribution the fractional transport rates are nearly the same: in other words, there is a close approach to the condition of equal mobility for those size fractions. Except at the highest bed shear stresses, however, the curves depart from the conditions of equal mobility: the fractional transport rates of both the finest fractions and the coarsest fractions are more difficult to transport. You might have guessed that the coarsest fractions would be harder to transport, but it is somewhat surprising that the same is true for the finest fractions.

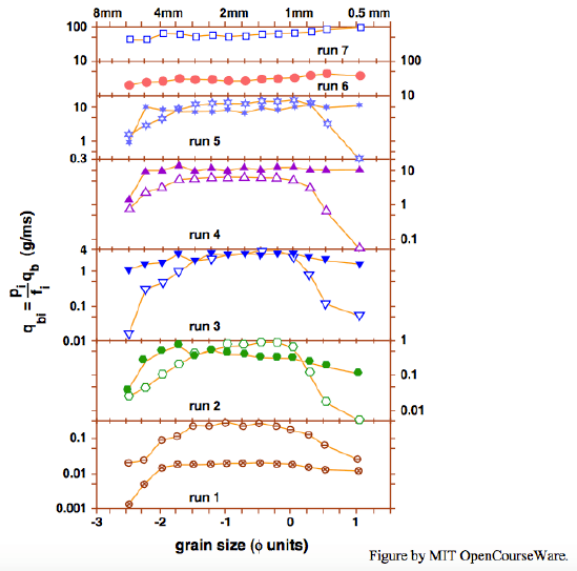


Figure 14.3.2: Fractional transport rate $(p_i/f_i)q_b$ vs. particle size for seven runs with increasing bed shear stress. The solid symbols are for initial fractional transport rates, and the open circles are for equilibrium fractional transport rates. (From Wilcock and Southard, 1988.)

Figure 14.3.2, also from Wilcock and Southard (1988), repeats the data in Figure 14.3.1 but also shows the data for the initial conditions in the runs (except for the two at the highest bed shear stresses). The main difference in the data between the two conditions is that at the initial condition the finest fractions approach the condition of equal mobility more closely than they do at the equilibrium condition. The explanation seems to be lie in a combination of two effects:

1. As time goes on, the finer particles find their way downward among the coarser particles to positions below the surface layer; and
2. As a coarse pavements develops on the bed surface, the finer particles are hidden from the flow more effectively.

The most widely cited data set on fractional transport rates in natural streams is that of Milhous (1973) from Oak Creek, a gravel-bed stream in Oregon. The Oak Creek data were used by Parker et al. (1982b) in their classic work on the concept of equal mobility.

Figure 14.3.3, a graph of the Oak Creek data on fractional transport rate shows, unsurprisingly, that the fractional transport rates are a steeply increasing function of flow strength. The dimensionless version of the fractional transport rate, called the dimensionless bed-load parameter W_i^*, is equal to $\gamma' q_{bvi}/f_i u_*^3$. (Note: the fractional transport rate, denoted here by q_{bvi}, is by sediment volume, not sediment mass.) The reason for the separation of the curves for the various size fractions is that the dimensionless variable on the horizontal axis, \tau_{i}^{*} (= \tau_{\text{o}}/ \gamma^{\prime}D_i), contains the particle size D_i of the given fraction.

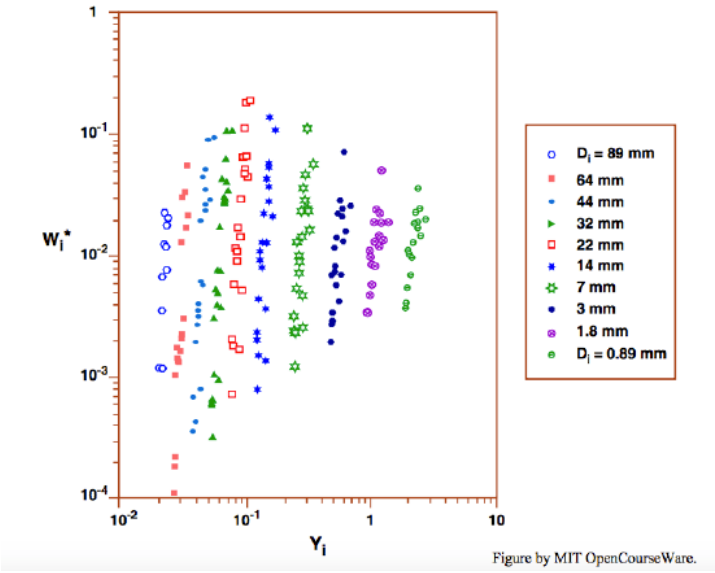


Figure 14.3.3: Plot of dimensionless bed-load parameter W_i^* vs. dimensionless bed shear stress τ_i^* for ten size ranges in the Oak Creek data. (From Parker et al., 1982b.)

Each curve in Figure 14.3.3 was extrapolated downward to find the threshold shear stress, defined as the value for which W_i^* was at an arbitrarily chosen reference value of 0.002 (chosen to conform to what would match the commonly accepted condition of movement threshold; see the discussion on the reference-transport rate method of defining the movement threshold, in Chapter 9). Then, in a plot of W_i^* versus τ_r^*/τ_{ri}^*, which Parker et al. denote by ϕ_i, all of the ten curves for fractional transport rate in Figure 14.3.3 collapse into a single curve—not perfectly, but to a fairly good approximation (Figure 14.3.4).

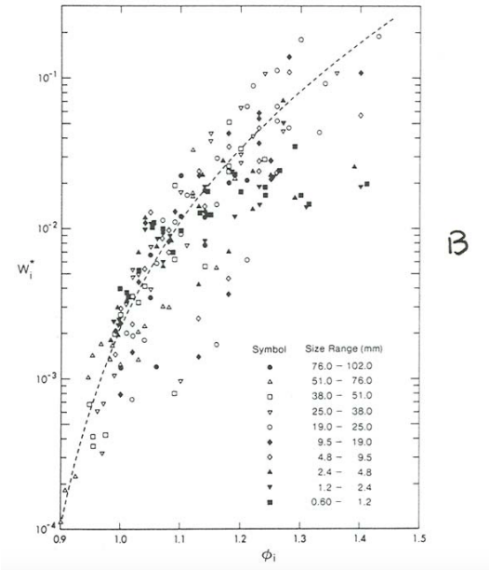


Figure 14.3.4: Courtesy of American Society of Civil Engineers. Used with permission. **A)** Plot of W_i^* *vs.* (\tau^{*}_{r}/\tau^{*}_{ri}\) *for the Oak Creek data.* ***B)*** *The same plot, with size ranges given. (From Parker et al., 1982b.)*

(Here, the dimensionless variable $\phi_i = tau_r^*/\tau_{ri}^*$ might need careful attention on your part: it is the reference value of the dimensionless bed shear stress at which the dimensionless total bed-load transport rate equals the reference total bed-load transport rate, divided by the reference value of the dimensionless bed shear stress of the ith size fraction at which the dimensionless bed-load transport rate of the ith fraction equals the reference bed-load transport rate of the ith fraction. (That long sentence requires careful reading.) Basically, it expresses the relative magnitude of the dimensionless bed shear stress at reference threshold condition for the bulk sediment, on the one hand, and the dimensionless bed shear stress at the reference condition for the ith fraction, on the other hand.)

What, then, is the significance of this “collapse” of the individual curves into a single curve? If you go back to the section on

the thought experiment and look at Figure 14.2.7, for the condition of perfect equal mobility, you can see that Figure 14.3.4 is of the same nature, because the effect of having the particle size in the denominator of the dimensionless bed shear stress is circumvented by taking the ratio of the two dimensionless bed shear stresses. The conclusion to be drawn is that also in the case of this natural gravel-bed stream the condition of equal mobility is approached, although not met exactly. We must conclude, then, that the effects of hiding–sheltering and rollability combine, in some way, to make the transport of the various size fractions more nearly equal, when normalized by the proportions of the fractions in the mixture, although there still is a tendency for the coarser fractions to be less easily transported.

This page titled 14.3: A Look at Some Real Data on Fractional Transport Rates, From the Flume and From the Field is shared under a CC BY-NC-SA 4.0 license and was authored, remixed, and/or curated by John Southard (MIT OpenCourseware) via source content that was edited to the style and standards of the LibreTexts platform.

14.4: Movement Threshold in Mixed-Sized Sediments

Introduction

It might seem like “putting the cart before the horse” to deal with movement thresholds after having already considered transport rates, but there is a certain logic to it, inasmuch as the most common way of identifying threshold conditions for mixed-size sediments is to measure transport rates for several values of boundary shear stress and then extrapolate downward to some chosen very low transport rate, called a **reference transport rate**, that corresponds approximately to what seems, by visual observations, to correspond to the boundary shear stress at which movement begins. The discussion in Chapter 9 on how to define the threshold condition in the first place is relevant here.

It is abundantly clear, from studies both in flumes and in natural flows, that the threshold shear stress for mixed-size sediments is different from that for unisize sediments. You should not expect to find that the threshold for movement of a certain size fraction in a mixed-size sediment is predictable by reference to the same sediment size in a relationship like the Shields diagram (Chapter 9), which is assumed to hold for unisize or very well-sorted sediment.

As with fractional transport rates, it is the outcome of the competition between the particle-weight effect, on the one hand, and the combination of the hiding–sheltering effect and the rollability effect, on the other hand, that is the key to movement threshold in mixed-size sediments. You should expect that to a first approximation the movement thresholds of the size fractions in a mixed-size sediment should be more nearly the same than would be predicted by, say, the Shields diagram for very well-sorted or unisize sediment. The question, again, as with fractional transport rates, is where the true situation lies between the end- member extremes of gradation independence (the threshold for each fraction is the same as for the same sizes of unisize sediment) and equal mobility (all of the size fractions of a mixed-size sediment begin to move at the same value of boundary shear stress).

Setting The Stage

Here is a useful framework for thinking about thresholds in mixed-size sediments, in light of what was just said about gradation independence and equal mobility:

Gradation independence: The threshold for each fraction is that same as if it were a unisize sediment, so τ_{ci}^* ($\tau_{oc}/\gamma' D_i$, the threshold value of the Shields parameter) is the same for all size fractions:

$$\tau_{ci}^* = \tau_{cj}^* \text{ for all } i, j \tag{14.4.1}$$

We can massage this by setting, arbitrarily, τ_{ci}^* equal to τ_{c50}^*, the threshold value for the 50th percentile of the sediment mixture. That is,

$$\tau_{ci}/\gamma' D_i = \tau_{c50}/\gamma' D_{50} \tag{14.4.2}$$

Dividing both sides by γ' and doing a bit of algebra then shows that

$$\tau_{ci}/\tau_{c50} = D_i/D_{50} \tag{14.4.3}$$

which expresses the condition of gradation independence. This would look like the graph in Figure $14.4.1$. We can carry this a bit further by use of the definition of τ^* : $\tau_{ci} = \gamma' D_i \tau_{ci}^*$ and $\tau_{c50} = \gamma' D_{50} \tau_{50}^*$, so the condition $\tau_{ci}/\tau_{c50} = D_i/D_{50}$ can be written

$$\tau_{ci}^*/\tau_{c50}^* = 1 \tag{14.4.4}$$

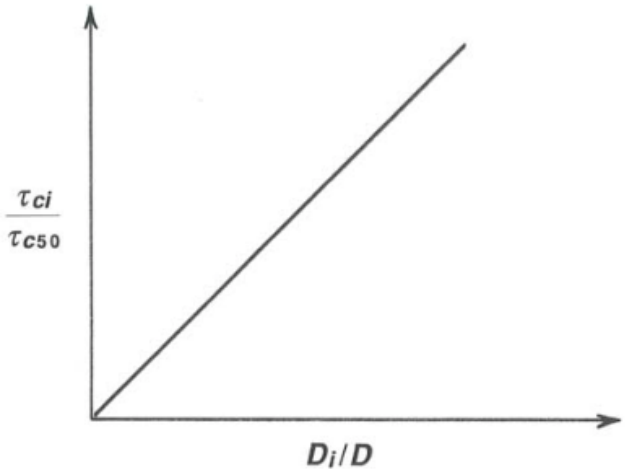


Figure 14.4.1: Graph of τ_{ci}/τ_{50} vs. D_i/D_{50} for the condition of gradation independence.

Equal mobility: each size fraction has the same movement threshold as all the others, and the particles of all of the size fractions start to move at the same value of τ_o:

$$\tau_{ci} = \tau_{cj} \text{ for all } i, j \tag{14.4.5}$$

Again we can massage this by setting τ_{ci} equal to τ_{c50}, for convenience, and then, with some algebra,

$$\tau_{ci}/\tau_{c50} = 1 \tag{14.4.6}$$

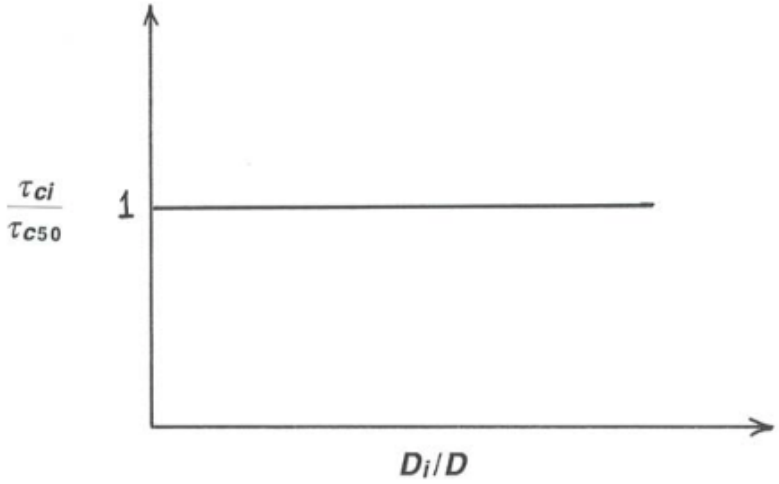


Figure 14.4.2: Graph of τ_{ci}/τ_{50} vs. D_i/D_{50} for the condition of equal mobility.

This would look like the graph in Figure 14.4.2. Again by use of the definition of τ^*_{ci} and τ^*_{c50}, the condition $\tau_{ci} = \tau_{c50}$ can be written

$$\tau^*_{ci}/\tau^*_{c50} = (D_i/D_{50}) - 1 \tag{14.4.7}$$

Finally, combining the results for both end-member cases, the contrast between gradation independence and equal mobility in graphic form is shown in Figures 14.4.3 and 14.4.4.

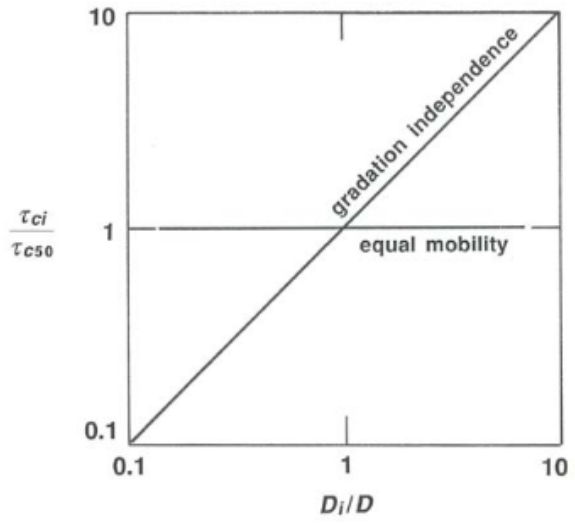


Figure $14.4.3$: Graph of τ_{ci}/τ_{c50} vs. \(D_{i}/D_{50}) for gradation independence and equal mobility.

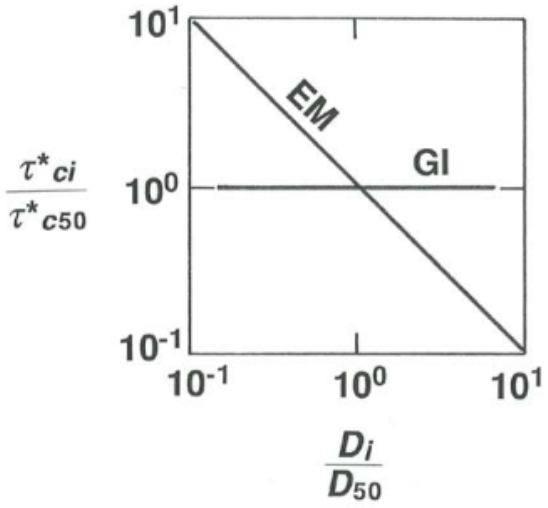


Figure $14.4.4$: Graph of τ^*_{ci}/τ^*_{c50} vs. \(D_{i}/D_{50}) for the conditions of gradation independence (GI) and equal mobility (EM).

Some Real Data on Thresholds in Mixed-Sized Sediments

Wilcock and Southard (1988), using the same experimental arrangement described above for fractional transport rates, studied movement thresholds in five batches of mixed-size sediments, made up specifically to represent a range of median size and sorting. The three main batches were chosen to have mean size of about $1.8\ \mathrm{mm}$ but with sorting ranging from very well sorted (phi standard deviation 0.20) to moderately poorly sorted (phi standard deviation 0.99). Also used were a well-sorted finer mixture, with mean size $0.66\ \mathrm{mm}$, and a well-sorted coarser mixture, with mean size $5.31\ \mathrm{mm}$. Movement threshold was determined by making several runs over a range of bed shear stress and extrapolating back to a reference transport rate chosen to correspond to a level of weak movement that would generally be agreed to represent threshold conditions.

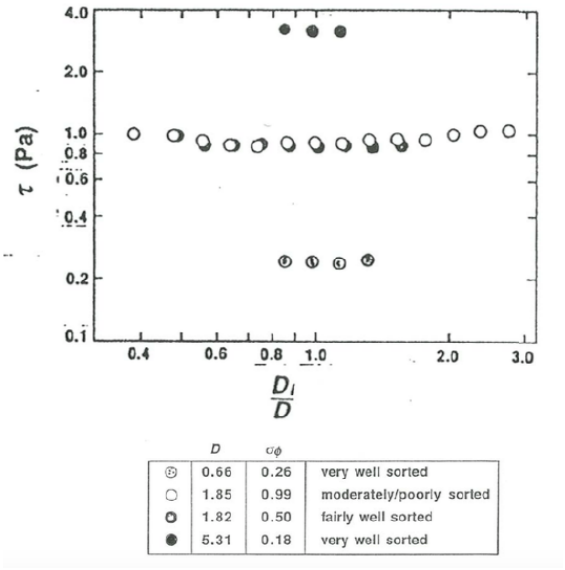


Figure 14.4.5: Plot of boundary shear stress τ_o against D_i/D, the ratio of the size of the ith fraction to the mean size of the sediment batch, for four of the sediment batches. (Modified from Wilcock and Southard, 1988.)

Figure 14.4.5 shows results for four of the sediment batches in a plot of τ_o against D_i/D_{50}, the ratio of the size of the given fraction to the mean size of the sediment batch. Owing to the differences in mean size, the curve for each sediment occupies a different range of τ_o, but what is interesting is that for each sediment the curves are nearly horizontal, indicating a close approach to equal mobility (see Equation 14.4.6 and Figure 14.4.2 above).

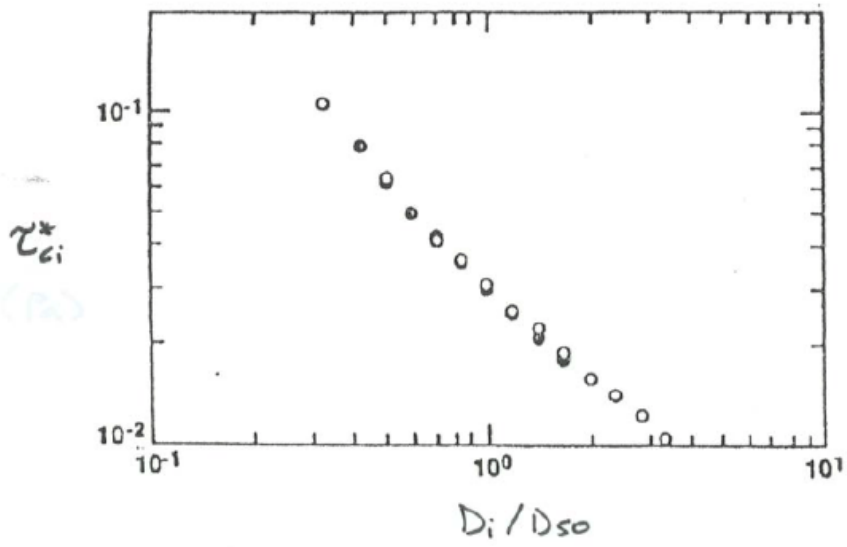


Figure 14.4.6: Plot of dimensionless threshold bed shear stress τ_{ci}^* against relative size D_i/D_{50} for two sediment batches with almost the same mean size but different sorting. Open circles, phi standard deviation $= 0.99$; solid circles, phi standard deviation 0.50. (Modified from Wilcock and Southard, 1988.)

Figure 14.4.6 shows results for movement threshold in a plot of τ_{ci}^*, the dimensionless threshold bed shear stress for the ith fraction, against D_i/D, the ratio of the size of the ith fraction to the mean size of the sediment batch. There are two noteworthy things about this graph:

1. The downward trend of the curves shows that the results correspond to a condition close to equal mobility, which is that of a straight line with a slope of -1 (compare with Equation 14.4.7 and with the graph in Figure 14.4.2B).
2. The two curves are almost identical, showing that the sorting of the sediment has little effect on the thresholds of the individual size fractions, once D_{50} and relative size D_i/D_{50} are accounted for.

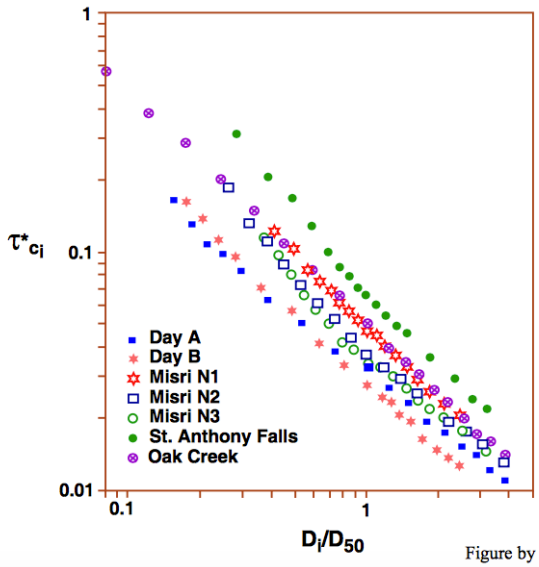


Figure by MIT OpenCourseWare.

Figure 14.4.7: Plot of dimensionless threshold bed shear stress τ_{ci}^* against relative size D_i/D_{50} for laboratory experiments (Day, 1980; Misri et al., 1984; Dhamotharan et al., 1980; Wilcock, 1987) and field studies (Milhous, 1973).

Figure 14.4.7 is a plot similar to that in Figure 14.4.6 for sediments from various laboratory and field studies. For these sediments as well, the condition of equal mobility, expressed as slope of -1 in the plot, is approached but not met.

An equivalent, but revealing, way of presenting the data in Figure 14.4.7 is to plot (Figure 14.4.7) the dimensionless threshold bed shear stress τ_{ci}^* against the dimensionless variable $D^3\gamma'\rho/\mu^2$ (taken to the one-half power here), which is a nondimensionalization of the particle size in a way that does not involve the bed shear stress. The Shield curve for movement threshold is replotted in this graph as the solid curve. The downward slope of each of the curves defined by the data points shows clearly that the finer fractions of the sediment mixtures have threshold values that lie above the Shields curve, and the coarser fractions have threshold values that lie below the Shields curve.

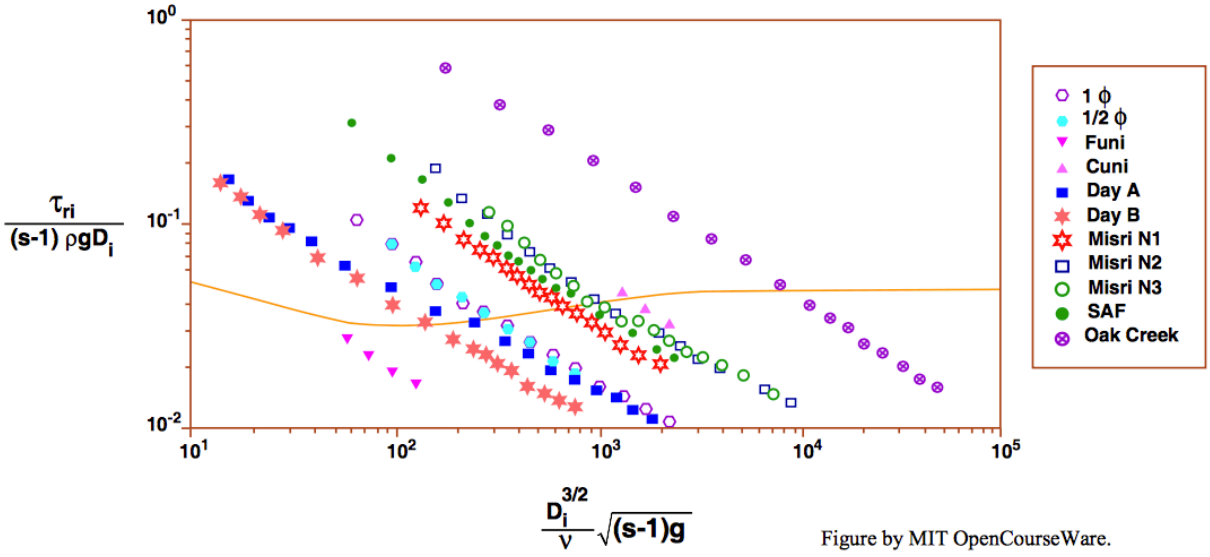


Figure by MIT OpenCourseWare.

Figure 14.4.6. The solid curve is the Shields curve, transformed into the coordinates of this plot. (From Wilcock and Southard, 1988.)

This page titled 14.4: Movement Threshold in Mixed-Sized Sediments is shared under a CC BY-NC-SA 4.0 license and was authored, remixed, and/or curated by John Southard (MIT OpenCourseware) via source content that was edited to the style and standards of the LibreTexts platform.

14.5: Deviations from the Condition of Equal Mobility

Some perspective is needed at this point. You have seen, from discussion of the various data sets presented in the preceding sections, that although the thresholds and transport rates of mixed-size sediments show a much closer approach to the condition of equal mobility than to the condition of gradation independence, there remains a deviation from the condition of equal mobility such that in general the coarser fractions are somewhat more difficult to entrain and transport than the finer fractions; in other words, the combined effects of hiding–sheltering and rollability are insufficient to counteract fully the effect of particle weight.

The incomplete approach to the condition of equal mobility leads to two related concepts: selective entrainment and partial transport. The term **selective entrainment** refers to differences in movement thresholds among the various size, shape, and density fractions of a sediment consisting of a mixture of particle sizes, shapes and densities. The emphasis here is on size-selective entrainment, although density-selective entrainment is one of the keys to the development of placers. Much of the work on selective entrainment is owing to Komar (1987a, 1987b, 1989).

A concept related to that of selective entrainment is that of **partial transport**: for a range of bed shear stresses above the condition of no particle movement, a given size fraction may comprise two populations:

1. Particles that are moved, occasionally, by the flow; and
2. Particles that are never moved by the flow, and remain motionless on the bed (Wilcock and McArdell, 1993, 1997).

The domain of partial transport lies between the range of bed shear stresses for which there is no motion of any of the particles of the given size fraction, on the one hand, and the range of greater bed shear stress for which all of the particles of the given size fraction are moved by the flow at one time or another. In general, the lower and upper limits of this range differ from size fraction to size fraction. A corollary is that, when all of the size fractions are considered, the domain of partial transport extends from the upper limit of bed shear stress for which no particles of any size fraction are moved by the flow, on the one hand, and the lower limit of bed shear stress for which at least some of the particles of all of the size fractions are moved at one time or another, on the other hand.

What is the relationship between partial transport and fractional transport rates? Insight into that question comes from flume experiments on partial transport by Wilcock and McArdell (1993, 1997). The sediment was unimodal but poorly sorted mixture with the distinctive feature that all of the particles of each of the size fractions was painted a different color, to facilitate observations of particle immobility and particle movement on the sediment bed. Observations of partial transport, as well as fraction transport rates, were made in several runs over a range of bed shear stress that bracketed the domain of partial transport as described above.

Figure $14.5.1$, a plot of fractional transport rate against particle size, shows the relationship between partial transport and fractional transport rates for each of five runs. In Figure $14.5.1$ the limiting value of the active proportion of particles in each size fraction, after a long running time, is denoted by Y_i. Each data point in Figure $14.5.1$ represents a given size fraction in a given one of the five runs. The proportion of the particles of the given fraction that are mobile increases from lower right to upper left for each curve.

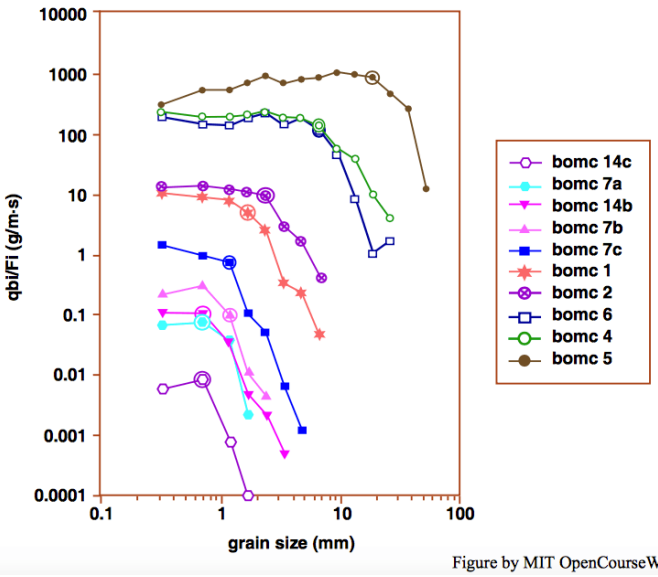


Figure by MIT OpenCourseWare.

Figure 14.5.1: Plot of fractional transport rate q_{bi}/F_i (where F_i is the proportion of size fraction i on the bed surface) against particle size. Bed shear stress ranges from the lowest values (solid diamonds) to the highest values (solid squares). The large open circles represent the largest fully mobilized particle size in each run. (From Wilcock and McArdell, 1993.)

The distinctive feature of the plot in Figure 14.5.1 is that the curves for fractional transport rate flatten to near horizontality (a condition approaching equal mobility) as flow strength increase. In other words, deviations from equal mobility are large within the domain of partial transport but become small for bed shear stresses above the domain of partial transport.

More on Sediment-Discharge Formulas: Subsurface-Based Models versus Surface-Based Models

All sediment-discharge formulas, including those described briefly in Chapter 13, make use, in one way or another, of the sediment size, usually the median size. Some such approaches have attempted to deal with mixed-size sediments by introducing a “hiding function” that takes account of the hiding– sheltering effect, but even those need to be based on a particular size distribution of the sediment.

The question then arises: which size distribution should be used? That of the sediment in the substrate, or that of the bed surface, which the flow actually sees? The latter would seem to be the more natural choice. As you have seen, in mixed-size sediments, especially those with both sand and gravel fractions, the sediment bed surface tends to become paved with sediment that is, on average, coarser than the substrate sediment. The problem is that the surface size distribution is itself a function of the flow. Moreover, only in carefully designed laboratory flume experiments is it possible to observe the surface size distribution, and only a few studies have succeeded in doing so. Up to now, only a few transport models based on the surface size distribution rather than the substrate distribution have been developed (Proffitt and Sutherland, 1983; Parker, 1990; Wilcock and Crowe, 2003).

Chapter 14 References Cited

Day, T.J., 1980, A study of the transport of graded streams: Wallingford, U.K., Hydraulics Research Station, Report IT 190.

Dhamotharan, S., Wood, A, and Parker, G., 1980, Bedload transport in a model gravel stream: University of Minnesota, St. Anthony Falls Hydraulics Laboratory, Project Report 190.

Milhous, R.T., 1973, Sediment transport in a gravel-bottomed stream: Ph.D. thesis, Oregon State University, Corvallis, Oregon.

Misri, R.L., Garde, R.J., and Ranga Raju, K.G., 1984, Bed load transport of coarse nonuniform sediment: American Society of Civil Engineers, Proceedings, Journal of the Hydraulics Division, v. 110, p. 312-328.

Parker, G., 1990, Surface-based bedload transport relation for gravel rivers: Journal of Hydraulic Engineering, v. 28, p. 417-436

Parker, G., and Klingeman, P.C., 1982, On why gravel bed streams are paved: Water Resources Research, v. 18, p. 1409-1423.

Parker, G., Dhamotharan, S., and Stefan, S, 1982a, Model experiments on mobile, paved gravel bed streams: Water Resources Research, v. 18, p. 1395-1408.

Parker, G., Klingeman, P.C., and McLean, D.L., 1982b, Bedload and size distribution in paved gravel-bed streams: American Society of Civil Engineers, Proceedings, Journal of the Hydraulics Division, v. 108, p. 544-571.

Proffitt, G.T., and Sutherland, A.J., 1983, Transport of non-uniform sediments: Journal of Hydraulic Research, v. 21, p. 33-43.

Wilcock, P.R., 1987, Bed-load transport of mixed-size sediment: Ph.D. thesis, Massachusetts Institute of Technology, Cambridge, Massachusetts.

Wilcock, P.R., and Crowe, J.C., 2003, Surface-based transport model for mixed-size sediment: Journal of Hydraulic Engineering, v. 129, p. 120-128.

Wilcock, P.R., and McArdell, B.W., 1993, Surface-based fractional transport rates: Mobilization thresholds and particle transport of a sand–gravel sediment: Water Resources Research, v. 29, p. 1297-1312.

Wilcock, P.R., and McArdell, B.W., 1997, Partial transport of a sand/gravel sediment: Water Resources Research, v. 33, p. 235-245.

Wilcock, P.R., and Southard, J.B., 1988, Experimental study of incipient motion in mixed-size sediments: Water Resources Research, v. 24, p. 1137-1151

Wilcock, P.R., and Southard, J.B., 1989, Bed load transport of mixed size sediment: fractional transport rates, bed forms, and the development of a coarse bed surface layer: Water Resources Research, v. 25, p. 1629-1641.

This page titled 14.5: Deviations from the Condition of Equal Mobility is shared under a CC BY-NC-SA 4.0 license and was authored, remixed, and/or curated by John Southard (MIT OpenCourseware) via source content that was edited to the style and standards of the LibreTexts platform.

15: DEPOSITION

15.1: Introduction to Deposition
15.2: Modes of Deposition
15.3: Why Deposition or Erosion?

This page titled 15: Deposition is shared under a CC BY-NC-SA 4.0 license and was authored, remixed, and/or curated by John Southard (MIT OpenCourseware) via source content that was edited to the style and standards of the LibreTexts platform.

15.1: Introduction to Deposition

The topic of deposition is an important one, because, obviously, every sedimentary sequence was deposited somehow. This section is meant to serve as background for our consideration of the current-generated physical sedimentary structures in real sedimentary deposits.

Let me pose a question for you: ***Why does deposition happen?*** I wonder whether this strikes you as a trivial question or as a difficult question. In one sense, we can supply a simple answer: sediment is carried by a flow, and when the conditions are such that the flow becomes overloaded, the sediment is deposited. But in another sense, this is a superficial answer, because it does not account for the conditions under which a flow becomes overloaded, and we have to look for a more fundamental answer. (By **overloading** I mean that the flow, at a given time, is transporting a greater sediment load than what it would be transporting if the sediment transport were in equilibrium with the given flow.)

The most straightforward process involved in deposition is **settling**: the downward fall of sediment particles through the surrounding fluid by the pull of gravity (see Chapter 3). Keep in mind, however, that there is far more to deposition than just settling of sediment particles: you have to worry about where the sediment came from, how it got to the site of deposition, and why it was that more sediment was falling out of suspension than was being resuspended at the site of deposition. Considerations like this are absolutely critical to a really fundamental understanding of sediment deposition, but in my opinion not nearly enough attention has been given to such matters in the literature on sedimentation, either by hydraulic engineers or by sedimentary geologists. This chapter makes only the barest start on addressing such matters.

This page titled 15.1: Introduction to Deposition is shared under a CC BY-NC-SA 4.0 license and was authored, remixed, and/or curated by John Southard (MIT OpenCourseware) via source content that was edited to the style and standards of the LibreTexts platform.

15.2: Modes of Deposition

Introduction

This section examines local modes of sediment deposition. Some of these modes may be observable in laboratory experiments or in field studies. Others may be difficult or impossible to observe with present technology, and we can only make deductions or speculations about them. (Keep in mind that deductions can be very dangerous in physical sedimentology, because the physics of the phenomena are so complex that we can easily fool ourselves into thinking that an unimportant process is important or that an important process is unimportant.) The treatment will be entirely qualitative.

Several distinctive modes of deposition, discussed in the sections below, can be recognized. These modes grade into one another; there are no sharp boundaries among the various processes involved. Keep in mind also that the terms used for these modes are only unofficial; you are not likely to find them in the published literature on sediment deposition. See Figure $15.2.1$ for cartoons that illustrate the various modes of deposition.

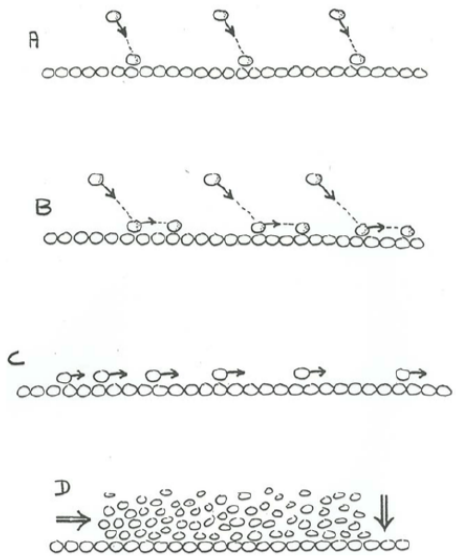


Figure $15.2.1$: Modes of deposition. **A)** Fallout without traction. **B)** Fallout with traction. **C)** Differential transport. **D)** Mass deposition.

Fallout Without Traction

In the simplest of depositional modes, sediment particles suspended in a flow by some earlier process or event settle to the bed and are not transported thereafter, either by traction or by suspension (Figure $15.2.1$A). This might be called **fallout without traction**.

Flows that deposit sediment by fallout without traction have velocities below the threshold for bed-load transport, which ranges from slightly less than $0.2\ \mathrm{m/s}$ to well over $0.3\ \mathrm{m/s}$, depending on the depth of the flow and the size of the sediment particles. In general, the weaker the flow, the finer the sediment that is being carried and deposited in this mode. The flow may even be nonexistent; in that case, the sediment must be supplied directly from above, as for example by fallout of eolian sediment into a standing body of water.

The size of the sediment deposited by fallout without traction is usually very fine, seldom coarser than very fine sand. The reason is that the flow would need to be much stronger to carry coarser sediment in suspension, and such flows would be strong enough to move the deposited sediment as bed load after the sediment lands on the bed.

In fallout without traction, the thickness of deposit is limited only by the quantity of sediment in suspension above the bed. At first thought this might seem like a severe limitation, but remember that there can be sedimentation systems in which new sediment

in suspension is introduced continuously some- where upcurrent in a steady flow (or, if not steady, episodic but long-continued), like an area offshore of the delta of a river carrying abundant suspended sediment. On the other hand, there is a definite spatial constraint: the downcurrent distance over which such deposition takes place is limited by the downstream loss of sediment from the flow. The finer the suspended sediment and the deeper the flow, the greater the distance over which there is deposition.

Fallout Without Traction

Sediment particles may settle onto the sediment bed from suspension and then be moved as bed load, or even be resuspended temporarily, before they eventually come to permanent rest and are buried by other particles as the bed builds up (Figure 15.2.1 B). This might be called **fallout with traction**.

Flows that deposit sediment by fallout with traction can have a wide range of velocities, from a small fraction of a meter per second to much greater than a few meters per second. Sediment size can range from silts to gravels. The only condition is that the flow is not so overloaded with suspended sediment that a well defined sediment–water interface cannot be maintained. The spatial and temporal constraints on the mode of deposition are largely the same as for fallout without traction.

Differential Transport

To non-geologists (and to some geologists as well!), if you mention deposition, what flashes into their minds is the kind of thing that happens when you suspend some sediment in a vessel of water and let it settle to the bottom. That was called, in the earlier section, fallout without traction. Yes, that is one mode of deposition, and it is important in many natural sedimentary environments. But there is an equally important mode of deposition that is much less intuitive. A sediment deposit can be formed without any fallout from suspension. At first thought this might seem strange, so we need to spend a little more time discussing this mode of deposition. Think about the consequences of a downstream change in sediment transport rate in a steady flow.

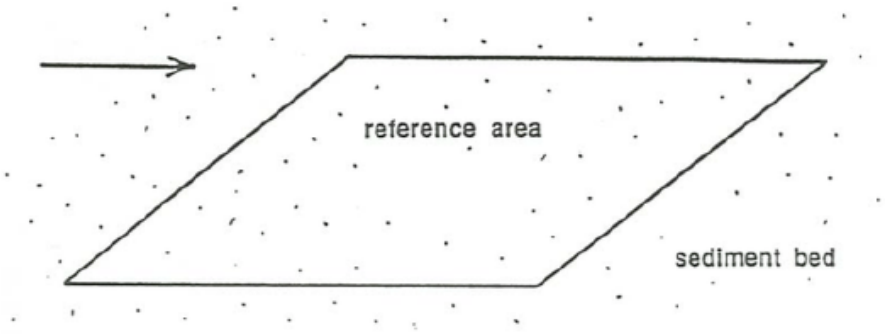


Figure 15.2.2: A small rectangular reference area on the sediment bed beneath a flow that is transporting sediment over the bed.

Look at a small rectangular reference area on the sediment bed beneath a flow that is transporting sediment over the bed (Figure 15.2.2). The edges of the reference area are parallel to and perpendicular to the flow direction. Because volume of sediment is neither created nor destroyed on the short time scales associated with sediment transport by traction or suspension, we can invoke the **principle of conservation of sediment volume** in accounting for what happens to the sediment.

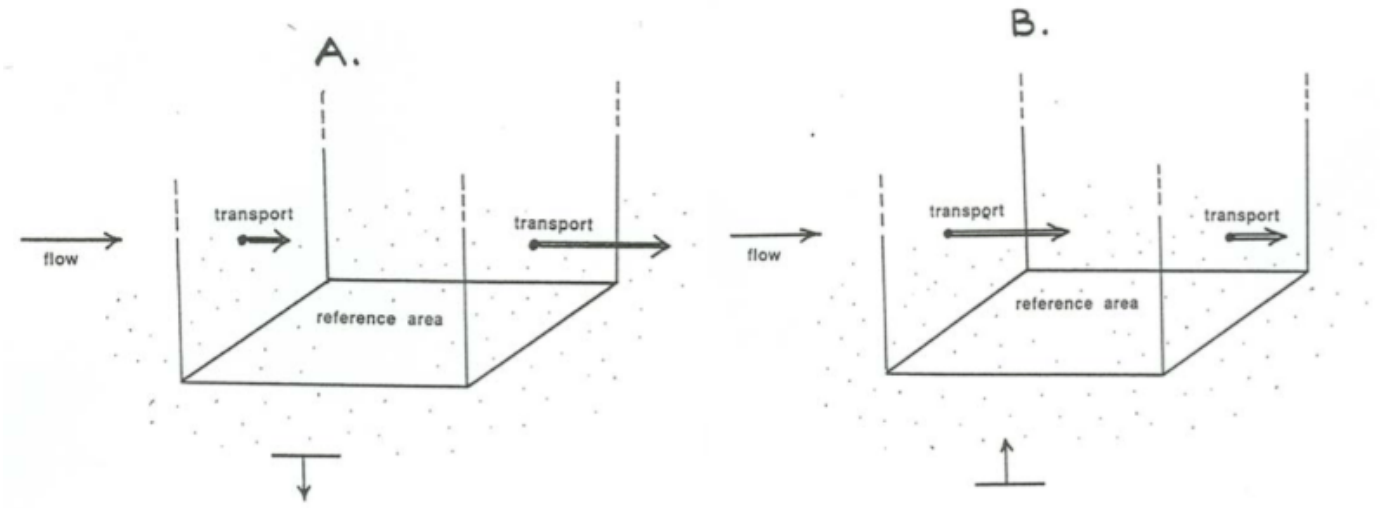


Figure 15.2.3: Sediment transport over the reference area. **A)** Sediment is being added to the flow from the bed somehow, resulting in net erosion. **B)** Sediment is being added to the bed from the flow somehow, resulting in net deposition.

If the total volume of sediment in traction and suspension passing across the plane extending upward from the upstream edge of the reference area is *less* than the total volume of sediment passing across the plane extending upward from the downstream edge of the reference area (Figure 15.2.3A), then sediment is somehow being *added* to the flow in the space above the reference area. The only place where that added sediment can come from is from the bed, and the only place where it can go is into the flow. So there must be *net erosion of the bed*.

On the other hand, if the total volume of sediment in traction and suspension passing across the upstream plane is *greater* than the total volume passing across the downstream plane (Figure 15-3B), then sediment is somehow being *extracted* from the flow in the space over the reference area. The only place where that extracted sediment can go is onto the bed, so there has to be *net deposition on the bed*. This mode of deposition might be called deposition by **differential transpor**t (Figure 15.2.1C). Figure 15.2.4 shows, in cartoon form, the conditions for deposition by differential transport.

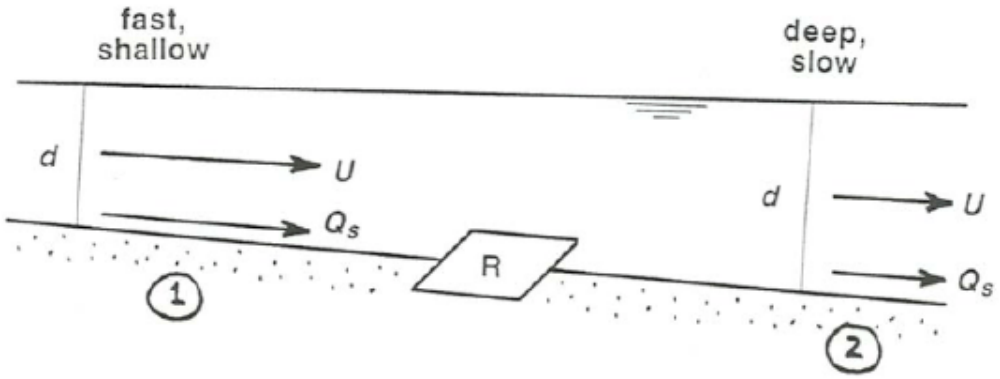


Figure 15.2.4: The conditions for deposition by differential transport. Sediment transport rate Q_s decreases downstream because mean flow velocity U decreases owing to a downstream deepening of the flow from cross section 1 to cross section 2. The result is aggradation on a reference area R on the sediment bed.

The consequence of the reasoning presented above is that there can be deposition on a sediment bed without any temporal change in the picture of sediment transport: the flow is steady, and the load and the sediment transport rate at every point do not change with time. There can be deposition, however, provided that the sediment transport rate is changing *spatially* by decreasing in the downstream direction.

Deposition by differential transport can take place entirely by downstream decrease in bed-load transport rate, even without any suspended sediment in the flow. This happens wherever the flow deepens slightly in the downstream direction (for any one or more of several reasons, which I will not discuss here), causing the flow velocity and therefore also the bed-load sediment

transport rate to decrease in the downstream direction.

Flows that deposit sediment by differential transport range widely in flow velocity, from a few tenths of a meter per second to well over two meters per second. Sediment size ranges from finer than sand size to well into the gravel size range. Clearly, the coarser the sediment the more likely it is that the process involves differential bed-load transport rather than differential suspended-load transport.

As with deposition by fallout, there are constraints on both the thickness and the downstream extent of deposition by differential transport, but they are not exactly the same as for deposition by fallout. For a given value of “input” transport rate (that is, at the upstream end of the reach of flow that is experiencing downstream-decreasing transport rate), there must be an inverse relationship between the distance along which there is deposition and the rate of deposition at points along the transport path—basically because deposition is everywhere using up the stock of sediment that is in transport. This will have application to the geometry and interpretation of cross-stratification produced by bed forms in unidirectional and combined flows; see Chapter 16.

Keep in mind also that deposition can be by a combination of fallout and differential transport. These two cases are only end members of a continuous spectrum of possibilities, depending upon the particular depositional setting (that is, the nature of the sediment supply and the nature of the current).

Mass Deposition

In many flows, the concentration of sediment is so high that there is no strong distinction, in sediment concentration or particle fabric, between the flow and the underlying immobile bed. In such cases it is common for deposition to take place by sudden or gradual freezing or immobilization of the flow. I will call this mode of deposition **mass deposition** (Figure 15.2.1D). This is in contrast to deposition by gradual buildup of the sediment bed when there is a well defined sediment-water interface. Mass deposition, discussed in this section, can therefore be counterposed to what might be called **interfacial deposition**, discussed in the preceding three sections. Treatment of the various processes involved in mass deposition, and the sedimentary textures and structures of the resulting deposits, are outside the scope of these course notes. The following brief comments will have to suffice.

Conditions during mass deposition are difficult to observe, because sediment concentrations are high and deposition is rapid. Also, the flows from which mass deposition occurs tend to be more powerful and on much larger scales than is the case with the other modes of deposition discussed above. Mass deposition is characteristic of strong sediment gravity flows, especially in their earlier stages.

It is my belief that mass deposition is important in two different but closely related depositional settings, both associated with sediment gravity flows:

- mass deposition *at the base of a heavily laden turbidity current*
- mass deposition by *freezing of a classical debris flow*, from the top down

Here are some brief comments about each of these settings.

When the region of the flow near the bed is overloaded with a high concentration of suspended sediment, as near the base of a large and powerful **turbidity current** carrying a high concentration of sediment both coarse and fine, the sediment settles to the bed with little space between adjacent sediment particles. A layer of the flow with a thickness that's orders of magnitude greater than the particle size becomes immobilized almost simultaneously as the shearing of the highly concentrated sediment-water mixture ceases (Figure 15.2.5).

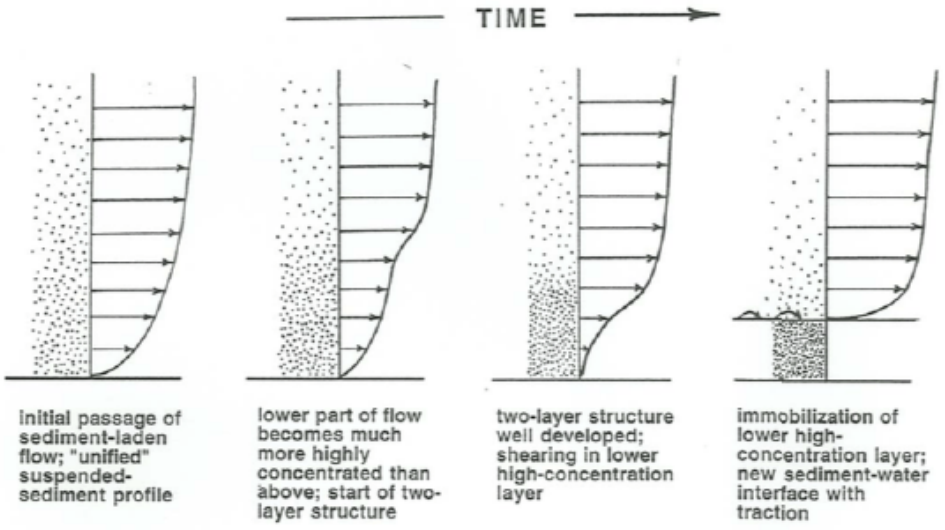


Figure 15.2.5: Development and immobilization of a lowermost higher- concentration layer at the base of a strong, high-concentration turbidity current.

During such mass deposition there is no well defined sediment–water interface; instead there is a gradual transition between the underlying already- deposited bed and the sheared, highly concentrated suspension above. Another way of looking at this is that the pore-water content of the mixture varies continuously upward from the already-deposited sediment bed into the still-moving sediment–water mixture.

The other setting for mass deposition is that of a high-concentration debris flow, in which the sediment concentration is near the “choke point” (the maximum possible for which the sediment–water mixture can still undergo shearing without the particles locking together). The mechanical properties of a **debris flow** are very different from those of clear water, but the velocity profile is qualitatively the same, in that the rate of shearing increases from zero at the free surface to a maximum at the base Note that the velocity profile is perpendicular to the bottom boundary at the surface and becomes more and more nearly parallel to the bottom boundary with depth in the flow. This is because at deeper and deeper levels in the flow, there is a greater and greater weight of overlying fluid that drives the fluid overlying the shear plane at that level in the downchannel direction. Also, highly concentrated mixtures of sediment and water are different from clear water also by having shear strength: it takes a certain nonzero shear stress acting across the shear planes for shearing movement to take place. The consequence for thick and highly concentrated debris flows is that as the flow decelerates it freezes from the top down, and when the freezing reaches the base, the flow comes to a halt (Figure 15.2.6), whereafter it sits motionless and slowly dewaters.

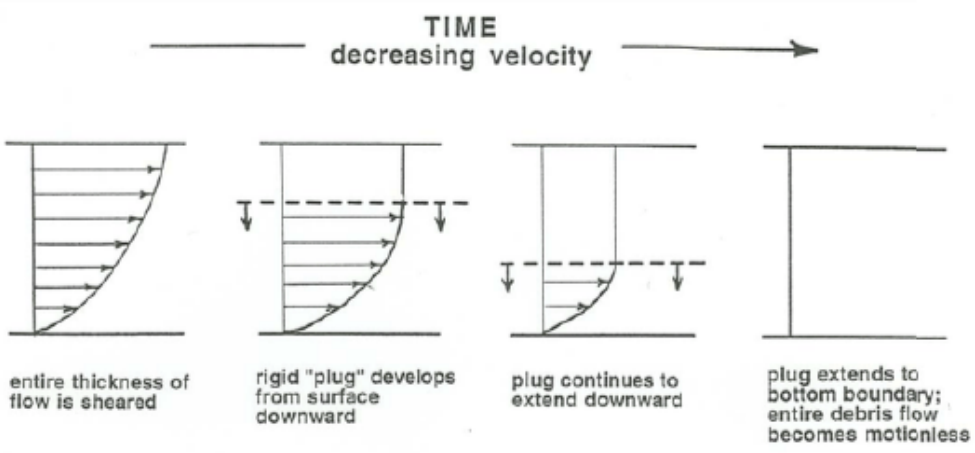


Figure 15.2.6: Freezing of a debris flow from the top downward, ending in complete cessation of movement.

This page titled 15.2: Modes of Deposition is shared under a CC BY-NC-SA 4.0 license and was authored, remixed, and/or curated by John Southard (MIT OpenCourseware) via source content that was edited to the style and standards of the LibreTexts platform.

15.3: Why Deposition or Erosion?

Introduction

This section provides some background on the basic nature of deposition and erosion. Some of it might seem elementary to you, but a clear understanding of it is fundamental to a productive view of the nature of sediment deposition and erosion. In this section, I will use the terms **aggradation** for increase in bed-surface elevation during deposition, and **degradation** for decrease in bed-surface elevation during erosion.

A Broad View of Sediment Deposition

Take as broad a view of sediment deposition as possible (Figure 15.3.1): sediment is derived from a *source*, mobilized, transported along a transport path, and deposited somewhere, which you could think of a *sink*. This is simple and elegant—but there is much more here than you might assume, at first thought.

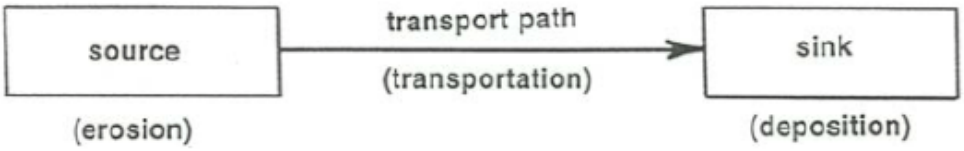


Figure 15.3.1: A broad view of sediment transport and deposition.

Sometimes the deposition is abrupt, as in the case of a Gilbert-style delta where a stream debouches into a lake Figured 15.3.2A). More commonly, deposition is gradual, in a spatial sense: it is spread out over a long distance. Figure 15.3.2B shows a common and important example.

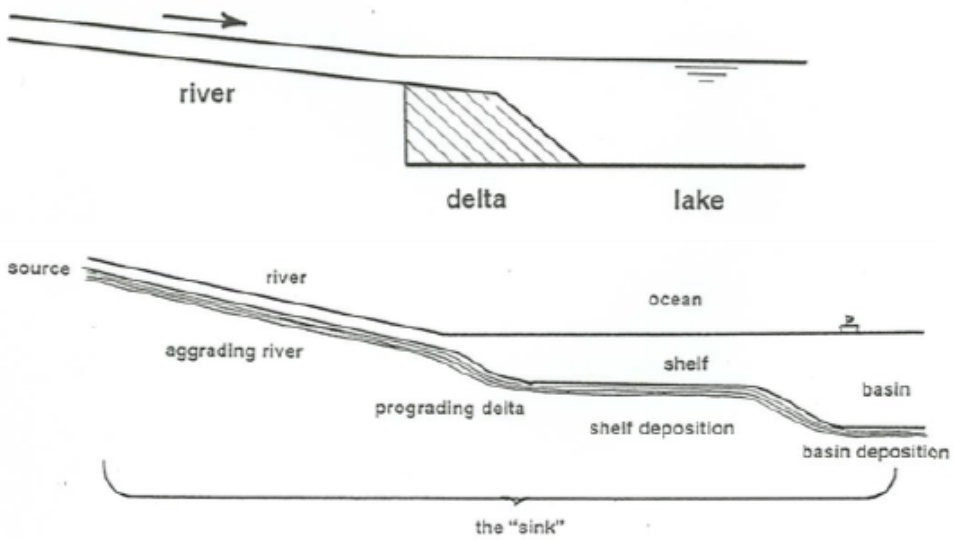


Figure 15.3.2: **A)** *(upper) A river enters and lake and builds a delta.* ***B)*** *(lower) Spatially gradual sediment deposition along a typical transport path.*

The Relationship Between the Load and the Deposit

This subsection makes some fundamental points about the relationship between the sediment load and the deposit in a

depositing flow. In my opinion, this material is fundamental to understanding the texture of a deposit, although it is not likely to tell you anything really practical.

Obviously (but importantly), whenever a deposit is being formed by a sediment-transporting flow, some percentage of the sediment load is being extracted from the flow and added to the bed, by one or more of the various processes discussed in the previous section. The ratio of sediment extraction to sediment passage or throughput can range from nearly zero, in the case of an almost uniform flow carrying fairly high concentrations of sediment in an almost nondepositional regime, to one hundred percent, when a flow dumps all its sediment in one place, as with certain kinds of debris flows. Just for convenience, I will call this ratio—unofficially—the **deposition ratio**. (Do not worry about how this ratio could be defined quantitatively.) Although you cannot read the value of the deposition ratio directly from beds in an outcrop, I think that it is one more of those things that are useful to think about as an aid in framing your interpretations.

This section deals with the relationship between the characteristics of the sediment load and the characteristics of the deposit left by the flow. As you learned back in Chapter 13, the sediment—whether in the substrate, in the active layer, on the bed surface, or in the sediment load—always has some joint probability distribution of particle size, particle shape, and particle density. You can never really characterize this distribution fully, even when you can obtain a good representative sample of the load, mainly because of the problem of the infinite variations in particle shape, but it is nonetheless real, and important.

When deposition takes place, some subset of the passing particles are selected from the flow to become part of the permanent deposit left behind by the flow. Here is what I consider to be the most fundamental question of sediment deposition: *How does the nature of the deposit depend upon the characteristics of the flow and the nature of the load?* If sedimentologists are ever going to be able to make interpretations about depositional conditions by examining the texture of the deposit, they are going to have to answer that question first.

The Active Layer

There is more to the selection process than might seem to you at first thought. First I would like to divide the sediment bed into two depth zones (Figure 15.3.3). The uppermost zone, extending some distance down from the bed surface, is called the **active layer**. The sediment in the active layer is subjected to repeated re-entrainment by the flow as the bed elevation at any given point rises and falls as a result of local erosion and deposition that is superimposed on the long-term net deposition. A good example of such temporary changes in bed elevation are those associated with the passage of bed forms. All the sediment within the active layer is recycled by the flow at least once by the flow before it is permanently buried. Below the active layer is the substrate, which might be called the **permanent deposit**. The sediment in the permanent deposit is below the reach of the local erosional processes of the flow, and it will never again be entrained by the flow unless the overall depositional regime changes into an overall erosional regime at some later time. (You thus have to take the word “permanent” to apply to a time that extends into the future only as far as the flow conditions remain fairly constant.)

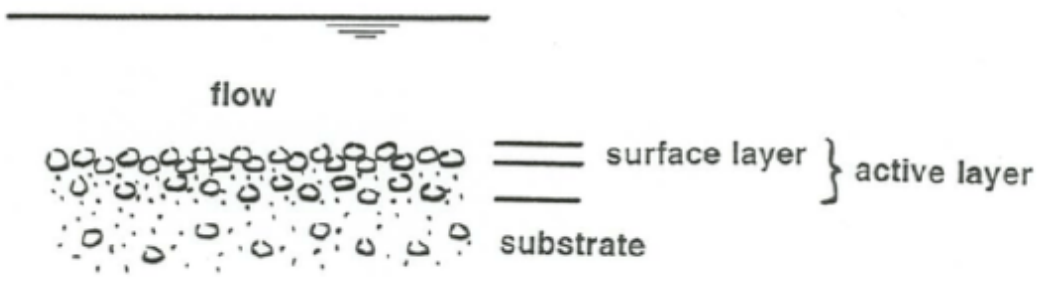


Figure 15.3.3: The surface layer, the active layer, and the substrate (the permanent deposit).

The thickness of the active layer may range from just several grain diameters, on an approximately planar bed undergoing aggradation, to many meters, when the bed is covered with very large bed forms that deposit and re- erode sediment as they move downstream.

When viewed in terms of the active layer, deposition therefore involves the burial of certain particles deeply enough within the active layer so that they are no longer moved by the flow again, whereupon they become part of the permanent deposit. During long-term aggradation at a point on the sediment bed, the active layer rises vertically, relative to some datum buried deeply in the substrate. Sediment particles are added to the active layer from the sediment load, by way of resting at least briefly on the bed

surface, and at the same time the base of the active layer rises upward through the deposit, as particles at the base of the active layer pass beyond the reach of the flow (or, in other words, as the probability of eventual re-entrainment by the flow becomes zero).

Fractionation

If we lived in a world of unisize (and "unishape" and "unidensity") sediment (a boring world, for sedimentationists!), then what has gone before in this section would be all that there is to it. In the real world, however, every sediment contains a range of particle sizes, shapes, and densities, as you have seen earlier in these notes. (Here, for convenience, I will refer to fractions in the three-dimensional joint frequency distribution of size, shape, and density as "SSD fractions".) This opens up the possibility of **fractionation**: the spatial segregation of different SSD fractions during transport and deposition.

The simplest kind of fractionation to understand is *lateral*: different SSD fractions can be deposited, or stored, along the "sides" of the transport path—as, for example, in overbank deposition in a river system. As a consequence, the SSF distribution of the transported sediment, which we might call the "throughput", evolves in the downstream direction.

Because only a subset of the particles of the load end up becoming part of the permanent deposit, there is the possibility of *fractionation* of the various SSD fractions between the load and the deposit. Obviously, such fractionation can take place only if there is some range of sizes, shapes, or densities in the load in the first place. But all natural sediments show at least some variation in size and shape.

The fractionation can be viewed as a multi-step process, from the load, to the bed surface, to the active layer, and finally to the permanent deposit. Figure 15.3.4 shows some general things about the course of this fractionation during deposition. The first step is fractionation between the load and the bed surface. As you saw in Chapter 13, most tractional flows the bed surface is coarser than the load, although that effect is most striking at weak transport rates and becomes much less at higher transport rates. The rest of the active layer, below the bed surface, is finer than the bed surface, but it can be either finer or coarser than the load. Although more work needs to be done, it seems clear that in weak flows the active layer as well as the bed surface is coarser than the load, but in strong flows carrying coarse sediment the active layer is actually finer than the load! The relationship between the active layer and the permanent deposit is still not well understood, but it does not represent the major effect in fractionation.

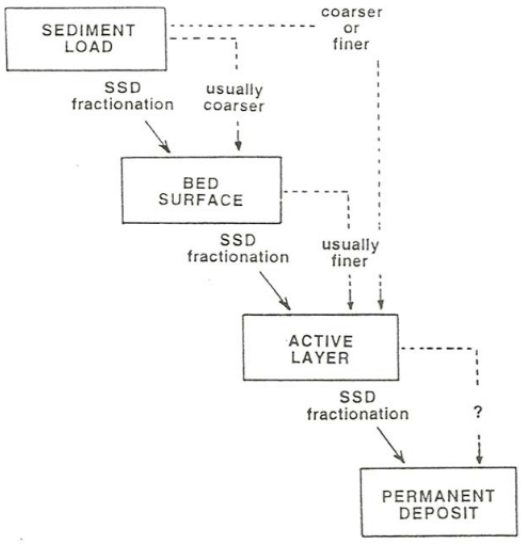


Figure 15.3.4: Steps in fractionation, from the sediment load to the permanent deposit.

In the strongest flows, with high concentrations of sediment traveling both as bed load and suspended load, the coarser particles less commonly find permanent resting places on the bed, so the deposit is much finer than the load. In weaker flows, on the other hand, under conditions not far above the threshold for particle transport, the mean size of the deposit is greater than the mean size of the load. One's first reaction is that the stronger the flow, the coarser the deposit. But just the opposite is true! (The qualification here is that we are considering a given supply of sediment that flows with a range of flow strength are constrained to carry.) Here is yet another example of how deduction or intuition can mislead us when it comes to the dynamics of sediment

transport by turbulent flows.

A Note on Degradation

Up to now in this chapter the focus has been on aggradation. Degradation is also important to consider, because in a succession of deposited sediment there might be thin intervals that represent periods of temporary degradation, and the nature of the SSD distribution in those intervals can be greatly different from the rest of the succession. In particular, density fractions that are more difficult for the flow to transport might become concentrated to form an economically important placer.

In the context of differential transport (see the earlier section on modes of deposition), if for whatever reason the sediment transport rate *increases* downstream in a given reach of the flow the bed elevation *decreases*, causing degradation. If the flow is able to transport all of the sediment that it encounters as it eats into the substrate, then the process can continue indefinitely, for as long as the large-scale changes that cause the degradation—like base-level lowering in a river—continue to operate. If the coarsest of the transported fractions are in the gravel size range, the bed is likely to be paved (see Chapter 13), but the coarser particles that constitute the pavement can be transported by the flow, and so, although the exact nature of the pavement might change with time, degradation can continue. If, however, during degradation the flow encounters size fractions that are so coarse that it cannot transport them, then the pavement evolves into armor, and degradation ceases.

This page titled 15.3: Why Deposition or Erosion? is shared under a CC BY-NC-SA 4.0 license and was authored, remixed, and/or curated by John Southard (MIT OpenCourseware) via source content that was edited to the style and standards of the LibreTexts platform.

16: CROSS STRATIFICATION

16.1: Stratification and Cross Stratification
16.2: The Nature of Cross Stratification
16.3: The Basic Idea Behind Climbing-Bed-Form Cross Stratification
16.4: Important Kinds of Climbing-Bed-Form Cross Stratification
16.5: Cross Stratification Not Produced by Climbing Bed Forms

This page titled 16: Cross Stratification is shared under a CC BY-NC-SA 4.0 license and was authored, remixed, and/or curated by John Southard (MIT OpenCourseware) via source content that was edited to the style and standards of the LibreTexts platform.

16.1: Stratification and Cross Stratification

I will probably be insulting your intelligence by pointing out that the term **texture** is commonly used in geology to apply to features of a sediment or a rock on the scale of individual particles, whereas the term **structure** is used for geometrical features on a scale much larger than particles. Stratification is one kind of sedimentary structure. A succinct way of defining **stratification** is *layering by sediment deposition*.

The nature and features of stratification in sedimentary rocks vary widely. This course focuses on aspects and features of stratification that are produced by physical processes. Chemical and biological processes are important for stratification as well, but they are outside the scope of this course.

You probably also know well that any individual layer in a sediment or a sedimentary rock that is produced by deposition is called a **stratum** (plural: **strata**). In terms of official terminology, a stratum that is less than one centimeter thick is called a **lamina** (plural: **laminae**), and a stratum that is greater than one centimeter thick is called a **bed** (plural: **beds**). Correspondingly, stratification is termed either lamination or bedding.

Stratification is manifested as differences in the nature of the deposit from stratum to stratum, in texture, and/or in composition, and/or even in sedimentary structures. Some features of stratification are immediately obvious—stratification is one of the most visible and striking features of sedimentary rocks—but some stratification is subtle, and requires care in observation. Lamination, in particular, is often subtle and delicate. Commonly, lamination is virtually invisible on fresh surfaces of sedimentary rocks but become apparent upon slight to moderate weathering of the surface. Likewise, lamination in well-sorted non-consolidated sands does not show up well on a cut and trimmed surface through the deposit until drying by the wind has etched some laminae more than others.

The focus of this part of the course is on physical stratification in the interior of strata. Transitions between successive strata in a succession of strata, when they are sharp, are usually caused by erosion, or at least nondeposition, before deposition of the overlying stratum. Such bounding surfaces have great significance in interpreting depositional conditions, but they are not considered in a systematic way in these course notes.

It is natural to think in terms of two kinds of physical stratification features within strata: *planar stratification* and *cross stratification*. Both are common features of sediments and sedimentary rocks. the present chapter deals with cross stratification; planar stratification is the topic of the following chapter.

The term **cross stratification** (often written with a hyphen: *cross-stratification*) is applied to any arrangement of strata that are locally inclined at some angle to the overall planar orientation of the stratification. That definition leaves some uncertainty about what is meant by the scales of “local” and “overall”, but that is usually not a problem in most instances of cross stratification. Cross stratification is commonly manifested as lamination, within a much thicker stratum, that is at least in some places at an angle to the bounding surface of the given thicker stratum. Corresponding to the official division of strata into beds and laminae, cross stratification can be classified as either **cross bedding** or **cross lamination**.

This page titled 16.1: Stratification and Cross Stratification is shared under a CC BY-NC-SA 4.0 license and was authored, remixed, and/or curated by John Southard (MIT OpenCourseware) via source content that was edited to the style and standards of the LibreTexts platform.

16.2: The Nature of Cross Stratification

Cross stratification varies enormously in geometry. This is presumably a reflection of the great diversity of bed configurations produced by fluid flows over loose beds of sediment.

More commonly than not, cross-stratified deposits are arranged as packets or **sets** of conformable laminae, planar or curving, that are separated from adjacent sets by erosional set boundaries or **truncation surfaces**. The laminae within the sets may be planar or curving. Concave-up laminae are more common than convex-up laminae. (You will see why in the course of this chapter.) The orientations of the truncation surfaces are usually different from the orientations of the laminae within the sets. Commonly the lateral scale of the sets may be not much greater than the vertical scale, or it may be much greater. Figure 16.2.1 shows two common varieties of cross stratification as seen in sections normal to the overall plane of stratification. In some cases, there are no truncation surfaces within the cross-stratified deposit; Figure 16.2.2 shows a common example.

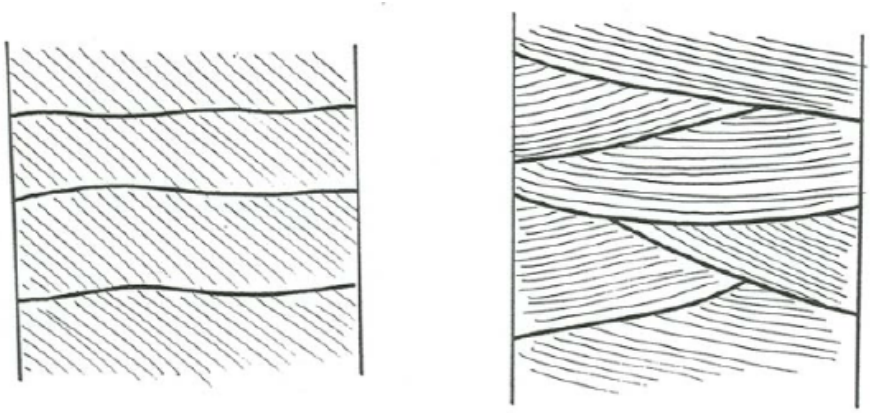


Figure 16.2.1: Two common varieties of cross stratification as seen in sections normal to the overall plane of stratification.

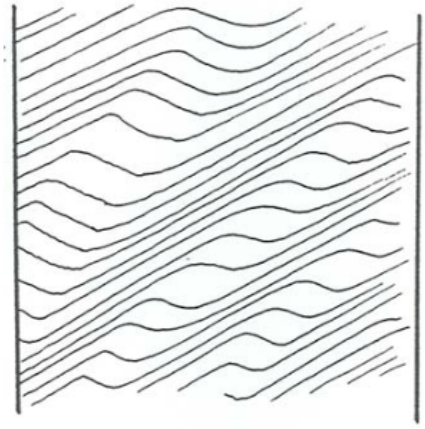


Figure 16.2.2: A common example of a cross-stratified deposit with no truncation surfaces.

In a given local volume of cross-stratified deposit, the geometry of cross stratification commonly looks different in differently oriented sections normal to the overall plane of stratification. I will use the unofficial term *anisotropic* for such cross stratification. Figure 16.2.3 is a common example. Usually in such cases the cross laminae have a preferred direction of dip. (Note that the cross stratification on the two faces of the block shown in Figure 16.2.3 are the same as those used in Figure 16.2.1, which you might have thought were entirely unrelated.) If the geometry of cross stratification looks about the same in differently oriented sections, I will use the unofficial term *isotropic*.

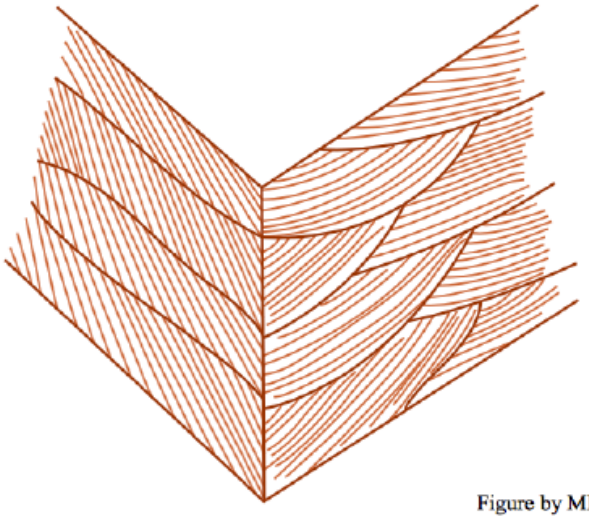


Figure 16.2.3: *A common example of anisotropic cross-stratification.*

Often a given cross-stratified bed may represent not just one depositional event but two or more separate depositional events, each one superimposed on the previous one. Such beds are said to be **amalgamated**. Sometimes it is easy to recognize the individual depositional events within the amalgamated bed; the stratification within each part of the bed can then be studied separately. But sometimes it is difficult to determine whether or not the bed is amalgamated.

Some General Points about Interpretation

In analogy with problems in geophysics, you might think in terms of the *forward problem* and the *inverse problem*. The forward problem in interpreting cross stratification that is generated by the movement of bed forms (arguably the most common kind) is that the flow generates moving bed forms, and the movement of the bed forms, together with a zero or nonzero rate of overall net aggradation of the bed, generates the stratification geometry (Figure 16.2.4A). The inverse problem is more difficult (Figure 16.2.4B): you start with the observed geometry of stratification and attempts to reconstruct the time history of bed geometry that generated that stratification. Then you attempt to reconstruct the flow conditions which were responsible for that time history of bed geometry.

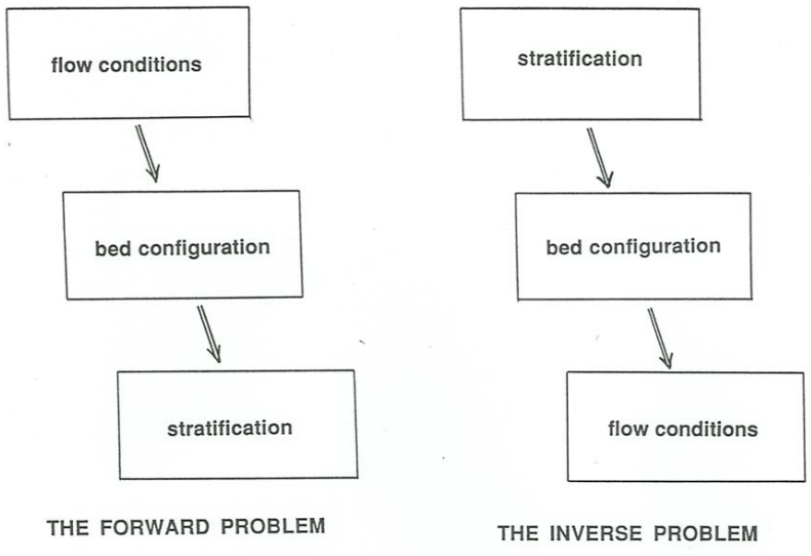


Figure 16.2.4: **A)** The forward problem and **B)** the inverse problem in interpreting cross stratification.

The difficulties in the inverse problem are that

1. Nature does not give us time markers in the deposit, so *information on time is lost* in the generation of cross stratification, and
2. In most cases some of the earlier-deposited sediment is eroded later as the cross stratification develops, so *information on bed geometry is lost*.

One way of circumventing the need to solve the difficult first step in the inverse problem (reconstructing the bed geometry from the stratification geometry) would be to have a complete catalog of the stratification geometries that are developed as a function of flow conditions and net aggradation rate (Figure 16.2.5). One could then mindlessly compare the observed example of cross stratification with the patterns in the catalog to find the set of conditions that must have produced the observed example. There are two serious problems with this approach, though:

1. We could never catalog all of the possible combinations of flow and aggradation rate; and
2. Two or more rather different sets of conditions of flow and aggradation rate might produce very similar geometries of cross stratification.

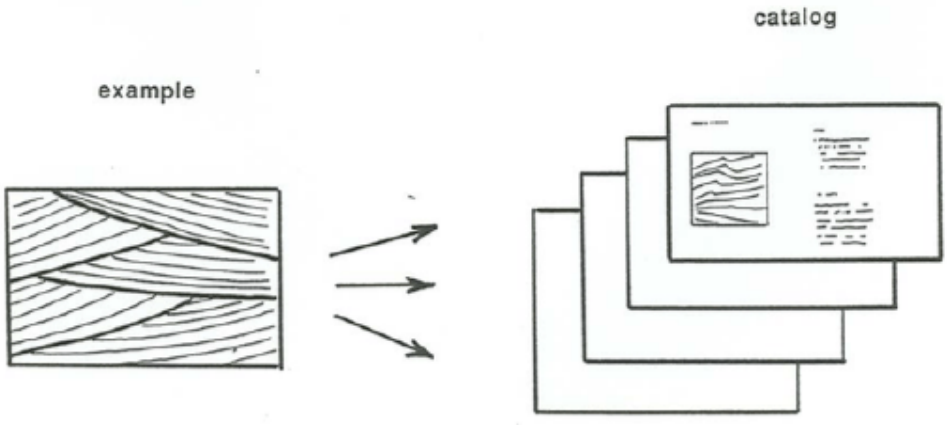


Figure 16.2.5: Catalog of stratification geometries that are developed as a function of flow conditions and net aggradation rate.

When you are on the outcrop it is valuable to try to develop an idea of the bed configuration that was responsible for an observed cross-stratification geometry. That would be an incomplete task, however, even if you were able to carve the outcrop into thin slices to obtain a complete three-dimensional picture of the geometry. (Only in certain semi-lithified deposits can that actually be done without a lot of difficulty.) The best you can do is to obtain some partial ideas by examining the available faces of the outcrop. Those ideas are certain to be useful in developing an interpretation, but they are unlikely to give you anything near a complete picture of the cross-stratification geometry.

In actual practice, the sedimentologist on the outcrop relies upon certain widely accepted models for the development of cross stratification. (But keep in mind that not all cross stratification fits naturally into the available models.) Recall from the section on bed configurations that there are a small number of important bed phases (distinctive kinds of bed configuration), like unidirectional-flow ripples or dunes, or small two-dimensional oscillation ripples, or large three- dimensional oscillation ripples. Each of these bed phases is associated with some distinctive range of conditions of flow and particle size. Such a range of conditions is expressed graphically as the stability region a given bed phase occupies in some appropriate bed-phase graph.

The models are based on what is known empirically, by observations in flumes or natural flows, about the relationship between the bed phase and the cross stratification. The hope for the future is that, as our base of such observations increases, we can make more and more specific interpretations, but the fact remains that at the present time the interpretations can seldom be very specific. The need for careful laboratory and field studies of the stratification produced by definite combinations of flow conditions and net aggradation rate is still great.

The next section is a fairly detailed analysis of what is probably the most common and important kind of cross stratification: that produced by the movement of bed forms while the bed as a whole is undergoing net aggradation, slow or fast. Cross stratification of that kind is common in unidirectional flows of both water and air, and also in combined flows of water, and even in purely oscillatory flows of water, because, even in purely oscillatory flows, even slight asymmetry of the oscillation causes the bed forms to shift laterally at non-negligible rates. I will unofficially term cross stratification of this kind **climbing-bed-forms cross stratification**. Bed forms are said to *climb* when there is overall aggradation of the sediment bed while the bed forms are moving; see a later section for details.

This page titled 16.2: The Nature of Cross Stratification is shared under a CC BY-NC-SA 4.0 license and was authored, remixed, and/or curated by John Southard (MIT OpenCourseware) via source content that was edited to the style and standards of the LibreTexts platform.

16.3: The Basic Idea Behind Climbing-Bed-Form Cross Stratification

In general terms, the fundamental idea about cross stratification is easy to state (Figure 16.3.1): as bed forms of one kind or other pass a given point on the bed, both the bed elevation and the local bed slope change with time. Consider a short time interval during the history of decrease and increase in bed elevation. After a temporary minimum in bed elevation is reached, deposition of new laminae takes place for a period of time, until a temporary maximum in bed elevation is reached. Then, as the bed elevation decreases again, there is complete or partial erosion of the newly deposited laminae and formation of a new truncation surface. After the next minimum in bed elevation, another set of laminae is deposited.

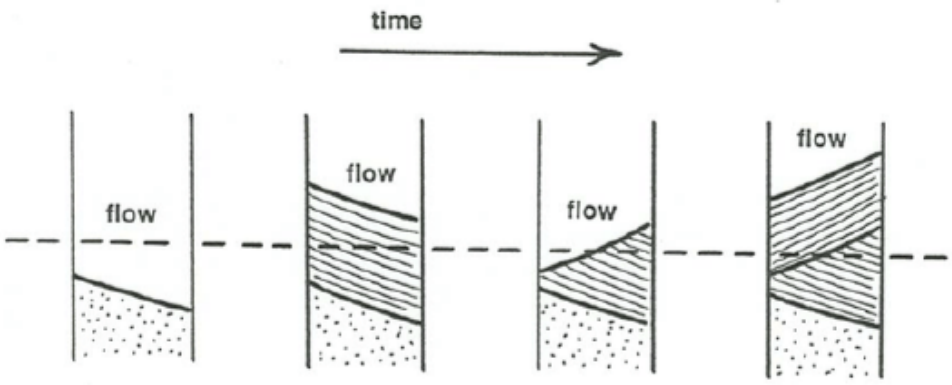


Figure 16.3.1: The fundamental idea about cross stratification.

The preceding paragraph is still too general to give you a concrete idea about how moving bed forms generate cross stratification. Now I will be more specific. Take as an example a train of downstream-moving ripples in unidirectional flow. (The picture would be similar for dunes.) Each ripple moves slowly downstream, generally changing in size and shape as it moves. Sediment is stripped from the upstream (stoss) surface of each ripple and deposited on the downstream (lee) surface.

In your imagination, cut the train of ripples by a large number of vertical sections parallel to the mean flow direction (Figure 16.3.2). The trough of a ripple is best defined by the curve formed by connecting all of the low points on these vertical sections where they cut the given trough (Figure 16.3.3). This curve, which I will unofficially call the **low-point curve**, is generally sinuous in three dimensions. The low-point curve moves downstream with the ripples, and it changes its shape as it moves, like a writhing dragon, because trough depths and ripple speeds change with time.

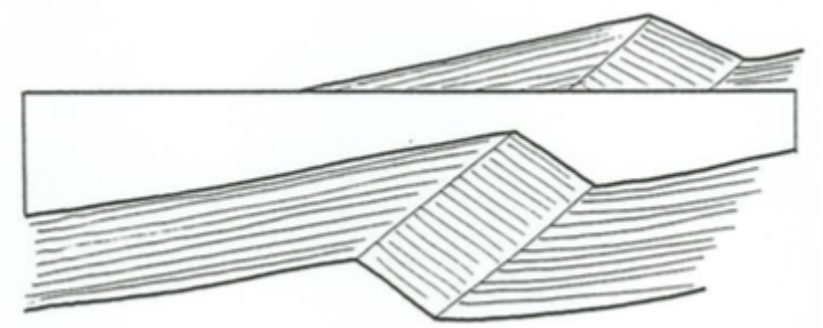


Figure 16.3.2: Cutting the train of ripples by a large number of vertical sections parallel to the mean flow direction.

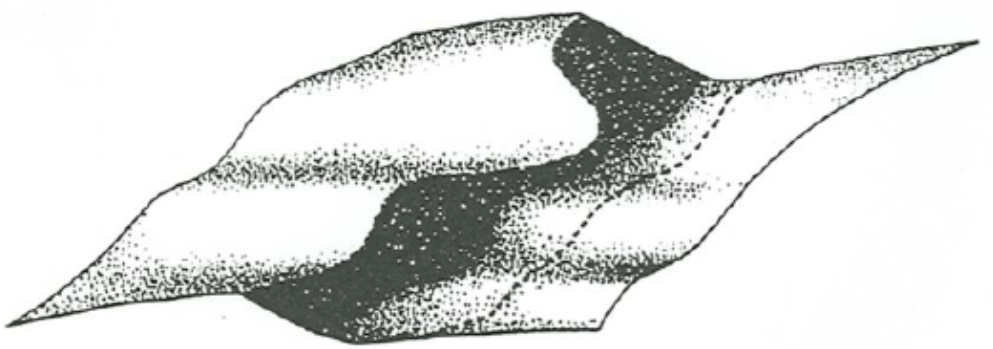


Figure 16.3.3: The trough of a ripple is best defined by the curve formed by connecting all of the low points on these vertical sections where they cut the given trough.

As the low-point curve shifts downstream, it can be viewed as having the effect of a cheese-slicing wire: it seems to shave off the body of the ripple immediately downstream for removal by erosion, and in that way it prepares an undulating floor or surface for the deposition of advancing foresets by the ripple immediately upstream.

Depending on flow conditions and sediment size, the foreset laminae laid down by an advancing ripple vary widely in shape, from almost perfect planes sloping at the angle of repose, to sigmoidal curves that meet the surface of the trough downstream at a small angle (Figure 16.3.4). Whatever their shape, these laminae are always deposited directly on the erosion surface that is formed, as just described above, by the downstream movement of the ripple trough into which the foresets prograde.



Figure 16.3.4: Geometries of foreset laminae.

If no new sediment is added to the bed while the ripples move, the average bed elevation does not change with time, and the invisible plane that represents the average bed surface stays at the same elevation. On the average, the foresets deposited by a given ripple are entirely eroded away again as the next trough upstream passes by (Figure 16.3.5). If new sediment is added everywhere to build the bed upward, however, the ripples no longer move parallel to the plane of the average bed surface but instead have a component of upward movement (Figure 16.3.6). The resultant direction of ripple movement is described by the **angle of climb**, denoted by θ in Figure 16.3.6. The tangent of θ is equal to the average rate of bed aggradation divided by the ripple speed.

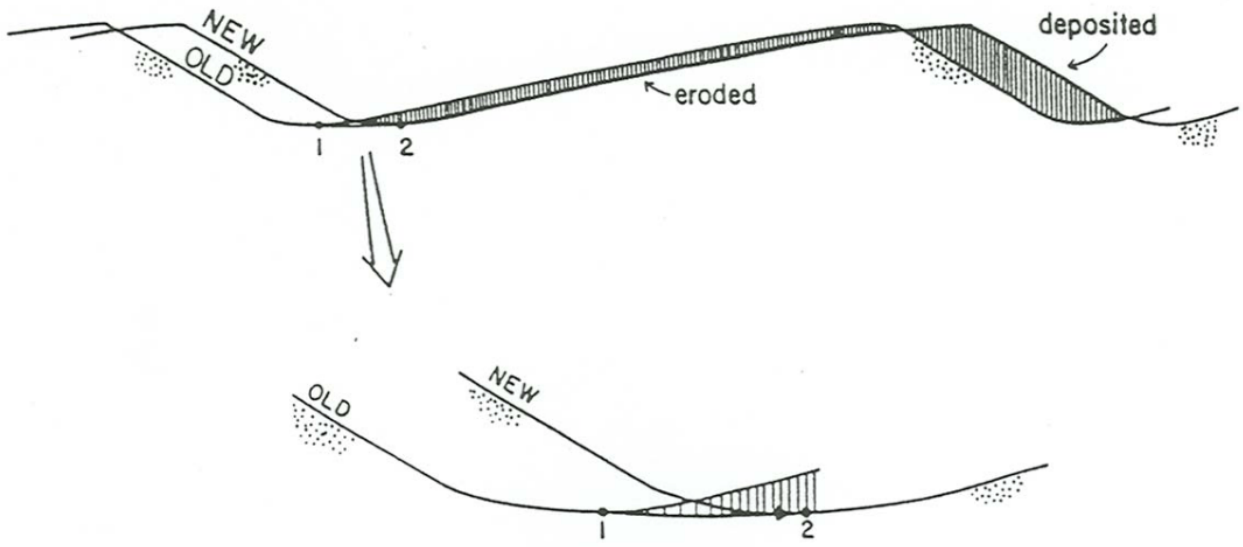


Figure 16.3.5: On average, the foresets deposited by a given ripple are entirely eroded away again as the next trough upstream passes by.

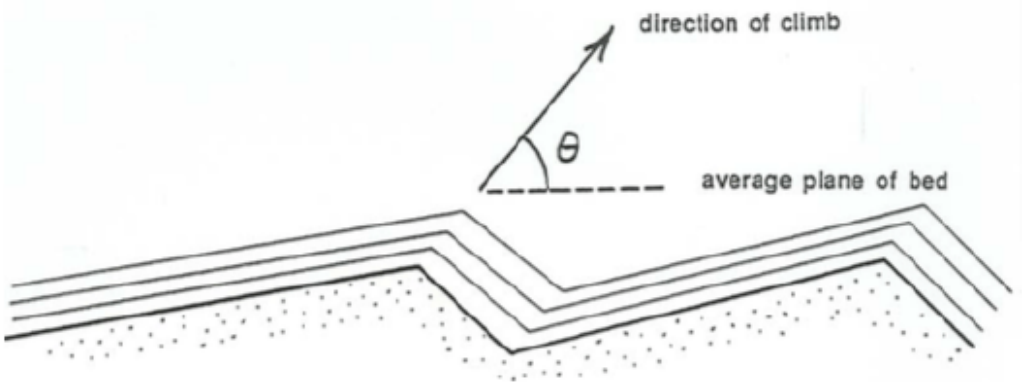


Figure 16.3.6: Climb of ripple-shaped bed forms.

As the ripples climb in space, as described above, their troughs climb with them, so the erosion surface associated with the downstream movement of the low-point curve in a given trough passes above the erosion surface that was formed when the preceding trough passed by. The lowest parts of the foresets deposited by the ripple that was located between those two troughs are then preserved rather than eroded entirely (Figure 16.3.7). This remnant set is bounded both above and below by erosion surfaces.

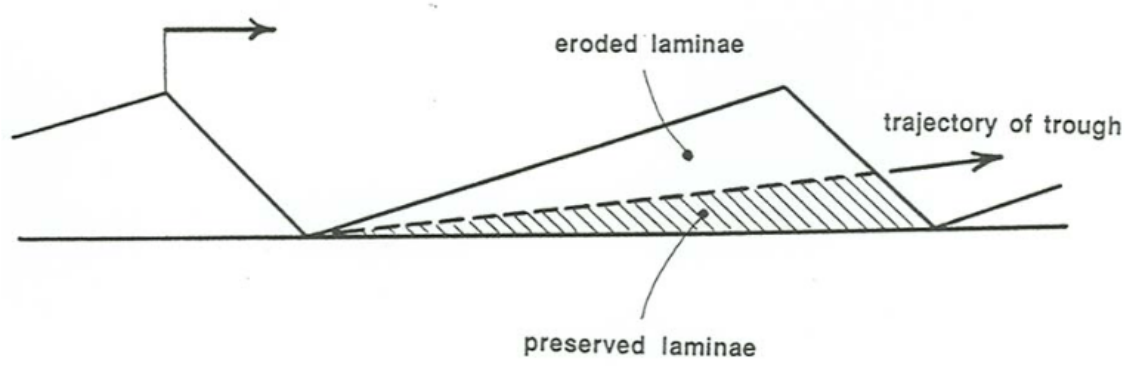


Figure 16.3.7: Partial preservation of ripple foresets as ripples climb at a small angle.

Figure 16.3.8 shows cross stratification in an ideally regular deposit produced by low-angle climb of a train of ripples. The heavy lines are erosion surfaces, and the light lines are foreset laminae. The profile of the ripple train as it existed at a given time is shown also. The upper parts of each ripple in the train, underneath the dashed part of the profile, were eliminated by later erosion. In real cross-stratified deposits of this kind, the erosion surfaces are irregularly sinuous because trough geometry changes with time, and the sets tend to pinch out both upstream and downstream because the ripples exist for only a finite distance of movement.

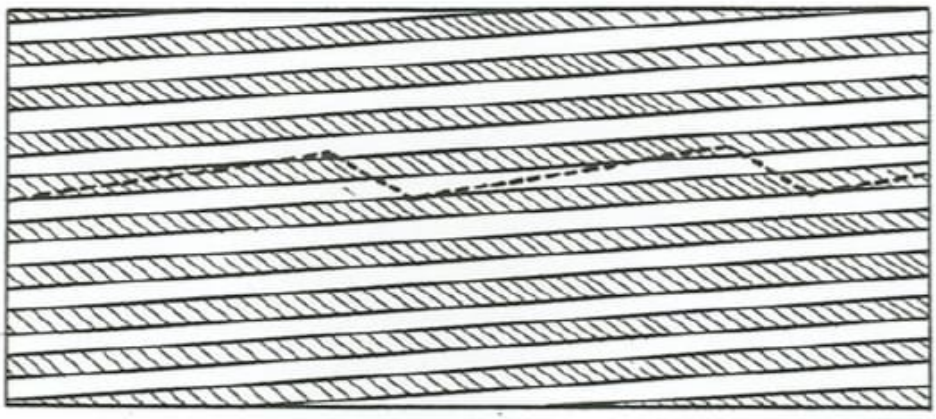


Figure 16.3.8: Erosional-stoss climbing-ripple cross stratification. For clarity, cross laminae are drawn in only half of the cross sets.

It is significant that what is most important in determining the geometry of this kind of cross-stratification is the geometry of the bed forms in the *troughs*, not near the *crests*. I should also point out that the height of the sets is always less than the height of the bed forms that were responsible for the cross stratification. If you compare the height of the cross sets with the height of the ripples in the dashed profile in Figure 16.3.8, you can see that for low angles of climb the set height is only a small fraction of the bed-form height.

The larger the angle of climb, the greater the fraction of foresets preserved. If the angle of climb of the ripples is greater than the slope angle of the stoss side of the ripples, then laminae are preserved on the stoss sides as well as on the lee sides, and the full profile of the ripple is preserved (Figure 16.3.9). This happens when the rate of addition of new sediment to the bed is greater than the rate at which sediment is transported from the stoss side to the lee side of the ripple. The differences in geometry between Figure 16.3.8 and Figure 16.3.9 seem great, but keep in mind that the differences in environmental conditions are not large. The only difference is in the value of the angle of climb.

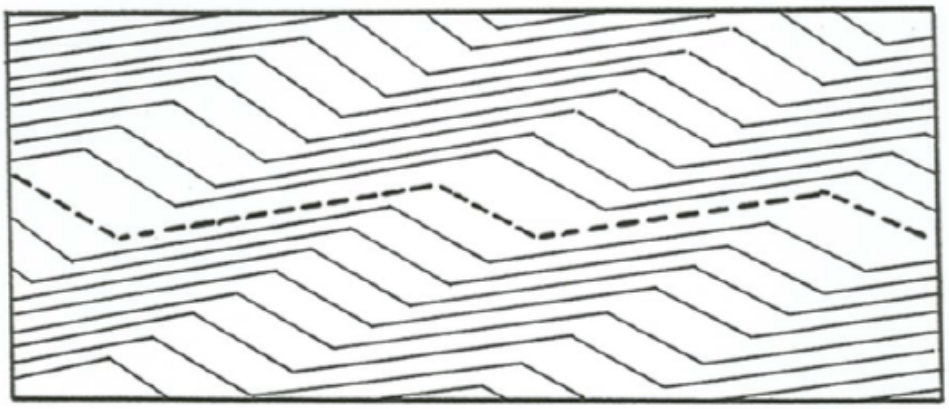


Figure 16.3.9: Depositional-stoss climbing-ripple cross stratification.

The lamination produced when ripples move with a positive angle of climb is called **climbing-ripple cross stratification**. Examples with angle of climb so small that the contacts between sets are erosional (as in Figure 16.3.8) might be called **erosional-stoss** climbing-ripple cross stratification, and examples with angle of climb large enough for preservation of the full ripple profile (as in Figure 16.3.9) might be called **depositional-stoss** climbing-ripple cross stratification.

Here is a recapitulation of some of the important points in this section. Cross stratification is formed by the erosion and deposition associated with a train of bed forms as the average bed elevation increases by net addition of sediment to some area of the bed. The angle of climb of the ripples depends on the ratio of rate of bed aggradation to speed of ripple movement. At high angles of climb, the entire ripple profile is preserved, and there are no erosion surfaces in the deposit. At low angles of climb, only the lower parts of foreset deposits are preserved, and the individual sets are bounded by erosion surfaces. The general nature of such stratification is common to moving bed forms of all sizes, from small current ripples to extremely large subaqueous or eolian dunes. Important differences in the details of stratification geometry arise from differences in bed-form geometry and how

it changes with time.

This page titled 16.3: The Basic Idea Behind Climbing-Bed-Form Cross Stratification is shared under a CC BY-NC-SA 4.0 license and was authored, remixed, and/or curated by John Southard (MIT OpenCourseware) via source content that was edited to the style and standards of the LibreTexts platform.

16.4: Important Kinds of Climbing-Bed-Form Cross Stratification

Introduction

Here I will present the substance of what the major kinds of cross stratification in the sedimentary record look like. They conveniently fall into (1) **unidirectional-flow cross stratification**, on a small scale corresponding to ripples and on a larger scale corresponding to dunes, and (2) **oscillatory-flow cross stratification**. Unfortunately there is little I can say at present about **combined-flow cross stratification**. I will make a few comments about that in the section on oscillatory-flow cross stratification.

Small-Scale Cross Stratification in Unidirectional Flow

Small-scale cross stratification formed under unidirectional flow is associated almost entirely with the downstream movement of current ripples. In accordance with the discussion of how moving bed forms produce cross-stratified deposits, discussed above, the general features of the cross stratification geometry depend on

1. The geometry of the ripples themselves, as well as how that geometry changes with time as the ripples move, and
2. The angle of climb.

For small angles of climb, the general geometry of the cross-stratified deposit is shown by the block diagram in Figure $16.4.1$. In addition to the actual rippled surface, Figure $16.4.1$ shows a flow-parallel section and a flow-transverse section perpendicular to the overall bedding. Figure $16.4.1$ is the real-life counterpart of Figure 16.3.8.

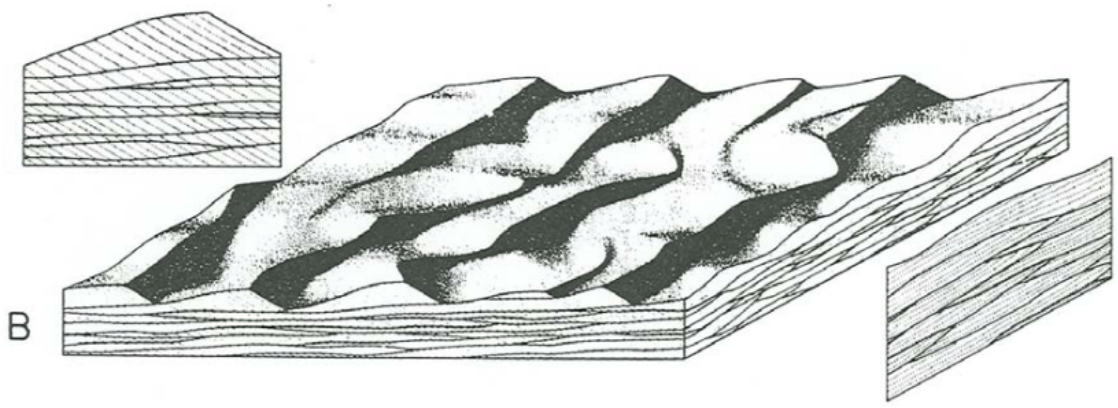


Figure $16.4.1$: Block diagram showing the geometry of climbing-ripple cross stratification produced at small angles of climb.

In sections parallel to flow (Figure $16.4.1$) you see sets of laminae dipping mostly or entirely in the same direction (which is the flow direction), separated by truncation surfaces. The height of the sets is seldom greater than $2–3\ \mathrm{cm}$, because it is always some fraction of the ripple height, which itself is seldom greater than $2–3\ \mathrm{cm}$. The set boundaries are sinuous and irregular, because of the changes in the ripples as they move. Sets are commonly cut out at some point in the downstream direction by the overlying truncation surface. This is a reflection of either (1) locally stronger erosion by a passing ripple trough or (2) disappearance of a given ripple as it moved downstream, by being overtaken or absorbed by another faster-moving ripple from upstream. New sets also appear in the downstream direction, reflecting the birth of a new ripple in the train of ripples.

In sections transverse to flow, the geometry of cross stratification is rather different (Figure $16.4.1$): you see nested and interleaved sets whose lateral dimensions are usually less than something like five times the vertical dimension. Each set is truncated by one or more truncation surfaces. These truncation surfaces are mostly concave upward. The laminae within each set are also mostly concave upward, but the truncation surfaces generally cut the laminae discordantly.

The key to understanding this cross-stratification geometry lies in the geometry of ripple troughs and the trough-filling process. Recall from Chapter 12 that fully developed current ripples have strongly three-dimensional geometry, and an important element

of that three-dimensional geometry is the existence of locally much deeper hollows or swales or depressions in ripple troughs, where the separated flow happens to become concentrated (because of the details of the ripple geometry upstream) and where scour or erosion is much stronger. As one of these swales shifts downstream, driven by the advancing ripple upstream, it carves a rounded furrow or trench, oriented parallel to the flow, which is then filled with scoop-shaped or spoon-shaped laminae that are the foreset deposits of the upstream ripple. Eventually the resulting set of laminae is partly or mostly or even entirely eroded by the passage of a locally deeper swale in some later ripple trough. This accounts for both the geometry of the sets and their irregular interleaving.

On the rare occasions when you are able to see a planar section through the deposit parallel to the overall stratification, you see a geometry that looks like Figure 16.4.2, which shows the truncated edges of sets of laminae that are strongly concave downstream, separated laterally by truncation surfaces. This has been called **rib and furrow** (not a very descriptive term). It is an excellent paleocurrent indicator.

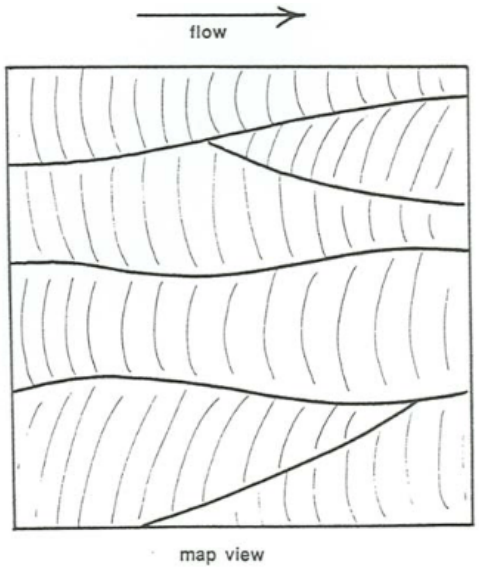


Figure 16.4.2: Planar section through a deposit of climbing-ripple cross stratification, parallel to the overall plane of stratification.

For large angles of climb, the general geometry of the cross-stratified deposit is shown by the block diagram in Figure 16.4.3. In addition to the actual rippled surface, Figure 16.4.3 shows a flow-parallel section and a flow-transverse section perpendicular to the overall bedding. Compare Figure 16.4.3 with Figure 16.4.1.

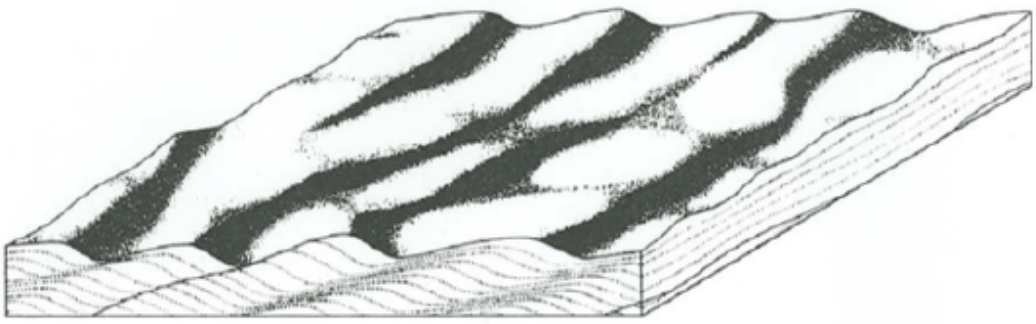


Figure 16.4.3: Block diagram showing geometry of climbing-ripple cross stratification produced at large angles of climb.

In sections parallel to flow, you see mostly continuous laminae whose shapes reflect the profiles of the ripples that were moving downstream while sediment was added to the bed. The local angles of climb vary from place to place in the deposit, because the speeds of the ripples are highly variable in time. So unless the overall angle of climb is very high, there are likely to be a few discontinuous truncation surfaces, where a particular ripple moved temporarily at a speed much greater than average.

In sections transverse to flow, you usually see just irregularly sinuous laminae that reflect the changing flow-transverse profiles of the ripples as they passed a given cross section of the flow.

Keep in mind that for intermediate angles of climb the stratification geometry is intermediate between the two end members presented above. As the angle of climb increases, the density and extent of truncation surfaces bounding the sets decreases, and the average set thickness increases.

For a given sand size, current ripples in equilibrium with the flow do not vary greatly in either size or geometry with flow velocity, so unfortunately there is little possibility of using the details of stratification geometry to say anything precise about the flow strength.

Large-Scale Cross Stratification in Unidirectional Flow

Large-scale cross stratification formed under unidirectional flow is associated mostly with the downstream movement of dunes. Again the general features of the cross-stratification geometry depend on the geometry of the dunes and the angle of climb.

Recall from Chapter 12 that dunes formed at relatively low flow velocities have a tendency to be two-dimensional: their crests and troughs are nearly continuous and fairly straight, and the elevations of the crests and troughs are nearly uniform in the direction transverse to flow. On the other hand, at relatively high flow velocities the dunes are moderately to strongly three-dimensional, in much the same way that ripples are three-dimensional. You should expect the geometry of cross stratification to vary greatly depending on whether the dunes were two-dimensional or three-dimensional.

Three-dimensional dunes produce cross stratification that is qualitatively similar in geometry to the small-scale cross stratification produced by ripples. You might reread the earlier section and apply it to the stratification produced by three-dimensional dunes.

Figure $16.4.4$ is a block diagram of cross stratification produced by three-dimensional dunes in unidirectional flows. It shows the dune-covered bed surface and sections perpendicular to the overall plane of stratification and parallel and transverse to the flow direction. Most of what I said about the analogous section in Figure $16.4.1$ for cross stratification produced by ripples at low angles of climb is applicable to Figure $16.4.4$ as well. Set thickness ranges from less than $10\ \mathrm{cm}$ to as much as a few meters.

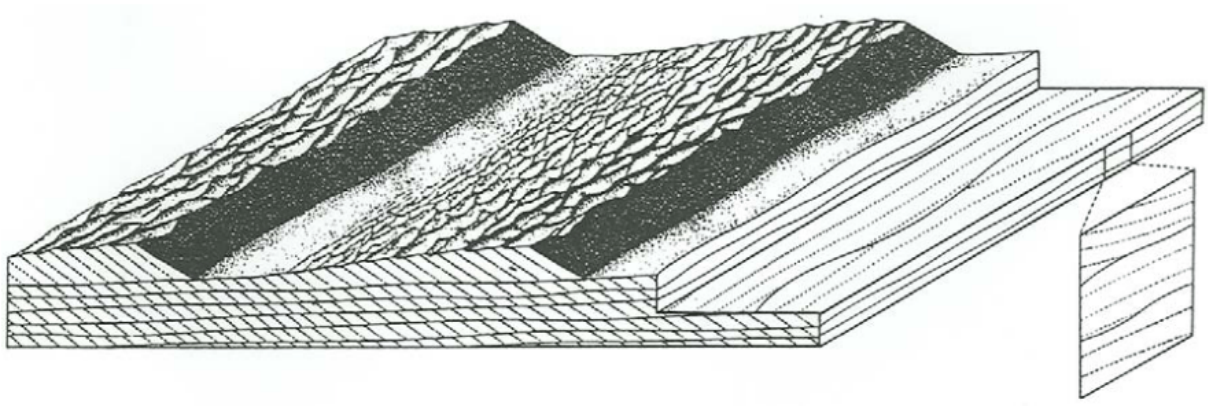


Figure $16.4.4$: Block diagram of cross stratification produced by almost perfectly two-dimensional dunes in unidirectional flows.

Figure $16.4.4$ is a corresponding block diagram of cross stratification produced by almost perfectly two-dimensional dunes in unidirectional flows. The stratification geometry is rather different from that in Figure $16.4.3$: in flow- parallel sections the sets extend somewhat farther and the set boundaries are less sinuous, but the greatest difference is in flow-transverse sections, where both the sets and the truncational set boundaries are much more extensive and show much less upward concavity. This is because of the absence of locally strong scour swales in the troughs of the dunes.

There is a whole spectrum of intermediate cases for which the cross- stratification geometry is less regular than the extreme case shown in Figure $16.4.5$ but not as irregular as in Figure $16.4.4$.

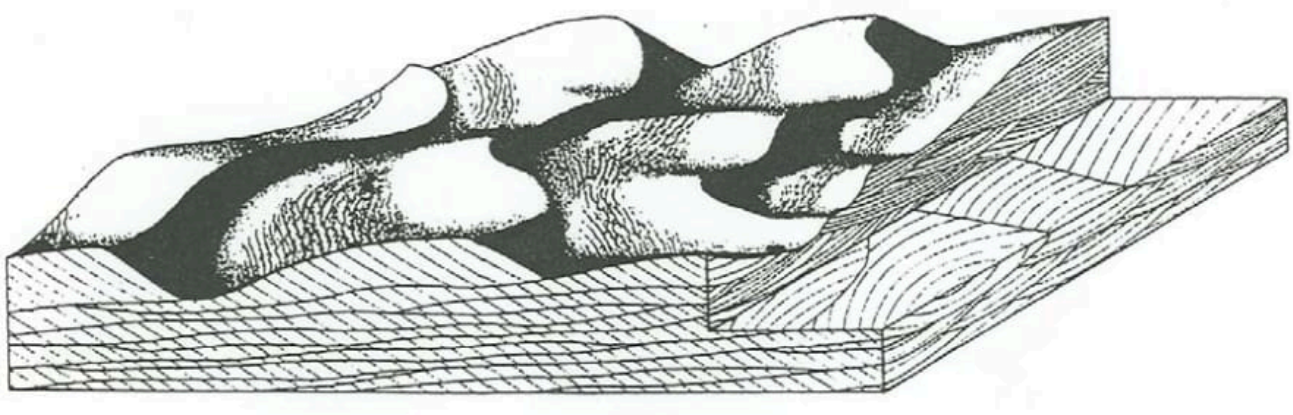


Figure 16.4.5: Block diagram of cross stratification produced by three-dimensional dunes in unidirectional flows.

In both Figure 16.4.4 and Figure 16.4.5, the angle of climb of the dunes is very small. Dunes sometimes climb at higher angles, but that is not nearly as common as for ripples, because it is uncommon for fairly coarse sediment to be settling abundantly out of suspension over large areas to build up the bed rapidly. In the very few cases I have seen, the geometry of cross stratification is very much like that shown in Figure 16.4.3.

Telling Bed-Form Size from Erosional-Stoss Climbing-Bed-Form Cross Stratification

From depositional-stoss climbing-bed-form cross stratification, you can find both the height and the spacing of the bed forms by direct measurement. With the more common erosional-stoss climbing-bed-form cross stratification, however, it is much more difficult to get an idea of either the height or the spacing of the bed forms, because their profiles are not directly reflected in the geometry of the cross stratification.

If you know, independently, the orientation of the overall plane of stratification—which you also cannot read from the geometry of the cross stratification itself, but which you might know from the upper and lower contacts of the cross-stratified bed—then in theory you can find the spacing by use of the simple equation

$$L = \frac{T}{\sin \theta} \tag{16.4.1}$$

where L is the bed-form spacing, T is the thickness of cross sets, measured perpendicular to the set boundaries, and θ is the angle of climb. (I invite you to try to derive this equation for yourself; it is not difficult to derive, by use of some trigonometry.) Figure 16.4.6 is a sketch that shows these variables, and the geometry of the climbing-ripple cross stratification. The trouble with Equation 16.4.1 is that it is applicable only when the cross sets are fairly regular in their thickness.

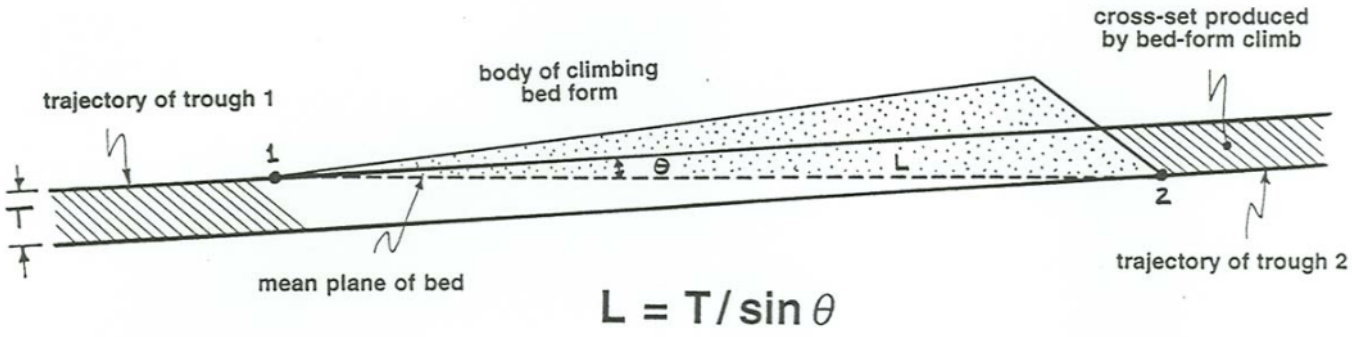


Figure 16.4.6: Sketch to aid in analysis of the problem of telling bed-form spacing from angle of climb and cross-set thickness.

That leads us to the problem of how to estimate the bed-form height from the preserved cross stratification. It should make good sense to you that, in a qualitative way, for a given bed-form size the smaller the angle of climb, the smaller the percentage of bed-form height represented by the set thickness. You can derive an equation similar to Equation 16.4.1 for bed-form height as a

function of set thickness and angle of climb, but it is more complicated, because the solution depends on the angle of the stoss slope and the angle of the lee slope as well as on T and θ:

$$H = \frac{T \tan \alpha \tan \beta}{\sin \theta (\tan \alpha + \tan \beta)} \tag{16.4.2}$$

But for an angle-of-repose lee slope (about 30°) and a stoss slope of between ten and fifteen degrees, Equation 16.4.2 specializes to

$$H \cong 0.15 \frac{T}{\sin \theta} \tag{16.4.3}$$

But all of the above applies only to regular bed forms climbing regularly. That is usually not the case, because, as you saw in Chapter 12, both large-scale and small-scale bed forms in unidirectional flow can be very irregular. In particular, the depth of scour in the troughs can vary greatly from place to place and from time to time, with the result that the sets vary greatly in thickness when viewed in flow-parallel section. Then the average set thickness is greater than given by Equations 16.4.2 or 16.4.3. You can appreciate that qualitatively just by realizing that, even at zero angle of climb, bed forms with temporarily deep troughs must leave thick, but localized, sets of cross-laminae. Paola and Borgman (1991) have calculated that, for bed forms with essentially random variability of trough depth, the average set thickness is only slightly less than the average bed- form height and is not very sensitive to the angle of climb. If you were able to measure the "negative" thickness of lamina sets now gone forever by erosion, they would balance out the "positive" thickness of the preserved lamina sets—but we see only the "positive" thickness, not the "negative thickness.) For bed forms that have elements of both regularity and randomness, the truth would lie somewhere in between the two approaches noted above. That does not help much in concrete situations, but it is the best we can do at this stage in our understanding. Figure 16.4.7 shows the two end-member cases of extreme regularity and extreme randomness in erosional-stoss bed-form climb.

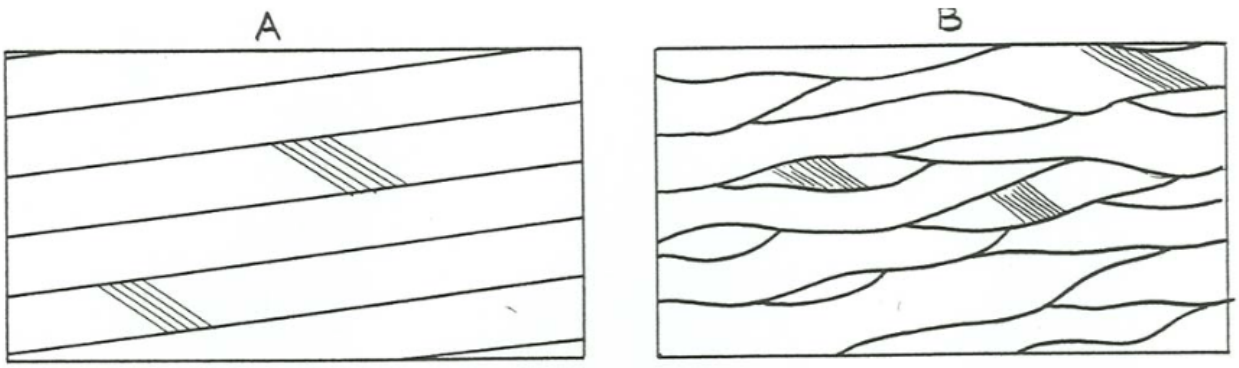


Figure 16.4.7: Erosional-stoss climbing-bed-form cross stratification produces by **A)** perfectly regular bed forms and **B)** bed forms that vary essentially randomly in trough depth with time.

Cross Stratification Produced by Antidunes

Antidunes do produce cross-stratification, but the lamination tends to be obscure, so the preservation potential is low. A number of studies in laboratory flumes (Jopling and Richardson, 1966; Hand, 1969, 1974; Shaw and Kellerhals, 1977; Cheel, 1990; Alexander et al., 2001) and in ancient sedimentary deposits (Walker, 1967; Hand et al., 1969; Skipper, 1971; Schmincke et al., 1973; Prave and Duke, 1990; Yagishita, 1994; Massari, 1996) have revealed or interpreted the existence of such stratification.

Cross Stratification in Oscillatory Flow

Recall from Chapter 12 that in truly symmetrical oscillatory flow at low to moderate oscillation periods and low to moderate oscillation speeds the bed configuration is symmetrical two-dimensional oscillation ripples. Under these conditions, the sediment transport is also strictly symmetrical in the two flow directions. You might expect the ripples to remain in one place indefinitely. Then, if sediment is supplied from suspension to build up the bed, symmetrical oscillation-ripple cross stratification with vertical climb would be produced (Figure 16.4.8). Although stratification of this kind is present in the sedimentary record, it is not common, presumably because even in purely oscillatory flow there is usually a minor degree of asymmetry of sediment transport, which

causes the ripples to move slowly in one direction or the other.

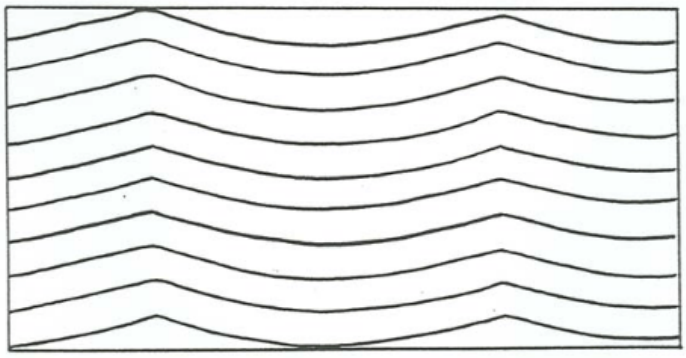


Figure 16.4.8: Cross stratification produced by vertical climb of symmetrical oscillation ripples.

Figure 16.4.9 is an attempt to account for types of oscillatory-flow cross stratification produced by the buildup of two-dimensional oscillation ripples as a function of the slow net rate of ripple movement and the rate of aggradation of the bed. Along the vertical axis, for zero ripple movement, is symmetrical oscillation-ripple cross stratification, of the kind that I mentioned above might be expected on the basis of deduction. The chevron-like interleaving of laminae at the ripple crests, shown schematically, results from minor shifts in crest position back and forth during aggradation. This is shown by the first box from the top in Figure 16.4.9.

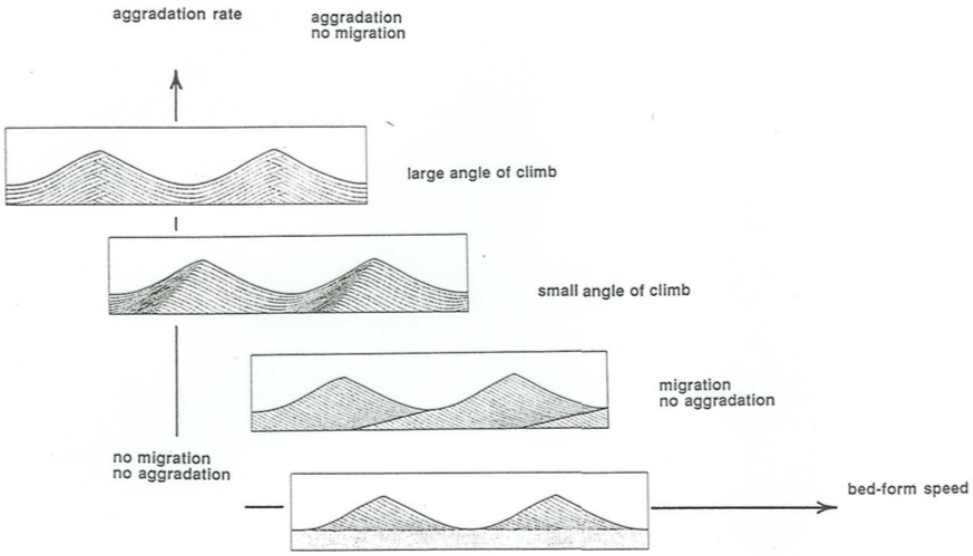


Figure 16.4.9: *Kinds of oscillatory-flow cross stratification produced by the buildup of two-dimensional oscillation ripples as a function of the slow net rate of ripple movement and the rate of aggradation of the bed.*

If the ripple speed is nonzero but slow relative to aggradation rate, the angle of climb is steep and the entire ripple profile is preserved (see the second box from the top in Figure 16.4.9). If the ripple speed is large relative to the aggradation rate, ripple troughs erode into previously deposited laminae, and the stratification shows laminae dipping in one direction only, in sets bounded by erosion surfaces (see the third box from the top in Figure 16.4.9). This last type is the most common in the sedimentary record. Finally, if a preexisting bed is molded into slowly shifting oscillation ripples without any net aggradation of the bed, the thickness of the cross-stratified deposit is equal to only one ripple height (see the bottom box in Figure 16.4.9).

Stratification that is represented by the third sketch from the top in Figure 16.4.9, for a small angle of climb such that the individual lamina sets are separated by truncation surfaces, differs only in detail, rather than in general features, from low-angle climbing-ripple cross stratification produced by ripples in unidirectional flows, discussed in the previous section. In the field it can be a challenge to tell the two kinds apart. The regularity of the sets is generally greater in the oscillatory-flow case, but newly developing climbing current ripples can show just as great a degree of regularity.

In the real world, oscillation-ripple stratification is likely to be more complicated, because wave conditions seldom remain the same for long. Commonly there are a large number of sets of laminae dipping more or less randomly in both directions.

The origin and classification of stratification produced by oscillatory flows at longer oscillation periods and higher oscillation velocities is less well understood, because there have been very few studies in natural environments in which first the bed configuration was observed while the flow conditions were measured and then the bed was sampled to see the resulting deposit. Also, there have been few studies of these bed configurations under laboratory conditions. Another element of complexity is that in the natural environment the oscillatory flows are likely to be more complicated than the regular and symmetrical bidirectional oscillatory flows that were assumed above, and not much is known in detail about the stratification types produced by these more complicated oscillatory flows.

In the face of this seemingly hopeless situation, I will take the following approach. I will describe in a general way a common style of medium-scale to large-scale cross stratification, called **hummocky cross stratification**, which is generally believed to be produced by an oscillatory flow of some kind, and I will present what evidence I can for the kinds of flows that might produce hummocky cross stratification.

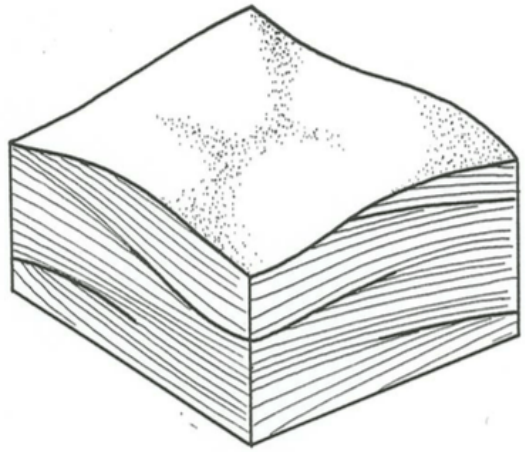


Figure 16.4.10: Block diagram of one of the common styles of cross stratification that has been called hummocky cross stratification.

Figure 16.4.10 is a block diagram of one of the common styles of cross stratification that been called hummocky cross stratification. It shows sets of laminae that are both concave upward and convex upward, bounded by broad truncation surfaces which themselves may be either concave or convex upward. Two characteristic small-scale features of the geometry of stratification are the fanning of truncation surfaces laterally into conformable sequences of laminae (Figure 16.4.11A) and, where the thickness of the bed is great enough to observe this, a tendency for convex-up sets of laminae to be succeeded upward by concave-up sets, and vice-versa (Figure 16.4.11B).

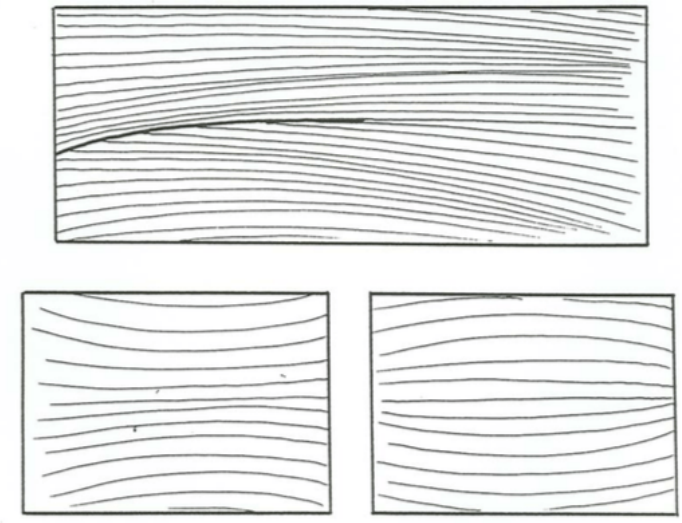


Figure 16.4.11: Characteristic small-scale features of the geometry of stratification in hummocky cross stratification formed by bed aggradation during maintenance of oscillatory-flow bed forms. **A)** Fanning of truncation surfaces laterally into conformable successions of laminae. **B)** Tendency for convex-up sets of laminae to be succeeded upward by concave-up sets, and vice versa.

Note that the two normal-to-bedding faces of the block are shown to have about the same style of stratification, and on each face there is no strongly preferred dip direction. In the rare cases where you can make serial sections of the deposit to ascertain the entire three-dimensional geometry of the deposit, it is clear that there is no preferred dip direction in the entire deposit. This is the kind of stratification I call isotropic.

The upper surface of the block diagram in Figure 16.4.10 is shown to be a bedding surface with a bed configuration that could be described as a collection of *hummock*s (locally positive convex-up areas) and *swale*s (locally negative concave-up areas). Sometimes, but not often, the upper surface of a bed with hummocky cross stratification can be seen to have just this bed geometry. The general belief is that isotropic hummocky cross stratification is produced by this kind of bed configuration, although it is seldom possible to actually demonstrate this.

Recent experiments (Dumas et al., 2005) have shown that bed configurations which in their general features are like those just described are produced by symmetrical bidirectional oscillatory flows at long periods and high oscillation velocities. This suggests that at least some isotropic hummocky cross stratification is produced by such flows. But it also seems likely that more complex oscillations with more than one oscillatory component would also produce qualitatively similar bed configurations and therefore similar cross- stratification. Much more work needs to be done before the origin of hummocky cross stratification is well understood.

The style of stratification that people call hummocky cross stratification covers a wide range in scale and geometry. It seems likely that hummocky cross stratification, used in the broad sense as a descriptive rather term than as a genetic term, is *polygenetic*: several distinctly different kinds of flow and sedimentation settings produce stratification that at least some workers would want to call hummocky cross stratification. There have even been published reports in recent times (Alexander et al., 2001) of a kind of stratification, which might be described, objectively, as a kind of hummocky cross stratification, that develops by aggradation of the bed while antidunes were present and changing their shape and position in some way.

Classification of hummocky cross stratification, in the wide sense of the term, is not in a very advanced state, and yet a rational classification would be useful, in view of the commonness and the multiplicity of origin of hummocky cross stratification. Figure 16.4.12 is my own unofficial attempt at such a classification. In my own examination of hummocky cross stratification I have found this classification to be a useful guide to my thinking about the origin of the stratification. The elements in the classification are as follows.

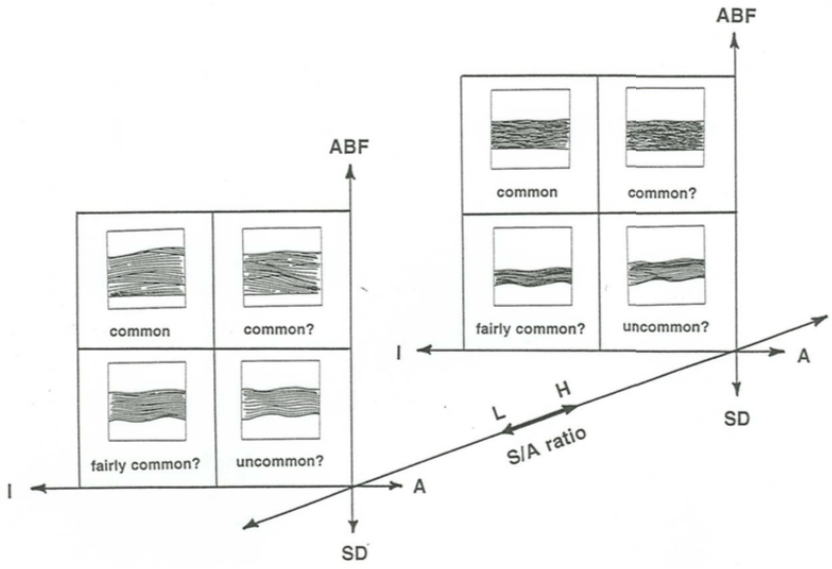


Figure 16.4.12: Unofficial classification of hummocky cross stratification. Key to symbols: ABF, aggrading bed forms; SD, scour and drape; I, isotropic; A, anisotropic; S/A, ratio of rate of lateral shifting of bed forms to rate of overall aggradation; L, low; H, high.

The eight varieties represented on the graph could be named as follows:

upper left, front: isotropic aggrading-bed-forms slow-shift HCS

upper right, front: anisotropic aggrading-bed-forms slow-shift HCS

lower left, front: isotropic scour-and-drape slow-shift HCS
lower right, front: anisotropic scour-and-drape slow-shift HCS

upper left, rear: isotropic aggrading-bed-forms fast-shift HCS

upper right, rear: anisotropic aggrading-bed-forms fast-shift HCS

lower left, rear: isotropic scour-and-drape fast-shift HCS
lower right, rear: anisotropic scour-and-drape fast-shift HCS

Isotropy vs. anisotropy: This has to do with the extent to which the cross sets have a preferred dip direction and/or dip angle. This must be controlled by the asymmetry of the oscillatory flow and/or the superimposition of a unidirectional flow component. As the stratification becomes more anisotropic, it might better be viewed as combined-flow stratification rather than as purely oscillatory-flow stratification.

Ratio of aggradation to bed-form shift: Depending mainly on the relative importance of bed-form shifting vs. rate of aggradation, sets may be very restricted in lateral extent and show mainly concave-up laminae (most workers would probably call this *swaly cross stratification*), or they may be continuous over a greater lateral distance and show more convex-up laminae.

Draping vs. bed-form maintenance: hummocky cross stratification can be formed by scouring of a hummocky–swaly bed topography initially and then draping of that irregular bed surface without the participation of oscillatory-flow bed forms that are in equilibrium, or not far out of equilibrium, with the flow. Alternatively, it can be formed by bed forms that are maintained by the flow during overall aggradation of the bed.

Scale: the scale of hummocky cross stratification ranges from quite small (what many would simply call three-dimensional wave-ripple cross stratification) to large (sets a few decimeters thick and with lateral extent of a meter or two). The scale must have a fairly direct link to the original size of the geometrical elements that existed on the sediment bed during deposition, although the vertical scale must depend also on the rate of net aggradation of the bed.

Extent of amalgamation: It is common to find single hummocky cross- stratified beds, but it is equally common to find sandstone beds that consist of two, three, or even more amalgamated beds, separated by through-going amalgamation surfaces, with each amalgamation unit showing hummocky cross stratification of one kind or other (or planar lamination, especially the

lowest amalgamation unit in the succession).

Of course, it is not possible to represent a five-dimensional classification graphically! What Figure 16.4.12 shows is a three-dimensional pigeonhole arrangement with the first three attributes in the above list, leaving scale and extent of amalgamation as additional descriptors.

Here are a few tentative comments about the classification shown in Figure 16.4.12.

- The four cartoons of scour-and drape hummocky cross stratification are end-member cases. What I think is much more common is stratification that is largely scour and drape but with bed topography changing at least slightly as the drape forms, so that the internal structure of the bed is not quite as regular and conformable as shown in the cartoons.
- When the stratification is largely of the scour-and-drape variety, I see no way to tell whether the S/A ratio was low or high; with aggrading-bed forms HCS, on the other hand, that is easier to do, at least in a qualitative way, by looking at the abundance and lateral extent of truncation surfaces.
- The case in the upper right rear ("anisotropic aggrading-bed-forms fast- shift hummocky cross stratification") might also be described as a kind of combined-flow trough cross-stratification, and as the importance of the unidirectional flow component increases and that of the oscillatory flow component decreases, this kind of stratification grades over into the trough cross stratification that is familiar to all.

Combined-Flow Cross Stratification

This brings us to the problem of combined-flow cross stratification. Unfortunately there is an almost complete lack of observational information on the origin of combined-flow cross stratification, so we have no actual models to guide interpretations. Up to now the recognition of combined-flow cross stratification has largely been a matter of deduction.

It seems convenient to think separately about the relatively small combined-flow ripples produced under combinations of relatively low oscillatory and unidirectional flow velocities, on the one hand, and the relatively large combined-flow ripples produced under combinations of relatively high oscillatory and unidirectional flow velocities, on the other hand.

When the combinations of oscillation period and oscillation velocity are such that in purely oscillatory flow the ripples would be at about the same scale as current ripples, there is a kind of *coherence* in the combined-flow ripples: they are on the same scale as unidirectional-flow ripples, but more nearly two- dimensional. Actual experiments indicate that only a very small unidirectional component is needed to make such ripples noticeably asymmetrical.

Figure 16.4.13 shows a series of flow-parallel profiles of ripples formed under a range of combined flows, from purely oscillatory to purely unidirectional One striking thing about such ripples is that it takes only a very slight unidirectional component for the ripples to shift slowly in their position, even though the profile is still virtually symmetrical. The top sketch in Figure 16.4.13, which is drawn as if the ripple stayed in the same place as it developed from the sandy substrate, is therefore a bit unrealistic, because even symmetrical ripples usually show one-way internal lamination. With even a fairly small unidirectional component the ripples become noticeably asymmetrical, as in the second sketch from the top in Figure 16.4.13. By the time the oscillatory and unidirectional components are both substantial, as in the third sketch from the top, the ripples do not look much different from those produced in purely unidirectional flows, except that the profile is typically a little more rounded and the slope of the lee side is somewhat less.

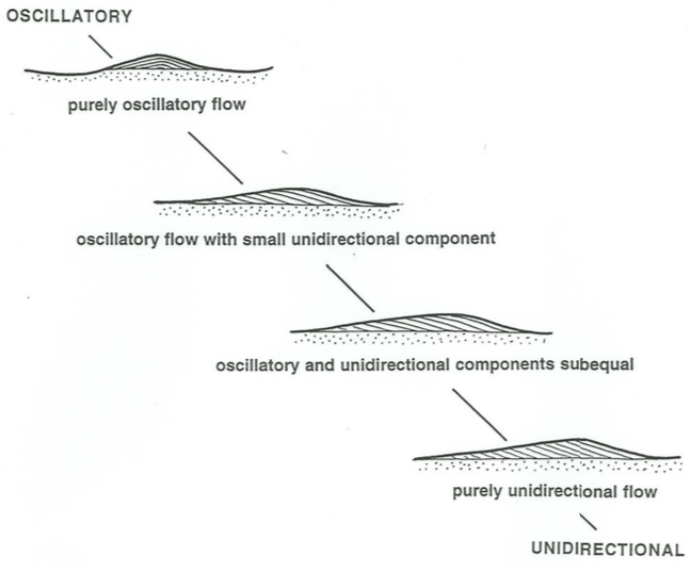


Figure 16.4.13: Profile shape and internal lamination in small-scale ripples in purely oscillatory flow, combined flow, and purely unidirectional flow.

For very short periods or very long periods, however, when the ripples that would be produced in purely oscillatory flow are much smaller or much larger than current ripples, the situation is more complicated, because in combined flows the bed configuration wants to be at two separate scales, and there is a complicated interaction between the two differing scales. There has not been much study of the stratification produced under these combined-flow conditions.

When the oscillation period is so small that the oscillation ripples are much smaller than current ripples, their dominantly oscillatory nature is clear. But there is still a problem, because the spacing of current ripples when they first become organized on a preexisting planar sand surface is no more than six or seven centimeters, and then they grow to their full size of something like fifteen to twenty centimeters. Only for ripples smaller than six or seven centimeters, therefore, can you be sure that you are dealing with dominantly oscillatory ripples and not unidirectional-flow-dominated ripples that are still growing toward equilibrium.

Eolian Cross Stratification

So far the discussion has implicitly been directed toward subaqueous bed configurations. Everyone knows that the shifting of eolian dunes produces large-scale cross stratification as well.

I can make a first-order statement here without fear of contradiction: eolian dune cross stratification is similar in gross aspects to large-scale trough cross stratification produced by water flows. Behind the gross similarity, however, are real differences. These differences are simply a consequence of the differing details of geometry of the dunes themselves.

Although I have looked at a fair number of cross-stratified eolian units, I find it difficult to be specific or concrete about how eolian dune cross stratification differs from subaqueous dune cross stratification. Here are some points of difference. (I do not pretend this to be an exhaustive list.)

- In eolian cross stratification there is a tendency for the laminae in the cross sets in the downwind part of the set to dip in the direction opposite to the dune movement. That tends to be in contrast to cross stratification produced by subaqueous dunes, for which an upcurrent dip direction of the laminae in the cross sets is much less pronounced. I think that that feature reflects the tendency for the troughs of eolian dunes to be filled by plastering of new trough laminae not just on the mean-upcurrent side, as is usually the case in subaqueous cross stratification, but on the lateral and mean-downcurrent sides as well.
- Eolian cross stratification is more likely to show greater dispersion of dip directions of cross sets, because of the greater variability of wind directions than of subaqueous current directions. (But this is not as strong a tendency as you might think, because most of the major eolian sand bodies preserved in the sedimentary record were probably produced in sand seas swept by winds fairly constant in direction.)
- The *nature of the lamination* in eolian cross-sets tends to be different from that in subaqueous cross-sets. The three basic kinds of laminae in cross-sets (see Hunter, 1977a) are:

- **grain-flow laminae**, produced by the downslope movement of grain flows to iron out the oversteepening of the foreset slope caused by deposition at the brink.
- **grain-fall laminae**, produced by the rain of sand grains onto the foreset slope after they are carried across the brink in saltation.
- **translatent laminae**, produced by the movement and very-low-angle climb of ripples on sand surfaces that are undergoing net aggradation.

The first two kinds of laminae are common to both subaerial and subaqueous cross sets, but they are much more distinctive and better differentiated in subaerial deposits. Translatent laminae are specific to subaerial deposits, because in subaqueous environments the scale and movement of ripples in dune-lee environments is such as to produce recognizable small-scale cross lamination rather than laminae so thin that the cross-stratified nature is undetectable, as in the eolian case.

Here is another, and rather different, consideration that can be useful in some cases in distinguishing subaerial from subaqueous cross stratification.
Think back to the velocity–size diagram for subaqueous unidirectional-flow bed phases. The minimum mean particle size for the existence of dunes is shown to be about $0.16\ \mathrm{mm}$. When the effects of water temperature and therefore water viscosity are taken into account, that translates (by a computational procedure that I will not describe here; see Southard and Boguchwal, 1990) into a range of minimum sizes from $0.20\ \mathrm{mm}$ at $0^{\circ}\mathrm{C}$ to $0.12\ \mathrm{mm}$ at $30^{\circ}\mathrm{C}$. If the mean size of the sediment in the cross sets in question is significantly finer than these sizes, then the deposits are almost certainly eolian rather than subaqueous. (How you estimate what the water temperature might have been is, of course, another matter.) There is an important qualification to this conclusion, however: you must be able to rule out the possibility that, if the cross stratification is subaqueous, it was indeed the result of the movement of dunes, and not of fluvial bars, whose sediment size might be finer than the lower limit associated with dunes. The overall geometry of the cross stratification usually makes that decision possible.

This page titled 16.4: Important Kinds of Climbing-Bed-Form Cross Stratification is shared under a CC BY-NC-SA 4.0 license and was authored, remixed, and/or curated by John Southard (MIT OpenCourseware) via source content that was edited to the style and standards of the LibreTexts platform.

16.5: Cross Stratification Not Produced by Climbing Bed Forms

After all of the voluminous material above on how to deal with cross stratification produced by trains of repetitive bed forms that climb at some angle owing to net aggradation of the bed, I think that it is important to point out here that not all cross stratification is produced by bed forms climbing at some angle— although I think it is fair to say that *most* of the cross stratification you see is indeed formed in that way.

One obvious case in point is rather obvious, and has been touched upon in the earlier part of this chapter:

> a train of flow-transverse bed forms is produced by a neutral flow (by "neutral" I mean that there is neither net aggradation or net degradation) over a loose sediment bed, then the flow stops, and later the train of bed forms is mantled or draped by sediment deposited in such a way as not to disturb that underlying train of bed forms (by fallout without traction, for the most part).

I might term this kind, unofficially, **single-bed-form-train cross stratification**.

I have already shown one example of single-bed-form-train cross stratification in Figure 16.4.9, wherein two-dimensional oscillation ripples are formed and shift slowly with no net addition of sediment to the bed. Single trains of unidirectional-flow ripples are more common. Cross stratification of this kind is especially common in deposits of distal turbidity currents. The situation is this: an almost exhausted turbidity current sweeps by a point, depositing fine sand, and molds that sand into a train of ripples. Although the bed is aggrading while the ripples are moving, the total thickness of sand added to the bed is not enough to form a layer more than one ripple thick (Figure 16.5.1A). In fact, in many such cases the ripples end up starved, in the sense that the difficultly erodible substrate is exposed in the ripple troughs (Figure 16.5.1B). Of course, as the total thickness of sediment added to be bed increases, the degree of overlapping of ripples (whereby ripples start climbing up the backs of others) increases (Figure 16.5.1C), and eventually the picture is as described in the earlier section on classic climbing-ripple cross stratification.

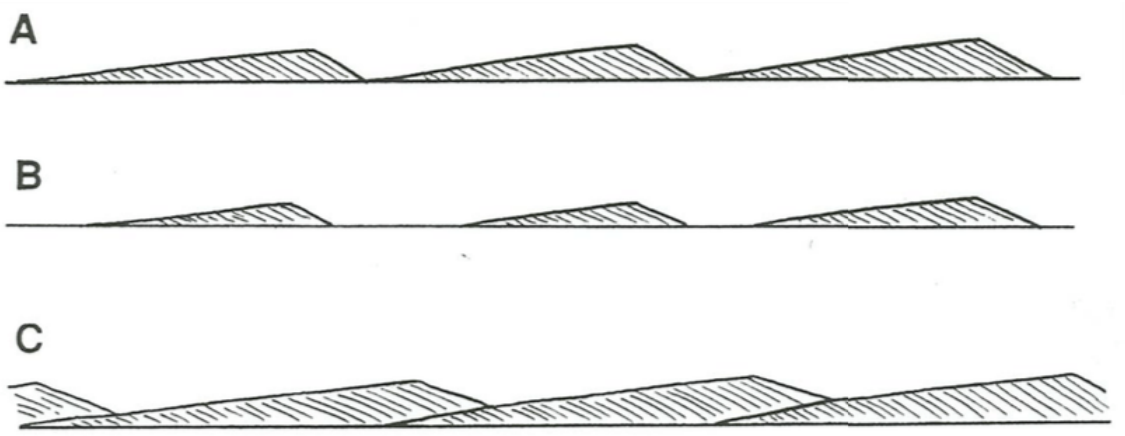


Figure 16.5.1: Single-ripple-train cross stratification. **A)** Full single train. **B)** Starved train. **C)** Ripples starting to overlap.

Usually the material presented so far in this section is relevant to small- scale bed configurations—ripples of various kinds—but sometimes single trains of much larger dunes are formed and then interred within different, or at least differently structured, sediment. When the dunes have large spacings and small height-to-spacing ratios, there is the added complication that you may on the outcrop see a segment of a dune that is very short relative to the dune spacing, and the cross stratification looks like a planar-tabular set with uniform thickness (Figure 16.5.2). I know of no way of knowing, just from looking at an outcrop like Figure 16.5.2, what the original spacing of the dunes was—or even if I am really dealing with a train of dunes in the first place!

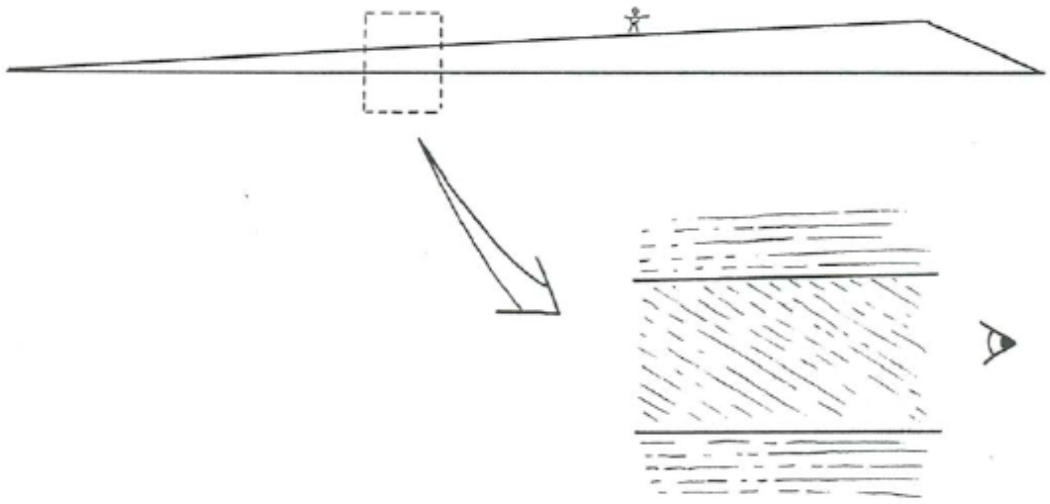


Figure 16.5.2: A planar-tabular cross set that represents a small part of single large dune-like bed form.

In a situation like that shown in Figure 16.5.2, there is also the problem of whether the full height of the dune is preserved. You might find features at the upper surface of the cross set that gives evidence of its having been the exposed upper surface of a dune, like superimposed smaller bed forms. Although that is not foolproof, it would suggest strongly that the dune was not eroded or shaved off by a later strong current after its own driving current ceased.

Finally, cross stratification can be formed by the progradation of the sloping surface of an isolated element of positive relief, like a fluvial sand bar or a submarine shoal or a delta body. Scales of such features can range up to very large. Deciding between this situation and the one described above (a small part of a single train of dunes) would be impossible without a degree of lateral control not usually available in outcrop.

Chapter 16 Reading List

Alexander, J., Bridge, J.S., Cheel, R.J., and Leclair, S.F., 2001, Bedforms and associated sedimentary structures formed under supercritical water flows over aggrading sand beds: Sedimentology, v. 48, p. 133-152.

Allen, J.R.L., 1963, The classification of cross-stratified units with notes on their origin: Sedimentology, v. 2, p. 93-114.

Allen, P.A., 1985, Hummocky cross-stratification is not produced purely under progressive waves: Nature, v. 313, p. 562-564.

Arnott, R.W.C., and Hand, B.M., 1989, Bedforms, primary structures and grain fabric in the presence of suspended sediment rain: Journal of Sedimentary Perology, v. 59, p. 1062-1069.

Bridge, J.S., 1997, Thickness of sets of cross strata and planar strata as a function of formative bed-wave geometry and migration, and aggradation rate: Geology, v. 25, p. 971-974.

Cheel, R.J., 1990, Horizontal lamination and the sequence of bed phases and stratification under upper-flow-regime conditions: Sedimentology, v. 37, p. 517- 529.

Dott, R.H., Jr., and Bourgeois, J., 1982, Hummocky stratification: Significance of its variable bedding sequences. Geological Society of America, Bulletin, v. 93, p. 663-680.

Duke W.L., Arnott, R.W.C., and Cheel, R.J., 1991, Shelf sandstones and hummocky cross-stratification: new insights on a stormy debate: Geology, v. 19, p. 625-628.

Dumas, S., Arnott, R.W.C., and Southard, J.B., 2005, Experiments on oscillatory-flow and combined flow bed forms: implications for interpreting parts of the shallow- marine sedimentary record: Journal of Sedimentary Research, v. 75, p. 501-513.

Hand, B.M., 1969, Antidunes as trochoidal waves: Journal of Sedimentary Petrology, v. 39, p. 1302-1309.

Hand, B.M., 1974, Supercritical flow in turbidity currents: Journal of Sedimentary Petrology, v. 44, p. 637-648.

Hand, B.M., Wessel, J.M., and Hayes, M.O.,1969, Antidunes in the Mount Toby Conglomerate (Triassic), Massachusetts: Journal of Sedimentary Petrology, v, 39, p. 1310-1316.

Harms, J.C., Southard, J.B., and Walker, R.G.,. 1982, Structures and Sequences in Clastic Rocks: Society of Economic Paleontologists and Mineralogists, Short Course 9, variously paginated.

Hill, P.R., Meulé, S., and Longuépée, H., 2003, Combined-flow processes and sedimentary structures on the shoreface of the wave-dominated Grande-riviére- de-la-Baleine delta: Journal of Sedimentary Research, v. 73, p. 217-226.

Hunter, R.E., 1977a, Basic types of stratification in small eolian dunes: Sedimentology, v. 24, p. 361-387.

Hunter, R.E., 1977b, Terminology of cross-stratified sedimentary layers and climbing- ripple structures: Journal of Sedimentary Petrology, v. 47, p. 697-706.

Jopling, A.V., and Richardson, E.V., 1966, Backset bedding developed in shooting flow in laboratory experiments: Journal of Sedimentary Petrology, v. 36, p. 821-825.

Leclair, S.F., 2002, Preservation of cross-strata due to the migration of subaqueous dunes: an experimental investigation: Sedimentology, v. 49, p. 1157-1180.

Lowe, D.R., 1988, Suspended-load fallout rate as an independent variable in the analysis of current structures: Sedimentology, v. 35 , p. 765-776.

Massari, F., 1996, Upper-flow-regime stratification types on steep-face, coarse-grained, Gilbert-type progradational wedges (Pleistocene, southern Italy): Journal of Sedimentary Research, v. 66, p. 364-375.

Nøttvedt, AS., and Kreisa, R.D., 1987, Model for the combined-flow origin of hummocky cross-stratification: Geology, v. 15, p. 357-361.

Paola, C., and Borgman, L., 1991, Reconstructing random topography from preserved stratification: Sedimentology, v. 38. p. 553-565.

Prave, A.R., and Duke, W.L., 1990, Small-scale hummocky cross-stratification: a form of antidune, stratification?: Sedimentology, v. 37, p. 531-539.

Rubin, D.M., and Hunter, R.E., 1982, Bedform climbing in theory and nature: Sedimentology, v. 29, p. 121-138.

Schmincke, H.-U., Fisher, R.V., and Waters, A.C., 1973, Antidune and chute and pool structures in base surge deposits of the Laacher See area, Germany: Sedimentology, v. 20, p. 553-574.

Shaw, J., and Kellerhals, R., 1977, Paleohydraulic interpretation of antidune bedforms with applications to antidunes in gravel: Journal of Sedimentary Petrology, v. 47, p. 257-266.

Sherman, D.J., and Greenwood, B., 1989, Hummocky cross-stratification and post- vortex ripples: length scales and hydraulic analysis: Sedimentology, v. 36, p. 981-986.

Skipper, K., 1971, Antidune cross-stratification in a turbidite sequence, Cloridorme Formation, Gaspé, Quebec: Sedimentology, v. 17, p. 51-68.

Southard, J.B., and Boguchwal, L.A., 1990, Bed configurations in steady unidirectional water flows. Part 2. Synthesis of data: Journal of Sedimentary Research, v. 60, p. 658-679.

Storms, J.E.A., van Dam, R.L., and Leclair, S.F., 1999, Preservation of cross-sets due to migration of current ripples over aggrading and non-aggrading beds: comparison of experimental data with theory: Sedimentology, v. 46. p. 189-200.

Walker, R.G., 1967, Upper-flow-regime bed forms in turbidites of the Hatch Formation, Devonian of New York State: Journal of Sedimentary Petrology, v. 37, p. 1052- 1058.

Yagishita, K., 1994, Antidunes and traction-carpet deposits in deep-water channel sandstones, Cretaceous, British Columbia, Canada: Journal of Sedimentary Research, v. 64, p. 34-41.

This page titled 16.5: Cross Stratification Not Produced by Climbing Bed Forms is shared under a CC BY-NC-SA 4.0 license and was authored, remixed, and/or curated by John Southard (MIT OpenCourseware) via source content that was edited to the style and standards of the LibreTexts platform.

17: PLANAR STRATIFICATION

Planar stratification is just as common as cross-stratification, if not more so, but the literature on it is not nearly as large. In a sense, the title of this chapter is misleading: it concentrates on the topic of planar lamination, not planar stratification in general.

17.1: Introduction to Planar Stratification

17.2: The Origin of Planar Lamination in Sands and Sandstones

17.3: Planar Lamination in Fine Sediments

This page titled 17: Planar Stratification is shared under a CC BY-NC-SA 4.0 license and was authored, remixed, and/or curated by John Southard (MIT OpenCourseware) via source content that was edited to the style and standards of the LibreTexts platform.

17.1: Introduction to Planar Stratification

Planar stratification is just as common as cross-stratification, if not more so, but the literature on it is not nearly as large. In a sense, the title of this chapter is misleading: it concentrates on the topic of planar lamination, not planar stratification in general.

It seems important at the outset to mention the distinction between beds with approximately planar and parallel bases and tops, forming tabular sediment bodies (I tend to call such beds *tabular* beds rather than *planar* beds), on the one hand, and **planar internal stratification**, within much thicker beds, either planar or not, on the other hand. Such internal stratification might be either technically bedding or lamination, technically, depending on stratum thickness, but the important point is that the relatively thick bed typically comprises a very large number of much thinner internal laminae. This distinction seems to me to be useful and sensible.

We need to deal with some more matters of terminology. First of all, the term "parallel" does not need to imply that the existence of straight lines or planes: the laminae might be curved, in three dimensions, but they are parallel in the sense of being *congruent*; that is, adjacent laminae have the same shape, or are at least close to having the same shape. I prefer, however, to reserve the term *parallel* for laminae that are close to being planes, and to use the term *congruent* for laminae that do not form planes but have approximately the same curved shape in a succession of laminae.

As far as I can tell, the terms *planar lamination* and *parallel lamination* are essentially identical. Such lamination is sometimes also called *even lamination* or *horizontal lamination*, although the latter term may carry some confusion, because the laminae may have been horizontal when deposited but are not now, or they could have been deposited with a non-negligible initial dip even though they were planar.

One could develop a geometrical classification of laminae in a lamina set (also called a laminaset) on the basis of three attributes:

- planar vs. congruent shape of the laminae
- tabular vs. non-tabular shape of the lamina set
- horizontal or non-horizontal orientation of the laminae

Rather than doing that here, however, I will just show the four most common categories that would arise in such a classification (Figure 17.1.1). What most workers consider planar lamination is the "planar; tabular set; ± horizontal" variety in Figure 17.1.1. That is the focus of this chapter.

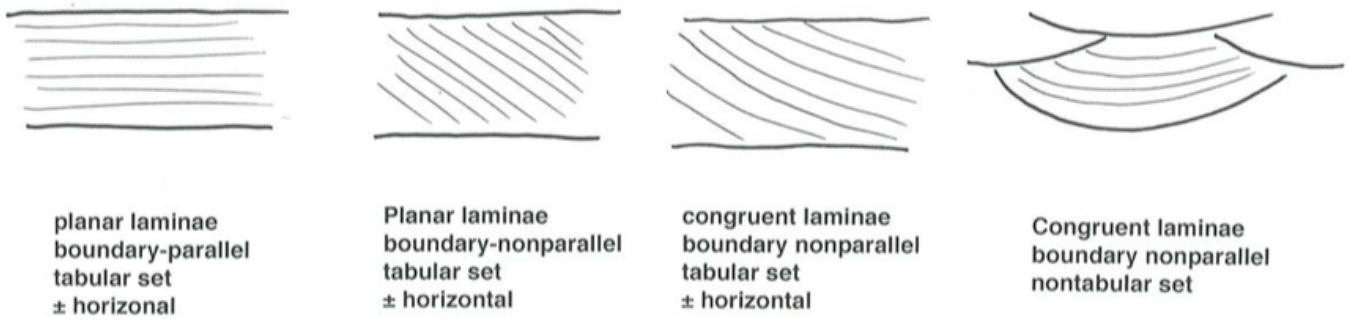


Figure 17.1.1: Four common kinds of beds with parallel or congruent internal lamination.

With regard to the three other items in Figure 17.1.1, most sedimentary geologists would call the laminae *cross laminae*, even though, according to the terminology I presented above, they would qualify as parallel (in the sense of *congruent*) laminae. I think most sedimentologists would agree that to a great extent such laminae owe their origin to processes that are specific to the lee regions of ripples or dunes: grain flows down angle-of-repose lee slopes; interleaving of grain-flow deposits and fallout deposits; and/or temporal variation in sediment supply to the lee region as a consequence of arrival of superimposed smaller bed forms to the brink region of the larger form.

In think that, similarly, most sedimentologists would agree that planar lamination in sands and sandstones is somehow associated

with the existence of a planar transport surface, in what I called in Chapter 11 the upper-flow-regime plane bed, over which abundant sediment is being transported in traction. Planar lamination is also very common in muds, mudrocks, and shales, and it seems clear that much—probably most—such lamination is formed under conditions of weak currents by fallout without traction. The distinction is usually clear from the overall context of the deposit, aside from the contrast in particle size. After a few comments on the possibilities for paleoflow interpretations, and then a brief section on the characteristic features of planar lamination, the rest of the chapter deals with the origin of planar lamination in sands and in fine sediments.

In terms of paleoflow interpretation, in the spirit of Chapter 16, on cross stratification, we might take the approach of trying to identify the entire range of flow conditions under which the bed configuration is a plane bed rather than a bed covered with rugged bed forms—on the theory that planar lamination in sands is associated with plane-bed transport in the upper flow regime. This would, however, give us only a partial idea of how to interpret the environmental significance of planar-stratified beds. The problem is that, in contrast to cross- stratified beds, there are no obvious internal geometrical features that vary with flow and sediment conditions within that overall range, so we cannot try to go on to be more specific about environmental conditions, as we can with much success with cross-stratified beds. Moreover, there is no natural basis for deciding among interpretations involving unidirectional flows, oscillatory flows, or combined flows, all of which feature plane-bed transport in an upper flow regime.

Owing to these problems, the observational fodder for interpretation of planar lamination would have to lie in textural attributes like particle size distribution and particle orientation, or in subtle variations in lamina thickness and spatial continuity. There is an offsetting advantage, however: the scale of planar lamination is so small that its features can be studied in even small laboratory flumes.

Features of Planar Lamination

- Laminae range in thickness from just a few particle diameters to over a centimeter (in which case they should not technically be called laminae any more!), equivalent to as much as hundreds of particle diameters.
- The essential feature of planar laminae is that their extent is much greater than their thickness. At a minimum, the lateral extent is an order of magnitude greater than the thickness, and it can range up to many meters, which is at least three orders of magnitude grater than the thickness.
- Laminae, almost by definition, vary in their textural features (particle size, sorting, and shape); they are commonly graded, either normally or inversely.
- On parting surfaces through planar-laminated sandstones, *parting lineation* (also called, somewhat more precisely, *parting-step lineation*) is characteristic, presumably reflecting a tendency for flow-parallel orientation of slightly elongated particles under upper-flow-regime conditions.

This page titled 17.1: Introduction to Planar Stratification is shared under a CC BY-NC-SA 4.0 license and was authored, remixed, and/or curated by John Southard (MIT OpenCourseware) via source content that was edited to the style and standards of the LibreTexts platform.

17.2: The Origin of Planar Lamination in Sands and Sandstones

Up until the late 1980s, the origin of planar lamination was an unsettled issue; a number of hypothesis had been proposed but none seems to have been widely accepted. Perhaps surprisingly, from the vantage point of the present, there were no reports of attempts to reproduce planar lamination experimentally in laboratory flumes, with the exception of the study by McBride et al. (1975). McBride et al. (1975), in shallow flow in a small flume, demonstrated that a variety of parallel lamination could be generated by the downstream movement of very low, depth-limited current ripples during slow overall aggradation of the sediment bed. They did not succeed, however, in producing parallel lamination under upper-flow regime plane-bed conditions—the flow condition under which it might be most natural to expect planar lamination to develop.

Early ideas on the development of planar lamination developed along two lines: downstream movement of very low-amplitude bed forms or bed waves under plane-bed conditions in the upper flow regime under conditions of slow aggradation of the bed, or the effect of features of the turbulence structure on sand transport. In a field study of a shallow sand-bed river, Smith (1971) was the first to report on development of planar lamination caused by downstream movement of low-amplitude bed forms. Models that invoke turbulence structure of the flow date back to that of Allen (1964).

The first attempt to develop a model that involves both of the effects describe above was that of Allen (1984). Later, on the basis of similar flume studies made at about the same time, Bridge and Best (1988) and Paola et al. (1989) (see also Best and Bridge, 1992, and Bridge and Best, 1997) developed a satisfying model in which the laminae are accounted for by downstream movement of very low-amplitude bed forms under upper-regime plane bed conditions, with the internal features of the laminae accounted for by the nature of the turbulence felt by the bed.

This page titled 17.2: The Origin of Planar Lamination in Sands and Sandstones is shared under a CC BY-NC-SA 4.0 license and was authored, remixed, and/or curated by John Southard (MIT OpenCourseware) via source content that was edited to the style and standards of the LibreTexts platform.

17.3: Planar Lamination in Fine Sediments

Planar lamination an develop wherever there is fallout of suspended sediment onto a planar sediment surface in the presence of currents that are too weak to transport the newly arriving sediment over the bed. This is what was called **fallout without traction** in Chapter 14. Planar lamination of this kind is at once the easiest to understand and philosophically the most natural. Whenever there is a planar bed surface with particles raining down from above, from a fluid that is not moving fast enough to transport the particles once they land, planar lamination is formed, provided only that the nature of the sediment that is raining out fluctuates in one or more ways with time. Such planar lamination is usually found in fine sediments—muds and silts—for the obvious reason that it is not easy to imagine scenarios in which sediment with substantial fall velocities can be carried for long distances by near-bed currents too weak to transport that sediment as bed load.

The floor of the deep ocean is exposed to bottom currents that in most (but not all) places and at most (but not all) times are well below the threshold for sediment entrainment. Slow settling of fine sediment onto the sea floor under those conditions leads to planar lamination if the nature of the settling sediment varies in some way with time—and also provided that bioturbation does not disrupt the lamination. I suspect that most marine sedimentologists would assert that by far the most planar lamination in the sedimentary record was formed in just such a way!

Most shales, if you inspect them closely enough, have planar lamination. The study of such planar lamination goes far beyond the scope of these notes, because it involves consideration of the physicochemical interactions among fine clay particles, as well as the microbiological setting.

One way of producing fallout-without-traction planar lamination in coarser sediments, like fine to medium sands, is to appeal to strong and sediment-laden hypopycnal flows in the ocean (or in saline lakes), from which sediment rains down into quieter water below. Such hypopycnal flows develop wherever the river flow that disgorges into the water body has bulk density lower than that of the water body. Provided that the concentration of suspended sediment is not so high as to make the bulk density of the river flow even grater than that of the saline water body—in which case a bottom-hugging density underflow develops—the river flow spreads out across the surface of the water body, from which it is largely uncoupled dynamically because of the tendency for the strong vertical density gradient to damp turbulent mixing.

References

- Allen, J.R.L., 1964, Primary current lineation in the Lower Old Red Sandstone (Devonian), Anglo-Welsh Basin: Sedimentology, v. 3, p. 89-108.
- Allen, J.R.L., 1984, Parallel lamination developed from upper-stage plane beds: a model based on the larger coherent structures of the turbulent boundary layer: Sedimentary Geology, v. 39, p. 227-242.
- Best, J., and Bridge, J., 1992, The morphology and dynamics of low amplitude bedwaves upon upper stage plane beds and the preservation of planar laminae: Sedimentology, v. 39, p. 737-752.
- Bridge, J., and Best, J., 1997, Preservation of planar laminae due to migration of low-relief bed waves over aggrading upper-stage plane beds: comparison of experimental data and theory: Sedimentology, v. 44, p. 253-262.
- Bridge, J.S, and Best, J.L., 1988, Flow, sediment and bedform dynamics over the transition from dunes to upper-stage plane beds: implications for the formation of planar laminae: Sedimentology, v. 35, p. 753-763.
- McBride, Shepherd, R.G., and Crawley, R.A., 1973, Origin of parallel, near- horizontal laminae by migration of bed forms sin a small flume: Journal of Sedimentary Petrology, v. 45, p. 132-139.
- Paola, C., Wiele, S.M., and Reinhart, M.A., 1989, Upper-regime parallel lamination as the result of turbulent sediment transport and low-amplitude bed forms: Sedimentology, v. 36, p. 47-59.
- Smith, N.D., 1971, Pseudo-planar stratification produced by very low amplitude sand waves: Journal of Sedimentary Petrology, v. 41, p. 69-73.

This page titled 17.3: Planar Lamination in Fine Sediments is shared under a CC BY-NC-SA 4.0 license and was authored, remixed, and/or curated by John Southard (MIT OpenCourseware) via source content that was edited to the style and standards of the LibreTexts platform.

INDEX

A

active layer
15.3: Why Deposition or Erosion?
8.1: Introduction to Sediments, Variables, and Flumes

aerodynamic threshold
11.2: Saltation I

aggradation
15.3: Why Deposition or Erosion?

Airy waves
6.3: Water Motions Due to Waves

amalgamation
16.2: The Nature of Cross Stratification

angle of climb
16.3: The Basic Idea Behind Climbing-Bed-Form Cross Stratification

angular velocity
7.2: The Coriolis Effect on the Earth's Surface

antidunes
12.2: Unidirectional-Flow Bed Configurations

armor
14.2: Several Consequences of Size

B

backwater curve
5.7: Gradually Varied Flow

barchans
12.7: Wind Ripples and Eolian Dunes

bed
16.1: Stratification and Cross Stratification

bed configuration
12.1: Introduction to Bed Configurations

bed forms
12.1: Introduction to Bed Configurations

bed load
10.1: Introduction to the Movement of Sediment by Water Flows
10.2: The Bed, the Flow, and the Load
10.4: Bed Load

bed phase
12.1: Introduction to Bed Configurations

bed state
12.1: Introduction to Bed Configurations

bedding
16.1: Stratification and Cross Stratification

Bernoulli equation
3.4: The Bernoulli Equation

boundary layer
3.5: Turbulence
3.6: Boundary Layers

boundary Reynolds number
4.6: Flow Resistance

boundary shear stress
4.6: Flow Resistance

brink
12.2: Unidirectional-Flow Bed Configurations

Buckingham's theorem
2.6: "Dimensional Analysis"

buffer layer
4.5: Structure of Turbulent Boundary Layers

buoyancy
1.2: Pressure

burst
4.8: More on the Structure of Turbulent Boundary Layers- Coherent Structures in Turbulent Shear Flow

C

Chézy coefficient
4.6: Flow Resistance

Chézy equation
4.6: Flow Resistance

coherent structures
4.8: More on the Structure of Turbulent Boundary Layers- Coherent Structures in Turbulent Shear Flow

combined flow
6.5: Combined Flow (Waves plus Current)

competence
9.1: Introduction to Threshold of Movement

conservation of sediment volume
15.2: Modes of Deposition

continua
1.1: The Nature of Fluids

core region
4.5: Structure of Turbulent Boundary Layers

Coriolis acceleration
7.1: Playing on a Rotating Table

Coriolis Effect
7.1: Playing on a Rotating Table
7.2: The Coriolis Effect on the Earth's Surface

Coriolis Force
7.1: Playing on a Rotating Table

Coriolis parameter
7.2: The Coriolis Effect on the Earth's Surface

creeping flow
3.2: Flow Past a Sphere at Low Reynolds Numbers

crest
12.2: Unidirectional-Flow Bed Configurations

critical flow
5.4: Energy in Open-Channel Flow

critical shear stress
9.1: Introduction to Threshold of Movement

cross bedding
16.1: Stratification and Cross Stratification

cross lamination
16.1: Stratification and Cross Stratification

cross stratification
16.1: Stratification and Cross Stratification
16.3: The Basic Idea Behind Climbing-Bed-Form Cross Stratification

D

debris flow
15.2: Modes of Deposition

degradation
15.3: Why Deposition or Erosion?

deposition ratio
15.3: Why Deposition or Erosion?

differential transport
15.2: Modes of Deposition

diffusion
1.4: Diffusion

dimensional analysis
2.6: "Dimensional Analysis"

dimensionless variables
2.4: How to Construct Dimensionless Variables

displacement height
12.3: Velocity Profiles over Ripples

drag
9.2: Forces on Bed Particles

drag coefficient
2.3: Some Dimensional Reasoning and its Consequences

drag crisis
3.8: Flow Past a Sphere at High Reynolds Numbers

drag force
3.2: Flow Past a Sphere at Low Reynolds Numbers

drag partition
8.5: Variables

dunes
12.2: Unidirectional-Flow Bed Configurations

dynamic pressure
1.2: Pressure

dynamically rough flow
4.6: Flow Resistance

dynamically smooth flow
4.6: Flow Resistance

E

eddies
3.5: Turbulence

eddy diffusion coefficient
4.7: Velocity Profiles

eddy viscosity
4.7: Velocity Profiles

Ekman Layers
7.6: Ekman Layers

Ekman spiral
7.4: The Ekman Spiral

elevation head
5.4: Energy in Open-Channel Flow

energy cascade
4.7: Velocity Profiles

energy grade line
5.4: Energy in Open-Channel Flow

energy gradient
5.4: Energy in Open-Channel Flow
5.7: Gradually Varied Flow

energy slope
5.4: Energy in Open-Channel Flow
5.7: Gradually Varied Flow

eolian sediment transport
11: Movement of Sediment by the Wind

equal mobility
14.2: Several Consequences of Size

equations of motion
2.7: Significance of Reynolds Numbers and Froude Numbers
equivalent sand roughness
4.6: Flow Resistance

F

fall velocity
3.9: Settling of Spheres
fallout without traction
17.3: Planar Lamination in Fine Sediments
fetch
6.3: Water Motions Due to Waves
flow intensity
10.1: Introduction to the Movement of Sediment by Water Flows
flow regimes
12.2: Unidirectional-Flow Bed Configurations
3.8: Flow Past a Sphere at High Reynolds Numbers
flow resistance
4.6: Flow Resistance
flow separation
12.2: Unidirectional-Flow Bed Configurations
3.7: Flow Separation
flowlines
3.4: The Bernoulli Equation
fluid threshold
11.2: Saltation I
flumes
8.6: Flumes
form drag
2.1: Introduction
8.5: Variables
fractionation
15.3: Why Deposition or Erosion?
free body
1.2: Pressure
free stream
3.6: Boundary Layers
free surface
4.2: Laminar Flow Down an Inclined Plane
5.1: Introduction to Open-Channel Flow
friction factor
4.6: Flow Resistance
friction velocity
4.6: Flow Resistance
Froude number
2.5: What if You Choose the Wrong Variables?
Froude Numbers
2.7: Significance of Reynolds Numbers and Froude Numbers

G

geophysical flows
7.1: Playing on a Rotating Table
Geostrophic Balance
7.5: Geostrophic Motion
Geostrophic Motion
7.5: Geostrophic Motion
gradation independence
14.2: Several Consequences of Size
gradually varied flows
5.7: Gradually Varied Flow
grain flows
10.4: Bed Load
granule ripples
12.7: Wind Ripples and Eolian Dunes
gravity waves
6.1: Introduction

H

hairpin vortices
4.8: More on the Structure of Turbulent Boundary Layers- Coherent Structures in Turbulent Shear Flow
head loss
5.4: Energy in Open-Channel Flow
Hjulstrom diagram
9.5: Recasting the Shields Diagram
horseshoe vortices
4.8: More on the Structure of Turbulent Boundary Layers- Coherent Structures in Turbulent Shear Flow
hummocky cross stratification
16.4: Important Kinds of Climbing-Bed-Form Cross Stratification
hydraulic jump
5.5: The Hydraulic Jump
hydraulic radius
4.2: Laminar Flow Down an Inclined Plane
hydrostatic balance
1.2: Pressure
hydrostatic equation
1.2: Pressure
hydrostatic pressure
1.2: Pressure
hypopycnal flows
17.3: Planar Lamination in Fine Sediments

I

impact creep
11.2: Saltation I
impact threshold
11.2: Saltation I
inertia circle
7.3: The Rossby Number and Inertia Currents
Inertia Currents
7.3: The Rossby Number and Inertia Currents
inertia period
7.3: The Rossby Number and Inertia Currents
interfacial deposition
15.2: Modes of Deposition
intermittent suspension load
10.2: The Bed, the Flow, and the Load
internal boundary layer
3.6: Boundary Layers
inviscid fluid
3.3: Inviscid Flow
isobaric surfaces
7.5: Geostrophic Motion
isobars
7.5: Geostrophic Motion

K

kinematic viscosity
4.6: Flow Resistance

L

Lagrangian velocities
3.5: Turbulence
lamina
16.1: Stratification and Cross Stratification
laminae
16.1: Stratification and Cross Stratification
laminar flow
3.5: Turbulence
laminar separation
3.8: Flow Past a Sphere at High Reynolds Numbers
lamination
16.1: Stratification and Cross Stratification
law of the wall
4.7: Velocity Profiles
lee surface
12.2: Unidirectional-Flow Bed Configurations
lift
9.2: Forces on Bed Particles
linear waves
6.2: The Nature of Waves
load
10.2: The Bed, the Flow, and the Load
13.2: The Sediment Load and the Sediment Transport Rate
loess
11.1: Introduction
logarithmic layer
4.7: Velocity Profiles
7.7: Planetary Boundary Layers- The Ekman Layer, The Logarithmic Layer, and The Mixed Layer
lower flow regime
12.2: Unidirectional-Flow Bed Configurations

M

Magnus effect
11.2: Saltation I
mass deposition
15.2: Modes of Deposition
mixed layer
7.7: Planetary Boundary Layers- The Ekman Layer, The Logarithmic Layer, and The Mixed Layer
momentum function
5.5: The Hydraulic Jump

N

nominal diameter
8.1: Introduction to Sediments, Variables, and Flumes
nonlinear waves
6.2: The Nature of Waves
normal depth
5.7: Gradually Varied Flow

O

oscillatory waves
6.2: The Nature of Waves
outer layer
4.5: Structure of Turbulent Boundary Layers
overlap layer
4.7: Velocity Profiles

overloading
15.1: Introduction to Deposition

P

parallel lamination
17.1: Introduction to Planar Stratification
partial transport
14.5: Deviations from the Condition of Equal Mobility
pathline
3.4: The Bernoulli Equation
pavement
14.2: Several Consequences of Size
Pi theorem
2.6: "Dimensional Analysis"
planar bed surface
12.2: Unidirectional-Flow Bed Configurations
planar lamination
17.1: Introduction to Planar Stratification
planar stratification
17.1: Introduction to Planar Stratification
planetary boundary layer
7.7: Planetary Boundary Layers- The Ekman Layer, The Logarithmic Layer, and The Mixed Layer
pocket
10.4: Bed Load
pressure
1.2: Pressure
pressure drag
2.1: Introduction
pressure head
5.4: Energy in Open-Channel Flow
pure drift currents
7.4: The Ekman Spiral

R

rapidly varied flows
5.7: Gradually Varied Flow
reattach
12.2: Unidirectional-Flow Bed Configurations
reference transport rate
14.4: Movement Threshold in Mixed-Sized Sediments
relative height
6.2: The Nature of Waves
relative roughness
4.6: Flow Resistance
6.4: Wave Boundary Layers
reptation
11.2: Saltation I
resistance diagram
4.6: Flow Resistance
Reynolds numbers
2.3: Some Dimensional Reasoning and its Consequences
2.7: Significance of Reynolds Numbers and Froude Numbers
3.5: Turbulence
Reynolds stress
4.4: Turbulent Shear Stress
rheological layer
10.4: Bed Load
rib and furrow
16.4: Important Kinds of Climbing-Bed-Form Cross Stratification
ripples
12.2: Unidirectional-Flow Bed Configurations
Robins effect
11.2: Saltation I
rollability effect
14.2: Several Consequences of Size
Rossby Number
7.3: The Rossby Number and Inertia Currents
roughness element
4.7: Velocity Profiles
roughness length
4.7: Velocity Profiles
roughness Reynolds number
4.6: Flow Resistance
Rouse number
10.5: Suspension in a Shear Flow- The Diffusional Theory of Suspension

S

saltation
10.1: Introduction to the Movement of Sediment by Water Flows
10.4: Bed Load
11.2: Saltation I
11.3: Saltation II
scale modeling
2.3: Some Dimensional Reasoning and its Consequences
sediment
8.1: Introduction to Sediments, Variables, and Flumes
sediment conservation equation
12.5: 2D Dunes and 3D Dunes
sediment discharge
13.1: Introduction to Sediment Transport Rates
sediment transport rate
13.1: Introduction to Sediment Transport Rates
selective entrainment
14.2: Several Consequences of Size
14.5: Deviations from the Condition of Equal Mobility
separation vortex
12.2: Unidirectional-Flow Bed Configurations
settling
15.1: Introduction to Deposition
settling velocity
3.9: Settling of Spheres
shear layer
12.2: Unidirectional-Flow Bed Configurations
shear stress
1.3: Viscosity
shear velocity
4.6: Flow Resistance
Shields curve
9.4: Movement Threshold
Shields diagram
9.4: Movement Threshold
Shields parameter
9.3: Balance of Forces and Dimensional Analysis
size fraction
14.1: Introduction
skimming flow
4.7: Velocity Profiles
skin friction
8.5: Variables
slip face
12.2: Unidirectional-Flow Bed Configurations
sorting
14.1: Introduction
8.1: Introduction to Sediments, Variables, and Flumes
spatial accelerations
8.3: Particle Motions vs. Turbulence
specific energy
5.4: Energy in Open-Channel Flow
specific head
5.4: Energy in Open-Channel Flow
specific weight
1.2: Pressure
spectral waves
6.3: Water Motions Due to Waves
splash function
11.2: Saltation I
stagnation points
3.3: Inviscid Flow
static pressure
1.2: Pressure
steady flow
4.1: Introduction to Flow in Channels
Stokes' law
3.2: Flow Past a Sphere at Low Reynolds Numbers
stoss surface
12.2: Unidirectional-Flow Bed Configurations
strata
16.1: Stratification and Cross Stratification
stratification
16.1: Stratification and Cross Stratification
stratified flows
5.1: Introduction to Open-Channel Flow
stratum
16.1: Stratification and Cross Stratification
streakline
3.4: The Bernoulli Equation
stream tube
3.4: The Bernoulli Equation
streamline
3.4: The Bernoulli Equation
structure
16.1: Stratification and Cross Stratification
subcritical flow
5.4: Energy in Open-Channel Flow
supercritical flow
5.4: Energy in Open-Channel Flow
surface creep
11.2: Saltation I
susceptibility
11.2: Saltation I
suspend load
10.1: Introduction to the Movement of Sediment by Water Flows
10.2: The Bed, the Flow, and the Load
suspension
10.4: Bed Load
sweep
4.8: More on the Structure of Turbulent Boundary Layers- Coherent Structures in Turbulent Shear Flow

T

temporal accelerations
8.3: Particle Motions vs. Turbulence

terminal velocity
3.9: Settling of Spheres

texture
16.1: Stratification and Cross Stratification

threshold shear stress
9.1: Introduction to Threshold of Movement

total head
5.4: Energy in Open-Channel Flow

traction
10.2: The Bed, the Flow, and the Load

traction carpet
10.4: Bed Load

transitionally rough flow
4.6: Flow Resistance

translatent laminae
16.4: Important Kinds of Climbing-Bed-Form Cross Stratification

translatory waves
6.2: The Nature of Waves

transport stage
10.3: Transport Mode Versus Flow Intensity

trough
12.2: Unidirectional-Flow Bed Configurations

truncation surfaces
16.2: The Nature of Cross Stratification

turbidity current
15.2: Modes of Deposition

turbulence
3.5: Turbulence

turbulence closure problem
4.4: Turbulent Shear Stress

turbulent diffusion
4.4: Turbulent Shear Stress

turbulent flow
4.3: Turbulent Flow in Channels - Initial Material

turbulent separation
3.8: Flow Past a Sphere at High Reynolds Numbers

turbulent shear flow
4.5: Structure of Turbulent Boundary Layers

turbulent shear stress
4.4: Turbulent Shear Stress

U

uniform flow
4.1: Introduction to Flow in Channels
5.3: Uniform Flow

unit sediment transport rate
13.2: The Sediment Load and the Sediment Transport Rate

upper flow regime
12.2: Unidirectional-Flow Bed Configurations

V

velocity defect law
4.7: Velocity Profiles

velocity head
5.4: Energy in Open-Channel Flow

Velocity Profile
4.7: Velocity Profiles

viscosity
1.3: Viscosity

viscous drag
2.1: Introduction

viscous length scale
4.6: Flow Resistance

viscous sublayer
4.5: Structure of Turbulent Boundary Layers

von Kármán's constant
4.7: Velocity Profiles

vortex ripples
12.6: Oscillatory-Flow and Combined-Flow Bed Configurations

vorticity
3.5: Turbulence
4.8: More on the Structure of Turbulent Boundary Layers- Coherent Structures in Turbulent Shear Flow

W

wake
3.6: Boundary Layers
3.7: Flow Separation

wash load
10.1: Introduction to the Movement of Sediment by Water Flows
10.2: The Bed, the Flow, and the Load

wave boundary layer
6.4: Wave Boundary Layers

wave friction factor
6.4: Wave Boundary Layers

wave steepness
6.2: The Nature of Waves

wave–current boundary layers
6.5: Combined Flow (Waves plus Current)

wavelets
6.2: The Nature of Waves

wind ripples
12.7: Wind Ripples and Eolian Dunes

This page titled Index is shared under a CC BY-NC-SA 4.0 license and was authored, remixed, and/or curated by John Southard (MIT OpenCourseware) via source content that was edited to the style and standards of the LibreTexts platform.

INDEX

A

active layer
15.3: Why Deposition or Erosion?
8.1: Introduction to Sediments, Variables, and Flumes

aerodynamic threshold
11.2: Saltation I

aggradation
15.3: Why Deposition or Erosion?

Airy waves
6.3: Water Motions Due to Waves

amalgamation
16.2: The Nature of Cross Stratification

angle of climb
16.3: The Basic Idea Behind Climbing-Bed-Form Cross Stratification

angular velocity
7.2: The Coriolis Effect on the Earth's Surface

antidunes
12.2: Unidirectional-Flow Bed Configurations

armor
14.2: Several Consequences of Size

B

backwater curve
5.7: Gradually Varied Flow

barchans
12.7: Wind Ripples and Eolian Dunes

bed
16.1: Stratification and Cross Stratification

bed configuration
12.1: Introduction to Bed Configurations

bed forms
12.1: Introduction to Bed Configurations

bed load
10.1: Introduction to the Movement of Sediment by Water Flows
10.2: The Bed, the Flow, and the Load
10.4: Bed Load

bed phase
12.1: Introduction to Bed Configurations

bed state
12.1: Introduction to Bed Configurations

bedding
16.1: Stratification and Cross Stratification

Bernoulli equation
3.4: The Bernoulli Equation

boundary layer
3.5: Turbulence
3.6: Boundary Layers

boundary Reynolds number
4.6: Flow Resistance

boundary shear stress
4.6: Flow Resistance

brink
12.2: Unidirectional-Flow Bed Configurations

Buckingham's theorem
2.6: "Dimensional Analysis"

buffer layer
4.5: Structure of Turbulent Boundary Layers

buoyancy
1.2: Pressure

burst
4.8: More on the Structure of Turbulent Boundary Layers- Coherent Structures in Turbulent Shear Flow

C

Chézy coefficient
4.6: Flow Resistance

Chézy equation
4.6: Flow Resistance

coherent structures
4.8: More on the Structure of Turbulent Boundary Layers- Coherent Structures in Turbulent Shear Flow

combined flow
6.5: Combined Flow (Waves plus Current)

competence
9.1: Introduction to Threshold of Movement

conservation of sediment volume
15.2: Modes of Deposition

continua
1.1: The Nature of Fluids

core region
4.5: Structure of Turbulent Boundary Layers

Coriolis acceleration
7.1: Playing on a Rotating Table

Coriolis Effect
7.1: Playing on a Rotating Table
7.2: The Coriolis Effect on the Earth's Surface

Coriolis Force
7.1: Playing on a Rotating Table

Coriolis parameter
7.2: The Coriolis Effect on the Earth's Surface

creeping flow
3.2: Flow Past a Sphere at Low Reynolds Numbers

crest
12.2: Unidirectional-Flow Bed Configurations

critical flow
5.4: Energy in Open-Channel Flow

critical shear stress
9.1: Introduction to Threshold of Movement

cross bedding
16.1: Stratification and Cross Stratification

cross lamination
16.1: Stratification and Cross Stratification

cross stratification
16.1: Stratification and Cross Stratification
16.3: The Basic Idea Behind Climbing-Bed-Form Cross Stratification

D

debris flow
15.2: Modes of Deposition

degradation
15.3: Why Deposition or Erosion?

deposition ratio
15.3: Why Deposition or Erosion?

differential transport
15.2: Modes of Deposition

diffusion
1.4: Diffusion

dimensional analysis
2.6: "Dimensional Analysis"

dimensionless variables
2.4: How to Construct Dimensionless Variables

displacement height
12.3: Velocity Profiles over Ripples

drag
9.2: Forces on Bed Particles

drag coefficient
2.3: Some Dimensional Reasoning and its Consequences

drag crisis
3.8: Flow Past a Sphere at High Reynolds Numbers

drag force
3.2: Flow Past a Sphere at Low Reynolds Numbers

drag partition
8.5: Variables

dunes
12.2: Unidirectional-Flow Bed Configurations

dynamic pressure
1.2: Pressure

dynamically rough flow
4.6: Flow Resistance

dynamically smooth flow
4.6: Flow Resistance

E

eddies
3.5: Turbulence

eddy diffusion coefficient
4.7: Velocity Profiles

eddy viscosity
4.7: Velocity Profiles

Ekman Layers
7.6: Ekman Layers

Ekman spiral
7.4: The Ekman Spiral

elevation head
5.4: Energy in Open-Channel Flow

energy cascade
4.7: Velocity Profiles

energy grade line
5.4: Energy in Open-Channel Flow

energy gradient
5.4: Energy in Open-Channel Flow
5.7: Gradually Varied Flow

energy slope
5.4: Energy in Open-Channel Flow
5.7: Gradually Varied Flow

eolian sediment transport
11: Movement of Sediment by the Wind

equal mobility
14.2: Several Consequences of Size

equations of motion
2.7: Significance of Reynolds Numbers and Froude Numbers
equivalent sand roughness
4.6: Flow Resistance

F

fall velocity
3.9: Settling of Spheres
fallout without traction
17.3: Planar Lamination in Fine Sediments
fetch
6.3: Water Motions Due to Waves
flow intensity
10.1: Introduction to the Movement of Sediment by Water Flows
flow regimes
12.2: Unidirectional-Flow Bed Configurations
3.8: Flow Past a Sphere at High Reynolds Numbers
flow resistance
4.6: Flow Resistance
flow separation
12.2: Unidirectional-Flow Bed Configurations
3.7: Flow Separation
flowlines
3.4: The Bernoulli Equation
fluid threshold
11.2: Saltation I
flumes
8.6: Flumes
form drag
2.1: Introduction
8.5: Variables
fractionation
15.3: Why Deposition or Erosion?
free body
1.2: Pressure
free stream
3.6: Boundary Layers
free surface
4.2: Laminar Flow Down an Inclined Plane
5.1: Introduction to Open-Channel Flow
friction factor
4.6: Flow Resistance
friction velocity
4.6: Flow Resistance
Froude number
2.5: What if You Choose the Wrong Variables?
Froude Numbers
2.7: Significance of Reynolds Numbers and Froude Numbers

G

geophysical flows
7.1: Playing on a Rotating Table
Geostrophic Balance
7.5: Geostrophic Motion
Geostrophic Motion
7.5: Geostrophic Motion
gradation independence
14.2: Several Consequences of Size
gradually varied flows
5.7: Gradually Varied Flow
grain flows
10.4: Bed Load
granule ripples
12.7: Wind Ripples and Eolian Dunes
gravity waves
6.1: Introduction

H

hairpin vortices
4.8: More on the Structure of Turbulent Boundary Layers- Coherent Structures in Turbulent Shear Flow
head loss
5.4: Energy in Open-Channel Flow
Hjulstrom diagram
9.5: Recasting the Shields Diagram
horseshoe vortices
4.8: More on the Structure of Turbulent Boundary Layers- Coherent Structures in Turbulent Shear Flow
hummocky cross stratification
16.4: Important Kinds of Climbing-Bed-Form Cross Stratification
hydraulic jump
5.5: The Hydraulic Jump
hydraulic radius
4.2: Laminar Flow Down an Inclined Plane
hydrostatic balance
1.2: Pressure
hydrostatic equation
1.2: Pressure
hydrostatic pressure
1.2: Pressure
hypopycnal flows
17.3: Planar Lamination in Fine Sediments

I

impact creep
11.2: Saltation I
impact threshold
11.2: Saltation I
inertia circle
7.3: The Rossby Number and Inertia Currents
Inertia Currents
7.3: The Rossby Number and Inertia Currents
inertia period
7.3: The Rossby Number and Inertia Currents
interfacial deposition
15.2: Modes of Deposition
intermittent suspension load
10.2: The Bed, the Flow, and the Load
internal boundary layer
3.6: Boundary Layers
inviscid fluid
3.3: Inviscid Flow
isobaric surfaces
7.5: Geostrophic Motion
isobars
7.5: Geostrophic Motion

K

kinematic viscosity
4.6: Flow Resistance

L

Lagrangian velocities
3.5: Turbulence
lamina
16.1: Stratification and Cross Stratification
laminae
16.1: Stratification and Cross Stratification
laminar flow
3.5: Turbulence
laminar separation
3.8: Flow Past a Sphere at High Reynolds Numbers
lamination
16.1: Stratification and Cross Stratification
law of the wall
4.7: Velocity Profiles
lee surface
12.2: Unidirectional-Flow Bed Configurations
lift
9.2: Forces on Bed Particles
linear waves
6.2: The Nature of Waves
load
10.2: The Bed, the Flow, and the Load
13.2: The Sediment Load and the Sediment Transport Rate
loess
11.1: Introduction
logarithmic layer
4.7: Velocity Profiles
7.7: Planetary Boundary Layers- The Ekman Layer, The Logarithmic Layer, and The Mixed Layer
lower flow regime
12.2: Unidirectional-Flow Bed Configurations

M

Magnus effect
11.2: Saltation I
mass deposition
15.2: Modes of Deposition
mixed layer
7.7: Planetary Boundary Layers- The Ekman Layer, The Logarithmic Layer, and The Mixed Layer
momentum function
5.5: The Hydraulic Jump

N

nominal diameter
8.1: Introduction to Sediments, Variables, and Flumes
nonlinear waves
6.2: The Nature of Waves
normal depth
5.7: Gradually Varied Flow

O

oscillatory waves
6.2: The Nature of Waves
outer layer
4.5: Structure of Turbulent Boundary Layers
overlap layer
4.7: Velocity Profiles

overloading
15.1: Introduction to Deposition

P

parallel lamination
17.1: Introduction to Planar Stratification
partial transport
14.5: Deviations from the Condition of Equal Mobility
pathline
3.4: The Bernoulli Equation
pavement
14.2: Several Consequences of Size
Pi theorem
2.6: "Dimensional Analysis"
planar bed surface
12.2: Unidirectional-Flow Bed Configurations
planar lamination
17.1: Introduction to Planar Stratification
planar stratification
17.1: Introduction to Planar Stratification
planetary boundary layer
7.7: Planetary Boundary Layers- The Ekman Layer, The Logarithmic Layer, and The Mixed Layer
pocket
10.4: Bed Load
pressure
1.2: Pressure
pressure drag
2.1: Introduction
pressure head
5.4: Energy in Open-Channel Flow
pure drift currents
7.4: The Ekman Spiral

R

rapidly varied flows
5.7: Gradually Varied Flow
reattach
12.2: Unidirectional-Flow Bed Configurations
reference transport rate
14.4: Movement Threshold in Mixed-Sized Sediments
relative height
6.2: The Nature of Waves
relative roughness
4.6: Flow Resistance
6.4: Wave Boundary Layers
reptation
11.2: Saltation I
resistance diagram
4.6: Flow Resistance
Reynolds numbers
2.3: Some Dimensional Reasoning and its Consequences
2.7: Significance of Reynolds Numbers and Froude Numbers
3.5: Turbulence
Reynolds stress
4.4: Turbulent Shear Stress
rheological layer
10.4: Bed Load
rib and furrow
16.4: Important Kinds of Climbing-Bed-Form Cross Stratification
ripples
12.2: Unidirectional-Flow Bed Configurations
Robins effect
11.2: Saltation I
rollability effect
14.2: Several Consequences of Size
Rossby Number
7.3: The Rossby Number and Inertia Currents
roughness element
4.7: Velocity Profiles
roughness length
4.7: Velocity Profiles
roughness Reynolds number
4.6: Flow Resistance
Rouse number
10.5: Suspension in a Shear Flow- The Diffusional Theory of Suspension

S

saltation
10.1: Introduction to the Movement of Sediment by Water Flows
10.4: Bed Load
11.2: Saltation I
11.3: Saltation II
scale modeling
2.3: Some Dimensional Reasoning and its Consequences
sediment
8.1: Introduction to Sediments, Variables, and Flumes
sediment conservation equation
12.5: 2D Dunes and 3D Dunes
sediment discharge
13.1: Introduction to Sediment Transport Rates
sediment transport rate
13.1: Introduction to Sediment Transport Rates
selective entrainment
14.2: Several Consequences of Size
14.5: Deviations from the Condition of Equal Mobility
separation vortex
12.2: Unidirectional-Flow Bed Configurations
settling
15.1: Introduction to Deposition
settling velocity
3.9: Settling of Spheres
shear layer
12.2: Unidirectional-Flow Bed Configurations
shear stress
1.3: Viscosity
shear velocity
4.6: Flow Resistance
Shields curve
9.4: Movement Threshold
Shields diagram
9.4: Movement Threshold
Shields parameter
9.3: Balance of Forces and Dimensional Analysis
size fraction
14.1: Introduction
skimming flow
4.7: Velocity Profiles
skin friction
8.5: Variables
slip face
12.2: Unidirectional-Flow Bed Configurations
sorting
14.1: Introduction
8.1: Introduction to Sediments, Variables, and Flumes
spatial accelerations
8.3: Particle Motions vs. Turbulence
specific energy
5.4: Energy in Open-Channel Flow
specific head
5.4: Energy in Open-Channel Flow
specific weight
1.2: Pressure
spectral waves
6.3: Water Motions Due to Waves
splash function
11.2: Saltation I
stagnation points
3.3: Inviscid Flow
static pressure
1.2: Pressure
steady flow
4.1: Introduction to Flow in Channels
Stokes' law
3.2: Flow Past a Sphere at Low Reynolds Numbers
stoss surface
12.2: Unidirectional-Flow Bed Configurations
strata
16.1: Stratification and Cross Stratification
stratification
16.1: Stratification and Cross Stratification
stratified flows
5.1: Introduction to Open-Channel Flow
stratum
16.1: Stratification and Cross Stratification
streakline
3.4: The Bernoulli Equation
stream tube
3.4: The Bernoulli Equation
streamline
3.4: The Bernoulli Equation
structure
16.1: Stratification and Cross Stratification
subcritical flow
5.4: Energy in Open-Channel Flow
supercritical flow
5.4: Energy in Open-Channel Flow
surface creep
11.2: Saltation I
susceptibility
11.2: Saltation I
suspend load
10.1: Introduction to the Movement of Sediment by Water Flows
10.2: The Bed, the Flow, and the Load
suspension
10.4: Bed Load
sweep
4.8: More on the Structure of Turbulent Boundary Layers- Coherent Structures in Turbulent Shear Flow

T

temporal accelerations
8.3: Particle Motions vs. Turbulence

terminal velocity
3.9: Settling of Spheres

texture
16.1: Stratification and Cross Stratification

threshold shear stress
9.1: Introduction to Threshold of Movement

total head
5.4: Energy in Open-Channel Flow

traction
10.2: The Bed, the Flow, and the Load

traction carpet
10.4: Bed Load

transitionally rough flow
4.6: Flow Resistance

translatent laminae
16.4: Important Kinds of Climbing-Bed-Form Cross Stratification

translatory waves
6.2: The Nature of Waves

transport stage
10.3: Transport Mode Versus Flow Intensity

trough
12.2: Unidirectional-Flow Bed Configurations

truncation surfaces
16.2: The Nature of Cross Stratification

turbidity current
15.2: Modes of Deposition

turbulence
3.5: Turbulence

turbulence closure problem
4.4: Turbulent Shear Stress

turbulent diffusion
4.4: Turbulent Shear Stress

turbulent flow
4.3: Turbulent Flow in Channels - Initial Material

turbulent separation
3.8: Flow Past a Sphere at High Reynolds Numbers

turbulent shear flow
4.5: Structure of Turbulent Boundary Layers

turbulent shear stress
4.4: Turbulent Shear Stress

U

uniform flow
4.1: Introduction to Flow in Channels
5.3: Uniform Flow

unit sediment transport rate
13.2: The Sediment Load and the Sediment Transport Rate

upper flow regime
12.2: Unidirectional-Flow Bed Configurations

V

velocity defect law
4.7: Velocity Profiles

velocity head
5.4: Energy in Open-Channel Flow

Velocity Profile
4.7: Velocity Profiles

viscosity
1.3: Viscosity

viscous drag
2.1: Introduction

viscous length scale
4.6: Flow Resistance

viscous sublayer
4.5: Structure of Turbulent Boundary Layers

von Kármán's constant
4.7: Velocity Profiles

vortex ripples
12.6: Oscillatory-Flow and Combined-Flow Bed Configurations

vorticity
3.5: Turbulence
4.8: More on the Structure of Turbulent Boundary Layers- Coherent Structures in Turbulent Shear Flow

W

wake
3.6: Boundary Layers
3.7: Flow Separation

wash load
10.1: Introduction to the Movement of Sediment by Water Flows
10.2: The Bed, the Flow, and the Load

wave boundary layer
6.4: Wave Boundary Layers

wave friction factor
6.4: Wave Boundary Layers

wave steepness
6.2: The Nature of Waves

wave–current boundary layers
6.5: Combined Flow (Waves plus Current)

wavelets
6.2: The Nature of Waves

wind ripples
12.7: Wind Ripples and Eolian Dunes

This page titled Index is shared under a license and was authored, remixed, and/or curated by LibreTexts.

GLOSSARY

S

Sample Word 1 | Sample Definition 1

This page titled Glossary is shared under a CC BY-NC-SA 4.0 license and was authored, remixed, and/or curated by John Southard (MIT OpenCourseware) via source content that was edited to the style and standards of the LibreTexts platform.

DETAILED LICENSING

Overview

Title: Introduction to Fluid Motions and Sediment Transport (Southard)

Webpages: 122

Applicable Restrictions: Noncommercial

All licenses found:

- CC BY-NC-SA 4.0: 94.3% (115 pages)
- Undeclared: 5.7% (7 pages)

By Page

- Introduction to Fluid Motions and Sediment Transport (Southard) - *CC BY-NC-SA 4.0*
  - Front Matter - *CC BY-NC-SA 4.0*
    - TitlePage - *CC BY-NC-SA 4.0*
    - InfoPage - *CC BY-NC-SA 4.0*
    - Table of Contents - *Undeclared*
    - Licensing - *Undeclared*
  - 1: Introduction - *CC BY-NC-SA 4.0*
    - 1.1: The Nature of Fluids - *CC BY-NC-SA 4.0*
    - 1.2: Pressure - *CC BY-NC-SA 4.0*
    - 1.3: Viscosity - *CC BY-NC-SA 4.0*
    - 1.4: Diffusion - *CC BY-NC-SA 4.0*
  - 2: Flow Past a Sphere I - Dimensional Analysis, Reynolds Numbers, and Froude Numbers - *CC BY-NC-SA 4.0*
    - 2.1: Introduction - *CC BY-NC-SA 4.0*
    - 2.2: Which Variables are Important? - *Undeclared*
    - 2.3: Some Dimensional Reasoning and its Consequences - *CC BY-NC-SA 4.0*
    - 2.4: How to Construct Dimensionless Variables - *CC BY-NC-SA 4.0*
    - 2.5: What if You Choose the Wrong Variables? - *Undeclared*
    - 2.6: "Dimensional Analysis" - *CC BY-NC-SA 4.0*
    - 2.7: Significance of Reynolds Numbers and Froude Numbers - *CC BY-NC-SA 4.0*
  - 3: Flow Past a Sphere II - Stokes' Law, The Bernoulli Equation, Turbulence, Boundary Layers, Flow Separation - *CC BY-NC-SA 4.0*
    - 3.1: Introduction and the Navier-Stokes Equation - *CC BY-NC-SA 4.0*
    - 3.2: Flow Past a Sphere at Low Reynolds Numbers - *CC BY-NC-SA 4.0*
    - 3.3: Inviscid Flow - *CC BY-NC-SA 4.0*
    - 3.4: The Bernoulli Equation - *CC BY-NC-SA 4.0*
    - 3.5: Turbulence - *CC BY-NC-SA 4.0*
    - 3.6: Boundary Layers - *CC BY-NC-SA 4.0*
    - 3.7: Flow Separation - *CC BY-NC-SA 4.0*
    - 3.8: Flow Past a Sphere at High Reynolds Numbers - *CC BY-NC-SA 4.0*
    - 3.9: Settling of Spheres - *CC BY-NC-SA 4.0*
  - 4: Flow in Channels - *CC BY-NC-SA 4.0*
    - 4.1: Introduction to Flow in Channels - *CC BY-NC-SA 4.0*
    - 4.2: Laminar Flow Down an Inclined Plane - *CC BY-NC-SA 4.0*
    - 4.3: Turbulent Flow in Channels - Initial Material - *CC BY-NC-SA 4.0*
    - 4.4: Turbulent Shear Stress - *CC BY-NC-SA 4.0*
    - 4.5: Structure of Turbulent Boundary Layers - *CC BY-NC-SA 4.0*
    - 4.6: Flow Resistance - *CC BY-NC-SA 4.0*
    - 4.7: Velocity Profiles - *CC BY-NC-SA 4.0*
    - 4.8: More on the Structure of Turbulent Boundary Layers- Coherent Structures in Turbulent Shear Flow - *CC BY-NC-SA 4.0*
  - 5: Open-Channel Flow - *CC BY-NC-SA 4.0*
    - 5.1: Introduction to Open-Channel Flow - *CC BY-NC-SA 4.0*
    - 5.2: Two Practical Problems - *CC BY-NC-SA 4.0*
    - 5.3: Uniform Flow - *CC BY-NC-SA 4.0*
    - 5.4: Energy in Open-Channel Flow - *CC BY-NC-SA 4.0*
    - 5.5: The Hydraulic Jump - *CC BY-NC-SA 4.0*
    - 5.6: Hydraulic Regimes of Open-Channel Flow - *CC BY-NC-SA 4.0*
    - 5.7: Gradually Varied Flow - *CC BY-NC-SA 4.0*
  - 6: Oscillatory Flow - *CC BY-NC-SA 4.0*
    - 6.1: Introduction - *CC BY-NC-SA 4.0*
    - 6.2: The Nature of Waves - *CC BY-NC-SA 4.0*
    - 6.3: Water Motions Due to Waves - *CC BY-NC-SA 4.0*
    - 6.4: Wave Boundary Layers - *CC BY-NC-SA 4.0*
    - 6.5: Combined Flow (Waves plus Current) - *CC BY-NC-SA 4.0*

- 7: Flow in Rotating Environments - *CC BY-NC-SA 4.0*
  - 7.1: Playing on a Rotating Table - *CC BY-NC-SA 4.0*
  - 7.2: The Coriolis Effect on the Earth's Surface - *CC BY-NC-SA 4.0*
  - 7.3: The Rossby Number and Inertia Currents - *CC BY-NC-SA 4.0*
  - 7.4: The Ekman Spiral - *CC BY-NC-SA 4.0*
  - 7.5: Geostrophic Motion - *CC BY-NC-SA 4.0*
  - 7.6: Ekman Layers - *CC BY-NC-SA 4.0*
  - 7.7: Planetary Boundary Layers- The Ekman Layer, The Logarithmic Layer, and The Mixed Layer - *CC BY-NC-SA 4.0*
- 8: Sediments, Variables, and Flumes - *CC BY-NC-SA 4.0*
  - 8.1: Introduction to Sediments, Variables, and Flumes - *CC BY-NC-SA 4.0*
  - 8.2: Hydrodynamic Perspective - *CC BY-NC-SA 4.0*
  - 8.3: Particle Motions vs. Turbulence - *CC BY-NC-SA 4.0*
  - 8.4: Observing Sediment Transport - *CC BY-NC-SA 4.0*
  - 8.5: Variables - *CC BY-NC-SA 4.0*
  - 8.6: Flumes - *CC BY-NC-SA 4.0*
- 9: Threshold of Movement - *CC BY-NC-SA 4.0*
  - 9.1: Introduction to Threshold of Movement - *CC BY-NC-SA 4.0*
  - 9.2: Forces on Bed Particles - *CC BY-NC-SA 4.0*
  - 9.3: Balance of Forces and Dimensional Analysis - *CC BY-NC-SA 4.0*
  - 9.4: Movement Threshold - *CC BY-NC-SA 4.0*
  - 9.5: Recasting the Shields Diagram - *CC BY-NC-SA 4.0*
  - 9.6: The Effect of Density Ratio - *CC BY-NC-SA 4.0*
- 10: Movement of Sediment by Water Flows - *CC BY-NC-SA 4.0*
  - 10.1: Introduction to the Movement of Sediment by Water Flows - *CC BY-NC-SA 4.0*
  - 10.2: The Bed, the Flow, and the Load - *CC BY-NC-SA 4.0*
  - 10.3: Transport Mode Versus Flow Intensity - *CC BY-NC-SA 4.0*
  - 10.4: Bed Load - *CC BY-NC-SA 4.0*
  - 10.5: Suspension in a Shear Flow- The Diffusional Theory of Suspension - *CC BY-NC-SA 4.0*
- 11: Movement of Sediment by the Wind - *CC BY-NC-SA 4.0*
  - 11.1: Introduction - *CC BY-NC-SA 4.0*
  - 11.2: Saltation I - *CC BY-NC-SA 4.0*
  - 11.3: Saltation II - *CC BY-NC-SA 4.0*
- 12: Bed Configurations Generated by Water Flows and the Wind - *CC BY-NC-SA 4.0*
  - 12.1: Introduction to Bed Configurations - *CC BY-NC-SA 4.0*
  - 12.2: Unidirectional-Flow Bed Configurations - *CC BY-NC-SA 4.0*
  - 12.3: Velocity Profiles over Ripples - *CC BY-NC-SA 4.0*
  - 12.4: Movement of Ripples and Dunes - *CC BY-NC-SA 4.0*
  - 12.5: 2D Dunes and 3D Dunes - *CC BY-NC-SA 4.0*
  - 12.6: Oscillatory-Flow and Combined-Flow Bed Configurations - *CC BY-NC-SA 4.0*
  - 12.7: Wind Ripples and Eolian Dunes - *CC BY-NC-SA 4.0*
  - 12.8: Works Cited and Reading List - *CC BY-NC-SA 4.0*
- 13: The Sediment Transport Rate - *CC BY-NC-SA 4.0*
  - 13.1: Introduction to Sediment Transport Rates - *CC BY-NC-SA 4.0*
  - 13.2: The Sediment Load and the Sediment Transport Rate - *CC BY-NC-SA 4.0*
  - 13.3: Predicting the Sediment Transport Rate - *CC BY-NC-SA 4.0*
- 14: Mixed-Size Sediments - *CC BY-NC-SA 4.0*
  - 14.1: Introduction - *CC BY-NC-SA 4.0*
  - 14.2: Several Consequences of Size - *CC BY-NC-SA 4.0*
  - 14.3: A Look at Some Real Data on Fractional Transport Rates, From the Flume and From the Field - *CC BY-NC-SA 4.0*
  - 14.4: Movement Threshold in Mixed-Sized Sediments - *CC BY-NC-SA 4.0*
  - 14.5: Deviations from the Condition of Equal Mobility - *CC BY-NC-SA 4.0*
- 15: Deposition - *CC BY-NC-SA 4.0*
  - 15.1: Introduction to Deposition - *CC BY-NC-SA 4.0*
  - 15.2: Modes of Deposition - *CC BY-NC-SA 4.0*
  - 15.3: Why Deposition or Erosion? - *Undeclared*
- 16: Cross Stratification - *CC BY-NC-SA 4.0*
  - 16.1: Stratification and Cross Stratification - *CC BY-NC-SA 4.0*
  - 16.2: The Nature of Cross Stratification - *CC BY-NC-SA 4.0*
  - 16.3: The Basic Idea Behind Climbing-Bed-Form Cross Stratification - *CC BY-NC-SA 4.0*
  - 16.4: Important Kinds of Climbing-Bed-Form Cross Stratification - *CC BY-NC-SA 4.0*
  - 16.5: Cross Stratification Not Produced by Climbing Bed Forms - *CC BY-NC-SA 4.0*
- 17: Planar Stratification - *CC BY-NC-SA 4.0*
  - 17.1: Introduction to Planar Stratification - *CC BY-NC-SA 4.0*
  - 17.2: The Origin of Planar Lamination in Sands and Sandstones - *CC BY-NC-SA 4.0*
  - 17.3: Planar Lamination in Fine Sediments - *CC BY-NC-SA 4.0*
- Back Matter - *CC BY-NC-SA 4.0*
  - Index - *CC BY-NC-SA 4.0*
  - Index - *Undeclared*
  - Glossary - *CC BY-NC-SA 4.0*

- Detailed Licensing - *Undeclared*

This page titled Introduction to Fluid Motions and Sediment Transport (Southard) is shared under a CC BY-NC-SA 4.0 license and was authored, remixed, and/or curated by John Southard via source content that was edited to the style and standards of the LibreTexts platform.